This Bachelor's Thesis consists of the development of an electronic device for non-destructive characterization of the Modulus of Elasticity (MOE) of wood in standing trees, logs and boards. This way, wood from forestry can be characterized and classified for different purposes.

To estimate the MOE, the Time-of-Flight (ToF) approach is used. This method consists of measuring the transit time of an acoustic wave travelling longitudinally through the wood by using piezoelectric transducers. The signal arrival is detected accurately by complex pos-processing algorithms.

The project comprises all stages of electronic product development, from conception and specification through design and manufacturing, and ending with the validation of a prototype. This thesis has a multidisciplinary scope, and it has been accomplished by using Engineering Design Process methodologies during all stages of development.

Juan Del Pino Mena is a Telecommunication Engineer specialized in Electronics Systems from Arriate, Spain. With this Thesis he ends his Bachelor's Degree at the University of Granada. In 2021 he joined GranaSat, where he was a member of the technical support team for the Esero CanSat 2022 competition.

https://www.linkedin.com/in/dpmj/
https://github.com/dpmj

Andrés M. Roldán Aranda is the academic head of the present project, and the student's tutor. He is a professor in the Departament of Electronics and Computers Technologies at the University of Granada, and in charge of GranaSat.

BACHELOR'S THESIS

Development of an acoustic measurement system of the Modulus of Elasticity in trees, logs and boards

Juan del Pino Mena

TELECOMMUNICATIONS ENGINEERING

2022

UNIVERSITY OF GRANADA
BACHELOR'S THESIS IN TELECOMMUNICATIONS ENGINEERING

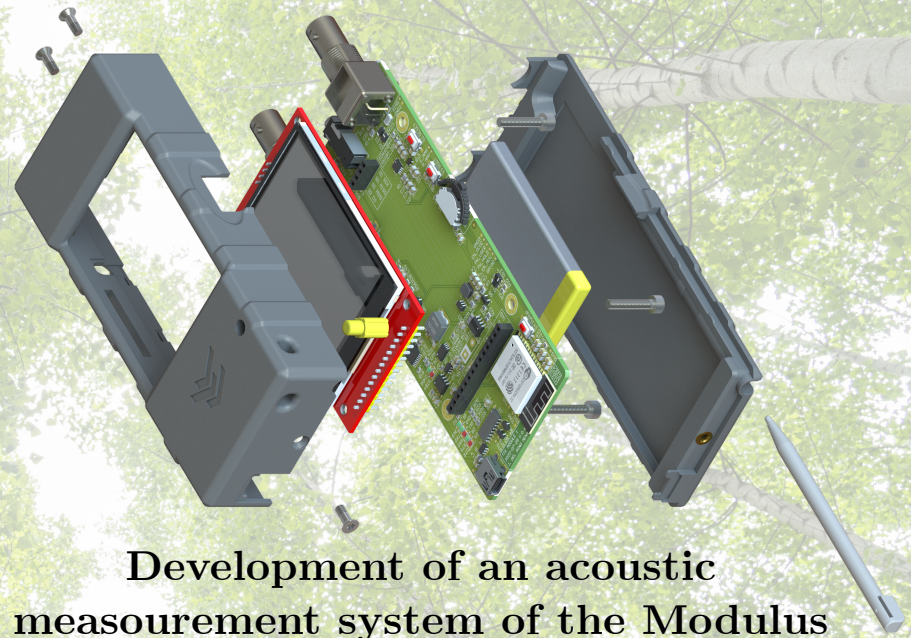

Development of an acoustic measourement system of the Modulus of Elasticity in trees, logs and boards

Juan Del Pino Mena

Academic course 2021/2022

SUPERVISOR:

Andrés María Roldán Aranda

Credits for the cover background: COMPOP/LWFF
Printed in Granada, September 2022

"Development of an acoustic measurement system of the Modulus of Elasticity in trees, logs and boards"

BACHELOR'S DEGREE IN TELECOMMUNICATION ENGINEERING

Bachelor's Thesis

"Development of an acoustic measurement system of the Modulus of Elasticity in trees, logs and boards"

ACADEMIC COURSE: 2021/2022

Juan Del Pino Mena

BACHELOR IN TELECOMMUNICATION ENGINEERING

"Development of an acoustic measurement system of the Modulus of Elasticity in trees, logs and boards"

AUTHOR:

Juan Del Pino Mena

SUPERVISED BY:

Prof. Andrés Roldán Aranda

DEPARTMENT:

Electronics and Computer Technologies

D. Andrés María Roldán Aranda, Profesor del departamento de Electrónica y Tecnología de los Computadores de la Universidad de Granada, como director del Trabajo Fin de Grado de D. Juan Del Pino Mena,

Informa:

Que el presente trabajo, titulado:

Development of an acoustic measurement system of the Modulus of Elasticity in trees, logs and boards

ha sido realizado y redactado por el mencionado alumno bajo mi dirección, y con esta fecha autorizo a su presentación.

Granada, a 7 de septiembre de 2022

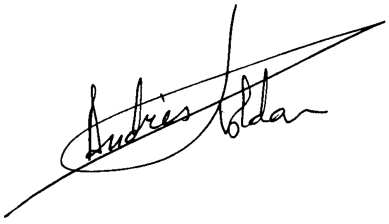

Fdo. Prof. Andrés María Roldán Aranda

Los abajo firmantes autorizan a que la presente copia de Trabajo Fin de Grado se ubique en la Biblioteca del Centro y/o departamento para ser libremente consultada por las personas que lo deseen.

Granada, a 7 de septiembre de 2022

Fdo. Juan Del Pino Mena

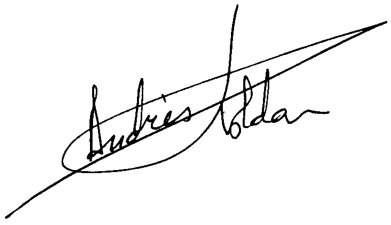

Fdo. Prof. Andrés María Roldán Aranda

"Development of an acoustic measurement system of the MoE in trees, logs and boards"

Juan Del Pino Mena

KEYWORDS:

Modulus of Elasticity (MOE), ToF, TIK, LIFE Wood For Future, ADIME, GranaSat, Poplar, NDT, Acoustic Wave, Piezoelectric Sensors, EDP, PCB, CAD, EDA, Firmware, Embedded System, RTOS, Reverse Engineering

ABSTRACT:

The objective of this Bachelor's Thesis is to develop a portable electronic device capable of quantifying the stiffness of the wood of standing trees, logs and boards using non-destructive testing (NDT) by means of acoustic wave analysis. As an indicator of stiffness, the Modulus of Elasticity (MOE) is used, a standard figure in the industry. This way, wood from forestry can be characterized and classified for different purposes.

This Thesis is part of LIFE Wood For Future, a project of the University of Granada (UGR) financed by the European Union's LIFE programme. LIFE Wood For Future aims to recover the cultivation of poplar *(populus sp.)* in the Vega de Granada, by proving the quality of its wood through innovative structural bioproducts. Recovering the poplar groves of Granada would have great benefits for the Metropolitan Area: creation of local and sustainable jobs, improvement of biodiversity, and increase in the absorption of carbon dioxide in the long term, helping to reduce the endemic air pollution of Granada. This Final Degree Project has been developed in collaboration with the ADIME research group of the Higher Technical School of Building Engineering (ETSIE) and the aerospace electronics group GranaSat of the UGR.

The goal of the developed device, named Tree Inspection Kit (or TIK), is to be an innovative, portable and easy-to-use tool for non-destructive diagnosis and classification of wood by measuring its MOE. TIK is equipped with the necessary electronics to quantify the Time of Flight (ToF) of an acoustic wave that propagates inside a piece of wood. In order to do this, two piezoelectric probes are used, nailed in the wood and separated a given distance longitudinally. The MOE can be derived from the propagation speed of the longitudinal acoustic wave if the density of the is known. For this reason, this device has the possibility of connecting a load cell for weighing logs or boards to estimate their density. It also has an expansion port reserved for future functionality.

A methodology based on the Engineering Design Process (EDP) has been followed. The scope of this project embraces all aspects of the development of an electronic product from start to finish: conceptualization, specification of requirements, design, manufacture and verification. A project of this reach requires planning, advanced knowledge of signal analysis, electronics, design and manufacture of Printed Circuit Boards (PCB) and product design, as well as the development of a firmware for the embedded system, based on a RTOS. Prior to the design of the electronics, a Reverse Engineering process of some similar products of the competition is performed; as well as an exhaustive analysis of the signals coming from the piezoelectric sensors that are going to be used, and the frequency response characterization of the piezoelectric probes themselves.

This project has as its ultimate goal the demonstration of the multidisciplinary knowledge of engineering, and the capacity of analysis, design and manufacturing by the author; his skill and professionalism in CAD and EDA software required for these tasks, as well as in the documentation of the entire process.

"Desarrollo de un sistema acústico de medida del MoE en árbol, troza y tabla"

Juan Del Pino Mena

PALABRAS CLAVE:

Módulo de Elasticidad (MOE), ToF, TIK, LIFE Wood For Future, ADIME, GranaSat, Chopo (*Poplar*), NDT, Onda Acústica (*Acoustic Wave*), Sensores Piezoeléctricos (*Piezoelectric Sensors*), EDP, PCB, CAD, EDA, Firmware, Sistema Empotrado (*Embedded System*), RTOS, Ingeniería Inversa (Reverse Engineering)

RESUMEN:

El presente Trabajo de Fin de Grado tiene como objetivo el desarrollo de un dispositivo electrónico portátil capaz de cuantificar la rigidez de la madera de árboles en pie, trozas y tablas usando ensayos no destructivos *(Non-Destructive Testing, NDT)* por medio del análisis de ondas acústicas. Como indicador de la rigidez se usa el Módulo de Elasticidad (MOE), una figura estándar en la industria.

Este TFG forma parte de LIFE Wood For Future, un proyecto de la Universidad de Granada (UGR) financiado por el programa LIFE de la Unión Europea. LIFE Wood For Future tiene como objetivo recuperar el cultivo del chopo *(populus sp.)* en la Vega de Granada demostrando la viabilidad de su madera a través de bioproductos estructurales innovadores. Recuperar las choperas de Granada tendría grandes beneficios para la zona del Área Metropolitana: creación de puestos de trabajo locales y sostenibles, mejora de la biodiversidad, e incremento de la tasa de absorción de dióxido de carbono a largo plazo, contribuyendo a reducir la contaminación endémica del aire en Granada. Este Trabajo de Fin de Grado se ha desarrollado con la colaboración del grupo de investigación ADIME de la Escuela Técnica Superior de Ingeniería de Edificación (ETSIE) y el grupo de electrónica aeroespacial GranaSat de la UGR.

El objetivo del dispositivo, denominado Tree Inspection Kit (TIK), es ser una herramienta innovadora, portátil y fácil de usar para el diagnóstico y clasificación no destructiva de la madera por medio de su MOE. TIK está dotado de la electrónica necesaria para medir el tiempo de tránsito (ToF) de una onda acústica que se propaga en el interior de una pieza de madera. Para ello, se utilizan dos sondas piezoeléctricas clavadas en la madera y separadas longitudinalmente una distancia conocida. De la velocidad de propagación de la onda longitudinal se puede derivar el MOE, previo conocimiento de la densidad del material. Por ello, este dispositivo cuenta con la posibilidad de conectarle una célula de carga y pesar trozas o tablas para estimar su densidad. También tiene un puerto de expansión reservado para funcionalidad futura.

Se ha seguido una metodología basada en el Proceso de Diseño de Ingeniería *(Engineering Design Process, EDP)*, abarcando todos los aspectos del desarrollo de un producto electrónico de principio a fin: conceptualización, especificación de requisitos, diseño, fabricación y verificación. Un proyecto de este alcance requiere de planificación, conocimientos avanzados de análisis de señales, de electrónica, de diseño y fabricación de Placas de Circuito Impreso (PCB) y de diseño de producto, así como el desarrollo de un firmware para el sistema empotrado, basado en un RTOS. Previo al diseño de la electrónica, se realiza un proceso de Ingeniería Inversa (Reverse Engineering) de algunos productos similares de la competencia; al igual que un exhaustivo análisis de las señales provenientes de los sensores piezoeléctricos que van a utilizarse y la caracterización en frecuencia de las propias sondas piezoeléctricas.

Este proyecto tiene como fin último la demostración de los conocimientos multidisciplinares propios de la ingeniería y la capacidad de análisis, diseño y fabricación por parte del autor; su habilidad y profesionalidad en el software CAD y EDA requerido para estas tareas, así como en la documentación de todo el proceso.

How many roads must a man walk down
Before you call him a man?

How many seas must the white dove sail
Before she sleeps in the sand?

Yes, and how many times must the cannonballs fly
Before they're forever banned?

The answer, my friend, is blowin' in the wind
The answer is blowin' in the wind

Bob Dylan

"Blowin' in the Wind"
On *The Freeewheelin' Bob Dylan*, 1963

Our Universe has never been so close.

25 December 2021	Launch of the James Webb Space Telescope.
12 July 2022	The James Webb Space Telescope officially enters service. Release of the first full-color images and spectroscopic data.

Cosmic Cliffs in Carina (NGC 3324) – Near Infrared Camera.
James Webb Space Telescope, 2022-07-12.

Acknowledgements

Sometimes we forgot the great importance of the people who are part of our life. This Bachelor's Thesis would not have been possible without them.

First of all, I want to thank my parents Maru and Juan and my sister María for their constant love, laughter, support and the happiness they imbue me with, and that I know I will always have.

To all my old and new friends, for all the great times we've had. To my classmates, who have made the degree more bearable during these intense years. And of course, thanks to the people who have put up with me the longest during this stage of my life, Arturo and Jorge. Wash the dishes, and do the laundry.

To my colleagues in the GranaSat laboratory for their help before and during the development of this Thesis (and for the delicious breakfasts). Special thanks to Irene Gil, who has been a great project colleague. Thanks to all the members of ADIME including, but not limited to, Elisabet Suárez, Antolino Gallego, Yaiza Fuentes and Miriam Castillo for their initiative and extraordinary work. And of course, thanks to Andrés Roldán, whose perseverance and ambition has allowed me to go further than I imagined, and in the process I found the vocation I was looking for.

Without a doubt, I must also thank the altruistic work of the thousand of communities and individuals that make free and accessible knowledge available on the Internet.

Thank you very much.

Agradecimientos

En ocasiones se olvida la gran importancia de las personas que forman parte de tu vida. Este Trabajo de Fin de Grado no hubiese sido posible sin ellas.

En primer lugar, quiero agradecer a mis padres Maru y Juan y a mi hermana María su constante cariño, risas, apoyo y la felicidad con la que me imbuyen, y que sé que siempre tendré.

A todos mis viejos y nuevos amigos, por todos los geniales momentos que hemos pasado. A mis compañeros de clase, que han hecho más llevadera la carrera durante estos intensos años. Y cómo no, también a las personas que más tiempo me han aguantado durante etapa de mi vida, Arturo y Jorge. Fregad los platos, y tended la lavadora.

A mis compañeros del laboratorio de GranaSat por su ayuda antes y durante el desarrollo de este Trabajo de Fin de Grado (y por los deliciosos desayunos). Un agradecimiento especial a Irene Gil, que ha sido una genial compañera de proyecto. Gracias a todos los integrantes de ADIME incluyendo, pero no limitado a, Elisabet Suárez, Antolino Gallego, Yaiza Fuentes y Miriam Castillo por su iniciativa y extraordinario trabajo. Y por supuesto, gracias a Andrés Roldán, cuya perseverancia y ambición me ha permitido llegar más lejos de lo que imaginé, y en el proceso he encontrado la vocación que buscaba.

Sin duda, debo agradecer también el trabajo altruista que realizan miles de individuos y comunidades que hacen posible un conocimiento libre y accesible en Internet.

Muchas gracias a todos.

Contents

List of Figures

List of Tables

Code Listings

List of Videos

Glossary

A | B | C | D | E | F | G | I | J | L | M | N | O | P | R | S | T | U | W

A

Acoustic Wave Also called *Sound wave*, it is a type of mechanical, elastic wave (see elastic deformation) that propagates by means of adiabatic loading and unloading. If it disseminate in an elastic and continuous medium, it generates a variation of pressure or density in said medium. The term "acoustic" refers to the frequency domain of the waves, which is comprised in the human-audible spectrum (usually defined between 20 Hz and 20 kHz) in contrast to ultrasonic waves [2].

Adiabatic process A kind of thermodynamic process in which the thermodynamic system does not exchange heat or mass with its surrounding environment.

ADIME (Acústica y Diagnóstico de Materiales y Estructuras, *Acoustics and Diagnosis of Materials and Structures*) Research group inside IDIE dedicated to the research of wood technology, structural wood materials, characterization of materials and non-destructive material tests and study of acoustic emission for structural monitoring [3].

Altium Designer® EDA software used to design Printed Circuit Board from schematics. It allows 2D and 3D Design, as well as simulation of the electronics.

Antenna A metallic structure that acts as an interface between radiated waves propagating through space and electronic circuits. Antennas can receive and/or transmit radio-frequency electromagnetic waves.

B

BJT (Bipolar-Junction Transistor) A type of semiconductor-based transistor that uses electrons and electron holes as carriers. The current flow between the "collector" and the "emitter" terminals is controlled by a small current injected at the "base" terminal.

Bypass capacitor A synonym for "decoupling capacitor".

C

C (C programming language) A high-level, cross-platform, compiled, imperative, structured, functional, procedural, static-type and general-purpose programming language with mechanisms to provide access to low-level functionality such as memory management.

C++ (C++ programming language) An evolution of the C programming language, matching all its features with the addition of objects (classes).

CAD (Computer-Aided Design) The usage of computer tools to aid during the process of creation, modification, analysis, or optimization of a design.

Choke An inductor specifically used to block high-frequency AC while passing low-frequency signals and DC.

Circuit topology The interconnections between the circuit components. Topology is not concerned with the physical layout of parts in a circuit, nor with their positions on a circuit diagram, but only what connections exist between the components. Different values or ratings of the parts are considered as being the same topology.

Conflict resource Natural resources whose systematic exploitation and trade in a context of conflict contribute to, benefit from or result in the commission of serious violations of human rights, violations of international humanitarian law or violations amounting to crimes under international law [4].

Coupling capacitor A capacitor used to couple an AC signal from one circuit phase to another, blocking the DC component. Functionally opposite to a decoupling capacitor.

D

Decoupling capacitor A decoupling capacitor removes unwanted AC components (noise and ripple) from a DC signal, making it more clean and stable. Usually 100 nF, ceramic, and located on the power input pins of an active device. This device is functionally opposite to a coupling capacitor. It's a common and effective technique for noise filtering on power traces. A bypass capacitor should be placed as close as possible to the pin of the component that uses such power rail. In addition, it provides a charge reserve physically near to the component itself, which supplies energy to the IC in case it has an irregular, pulsed power consumption characteristic. Thus preventing the supply voltage from decaying in short pulses and mitigating the effects it may have on the rest of the components connected to the same power rail.

Differential Pair A pair of parallel conductors of identical impedance carrying differential signals, which are two opposite, complementary signals. The receiving circuit responds to the difference between the two signals. This technique is used for example in high-fidelity audio and high-speed digital lines, with many advantages such as improving signal integrity, noise rejection and equalizing the time of arrival of delicate signals.

Diode An electronic component formed by a P-N semiconductor junction with two terminals ("anode" and "cathode"). It has low resistance in the *forward* direction (thus conducting current), and high resistance in the *reverse* direction.

Duty Cycle In a PWM signal, the duty cycle is the ratio of time the signal is HIGH with respect to the time it is LOW, in one period.

E

EDA (Electronic Design Automation) Also known as ECAD, (Electronic CAD), is a category of software tools for designing electronic such as s and Printed Circuit Boards.

Elastic Deformation Transitory strain that appears while applying a stress and disappears immediately upon removal of it [5].

Embedded System Systems which offers specialized and restricted functions. Their software and hardware resources are limited, and they are sized to your application. There are usually real-time constraints.

EMC (Electro-Magnetic Compatibility) the capability of electrical and electronic systems, equipment and devices to operate in their intended electromagnetic environment within a defined margin of safety, and at design levels of performance without suffering or causing unacceptable degradation as a result of Electro-Magnetic Interference [6].

EMI (Electro-Magnetic Interference) the process by disruptive electromagnetic energy is transmitted from one electronic device to another, via radiated or conducted paths (or both) [6].

F

Fakopp (Fakopp Enterprise Bt.) A company established in 2005 in Ágfalva, Hungary. The company is dedicated to the development and production of testing equipment for forestry and the wood industry.

Ferrite Bead A type of choke made of ferritic material that filter high-frequency AC and noise in a circuit.

FET (Field-Effect Transistor) A type of semiconductor-based transistor that uses an electric field to control the flow of current through the "drain" and "source" terminals by setting a voltage on the "gate" terminal.

Fiducial marks On a Printed Circuit Board, fiducial marks are pads of a determined size which act as reference points stencil alignment, computer vision automated component placement by pick and place machines and optical inspections systems. Usually found as round SMT pad of 1 mm in diameter, with solder mask expansion of 3 mm in diameter. To achieve the best measurement precision, fiducials should be placed as far from each other as possible, and no more than 3 should be placed in a single layer.

Filter A device or process that removes some components from a signal, like noise.

Firmware The software for an Embedded System.

Footprint A synonym for Land pattern, is the arrangement of pads used to physically and electrically attach a component to a Printed Circuit Board.

Form factor The size and shape of a Printed Circuit Board. Aspects such as the chassis, mounting schemes and standards are taken into consideration for defining a board form factor [7].

FR-4 (Flame Retardant 4) A designation for fiberglass-reinforced epoxy laminate material that it is self-extinguishing. Commonly used as an electrical insulator for electronic devices and Printed Circuit Board fabrication for its fire resistance, nearly zero water absorption and high mechanical strength.

FreeRTOS An open source RTOS for microcontrollers and small microprocessors [8].

G

GND (Ground) The reference net of an electronic circuit..

GNU/Linux A family of open source Unix-like OSes (called *"distributions"*) based on the Linux kernel and accompanied by GNU's software and libraries.

GPIB (General Purpose Interface Bus) A multi-master interface bus specification, based on the IEEE-488.2 standard. The bus is meant for parallel, short-range digital communications. Originally developed in the 1960s by Hewlett-Packard as HP Interface Bus(HP-IB), it's very common among old electronic instrumentation..

GranaSat *Electronics Aerospace Group.* An academic project from the UGR. This organization has an electronics laboratory where students from different degrees and education levels develop multidisciplinary projects [9].

Green wood Timber wood that has been recently cut and still has a significant amount of internal moisture.

I

IC (Integrated Circuit) A monolithic set of electronic circuits integrated onto a small flat piece of semiconductor material, usually silicon.

IDIE (Investigación y Desarrollo en Ingeniería de Edificación, *Research and Development in Building Engineering*) R&D group inside the Building Engineering department of the UGR. It has two separate lines of research: IDIE-ADIME and IDIE-IE [10].

IPython (Interactive Python) is a command shell for originally developed for Python (but nowdays it supports many other programming languages). It offers an interactive shells, debugging, media support, a browser-based notebook interface and parallel computing..

Isotropic material A material whose mechanical and thermal properties are the same in all directions.

J

Jupyter Lab A web-based interactive development environment for notebooks, code, and data. It an open, flexible environment with support for extensions. Jupyter supports multiple programming languages, but the main one is Python, which uses IPython as a interpreter and kernel.

L

Land pattern The arrangement of pads used to physically and electrically attach a component to a Printed Circuit Board.

Layer stackup Arrangement of conductive and insulating layers in a Printed Circuit Board.

Lead Can be referred to:
1. The chemical element with the symbol *Pb*, and atomic number 82. It is a heavy metal, very dense, malleable and with a relatively low melting point. It is also a toxic substance.
2. A length of rigid wire designed to electrically connect two spots.

LED (Light-Emitting Diode) A semiconductor diode that emits visible light when current flows through it. Photons are released by the recombination of electrons with electron holes. The color of the light is determined by the amount of energy that electrons require for crossing the band gap of the semiconductor.

LWFF (LIFE Wood For Future) The LIFE Wood For Future project aims to recover the poplar cultivation in the Vega de Granada to enhance biodiversity and long-term carbon sequestration through structural bioproducts. LWFF is financed by the EU's LIFE programme (code LIFE20 CCM/ES/001656).

M

Microcontroller A standalone computer which contains one or more CPUs or cores along with memory and peripherals on a single Integrated Circuit. Is similar to, but less sophisticated than, a SoC. These chips are meant for embedded devices, in opposition to the microprocessors used in general purpose applications.

Microprocessor A type of IC circuit that contains the arithmetic-logic and control blocks required to perform the tasks of a CPU.

Microsoft Windows A proprietary OS developed by Microsoft.

Microwaves The name given to electromagnetic waves with frequencies between 300 MHz and 300 GHz. In this range, the wavelengths vary between one meter and one millimeter, respectively.

Mil Unit of length equal to 0.001 inches, or 0.0254 mm.

Mixed Technology On a Printed Circuit Board, the usage of both SMT and THT [11] [12].

MOE (Modulus Of Elasticity) Also known as Elastic Modulus, is the resistance of an object or substance to being elastically deformed (elastic deformation) when a stress is applied to it [5].

Mounting Holes Drill holes on a Printed Circuit Board meant to mechanically support the board inside a enclosure or surface, or for the mechanical attachment of components to the Printed Circuit Board [12].

N

Noise Unwanted and unpredictable disturbance in a signal.

O

OpAmp Un amplificador operacional es un bloque de amplio uso en el diseño analógico formado por un amplificador de tensión de alta ganancia acoplado en DC a la entrada diferencial y con salida simple. La tensión que genera a la salida es cientos de miles de veces mayor que la diferencia de tensión entre los terminales de la entrada.

Open Hardware The philosophy of open source but applied to mechanical, electric and electronic resources.

Open Source An initiative in which the developer licenses a software or resource to grant users the rights to use, change, make derived work and freely distribute the software and its source code [13].

P

PC Oscilloscope A type of digital oscilloscope which relies on a PC for waveform display and instrument control. Most high-end digital oscilloscopes integrate a computer for this purpose, but they also exist external oscilloscopes which connect via USB or Ethernet to a PC .

PCB (Printed Circuit Board) A rugged, non-conductive boards built on a dielectric substrate structure used to provide electrical connection between the components of a electronic circuit, as well as mechanical support for those components [7].

PDF3D A PDF which contains an embedded 3D model.

Pick and Place machine A machine with a robot arm and computer vision for picking components from a feeder and inserting them into a specific site on the Printed Circuit Board [12].

PicoScope Series of external PC Oscilloscopes from Pico Technology. This term can also refer to the real-time signal acquisition software for these devices.

Piezoelectricity The property of certain materials to generate an electric charge in response to a mechanical stress, and vice versa: they have the ability to generate a mechanical movement or vibration in response to an electric stimulus.

Plastic Deformation Strain that appears when a stress is applied and does not disappear when the stress is removed. The level of stress needed to initiate plastic deformation is known as the *yield strength* [5].

Poisson's Ratio The measure of the deformation of a material perpendicular to the direction of loading.

Poplar (In Spanish: *álamo, chopo*) Common name for *Populus sp.*, a genus in the family *Salicaceae*. These trees are generally tall, straight and grow fast.

Python A high-level, cross-platform, interpreted, dynamically-typed, garbage-collected, general-purpose programming language. Has strong emphasis in code readability and includes a comprehensive standard library. It supports structured, object-oriented and functional programming paradigms.

R

RE The analysis of a device or piece of software to determine how it functions, with very little insight into exactly how it does so, and with the intent of recreating or modifying it.

Re-flow soldering The process consists on joining components to substrates by placing the parts into solder paste and then warming the paste up to its melting point for a short period of time, in order to achieve re-flow and the interconnection between a component terminal and a Printed Circuit Board pad [12].

Resonance A phenomenon of increased amplitude that occurs in object free-to-vibrate objects when the frequency of an applied periodic force matches the object's natural (or resonant) frequency.

Ripple A residual, periodic variation of a DC voltage due to incomplete suppression of the AC signal after rectification.

RoHS (Restriction of Hazardous Substances) European normative that restricts the use of the following hazardous substances in electrical and electronic equipment: lead (Pb), mercury (Hg), cadmium (Cd), hexavalent chromium (Cr6+), polybrominated biphenyls (PBB), polybrominated diphenyl ether (PBDE), bisphthalate (DEHP), butyl benzyl phthalate (BBP), dibutyl phthalate (DBP) and diisobutyl phthalate (DIBP) in a concentration no larger than 1000 ppm [14].

S

SCPI (Standard Commands for Programmable Instruments) A standard command syntax designed for controlling instruments.

Silkscreen Also called *"overlay"*, is the layer of shapes and text printed above the solder mask.

Silviculture The cultivation of trees.

SoC (System on Chip) that integrates all the components within a chip including analog, digital, mixed and even radio frequency functionality.

Solder mask The insulating polymer coating used to mask or protect the Printed Circuit Board's copper tracks from chemical and abrasive damage, such as corrosion and oxidation, dirt, dust, and fingerprints. It also masks off a PCB surface and prevents masked areas of being poured by solder during wave reflow soldering and other processes such as etchant or plating. This way, only the desired pads are soldered and no shorts are created between tracks [15]. Solder mask is also colored, giving the PCBs a distinct colour, being usually green.

Solder paste A sticky mixture of powdered solder (the fusible metal alloy which bonds pads and components) and flux (a viscous chemical cleaning agent).

SolidWorks® CAD software from Dassault Systèmes for 3D Mechanical Design.

Stencil A sheet of material (usually plastic or stainless steel) with openings according to the solder mask. The apertures are the same shape and size as the SMD component pads, and are placed in their corresponding position. With the stencil it is easy to deposit the right amount of solder paste accurately and repeatably.

Strain Elongation or dimensional change of an object or substance from its original dimensions [5].

Stress Load or force per unit area. In a material, application of stress causes strain [5].

T

Test Point In a PCB, a test point is a special THT or SMT pad used to inspect or inject signals on a circuit. During the manufacturing process, test points are used to verify that a electronic device is working correctly. Test points may also be used subsequently to repair a device if it malfunctions or if it needs a calibration.

Transistor A device capable of amplifying and/or switching electric signals or power. A voltage or current applied to a pair of its terminals controls the current through another pair.

U

Ultrasonic wave Equivalent to sound waves (acoustic waves), but with a frequency spectrum higher than the upper audible limit of human hearing (20 kHz).

UNIX A family of OSes which derive from the original Unix developed at the Bell Labs Research Center.

W

Wave soldering A standard method for industrial, mass soldering of leaded THT components onto Printed Circuit Boards. Consists of passing loaded boards over a wave of liquid solder. This soldering can be used successfully for assembly of Mixed Technology boards [11].

Acronyms

A | B | C | D | E | F | G | I | L | M | N | O | P | Q | R | S | T | U | V | W

A

ABS Acrylonitrile Butadiene Styrene.

AC Alternating Current.

ADC Analog-to-Digital Converter.

AGPL GNU Affero General Public License.

AIC Akaike Information Criterion.

ASIC Application-Specific Integrated Circuit.

AWGN Additive White Gaussian Noise.

B

BGA Ball Grid Array.

BLE Bluetooth Low-Energy.

BMS Battery Management System.

BNC Bayonet Neill–Concelman.

BOM Bill Of Materials.

BSD Berkeley Software Distribution.

BT Bluetooth.

C

CC-BY-SA Creative Commons Attribution-ShareAlike.

CE Conformité Européenne.

CLI Command Line Interface.

CNC Computer Numerical Control.

CPU Central Processing Unit.

CSV Comma-Separated Values.

CTS Clear To Send.

D

DAC Digital-to-Analog Converter.

DBH Diameter at Breast Height.

DC Direct Current.

DCD Data Carrier Detect.

DDS Direct Digital Synthesis.

DHCP Dynamic Host Configuration Protocol.

DMA Direct Memory Access.

DPAK Decawatt Package.

DSR Data Set Ready.

DTR Data Terminal Ready.

DUT Device Under Test.

E

EDP Engineering Design Process.

EEA European Economic Area.

EEE Electric and Electronic Equipment.

EMD Empirical Mode Decomposition.

ESD Electro-Static Discharge.

ESL Equivalent Series Inductance.

ESP-IDF Espressif IoT Development Framework.

ESR Equivalent Series Resistance.

EU European Union.

EULA End User License Agreement.

F

FAO Food and Agriculture Organization.

FFT Fast Fourier Transform.

FIR Finite Impulse Response.

FOSS Free Open Source Software.

FSM Finite State Machine.

G

GBL Gerber Bottom Layer.

GBO Gerber Bottom Overlay.

GKO Gerber Keep Out.

GNU GNU's Not Unix!.

GPIO General Purpose Input/Output.

GPL GNU General Public License.

GTL Gerber Top Layer.

GTO Gerber Top Overlay.

GTS Gerber Top Solder.

GUI Graphical User Interface.

I

I2C Inter-Integrated Circuit.

I2S Inter-Integrated Sound.

IDE Integrated Development Environment.

IEEE Institute of Electrical and Electronics Engineers.

IIR Infinite Impulse Response.

IoT Internet of Things.

IP Internet Protocol.

L

LAN Local Area Network.

LCD Liquid-Crystal Display.

LDO Low Drop-Out regulator.

LGPL GNU Lesser General Public License.

Li-Ion Lithium-Ion.

Li-Po Lithium-Polymer.

LIFE L'Instrument Financier pour l'Environnement.

LSB Least Significant Bit.

LVGL Light and Versatile Graphics Library.

M

MATLAB MATrix LABoratory.

MCU Micro-Controller Unit.

MIT Massachusetts Institute of Technology.

MLCC Multi-Layer Ceramic Capacitor.

MMC Multi-Media Card.

MODEM MOulator-DEModulator.

MOSFET Metal-Oxide-Semiconductor Field-Effect Transistor (FET).

MSOP Mini Small Outline Package.

Mutex Mutual Exclusion.

N

NC Drill Numeric Control Drill.

NDT Non-Destructive Test/Testing.

Ni-Cd Nickel-Cadmium.

Ni-MH Nickel-Metal Hydride.

Nmap Network Map.

NTC Negative Temperature Coefficient.

O

OMTP Open Mobile Terminal Platform.

OS Operating System.

OTG On-The-Go.

P

PA12-CF Polyamide 12 (a.k.a. Nylon12) - Carbon Fiber reinforced.

PC Personal Computer.

PCBLIB Printed Circuit Board Library.

PDF Portable Document Format.

PDS Power Delivery System.

PETG Polyethylene Terephthalate Glycol-modified.

PGA Programmable-Gain Amplifier.

PLA Poly-Lactic Acid.

PSF Python Software Foundation.

PWM Pulse-Width Modulation.

Q

QFN Quad-Flat No-leads package.

QFP Quad-Flat Package.

R

R&D Research and Development.

RAM Random Access Memory.

RF Radio Frequency.

RGB Red Green Blue.

RI Ring Indicator.

RTOS Real-Time Operating System.

RTS Request To Send.

S

SBC Single-Board Computer.

SCHLIB Schematic Library.

SD Secure Digitaly.

SDK Software Development Kit.

SKU Stock Keeping Unit.

SMA SubMiniature version A.

SMD Surface-Mount Device.

SMP Symmetric Multi-Processing.

SMT Surface-Mount Technology.

SNR Signal to noise ratio.

SoC System on Chip / State of Charge.

SOP Small Outline Package.

SOT Small Outline Transistor.

SPI Serial Peripheral Interface.

SPICE Simulation Program with Integrated Circuit Emphasis.

T

TARB True ARBitrary.

TFT Thin-Film Transistor.

THD Through-Hole Device.

THT Through-Hole Technology.

TIK Tree Inspection Kit.

ToF Time of Flight.

TPU Thermoplastic Polyurethane.

TSSOP Thin Shrink Small Outline Package.

TX Transmitter / Transmission.

U

UART Universal Asynchronous Receiver/Transmitter.

UGR University of Granada.

UI User Interface.

ULP Ultra Low Power.

USB Universal Serial Bus.

V

VAT Value Added Tax.

W

WBS Work Breakdown Structure.

Chapter 1

Introduction

This Thesis is presented as the result of the knowledge acquired in the Bachelor's Degree in Telecommunications Engineering, and specially during the development process of this project. This document aims to reflect the engineering process behind an electronic product: from conception and analysis to specification, system design, implementation, fabrication and verification. The overall goal of the project is to develop a measuring instrument (called TIK, *Tree Inspection Kit*) to find the Modulus of Elasticity of standing trees, logs and wood boards.

The MOE (*Modulus of Elasticity*, or *Elastic Modulus*) is the resistance of an object or substance to being elastically deformed when a stress is applied to it. The elastic deformation is a transitory strain that appears while applying a stress and disappears immediately upon removal of it (in opposition to plastic deformation) [5]. The MOE of a material gives us an indication of its stiffness: the higher the MOE, the higher the stiffness. For structural applications, one of the quality markers of wood is stiffness [16].

This project has been carried out within the framework of *C4 Action: "Development of the Tree Inspection Kit (TIK) tool to assess the quality of wood"* of the European project LIFE Wood For Future (code: LIFE20 CCM/ES/001656) *"Recovery of Granada-Vega poplar groves to boost biodiversity and long-term carbon capture through structural bioproducts"* [17, 18]. LWFF is in turn part of the European LIFE programme. LIFE is the European Union's funding programme dedicated to environmental, climate and energy objectives. It encourages the shift towards a clean, circular, energy efficient, climate-neutral and climate-resilient economy [19].

The action consists of the creation of a first prototype, an engineering model, which begins the development of the TIK tool. TIK's goal is to be an innovative, portable and easy-to-use equipment for the diagnosis and non-destructive classification of wood, by measuring its MOE.

(a) *The LIFE programme logo.*

(b) *The LWFF project logo.*

Figure 1.1 – *The LIFE and LWFF logos.*

1.1 Motivation

1

The Metropolitan Area of Granada has one of the worsts grades of contamination in Spain according to the 2020 report of air quality in Spain [20] only after Madrid and Barcelona, the two largest cities in the country. In this regard, Granada has the geographical disadvantage of being surrounded by Sierra Nevada: the mountain range makes natural wind ventilation difficult, favoring thermal inversion. But this alone is not enough reason, as highly polluting human activities are not being addressed: the high traffic of vehicles, the use of highly contaminating heating systems in winter and the burning of pruning remains and stubble [21]. This has been a well-known problem from a long time, but little action has been taken [21, 22, 23, 24].

In a contradictory way, in the last 20 years the poplar silviculture in the Vega de Granada has been severely reduced. This is mostly caused by the loss of economic competitiveness of the poplar trees compared to crops, along with a absence of association in the sector and a lack of appreciation of the environmental advantages of poplar trees [25]. In this line, poplar trees provide multiple environmental benefits: they have a high carbon sequestration capacity and thus they improve the quality of the air, they help to conserve the quality of the soil (absorbing nitrogen and phosphorus) and act as water cycle regulators (they filter the water before it reaches aquifers, moderate river floods and protect against erosion...).

With the development of innovative manufacturing processes of structural wood, a great chance arises for the Vega de Granada to develop a local industry with a nearly zero ecological footprint while acting as a contamination absorption ring for the Metropolitan Area of Granada. For this, it is necessary that its wood is of quality and is exploited efficiently: the price of wood is directly related to its quality, which depends on properties such as density, fiber orientation, rigidity and mechanical resistance [16].

Nowadays, the EU legislation on energy efficiency requirements of buildings (directives 2010/30/EU [26] and 2012/27/EU [27]) positions wood as a key material in the construction sector with the appearance of the concepts such as *sustainable construction* and *Nearly Zero Energy Buildings*. Also, the incorporation of wooden materials into Mediterranean structures can have beneficial results such as better winter performance (and therefore energy savings), cost-effectiveness, comfort and lower exploitation of environmental resources [28]. For structural applications, wood is selected based on its stiffness. Thus, knowing its properties and classifying wood as early as possible is of great value.

With all of the above, the need for adequate characterization tools is indisputable. It is at this point that the purpose of this project arises: the development of a measuring instrument to find the Modulus of Elasticity in standing trees, trunks and wooden boards; since the MOE and the stiffness are directly related.

From the perspective of Telecommunications and Electronics Engineering, this is an opportunity to develop all the aspects of an electronic product from start to finish. Addressing a project of this reach requires advanced knowledge of signal acquisition, analysis and processing, electronics, Printed Circuit Board design and fabrication, mechanical considerations and the firmware development for an embedded system.

(a) *Pollution haze in Granada, by Alfredo Aguilar.* **(b)** *Poplars in the Vega de Granada. Credits: [29]*

Figure 1.2 – *Two typical landscapes of Granada.*

1.2 State of the Art

This section serves as an introduction to the current situation of poplar cultivation, provides the theoretical basis for the non-destructive measurement of wood properties using acoustic waves, and presents a view of the current state of competing electronic equipment.

1.2.1 Poplar cultivation

The poplar is a species highly demanded by farmers around the world and the wood industry; being fast growing and short cycle (they can be harvested from 9 years old to 18 years old). Its cultivation is recommended by the FAO, which has created the International Commission on Poplars and Other Fast-Growing Trees (IPC) as sustainable forest exploitation, re-population and for combating desertification [30].

Poplar wood has been traditionally used in pulp, plywood, reconstituted wood panels and engineered lumber, but also matches, furniture, and fuelwood [31]. At present, new innovative applications are being investigated by the COMPOP research project (code: BIA2017-82650-R) [32], through engineering products made in combination with other woods and synthetic materials such as carbon fiber [33, 34, 35].

1.2.1.1 Poplar cultivation in the World, Europe, Spain, Andalusia and Granada.

In 2011, the total area of poplars in the world was estimated in 87 Mha (an increase of 8.5 Mha from 2007). Of which, the 88 % are found in natural forests and 9 % in plantations. Indigenous poplar forests cover significant areas in northern hemisphere countries with vast land areas and rich forest resources, such as Canada (30.3 Mha), Russia (24.7 Mha), USA (17.7 Mha) and China (2.5 Mha) [36]. At the plantations level, the leading two world regions are South Asia, with significant investments made by India and China (the latter having the most dedicated area in the world, 7.6 Mha); followed by Europe [36].

The total poplar area reported by 14 EU countries in 2015 ascends to over 800 000 ha, of which 611 000 ha (76 %) are plantations. The three leading countries are France (360 000 ha), Spain (144 500 ha) and Italy (134 300 ha) (see Figure 1.3). Of the total European poplar area, 609 000 ha (76 %) serve as wood resources for industries and biomass; and 209 000 ha (26 %) provide environmental functions (protection of the soil, carbon sequestration...) [37].

In Spain, the poplar harvesting industry provides employment to 11 000 workers in direct and indirect jobs; and the industrial sector that uses poplar as a raw material exceeded 350 M€ in 2017 [38, 39]. The poplar wood consumption is expected to increase in the coming years. However, statistics indicate that production is declining due to the consequences of the 2008 economic crisis, the absence of public subsidies, canon policies, and delays in the issuance of planting/cutting permits. This situation has discouraged private owners, who have opted for more cost-effective crops [38, 39]. A considerable increase in plantations is needed in the next few years to cover the industry needs and prevent its disappearance.

As we can see in Figure 1.3b, there are great regional differences in Spain. The vast majority of the national poplar wood comes from the Duero and the Ebro basins. As of 2018, Andalucía contributed only 7 % of the national yield. On the other hand, Granada generated 85 % of the total Andalusian output.

The In 2002, the area was estimated at 12 000 ha in the province of Granada. In 2018, it is estimated between 2 000 and 4 000 ha [39]. This is again due to economic viability issues: small and disseminated plantations, lack of organization of the poplar farmers, and local wood is perceived by the industrial sector as low quality, so it is used to make pallets and assembly boxes. Low wood prices equals low profitability.

The majority of poplars are standardized hybrids of the *populus* genus such as the I-214 clone, which is very extended for its high resistance to diseases [31]. However, for structural applications and overall quality of wood, the MC clone is preferred for its higher MOE in less growth time [40].

1

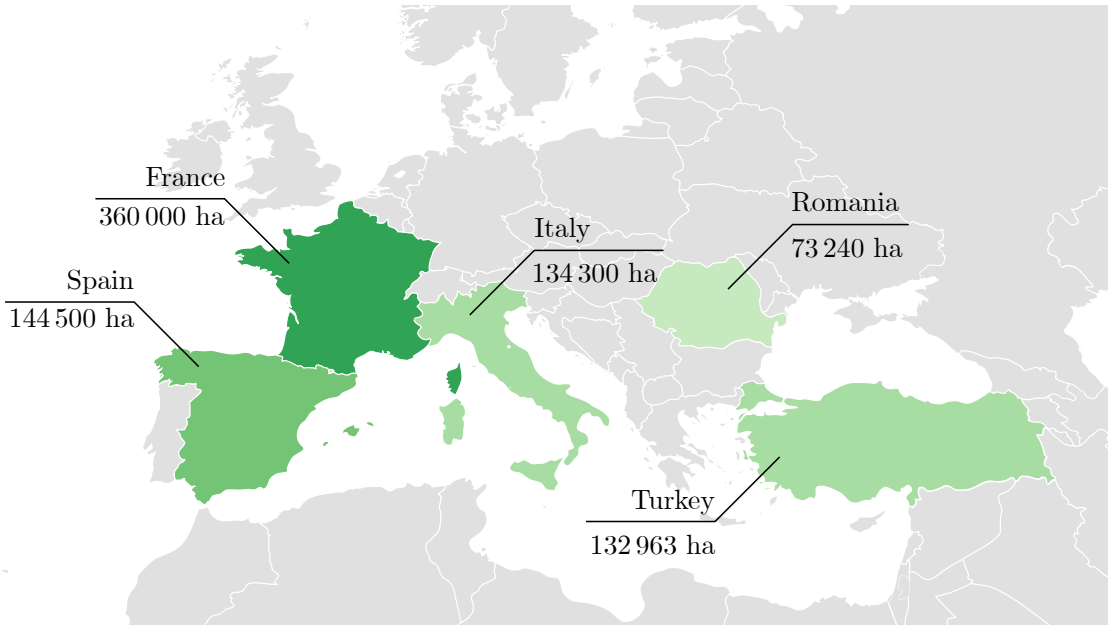

(a) *The 5 countries with the largest cultivated poplar area in Europe. Figures from the period 2008-2011 (Turkey and Romania) and 2012-2015 (remaining). Data from the latest public-available statistics by the International Poplar Commission [41, 37]. Empty world map credits: [42].*

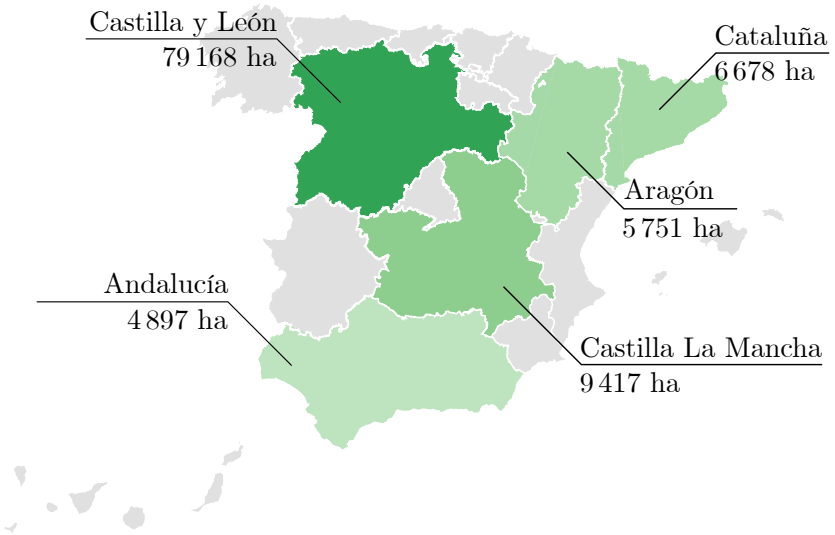

(b) *The 5 Autonomous Communities of Spain with the largest poplar area. Data from the 2019 survey on surfaces and crop yields (ESYRCE) [43]. Empty map of Spain credits: [44]. Important note: this data are significantly newer than the map above.*

Figure 1.3 – *Maps on poplar cultivation in Europe and Spain.*

1.2.2 Non-destructive testing of wood

A non-destructive test is the examination or evaluation performed on any type of sample object without altering or damaging it. NDT is based on the indirect determination of a physical property. This type of test is therefore very advantageous, since it can be carried out at any stage of the production, and even on products and structures once they have been put into service. [45] There are 3 major areas of NDT [16]:

- **Defectology.** Determine the absence or presence of conditions or discontinuities that may have an effect on the usefulness or serviceability of that object.
- **Metrology.** Measurement of the geometry, dimensions, configuration and assembly.
- **Characterization of materials.** Identification of physical and chemical properties of substances.

In this Thesis, we are interested in the latter. In particular, in the measurement of MOE, a physical property of materials directly related to their stiffness, so that wood can be classified for use in structural applications. We will resort to acoustic methods, widely used in the industry for its portability and cost-effectiveness. The following sections delve into the types of measurements and their fundamentals.

1.2.2.1 Acoustic wave propagation in wood

Material evaluation by acoustic methods has become widely accepted in the forest products industry as a non-destructive way of measuring the intrinsic properties of wood and classifying it according to its quality [46]. There are different methods, some more appropriate and accurate depending on whether it is measured on logs and boards or in standing trees.

An acoustic wave is a type of elastic wave which is propagated in a medium, and its frequency domain does not exceed the upper limit of the human audition, usually defined as 20 kHz. An ultrasonic wave is equivalent to an acoustic one, but whose frequency spectrum is higher than the human-audible range, but are still propagated as waves of particle vibrations. These waves travel long distances in uniform solid materials and low-viscosity liquids. On the other hand, voids gases such as air quickly attenuate them. Their velocity is constant in homogeneous materials [47].

Ultrasonic waves can be generated by radio-frequency electromagnetic waves or pulses driving a piezoelectric crystal. This technique is usually used to analyze the reflections received by the piezoelectric transducer to measure depth, thickness or to analyze a material in search of flaws or internal fractures. The waves can also be generated by a physical hit and then picked up by electronic tools. When wood surface is knocked, the generated acoustic or ultrasonic waves travels through the wood as stress waves in different modes [46, 48] (see Figure 1.4 and Figure 1.5):

- **Longitudinal waves (or P-waves).** These waves correspond to the motion of the particles back and forth along the direction of wave propagation, such that the particle velocity is parallel to the wave velocity. Longitudinal waves are compressional.
- **Distortional waves (or shear waves).** In which the movement of the particles transporting the wave is perpendicular to the direction of propagation of the wave itself.
- **Surface waves (or Rayleigh wave).** A disturbance in the material surface, restricted to the region adjacent to the impact as particle velocity decays exponentially. Similar to water surface waves, particles move both up and down and back and forth in elliptical trajectories.

Although most of the impact energy is transmitted by surface and shear waves, the longitudinal wave travels faster and is the easiest to detect by instruments. Therefore, the longitudinal wave is the most used for the characterization of materials, and especially wood [46].

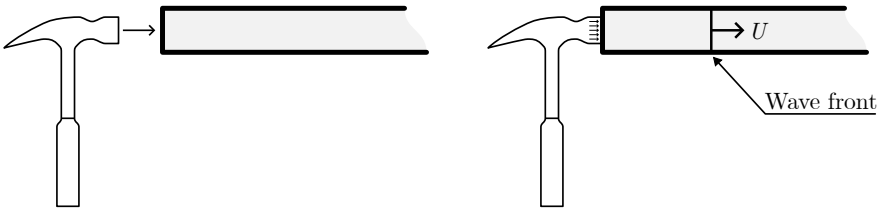

(a) *Hammer impacting slender body. Only the longitudinal wave is drawn, which propagates in a wave front.*

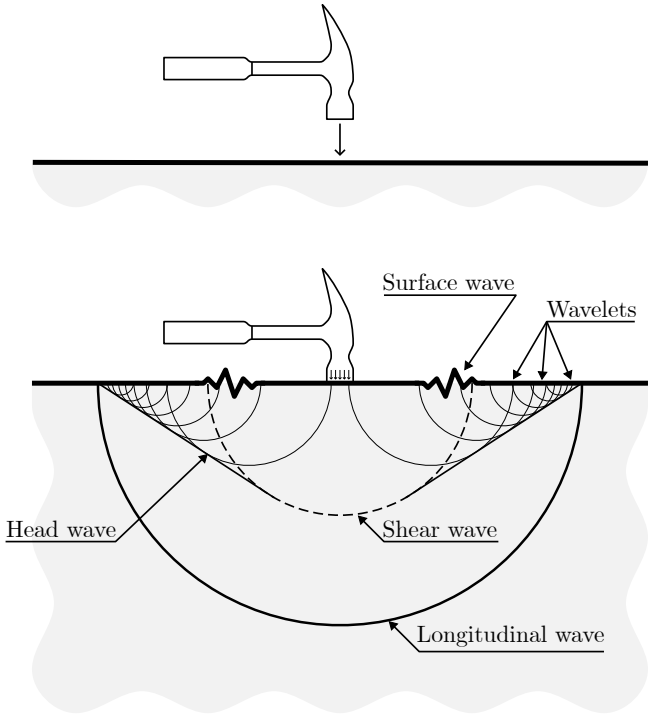

(b) *Hammer impacting semi-infinite body. Notice the formation of longitudinal, shear and surface waves.*

Figure 1.4 – *Propagation of waves in slender body and in a semi-infinite body. Own work, based on [48] (figure 2.5).*

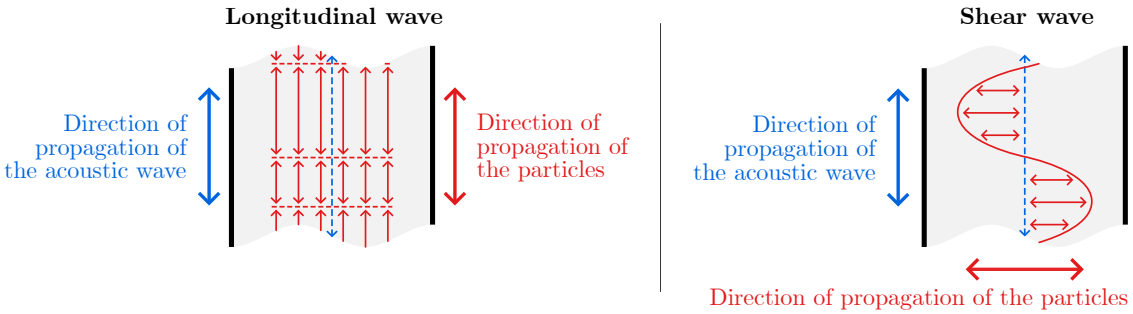

Figure 1.5 – *Comparison between longitudinal waves and shear waves. Own work, based on [16] (figure 1).*

1.2.2.1.1 Relationship between wood properties and longitudinal wave velocity

Some approaches based on wave theory proposed in the literature are presented below:

- **One-dimensional wave approach.** In a long, thin, isotropic material, strain and inertia in the transverse direction can be ignored; and therefore it can be considered that longitudinal waves propagate in a planar wave front. Its velocity can be approximated by Equation 1.2.1 [46]:

$$C_0 = \sqrt{\frac{E}{\rho}} \tag{1.2.1}$$

  Where C_0 is the wave velocity in the longitudinal axis, E is the MOE and ρ is the material density. For green wood, green density is used, which is found by destructive analysis. Green density varies with the species and from tree to tree, but characteristic values can be used [49].

- **Three-dimensional wave approach.** In an infinite, isotropic, elastic medium the wave front of the longitudinal wave cannot be considered planar and the velocity of the three-dimensional longitudinal wave (also known as *dilatational* wave) is defined by Equation 1.2.2 [48]:

$$C = k \cdot \sqrt{\frac{E}{\rho}} \quad ; \quad \text{Where} \quad k = \sqrt{\frac{1-\nu}{(1+\nu)\cdot(1-2\nu)}} \tag{1.2.2}$$

  C is the velocity of the dilatational wave and ν is the Poisson's Ratio of the material, usually acquired by destructive analysis. Since common materials are in the range of $\nu \in [0, 0.5]$, $k \geq 1$ and so $C \geq C_0$: the velocity of the dilatational wave is always greater of equal to the velocity of the planar longitudinal wave. As ν increases, so does the deviation of C from C_0.

  Poisson's ratio of green wood is not explicitly known, but as with green density, some studies have given characteristic figures according to its species [49]. An average value of $v_{LR} = 0.37$ has been suggested for softwoods and hardwoods [46].

As we can see, the elasticity and density of an isotropic material determines the wave velocity. Therefore, if we can measure the density and propagation speed of the longitudinal wave, we will find the MOE. However, the above approaches have a handful of important setbacks:

- The approximations are conditioned to homogeneous and isotropic materials, and wood is neither of them. Besides, other factors such the log diameter, age, temperature, and moisture can alter the longitudinal velocity on trees and logs [46].

- Wood properties vary with depth from the bark and from the base to the top of the tree. Soil and environmental conditions can create differences among the same species and even clones [46].

- Since wood is a non-isotropic medium, by extracting the MOE from a measurement along the longitudinal axis, we are actually finding the longitudinal Modulus of Elasticity. Due to frequent use and economy of language, the longitudinal MOE is often referred to simply as MOE in the industry. This will also be done in this document from now on.

The consequences of the previous statements, as well as a reflection on the accuracy of the models, will be commented on later, in Section 1.2.2.3: Discussion.

1.2.2.2 Measurement procedures

The measurement methods focus on obtaining the speed of the longitudinal acoustic wave of the wood, and from this data the Modulus of Elasticity is derived. Usually, the Time of Flight (ToF) method is used for standing trees due to the inability to access the trunk section, and a resonance-based approach for logs and boards due to its accuracy. In both techniques the acoustic wave is generated by an impact.

1.2.2.2.1 Time of Flight

In this approach two sensor probes (one labelled as *emitter* and the other as *receiver*) are inserted into the sapwood, and then mechanical energy is introduced into the wood through a hammer impact on the *emitter* probe. The ToF method essentially consists of measuring the travel time of the stress wave between two points, from the *emitter* to the *receiver*. The velocity of the acoustic wave is then calculated from that time span using Equation 1.2.3:

$$C_T = \frac{d}{\Delta T} \tag{1.2.3}$$

Where C_T is tree acoustic velocity, d is distance between the two probes and ΔT is the travel time.

During field measurement, probes are inserted around 25 mm into the tree trunk so they pierce bark and cambium and enter sapwood (see Figure 1.6). Probes are inserted in a 45º angle towards each other and aligned vertically to promote the propagation of longitudinal waves. The distance span between the probes is standardized for our measures: 60 cm (unless otherwise noted). On a standing tree, the center of the span is determined from a practical standpoint, typically set at 1.3 m (the same as for DBH measurements). This way the probes are at a comfortable height for the operator [50]. See Figure 1.7a.

But because acoustic waves are introduced from the side surface of the stem in an angle, the stem is being stressed obliquely and not longitudinally. One-dimensional wave equation is therefore no longer valid for trees [46]. Additionally, trees have variable external and boundary conditions that create repeatability concerns. These problems will also be engaged at Section 1.2.2.3: Discussion.

1.2.2.2.2 Resonance analysis

In this method an acoustic sensor is mounted on one end of a slender wood members such as logs, poles, timber or boards. A stress wave is initiated by a mechanical impact on one end and the stress waveforms are detected by a piezoelectric sensor (see Figure 1.7b.). This approach is based on the record of oscillations product of hundreds of acoustic pulses resonating longitudinally inside the wood. By using the registered fundamental frequency in the calculus of this wave velocity, we effectively provide a weighted average travel time (equal to twice the period) [46]. The velocity is then derived by applying Equation 1.2.4:

$$C_L = 2 \cdot f_0 \cdot d = \frac{2 \cdot d}{T_0} \tag{1.2.4}$$

Where C_L is log acoustic velocity, d is the end-to-end log length and f_0 the fundamental frequency of the received acoustic signal and T_0 is the fundamental period, the inverse of f_0. Note the similarities between this expression and ToF's Equation 1.2.3.

This results in a very accurate and repeatable velocity measurement. The robustness of this method is very advantageous over ToF. Because of this, the acoustic velocity of logs obtained by resonance has been used to validate ToF measurements in standing trees [46].

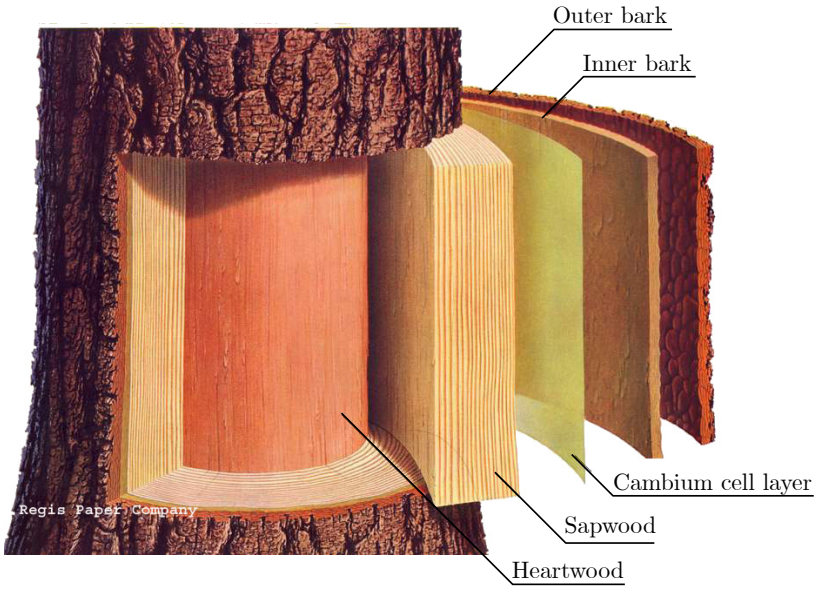

Figure 1.6 – *Layers of a tree trunk. Credits: [51].*

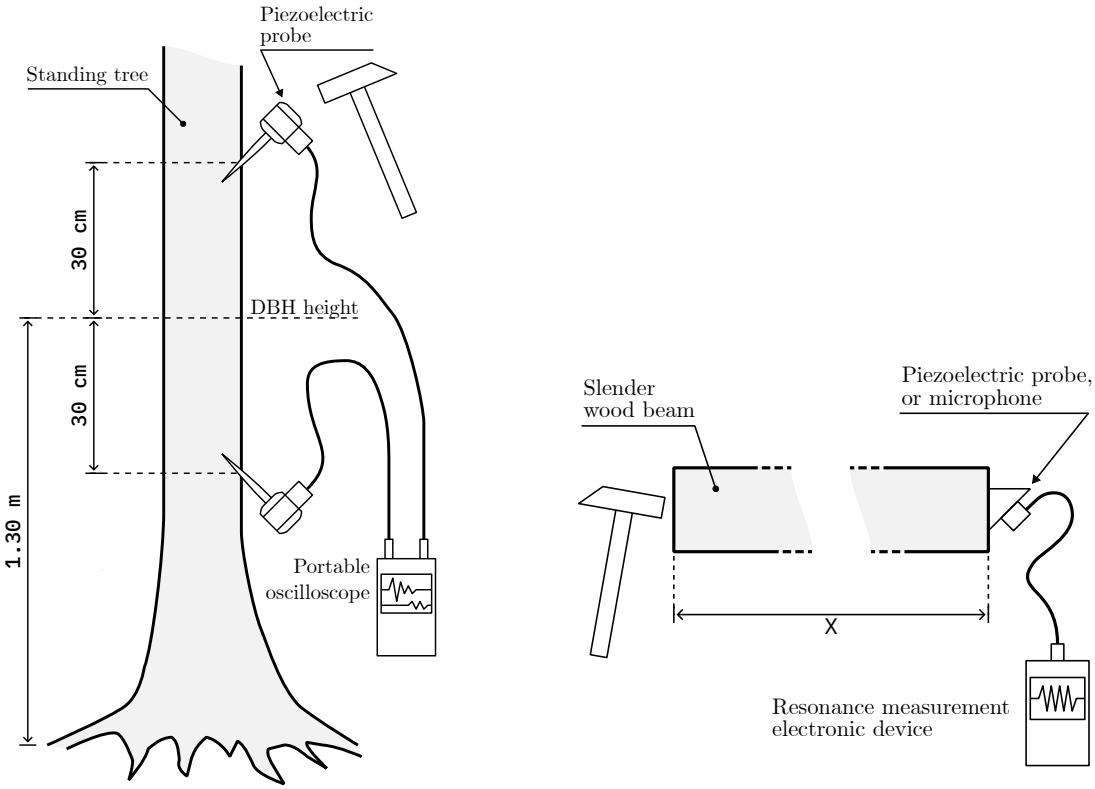

(a) *ToF measurement procedure on standing trees.* **(b)** *Resonance measurement procedure on logs.*

Figure 1.7 – *Illustrations of the two measurement methods. Own work.*

1.2.2.3 Discussion

In spite of the flaws listed at the end of paragraph 1.2.2.1.1, studies have shown that the one-dimensional wave velocity equation (Equation 1.2.1) is adequate to characterize the wave propagation behavior in wood that are in a long, slender form [52]. Thus, this approach can be successfully applied directly on logs and boards, where there is access to an end surface.

Unfortunately, this is not true for measurements on trees, and the speed calculated using the ToF method are usually significantly higher than those found by the resonance method. Studies show that ToF is probably dominated by dilatational waves rather than one-dimensional waves [53]. Given this circumstance, ToF measurement results must be interpreted differently than resonance ones. That is, ToF results can be used to compare woods measured with the same *modus operandi*, as long as it is taken into account that the obtained MOE is not the real one. A correction factor can also be applied, which seems to depend on the Poisson's ratio [53] as the theory says (Equation 1.2.2).

However, as we will see in later sections, repeatability of the ToF reading is poor; since many factors influence the measurement, including the acoustic tool, probes and how they were positioned in the stem, inconsistency in manual hammer tapping. Nevertheless, the effect can be minimized by taking multiple measurement samples and using the average value for a tree. In ADIME's measurement procedure [50] a total of 10 measurements are taken, 5 on the south face and 5 on the north face, and the average is considered the ToF of that tree.

1.2.3 Measurement devices on the market

In this section, a list of TIK's closest competitors will be presented to give perspective to the measurement approaches of the competition, their degree of sophistication and their prices. It will also give us an idea of the functions that TIK can include. We will focus on portable and handheld tools.

- **Fakopp microsecond timer** (Figures 1.8a and 1.8d). It's a very popular but simple device which measures the transit time between its probes in microseconds. This device is accompanied by Fakopp's SD-02 piezoelectric sensors. These transducers are identical and interchangeable between emitter and receiver. The measurement method involves tapping the start probe with a hammer. This equipment gives results very fast, immediately after the hit which indicates that no signal post-processing is done whatsoever. For a new measurement, the reset button has to be pressed. The device cannot give any other derived measurements. User interface consists only of a 4-digit, 7-segment display. The device works with regular 9-volt PP3 non-rechargeable batteries.

  The manufacturer claims that this tool can be used for ToF measurements and for trunk defect detection [54]. Additionally, Fakopp also sells a (not included) metal reference rod, for verifying that the microsecond timer is working correctly (Figure 1.8e).

  The price of this tool is 490 € excluding VAT and includes two probes.

- **Fakopp portable lumber grader** (Figures 1.8f and 1.8g). This is a toolkit comprised of hardware (load cell, load cell amplifier, microphone) and software (a PC program) which directly grades wood boards according to the EN-338 standard by its MOE, computed using a resonance approach. The microphone is put close and directed towards the wood board. Then, the operator hits the side of the lumber. The microphone listens to the vibrations and determines the fundamental resonance frequency, which is used to calculate the acoustic wave velocity. The user then introduces the tree species and the plank's size (WxHxL) in the program. Given that the board is also being weighted by a load cell, the exact density is found and the MOE and grading is shown to the operator [54].

  This instrument requires many different devices, including a computer for analysis, which makes it inconvenient. This toolkit is manufactured and shipped under demand. The price is unknown.

- **Brookhuis MTG timber grader** (Figures 1.8c and 1.8h). It's similar to Fakopp's portable lumber grader, but much more convenient for the operator as it grades planks in a single handheld device. The design of this unit is considerably more ergonomic than previous options and it has a more professional manufacture and finish (see Figure 1.8c). This handheld device has a back-lighted, 2-color, 122x16 pixels LCD in which the and gives more information of the analyzed wood such as the EN-338 class. UI navigation is done by pressing the 6 buttons on the front. This device is battery-operated.

  This device makes an interesting approach: it integrates a microphone to listen to the resonance, but also a solenoid which performs the impact on the wood (although it can also be hit with a hammer, Figure 1.8h). This is very convenient since the operator only has to bring the device to the side of a table, press a button and the device does the rest, making it very quick to use and suitable for a production line. The drawback is that the stiffness calculation is based on density according to the species, or provided by the operator [55].

  The price is approximately 550 € excluding VAT. The device does include (optionally) a reference methacrylate board for calibration (Figure 1.8i).

- **Controls Pulsonic 58-E4900 ultrasonic pulse analyzer** (Figure 1.8b). The most advanced device on this list. It is essentially a digital oscilloscope, but specialized in ultrasonic measurements. It provides multiple signal arrival detection algorithms and FFT. The user interacts with the device via a GUI on a 6-inch touchscreen. This instrument is powered by a battery.

  The measurement method is by excitation of an emitting piezoelectric sensor with a high-voltage pulse, but it can also measure resonance and time of arrival of acoustic waves performed by a hammer impact. The receiver has programmable gain via a PGA. This tool is used for the detection of acoustic emission of materials (in search of internal fractures), voids, cracks and strength grading (via MOE) of various construction materials such as concrete [56].

  The price rounds 1700 € excluding VAT, which makes it more inaccessible than the rest of the options presented before.

In chapter 2 we will dive into a detailed process of reverse engineering two of the aforementioned devices: the Fakopp microsecond timer and the Brookhuis MTG handheld device.

1.3 Scope of this Thesis

As seen, the field of non-destructive testing of wood is broad. Thus, the scope of this Thesis needs to be limited in order to be manageable by a single student. This document contains the process of analysis, specification, design and manufacture of a device capable of measuring the ToF of an acoustic wave in standing trees, logs and wood boards. This tool has been codenamed Tree Inspection Kit Module 1 and it serves as a basis for further development.

The resonance method is researched in parallel by Irene Gil Martín in her Master's Thesis [58]. She has designed a second device called TIK Module 2 for resonance analysis, which connects to and works as an extension of the first.

1

(a) *Fakopp µs timer.*

(b) *Controls Pulsonic 58-E4900 [56].*

(c) *Brookhuis MTG [55].*

(d) *Fakopp µs timer in action [54].*

(e) *Fakopp testing bar in a lab stand.*

(f) *Fakopp PLG during measurement [54].*

(g) *PLG's microphone and load cell.*

(h) *Brookhuis MTG during measurement [57].*

(i) *MTG calibration bar.*

Figure 1.8 – *Photos of some competing products.*

1.4 Engineering Design Process

The work of an engineer is largely concerned with design. Design establishes and defines solutions for problems not solved before, or new solutions to problems which have previously been solved in a different way [59]. Good design requires creativity, decision-making based on many parameters and compromises between conflicting requirements. Design is the product of planning and work, and is usually carried out by decomposing the problem into manageable parts.

The Engineering Design Process, or EDP, is a series of steps that engineers follow in order to solve a problem. The EDP can be summarized in the following stages [59, 60] (Figure 1.9):

- **Definition of the problem.** The response to what is the problem, who has it and why it is important to solve. In this Thesis, Chapter 1: Introduction addresses these questions.
- **Background research and analysis.** Consists of taking a closer look at the problem, finding out what is the state of the art and other existing solutions, and avoid mistakes that were made in the past. Chapter 1: Introduction, Chapter 2: Reverse Engineering of competing products and Chapter 3: Signal analysis and processing can be included in this stage.
- **Requirements Engineering.** Consists on requirement analysis and specification to establish the system behaviour, its functions and operating constraints.
- **Brainstorming and evaluation of concepts.** Proposal of many possible and creative solutions. An evaluation of the advantages and disadvantages of each alternative must be made. Then, the unfeasible and the ones which do not meet the requirements are discarded.
- **Specify the product's architecture.** What technologies is the solution going to use, and in which configuration.

  Last 3 steps are diluted in Chapter 4: System specification
- **Development and prototyping.** The implementation, refinement and improvement of the chosen solution in physical architecture, hardware and software. A prototype is an testing operating version of the solution which allows the designer to test the solution before production. This appears in Chapter 5: System design and Chapter 6: Fabrication, testing and validation.
- **Testing and validation.** Testing and evaluation of whether the prototype meets the user needs and requirements; and identification and solution of design issues. This step is tackled in Chapter 6: Fabrication, testing and validation.
- **Feedback.** The design process involves multiple iterations and redesigns of the final solution. Problems will appear during the prototype testing, so changes will be made at different levels of the design process, and new solutions will be tested before settling in a final solution.
- **Communication of results.** As a last step, the results of one or various iterations are shared. This Bachelor's Thesis records and serves as proof of the entire engineering process. This step also includes the generation of technical documentation for manufacturing, included in the annexes of this document.

1

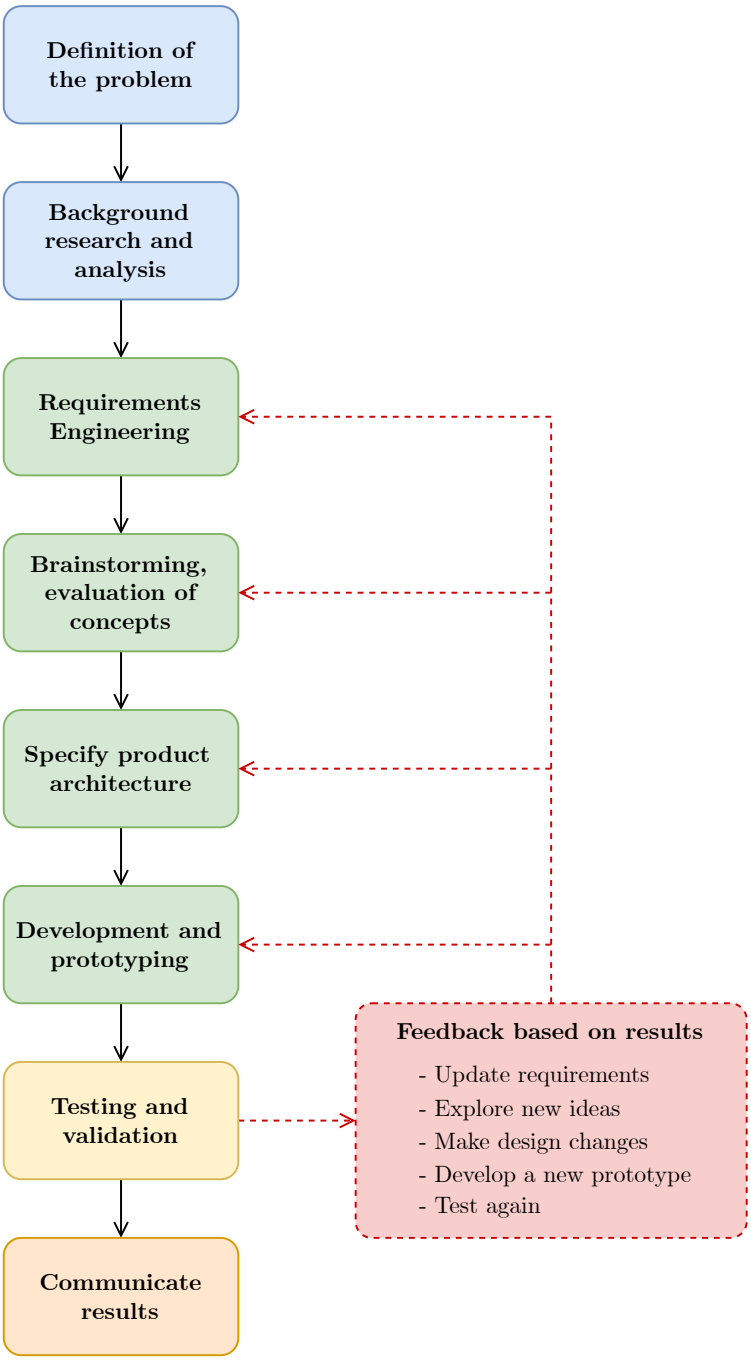

Figure 1.9 – *The Engineering Design Process.*

1.5 Project goals and objectives

After introducing the motivation of this Bachelor's Thesis, this section outlines the main, top-level, non-technical goals of the project, which are listed in Table 1.1. These are the Thesis execution's expected results, in a pure academic and professional terms.

Obj. Nº	Description
Obj. 1	To successfully develop an electronic product going through all the necessary steps: from conception, research and analysis to specification, design, implementation, manufacturing and validation with all the effort that it entails.
Obj. 2	To gain familiarity, skill and confidence with professional EDA and CAD software for electronic and mechanical design.
Obj. 3	To acquire ability in handling electronic instrumentation.
Obj. 4	To prove the student's capabilities of organizing and carrying out an engineering project.
Obj. 5	To document the entire process, which may be necessary during the development itself or useful for the future of the project and research line.
Obj. 6	To demonstrate the knowledge acquired during the Bachelor studies in Telecommunications Engineering, as well as the multidisciplinary abilities gathered during the development of this Thesis.
Obj. 7	To participate into the GranaSat laboratory work environment to consolidate the training of the Bachelor's Degree.
Obj. 8	To successfully conclude the Bachelor's Degree in Telecommunications Engineering with this Thesis.

Table 1.1 – *Top-level objectives of this Bachelor Thesis.*

1.6 Project structure

This document is divided into seven chapters and six appendixes. The chapters progressively expound all the stages of the development of the proposed device, while the addenda include complementary material of the project: costs, schematics, renderings, simulations, etc.

1. **Chapter 1: Introduction.** This first chapter is intended as groundwork to the subject at hand, and to show the objectives and motivations of this project. It includes some definitions, the state of the art and an introduction to the engineering methodology followed throughout this project.
2. **Chapter 2: Reverse Engineering of competing products.** This chapter offers a more thoughtful analysis of the existing commercial competing products mentioned in the introduction. It also addresses a process of Reverse Engineering in order to gain understanding of the advantages and limitations of their technology so we can synthesize our own and superior product.
3. **Chapter 3: Signal analysis and processing.** The third chapter dives into the analysis of signals captured from a multitude of experiments in wood such as in standing trees and trunks, but also in a reference aluminum rod. The analysis help us to characterise and to understand the signal's nature, as well as to delineate some requirements of the electronics.

4. **Chapter 4: System specification.** This chapter aims to define all the requirements that our electronic device must fulfil from the point of view of Requirements Engineering. Once depicted the specs, we will delve into the study of the device's hardware, software and mechanical architecture.
5. **Chapter 5: System design.** This chapter describes all the aspects of the system design: the electronic circuits, firmware, the Printed Circuit Board and mechanical design.
6. **Chapter 6: Fabrication, testing and validation.** This sixth chapter details the fabrication options, manufacturing process and testing of the electronics and verification of the systems' correct operation.
7. **Chapter 7: Conclusion and future lines.** Lastly, the final chapter brings to an end the main contents of this Bachelor's Thesis, reviews the achieved milestones and establishes future lines of work that have emerged from the development process.

On the other hand, the addenda is divided in:

A. **Appendix A: Project costs.** Detailed cost of this project, including materials and human costs.
B. **Appendix B: Circuit schematics.** In this appendix is attached the complete circuit schematics.
C. **Appendix C: Circuit simulations.** Explanation of simulation parameters and constraints, and circuit simulation results.
D. **Appendix D: PCB.** Printed Circuit Board drawings, mechanical information and renders.
E. **Appendix E: Case.** Mechanical drawings, information and renders of the case parts and the product assembly.
F. **Appendix F: Handling of electronic instrumentation.** Description of the operation of the used electronic instrumentation. Includes the developed Python code (and examples) for instrumentation automation using SCPI commands.

1.7 Project tasks and organization

A Work Breakdown Structure (WBS) is a hierarchical decomposition of the tasks of a project in order to accomplish the desired objectives. In Figure 1.10 the WBS of the project is presented. This schema is product of the definition of system requirements in Chapter 4: System specification and iteration with the design process elaborated on Chapter 5: System design.

On the other hand, a *Gantt chart* is a management tool in which a list of tasks is outlined in a timeline. Color bars represent working on tasks. The balloons indicate milestones, and dependencies between tasks are denoted with arrows. Figure 1.11 shows the Gantt chart of the project's development process.

It is important to point out that besides the tasks, meetings are also included since they were a fundamental part of the development process. These meetings not only served as a form of reviewing results and controlling the development, but they were essential to define the project requirements (elaborated in chapter 4) and allowed us to coordinate tasks between IDIE-ADIME and GranaSat teams.

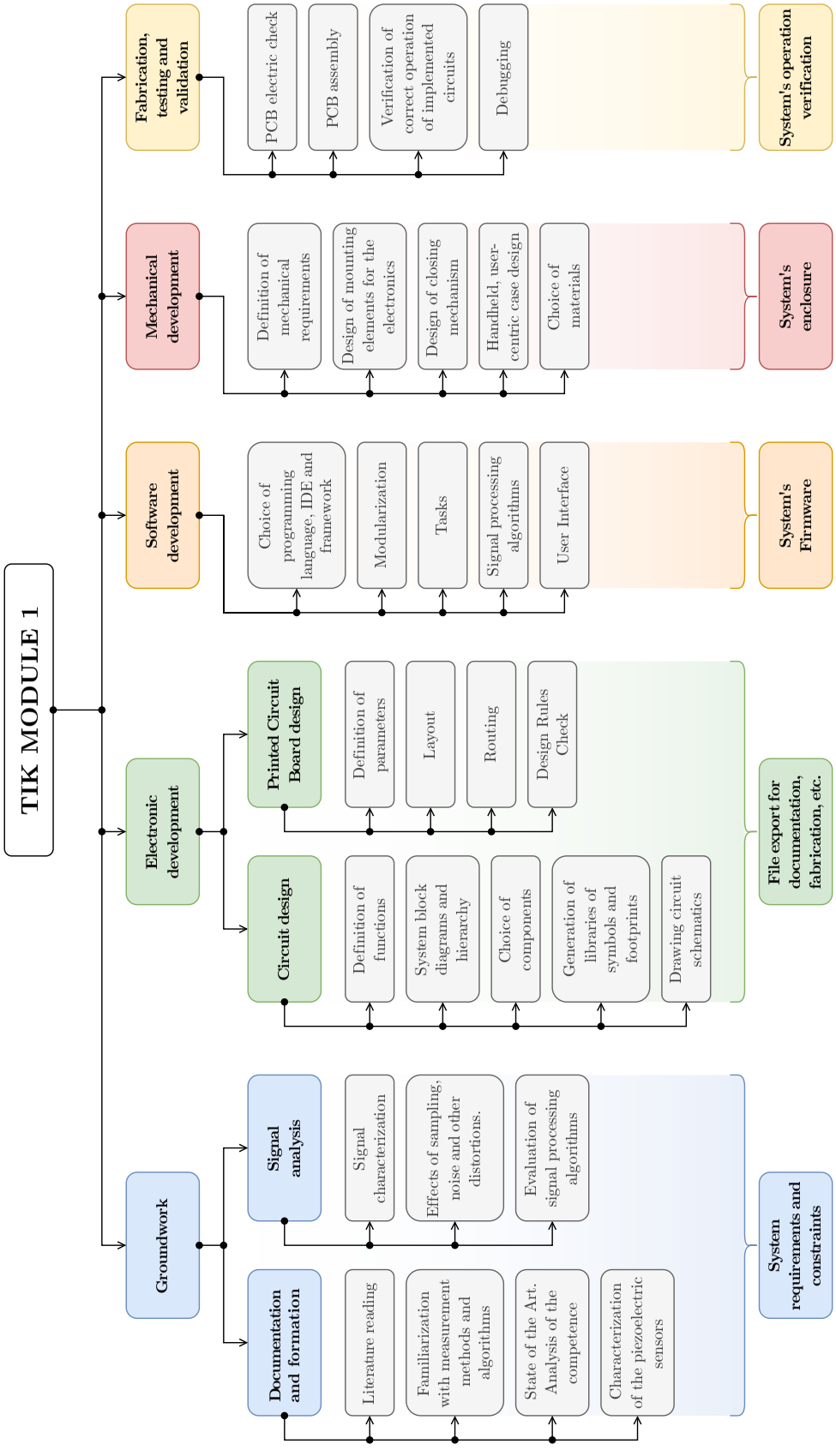

Figure 1.10 – *Work Breakdown Structure of the project.*

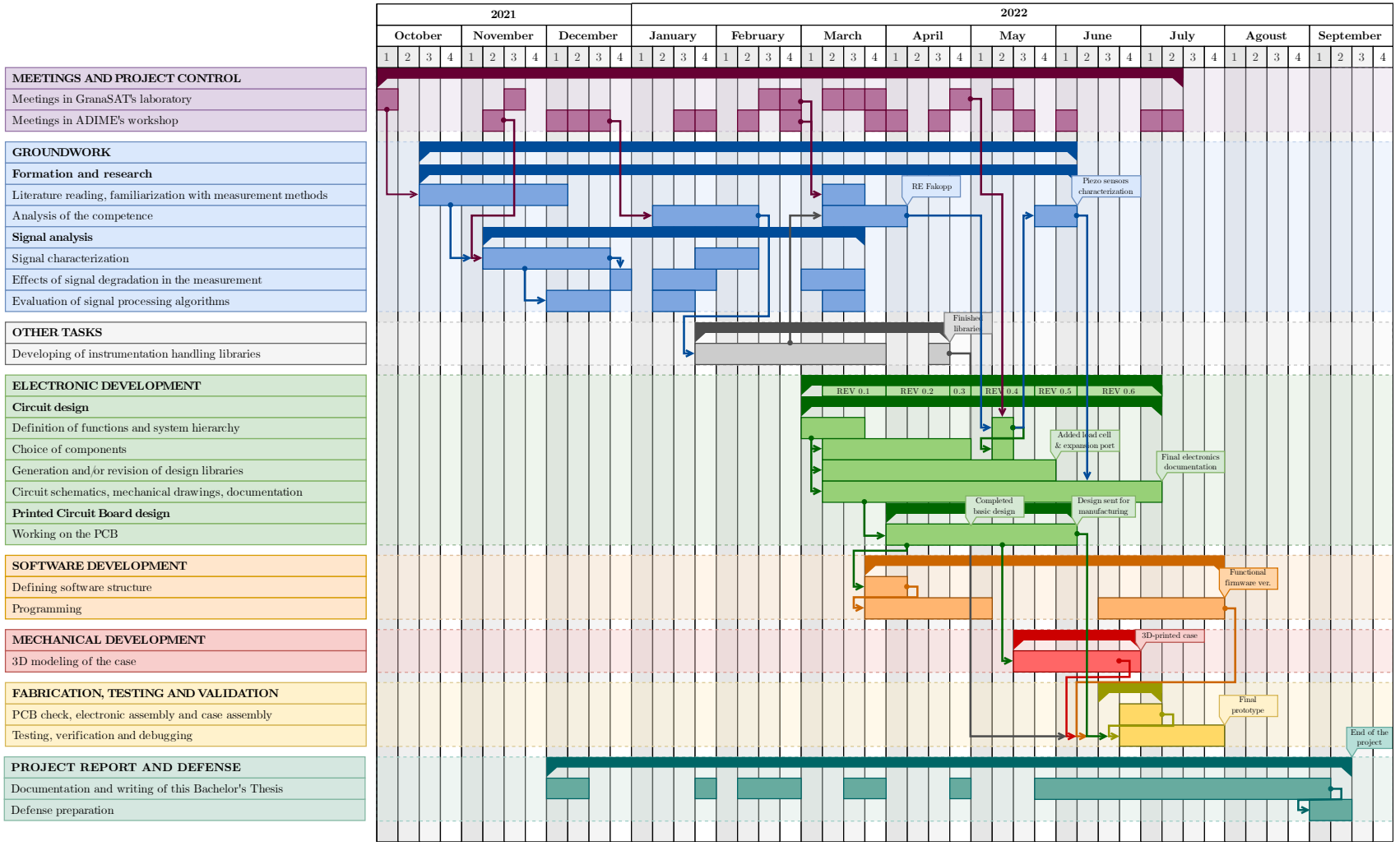

Figure 1.11 – *Gantt chart of the project.*

Chapter 2

Reverse Engineering of competing products

This chapter helps to understand the followed measurement method, as well as to provide examples on how to approach the measurements in the device that is going to be developed throughout this thesis. For this, a Reverse Engineering process was carried out together with Irene Gil Martín on two competing products similar to TIK and competitors in its market niche: **Fakopp's Microsecond Timer** and **Brookhuis's MTG Timber Grader**. These products were already presented in Section 1.2.3: Measurement devices on the market. This chapter aims to delve into the operation of these devices both at the level of operation and design decisions and technological level. Please note that this process is not yet fully completed, there is missing information and may contain mistakes and misconceptions.

Additionally, the **Fakopp SD-02 piezoelectric transducers** are analyzed and the results of electrical characterization are presented.

2.1 Fakopp microsecond timer (µstimer)

A tool that measures the transit time between its probes in microseconds, which are shown in a simple 4-digit, 7-segment display. The manufacturer-provided specifications of this device can be found in Table 2.1.

The measurement method of this device only involves nailing its probes in the wood with a rubber hammer and then tapping the start probe with a light metal hammer. The result should appear on screen in a few seconds. For clearing the screen and doing a new measurement, the reset button has to be pressed. The device does not accept user input other than the on/off switch and the reset button. The device works with regular 9-volt PP3 non-rechargeable batteries. This is a questionable choice, although it has the advantage of being able to change the battery for a full one immediately in case it runs out.

The results are immediate, which indicates to us that the equipment is most probably measuring the delay between signal flanks without digital signal processing. This tool does not give any other derived measurements, requiring the user to do the math.

Fakopp includes two SD-02 piezoelectric sensors, which will be described and characterized in section 2.3. Additionally, Fakopp also sells an aluminum reference rod for verifying that the microsecond timer is working correctly. We will use this rod in Chapter 3: Signal analysis and processing.

The device has a very simple shape, is light, and all the ports are located on the top. This, however, leaves little room to manipulate the BNCs with ease.

2

Spec	Value
Dimensions	29x80x156 mm
Weight (without battery)	220 g
Battery	PP3, 9 V
Power consumption[1] (before reset)	15 mW
Power consumption[1] (after reset)	50 mW
Enclosure material[2]	Plastic
Water resistant	No
Display	4-digit, 7-segment LCD, no backlight
Standard deviation[3]	± 1 µs
RS232 baudrate	2400 bps
RS232 port connector	D-SUB 9, male
Operating temperature	-10ºC to 40ºC

Table 2.1 – *Manufacturer-provided Fakopp's microsecond timer technical data according to its user's manual [61].*
[1] *In constrast, Fakopp's website specifies a power consumption of 320 mW.*
[2] *Plastic type unknown.*
[3] *Fakopp's website states ± 3 µs.*

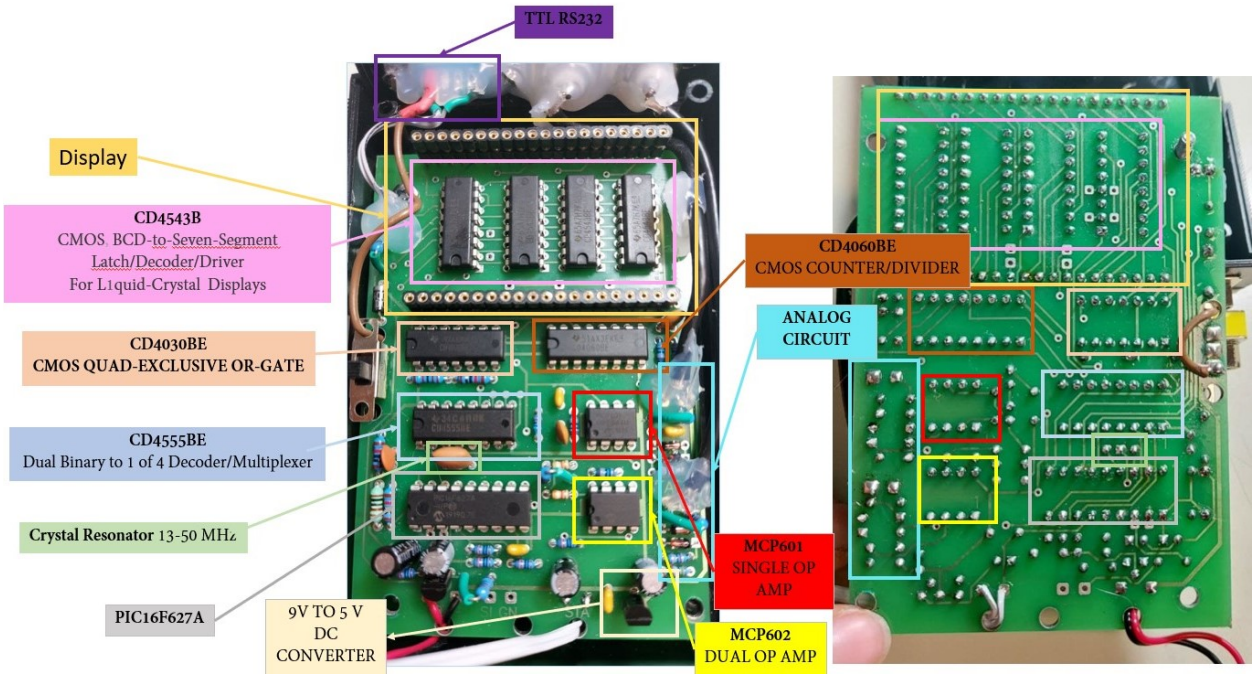

Figure 2.1 – *Identification of the components inside the Fakopp µstimer. Credits: Irene Gil Martín.*

2.1.1 Circuit analysis

Upon removal of the cover of the device, we find the electronics in figure 1.

The technology of this device is old: all the components are THT, the PCB is double-sided, simple, without polygons or planes and without silkscreen. The manufacturing seems to be manual, evident by the insides' simplicity and by the use of silicone to secure the cables and ports.

Several blocks are identified:

- **Power on and supply system.** The device is powered by a 9V type PP3 battery. In series with it is a switch that turns on the system, and a reverse polarity protection diode. Next, a TY5050TI LDO regulates the voltage to a fixed 5V, which is the main supply of the system.
- **Processor.** The heart of the device is a PIC16F627A. Nowadays it is a underpowered and obsolete microcontroller, whose feature that will interest us the most is that it has two comparators accessible from its pins. The microcontroller sends the results through an RS232 interface. Fakopp currently delivers an RS232 to Bluetooth adapter with the microsecond timer to provide this device with wireless communication.
- **Screen system.** Composed of four CD4543BE that contains the necessary logic to convert a number in BCD format to the one required by the 7-segment display, a CD4555BE multiplexer to drive them, and some auxiliary ICs such as the CD4030 (four XOR logic gates) and a CD4060BE (digital counter, whose functionality is not yet known).
- **Analog signal processing.** It seems that the signals from the BNCs are processed analogically by a series of Operational Amplifiers. Their circuits will be discussed next.

We will focus on the description of the signal capture, adequacy and processing circuit since we are mainly interested in that part. The rest of the circuit will not be discussed in this work, since it is of no interest.

2.1.1.1 Description of the analog signal processing circuit

Figure 2.2 describes the circuit inferred from the visual inspection, the sounding of it with a multimeter and the consultation of the components' datasheets. The circuit for the emitter and the receiver are different, because as we will see in chapter 3 they have very different properties.

- First, the voltage provided by the LDO is divided with resistive networks into bias voltages that will be used by the operational amplifiers and comparators.
- Both emitter and receiver have an input circuit that clip the signal to an offset voltage $\pm V_f$ ($\approx 0.7\,\mathrm{V}$) of the anti-parallel 1N4148 diodes.
- The receiver signal is amplified in two feedback stages with a strange topology. However, once this is done, the resulting voltage is fed into a pin of one of the PIC16's comparators, where it is compared to one of the bias voltages.
- On the other hand, the emitter circuit simply clips the signal to a safe voltage and feeds it into the other comparator, since this signal has much more amplitude and does not need amplification.

In summary, the PIC16 seems to counts the time between activations of its comparators triggered by the sensors' signals.

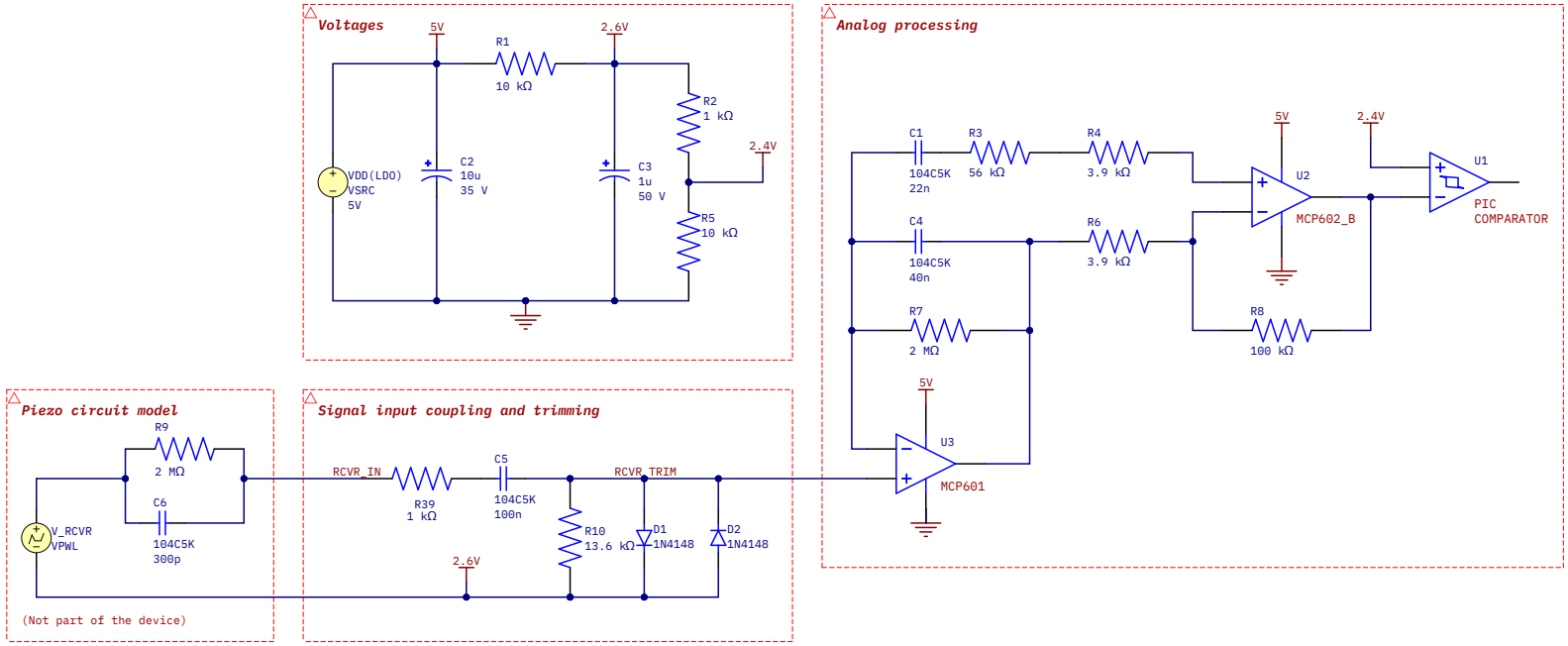

(a) *Circuit for the Receiver port, and detail of bias voltages.*

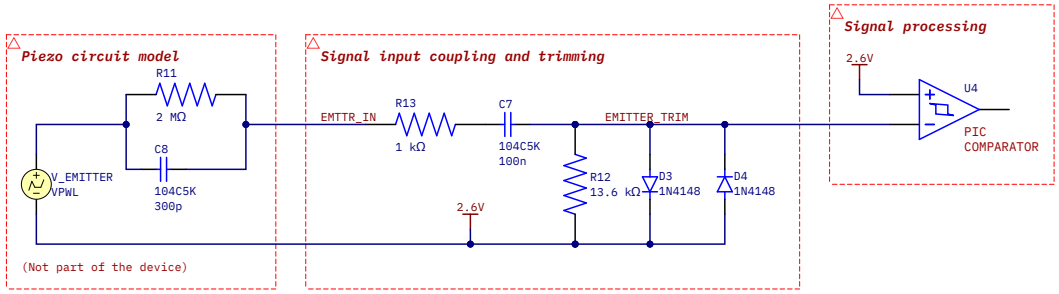

(b) *Circuit for the Emitter port.*

Figure 2.2 – *Signal processing circuits of Fakopp's µs timer.*

2.2 Brookhuis Mechanical Timber Grader (MTG)

The Mechanical Timber Grader (MTG) is an ergonomic measuring instrument that measures by analyzing the sound waves of an impact against a plank or wood beam. For hitting the wood, this device contains a solenoid. The sound of the hit will then be recorded by a microphone and analyzed. The reverse engineering of this product is of interest for the development process of the resonance-based device for classification of wood planks, which will be incorporated to TIK Module 2.

The shape of the device is comfortable in the hand, but it is a hefty device and it gets very hot when charging. It is undoubtedly a much more modern, advanced and professional-looking product compared to the Fakopp microsecond timer in appearance, functionality, mechanical design and electronics.

The device has Bluetooth to send the results, and the manufacturer has also developed a licensed PC application to organize and analyze the results.

2.2.1 Circuit analysis

As we can see in Figure 2.3, several areas are identified: the power supply, the electret microphone and its amplifier, the microprocessor area, the wireless communication module, the solenoid driver and finally the LCD PCB. Now that we have a general picture of the electronics stages, we are going to analyze each one separately.

2.2.1.1 Power supply

This stage contains the battery charger and voltage conversion. The modules that this stage contains are the one shown in Figure 2.4a.

- Two-cell Li-Po battery, which have a nominal voltage of 7.4 V and unknown capacity.
- Texas Instruments BQ42005 two-cell Li-Ion battery charger IC. Powered by 8.4 V to 10 V from an external power supply, can provide up to 2 amps.
- Texas Instruments LM117 LDO adjustable voltage regulator. Set to output 3.3 V, at a maximum of 800 mA.
- Maxim Integrated MAX660M switched capacitor voltage converter. May be used to generate a symmetrical (dual-supply) voltage for the microphone amplifier circuit. Is powered by 3.3 V, and can output up to 100 mA.

With the previous information and the identification of the connections by means of a multimeter, it is believed that the battery voltage is regulated directly by the LDO to supply the rest of the modules. This is inefficient, and depending on the current consumption it may result in the generation of a large amount of heat.

2.2.1.2 Microprocessor, wireless communication module and solenoid driver

The modules contained in this area are shown in Figure 2.4c. This stage comprises the the microcontroller IC, the Bluetooth module and the solenoid driver.

- MSP430F016 mixed-signal microcontroller. It Is powered by the 3.3 V rail from the LDO.
- 32.768 kHz crystal oscillator for the microcontroller.

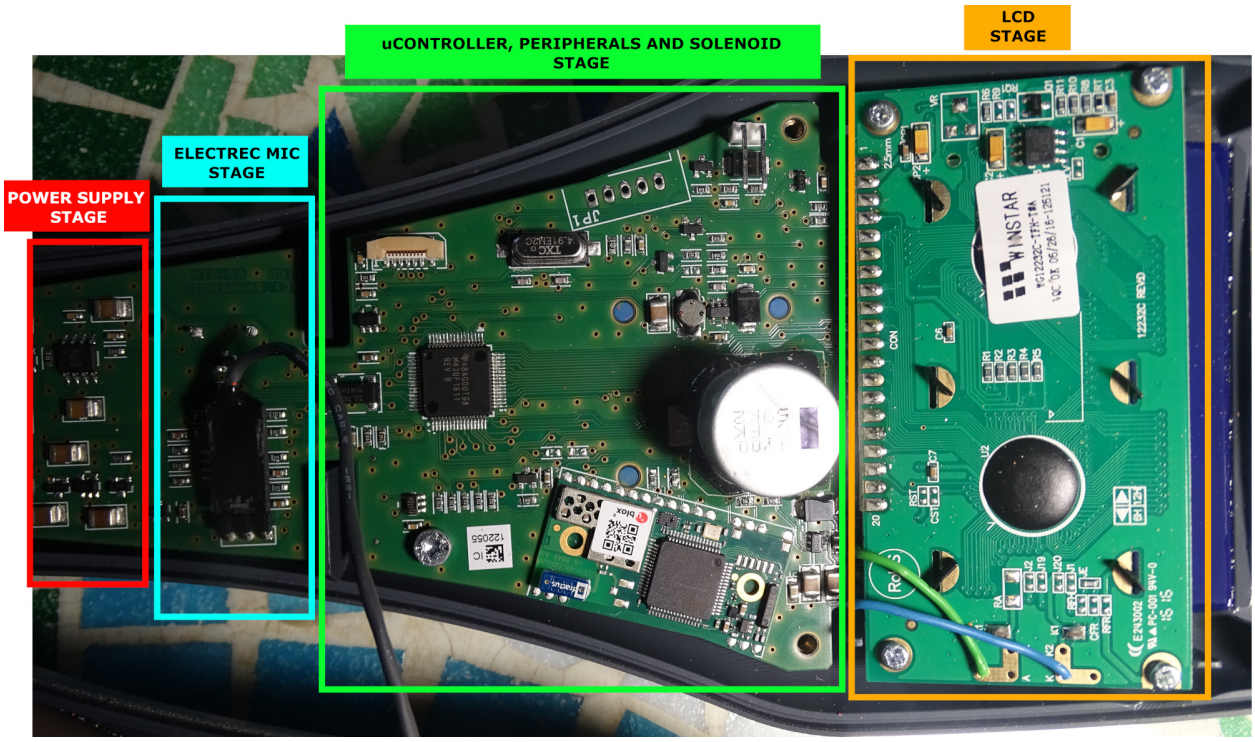

(a) *Identification of the MGT's PCB areas.*

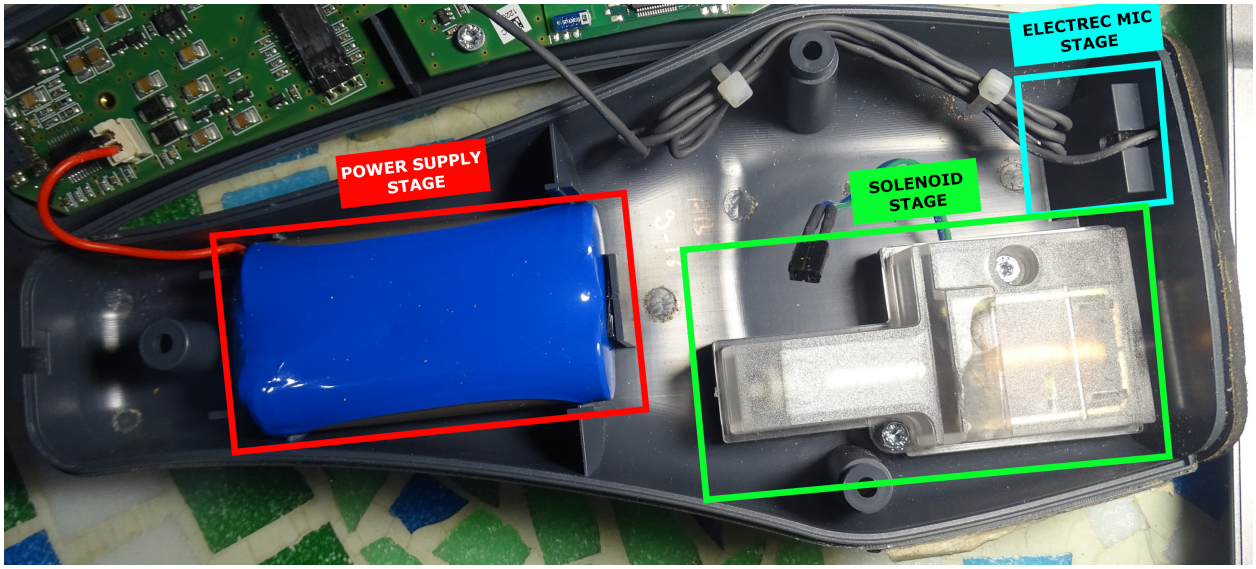

(b) *Connection of the MGT's electronics placed in the back cover to the PCB areas.*

Figure 2.3 – *First look at the insides of Brookhuis MGT. Credits: Irene Gil Martín.*

- TJ660 charge pump voltage converter, which provides the needed voltage for the LCD backlighting.
- 4700 uF, 16 V electrolytic capacitor. Slowly charged, serves as a energy storage, which is suddenly released when the solenoid is actuated.
- Unidentified (and obfuscated) Ublox connectBlue Bluetooth module.

We think that the solenoid is driven at 12 V (a typical value for a solenoid and just below the maximum capacitor voltage). To reach this high voltage, a DC/DC boost converter is used.

2.2.1.3 Electret microphone

Pictured in Figure 2.4d, we have not been able to acquire much information from this stage yet. We will only remark that the microphone is placed on the front part of the MTG, and that is protected by a thin film that allows the sound to pass through while protecting the microphone itself from dust.

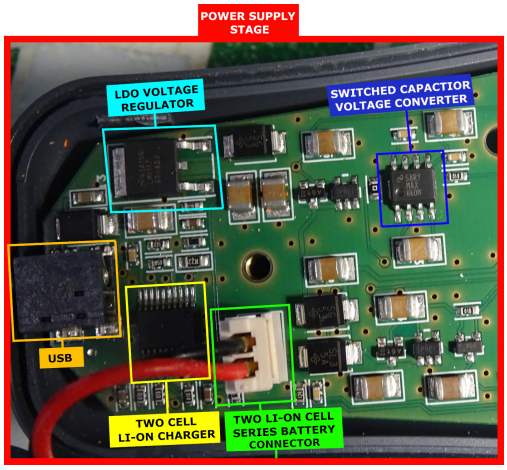

(a) *Power stage detail.*

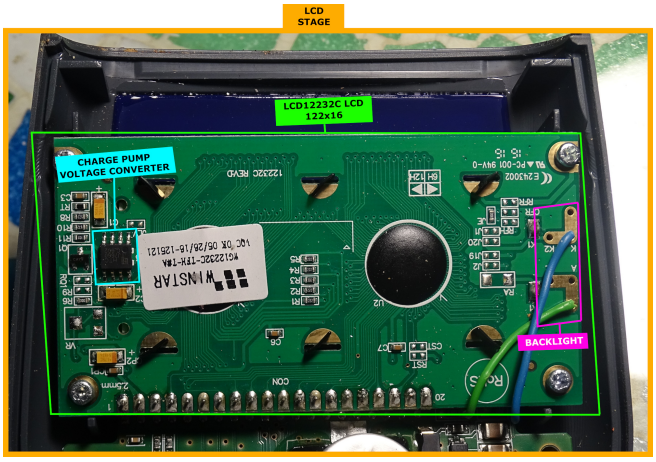

(b) *LCD module detail*

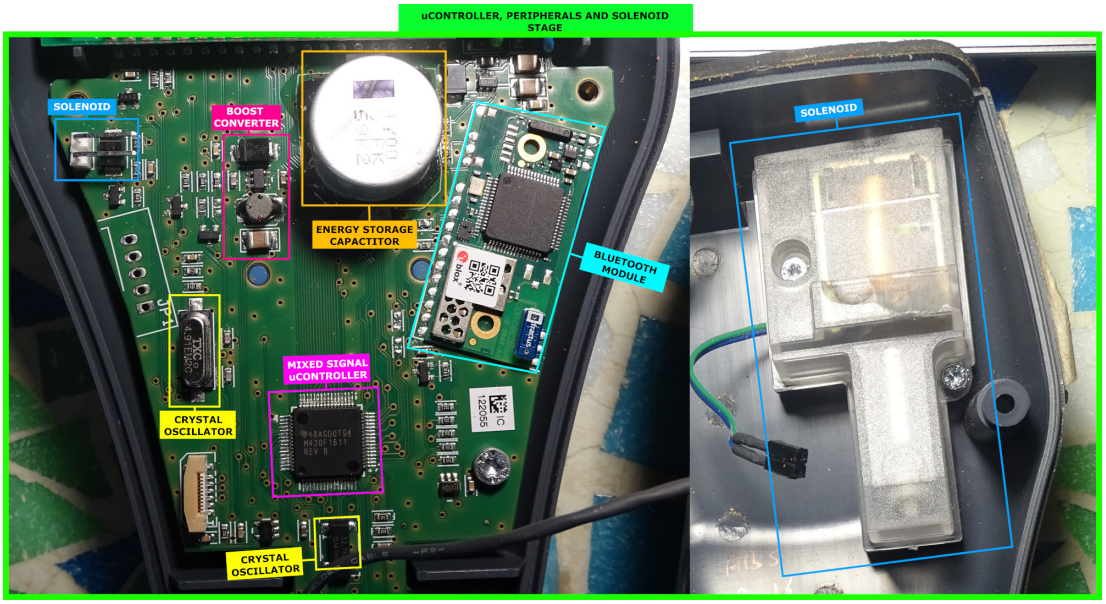

(c) *Digital, communication and solenoid stage detail.*

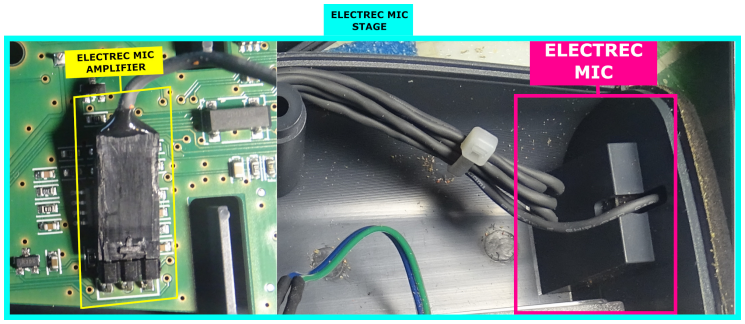

(d) *Electret microphone stage detail.*

Figure 2.4 – *Detail of the different areas of the PCB of the Brookhuis MTG. Credits: Irene Gil Martín.*

2.3 Fakopp SD-02 piezoelectric transducers

In this project, we are going to use the Fakopp SD-02 probes (Figure 2.5) that are included with the microsecond timer as sensors for the TIK. Therefore, it is of great interest for the success of the project to know as much data as possible about these sensors. In this section, we take care of a thorough inspection and characterization of the properties of these probes.

The sensors are made up of two parts: a head that is nailed to the wood, and a coaxial cable with a male BNC termination. The outer shell of the sensors is made of at least 3 pieces of indeterminate metal riveted together. The tip is very sharp to facilitate nailing into the wood. The tip appears to follow a conical or *spline* (parametrical) curve, not a circular one. Table 2.2 shows the technical data of the probes specified by the manufacturer. However, in our actual measurements we found certain discrepancies that are discussed below:

- To begin with, the measurements are not correct. The probe has been measured with a caliper in order to create a 3D model replica, and the dimensions obtained are roughly 92x20x35 mm. The created model dimensions can be consulted in Figure 2.7. See Figure 2.6 for a profile comparison between the real probe and the 3D model.
- The ADIME team has many SD-02 piezoelectric probes with cables of different lengths: 50 cm (the broad majority, which are described in the manual, figures 2.5a and 2.5b) and 200 cm (they have only 2, and they are not listed by the manufacturer anywhere, figures 2.5c and 2.5d).
- As will be seen in Section 2.3.1: Characterization of the piezoelectric sensors, the resonant frequency of the probes seems to vary greatly from that specified by the manufacturer: from 23 kHz according to Fakopp to 80 kHz according to our tests, for both the probes with 50 cm and 200 cm cables.
- In the aforesaid section it will also be checked that the capacitance of both types of probes seems to be in line with the specifications.

Unfortunately, we do not have a way to validate the sensitivity of the probes. In any case, this datum does not seem useful, because it is specified for a very low frequency (160 Hz) when the spectrum of the

Spec	**Value**
Dimensions[1]	99x40x20 mm
Weight	22 g (sensor only)
Resonance frequency (typical)[1]	23 kHz
Charge sensitivity @ 160 Hz	1.35 pC/m/s^2 typ.
Force sensitivity @ 160 Hz	23 pC / N
Sensor capacitance	260 pF/m ± 5 %
Cable capacitance	100 pF/m ± 5 %
Cable length	50 cm
Piezoelectric polarity	Positive for shock from the tip, Negative for shock from the back.
Operating temperature	-30ºC to 70ºC

Table 2.2 – *Manufacturer-provided Fakopp's SD-02 piezoelectric transducers technical data [61].*
[1] *Entries that do not correspond to the result of our tests.*

captured signals predominates around 10 kHz and can expand to hundreds of kHz (see Chapter 3: Signal analysis and processing).

Changing the subject, the cables of the short (50 cm) probes have the following inscription:

```
RG 58A/U 21 AWG UL TYPE CL2 SHIELDED
```

Which means it is an Alpha Wire RG-58 coaxial cable, model P/N 9058AC, with a characteristic impedance of $50 \pm 2\,\Omega$. The capacitance coincides with Fakopp's manual, of 101 pF/m. The signal propagation speed is $0.66c$, and the losses are 19 dB/100m at 100 MHz [62]. The 200 cm cables do not have any inscription, or it has been erased.

2.3.1 Characterization of the piezoelectric sensors

Therefore, they will be electrically characterized to allows us to have an accurate circuit model of the probes, which will be useful for TIK's circuit design and simulation. Below are graphs resulting from the characterization of five Fakopp SD-02 probes, three with short cables (50 cm) and two with long cables (200 cm). These sensors were provided by ADIME.

To find the circuit equivalent of the piezoelectric sensors in frequency it was used an Agilent/HP 4192A LF impedance analyzer. This equipment allows us to characterize an electrical impedance in frequency, that is, to find the resistance, reactance, capacitance, inductance, absolute impedance or phase of a DUT at a given frequency.

An electrical impedance (Z) is an opposition to the flow of current. It is described by a real component (R, resistance) and an imaginary component (X, reactance); or in terms of absolute impedance ($|Z|$, modulus of the impedance, or magnitude) and phase (Φ), the angle between the real and imaginary parts.

$$Z = R + j \cdot X = |Z| \angle \Phi \quad ; \quad \text{where:} \quad \Phi = \arctan\left(\frac{X}{R}\right) \tag{2.3.1}$$

If the reactance is predominantly capacitive, the imaginary part will be negative, and so will the phase; while for the predominant inductance they are positive.

Thus, by Ohm's law, the complex impedance of a two-terminal circuit element can be measured by observing the amplitude and phase of AC voltage and current flowing through it, and this is what the HP4192A does. The probes were characterized in the range of 1 kHz (below this frequency the readings have too much noise) up to 13 MHz (the maximum of the measurement equipment). More information about the setup, calibration and operation of the HP4192A can be consulted in Appendix F: Handling of electronic instrumentation, Section F.3: Agilent/HP4192A LF impedance analyzer.

Next, we proceed to comment on the results obtained, as well as to reflect on them. Figures 2.8, 2.9, 2.10, 2.11 and 2.12 correspond to the individual characterization of the resistance and capacitance of each one of them. Later, several datum (capacitance: 2.13, resistance: 2.14a, reactance: 2.14b, impedance: 2.15a and phase: 2.15b) of the five probes are combined, as a way of comparing the results.

Some important conclusions to be drawn from the obtained results:

- As we can see in the individual characterizations (Figures 2.8, 2.9, 2.10, 2.11 and 2.12), the frequency response of the probes is very characteristic: The resistance decays with frequency, but the capacitance mostly stays stable. This is until approximately 50 kHz, where irregular peaks and fluctuations appear in both parameters. A peak, that may be identified as the probes' resonant frequency, appears in both resistance and capacitance at about 80 kHz.

(a) *Probe Nº1, with 50 cm long cable.*

(b) *Probe Nº2, with 50 cm long cable.*

(c) *Probe Nº4, with 200 cm long cable.*

(d) *Probe Nº5, with 200 cm long cable.*

(e) *Detail of the probes' male BNC connector.*

Figure 2.5 – *Photos of several Fakopp SD-02 probes with short and long cables.*

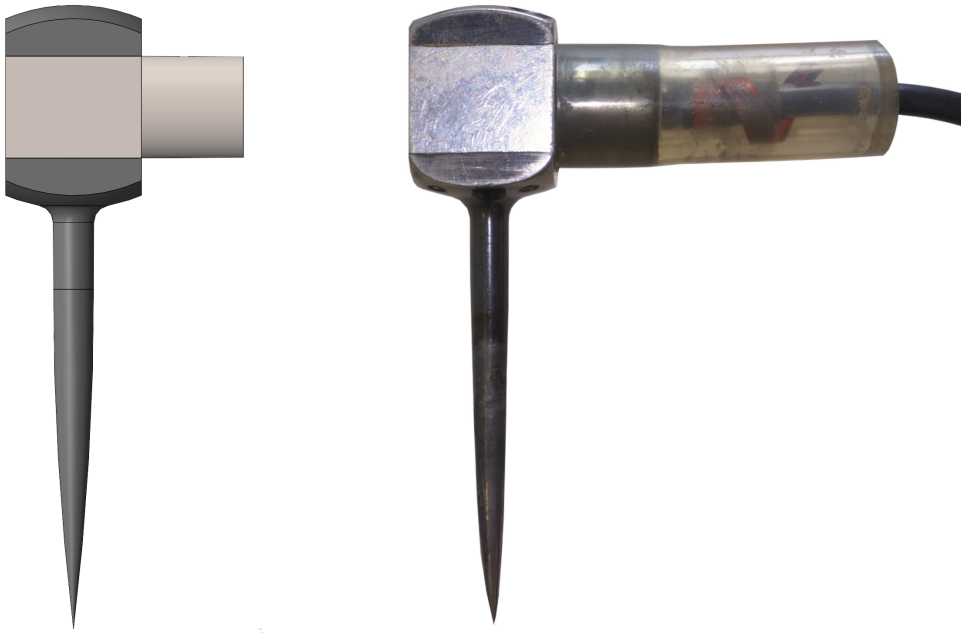

Figure 2.6 – *Comparison of the profile of a real probe with the 3D model.*

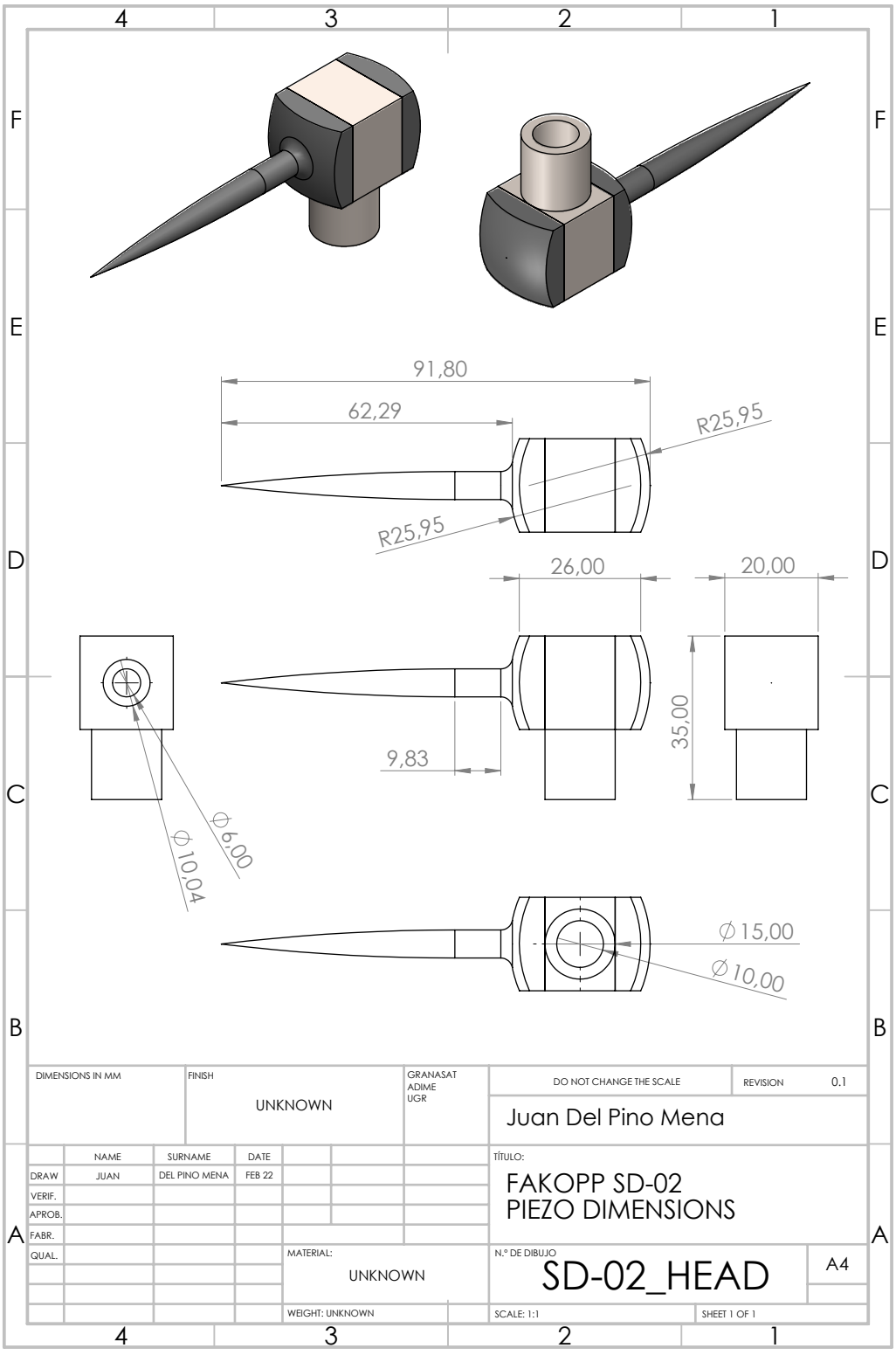

Figure 2.7 – *Schematics of the SD-02 sensors. 3D model done in SolidWorks from measurements.*

- It is important to note that the manufacturer-specified probe capacitance of approximately 260 pF is met for short-wired probes up to 50 kHz, while long-wired probes have a higher capacitance of around 400-450 pF (see Figure 2.13). This is most likely due to the extra capacitance of the cable, which according to Fakopp is 100 pF per meter.

  The difference in capacitance between the probes types can be clearly seen in Figure 2.13. In this figure it can also be observed how all follow the same behavior, even the small fluctuations are comparable.

- However, the probes' resonant frequency specified by Fakopp as 20 kHz is not correct according to our measurements. None of the graphs obtained shows a significant variation at that frequency. Moreover, the response in said range is almost like a capacitor's.

- The probes' resistance generally decreases with frequency, except in fluctuations, where it rises irregularly. However, the resistance of the sensors with the long cables remains consistently lower than the probes with short cables (Figure 2.14a).

- The overall lower resistance and higher capacitance of the probes with 200 cm long cables results in a lower overall absolute impedance ($|Z|$) over the ones with 50 cm long cables, as can be seen in Figure 2.15a. These discrepancies, coupled with the capacitance discrepancy, indicate that the probes are similar but not equal, and that sensors with different cable length may have had different manufacturing processes.

  This plot also reveals that the probes generally function as a capacitor up to 6 MHz to 10 MHz, where inductance begins to take over capacitance. This is visible by the minimum that appears in this region, and the consequent impedance rise caused by inductance.

- At the highest crest around 80 kHz, some points are missing from the peak in the capacitance graphs, since the HP 4912A identified the reactance in these points as negative capacitance. That is to say: a momentary phase change occurs, and so the behavior at those points changes to inductive (from negative phase to positive phase, as it can be seen on Figure 2.15b). The value of the coil moves in the hundreds of microhenries and a few millihenries.

  To represent these missing points on a logarithmic plot, the absolute value of reactance ($|X|$) is presented in Figure 2.14b.

- Although no clear conclusion can be drawn from the phase graph (Figure 2.15b), since it is very chaotic, it clearly shows us how all the probes suffer a significant phase shift at 80 kHz, reaching phase zero and even positive phase. Also, all the phases follow the same form and peaks. Though again, the 200 cm probes seem to stay more capacitive (phase stays more negative) than their 50 cm siblings.

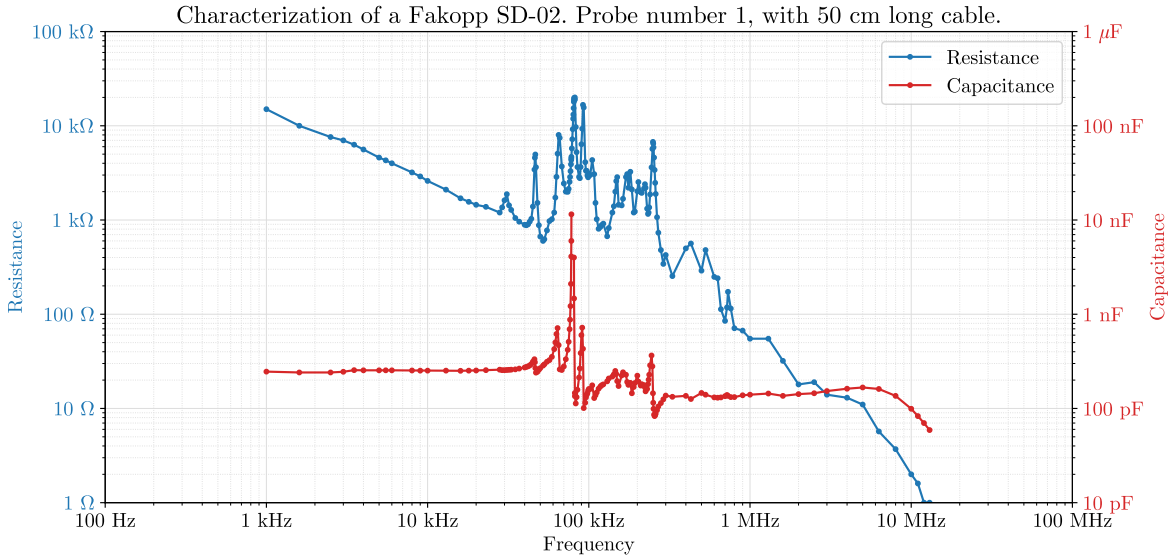

Figure 2.8 – *Resistance and capacitance characterization of Fakopp SD-02 probe number 1, with a 50 cm cable.*

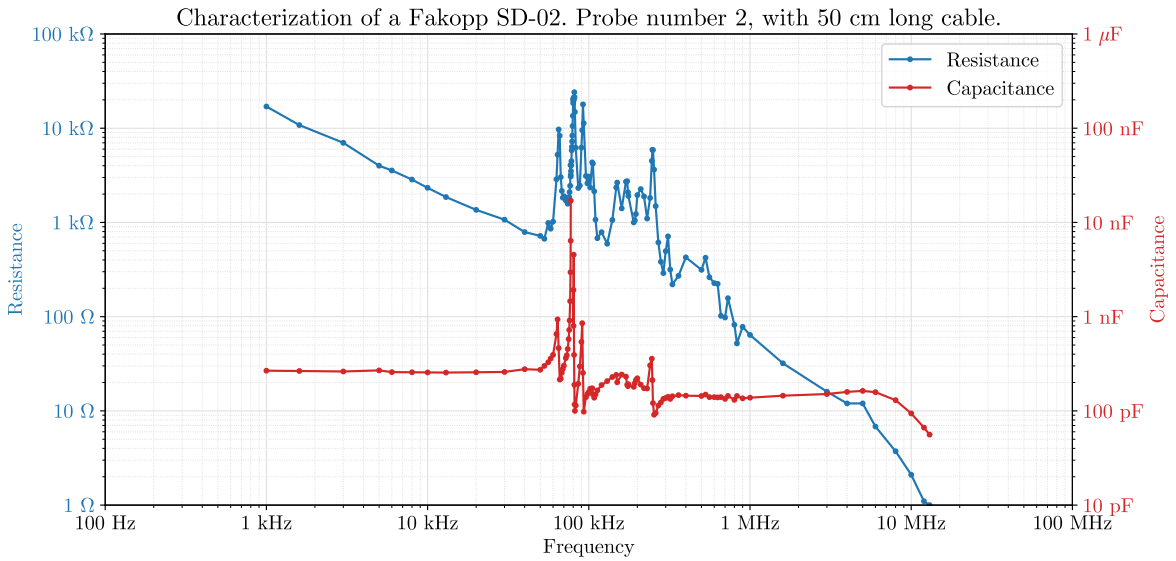

Figure 2.9 – *Resistance and capacitance characterization of Fakopp SD-02 probe number 2, with a 50 cm cable.*

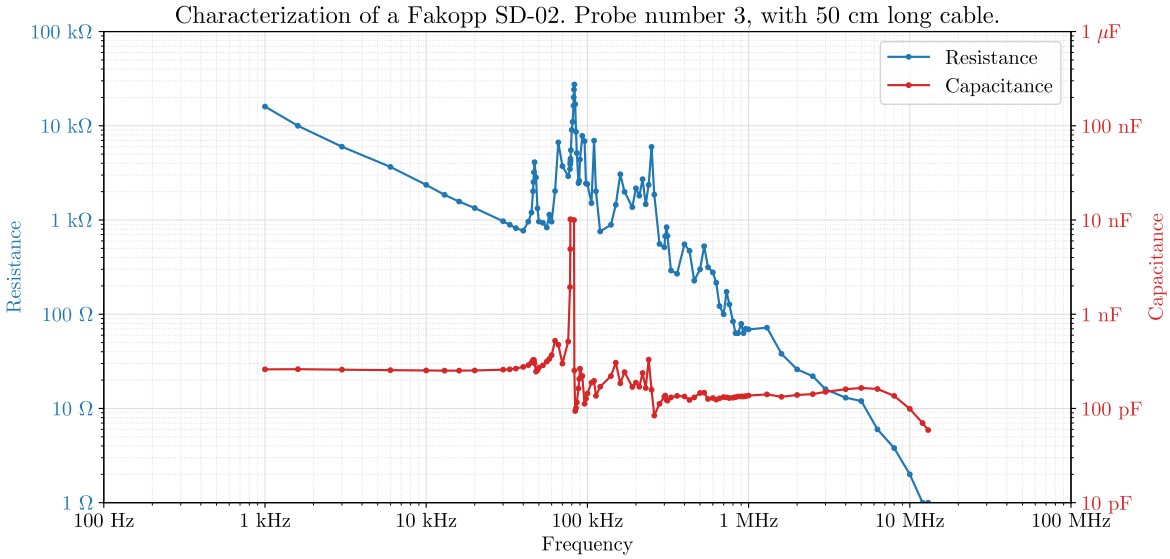

Figure 2.10 – *Resistance and capacitance characterization of Fakopp SD-02 probe number 3, with a 50 cm cable.*

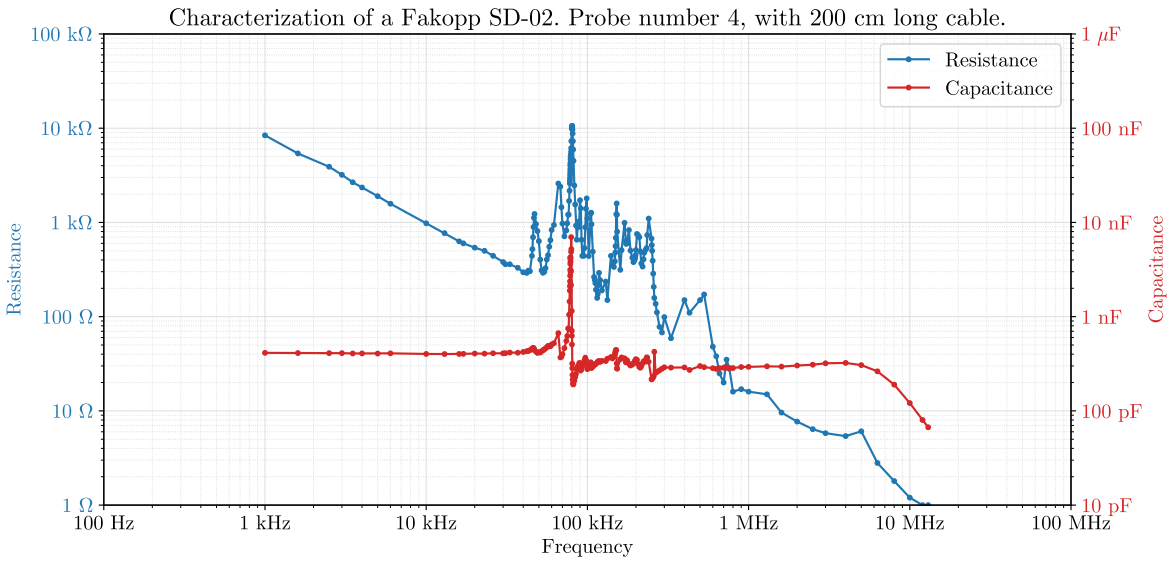

Figure 2.11 – *Resistance and capacitance characterization of Fakopp SD-02 probe number 4, with a 200 cm cable.*

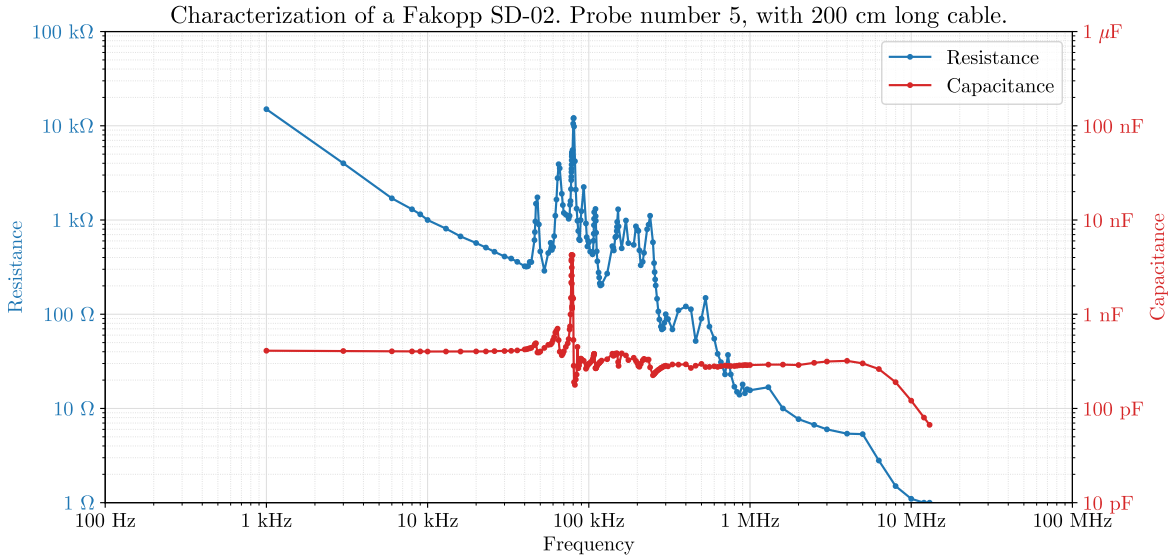

Figure 2.12 – *Resistance and capacitance characterization of Fakopp SD-02 probe number 5, with a 200 cm cable.*

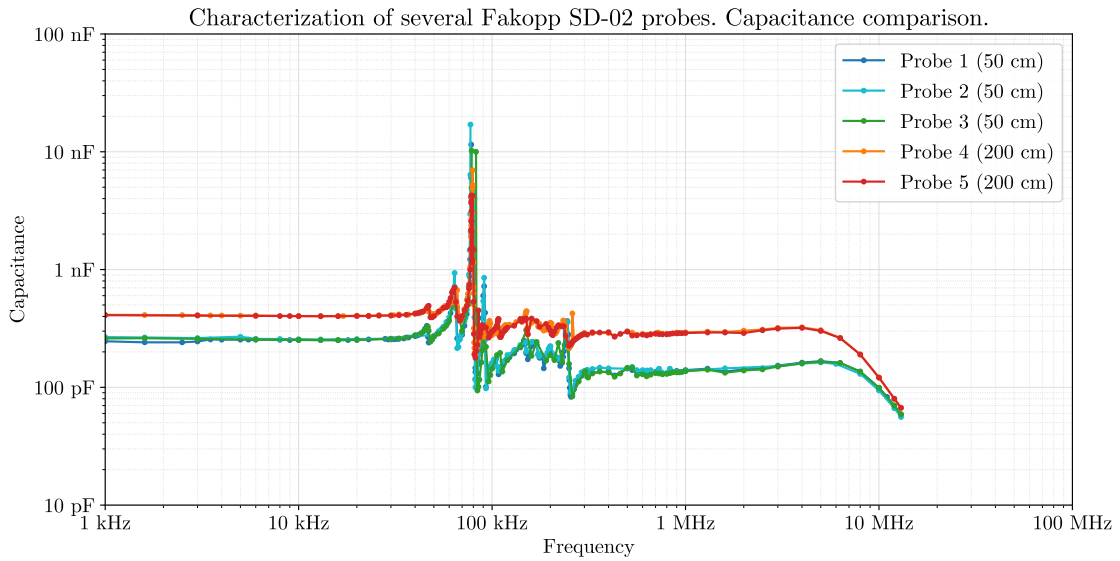

Figure 2.13 – *Comparison of the capacitance of the five Fakopp SD-02 probes.*

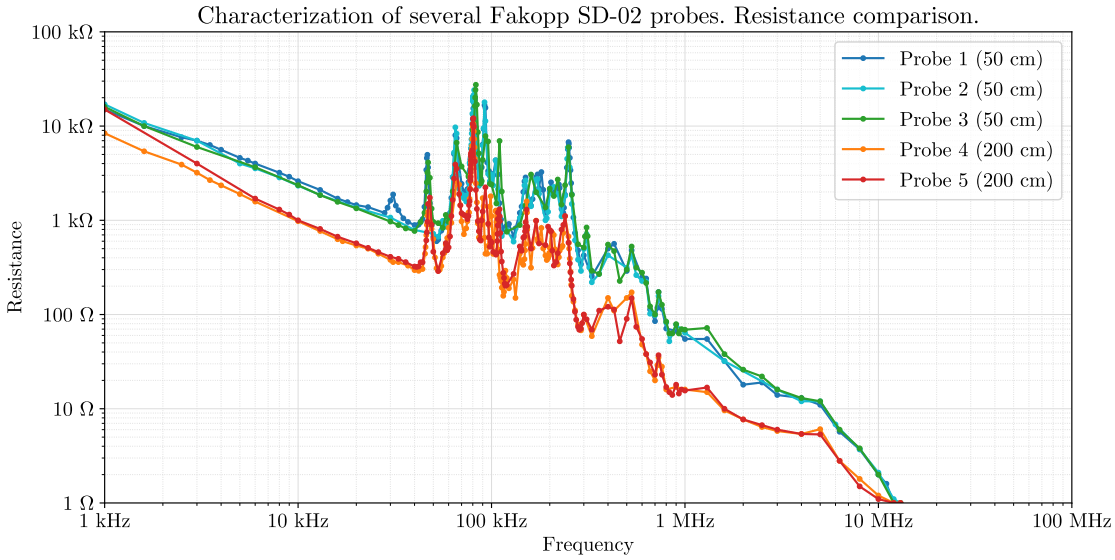

(a) *Resistance of the five probes.*

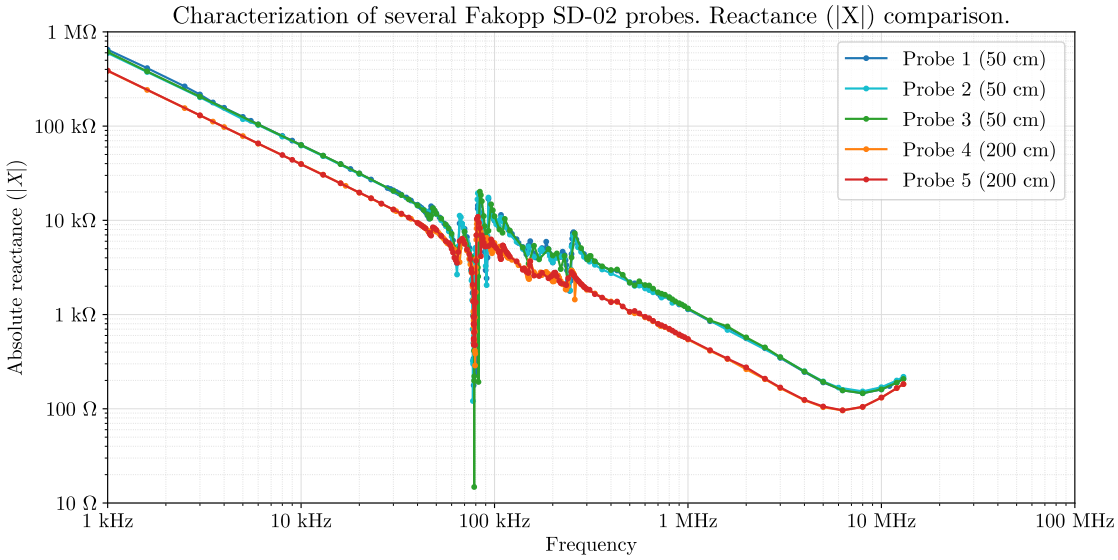

(b) *Reactance of the five probes.*

Figure 2.14 – *Comparison of resistance (R) and absolute reactance (|X|) of the five Fakopp SD-02 probes.*

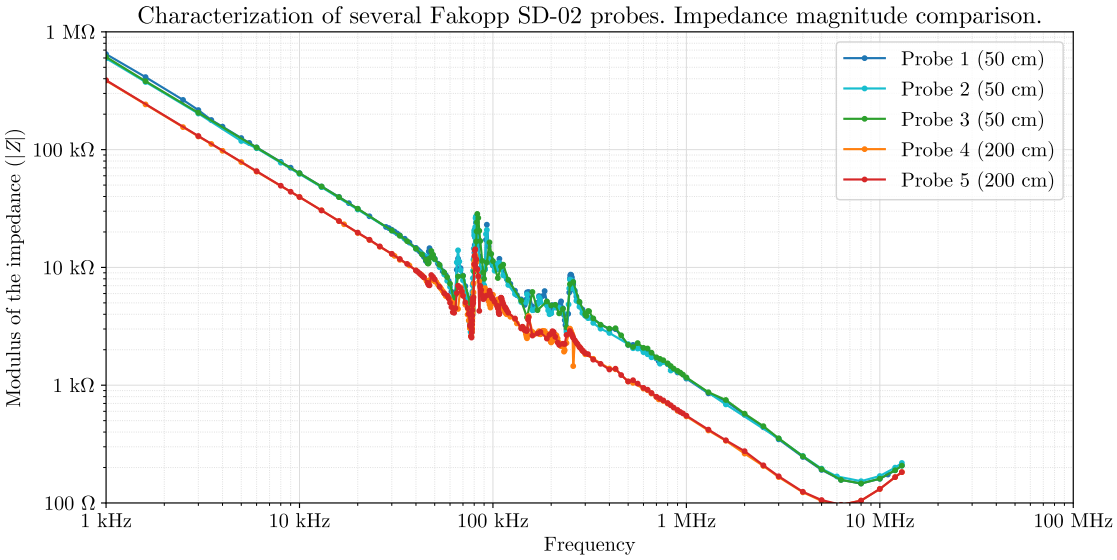

(a) *Magnitude of impedance (|Z|) of the five probes.*

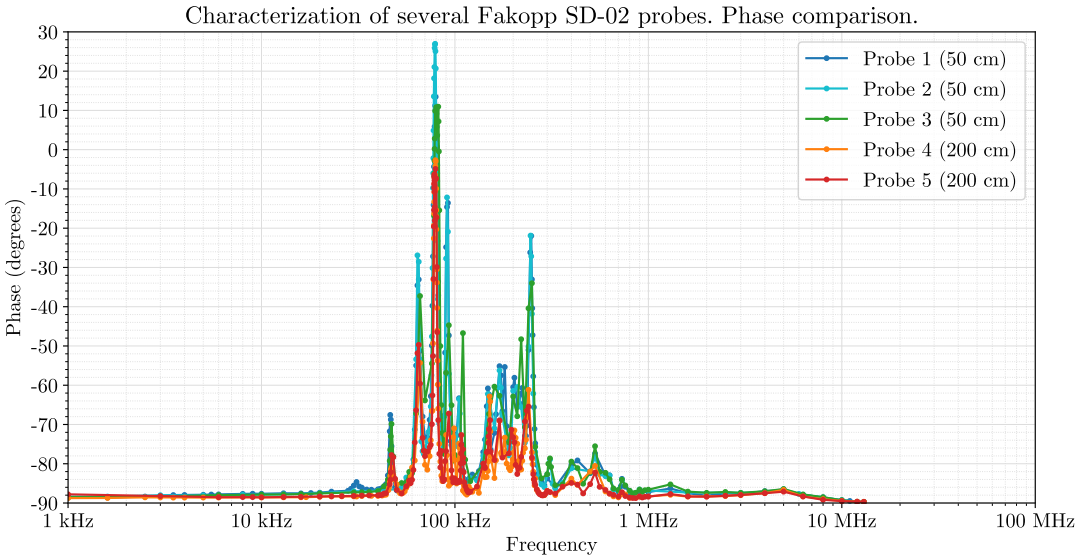

(b) *Phase of the five probes.*

Figure 2.15 – *Comparison of the absolute impedance (|Z|) and phase (Φ) of the five Fakopp SD-02 probes.*

Chapter 3

Signal analysis and processing.

The third chapter dives into the analysis of signals captured from a multitude of experiments in wood such as in standing trees and trunks, but also in a Fakopp-provided reference aluminum rod.

The analysis help us characterise and understand the signal's nature, as well as defining some requirements for the electronics. These signals were captured using ADIME a PicoScope PC Oscilloscope and Fakopp SD-02 piezoelectric sensors.

3.1 Test setup

This section details the measurement method, and lists the experiments performed.

- **Experiments on standing trees.** These measurements were taken in several poplar cultivations by the ADIME team before they were cut.
- **Experiments on a cut log.** One of the cut poplars was sent to ADIME's workshop to be dedicated to testing. This log serves as extensive experimentation for our research, since it has practically the same properties as a tree, but with the convenience of measuring without having to go to a plantation.

  The procedure for inserting the probes in each the log can be seen in Figure 3.1a and Figure 3.1b, according to the procedure described in [16, 50]. Since the probes are nailed 60 cm apart and 2.5 cm deep in the trunk, the *effective* distance between the tip of the probes is:

$$d_{\text{eff}} = 60\,\text{cm} - 2 \cdot 2.5\,\text{cm} \cdot \sin\frac{\pi}{4} \approx 56.46\,\text{cm} \tag{3.1.1}$$

- **Experiments in the Fakopp validation rod.** Fakopp optionally provides with the Microsecond Timer a cylindrical, aluminum test bar with two wooden stops or plugs at its ends, with the purpose of inserting two SD-02 probes into them. This bar is for device validation purposes, not a calibration bar, since the Microsecond Timer cannot be calibrated. The purpose of testing on the bar is to serve as a reference since it is assumed to be a more ideal medium and with more repeatable results than a log. In addition, it serves as a direct comparison with Fakopp results.

  The rod is 440 mm in length and 22 mm in diameter. The wooden stops are inserted 28 mm into the rod and are 13 mm in diameter. The Fakopp manual ensures that the rod is made of aluminum but does not specify what alloy. We will consider then the most probable alloy: aluminum 6061, with a density of $2700\,\text{kg/m}^3$ and with an approximate MOE of 69 GPa.

  The specified transit time is $89 \pm 2\,\mu\text{s}$ when the probes are nailed 12 mm deep in the wooden plugs [61]. So, the *effective* longitudinal travel length is 416 mm. Thus, with this information we can calculate

the theoretical longitudinal MOE of the rod applying the one-dimensional wave approach and the ToF method for a long, thin and isotropic material. Solving E (the MOE) from Equation 1.2.1:

$$\mathrm{E} = \frac{\rho \cdot d^2}{\Delta t^2} \tag{3.1.2}$$

The expected MOE is 59 ± 3 GPa (giga-pascals). However, this result is only testimonial, since we do not know the density of the bar and its real MOE and how much the wooden plugs influence it.

This serves as a prelude to the inconsistencies that we found between the specifications of this validation bar and our experiments in Section 3.4.1, both measured with Fakopp and with the PicoScope.

All experiments have been performed using Fakopp SD-02 piezoelectric sensors. Photos of the experiments can be seen in Figure 3.2.

Some experiments have been measured two times: with the probes connected to channels A and B of a PicoScope 4424 and a PC running its software (version 6); and another with Fakopp microsecond timer to compare results with.

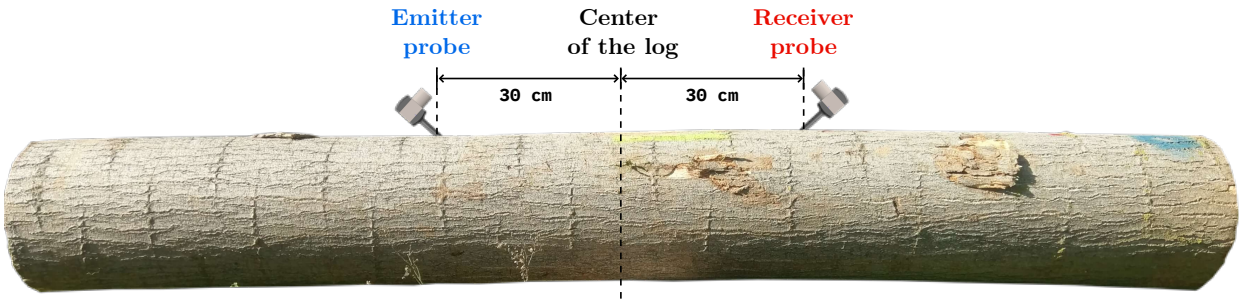

(a) *Placing the probes in a tree or log. The position of the transmitter and receiver is interchangeable.*

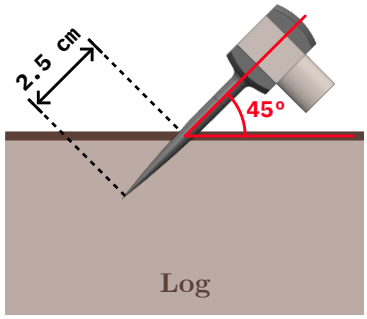

(b) *Detail of how the probes should be nailed into a tree or log.*

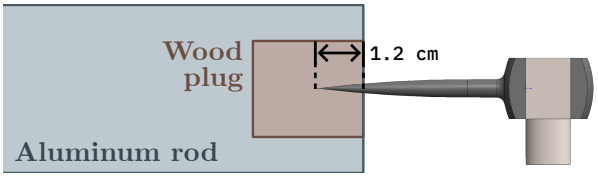

(c) *Detail of how the probes should be nailed to the rod.*

Figure 3.1 – *Diagrams of how to nail the probes into the trees, logs and rod.*

(a) *Measurements in log with the Picoscope 4424.*

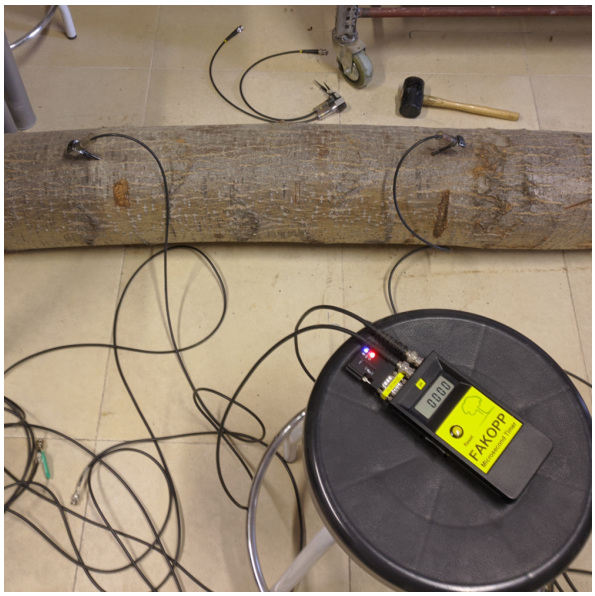

(b) *Measurements in log with the Fakopp Microsecond Timer.*

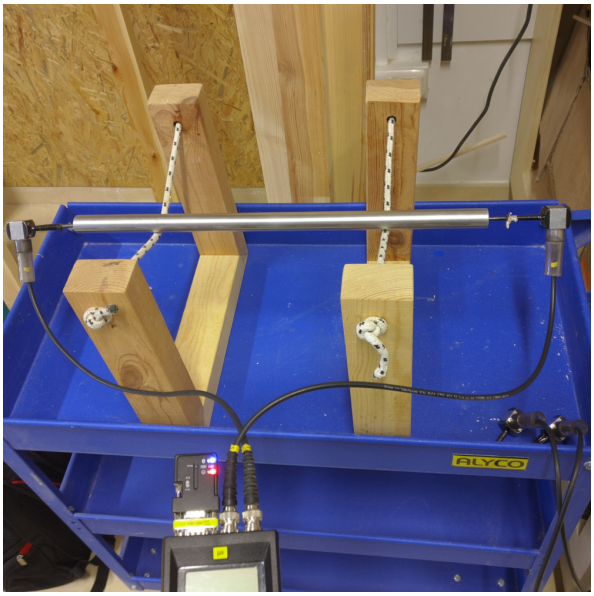

(c) *Fakopp validation bar. Horizontal mounting suspended on ropes.*

(d) *Fakopp validation bar. Vertical mounting supported by lab stand.*

Figure 3.2 – *Photos of several experiments.*

3.2 Typical properties of the signals

In Figure 3.3 are some representative graphs of a typical signal captured with Fakopp SD-02 transducers and a PicoScope 4424 in a tree log. The purpose of these is to familiarize the reader with the waveform and properties of the signal before moving on to a discussion of post-processing methods and further analysis.

Observing Figure 3.3a in the first place, the first big difference is their waveform and amplitude. The emitter signal reaches several tens of volts at its initial edge and then quickly fades. The receiver only reaches a few hundred millivolts, but maintains the level for longer.

The signal from the emitter always has a large falling edge. This is because, as discussed in Section 2.3: Fakopp SD-02 piezoelectric transducers, its polarity is negative if impacted from the rear. The signal from the receiver always starts positive, since it receives the vibration at its tip. In addition, the receiver starts much softer and progressive.

On the other hand, as can be seen in the Voltage Spectral Densities graphed in Figure 3.3b, the spectrum of these signals dominates in the acoustic zone, in the decade from 1 kHz to 10 kHz, although it is true that there are frequency components that expand up to the decades of kilohertzs and even 100 kHz in the case of the emitter. In the spectrogram of figure 2, we can see how the frequencies are distributed over time in each signal.

In Figure 3.3b the emitter signal appears to have a higher background noise level, but this is due to the configured input range in the PicoScope for each signal: $\pm 50\,\mathrm{V}$ for the emitter, and only $\pm 1\,\mathrm{V}$ for the receiver. Whatever the input range is, it is divided by the 12-bit resolution of ADC. The Emitter channel has lower resolution in millivolts than the Receiver channel, but the same in LSB, and therefore its noise level is registered as higher.

In the spectrograms of Figure 3.4, we can see how the frequencies are distributed over time in each signal. In order to illustrate this spectrogram, the above signals have been downsampled from 20 MHz originally down to 1 MHz. As we can see, the emitter exhibits many frequency components during the duration of the high amplitude flanks that we saw in Figure 3.3a, reflecting the rapid change of the signal in this interval. When the large fluctuations decay, oscillations are established in a frequency range similar to those of the receiver. For its part, the receiver signal presents a more homogeneous behavior from the moment the signal appears until it fades.

3.3 Signal arrival detection post-processing algorithms

Once the signals are captured with the PicoScope and stored as `.CSV` files. These are subsequently analyzed using different arrival detection algorithms or *pickers* (since they *pick* a sample as the signal's starting point). The signal analysis has been carried out in MATLAB.

3.3.1 Threshold detection picker

This method detects when the signal exceeds a certain level, which can be fixed or proportional to some feature of the signal (e.g.: the maximum value). The simplest and also the least precise given the characteristics of our signals, especially the receiver, which has a very weak and slow start.

Thus, algorithm is discarded because it is not considered appropriate, but it will be used as an auxiliary method to establish, for example, the limits of the calculation window for the next method.

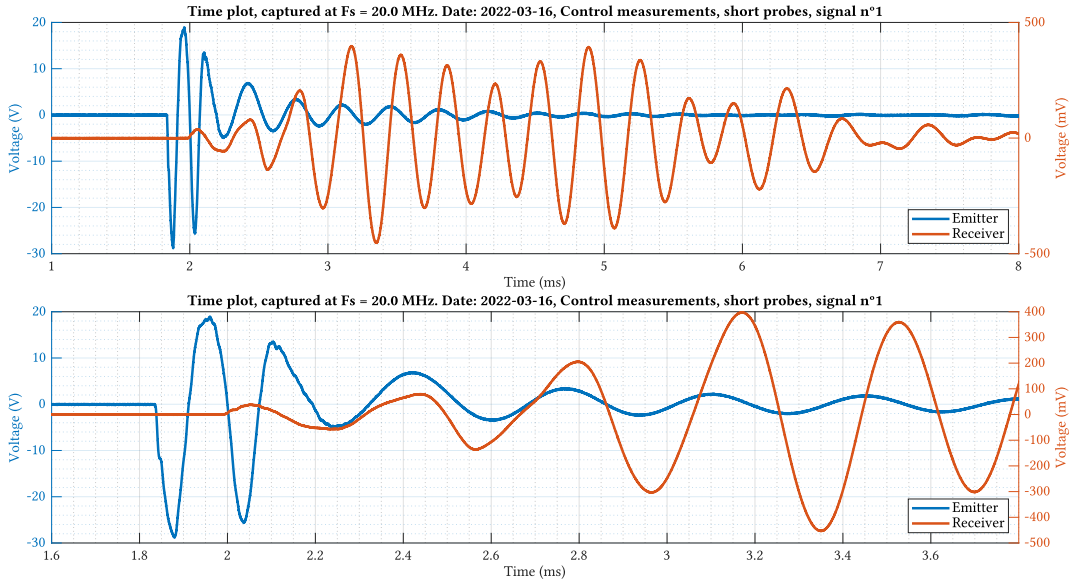

(a) *Typical transient response, captured on a log, zoom-out and detail of the signal's start.*

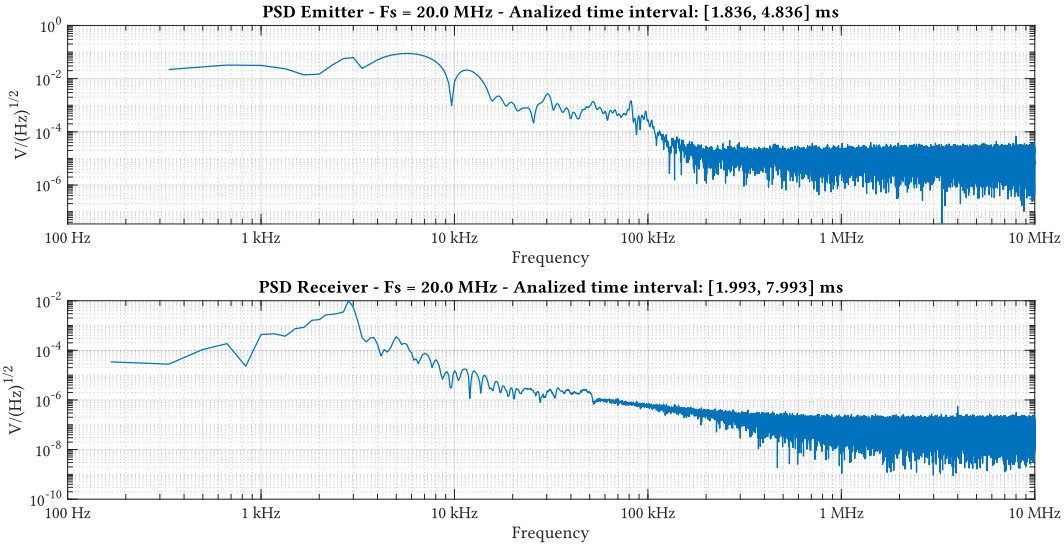

(b) *Voltage Spectral Density (VSD) of the prior signal. Only the regions of interest have been analyzed.*

Figure 3.3 – *Typical time and spectral characteristics of a signal captured with Fakopp's SD-02 sensors on trees and logs.*

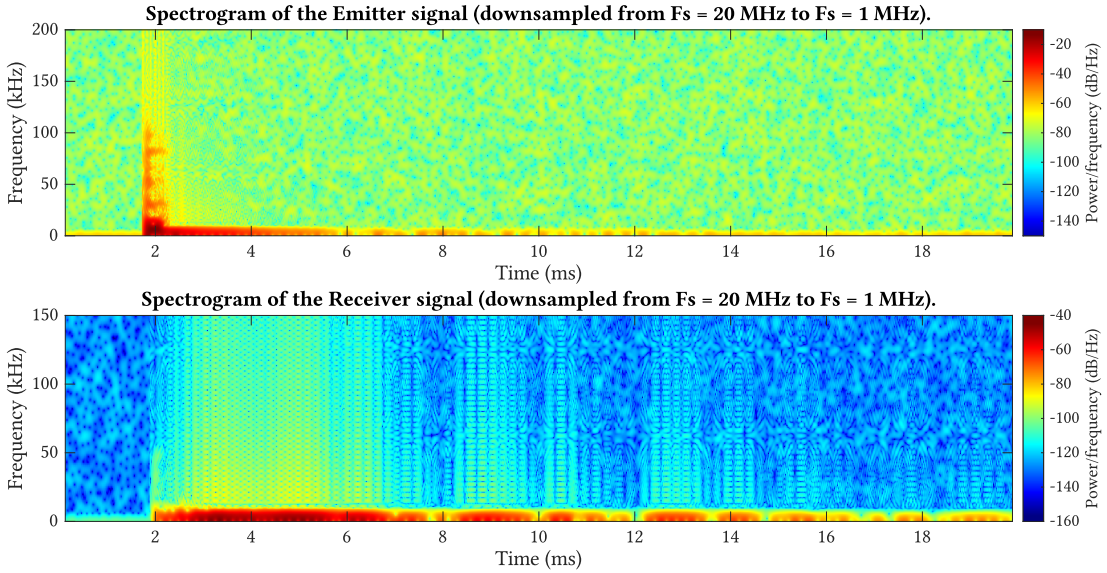

Figure 3.4 – *Spectrogram of the example signal from Figure 3.3.*

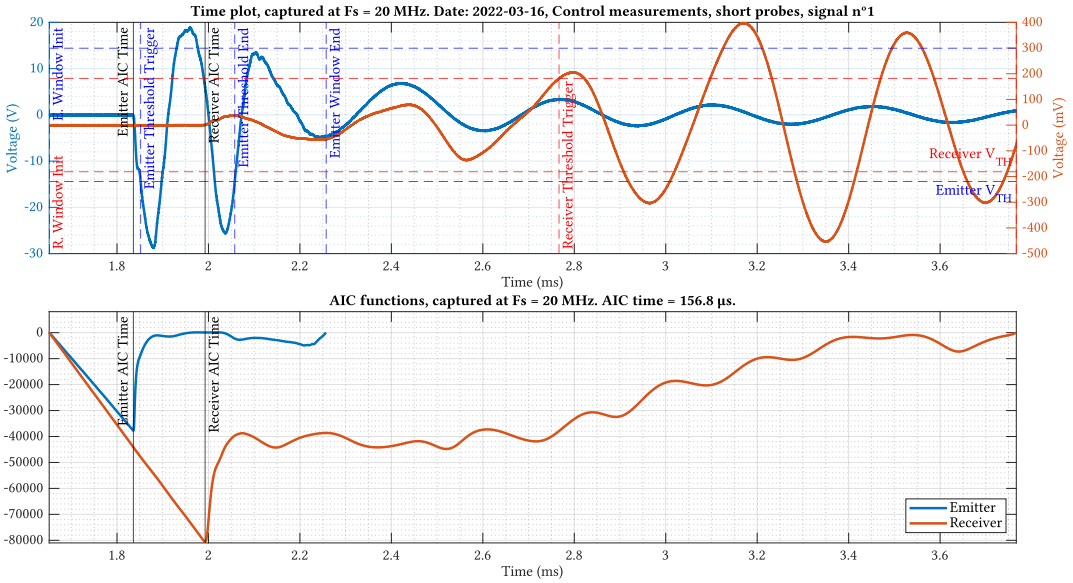

Figure 3.5 – *Analysis example of a tree log signal to which has been applied the AIC picker. Detail of the selected window in the time domain, and AIC functions.*

3.3.2 Akaike Information Criterion picker

The Akaike Information Criterion (AIC) picker supposes that the intervals before and after the arrival are two different stationary time series and detects the change. It is an arrival method widely used in other disciplines such as seismography. This algorithm analyzes the information contained in the signal by applying the following formula [63]:

$$\mathrm{AIC}(k) = k \cdot \log\left(\mathrm{var}(x[1,k])\right) + (N-k-1) \cdot \log\left(\mathrm{var}(x[k+1,N])\right) \tag{3.3.1}$$

Where $\mathrm{var}(x[1,k])$ is the variance of time series $x(1)$, $x(2)$, ..., $x(k)$, and $\mathrm{var}(x[k+1,N])$ is the variance of time series $x(k+1)$, $x(k+2)$, ..., $x(N)$. k must be always be equal or greater than 2 in order to avoid computing the variance of a single number, which is zero, and that would cause the logarithms to be equal to minus Infinity.

The AIC(k) vector, also called the AIC function, will present an absolute minimum when it considers a signal has arrived (see Figure 3.5). This method is very accurate for signals with clear beginnings, and useful in detecting the beginning of weak signals. However, the biggest disadvantage of this method is how relatively low SNR and other signal degradations may cause it to have large errors, as we will see in Section 3.5: Effect of signal degradations in the AIC picker.

3

3.4 Experiments

Some results of the most interesting experiments carried out during the development of this project are detailed below.

3.4.1 Comparison of results with different probes and cables on a tree log

This section details experiments performed to determine whether measuring with the short 50 cm or long 200 cm probes has an effect on the results on log measurements. In addition, ADIME uses a 6-meter coaxial cable to perform field measurements faster. This cable has the following inscription on its side:

```
TASKER RG58 CU MIL C/17 F 50 OHM ITALY
```

It is a Tasker cable with a characteristic impedance of 50 Ω and a capacitance of 100 pF/m [64]. At 6 meters, this is a total of 600 pF, which could be significant enough to skew the measurements.

Four measurements are taken: with the short probes with and without an extension cable, and with the long probes with and without an extension cable; following the indications given in Figure 3.1.

The results are directly represented in the form of bar graphs in Figure 3.6 (time) and Figure 3.7 (derived MOE). The results presented are the average of 10 realizations. The uncertainty is equal to the standard deviation of these realizations.

In view of the results, it cannot be ensured that there is a palpable difference between the cables used, since the uncertainty is too high. Fakopp's time is consistently lower, which gives the trees a MOE that is abnormally high for their species (the average for the poplar is around 6000 to 9000 MPa, which is the result we obtain with AIC).

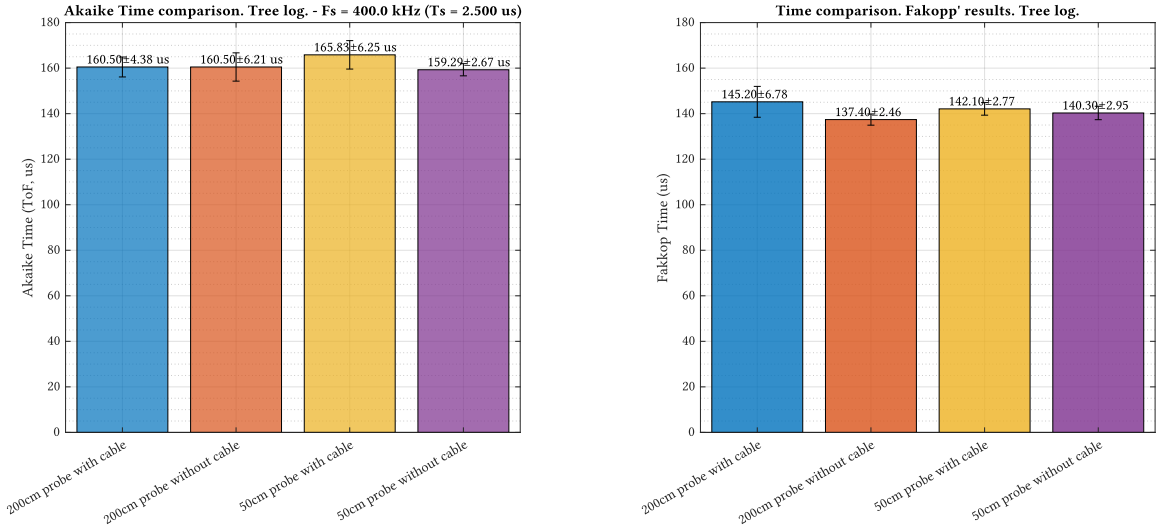

(a) *Transit time of the tree log, computed by the AIC method.* **(b)** *Transit time of the tree log, measured by Fakopp µstimer.*

Figure 3.6 – *Transit time of the tree log by AIC and Fakopp µstimer.*

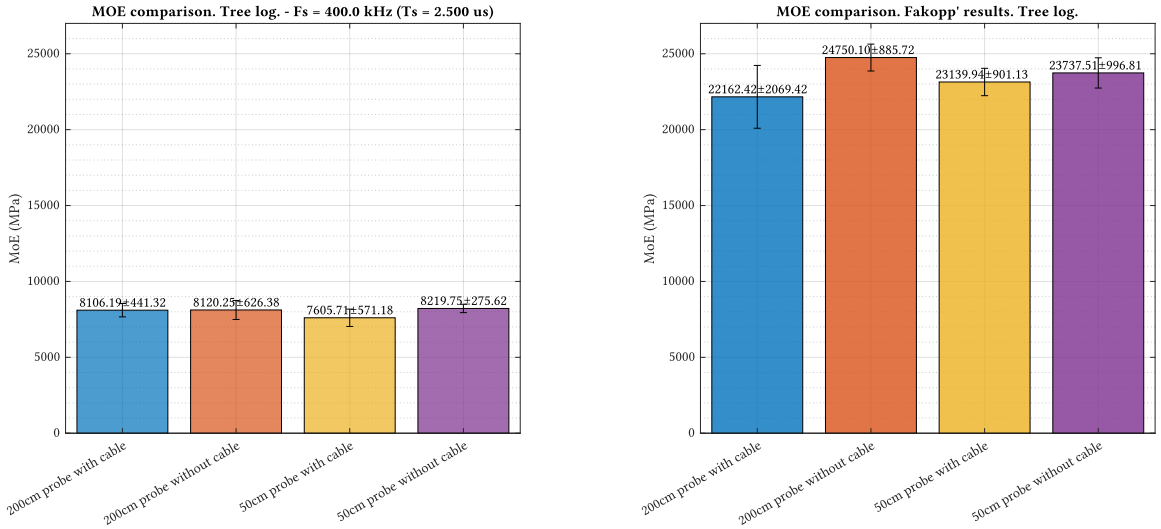

(a) *MOE derived from AIC results.* **(b)** *MOE derived from Fakopp's µstimer results.*

Figure 3.7 – *Derived MOE of the tree log by AIC and Fakopp µstimer. Assuming* $\rho = 653.62\,\mathrm{kg/m^3}$ *(measured destructively by ADIME).*

3.4.2 Comparison of results with different probes and cables on Fakopp's test rod

This experiment is identical to the previous one, but measured on Fakopp's aluminum testing rod. The properties of the bar have already been reviewed in section 3.1. The results can be seen in Figure 3.8 (time) and Figure 3.9 (derived MOE).

Again, a clear trend cannot be inferred from these results according to the type of probe and cable, the results overlap each other due to the margin of error.

However, neither of the two methods meets the transit time specified by Fakopp in its manual. Although it is true that the Fakopp is much closer, it is still around 10 µs higher than the expected result, leaving by a far margin the bounded error of 89 ± 2 µs of the manual.

As for the question of how is this low time even measured by the µstimer is a mystery. The electrical signals that we visually inspection on the oscilloscope take around the same time that has been calculated by the AIC algorithm. The possibility arises that the microcontroller is subtracting a fixed number of microseconds from each measurement, in order to compensate for its own processing time; but if that is the case, it is clearly overcompensating.

When contacting Fakopp about the discrepancies, they simply instructed us to subtract the difference from all measurements to match the specified transit time. But, with the permission of the reader, that makes no logical sense. What is more, if 10 µs were subtracted from all measurements including those of trees, the obtained MOE would be even higher than it is now.

Given this situation, both the results of this Fakopp µstimer and the manual specifications are suspected of being incorrect.

3.5 Effect of signal degradations in the AIC picker

As we saw in Equation 3.1.2, the MOE depends on the inverse of the time squared, so a small deviation in the time measurement generates large deviations in the MOE. Thus, ensuring accurate timing is of paramount importance. In this section, we study several degradations that affect the Akaike Information Criterion picker in particular.

3.5.1 Effect of noise

In this section, the noise resistance of the AIC method is tested. To do this, we inject AWGN noise in the captured signals. The noise bandwidth is filtered to that of the signal, to avoid artificially incorporating noise above $F_s/2$. The effect in the time domain can be seen in Figure 3.10. The consequences of the AWGN are more detrimental in the receiver, since having lower amplitude causes the SNR to also be lower at the same noise level as the emitter.

Figure 3.11 shows three cases to illustrate how the Akaike function in the receiver is modified as the noise level increases. We can observe how the minimum of the receiver becomes less and less evident, losing angle and simultaneously increasing the detection minimum in the positive X-axis direction, and causing the AIC-computed time result to increase. This is the visual representation of the difficulty the algorithm faces in distinguishing the beginning of the signal from the noise.

Noise can be extremely harmful to this algorithm, as we can see in Figure 3.12. Said figure represents the average AIC time of 10 realizations and its standard deviation, as a function of the amount of noise injected into the signals. The multi-sampling dampens the effect of noise, so the measurements do not vary too much until just before 100 µVrms, when the results begin to draw an upward trend with respect to the reference AIC time (the one obtained without adding noise). Above 1 mVrms, the discrepance skyrockets.

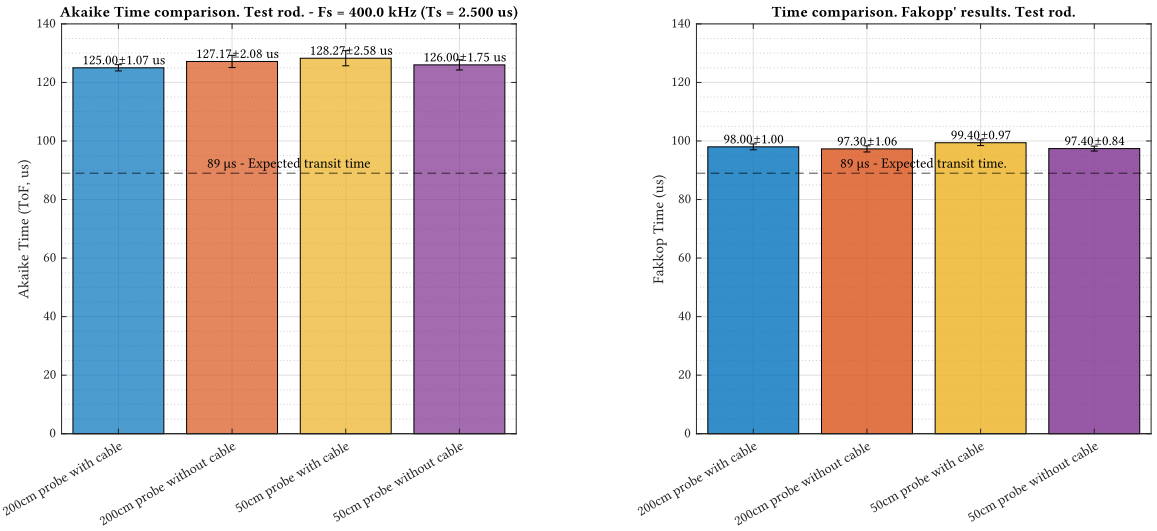

(a) *Transit time of the test rod computed by the AIC method.* **(b)** *Derived MOE of the test rod measured by Fakopp µstimer.*

Figure 3.8 – *Transit time of the testing rod by AIC and Fakopp µstimer.*

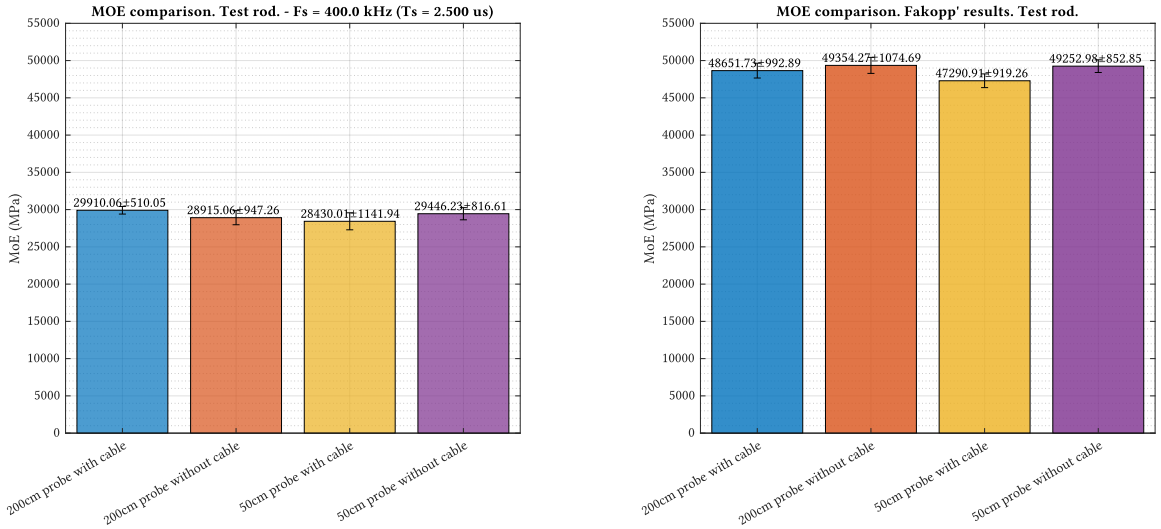

(a) *MOE derived from AIC results.* **(b)** *MOE derived from Fakopp's µstimer results.*

Figure 3.9 – *Derived MOE of the test rod by AIC and Fakopp µstimer. Assuming* $\rho = 2700\,\mathrm{kg/m^3}$.

A high level of noise makes results unacceptable. In the electronic design it will be necessary to guarantee low-noise conditions. Nevertheless, it would be convenient to seek a way to increase the robustness of this method, or use another procedure more noise-resistant.

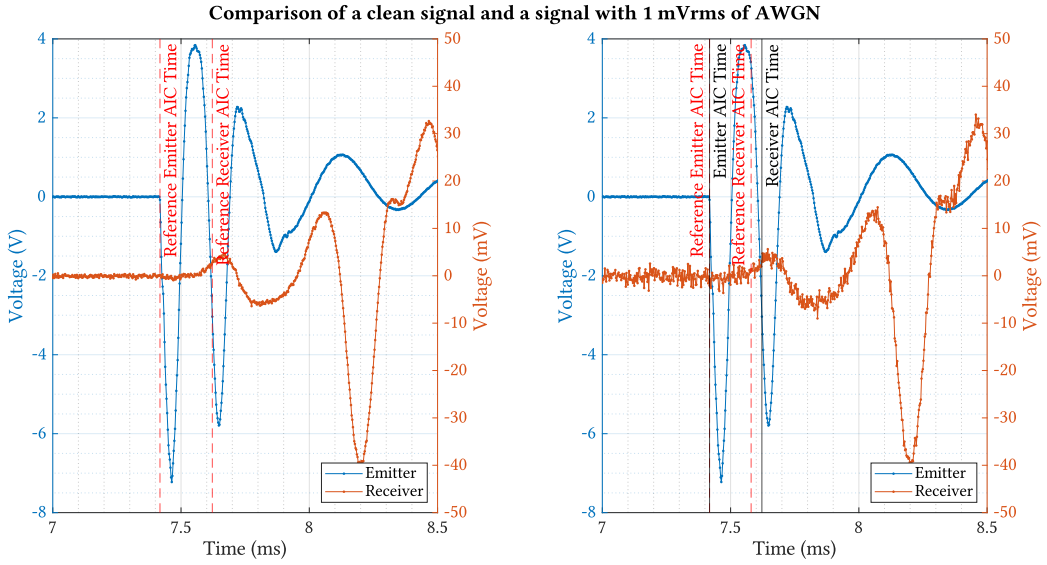

Figure 3.10 – *Comparison of a signal with no added noise and one with 1 mV (rms) of AWGN.*

3.5.2 Effect of the sampling frequency

At first glance of the spectrum in Figure 3.3b, we could think that the sampling rate (F_s) can be greatly reduced. However, the precision of any *picker* is tied to the sampling period (T_s), because they select a sample of the signal as the beginning, and measure the delay as the time difference between those two samples, which are forcibly separated a multiple of T_s.

So, the higher the sampling frequency, the more precision we will have. To demonstrate this, Figure 3.13a shows the Akaike time obtained in a single measurement, according to the samplig frequency. The base signals were sampled at 20 MHz, then downsampled by using the `downsample(X, N)` function in matlab, which does not introduce any filtering or extra processing. As we can see, the lower f_s, the higher the discrepancies with the reference value. Logically, the higher the f_s, the higher computation time required (Figure 3.13b).

The more immediate solution to this situation is to use multi-sampling, which greatly palliates the effects of a low sampling frequency (Figure 3.14), although the standard deviation does increase, and this method has a clear limit below 100 kHz. In our developed device, a compromise between sampling frequency and measurement quality must be found.

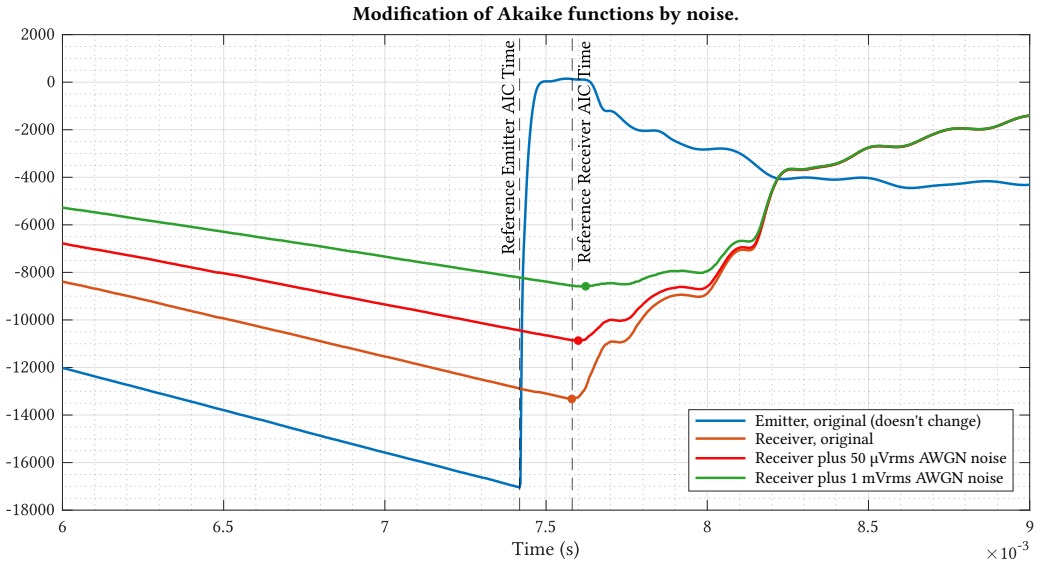

Figure 3.11 – *Comparison of how the the Akaike functions change with noise.*

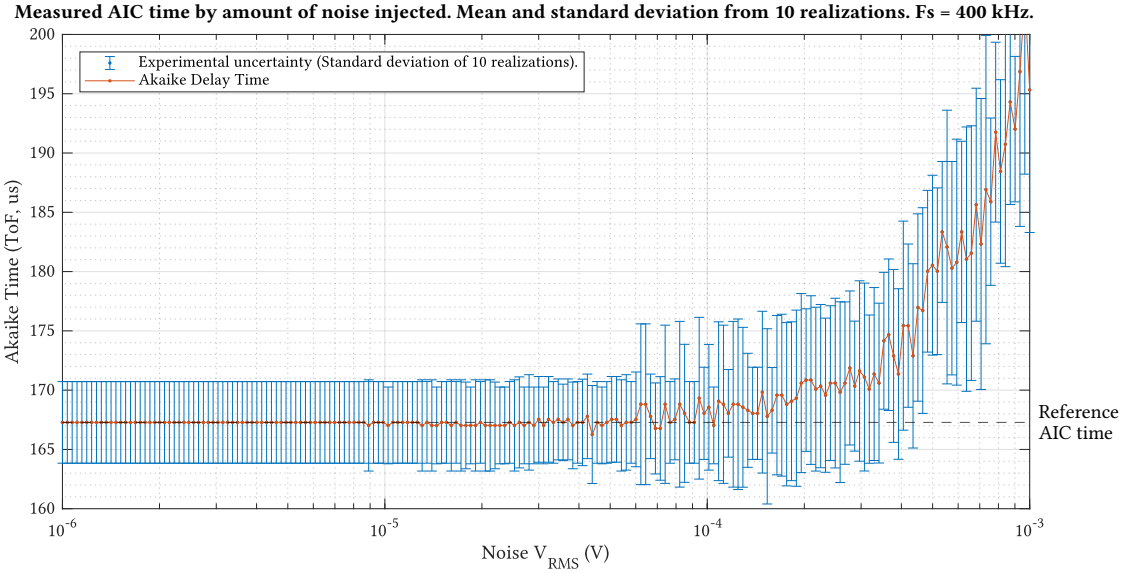

Figure 3.12 – *Measured AIC time by amount of noise injected. Mean and standard deviation from 10 realizations. Fs = 400 kHz.*

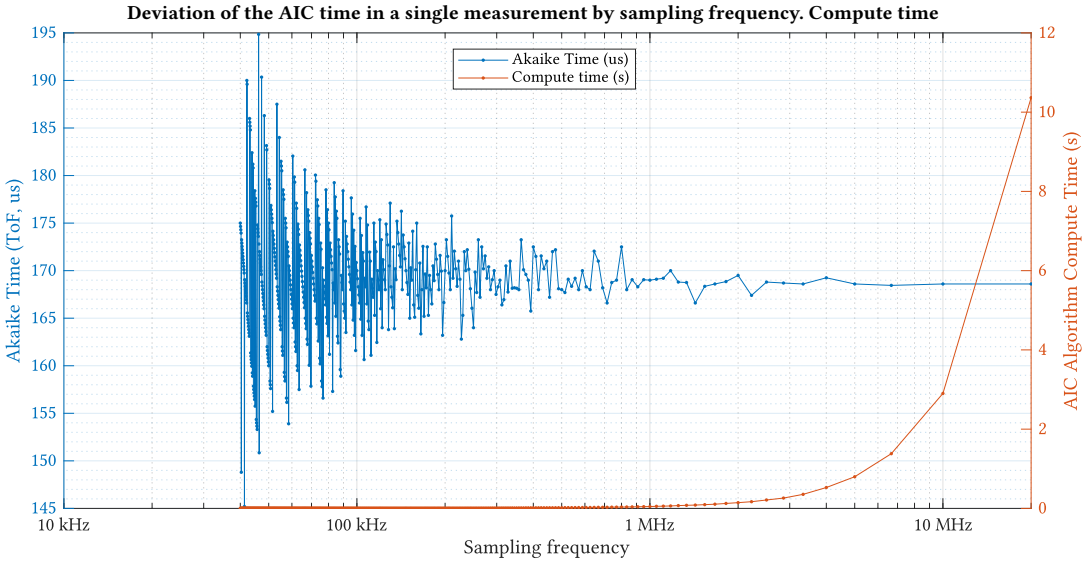

(a) *MOE derived from AIC results.*

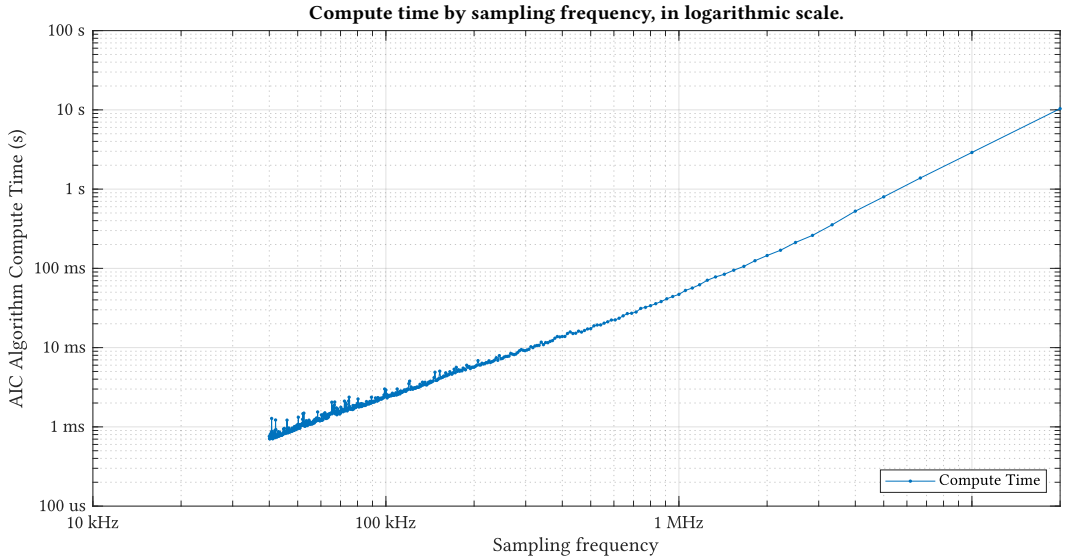

(b) *MOE derived from Fakopp's µstimer results.*

Figure 3.13 – *AIC time of a single measurement and compute time.*

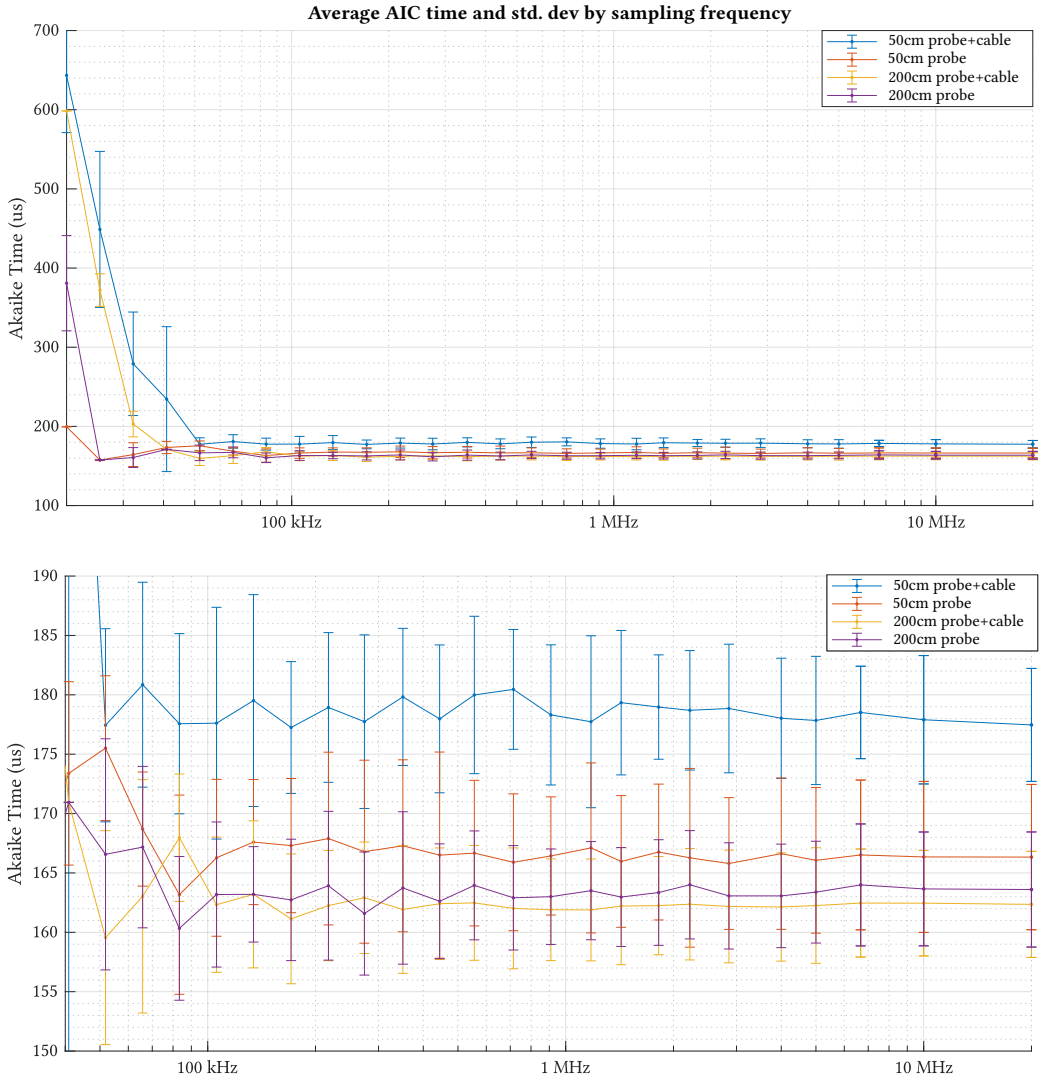

Figure 3.14 – *Average AIC time and standard deviation in 10 measurements, according to the sampling frequency. Zoom-out and detail views.*

Chapter 4

System specification

After establishing the scope and goals of the project, inspecting the signal properties and succeeding the reverse-engineering of some competing products; we must delve into the specification process, which consists of setting the functions, limits and needs of the device under development at different levels of abstraction. This chapter is divided into two distinct parts:

- **4.1: Requirements Engineering.** The first part aims to define all the requirements that our electronic device must fulfil, and to show the design strategy and concepts.
- Following the requirement specification comes the **product specification**. This second part of the chapter is split into 3 sections:
  - **4.2: Electronic architecture.** In the first section we will focus on the study of the device's electronic architecture, starting from a high-level, functional block diagram. All the relevant electronic components will be selected after an exhaustive comparison, checking that every element meet the requirements.
  - **4.3: Software architecture.** Once defined the hardware platform, we will approach its software structure, defining which programming language, framework, operating system, etc. to use.
  - **4.4: Mechanical architecture.** At last, the final section of the second part tackles the mechanical considerations of the product.

It's important to note that, whereas this chapter is encapsulated as the *specification* process, many times we will inevitably cross the line with the *design* process. They are not separate parts, but rather complementary, and developing an electronic product is not a sequential process, but an iterative process in which activities feedback one another and are interleaved. Having said this, most of the design process can be found in the next chapter, Chapter 5: System Design.

4.1 Requirements engineering

Requirements engineering is the process of establishing the system behaviour, functions, services that the final users or clients need, and the constraints under which the system operates. The requirements themselves are the descriptions of the system services and constraints [65]. We can distinguish different levels of description:

- **User requirements:** natural language statements and high-level descriptions and diagrams of what

services the system is expected to provide, and defines the usage environment. These are the subject of matter of this first part of the chapter.

- **System requirements:** A more detailed description of the system's functions and operational constraints. The second part of this chapter addresses this task, although this definition blurs with the product design process.

4.1.1 Working constraints. Portability and robustness

The first design point of importance is that the device has to be portable. Users are going to make use of the device in an environment where there is no power infrastructure. This has obvious consequences: a battery is mandatory and power consumption is restricted to maintain a good autonomy. The device must be capable of keep working without charging for a few hours at least; and charging the battery should not take several hours. In addition, a standard, non-privative port should be used as power input.

Another important aspect is that the device has to be robust. The environment in which it will be used can be very harsh: humidity and splashes, dirt, dust, sawdust, etc. A rugged casing will be designed and electronics should be protected within the possibilities.

4.1.2 User interface

The device should present the user with a friendly and easy to use interface. The obvious go-to option is a screen. Screens of competing products are generally simple: Fakopp's microsecond timer has only a 4-digit 7-segment display and Brookhuis's MTG has a basic 2-color 122x16 pixel LCD. In order to improve the attractiveness, usability and to maximize the amount of information presented to the user, a bigger, more advanced LCD should be used.

From an user's point of view, is taken for granted that a big display in a handheld device means it's a touchscreen, since it has undoubtedly become a standard nowadays. Thus, touch support is an interesting feature to add in terms of ease of usage and natural interaction.

But remembering the harsh environment, a parallel, physical interface using buttons or rotary encoders should be added in order to navigate the UI but without sacrificing user friendliness and quick, precise interaction. This is required if, for example, the operator is using gloves or if it's manipulating the device with only one hand.

4.1.3 Signal analysis

An adaptation circuit must be designed for the piezoelectric sensors, so that appropriate electrical signals are obtained for their capture and analysis by the system's microprocessor. For this, the electronic literature on the subject must be consulted, and what has been learned during the reverse-engineering process.

In addition, the processing unit must have the right specs in order to capture, store and process the signals coming from the adequation circuit.

4.1.4 Results storage and transference

The device must have a way of saving the analysis results and/or raw data to an external storage device for subsequent study. This device can be for example an USB drive or a SD card.

On top of that, wireless connectivity for data transfer is an attractive selling point, as well as modern and convenient from the user's point of view. The chosen wireless technology should be compatible with most

common portable devices, such as smartphones and laptops, and work only at close range. *Id est*, Wi-Fi (IEEE 802.11) and Bluetooth (IEEE 802.15.1).

4.2 Electronic architecture

This section contains some definitions of interest about printed circuit technology. They serve as an introduction to the technology that will be used to design and manufacture the device, and the concepts presented are necessary to understand the subsequent sections.

We will then go into detail about the chosen electronic architecture and component selection. The choices made are a merge of the iterative process of requirements engineering, circuit design (elaborated on subsection 5.1.2) and Printed Circuit Board design (subsection 5.1.3).

4.2.1 Printed Circuit Boards (PCB)

Printed Circuit Boards (Printed Circuit Boards) are the undisputed standard for the implementation of physical electronic circuits. PCBs are rugged, non-conductive boards built on a dielectric substrate structure. They are used to provide electrical connection between the components of a electronic circuit, as well as mechanical support for those components. [7]

PCBs are organized in planar layers, separated by dielectric material. The connection among the components on a PCB layer are established with copper paths called *traces* or *routes*. The connection points for components are called *pads*. The interconnect accesses for establishing the electrical connection through two or more layers of the circuit board are called *vias*. [7]

The arrangement of copper and insulating layers is stack-up refers to the arrangement of copper layers and insulating layers is named layer stackup. The distance between layers and the role of the layer copper can severally affect board performance in different ways. For example, a good stack-up can reduce the impedance of the board ground (GND) and reduce various kinds of . [66]

There are two technologies for mounting components to a PCB: [7]

- **Through-Hole Technology (THT):** The assembly process in which the leads of electrical components are inserted into holes on the boards, and fixed through soldering (typically wave soldering). Its main disadvantages are low component density and obstruction to miniaturization, as well as working frequency limitations by the leads' parasites and the circuit physical size. It is considered an obsolete technology, and nowadays is only used in specific cases such as some power electronics and to provide mechanical support for components that may suffer stress; usually included in a mixed-technology design with Surface-Mount components. An advantage of this technology is lower assembly costs, easy of manipulation and mechanical robustness.
- **Surface-Mount Technology (SMT):** Components are placed on one side or both sides of a board. These are called Surface-Mount Devices (SMD). The major advantage of SMT is that greatly increases board density with smaller components. SMT also allowed a big improvement of frequency performance as well as noise reduction, as SMD components have generally less parasites than THT and PCB traces are finer and shorter.

The size and shape of a PCB is called form factor. While determining a form factor of a PCB, aspects such as the product chassis, mounting schemes and standards are taken into consideration. PCBs can also include mounting holes, which have a mechanical function rather than an electrical. A drilled hole in a PCB can be *plated* or not. The term "plated" refers to the deposit of conductive material onto the interior walls. [7, 67].

Solder mask is a insulating polymer coating used to mask or protect the untinned copper tracks from chemical and abrasive damage. It also masks off a PCB surface and prevents masked areas of being poured by solder during soldering. This way, only the desired pads are soldered and no shorts are created between tracks [15]. Solder mask also give the PCBs a distinct colour. Their traditional tone is green, as seen on Figure 4.1. The layer of white shapes and text printed above the solder mask is called silkscreen or overlay.

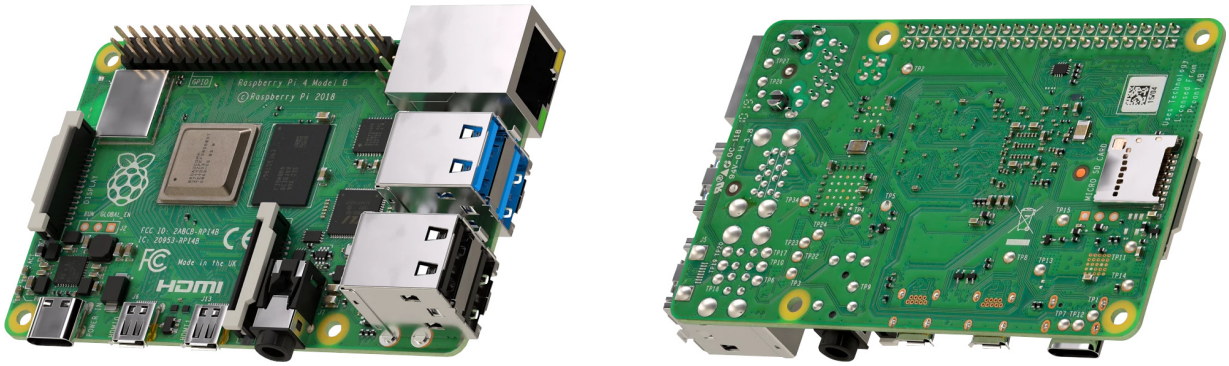

(a) *Front-side view.* **(b)** *Back-side view.*

Figure 4.1 – *Raspberry Pi 4 Model B SBC. An example of a device with a multi-layer Printed Circuit Board layer stackup, green solder mask, an mixed-technology components; all in a a standardized size, port layout and position of the mounting hole (the "model B" form factor). Images extracted from: [68].*

4.2.2 European legislation

Before choosing the electronic components, we must attend to the existing regulations. The most relevant European legislation in our field is compliance with the RoHS directive and the inclusion of the CE marking.

4.2.2.1 Restriction of Hazardous Substances (RoHS) European directive

The Restriction of Hazardous Substances (RoHS) directive lays down rules on the restriction of the use of hazardous substances in electrical and electronic equipment with the objective of reducing pollution, preventing environmental damage and reducing the health risks associated with these materials [14]. Any EEE sold on the EEA must comply with this regulation. Therefore, we must carefully select components that fit this directive, and comply with the normative during the fabrication process.

(a) *Example of logos showing that the product is lead-free and RoHS compliant [69].* **(b)** *The CE marking [70].*

Figure 4.2 – *Lead-free, RoHS and CE marking logos.*

4.2.2.2 CE (Conformité Européenne) marking

On a product such as electronic equipment, the CE marking (Figure 4.2b) indicates that the manufacturer affirms the good's conformity with European health, safety, and environmental regulations. The CE marking is required for a product in order to be sold in the EEA [71]. It is not a quality assurance nor a certification mark, it simply means that the product meets the requirements to be sold in the EU [72].

4.2.3 Electronic system block diagram

We are now ready to define a high-level block diagram of the system to outline the relations between subsystems and hierarchically organize the electronic design. In Figure 4.3 this chart is presented. Once again, the diagram is product of an iterative process in which requirements, design and implementation constraints have been part of. Nevertheless, this schema represents a conceptual approach at the project's current state, and should be taken as the initial planning and not the definitive block diagram of the electronics.

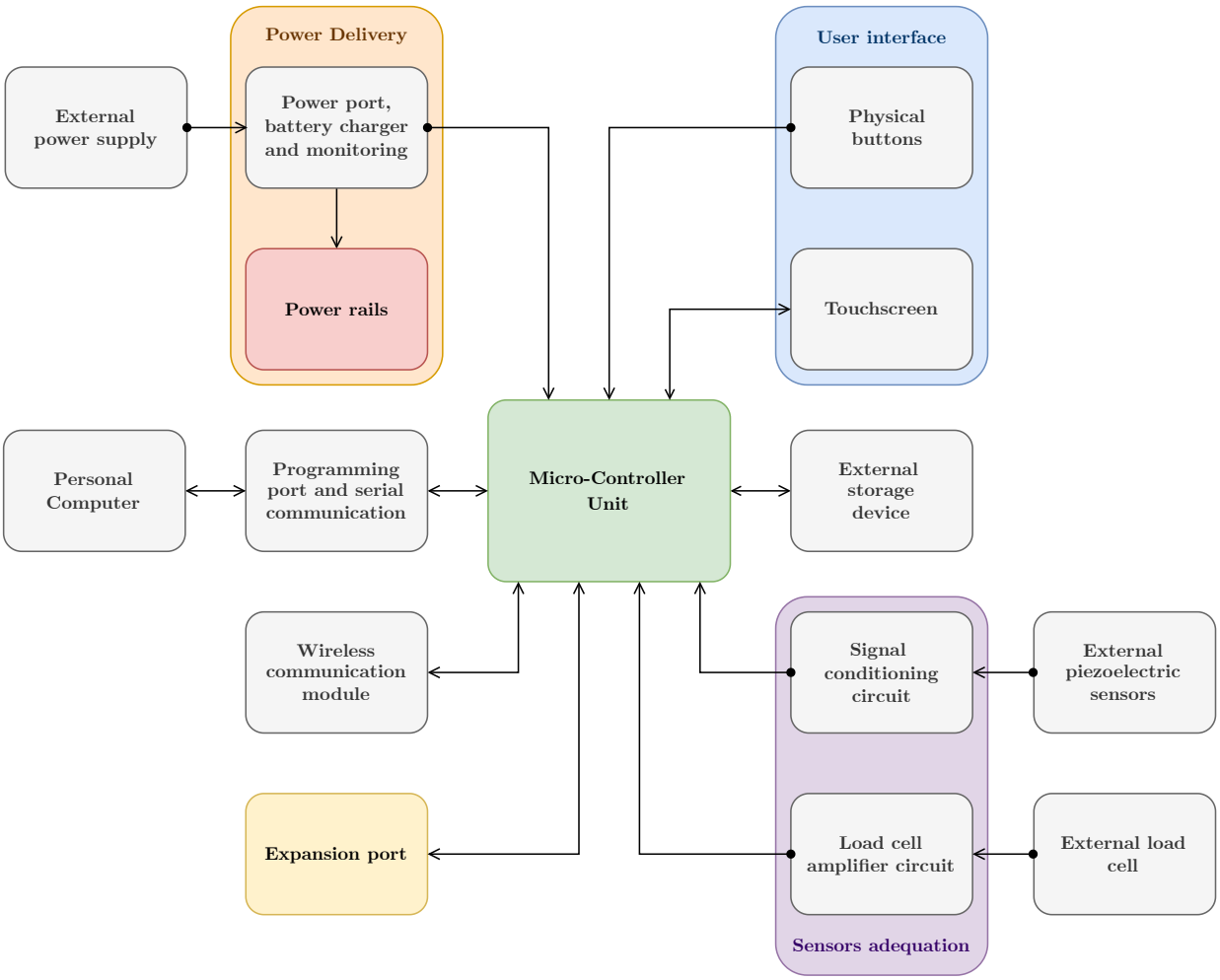

Figure 4.3 – *Initial, high-level block description of the necessary electronic subsystems.*

4.2.4 Component selection

Once defined the system blocks, we can proceed to choose the necessary components for the desired functions. In this section we will compare different component alternatives that are suited for our use case. These comparisons include the juxtaposition of specifications, price and analysis of the complexity of the needed circuit topologies.

On behalf of all the advantages enumerated before, SMD components are preferred over THD parts, these being relegated to components that need mechanical mounting firmness.

4.2.4.1 Passive components

It is easier to define what a passive component is through the description of what is an active component. Active components are those that have the ability to control the flow of current, requiring for this task a power source. They can be a source of power in the circuit like a battery, or provide an electrical switching or amplification, such as diodes, a transistor or a relay. Passive components are simply those which are not active. This category includes resistors, capacitors and inductors, transformers but also switches, thermistors and a good number of transducers such as speakers and microphones.

For simplicity, this section only addresses the passive components used in this project, which are:

- **Resistors:** SMD chip resistors come in a variety of rectangular, standard sizes.

  These are identified by a numeric code such as 0603 or 0805, whose units can be in the metric measurement system (in *tenths of a millimeter*) or in the imperial system (in *tens of mil*). Regarding the nomenclature, the first half of the code indicates the length, and the second the width. So, when we say that a resistance is 0603 in imperial units, it means that its measurements are 60 x 30 mil, or what is equivalent, 1.6 x 0.8 mm (and therefore the correspondent metric code is 1608). Figure 4.4 shows the relative size of these components and their respective codes in imperial and metric units.

  As a high precision of the resistance value will not be needed in our circuits, thick film resistors will be used.

- **Capacitors:** Non-polarized ceramic SMD chip capacitors such as MLCC follow with the same sizes and codes as SMD resistors. However, polarized, electrolytic capacitors such as aluminum-based and tantalum-based come in other formats (see Figure 4.4).

  As we will see, big capacitors will not be needed in our design and thus electrolytic capacitors. The intrinsic asymmetry and chemistry of an electrolytic capacitors make them more hazardous than ceramic if not used correctly. So, by not using it we avoided a potential (but not likely) risk.

  Also, we will avoid tantalum, a conflict resource which is extracted from coltan, a mineral infamous for being mined in conditions of armed conflict and human rights abuses [73].

- **Inductors:** These components can come in a variety of form factors, smaller ones in the same formats as SMD resistors, but as inductance and current rating grows they come in wire bound around a ferritic core, and usually in a square footprint. These inductors can be shielded using a metal covering for considerations.

- **Ferrite Bead:** Ferrite beads are a type of choke that suppresses high-frequency electronic noise in electronic circuits. Chip ferrite beads usually come in the same formats as SMD chip resistors and capacitors.

Active components come in a broader, more complex packaging variety. In the coming sections we will tackle Integrated Circuits and other active components and its form factors and footprints. For a list of common circuit symbols, see table 5.1 on section 5.1.2.1. For a reference on component packaging and sizes, see Figure 4.4.

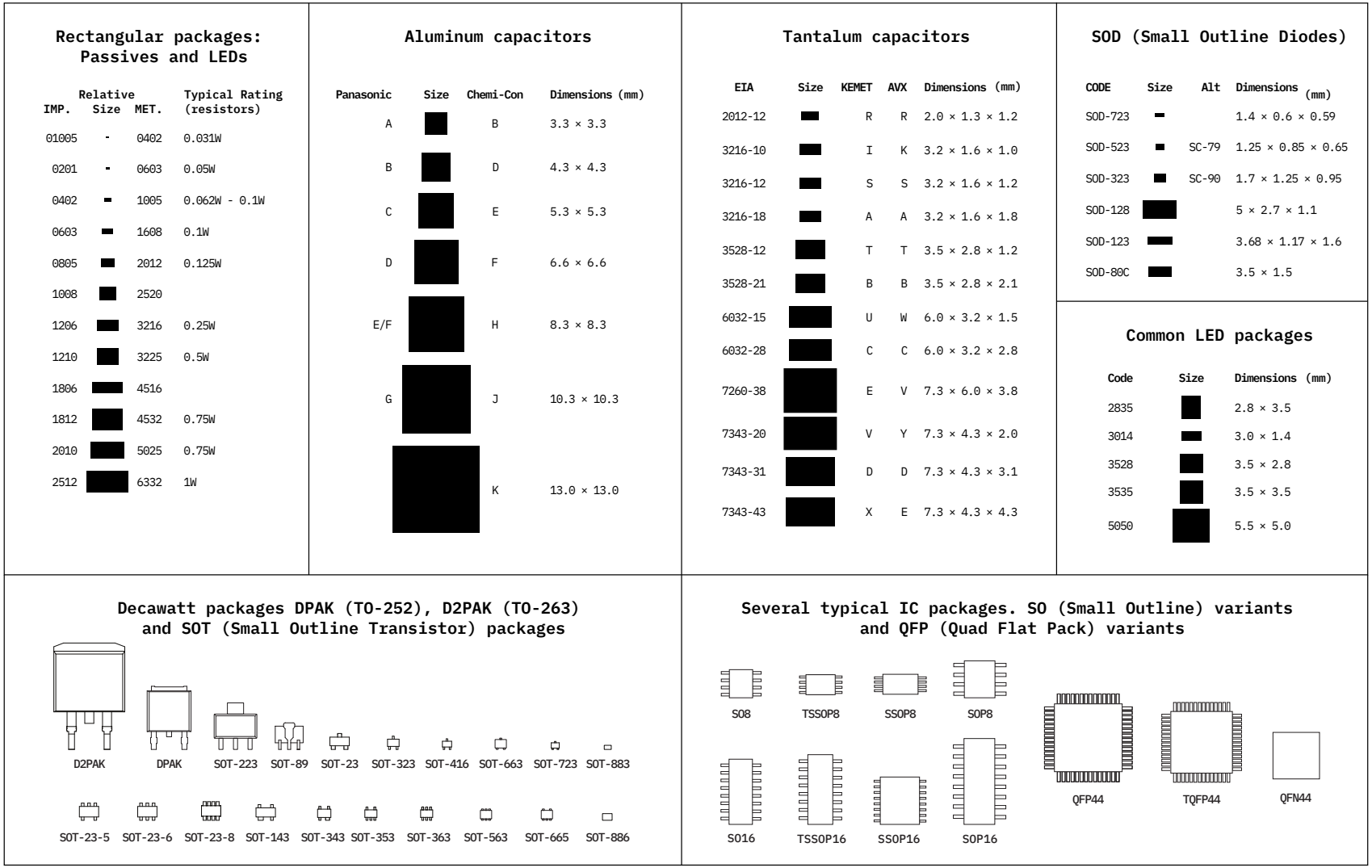

Figure 4.4 – *Common packaging sizes of different types of electronic components (extracted from [74]).*

4.2.4.2 Microprocessor

The microprocessor must have sufficient processing power to run the signal processing algorithms that will be used in a relatively short time, as well as simultaneously handling I/O ports and peripherals such as the touchscreen. For ease of implementation, we look for microcontroller modules or SoCs that include a complete system with one or various cores, decent amount of memory and a variety of convenient peripherals such as I2C, SPI, UART, ADC, PWM, etc.

Especially if built-in wireless connectivity is desired, Espressif System's ESP series are well suited, and currently hold a predominant position in both the professional IoT and hobby DIY worlds. In the Table 4.1 and Table 4.2 (cont.) the different specifications of these chip series are discussed, along with various SoC SKUs from other relevant manufacturers in the industry. Images of the different options are shown in Figure 4.5.

Mounting the chips directly on the PCB is ruled out. Instead, a standalone module is preferred for ease of implementation. This avoids dealing with unleaded QFN-type footprints, which are difficult to solder and debug with the means we have in the GranaSat laboratory. Besides, a module with a built-in antenna shortens development time by saving us from having to design, incorporate and verify a fairly complex microwave antenna into our PCB.

We must reach a compromise between power consumption, processing power and clock speed, available memories, number of GPIOs, the amount of area used by the module, wireless connectivity and peripheral availability. Nevertheless, we cannot forget the software support. Without resources and programming tools, a good SoC is useless.

With that said, we can begin to discuss the proposed options:

- STMicroelectronics' **STM32WB55** series is a ULP platform, which is good for our use case. However, because of this, it fails short on processing power and memory, since it is focused on low-power IoT applications such as sensor networks, as evidenced by the wireless protocols it supports.
- Even though the **CC3200** is the oldest series, it is still marked as active by Texas Instruments. However, it is also the most limited in functionality, and it is not particularly fast nor efficient.
- The **WFI32E01PC** standalone module is a modern and performing bet from MicroChip with moderate power consumption. Sadly, the device is still in its preliminary stage and in the time of writing not many resources are available to the public.

Given the above facts, only Espressif's options remain:

- Unlike its peers, the **ESP8266** does not support bluetooth. In addition, it is the one with the least power, memory and pins of the 3 options.
- The **ESP32-S3** is the most recent series from Espressif. It contains a good amount of peripherals, processing power, and connectivity as well as modern wireless security functionality. However, the modules are more expensive than the ESP32 series and since it has been released relatively recently, it is less documented and has fewer resources than it counterparts.
- The remaining option is the **ESP32 series**. This series and in special its modules offer a good compromise between hardware functionality, price and stock availability, while being very close, when not equal, in specifications with the already discussed ESP32-S3. The major downside of this series is that its maximum power consumption is high.

  Amidst the available modules, the ESP32-WROOM-32U is discarded as it does not have an integrated antenna. On another hand, the ESP32-WROVER-E is not very attractive as it takes up more area than the ESP32-WROOM-32D without offering any clear advantage.

Although it has recenty been marked as Not Recommended for New Designs (NRND), the ESP32-WROOM-32D module and its ESP32-D0WD chip have an extensive documentation by Espressif, including a technical reference manual [75], hardware information [1] and various programming guides [76, 77], not to mention Espressif's modified version of FreeRTOS to support SMP (this will be discussed in more detail in Section 4.3: Software architecture).

Furthermore, the ESP32-WROOM-32D module and its evaluation boards (ESP32-DEVKIT) have been available for a long time, during which time they have become well-known devices, with a large community of hobbyists and professionals. This community gives us access to many online resources, third-party libraries, and troubleshooting help.

Of all the exposed options, it is concluded that the ESP32-WROOM-32D module is the most appropriate and advantageous for this project.

4.2.4.3 Acquisition circuitry

The acquisition system, necessary to record the sensors' signals needs the following number of parts:

4.2.4.3.1 Analog-to-Digital Converter (ADC)

Its need is evident, since the signal processing is carried out in the digital domain and a posteriori (post-processing). The catalog of ADCs offered by renowned manufacturers such as Texas Instruments, Maxim Incorporated, Microchip and Analog Devices was consulted. Some promising SKUs were: AD7367, AD7386, LTC2306, ADS9226, ADS8355 and ADS7067.

However, due to the difficulty of finding a model in stock and at a reasonable price at the design stage that would satisfy all the requirements (high sampling rate ($\geq$ 0.5 kHz), 2 or more channels, single-ended (not differential), with an integrated voltage reference, which worked on 3.3 volts, single-supply, with an adequate footprint, and with supports for SPI or I2C for communication), the conclusion reached was that the most appropriate solution in terms of cost-effectiveness and implementation time was simply to use the ESP32's integrated ADC units. In our tests, the ESP32's ADCs reached 500 kSps by using DMA, an acceptable sampling frequency. The specifications of the ESP32's ADCs are [78, 79]

- Successive-Approximation ADC (SAR) with 12 bits of resolution, last 3 LSB can be discarded as noise.
- Theoretical maximum. sampling rate of 200 kSps with the RTC controller, 2 MSps with the DIG controller.
- Reference voltage is 1100 mV, however the true reference voltage can range from 1000 mV to 1200 mV amongst different ESP32s. Supposedly, on newer ESP32s this value is calibrated at the factory.
- Input range from 0 to supply. Maximum useful input range from 150 mV to 2450 mV due to non-linearity and noise at the extremes.
- ADC2 is unusable when using wifi due to pin conflicts. Additionally, some of the ADC2 pins are used as strapping pins (GPIO 0, 2 and 15) thus cannot be used freely.
- ADC1 supports DMA, but ADC2 does not.

As we can see, the characteristics are not the most appropriate for the acquisition of sensitive signals. However, since the non-linearity affects only the extremes of the input range and we only need the wave form that will be centered on a DC offset (see Section 4.2.4.3.2: Signal adequation circuit), it is likely that this ADC will suffice for these tasks.

Device series	ESP8266	ESP32	ESP32-S3	STM32WB55	CC3200	WFI32E01PC
Vendor	Espressif Systems	Espressif Systems	Espressif Systems	ST Microelectronics	Texas Instruments	Microchip
Release	2014	2016	2020	2019	2013	2020
CPU	Tensilica L106, 32 bit, up to 160MHz, single core	Tensilica Xtensa LX6, 32 bit, up to 240MHz, single/dual core	Tensilica Xtensa LX7, 32 bit, up to 240 MHz, dual core	ARM Cortex-M4, 32 bit, 64 MHz single core	ARM Cortex M4, 32 bit, 80 MHz, single core	MIPS32, 32 bit, 200 MHz, single core
SRAM	160 KiB	520 KiB	512 KiB	up to 256 KiB	up to 256 KiB	256 KiB
ROM	None, program on flash	448 KiB	384 KiB	None, program on flash	None, program on flash	None, program on flash
Flash	None, or 1 MiB (ESP8285)	None, 2 or 4 MiB	None, or 4 MiB	512 KiB or 1 MiB	None, or 1 MiB (CC3200SF)	1 MiB
Cache	32 KiB for instructions, 80 KiB data	64 KiB (32 KiB per core)	32 KiB for instructions, 64 KiB for data	?	?	16 KiB for instructions, 16 KiB for data
ULP co-processor	No	ULP FSM	PicoRV32, ULP FSM	No	No	No
Wireless capabilities	Wi-Fi 802.11 b/g/n	Wi-Fi 802.11 b/g/n, Bluetooth v4.2, BLE	Wi-Fi 802.11 b/g/n, Bluetooth v5.0, BLE	BLE v5.2, BT Mesh, Zigbee 3.0, OpenThread	Wi-Fi 802.11 b/g/n	Wi-Fi 802.11 b/g/n
Nº of SPI	2	4	4	2	1	2
Nº of I2C	1	2	2	2	1	2
Nº of I2S	1	2	2	No	No	No
Nº of UART	2	3	3	2	2	3
Nº of GPIO	17	34	45	Up to 47	Up to 27	62

Table 4.1 – *Comparative of some microcontrollers with wireless capabilities* ***(part 1 of 2)****. Sources: [78, 80, 81, 82, 83, 84, 85, 86, 87, 88, 89, 90, 91].*

Device series	ESP8266	ESP32	ESP32-S3	STM32WB55	CC3200	WFI32E01PC
Nº of PWM	5	16	8	?	4	?
USB OTG	No	No	Yes	Yes	No	Yes
SD/MMC controller	No	Yes	Yes	No	Yes	No
Nº of ADC	1, 10 bit SAR	2, 12 bit SAR, up to 18 channels	2, 12 bit SAR, up to 20 channels	1, 16 bit, up to 19 channels	1, 12 bit, 4 channels	2, 12 bit SAR, 20 channels
Nº of DAC	No	2, 8 bit	No	No	No	No
Timers	2, 23 bit	4, 64 bit	4, 54 bit	6, 5x 16 bit, 1x 32 bit	4	7x 16 bit or 3x 32 bit
Supply voltage	2.3 V min, 3.3 V typ, 3.6 V max	2.3 V min, 3.3 V typ, 3.6 V max	1.7 V min, 3.3 V typ, 3.6 V max	1.7 V min, 3.3 V typ, 3.6 V max	2.3 V min, 3.3 V typ, 3.6 V max	3.0 V min, 3.3 typ, 3.6 V max
Current consumption	up to 240 mA	up to 240 mA	up to 240 mA	up to 10 mA	up to 250 mA	up to 240 mA
Ambient temperature	-40 to +85 ºC	-40 to +85 ºC	-40 to +85 ºC	-40 to +105 ºC	-20 to +70 ºC	-40 to +85 ºC
Packaging	**- As chip:** QFN-32, 5x5 mm **- As module:** ESP-WROOM-02D 18 pin, 18x20 mm, with antenna ESP-WROOM-02U 18 pin, 18x14.3 mm, without antenna ESP-WROOM-S2 20 pin, 18x32 mm, with antenna	**- As chip:** QFN-48 (5x5 mm or 6x6 mm) **- As module:** ESP32-WROOM-32D (38 pin, 18x25.5 mm, with antenna) ESP32-WROOM-32U 38 pin, 18x19.2 mm, without antenna ESP32-WROVER-E 38 pin, 18x31.4 mm, with antenna	**- As chip:** QFN-56, 7x7mm **- As module:** S3-WROOM-1 38 pin, 18x25.5 mm, with antenna) S3-WROOM-1U 38 pin, 18x19.2 mm, without antenna	**- As chip:** UFQFPN-48, 7x7mm UFQFPN-68, 8x8mm **As module:** STM32WB5MMG SiP-LGA, 86 pins, 7.3 x 11mm, with antenna	**- As chip:** QFN-64 9x9-mm **- As module:** CC3200MOD 20.5x17.5mm, with/ without antenna	**- As module:** WFI32E01 54-pin, 20.5x24.5mm, with antenna

Table 4.2 – *Comparative of some microcontrollers with wireless capabilities* ***(part 2 of 2)****. Sources: [78, 80, 81, 82, 83, 84, 85, 86, 87, 88, 89, 90, 91].*

4.2.4.3.2 Signal adequation circuit

The literature [100] indicates that we must implement a charge-mode amplifier circuit: charge mode amplification is used when the amplifier is remote to the sensor as in our case, where there may be several meters of cable between the sensor and the amplifier circuit. A charge-mode amplifier circuit is very similar to an integrator (see Figure 4.6b). In the circuit, the piezoelectric *charge model* is being used to represent the piezoelectric transducer, however we will prefer the *voltage model* (Figure 4.6a) for the circuit's simulation.

In the charge-mode amplifier circuit of figure Figure 4.6b, we account for the parasitic capacitance of the cable, represented by Cc. Resistor Ri provide both an input impedance (given that Ri << Rf) and ESD protection. Cp is the piezoelectric sensor's capacitance. Cp and Cc combine and affect the upper cutoff frequency. Given that our system is single-supply, the $V_{CC}/2$ biasing shown in the figure is necessary to center the output voltage around this DC offset level.

However, we will not use the OpAmp model that appears in the Figure 4.6b, since we need one according to our needs. In particular: dual (in the same package have two symmetrical OpAmps), with a suitable frequency response for our signals, that works in single-supply mode and at low voltage (3.3 V) and, if possible, that is rail -to-rail to take full advantage of the ADC input range. The Texas Instruments LMV358 dual OpAmp in a MSOP-8 package perfectly meets the requirements and even it features its own ESD protection. As we can see in Figure 4.7, it assures a maximum gain of 20 dB to just under 300 kHz.

On the other hand, it is also necessary to introduce protection circuits that limit the input voltage in the adjustment circuit, given that, as has been seen previously, the sensors can generate maximum peaks of tens of volts. Looking at the Fakopp microsecond timer, we could use the same method: two diodes in antiparallel over the DC offset voltage (V_{bias}) that clip the signal to their respective forward voltages (V_f). A suitable option is to use 1N41418W diodes, which are general purpose, well known and with a large repetitive peak reverse voltage (V_{rrm}) of 100 V.

4.2.4.4 Load cell amplifier

One of the best known load cell amplifiers in the community is the HX711 IC from Avia Semiconductor [102]. This device has gained recognition due for its 24-bit ADC precision, very low price, reliability, and easy operation, with the communication bus being similar to I2C. It has gained recognition and third party support since Sparkfun's released its load cell amplifier open hardware module [103], based on the HX711. Alternatives to this device are precision ADCs, such as the Analog Devices AD7794 or AD7124, which are considerably more expensive.

4.2.4.5 User interface

We define User Interface (UI) as any form of interaction and display of information that is offered to the user: screens, buttons, switches, lights, sounds, vibration, joysticks, etc. In our device, it is proposed to use a touch screen, push-buttons, and a dial-type button as an alternative way to easily navigate the Graphical User Interface (GUI) without needing to press the touch screen.

4.2.4.5.1 Touchscreen

We are looking for a touch screen, of a medium size so that it is comfortable but does not greatly extend the dimensions of the device. The LCD screen must also be suitable for the capabilities of the chosen microcontroller: it cannot be high resolution nor can it have great color depth due to memory and processing power restrictions. Additionally, the display should not not make use of too many microcontroller pins, which is the same as saying that serial and not parallel communication, must be used.

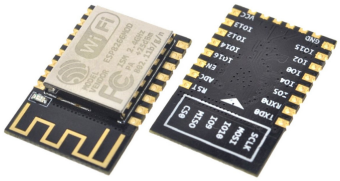

(a) *Espressif ESP8266MOD package. Extracted from: [92].*

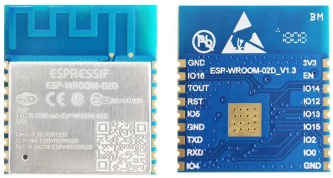

(b) *Espressif ESP-WROOM-02D. Extracted from: [93].*

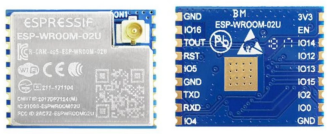

(c) *Espressif ESP-WROOM-02U. Extracted from: [93].*

(d) *Espressif ESP32-WROOM-32D. Extracted from: [94].*

(e) *Espressif ESP32-WROOM-32U. Extracted from: [95].*

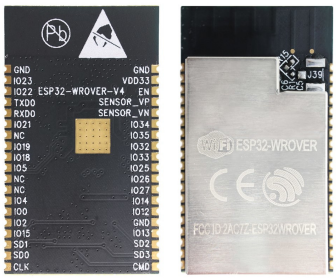

(f) *Espressif ESP32-WROVER-x series package. Extracted from: [96].*

(g) *Microchip WFI32E01PE-I. Extracted from: [97].*

(h) *STMicrocontrollers STM32WB5-MMG. Extracted from: [98].*

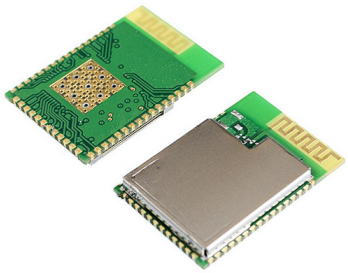

(i) *Texas Instruments CC3200MOD. Extracted from: [99].*

Figure 4.5 – *Images of some of the micro-controller with wireless communication modules selected for comparison.*

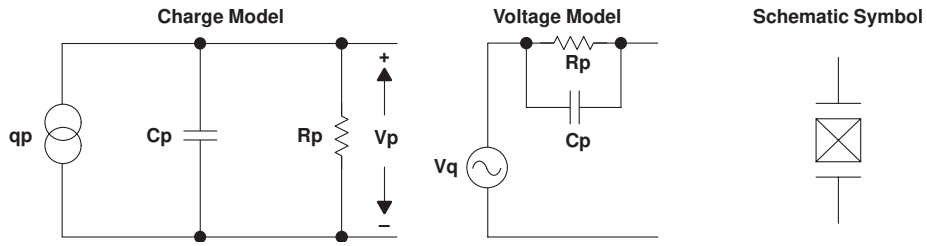

(a) *Sensor circuit models.*

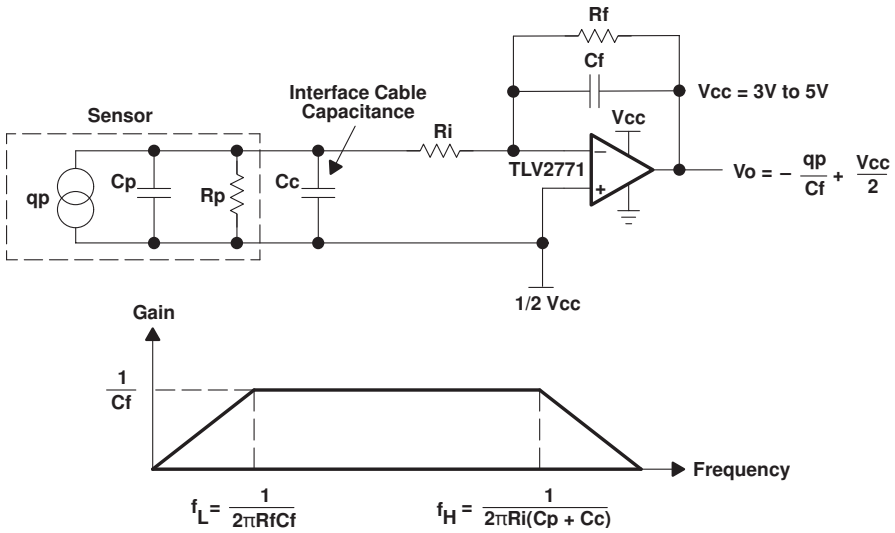

(b) *Charge mode amplifier circuit and approximated frequency response.*

Figure 4.6 – *Signal conditioning of piezoelectric sensors: Sensor models and charge mode amplifier circuit [100].*

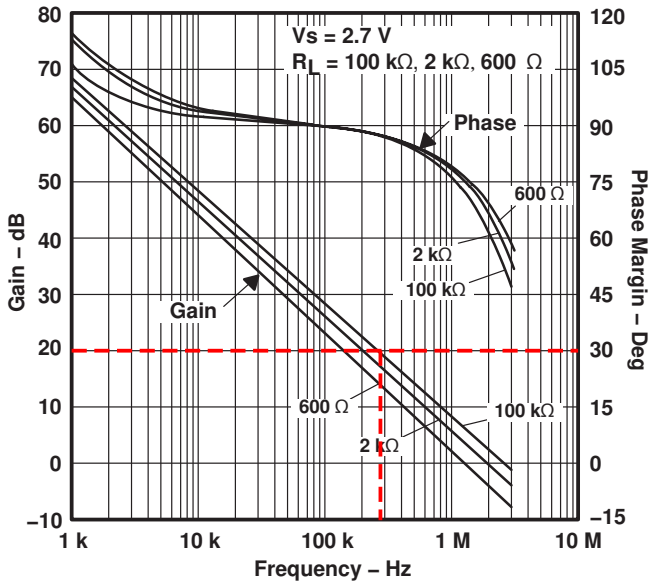

Figure 4.7 – *Frequency gain of the LMV358 OpAmp depending of the output load. Extracted from: [101].*

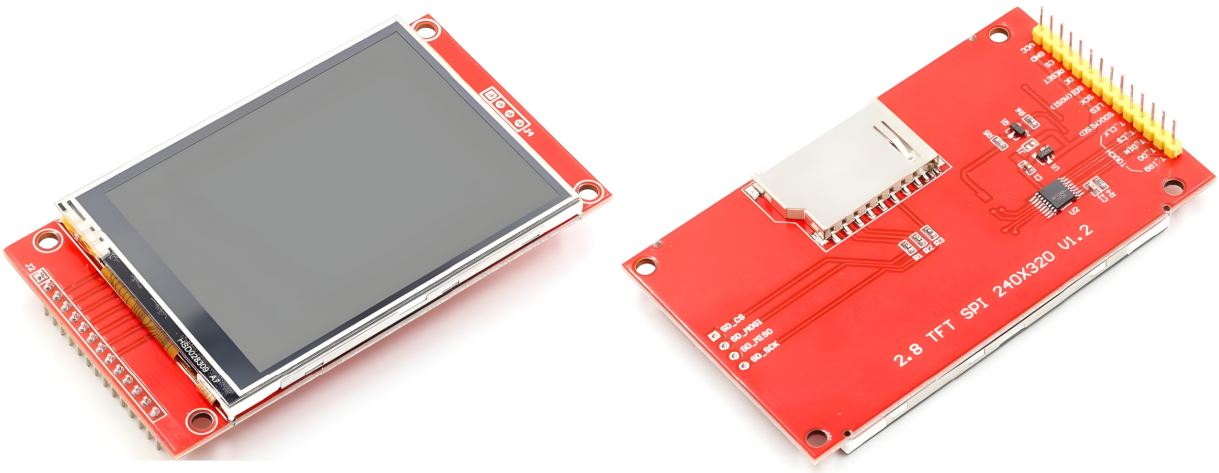

Figure 4.8 – *The chosen variant of the ILI9341 2.8" TFT LCD module.*

Certain modules that meet these qualities have become popular on the Internet: TFT LCD modules based on the ILI9341 display driver and XPT2046 touchscreen controller (they are similar to the one pictured in Figure 4.8). These touchscreens are perfect for our use: they have resolutions from 240x320 pixels to 360x480 pixels (aspect ratio of 3:4), in sizes from 2.4" to 4" (from 6 cm to 10 cm, in diagonal), can be used in vertical and horizontal, are RGB, they can produce up to 65 k different colors, are white-backlighted, and do support 3.3 V for both supply and logic. These modules also usually include a convenient SD card slot that we could use as external storage. Touch detection is very basic: it is based on a resistive mesh (not capacitive), requires calibration and only detects one touch at a time, making it difficult to implement gestures. Therefore, although it detects fingers without any problem, it is much more accurate to use a stylus. We will take this into account in the mechanical considerations in Section 4.4: Mechanical architecture. In addition, the boards of these modules have four M3 mounting holes.

A great advantage of the integrated driver ICs and the SD card is that they all support SPI (serial), only taking 3 shared pins for the bus (`MISO`, `MOSI` and `CLK`), and one more pin for chip select (`CS`) for every corresponding slave device in the bus. This is, 6 pins in total for the display, touchscreen and SD card. Therefore, we will avoid models that are configured to use parallel communication (usually 8 or 16 wires plus signaling).

Given the above, it has been decided to opt for a model with a 2.8" screen, 240x320 pixels, a compromise between screen size, resolution, pixel density and power consumption (said module is shown in Figure 4.8).

4.2.4.5.2 Buttons

4.2.4.5.2.1 Power-up button

Nowadays, many electronic devices include a push-button for the power-up instead of a on/off switch. Its operation is natural by the user. A button can be managed via software, so we can request a confirmation to avoid accidental shutdowns and the loss of information. The button also has the mechanical advantage of being lower in profile than a switch, making it easier to integrate it into a case, and to be potentially more attractive. For more details about the circuit implementation, see Section 5.1.1.8: Power-up button.

4.2.4.5.3 UI navigation dial

As discussed above, we want to include a dial as an alternative way of navigating the user interface. Some options are discussed next:

- **Rotary encoder.** This device converts angular position or circular motion to an electrical signals. There are two variants: absolute (indicates the axle position or angle) and incremental (detects the motion of the shaft and its turn direction). Normally there are two possible mounts: vertical (Figure 4.9a) and at an 90-degree angle (Figure 4.9b). For our use case the appropriate one is a digital, incremental rotary encoder. These components are widely used in multiple electronic devices such as dials, they are robust and durable and many incorporate a button on the axis, which makes navigation through a user interface natural.

  However, they have the disadvantage of being large devices, so they do not fit well in a low-profile device, and they can also be a significant expense.

- **Multi-direction "thumb" button.** A lesser-known type of component, but widely used in products such as reflex cameras (see Figure 4.9c). The angular movement is somewhat similar to that of a joystick, but limited: they can be rotated through a restricted angle, clockwise and counterclockwise; and once released they return to the center position. In addition, they have a push button actionable from the center position. It allows you to navigate through the user interface in an intuitive way. They are normally horizontally-mounted, are lighter, cheaper and take up considerably less space than a rotary encoder. In addition, they do not require the decoding of digital signal: the inclination is detected as it was the press of a push button.

For the reasons stated, it is decided to include a button in the product. In particular, we selected a low-profile device with a simple footprint: the HRO Electronics K1-1502SA-01 [104] (Figure 4.9c).

4.2.4.6 Ports

This section is dedicated to the discussion of which ports are most appropriate for each function specified in the requirements and in the block diagram of the device structure (Figure 4.3).

4.2.4.6.1 Charging and programming

In today's devices, ports often take on multiple functions. The most obvious example of this kind of versatility is the USB due to its omnipresence. USB cables and connectors were conceived for data transfer, but they have become the most universal connector for power delivery as well, being able to supply several amps under adequate conditions. This makes it suitable for charging batteries, which is our use case. The choice of connector type is important, and is discussed below.

USB connectors types can be divided into two classes: downstream and upstream. The downstream is the one that connects to the master device, such as a PC. This is the case of USB Type-A (Figure 4.10a). Other variants are connected to peripheral devices, such as the case of USB Type-B (Figure 4.10b), Mini-B (Figure 4.10d) and Micro-B (Figure 4.10c). We will discard the Micro and Mini *superspeed* variants, as the extra bandwidth is not needed for our use case. USB Type-C (Figure 4.10e) is a change in USB idiosyncrasy, as it is used for both upstream and downstream. With that said, we focus on the options detailed in Table 4.3. The USB Type B is automatically ruled out because of its large size. The most suitable for a handheld device are the following 3 options:

- **Mini-B.** A somewhat outdated connector meant for small, portable devices. but which has the advantage of having a relatively simple footprint and its construction is very robust.

(a) *Vertical rotary encoder (CUI Devices ACZ11BR1E-15FD1-12C).*

(b) *Horizontal rotary encoder (CUI Devices ACZ11BR1E-20FA1-20C).*

(c) *Multi-functional switch (HRO Electronics K1-1502SA-01)*

Figure 4.9 – *Various options contemplated for the dial.*

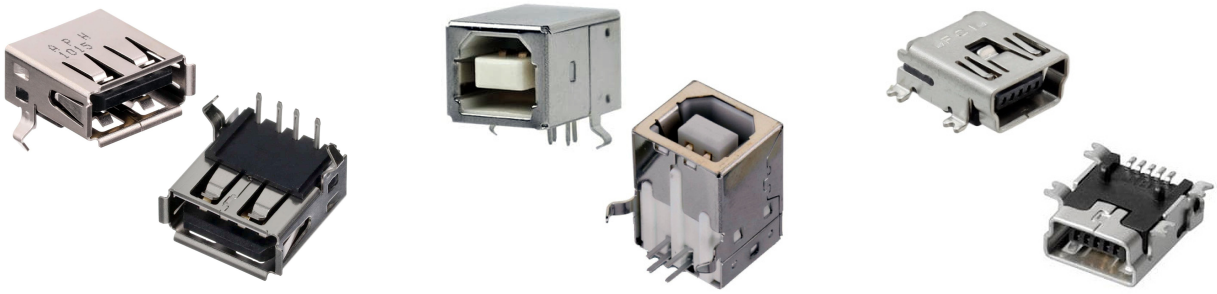

(a) *Type-A (GCT USB1135).*

(b) *Type-B (CUI Devices UJ2-BH-TH).*

(c) *Mini-B (GCT USB2066).*

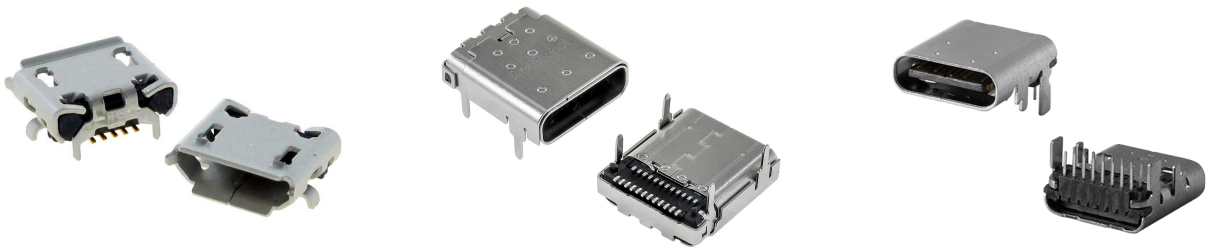

(d) *Micro-B (HRS ZX62D-B-5PA8-30).*

(e) *Type-C USB > 3.0 (Amphenol C-12401598).*

(f) *Type-C USB 2.0 (CUI Devices UJ20-C-H-G-SMT-TR).*

Figure 4.10 – *Some female, right angle, USB connectors for PCB mount.*

- **Micro-B.** Former universally-used connector, similar to Mini-B, but approximately half the thickness, enabling their integration into thinner devices. It is generally more fragile than the Mini-B.
- **Type-C.** A reversible, modern connector that is currently replacing the rest. However, it has many pins (from 16 to 24) in contrast to the previous ones (4 or 5). This makes its footprint complex: more pads, less clearance between them; and more difficult design and soldering than previous alternatives. This option is discarded for now.

Due to its mechanical robustness, low price, availability and ease of implementation, it was decided to opt for the USB Mini-B connector.

Since we have added an USB port, we must respect its communication protocol. However, the differential pair USB data lines cannot be connected directly to the ESP32, since it does not have the necessary hardware to decode it. Therefore, an intermediate Integrated Circuit for translating the USB to UART protocol is necessary. For that matter, the CH340C chip is selected, since it is available on Granasat's laboratory; and we have designs, implementation details and proof of its capabilities in other students' work [105, 106] and Sparkfun's open hardware resources of its CH340C serial basic breakout board [107].

Spec	Type-B	Mini-B	Micro-B	Type-C
Supported standards	USB 1.1/2.0	USB 1.1/2.0	USB 1.1/2.0	USB 2.0/3.0/3.1/3.2/4.0
Maximum standard data transfer speed	12/480 Mbps	12/480 Mbps	12/480 Mbps	480 Mbps 5/10/20/40 Gbps
Receptacle dimensions (LxWxH)	16.2x12.1x11 mm	7.5x5x2.5 mm	9.2x7.7x4 mm	10.5x9x3.3 mm
Type	THT pads, THT mounting	SMT pads, THT mounting	SMT pads, THT mounting	SMT pads, THT mounting
Number of pins	4 pins	5 pins	5 pins	USB 2.0: 16 pins. USB > 3.0: 24 pins
Pin-to-pin pitch	2.5 mm, 2 rows Row sep.: 2 mm	0.8 mm	0.65 mm	USB 2.0: 0.5 mm, 2 rows Row sep.: 1.7 mm USB > 3.0: 0.85 mm, 2 rows Row sep.: 1.35 mm
Pin width	0.65 mm	0.4 mm	0.25 mm	USB 2.0: 0.25 mm USB > 3.0: 0.2 mm

Table 4.3 – *USB connectors comparison. Sources: [108, 109, 110, 111, 112].*

4.2.4.6.2 Piezoelectric sensors connectors

This choice is straightforward: since we are going to adopt Fakopp's SD-02 piezoelectric sensors, we need female BNC connectors. In opposition to the Fakopp Microsecond Timer connectors, we will use metal, shielded, right-angle, PCB-mount BNCs, as seen in Figure 4.11a.

4.2.4.6.3 Load cell connector

Load cells typically have four wires, connected to each vertex of a Wheatstone bridge, and sometimes they include a fifth lead connected to both the metal structure of the load cell and the cable shield. However, there is no standardized connector for load cells. Some manufacturers use 6-pin RJ-11 connectors, and so a female socket was first integrated into our PCB (Figure 4.11b). Unfortunately, it turned out to be too big for the space available on the board, so it was necessary to change it for a smaller one.

The alternative that was evaluated as suitable is a 3.5 mm jack socket, since there are variants with four contacts. In particular, the SJ-43516-SMT from CUI Devices (Figure 4.11c) is suitable due to its robustness; and it also includes two switches which allow to detect when a cable has been plugged in.

4.2.4.6.4 Expansion port

The expansion port is intended to be a way to expand the capabilities of the TIK module 1. In her Master's Thesis [58], Irene Gil has worked in parallel on the development of the TIK module 2, which analyzes wood using the resonance method (see Section 1.2.2.2: Measurement procedures). Instead of developing another device from scratch, she uses the TIK module 1 as a base. For this to be possible, some functionality needs to be exposed via said expansion port. In this case, two power pins and two signal pins.

A very interesting option is to use magnetic connectors with *pogo pins* (spring-loaded pins), in the style of the ones in Figure 4.11d. These connectors are low profile, waterproof and are held by magnets. The disadvantage of these components is the inclusion of rare earth materials, their high price and low stock. For these reasons, they are ruled out for the time being. Instead, we can use the same 3.5 mm jack connector as for the load cell (Figure 4.11c), since it has the necessary number of pins, it is robust and we do not increase the number of different parts.

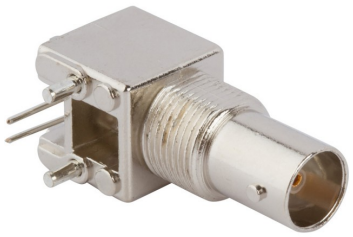

(a) *Right-angle, female BNC connector (Amphenol 31-71043).*

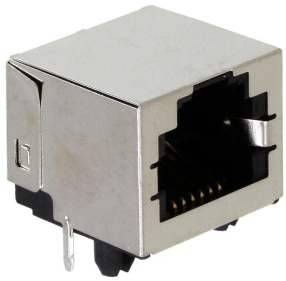

(b) *Right-angle, female RJ-11 connector (Molex 0438600026).*

(c) *3.5 mm female jack connector (CUI Devices SJ-43516-SMT).*

(d) *Example of 4-pin, magnetic pogo-pin male and female connectors (HytePro M417P).*

4.2.4.6.5 External storage

Since the selected TFT LCD screen module already has a built-in SD card reader (see Figure 4.8), we have chosen to use this reader for space savings and less complexity.

4.2.4.7 Power Delivery System

This section explains the Power Delivery System specification process. This system is critical in any electronic product. The PDS is in charge of the correct provisioning, conversion and distribution of the energy that feeds the rest of the subsystems. In this case, as it is a battery-powered handheld device, there are certain challenges and design peculiarities.

4.2.4.7.1 Early power budget estimation to dimension the Power Delivery System

To correctly size the power supply system of the device, it is necessary to balance the typical and maximum expected consumption. As we still do not have the circuits defined, we will only take into account the given consumption of the main Integrated Circuit; who will be the largest power consumers. This way we get an estimate of the magnitude of consumption to expect. We will use the figures offered by the manufacturers in their respective datasheets.

Figure 4.11 details the consumption of the main ICs chosen in previous sections. There will be only a single 3.3 V rail. This voltage is standard in electronic design, and our ICs are rated for that voltage.

The TFT LCD module is not documented so we had to measure its power consumption. The ESP32 consumption can vary greatly with the tasks the CPU is executing so it was also measured. To benchmark these components, we used a demo program designed to stress both the screen and the CPU. The program was running in a ESP32-DevKit board connected to a LCD module. For more information about the testing method, see Section 5.1.1.3.5: Detailed typical and maximum power budget.

The expected typical consumption is around 130 mA, and the maximum is close to 400 mA. As will be seen in the aforementioned section, this estimate is close to reality. Therefore, in Figure 4.11 it has been indicated that the 3.3 V rail must be able to supply at least 500 mA. This is a safety margin, so that the power supply is capable of responding to consumption peaks.

4.2.4.7.2 Battery chemistry and capacity

In this section we discuss the different battery technologies that may be appropriate for portable devices, and later we will discuss which is the most adequate for our product.

- **Nickel-Metal Hydride (Ni-MH).** Ni-MH batteries replaced the Ni-Cd batteries a few decades ago, since they are less expensive and eco-friendlier (cadmium is banned by the RoHS directive). Ni-MH batteries have low memory effect, excellent cycle life (500 to 3000 cycles), are very safe, have high charge rates and its energy density approaches that of the Lithium-based batteries [116].

  The drawbacks of Ni-MH batteries is their high self-discharge rate (which pose a severe limitation for occasionally-used devices), low nominal voltage of only 1.2 V per cell, and its form factor, which is usually cylindrical. The last two reasons force us to use at least a 3-cell battery pack to reach over 3.3 V. A battery pack can be bulky and therefore make the developed device thicker and less attractive to the end user.

- **Lithium-ion (Li-Ion).** One of the most commonly used rechargeable batteries nowadays. Li-Ion batteries have high energy density, low self-discharge rates, a high nominal voltage (3.7 V) and good

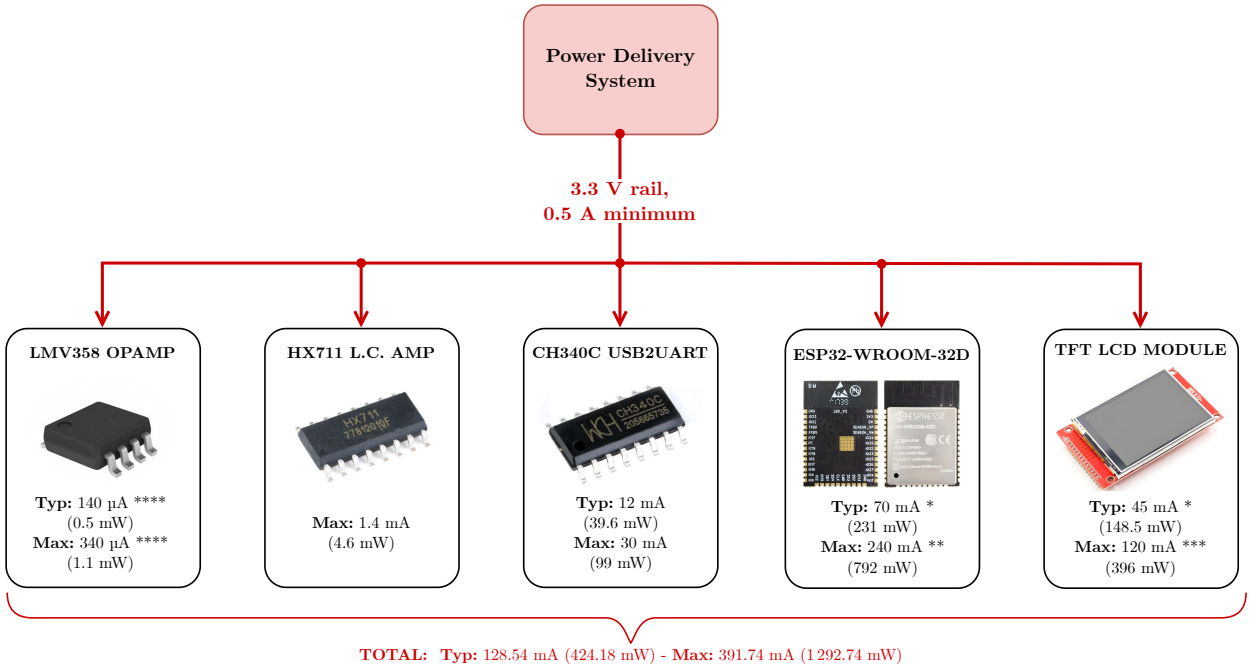

Figure 4.11 – *Early power budget estimation, in order to correctly dimension the Power Delivery System. Sources: [101, 102, 113, 78]. *Average, ***maximum power consumption measured, running demo program. **Manufacturer-provided figure, spikes during wireless TX [78] (table 15). ****With no load/High Z load. A more detailed itemization of the power consumption will be shown in later sections (see Table 5.5).*

(a) *Common standard cylindrical battery sizes. Used for Li-Ion, Ni-MH, LiFePo4, etc. Credits: [114]*

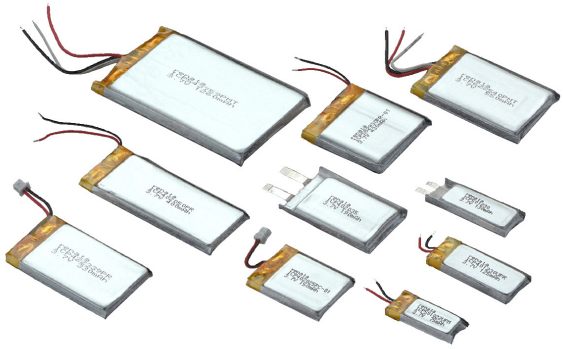

(b) *Common flat-type Li-Po sizes. Credits: [115]*

Figure 4.12 – *Common battery sizes for portable devices.*

cycling performance (300 to 500 cycles) [116]. The downside of these batteries are safety concerns, as they have poor thermal stability and can begin thermal runaway if damaged [117]. Besides, due to its internal chemistry and manufacturing, the shape of these batteries is mostly cylindrical or rectangular which is undesirable in our use case as mentioned above.

- **Lithium-polymer (Li-Po).** This technology is very similar to the former, but its fabrication process and chemistry make them safer, thinner and more flexible. The nominal voltage is still 3.7 volts per cell with slightly less energy density and shorter lifespan than Li-Ion [117]. Li-Po batteries are by far the most widely used technology in portable devices today [116].
- **Lithium iron phosphate (LiFePO4)** Another type of Li-Ion technology, which has received attention lately. They have good energy capacity and solve the traditional Li-Ion safety issues by being less affected by overheating (the phosphate is not flammable), while also providing a longer lifespan and cycle life. However, they have a lower nominal voltage of 3.2 V, greater self-discharge and reduced capacity in comparison to Li-ion and LiPo [117]; and they are not suitable for portable devices like ours because of their cylindrical form factor.

As we are developing an electronic tool that is going to be used in the outdoor fields, an important requirement of the battery is that it be safe, withstand a wide temperature range (in case the device is exposed to direct sunlight), and must provide many hours of continuous operation to our device, given that there is no electrical infrastructure at the measurement sites. In addition, we value and that the battery has a long period of life.

That said, project meetings failed to come up with a clear choice, leaving a technical tie between Ni-MH batteries for their long cycle life and reliability; and Li-Po, due to its high energy density, low profile and improved safety compared to other lithium batteries. Due to this situation, it was decided to integrate two chargers in the same prototype. That is, the two chargers are designed, but only the components of one of them are populated at a time. In this way, on the same PCB we can evaluate two types of battery technology and decide on the most advantageous option once tested.

4.2.4.7.3 Battery chargers

4.2.4.7.3.1 Lithium-Ion and Lithium-Polymer battery charger

We are going to implement a loader based on the NanJing Top Power TP4056. The TP4056 is a SOP-8 charger for both single-cell Li-Ion and Li-Po batteries which can *fast-charge* up to 1 amp to the battery. This ASIC is present in many charger modules that can be found on the Internet, due to its ease of use and implementation, and because it is convenient since it is designed to charge from the voltage offered by a USB. Many modules based on this ASIC implement the datasheet reference design [118] almost verbatim. This IC regulates its output to 4.2 V while charging, and detects that the battery is full based on the current it draws. However, it lacks any type of control other than the maximum charge current, and also it does not have any type of battery protection circuitry. So, as an additional protection measure, an over-discharge and over-charge protection IC is added, the DW01A. According to its reference design [119], this IC requires two MOSFETs to disconnect the low side of the battery. For this we chose the FS8205A, which includes two power NMOS in a single package [120].

4.2.4.7.3.2 Nickel-Metal Hydride battery charger

The Linear Technologies LTC4060 from is a well-known charger IC for both Ni-Cd and Ni-MH in a TSSOP-16 package. We can control the chemistry, number of cells and charging current up to 2 A. For charging termination, it can use any of the ΔV (voltage), Δt (time) and ΔT (temperature) methods, or a combination of them. This IC also requires some complementary parts, most notably a power PNP pass

transistor for voltage regulation and current supply. In the typical applications [121], the MJD210 or the FZT948 power BJTs are recommended.

This IC was selected over other options such as the MCP1630, BQ24401, CJC5288 and MAX712 because they require significantly more complex circuits to operate.

4.2.4.7.4 Current consumption monitor

Both of the above chargers give very limited battery status information: they simply indicate when they are charging and when the charge is 100% complete. We want to offer in the GUI the State of Charge (SoC) of the battery. To do this, there are various alternatives:

- **Voltage translation.** This method consists on measuring the battery voltage and estimating the SoC from a pre-established curve that relates the voltage and the charge level. The voltage could be read by ESP32 itself using a resistive divider on one of the ADC pins.

  However, for this it would be necessary to characterize the discharge curve of the specific battery model. And even so, although it can give a rough estimate, if we want to be accurate it would not be valid, since this curve can vary with both the discharge current and operating temperature especially in lithium batteries [122]. Besides, the discharge curve of lithium batteries is also very flat and hold an operating voltage very close to the exhaustion voltage, which makes this method very inconvenient and unsafe.

- **Coulomb counting (current integration).** This method consist of constantly monitoring the current in and out of the battery. This gives us the relative value of its charge. If the total capacity and initial charge in the battery is known, from then on *Coulomb Counting* can be used to calculate its SoC [122].

  For example, if a battery is discharging at 500 mA for 2 hours, we would have counted $-500\,\text{mA} \cdot 2\,\text{hours} = -1000\,\text{mAh}$ out of the battery charge. If the total battery capacity is 1500 mAh, that would have decreased its SoC by $1000\,\text{mAh}/1500\,\text{mAh} \cdot 100\,\% = 66.67\,\%$. But without knowing what the original SoC was, we do not know the actual SoC. However, since chargers do report end of charge, we can assume that is a 100% point, and count down from there.

This justifies the inclusion of an current sense IC. The alternatives will be discussed next. We proceed to choose by discarding the options contemplated in Table 4.4. The INA231 has a BGA-type package, which is not very convenient. And together with the LTC4151, they have a limited shunt measurement range compared to the rest. Besides, the latter cannot even be powered at 3.3 V. On the other hand, although it has more precision, the LTC2990 is ruled out by its package, which occupies more area than necessary, and has a slightly higher consumption. The remaining options are very similar and practically equivalent. Although in other conditions the INA226 would be chosen because it is slightly better, the INA219 is ultimately chosen for its availability in the GranaSat laboratory.

4.2.4.7.5 Main 3.3 V power rail

As said before, the main power rail will be 3.3 V, since all other subsystems' ICs have been selected to work at that voltage. Since the system is portable and battery powered, the efficiency of the supply is a key design element. In this regard, nothing is more suitable than a DC/DC step-down converter. Linear regulators are ruled out due to their low efficiency. The disadvantage of DC/DC converters is that they are switching regulators, so they will inevitably introduce noise in its output voltage. To reduce its effects we must be careful in the design stage, including decoupling capacitor and with an adequate component layout on the PCB.

Spec	LTC2990	LTC4151	INA219	INA226	INA231
Supply voltage range	2.9 V to 5.5 V	7 V to 80 V	3 V to 5.5 V	3 V to 5.5 V	2.7 V to 5.5 V
Sense pins voltage range	-0.3 V to supply + 0.3 V	-0.3 V to supply + 0.3 V	-0.3 V to 26 V	-0.3 V to 26 V	0 V to 28 V
Measurement channels	2	1	1	1	1
Bidirectional current sensing	Yes	Yes	Yes	Yes	Yes
Maximum shunt voltage	300 mV	81.92 mV	320 mV	320 mV	81.92 mV
Selected package	MSOP-10 (4.9x3 mm)	MSOP-10	SOIC-8 (4.9x3.9 mm)	VSSOP-10 (3x3 mm)	DS-BGA-12 (1.65x1.39 mm)
ADC resolution	14 bits	12 bits	12 bits	12 bits	16 bits
Communication protocol	I2C	I2C	I2C	I2C	I2C
Current sense side	High side	High side	High side	High/low side	High/low side
Power consumption (typ/max)	1.1 / 1.8 mA	1.2 / 1.7 mA	0.7 / 1 mA	0.33 / 0.42 mA	0.33 / 0.42 mA

Table 4.4 – *Comparison of some digital current monitor alternatives. Sources: [123, 124, 125, 126, 127].*

Spec	MIC22205	LM3671	TLV62569	AP3429K
Input voltage range	2.9 V to 5.5 V	2.7 V to 5.5 V	2.5 V to 5.5 V	2.7 V to 5.5 V
Output voltage range	0.7 V to supply	1.1 V to 3.3 V	0.6 V to supply	0.6 V to supply
Max. Outpu current	2 A	600 mA	2 A	2 A
Switching frequency	0.8 to 1.2 MHz	2 MHz fixed	2.5 MHz fixed	1 MHz fixed
Selected package	MLF (3x3 mm, no leads)	SOT-23-5 (2.9x1.6 mm)	SOT-23-5	SOT-23-5
Expected efficiency at 3.3 V, 100 mA	$\sim$ 90 %	$\sim$ 96 %	$\sim$ 95 %	$\sim$ 95 %
Expected efficiency at 3.3 V, 500 mA	$\sim$ 95 %	$\sim$ 92 %	$\sim$ 95 %	$\sim$ 96 %

Table 4.5 – *Comparison of some DC/DC step-down alternatives. Sources: [128, 129, 130, 131].*

At this stage of development, we still do not have a clear figure of the extra consumption magnitude of the rest of the components (the ones not contemplated on Figure 4.11), it is decided to over-dimension the PDS. Therefore, the selected devices that appear in Table 4.5 can withstand higher current draws than the maximum expected consumption. This extra current can also help to charge the capacitors quickly during system power-up without dropping the supply voltage (a phenomenon known as *inrush current* or *switch-on surge*); and supply the ESP32 without problems if its consumption characteristic presents large current peaks during transmission or reception.

The two most suitable components due to the simplicity of their recommended circuits and their convenient SOT-23-5 footprints were the Diodes Incorporated AP3429K and the Texas Instruments TLV62569. Both are very advantageous because of their pin-to-pin compatibility, and even their typical applications are the same. In the assembled PCBs, we used AP3429K converters already available on the GranaSat laboratory. However, since at the moment of writing there is no stock of this SKU in any online store, for production we will have to resort to the Texas Instruments alternative.

4.2.4.7.6 Bias voltage for the acquisition circuit

As Figure 4.6b, a voltage is necessary to offset the signals coming from the piezoelectric sensors, which are centered at zero. This avoids the signal to be clipped by the extremes of the supply voltage. This offset, called *bias* voltage, should be $V_{CC}/2$ or close to it. We have several options to consider:

- **Implement another DC/DC converter.** An efficient option, but considering that this voltage is not going to power any component but simply establishes an offset voltage, it is simply overkill. Furthermore, it adds unnecessary complexity, and the output will have switching noise, which will negatively affect the acquisition system.
- **Use a Low-DropOut Regulator (LDO).** A simple and direct way to create a voltage with only one IC through linear regulation. It is not as efficient as a DC/DC converter, since this voltage is not going to have a load (the current consumption is minimal), the linear regulation is going to dissipate hardly any power.
- **Use a voltage divider.** This is the solution used by Fakopp, as we have already seen in his circuit. It is undoubtedly the cheapest, simplest and most flexible alternative. We must bear in mind that in order for the analog signal to be a voltage from a source, it must be filtered through multiple bypass capacitors. Also, we must be careful not to add a load to this voltage. If so, it will decline.

Once the alternatives have been explained, we only have to decide which one to incorporate into the design. The voltage source feature that the LDO has is very advantageous, but it is a less flexible option than a resistive divider. As the exact effect that the piezoelectric sensors will have on the voltage divider is unknown, both options will be implemented: an LDO is mounted and additionally the necessary pads for a voltage divider, only one of the options being populated at a time.

The chosen option is the NCP562-series regulators, which are fixed-voltage LDOs, small (SC82-AB package, 4-pin, 2x1.25 mm), low-power (maximum output of 80 mA), and the available output voltages are 1.5, 1.8, 2.1, 2.5, 2.7, 2.8, 3.0, 3.3, 3.5 and 5.0 volts. Since our supply is 3.3 V, $V_{CC}/2 = 1.65\,\text{V}$, so both the 1.5 V and 1.8 V options are 0.15 V away from $V_{CC}/2$. The 1.8 V option is chosen (model NCP562SQ18T1G) because it is already available in GranaSat's laboratory.

4.3 Software architecture

In this section we will go into detail about the selection of the programming language, development platform, SDK framework, IDE, and third-party libraries; for writing the firmware of our system. The choices made are a combination of the characteristics of the chosen processor, the quality and quantity of support and the documentation available, and the ease of use and speed of development.

4.3.1 Programming language and SDK selection

The ESP32 supports various programming languages and SDKs. We must choose the appropriate ones according to the requirements and objectives of this project.

- **C/C++.** The salient features of these are their speed, reliability, and ease of access to low-level functionality. For this reasons, C and C++ are still two of the most popular programming languages for embedded devices according to the IEEE Spectrum annual survey of 2021 [132]. Moreover, they are the manufacturer's recommended languages. Consequently, C and C++ are the most widely used programming languages in the ESP32 community. There are two open source, officially supported C/C++ SDKs to choose from:

  - **Espressif IoT Development Framework (ESP-IDF).** Includes many software components such as an own implementation of FreeRTOS with SMP, peripheral drivers, networking stack, various protocol implementations, etc. ESP-IDF is extensively documented [76] and has many examples available on its github repository [133].

  - **Arduino Core Framework.** Is an Arduino-like SDK to ease development on Espressif hardware. Integrates all the common Arduino built-ins. It's built on top of the ESP-IDF and maintains some level of compatibility with it, as many functions from the latter are available or can be imported into Arduino Core. It is also documented by Espressif [77].

    This SDK has the advantage of the broad library support the Arduino environment has. Many Arduino libraries can work out-of-the-box, and other have specifically added support and optimizations for this framework.

- **MicroPython.** MicroPython is a lightweight implementation of Python aimed at micro-controllers. It maintains many Python conventions, it's simplicity, flexibility and convenient built-in libraries.

  Unlike Python itself, MicroPython code is compiled to bytecode, and an underlying C-based runtime executes it on the target. In fact, the MicroPython port for the ESP32 is implemented on top of the ESP-IDF. For this reason, the code execution and access to peripherals won't be as fast as using C/C++ directly, and memory usage is expected to be less efficient. Besides, not all the micro-controller's functionality is yet ported. And while an ESP32-specific documentation exists [134], it's not as extensive nor mature as the ESP-IDF or Arduino Core's.

- **Other options** such as Espruino (JavaScript), Zerynth (Python), MRuby (Ruby) and NodeMCU (Lua) are discarded because they make use of interpreted languages, are aimed at IoT applications, and are developed by third parties. This will negatively affect the level of control over the micro-controller and the program's execution speed and efficiency.

Based on the above, the C/C++ Arduino Core framework seems to be most advantageous option, specially considering the optimization, low-level control, official support by Espressif, ESP-IDF compatibility and extensive third-party library support.

4.3.2 Development platform and IDE selection

Espressif offers a standalone toolchain and scripts for compiling and uploading a program to a supported board. Also, an ESP-IDF extension for Eclipse and Visual Studio Code is available. However, the installation and configuration is manual and can be tedious. Visual Studio Code (or VS Code for short) is a multi-purpose and extensible IDE developed by Microsoft as open source.

A very popular alternative is PlatformIO, an open source platform for embedded development which supports many architectures from many vendors. Among them are the ESP32 series. In PlatformIO we can select between both the ESP-IDF and Arduino Core frameworks, and it automatically sets up all the needed components and toolchains. PlatformIO can be used as a CLI utility or as a Visual Studio Code extension. This last option gives PlatformIO a convenient and easy to use HTML-based GUI.

On the other hand, Arduino provides an open source IDE to program its devices, with the possibility of installing support for new *boards* through plugins. Among those *boards* supported, is the ESP32. However, the use of Arduino IDE was discarded since in its current stable version it has very poor management of code and project and library files, which is essential. In addition, the program's configuration is very limited and it does not include code inspection tools, auto-completion suggestions or many other basic and convenient tools for software development.

In view of the above, PlatformIO was chosen and installed as a VS Code extension. VS Code is considered as the best IDE alternative for the development of this project's firmware.

(a) *The Visual Studio Code logo. Credits: [135].*

(b) *The PlatformIO logo. Credits: [136].*

(c) *The Arduino IDE logo. Own work, based on: [137].*

(d) *The FreeRTOS logo. Credits: [8].*

Figure 4.13 – *The logos of the discussed software tools for embedded development.*

4.3.3 Real-Time Operating System (RTOS)

As aforementioned, Espressif has developed its own implementation of FreeRTOS (an open source Real Time Operating System for microcontrollers) with support for SMP, since the ESP32 processor has two symmetrical cores that can run independently and simultaneously.

The ESP32 SDKs are conceived for the use of this operating system, there is no reason not to use it. Although we don't explicitly import it in our code, it always underlies our program, managing the system routines. In addition, the well-known Arduino `setup()` and `loop()` functions are already implemented as FreeRTOS tasks transparently to the programmer.

There is no reason not to use it. Besides, it is the only way to utilize both cores of the ESP32. Furthermore, the alternative to using an RTOS would be a cyclic executive, with pre-designed, fixed task scheduling. Considering the nature of the program to be developed and in particular the complexity of the user interface, with a large number of tasks to manage, a cyclic executive would be incredibly difficult to schedule, implement, maintain and expand; requiring constant replanning at every change. These problems will be more evident in Section 5.2: Firmware design.

4.3.4 Libraries and examples

To greatly facilitate the software development work, some third-party libraries are used. Among them, the one that stands out for its importance is the LCD touchscreen management library. Two popular options are proposed:

- **TFT_eSPI.** An open source library developed by "@bodmer" et al. on GitHub [138]. This library is lightweight and simple, but with many possibilities since it controls both the graphics and the touch panel and it has broad LCD modules support, including ours. The graphics on screen are composed by commands sent directly to the LCD controller witch draw basic geometric shapes, without any sync or buffering; and stay drawn until erased by another command. This library is compatible with ESP32, but only through the Arduino Core Framework. The biggest drawback is its non-existent documentation. However, its absence is made up for by the immense number of examples included in this library that teaches almost all of its class methods.
- **LVGL (Light and Versatile Graphics Library).** Another open-source alternative developed by the LVGL group [139]. This library gives the opportunity to develop much more advanced and appealing GUIs by combining preexisting widgets. It has support for both the ESP32 and our LCD module, but introduces more complexity in the firmware design: it requires to code the application around its own components. Also, the full version of LVGL requires more flash and RAM memory than TFT_eSPI.

On the other hand, our code for the acquisition of signals through the ADC integrated in the ESP32 and using I2S to load the samples to a buffer using Direct Memory Access (DMA) is based on the example developed by Christopher Greening ("@cgreening" on GitHub) [140].

For the HX711 we will use an Arduino-compatible library to interface the amplifier for reading load cells and weight scales. This library already supports the ESP32 architecture through PlatformIO. Said library is developed by "@bogde" on GitHub [141].

Additionally, the official ESP-DSP library could be useful [142]. It includes implementations of common digital signal processing operations such as matrix multiplication, dot product, vector math, FFT, and IIR, FIR, and Kalman filters. These operations are optimized for the ESP32.

4.3.5 Language support

It is planned to include translation of the software for several languages, to facilitate the entry of the product in foreign markets. Considering the cultivation indices of the EU countries presented in Section 1.2.1.1: Poplar cultivation in the World, Europe, Spain, Andalusia and Granada, the languages proposed in a meeting with the ADIME team were English, Spanish, Italian and French. English is included and set to default since it is the *lingua franca* of science and engineering.

4.4 Mechanical architecture

4.4.1 Handheld device philosophy and design constraints

As we saw on Section 1.2.3: Measurement devices on the market, several competing products are handheld devices, and we will adopt that philosophy. It allows ease of usage and benefits portability, but it also means that the size, weight and autonomy are of special concern. We must be careful that our design is light, easy to carry and to manipulate.

Some design concepts are exposed below:

- The design must be rugged, since the operating conditions can be adverse: shocks, falls, dust, splashes and humidity...
- The size should not be too big. It must be possible to pick it up and manipulate it with just one hand.
- Due to the width restriction, the screen will be placed in portrait (vertical) orientation.
- The device can operate in the sun, so a visor can enhance the display visibility, as well as offer extra protection to the touchscreen.
- It must have a shape that benefits grip, preventing it from slipping.
- The BNCs must go on top, just like in the Fakopp Microsecond Timer, but with more separation between the connectors to facilitate handling.
- The charger port should be at the bottom.
- It should include a space to store a stylus.
- The power button will be clearly visible, and on the front.
- The addition of an anchor point for a strap is interesting, as the operator can then hang the strap around their neck, preventing the device from falling and leaving the user's hands free when they are not actively using it.
- The connectors must have enough margin so as not to collide with others or with the casing's wall itself.
- The multi-direction *'thumb'* button should be placed on the right, since the majority of the population is right-handed. The position of the button should be comfortable for the thumb. In order to make the button easy to find by touch, a groove or texture can be added to the wall of the device.
- That the screws are not very visible, or at least that they do not protrude from the profile of the case, is appreciated for aesthetic reasons and for user comfort.

As a first prototype, we chose a basic shape, a rectangular prism with smooth edges and grooves to make the walls more resistant and at the same time make it easier to grip the device. A sketch that combines the previous concepts can be seen in Figure 4.16 (it is only a concept, not the final design; which will be seen in later sections). Additionally, a render of the model is available in Figure 4.14

The dimensions of the product ultimately condition the dimensions of the PCB, which will consequently be narrow and elongated. A rectangular form factor is chosen, with slightly rounded corners. The position of the four mounting holes of the LCD screen is adopted, so that the module and the PCB can be fastened with the same screws (see Figure 4.15).

We will use M3 size screws, which corresponds to the size of the mounting holes. Regarding the length, type of head, etc. it will depend on the direction the final design takes.

Figure 4.14 – *3D rendering of the early conception of the TIK case design.*

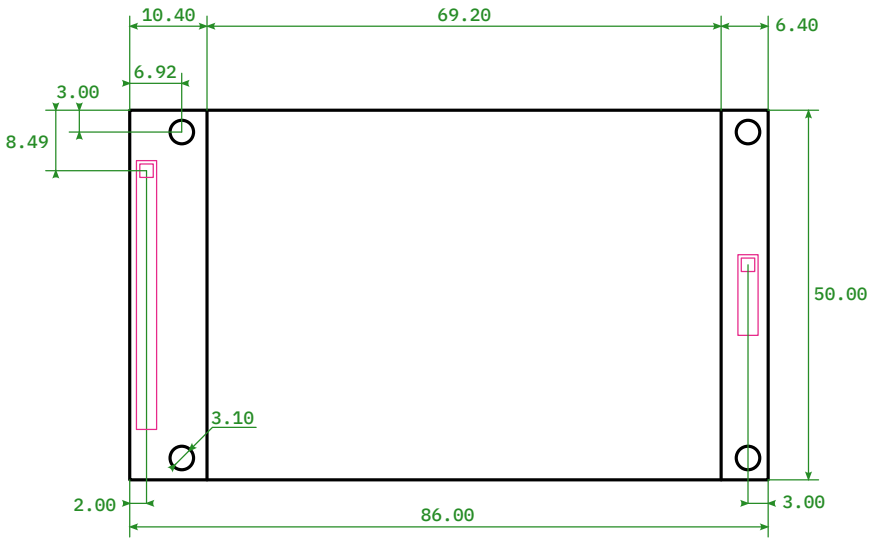

Figure 4.15 – *Dimensions of the 2.8" ILI9341 LCD TFT module.*

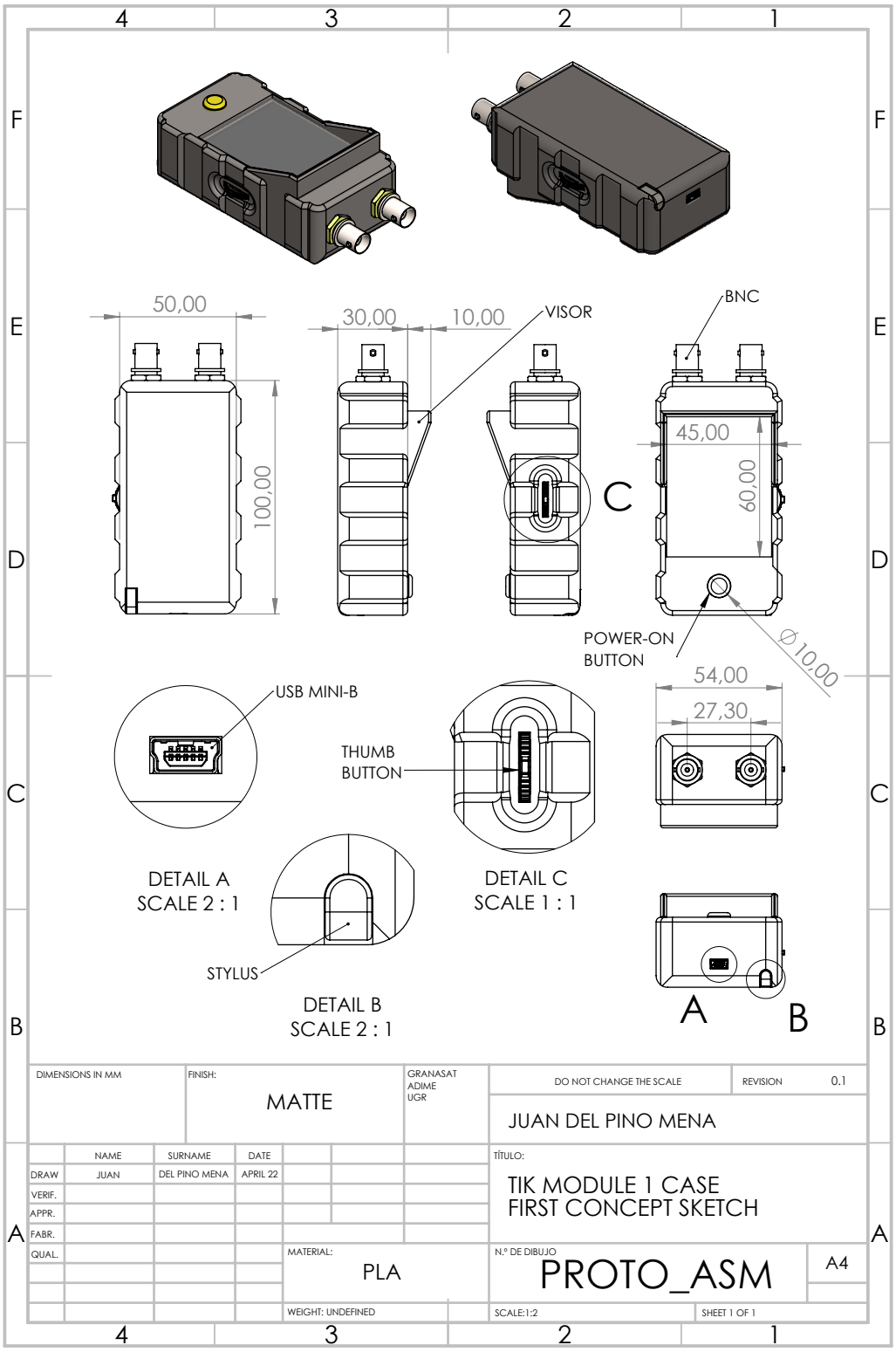

Figure 4.16 – *Early conception of the TIK case design. Schematic and dimensions.*

4.4.2 3D CAD software and fabrication material

The 3D CAD program to be used is SolidWorks. The decision is due to the fact that it is widely used in professional environments, which offers endless possibilities for industrial 3D design and simulation. In addition, the author is very familiar with his environment thanks to a course offered by the UGR, called *"Diploma in mechanical design and thermal and structural simulation with SolidWorks"* (code 21/D/028).

For the first approximation we will use 3D printing to create the case in PLA filament (Figure 4.18) and using Ultimaker Cura software (more information about the program in Section 6.2: Case 3D printing). 3D printing allows us to design, prototype, test and rectify designs quickly and cheaply; but it also adds restrictions to design freedom, and we already know that the 3D-printed case will not be resistant to dust or water. For the final device to be sold and manufactured in series, another more professional, more rugged and of more quality manufacturing process (such as plastic molding) will be required.

(a) *SolidWorks logotype, extracted from: [143].*

(b) *Ultimaker Cura logotype (own work).*

Figure 4.17 – *SolidWorks and Ultimaker Cura logotype.*

Figure 4.18 – *1 kg spool of PLA filament of 1.75 mm in diameter, from SmartMaterials [144].*

Chapter 5

System design.

After the foregoing chapters of analysis and requirements, this chapter will dig into the system design of the TIK device. As in the previous chapter, this one is divided into 3 well-differentiated parts: the **Electronic design** (which in turn consists of the circuits design and PCB design), the **Firmware design**, as well as the physical product's **Mechanical design**.

5.1 Electronic design

This section details all aspects of the electronic design of the TIK. This section is long and it is comprised of several differentiated parts:

- **The circuit design section** explains the symbols, nomenclature and conventions followed, and develops all the needed circuits.
- **The PCB design section** details all the characteristics of the printed circuit board designed and manufactured for this project.

5.1.1 EDA Software

All electronics have been developed in Altium Designer with sporadic help of KiCad and EasyEDA. Altium Designer is a professional and state-of-the-art EDA for electronic product design. It allows a co-design of the circuit schematics and the Printed Circuit Board itself, making the development fast and convenient. It can generate project documentation such as circuit schematics and PCB prints, as well as fabrication files, renders and videos, 3D models, PDF3Ds, BOMs, etc.

Altium Designer works with component libraries. There are two kinds of libraries: symbol libraries (SCHLIBs) and footprint libraries (PCBLIBs). Altium Designer matches each symbol that appears on schematics to a footprint in the PCB editor. These libraries are either generated by the manufacturers and users, or created by ourselves. Since the first option usually results in an inconsistent style of the schematics and footprints, we have chosen to create each one of the schematic symbols by ourselves. In the case of the footprints, own designs have been generated or modified from the *"Celestial Altium Library"* developed by "@issus" and available on Github [146].

Figure 5.1 – *Altium Designer logotype, extracted from: [145].*

5.1.2 Circuit schematics

This part of the chapter expounds in detail the synthesized circuitry for the project. Prior to the explanation, the symbols, nomenclature, practices and conventions followed in the development of electronic circuits are detailed.

5.1.2.1 Circuit symbols and nomenclature

In order to ease the understanding of the circuit diagrams for readers not familiar with the symbology used in electronics, this introductory section will address the component symbols, the industry *de facto* naming convention, as well as the parameter sets and common practices.

5.1.2.1.1 Common electric components symbols

Most common electric components schematics symbols follow the IEEE-315 *"Graphic Symbols for Electrical and Electronics Diagrams"* standard [147]. In table 5.1 is shown a collection of symbols of electric parts used in this project.

5.1.2.1.2 IC symbols

An Integrated Circuit's symbol is usually comprised of a rectangular box with pins sticking out of the perimeter. In Figure 5.2a we can see the parts that make up a generic IC symbol. In this case, it's an example from the USB ESD protection Integrated Circuit extracted from Section 5.1.2.5: USB port. The pins are divided in 3 parts:

- The first one is the pin line itself, which at the end of it resides the electrical connection terminal which can be used to connect that pin to a net.
- The second part is the pin number, which identifies the pin itself and links the pin with its correspondent pad on the footprint.
- Lastly, the third part is the pin name, which indicates the pin function(s).

Component symbols can be decorated with non-functional drawings that provide a visual representation of how the integrated circuit behaves or how the pins are related to one another (an example can be seen in Figure 5.2a). Over the symbol we can find the component designator. Below it we can find information about the part such as the IC name or model, packaging, and a brief description about the part itself.

Symbol	Description
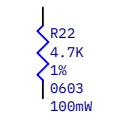	**Resistor.** Along with the designator, the symbol text comprises the resistance value, tolerance, package and maximum dissipated power.
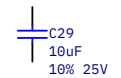	**Non-polarised capacitor** (ceramic, MLCC). As before, the designator is accompanied with the capacitance value, the tolerance, maximum rated voltage between the capacitor extremes, and the package. Other info that may also appear is the ceramic type: X7R, X5R, C0G...
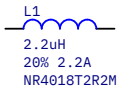	**Inductor.** Next to the designator we find the inductance value, the tolerance and maximum rated current and some more information about the specific model and the physical coil size.
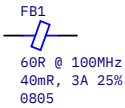	**Ferrite Bead.** The symbol displays the typical impedance at the given frequency, the DC resistance, the rated current and tolerance and the footprint size.
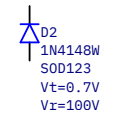	**General-Purpose diode.** Apart from the designator, the model, footprint and estimated forward voltage (V_f) and reverse breakdown voltage (V_r) are shown.
	**Light-Emitting Diode (LED).** The symbol contains the part designator, packaging and light color.
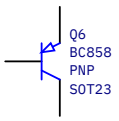	**Bipolar junction transistor (BJT).** In this case, a PNP type BJT. Attached info includes the designator, model, type and package.
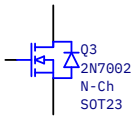	**Field Effect Transistor (FET).** In this case, a 3-pin N-Channel MOSFET with already connected source and substrate. The symbol also includes an additional diode (parallel to the intrinsic and worse body diode) to reduce the reverse recovery time of the transistor. Attached info includes the designator, model, type and package.
	**A generic push-button switch.** This symbol indicates that the button is normally-open and the two extremes of the switch will be shorted when pressed.
	**Test Point**. Indicates the presence of a test point in the net. Designator can include information about the net that is connected to. In this project, we used THT pads to make test points available in both the top and bottom layers.
	**Fiducial marks**. A special mark for the manufacturing process. Designator is not relevant, so it usually does not appear in the PCB.

Table 5.1 – *Legend of various components used in the schematics of this project.*

5.1.2.1.3 Reference designators

A reference designator identifies a component in an electrical schematic or/and in a PCB. The reference designator usually consists of one, or more letters followed by a number, e.g.: R2, D2, C418, FB52. This nomenclature for electrical and electronic components is also defined by the IEEE-315 [147]. However, the standard is not always followed [148]. In table 5.3 all the designators used in the schematic sheets are shown.

5.1.2.1.4 Nets and net names

In a schematic, components are connected via *nets* (or *networks*), a metaphor of wires. In the schematic sheets nets are lines which run from a component pin to another. Relevant nets are given a name which is put close above the net line itself. Two separate nets with the same name indicate that they are the same network, even on different schematic sheets. In table 5.2 we can see the net power symbols used to identify power nets in the circuit schematics.

5.1.2.1.5 Net classes, parameters sets and net highlighting

A *parameter set* is a collection of guidelines, design rules or constraints that we impose over a set of nets. A parameter set applies its properties to the net it's connected to. For including various nets under the same parameter set, we use a blanket, which is the red dashed area in Figure 5.2b.

In the other hand, a net class is a set of networks that share common characteristics, such as being a communication bus or a network connected to the power supply. The class is indicated by the red text above the parameter set. Arranging networks into classes allows the PCB designer greater organization and ease of manipulating networks as well as their parameters.

A Differential Pair is indicated with a special symbol and specific net nomenclature. In Figure 5.2c we can see an example of a differential pair. Notice how the net names end in `_N` or `_P` depending on whether it is the positive or negative pair.

5.1.2.2 Circuits structure block diagram

Figure 5.3 shows the complete block diagram of the system circuits indicating both the connections between the blocks and their hierarchy. This is a more advanced lower-level block diagram than the one presented in Figure 4.3, in which an initial structure was suggested that allowed us to start designing the system from a high-level perspective and choose the required parts.

However, although the diagrams correspond to different stages of development of the project, both are very similar since we built the second on the structure proposed in the first.

In the coming sections every block will be described in detail.

Symbol	Description
	Ground, as in the voltage reference. In this project, this symbol is the system's global GND.
	Another symbol for ground. In this project, this is used as the battery negative terminal to avoid confusion with the system's global GND.
	Indicates that the net is a power rail, connected to a voltage supply.
	Another symbol for a power rail. In this project, it's used only for the battery positive terminal to quickly identify it.

Table 5.2 – *Description of power net symbols used in the diagrams of this project.*

Type	Component	Designator
Passive	Resistor	R
	Capacitor	C
	Inductor	L
	Ferrrite Bead	FB
	Connector	J
	Switch	S
	Thermistor	RT
Active	Diode	D
	Transistor	Q
	Integrated Circuit	U
	Microcontroller	MCU
	Battery	BAT
Other	Test Point	TP
	Fiducial	F

Table 5.3 – *Legend of designators used in the schematics of this project.*

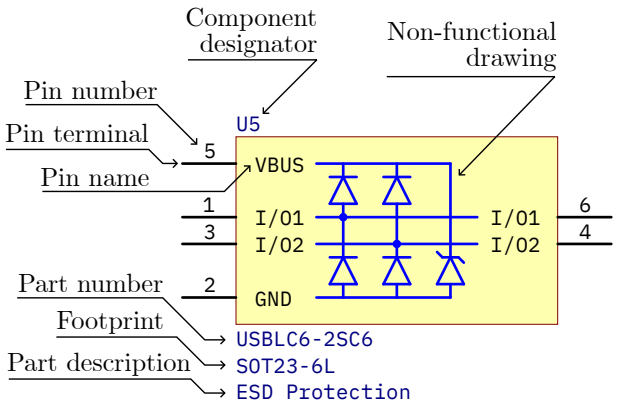

(a) *Parts of a integrated circuit symbol.*

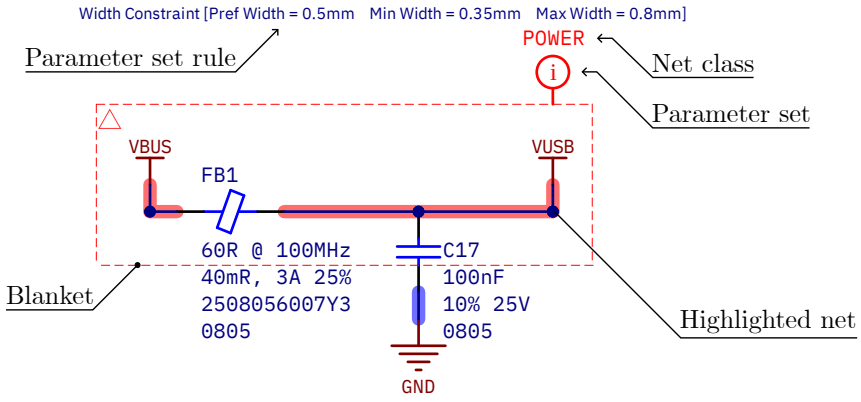

(b) *Parameter set usage with a blanket and assigned attributes. Net highlighting.*

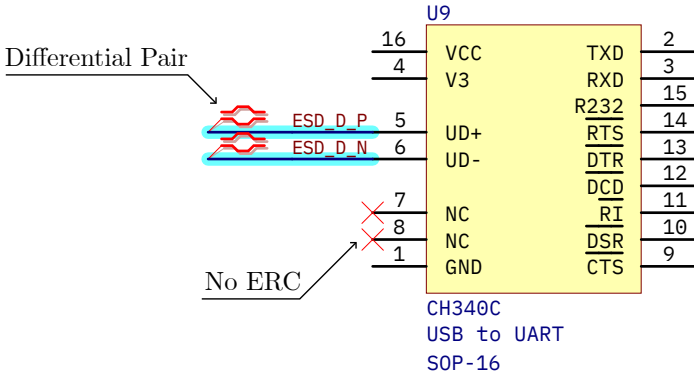

(c) *Specification of a differential pair and the no Electrical Rule Check parameters.*

Figure 5.2 – *Description of the component symbols and parameters.*

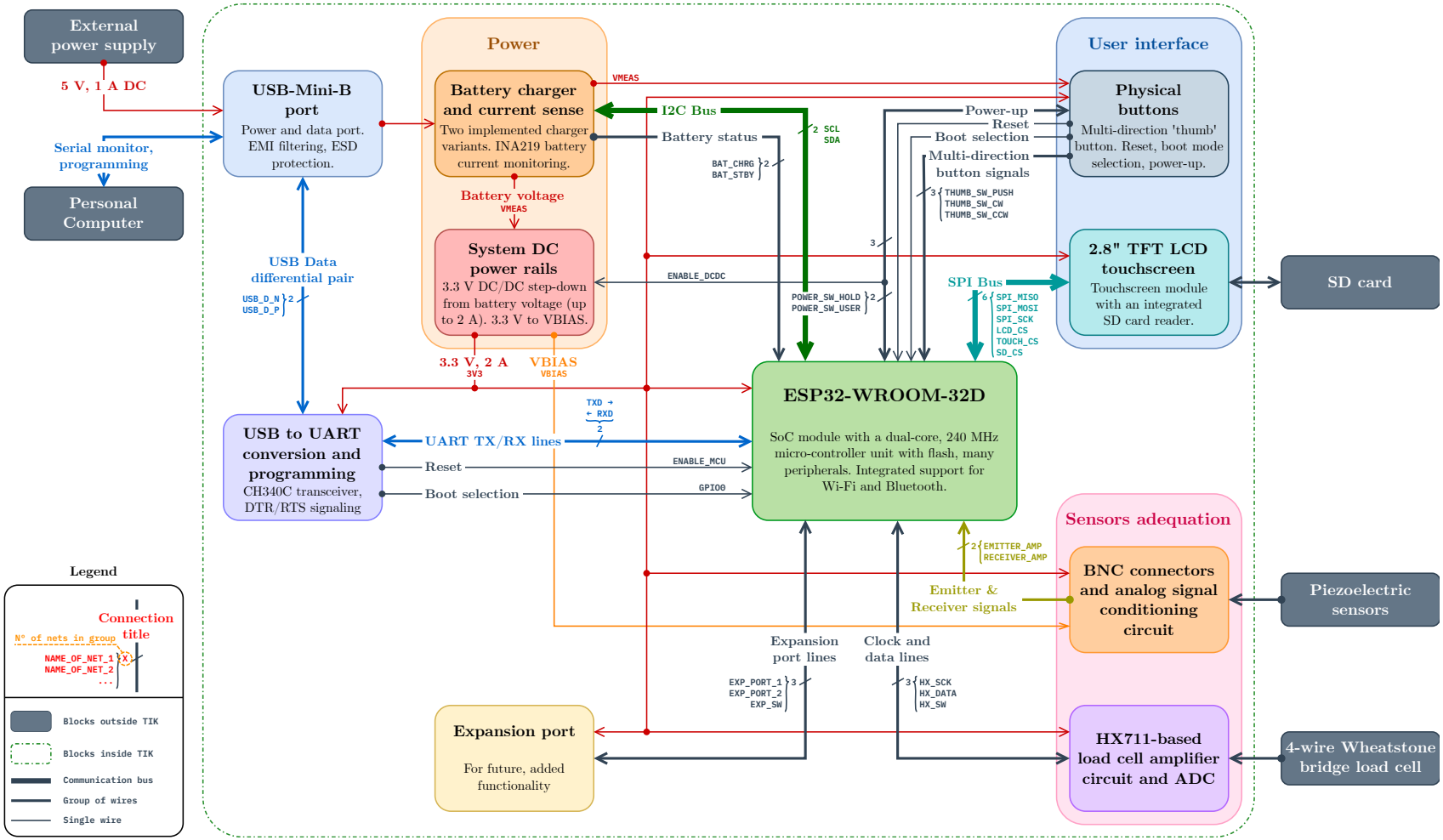

Figure 5.3 – *Circuit's block diagram.*

5.1.2.3 Power Delivery System

5.1.2.3.1 Structure of the Power Delivery System

Since the PDS of the developed prototype has multiple stages, its understanding can be complex. Figure 5.4 details its structure in the form of a block diagram. The PDS is divided in the following blocks:

- **The Battery.** The portable voltage source that supplies the system.
- **The Battery protection circuit.** The chemical characteristics and charge density of the lithium-based batteries make them more unstable than other types of batteries. In case of over-charging, the battery may lose effective charge and reduce its life time. In case of extreme over-discharging, the battery can swell and explode. The charger is responsible for cutting off the charge when it is full. The protection circuit monitors the battery voltage, and when it is too low it disconnects the negative pole of the battery to prevent over-discharging.
- **The Battery current sense.** This circuit contains an IC capable of monitoring the voltage on both extremes of a small $0.2\,\Omega$ resistor in series with the battery, and thus monitoring the current through it. This way we can know the current that is being consumed or supplied to the battery when required. In addition, we can estimate the battery charge level through continuous monitoring of the battery voltage and current, and applying the method of current integration (also known as *coulomb counting*).
- **The DC/DC step-down converter.** This circuit is responsible for reducing the voltage coming from the battery after the current measurement (V_{meas}) to a constant supply voltage of 3.3 volts, and it is rated for a maximum supply current of 2 amps. By using a DC/DC and not a linear regulator, this voltage conversion is quite efficient and does not generate as much heat.

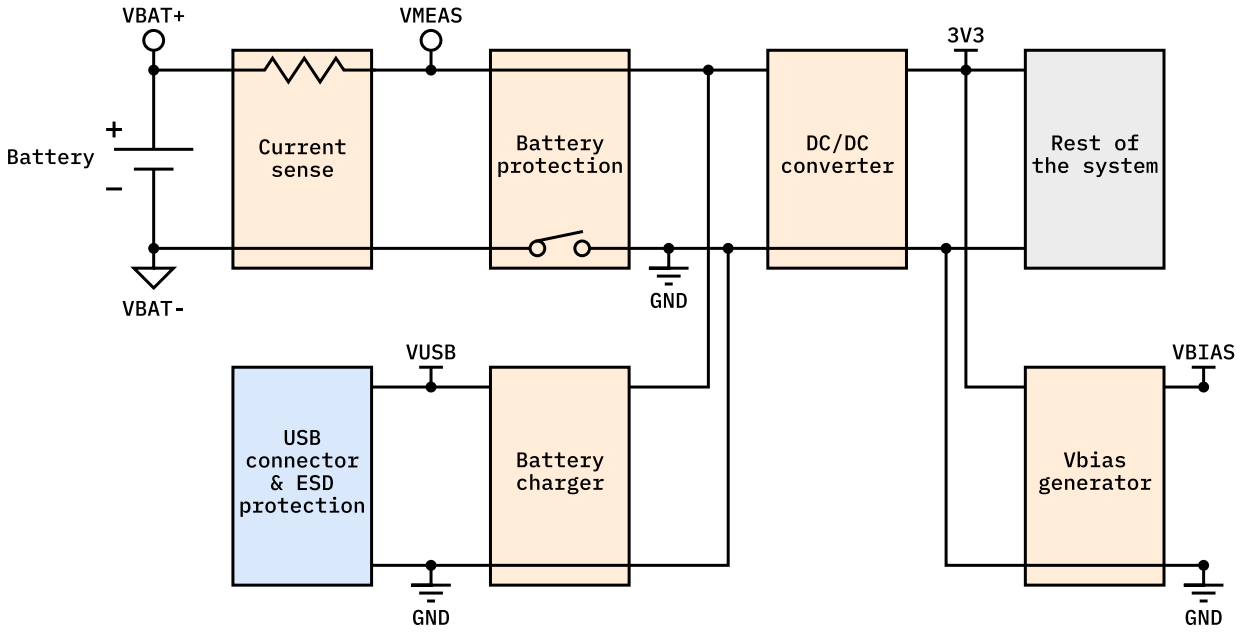

Figure 5.4 – *Block diagram of the TIK's Power Delivery System.*

- **The Vbias-generator circuit.** This circuit generates V_{bias} (forgive the redundancy) necessary for the signal conditioning circuit.

- **The battery charger.** As its name suggests, this circuit is responsible for charging the battery. When there is a voltage on the `VUSB` net (when the USB cable is plugged into the port), the circuit is activated and automatically starts charging the battery using the externally supplied energy.

- **The USB connector.** Apart from the USB port, this block contains a protection IC to avoid damaging the TIK internals with an ESD.

5.1.2.3.2 Power rails

The main power rail of the TIK prototype is a 3.3 V supplied by a DC/DC step-down converter from the battery. Also, a LDO regulator (optional, bypassable by a voltage divider) is used in order to generate the V_{bias} voltage for the signal conditioning circuit.

5.1.2.3.2.1 DC/DC step down for the main system power

The system's main power rail is supplied by the Diodes Incorporated AP3429KTTR-G1 DC/DC step-down converter. Another equivalent option is the aforementioned Texas Instruments TLV62569, which is pin-to-pin compatible with the AP3429K (Table 5.4) but more expensive (see Appendix A: Project costs: Electronic components). The circuit follows the typical application from the AP3429K's datasheet [131].

The Integrated Circuit takes care of the power switching with various integrated power MOSFETs, and also controls the MOSFETs according to its feedback pin. This pin is connected to an error amplifier and fixed at a reference 0.6 V by the IC itself. This way, when the voltage on the converter output tries to drop or rise, the IC will compensate by increasing or decreasing its power MOSFETs' PWM duty cycle.

Since this circuit can supply up to 2 amps, so components must be selected with special attention to their rated current and/or dissipated power. In special, the inductor must be rated at least for the maximum current without experiencing saturation. Input and output capacitors should be placed physically close to the converter chip, and the overall circuit should be traced in short loops to avoid noise coupling.

The feedback resistor network has been set up to output 3.3 V:

$$V_{\text{FB}} = \frac{R_2}{R_1 + R_2} \cdot V_{\text{out}} \quad ; \quad V_{\text{out}} = \frac{R_1 + R_2}{R_2} \cdot V_{\text{FB}} \tag{5.1.1}$$

And since $V_{\text{out}} = 3.3\,\text{V}$ and $V_{\text{FB}} = 0.6\,\text{V}$:

$$R_2 = \frac{2}{9} \cdot R_1 \tag{5.1.2}$$

Resistor values should be chosen in the order of magnitude of tens to hundreds of ohms, to have a very small current consumption in the feedback loop. A pair of appropriate resistor values are:

$$R_1 = 150\,\text{k}\Omega \quad ; \quad R_2 = 33\,\text{k}\Omega \tag{5.1.3}$$

Which should result in a typical output voltage of 3.33 V.

Pin	Pin name on the AP3429K	Pin name on the TLV62569	Type	Description
1	EN	EN	Input	Enable control input (active high). A voltage above 1.5 V enables the device, and below 0.4 V shuts it down. Must not be floating.
2	GND	GND	Power	Ground.
3	LX	SW	Power	Connected to the internal FET switches' drains of the main, synchronous power MOSFETs responsible for the switching. An inductor must be connected to this pin.
4	VIN	VIN	Power	Power supply voltage input.
5	FB	FB	Input	Feedback pin for the internal control loop. Connected to the internal error amplifier. Fixed at 0.6 V. Must be connected to a voltage divider.

Table 5.4 – *AP3429K and TLV62569 DC/DC step-down converters pins description [131, 130].*

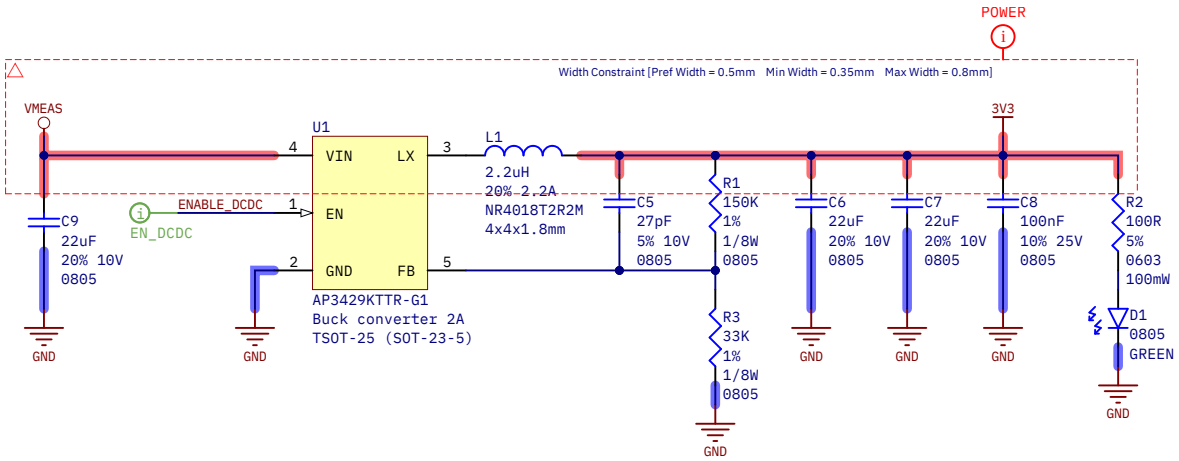

Figure 5.5 – *AP3429K DC/DC step-down converter circuit, which supplies the 3.3 V rail.*

5.1.2.3.2.2 Low-DropOut regulator for bias voltage

A NCP562SQ18T1G provides the V_{bias} voltage for the piezoelectric sensors' adequation circuit. The LDO circuit is simple (Figure 5.6), with only a few capacitors needed to smooth the input and output and reduce ripple and noise. Capacitor values are the recommended ones in the product's datasheet [149].

The zero-ohm resistors at the right in Figure 5.6 are a V_{bias} bypass. They allow to short V_{bias} to ground or 3.3 V if needed (but do not do it simultaneously). The resistors also allow to set any other intermediate voltage if needed by using a simple voltage divider. Even if the resistor divider is used in place of the NCP562SQ18T1G, the output capacitors should be populated to make the node a fixed DC voltage source in the eyes of the analog signal.

5.1.2.3.3 Battery and current monitor

The battery is the voltage source that supplies the system for a given time. The battery output is directly connected to the current sense resistor in series, so all the current that goes through the battery (in or out) also goes through said resistor.

The value of the current sense resistor is selected based on the INA219's specifications [125] and a compromise between voltage readability and dissipated power. By choosing the maximum possible (and default) PGA value of 8, we can measure up to 320 mV between the `VIN+` and `VIN-` pins. So, by choosing $R_{\text{sense}} = 200\,\text{m}\Omega$, the maximum detectable current is:

$$I_{\text{max}} = \frac{V_{\text{max}}}{R_{\text{sense}}} = \frac{320\,\text{mV}}{200\,\text{m}\Omega} = 1.6\,\text{A} \tag{5.1.4}$$

Which is larger than the maximum expected current specified in Section 4.2.4.6.1: Early power budget estimation and Section 5.1.2.3.5: Detailed power budget. The absolute maximum dissipated power in the shunt would be:

$$P_{\text{d,max}} = \frac{V_{\text{max}^2}}{R_{\text{sense}}} = I_{\text{max}}^2 \cdot R_{\text{sense}} = (1.6\,\text{A})^2 \cdot 0.2\,\Omega = 0.512\,\text{W} \tag{5.1.5}$$

An usual dissipated power rating for a 1206 power resistor is 0.5 W, so we exceed that amount by very little. But given the TIK's typical expected current consumption is only 142 mA and the maximum just 405 mA (see Section 5.1.2.3.5: Detailed power budget), the maximum dissipated power in R_{sense} will be from 4 mW to 33 mW (ten to a hundred less power) in normal conditions.

The current measurement resolution on the default 12-bit ADC configuration is then:

$$\Delta I = \frac{I_{max}}{N_{\text{ADC}}} = \frac{1.6\,\text{A}}{2^{12}\ \text{counts}} = 390.625\,\mu\text{A} \tag{5.1.6}$$

And since both the typical and maximum consumption are 3 orders of magnitude higher, the measurement accuracy is very good.

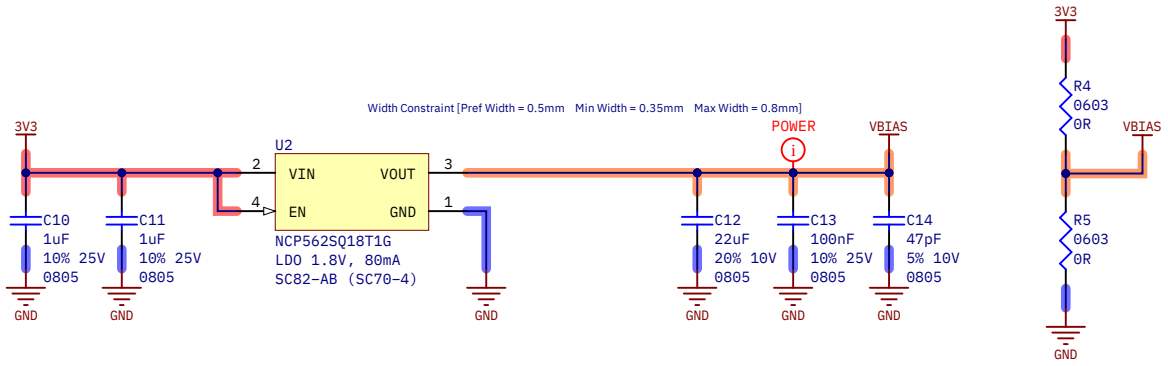

Figure 5.6 – *V_{bias} voltage rail provider circuits. Option 1: NCP562SQ18T1G LDO regulator (left). Option 2: V_{bias} bypass resistors (right).*

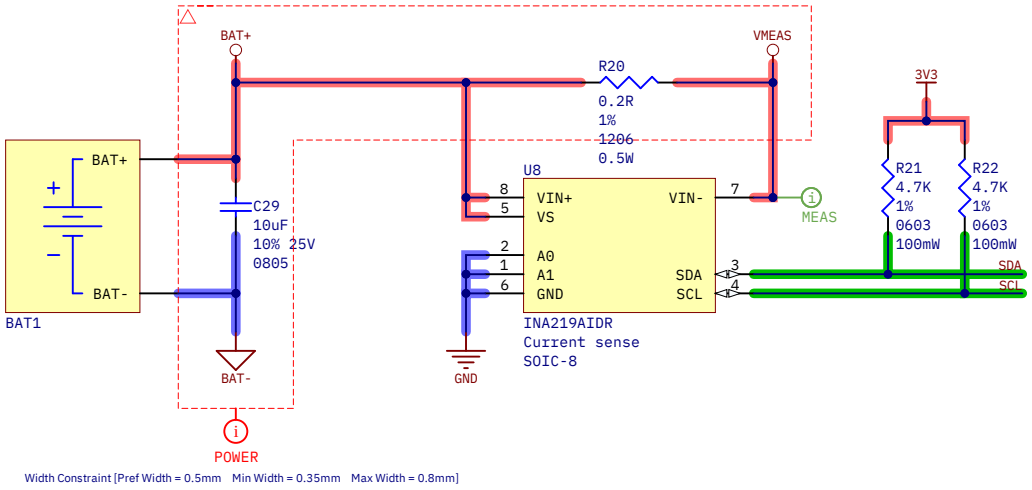

Figure 5.7 – *INA219 current sense circuit for battery current monitoring.*

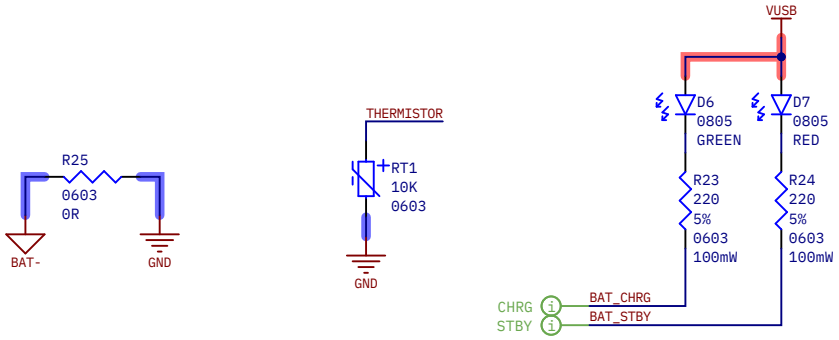

Figure 5.8 – *Additional charger components: resistor for charger selection (Lithium battery protection bypass) (left), battery charger status (charging and standby) (center) indicators and connector for the battery thermistor (right).*

5.1.2.3.4 Battery chargers

In this section, the two implemented battery chargers alternatives are presented.

5.1.2.3.4.1 Nickel-Metal Hydride battery charger

One of the manufacturer's recommended topology is used as specified in the LTC4060's datasheet (Figure 5.9) [121].

R_{prog} (R_{19}) sets the maximum charge current, which obeys the following equation:

$$R_{\text{prog}} = \frac{1395}{I_{\text{max}}\ (\text{amps})} \tag{5.1.7}$$

Thus, to set a maximum of 1 A we need a 1.395 kΩ resistor. The nearest commercially available value is 1.5 kΩ, which corresponds with a charge current of 950 mA. Although the charger ideally supports up to 2 amps, the limit it has not been raised higher due to safety concerns during the charging process: the metal fin of Q2 (the MJD210 pass transistor, with a DPAK package) is not connected to a ground plane, so it cannot dissipate so much heat and could be damaged.

On the other hand, C_{timer} (C_{28}) sets the charger's timer limit:

$$C_{\text{timer}} = \frac{t_{\text{max}}\ (\text{hours})}{1.567 \times 10^6 \cdot R_{\text{prog}}\ (\text{ohms})} \tag{5.1.8}$$

For example, a 1 nF capacitor sets a limit of 2 hours and 20 minutes.

R_{18} is a resistor which must form a voltage divider with a 10 kΩ NTC thermistor in order to monitor the battery voltage. However, the recommended R_{18} value is very specific (and expensive): 4.42 kΩ. So, we have selected a 4.7 kΩ resistor as a replacement. The consequence is that the temperature protection will act sooner than with the recommended resistor. It can also be left unpopulated to disable temperature detection. In that case, the NTC should not be connected (given the battery has one).

5.1.2.3.4.2 Lithium-Ion and Lithium-Polymer battery charger

As said in the previous chapter, we have selected the TP4056 Li-Ion and Li-Po charger. Datasheet recommends to connect a resistor of 300 mΩ to 500 mΩ in series between `VUSB` and the `VCC` pin [118]. It does not explain why, but probably due to chip temperature concerns: the small resistor reduces the input voltage and thus the dissipated power by the chip. However, we have omitted it for cost reasons, and we are confident on this decision because not a single commercial TP4056-based module uses any series resistor.

The rest of the implemented circuit follows the datasheet's typical application (Figure 5.10a). R_8 selects the charging current. For 1.2 kΩ, it is the maximum the TP4056 supports: 1.0 A. Since our battery is 1500 mA, charging occurs at a maximum of 0.67C. A full charge shouldn't take more than 1.5 to 2 hours.

In addition to the charger, the protection circuit for lithium batteries is also included (Figure 5.10b). Many Li-Po batteries already havea similar protection circuit (such as ours), but it was decided to add one for the sake of redundancy and security. The protection circuit follows the DW01A's recommended application [119]. The DW01A is the protection circuit itself, and cuts the low-side of the battery if it detects an overcharge (OC) or a over-discharge (ODC). The FS8205A is IC that contains two NMOS which are the switch to connect `BAT-` and `GND` together (and allow the circuit to be powered up).

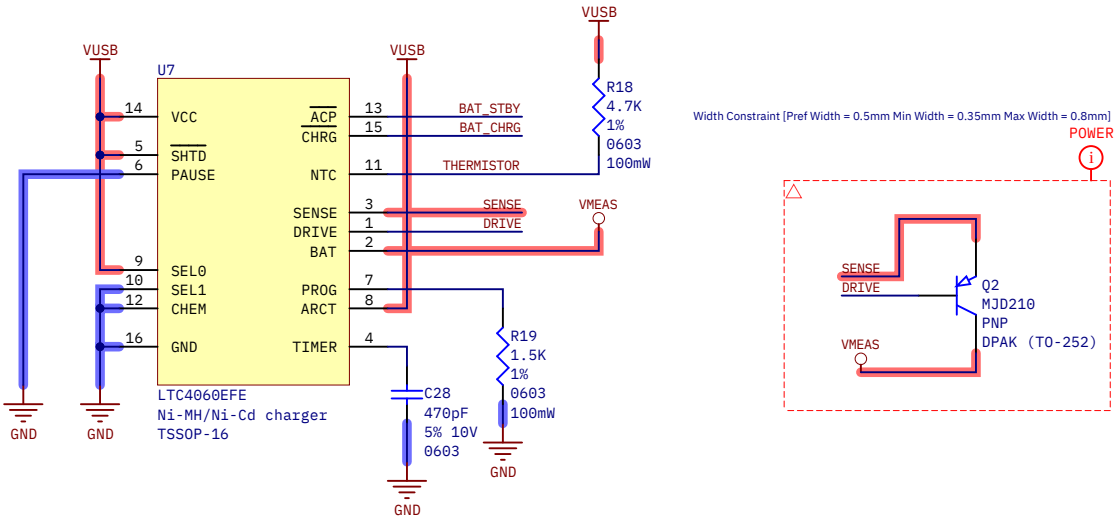

Figure 5.9 – *Charger circuit variant 1, for Ni-MH batteries.*

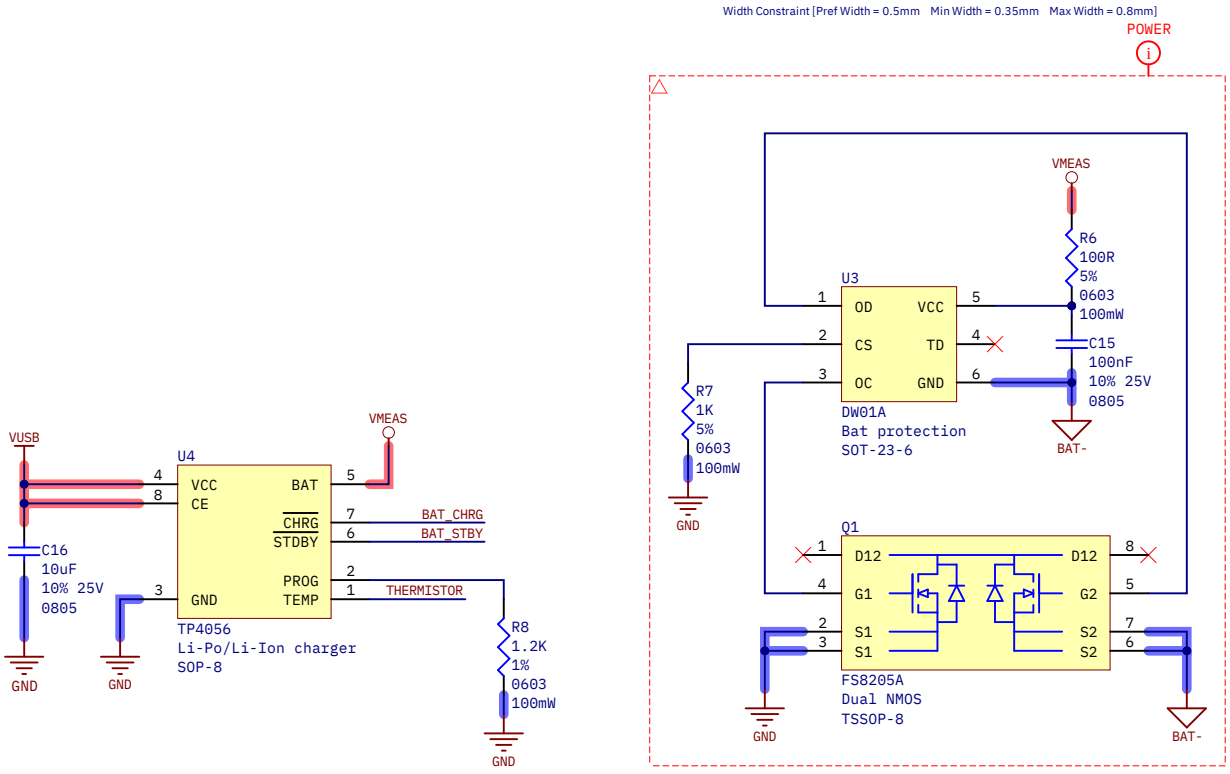

(a) *TP4056 charger IC.*

(b) *DW01A and FS8205A battery protection circuitry.*

Figure 5.10 – *Charger circuit variant 1, for single cell Lithium-based (Li-Ion or Li-Po) batteries, including a battery protection circuit.*

5.1.2.3.5 Detailed typical and maximum power budget. Estimated battery life

Table 5.5 contains an exhaustive power consumption approximation based on manufacturers' figures, except for the ESP32 and the TFT LCD module, whose average power consumption was measured and resulted around 70 mA and 45 mA respectively. This is in line with the ESP32's manufacturer-specified typical power consumption of 68 mA [78]. Section 6.4.8: Power consumption includes details about the procedure and the results of the measurements.

Table 5.6 adds up all the consumption of the components that are powered by the system battery. This excludes the chargers, whose consumption comes from the external USB power supply, see Table 5.7.

Expected typical sustained current draw on the TIK prototype is 139.6 mA in the 3.3 V rail, and the maximum is 402.9 mA. The estimated typical power consumption is 469.6 mW (in all rails) and the maximum 1342 mW. These figures allow us to approximate the duration of the battery knowing its nominal voltage, energy capacity, and assuming a linear consumption. A MIKROE-4473 MLP604060 Li-Po battery with a nominal voltage of 3.7 V and 1500 mAh of rated capacity has been mounted on the prototype:

$$3.7\,\mathrm{V}\cdot 1.5\,\mathrm{Ah} = 5.55\,\mathrm{Wh} \quad ; \quad \begin{cases} \text{Typical:} & \frac{5.55\,\mathrm{Wh}}{0.4696\,\mathrm{W}} = 11.82\,\mathrm{hours} \quad (11 \text{ hours, } 49 \text{ minutes}) \\ \text{Minimum:} & \frac{5.55\,\mathrm{Wh}}{1.342\,\mathrm{W}} = 4.14\,\mathrm{hours} \quad (4 \text{ hours, } 8 \text{ minutes}) \end{cases} \tag{5.1.9}$$

(Assuming a sustained and linear discharge)

The real battery time is probably less than the typical, because the battery may has less actual charge than specified, or because it is dangerous for the battery to be very discharged. In either case, it's clear that the device would last a reasonable number of hours under continuous usage.

5.1.2.3.6 Power dissipation and efficiency of the battery chargers

Since battery charging requires the charging voltage to be regulated to that of the battery, calculating the efficiency of the implemented chargers is interesting. An estimate of the worst-case efficiency of the chargers is presented in Table 5.8.

As it can be seen, both have fairly low efficiencies and dissipate about 2.2 to 2.7 W of power in the worst case, so both designs are expected to get quite hot during charging. However, of the two alternatives the lithium charger based on the TP4056 chip has a significantly better efficiency (62.2 %) over the LTC4060 one (53.8 %); mainly due to lower consumption by the charger components themselves, the fact that it does not use an external BJT for voltage regulation, and by the slightly higher programmed charging current.

Block	Component	Description	Supply voltage (V)	Current per unit		Units	Total power	
				Typical	Maximum		Typical	Maximum
MCU	ESP32-WROOM-32D	MCU + wireless comm. module	3.3	70 mA *	240 mA **	1	231 mW	792 mW
Power rails	AP3429	DC/DC Buck converter IC	4.2	90 µA		1	378 µW	
	NCP562SQ18T1G	Low-Dropout regulator IC	3.3	3 µA		1	9.9 µW	
	150+33 kΩ voltage divider	FB pin feedback.	3.3	18 µA		1	59.4 µW	
	[Optional] voltage divider	Assuming 3V3/2, 10 kΩ resistors	3.3	165 µA		1	544.5 µW	
	Generic 0805 LED	Assuming Vf = 2V & 1 kΩ series resistor	3.3	1.3 mA		1	4.3 mW	
Battery and current sense	INA219	Voltage & current sense IC	4.2	0.7 mA	1 mA	1	3 mW	4.2 mW
	Generic 0805 LED	Assuming Vf = 2V & 1 kΩ series resistor	5.5	1.3 mA		2	8.6 mW	
	I2C pull-up resistor	Assuming line level is LOW, with 4.7kΩ resistors	3.3	0.7 mA		2	4.6 mW	
USB connector	USBLC6-2SC6	USB ESD protection IC	5.5	10 nA	150 nA	1	55 nW	825 nW
Programming	CH340C	USB to UART converter IC	3.3	12 mA	30 mA	1	39.6 mW	99 mW
	2N7002	G.P. NMOS. Ib=0 A, Vds=3.3 V, Ids=330 µA (during conmutation)	–	–		2	1 mW	
	Generic 0805 LED	Assuming Vf = 2V & 1 kΩ series resistor	3.3	1.3 mA		4	17.2 mW	
Buttons	Pull-up resistors	Assuming line level is LOW, 10kΩ resistors	3.3	330 µA		5	5.4 mW	
Power-up button	BSS84AK	G.P. PMOS. Rsd(on) = 7.5 Ω, Ib=0, Isd = 77 µA	–	–		1	45 nW	
	1N4148W	Small signal diode. Vf=0.7 V, If=26 µA	–	–		2	36.4 µW	
	100 kΩ pull-up resistor	100 kΩ pull-up resistor	4.2	42 µA		1	176.4 µW	
Display	LCD TFT ILI9341 module	320x240p LCD (Measured)	3.3	45 mA *	120 mA ***	1	148.5 mW	396 mW
Signal conditioning	LMV358DGKR	General purpose dual OpAmp, with high-Z load	3.3	140 µA	340 µA	1	462 µW	1.1 mW
	1N4148W	Small signal diode. Vf=0.7 V, If= ? A	–	–		4	–	
Load cell amplifier	HX711	Load cell amplifier & ADC IC	3.3	1.4 mA		1	4.6 mW	
	BC858	General purpose PNP BJT. Vce=1.8V, Ice=? A	–	–		1	–	
	22+10 kΩ voltage divider	VFB, AVDD=1.82 V regulation	1.82	57 µA		1	103.7 µW	

Table 5.5 – *Typical and maximum estimated power consumption. Figures from the correspondent datasheets, except when specified. *Average, ***maximum power consumption measured, running demo program. **Manufacturer-provided figure, spikes during wireless TX [78] (table 15).*

Total current consumption in the 3V3 rail)	
Typical	**Maximum**
139.6 mA	**402.9 mA**

Total dissipated power	
Typical	**Maximum**
469.6 mW	**1342 mW**

Table 5.6 – *Total current consumption in the 3.3 V rail and total system power consumption of all the battery-powered components.*

Block	Component	Description	Supply voltage (V)	Current per unit		Units	Total power	
				Typical	Maximum		Typical	Maximum
NiMH charger	LTC4060EFE	NiMH/NiCd charger IC	5.5	2.9 mA	4.3 mA	1	16 mW	23.7 mW
	MDJ201	Power PNP BJT. Ice=0.95A, Ibe=120mA, Vce=1.8V, Vbe=0.7V	–	–		1	1.71 W + 84 mW ≈ 1.8 W	
	4.42 kΩ+NTC voltage divider	NTC pin. Assuming NTC at 50ºC (3.54 kΩ)	5.5	691 µA		1	3.8 mW	
Li-Ion/Li-Po charger	TP4056	Li-Ion/LiPo charger IC, Vbus-Vbat=1.8 V, Ibat=1 A	5.5	150 µA	500 µA	1	1.8W + 2.8 mW ≈ 1.8 W	
	DW01A	Battery protection IC	4.2	3 µA	6 µA	1	12.6 µW	25.6 µW
	FS825A	Dual power NMOS, Rds(on)=25 mΩ, Ibat=1 A	–	–		1	50 mW (both NMOS)	

Table 5.7 – *Typical and maximum estimated power consumption of both battery charger variants. These numbers do not contribute to the power budget, as the chargers are powered by the external supply used for charging the battery.*

Ni-MH charger worst-case efficiency			
Max. Input voltage	**Max. Input current**	**Min. Output voltage**	**Output current**
5.5 V	0.95 A + 111.5 mA	3.3 V	0.95 A
Maximum power in		**Minimum power out**	
5.84 W		3.14 W	
Worst-case efficiency			
53.77%			

Lithium charger worst-case efficiency			
Max. Input voltage	**Max. Input current**	**Min. Output voltage**	**Output current**
5.5 V	1.0 A + 52.8 mA	3.6 V	1.0 A
Maximum power in		**Minimum power out**	
5.79 W		3.6 W	
Worst-case efficiency			
62.20%			

Table 5.8 – *Worst-case efficiencies of both battery chargers. The calculus takes the maximum possible power input (both VUSB voltage and current consumption of the chargers' components, plus the programmed battery charging current) and the lowest output power (low battery voltage plus the programmed battery charging current).*

5.1.2.4 ESP32-WROOM-32D micro-controller, Wi-Fi and Bluetooth module

This block comprises the hardware configuration and GPIO pins connections of the ESP32-WROOM-32D module. The capabilities of this device have already been discussed at length in previous sections. Therefore, we will focus on its implementation particularities. In Figure 5.11 we can see the ESP32's symbol and connections, which is described on the following lines:

5.1.2.4.1 Decoupling capacitors

The capacitors below the ESP32 are decoupling capacitors, also called bypass capacitors. A decoupling capacitor removes unwanted AC components from a DC signal, making it more clean. It's a common and effective technique for filtering noise and ripple on power traces. A bypass capacitor should be placed as close to the IC's power pins as possible, to avoid trace inductance, noise coupling and guarantee voltage stability.

The ESP32 has an irregular, pulsed power consumption characteristic, accentuated when using radio communication. Big decoupling capacitors provide a charge reserve physically near to the component itself, which supplies energy to the SoC and prevents the supply voltage from decaying in short pulses. Thus, mitigating the effects of noise and supply voltage fluctuation that may appear on the rest of the components connected to the same power rail.

Recommended values for the bypass capacitors are two parallel 100 nF and 10 µF, ceramic and with low ESR [80] (page 21). They should be placed as close to the chip as possible, with short return paths.

An extra MLCC 22 µF capacitor was added as a charge reserve to filter out current spikes during ESP32 radio usage. The 47 pF was placed with the purpose of being more effective filtering high frequency components (such as radio communications or the CPU clock).

A real capacitor does not have an ideal frequency characteristic, in which its impedance decreases indefinitely with frequency. Instead, they have a clear resonance frequency caused by a Equivalent Series Inductance (ESL) which prevails at higher frequencies, an thus the magnitude of the impedance of the capacitor increases, as it can be seen in Figure 5.12. In addition, real capacitors posses a small series resistance (ESR) that also changes in frequency. SMD parts tend to have small ESL values thanks to the lack of leads. Also, smaller-value capacitors have smaller ESR and ESL values, making them suitable for decoupling high-frequency noise (and vice-versa).

Therefore, the reason behind using several capacitors of different order of magnitude in parallel is not adding their capacities, but due to their combined impedance and ESR frequency response. In Figure 5.12 we can also see the aggregate of the impedance modulus and ESR of the selected decoupling capacitors. As shown, a lower overall series resistance and impedance is achieved on a broad frequency range.

This curve is especially favorable since it presents its minimum impedance and ESR in the range of 1 to 2 MHz, where the DC/DC step-down power supply circuit works, which should help to efficiently filter switching noise. However, we must keep in mind that a series of resonances are drawn at 16 MHz and 830 MHz. Also, parasites gather significant value in both the sub-kilohertz and gigahertz regions. Fortunately, both the CPU working frequency (80 MHz to 240 MHz) and the RF frequency (the 2.4 GHz band) are not severely affected.

5.1.2.4.2 Pin restrictions

Some ESP32's GPIO pins behave in a way that prevent using them freely or under certain circumstances. They are marked on the legend on the ESP32 symbol (Figure 5.11).

- **GPIOs whose usage is not recommended.** According to the ESP32-WROOM-32D datasheet, GPIO6 to GPIO11 (pins 17 to 22) are connected to the integrated SPI flash memory and their usage is not recommended [80] (page 9). These pins are marked in red in Figure 5.11.

  However, we were forced to use a couple of these pins to implement some functionality. We were cautious selecting the pins: according to previous work carried out in Irene Gil's bachelor thesis [105], GPIO6 and GPIO8 are safe to use when the booting sequence is completed. These pins are pulled down once the PWM signal stops (Figure 5.13). Besides, the function of these pins will be input-only and attached to non-sensitive signals: two plug insertion detection switches from two different jack ports (see Expansion port and Load cell amplifier sections).

  On the However, as will be seen in Section 6.3: Verification, the use of these pins caused problems when trying to program the device due to a conflict with the SPI flash memory. Nevertheless, it is a fixable bug in later hardware revisions.

- **The ADC2 peripheral is unavailable if using radio.** The ADC2 peripheral is unusable while using Wi-Fi or Bluetooth, and should be left unused if not necessary. Digital input/output work on those pins while radio is ON [79]. These pins are crossed out in red in Figure 5.11.

- **Strapping pins.** Strapping pins are pins whose digital state are registered during boot. They modify the booting sequence parameters according to the table shown in Table 5.9. We must make sure that if pull-up/down resistors are connected to these pins (e.g. for buttons) they do not alter the default configuration unintentionally. These pins are marked with blue in Figure 5.11.

- **Input-only GPIOs.** GPIO34, GPIO35, GPIO36 and GPIO39 cannot be used for output. Since they are connected to the ADC unit 1, they will be used for reading the piezoelectric sensors' analog signals. These pins appear with a triangle pointing to the ESP32, whereas input/output GPIOs are marked with two triangles in Figure 5.11.

- **Pins which output of digital/PWM signals during boot.** Apart from the non-recommended GPIOs, other pins also have some kind of digital activity during boot [150]. These pins are marked with a green frame in Figure 5.11. Therefore, these pins are used for input or for non-critical outputs such as the SPI chip selects (since the rest of the SPI bus pins do not have this problem, no activity will occur on the bus).

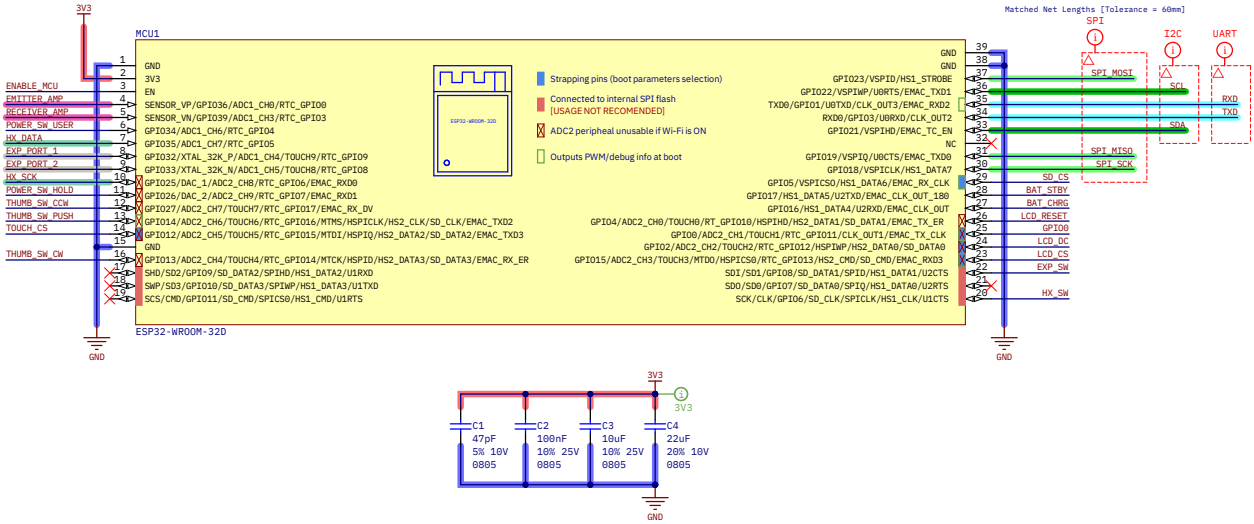

Figure 5.11 – *ESP32-WROOM-32D module circuit symbol and connections.*

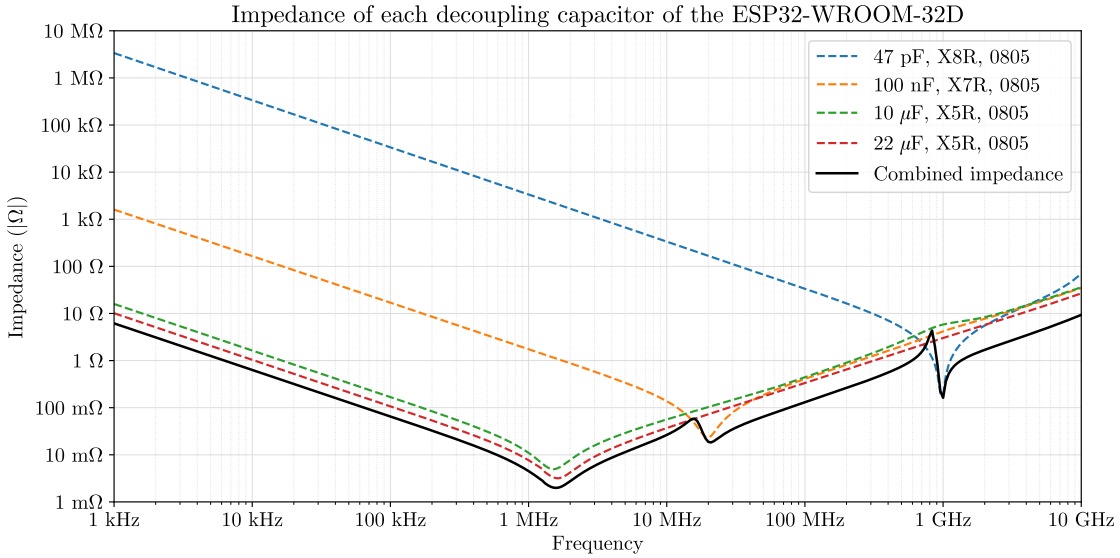

(a) *Modulus of the impedance of the individual capacitors.*

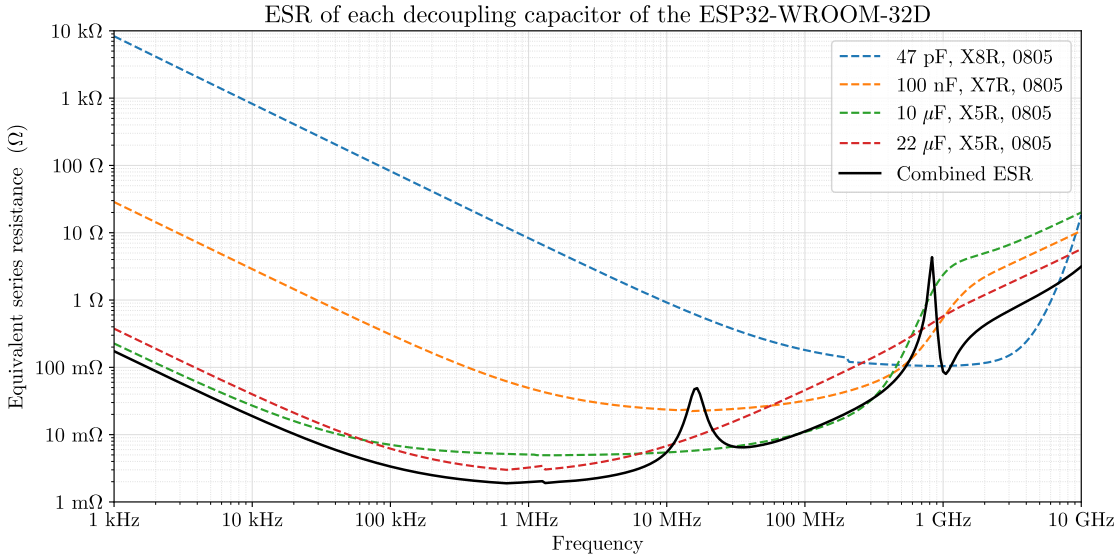

(b) *ESR of every capacitor.*

Figure 5.12 – *Curves of the magnitude of the impedance and Equivalent Series Resistance of the selected decoupling capacitors for the ESP32-WROOM-32D module; and the combined impedance and ESR of all of them (in parallel). Data extracted from Kemet K-SIM 3 simulator [151]. The 47 pF (C0805C470K8HAC) and 100 nF (C0805C104K4RACAUTO) capacitor models used for this representation are the exact parts placed on the PCB; whereas for the 22uF and 10uF capacitors equivalent Kemet models were used (22uF: C0805C226K8PAC and 10uF: C0805C106K8PACAUTO, instead of Samsung's CL21A226KPCLRNC and CL21A106KPFNNNF, respectively).*

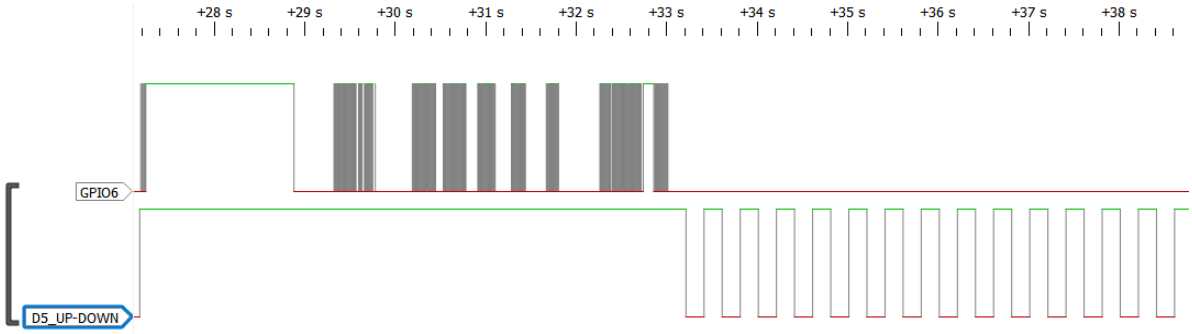

(a) *Registered logic levels on GPIO6 during boot.*

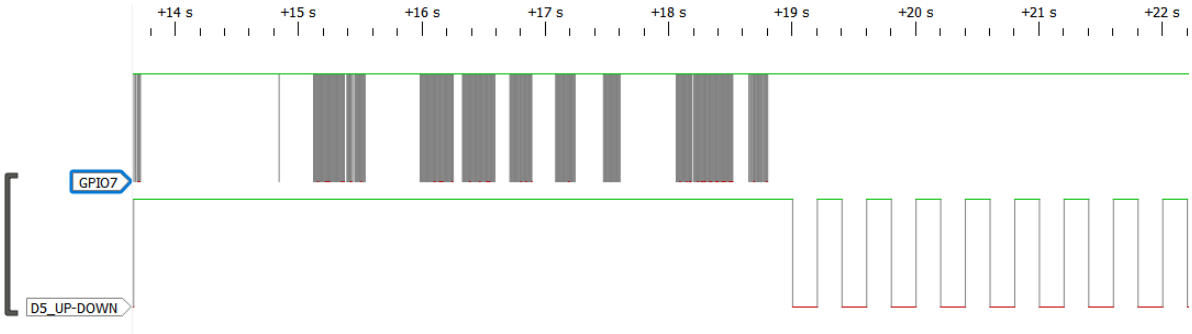

(b) *Registered logic levels on GPIO7 during boot.*

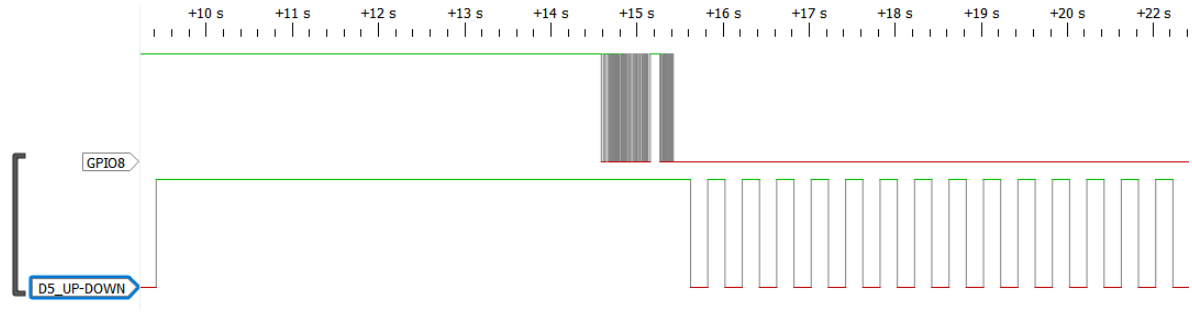

(c) *Registered logic levels on GPIO8 during boot.*

Figure 5.13 – *Pin behaviour of GPIO6 to GPIO11 during boot of an ESP32-WROOM-32D* ***(part 1 of 2)****. Extracted from Irene Gil's Bachelor Thesis [105] (figure 4.4, page 87). The images show the recording of signals with a logic analyzer. The program uploaded to the ESP32-WROOM-32D consists of turning on and off a LED (named D5) with the respective GPIO every second.*

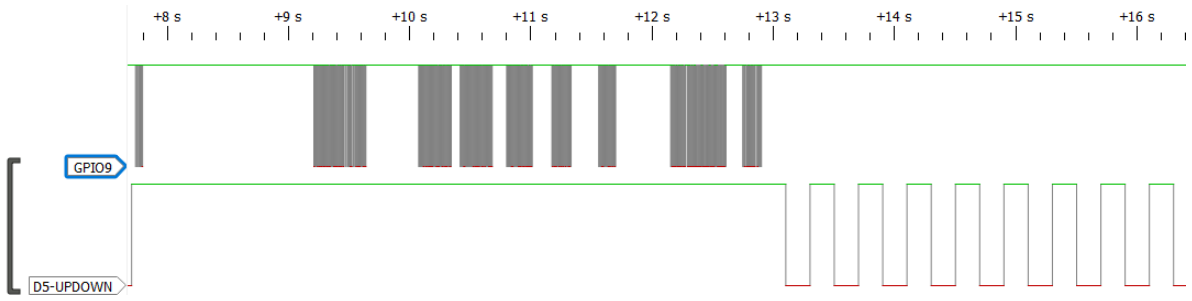

(a) *Registered logic levels on GPIO9 during boot.*

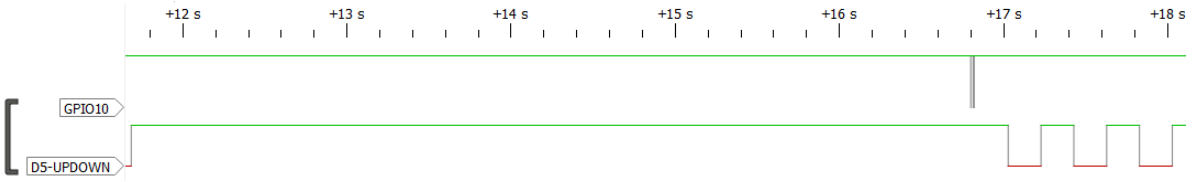

(b) *Registered logic levels on GPIO10 during boot.*

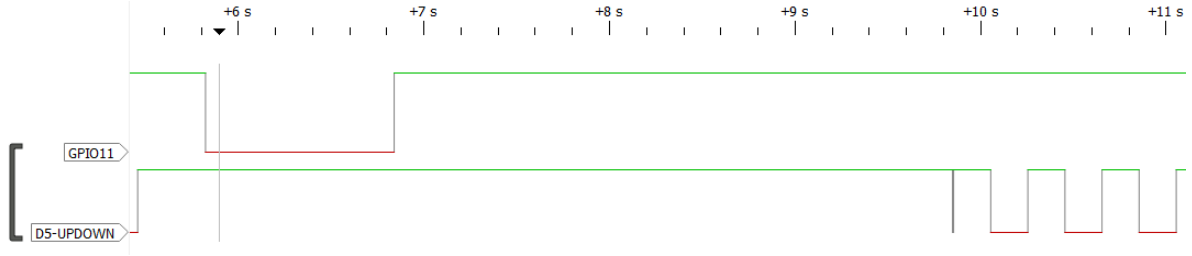

(c) *Registered logic levels on GPIO11 during boot.*

Figure 5.14 – *Pin behaviour of GPIO6 to GPIO11 during boot of an ESP32-WROOM-32D* ***(part 2 of 2)****. Extracted from Irene Gil's Bachelor Thesis [105] (figure 4.4, page 87). The images show the recording of signals with a logic analyzer. The program uploaded to the ESP32-WROOM-32D consists of turning on and off a LED (named D5) with the respective GPIO every second.*

5.1.2.5 USB port

Figure 5.15 specifies the USB port pin connections. `VBUS` is the USB bus voltage, expected between 4.5 V to 5.5 V. The USBLC6-2SC6 protection IC puts a limit of 5.5 V to the `VBUS` thanks to its integrated Zener diode. This device is also responsible for protection against Electro-Static Discharge up to 15 kV. The ESD protection IC should be as close as possible to the USB connector to prevent the pulse from traveling through the board and damaging other circuits. Additionally, a Ferrite Bead is placed in series in the power net as an Electro-Magnetic Interference suppressor.

The cable ground is connected to our system's global GND. `SH` pads are the USB's connector metal casing, which connects to the USB cable's metal shielding (in case it has one). These pads provide mechanical integrity to the port. This particular connector has 4, what makes it very robust. Shield pads are not connected to any circuit traces, not even ground. In any case, they should be connected to the device's metal chassis (as a Faraday cage, which we do not have). Connecting the cable shield to GND could increase EMI as the cable would work as an antenna.

On the other hand, both the USB Mini-B and the CH340C USB-to-UART conversion IC are USB 2.0 capable. The USB 2.0 specification places the maximum bus speed at 480 Mbps. Although we may not use all of its capabilities the data traces are parameterized as differential.

5.1.2.6 USB to UART and auto-programming circuit

The CH340C is an USB bus conversion chip which can translate from USB 2.0 to UART and vice-versa. It also can send the RTS, DTR, DCD, RI, DSR and CTS MODEM signals. RTS and DTR are used by the ESP32 program uploader tool to reset and select the boot mode according to Table 5.9, allowing the automatic programming of the MCU from a PC without needing to press the Boot Selection button. Consult the implemented circuit in Figure 5.16.

The CH340C has an integrated oscillator, which eliminates the need for an external crystal. Also, it can be powered by 3.3 V or 5 V. In the case of being powered by 3.3 V the `V3` pin must be connected to the supply voltage and a Bypass capacitor must be placed [113]. LEDs on TX/RX and RTS/DTR signals are for debugging purposes, but they proved to be not very useful (see Section 6.3: Verification). The values of the LED's resistors are a placeholder, they will be higher in a mounted board (ranging from 470 Ω to 1 kΩ).

5.1.2.7 Reset and boot selection buttons

As its name suggests, the reset button force a reset on the ESP32 by pulling down its Enable pin (pin nº3, named "EN"). The boot selection (or *bootsel* for short) forces entering the Download boot if it is pressed after a reset, by pulling down the GPIO0 strapping pin (see Table 5.9 and Figure 5.17). Both buttons are generic 2-lead SMD buttons. The HRO Electronics K2-1107ST [152] has been followed as a reference. Both of these buttons are for debugging purposes, and will not be available for the user.

Both buttons have a 100 nF *de-bouncing* capacitor in parallel, which is intended to palliate the buttons' contact bounces. The `ENABLE_MCU` net also has an extra 1 µF to ensure power stability to the microcontroller during powerup. This capacitor is recommended by the manufacturer [78] (page 22). The 10 kΩ R12 pull-up and the 1 µF C19 capacitor form a RC filter which introduces a delay on the Enable pin:

$$\tau = R \cdot C = 10\,\text{ms} \quad \Longrightarrow \quad t_{10\%-90\%} = \tau \cdot (\ln(0.9) - \ln(0.1)) \approx 22\,\text{ms} \tag{5.1.10}$$

This gives the PDS enough time to stabilize the supply voltage before the MCU is enabled. This delay is visible in circuit simulations (Appendix C: Simulations) and in validation tests (Section 6.4: Verification).

Voltage of internal LDO (VDD_SDIO)			
Pin	Default	VDD_SDIO = 3.3 V	VDD_SDIO = 1.8 V
GPIO12/MTDI	Pull-down	0	1

Booting mode			
Pin	Default	SPI boot	Download boot (programming)
GPIO0	Pull-up	1	0
GPIO2	Pull-down	Don't care	0

Enabling/Disabling debugging log print over UOTXD (UART TXD) during boot			
Pin	Default	U0TXD Active	U0TXD Silent
GPIO15/MTDO	Pull-up	1	0

Timing of SDIO slave					
Pin	Default	FE Sampling FE Output	FE Sampling RE Output	RE Sampling FE Output	RE Sampling RE Output
GPIO15/MTDO	Pull-up	0	0	1	1
GPIO5	Pull-up	0	1	0	1

Table 5.9 – *Strapping pin configuration during boot on the ESP32. Extracted from ESP32's data sheet [78] (Table 5, page 21). FE: Falling Edge, RE: Rising Edge.*

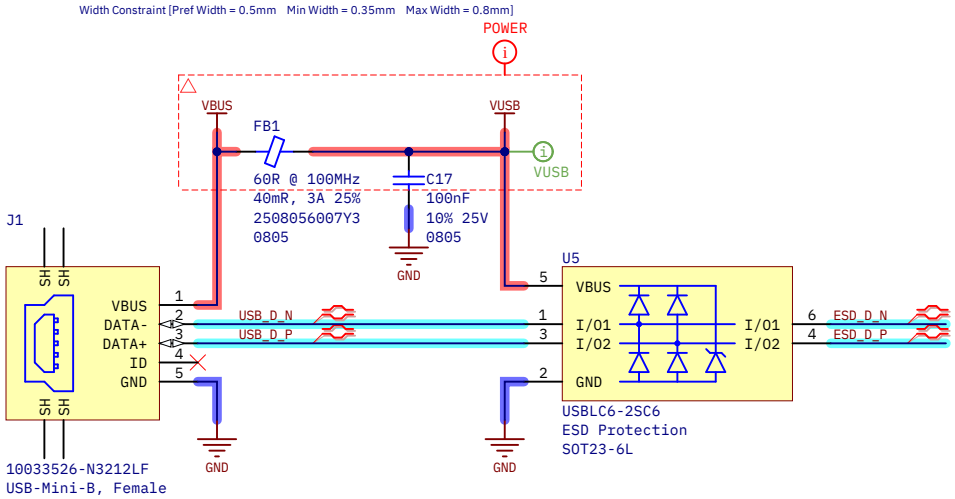

Figure 5.15 – *USB-Mini-B port connections and ESD protection IC.*

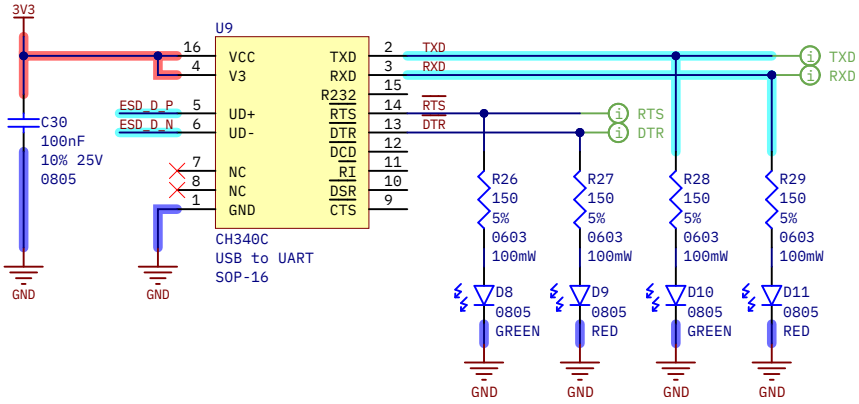

(a) *CH340C USB to serial converter. s' series resistors are only placeholders, and its values will be higher in reality (from* $470\,\Omega$ *to* $1\,\mathrm{k}\Omega$*).*

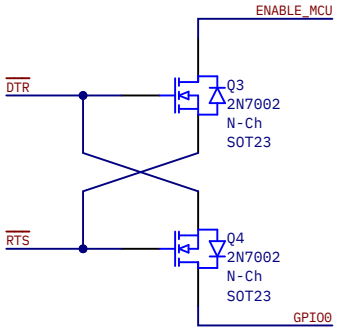

(b) *Auto-programming signaling circuit (right).*

Figure 5.16 – *CH340C USB to serial converter and auto-programming circuit.*

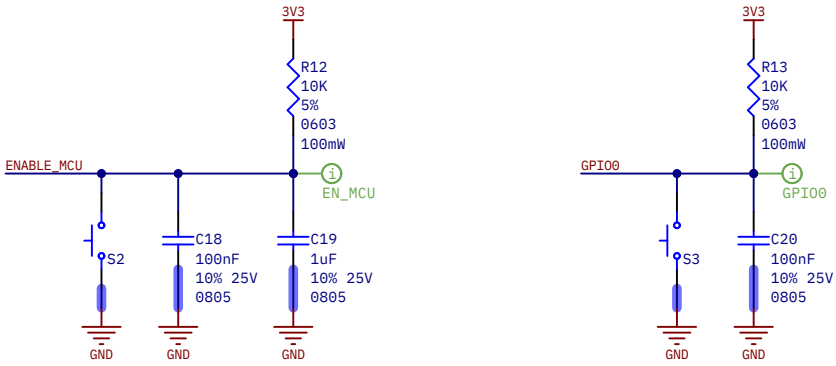

Figure 5.17 – *Reset (left) and boot selection (right) buttons.*

5.1.2.8 Power-up button

Instead of a traditional power switch, it has been decided to mount a power-on circuit based on a push button. Nowadays, this is taken for granted and appears in a large number of electronic devices. Usually, it is natural for the user and goes unnoticed, but the implementation has some complexity and requires a combination of hardware and software. Additionally, the button gives the considerable advantage of being able to manage the shutdown via software. This way, we can request a shutdown confirmation by the user to avoiding accidental power downs and the loss of information that may entail.

The power button circuit (Figure 5.18) operating principle is as follows:

1. When the button is not pressed, the tension in PMOS gate will be pulled up and approximately equal to V_{meas} (the battery voltage after the current measurement); and thus V_{SG} is not greater than V_{th} and so the PMOS is off.

2. When the button is pressed, gate voltage is pulled down, so V_{SG} will be greater than V_{th} and the PMOS allows current to pass through its source and drain.

3. The voltage rises on D12's anode, and since the `ENABLE_DCDC` node is weakly pulled down, the voltage difference on the diode will be greater than its V_{f}, so it allows current to flow and elevates the voltage on the `ENABLE_DCDC` net.

4. A voltage above 1.5 volts is sufficient to enable the AP3429K [131]. For the TLV62529 the margin is narrower at 2.5 volts [130].

5. The 3.3 V rail is now active, which turns on the rest of the system, including the ESP32.

6. The microcontroller boots over after the button has been pressed for a few moments, and immediately pulls up the pin connected to the `POWER_SW_HOLD` node. This maintains the `ENABLE_DCDC` net on high.

7. The user can release the power-up button now. The system will be on until the user sends a shutdown signal by GUI interaction or by pressing this button again (both ways the shutdown is via software).

8. When the shutdown is confirmed by the user, the ESP32 will get ready for power off. As last step, it pulls down the pin connected to `POWER_SW_HOLD`, and the system powers down completely.

5.1.2.9 Navigation "thumb" button

The HRO Electronics K1-1502SA [104] multi-function two-directional rotary slider and button provides a convenient way to navigate the GUI without using the touchscreen. Its circuit is shown on Figure 5.19.

It has five pins: three to detect when the user has performed one of the 3 possible actions, one for GND and the other for mechanical union. Pin 1 identifies a counterclockwise (CCW) turn, pin 2 a clockwise (CW) turn, and T registers a button press. All 3 lines are connected to GND when activated, so 3 corresponding pull-up resistors have been added. In contrast, only pin T needs a de-bouncing capacitor.

5.1.2.10 TFT LCD touchscreen and SD card reader module

The ILI9341 2.8" TFT LCD module has has the bigger footprint of all the components, with two separated jumpers, one on each board extreme. Note how the SPI bus is connected to 3 different set of pins, as it will interface with 3 different devices in the same module: the SD MMC, the ILI9341 display controller and the XPT2046 touchscreen controller.

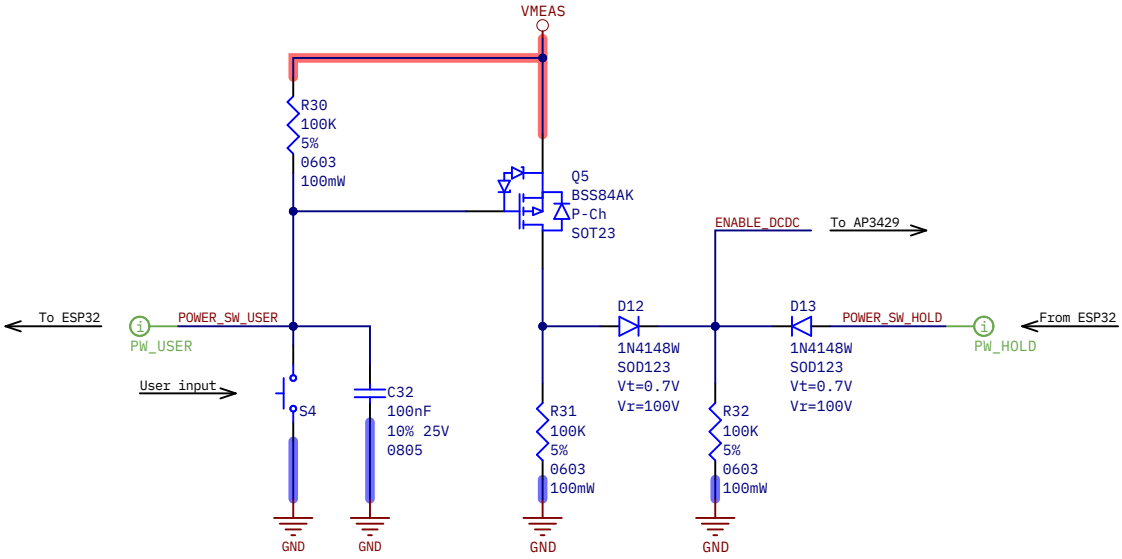

Figure 5.18 – *Power-up button circuitry.*

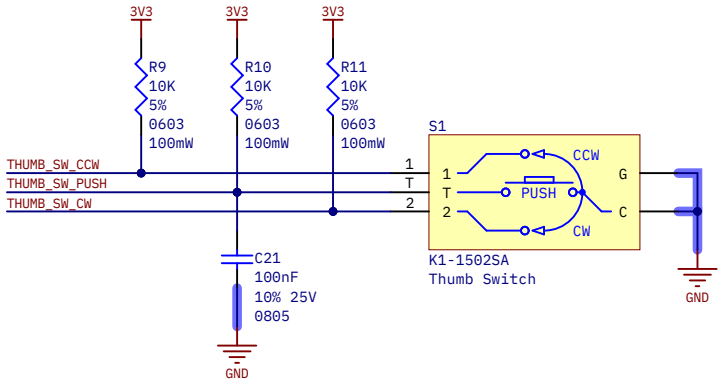

Figure 5.19 – *Multipurpose, multidirection "thumb" switch.*

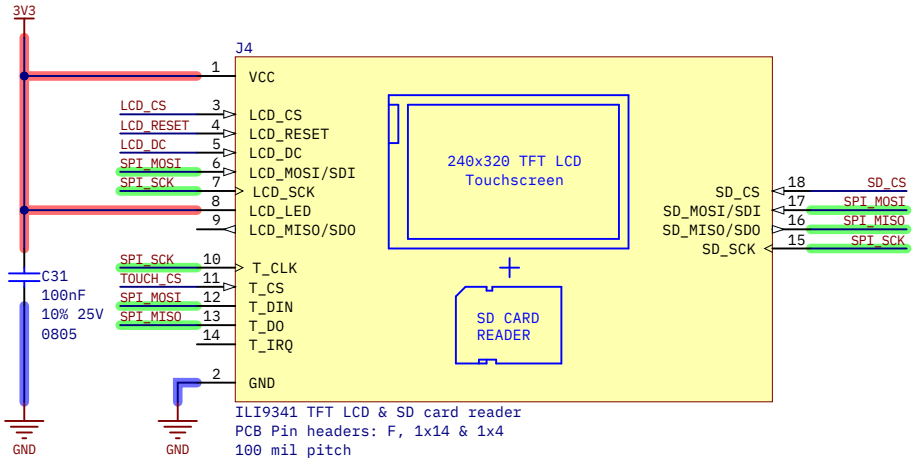

Figure 5.20 – *TFT LCD touchscreen and SD card reader module connections.*

The display module also needs mechanical support, and it has four mounting holes for it. Our PCB will inherit the position of said holes. The form factor of the PCB will in turn be affected by the screen dimensions. See Subsection 5.1.3.3: Form factor. Dimensions and mounting holes for more detail.

5.1.2.11 Signal conditioning

As seen in Chapter 3: Signal analysis and processing, the pulse of the emitter signal will be in the range of 15 V to 100 V. Therefore, to avoid damaging the rest of the electronics, the 1N4148W diodes placed in antiparallel clip the input signal to a safe range of $V_{\text{BIAS}} \pm V_f$; where $V_f \approx 0.7\,\text{V}$. Although such a wide voltage range is not expected to happen normally at the receiver, a pair of diodes are also placed for safety.

The dual LMV358 OpAmp will amplify the emitter signal to saturation of the supply rails, creating very steep slopes so that the instrument can easily detect them as a flank. On the other hand, the receiver signal has a much lower amplitude and the circuit is also designed with a more plain and restrained gain. This is due to avoid any distortion that could interfere with the arrival detection. This signal will probably be amplified without saturation.

For a more detailed explanation on the simulation's constraints and a deeper understanding of the functioning of the adequation circuit, see Annex C: Simulations.

5.1.2.12 Load cell amplifier

The circuit on Figure 5.22 is based on Sparkfun's open hardware HX711 breakout board [103] and AVIA Semiconductor's reference schematic [102].

A CUI Devices SJ-43516-SMT [153], a 4-pole, 6-pin, 3.5 mm female jack connector with two switches for plug insertion detection is used as a load cell port (for an explanation of switch operation, see the next section). The downside of this receptacle is that it does not provide a fifth connection for the shield that some load cells have (usually is a yellow cable). Although recalling the explanation given in Section 5.1.2.5: USB port, the shield would not be connected to any net.

Resistors in series with the `A+`–`INA+` and `A-`–`INA-` serve as short-circuit protection, limiting the current on both pins. They also set an input impedance. The capacitor between `INA+` and `INA-` removes differential-mode noise without affecting the measurement since signals from load cells change very slowly. For noise and EMI filtering on `AVDD`, Sparkfun's design uses a 2.2 uH chip inductor. Instead of this, we use a Ferrite Bead which serves the same function. Additionally, a set of bypass capacitors for noise filtering and voltage stabilization are placed on the 3.3 V power rail.

The HX711 `VBG` and `VFG` pins are connected to the same voltage reference fixed as 1.25 V. `VBG` capacitor is mandatory to guarantee voltage stability [102]. `AVDD` is the analog voltage source generated by the HX711's internal regulator with the aid of Q6, a BC858 PNP BJT pass transistor. The output voltage is configured by this relation:

$$V_{\text{AVDD}} = V_{\text{VGB}} \cdot \frac{\text{R36} + \text{R38}}{\text{R38}} \tag{5.1.11}$$

Which always should be less than `VSUP` - 100 mV. In our this design:

$$V_{\text{AVDD}} = 1.25\,\text{V} \cdot \frac{22\,\text{k}\Omega + 10\,\text{k}\Omega}{22\,\text{k}\Omega} = 1.82\,\text{V} \tag{5.1.12}$$

HX711 will transmit its measurements in 24 bit, 2's complement, raw ADC data continuously when enabled by a clock signal. Before operation, the system needs a software calibration with a known weight for

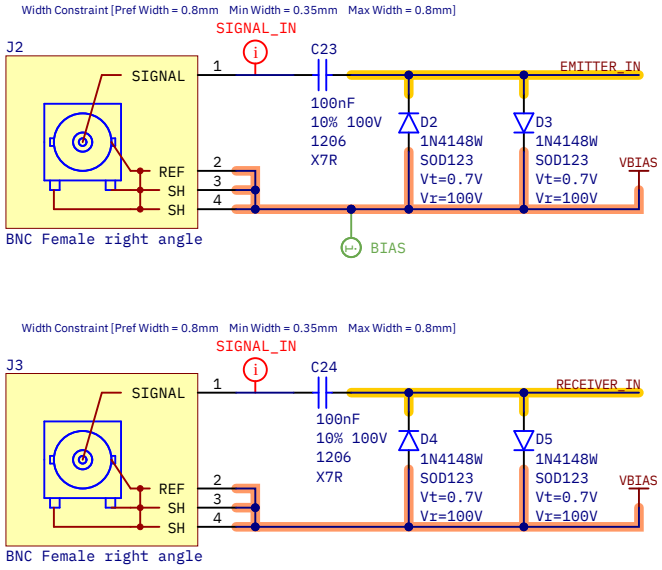

(a) *BNC connectors, coupling capacitor and diode input voltage limiting.*

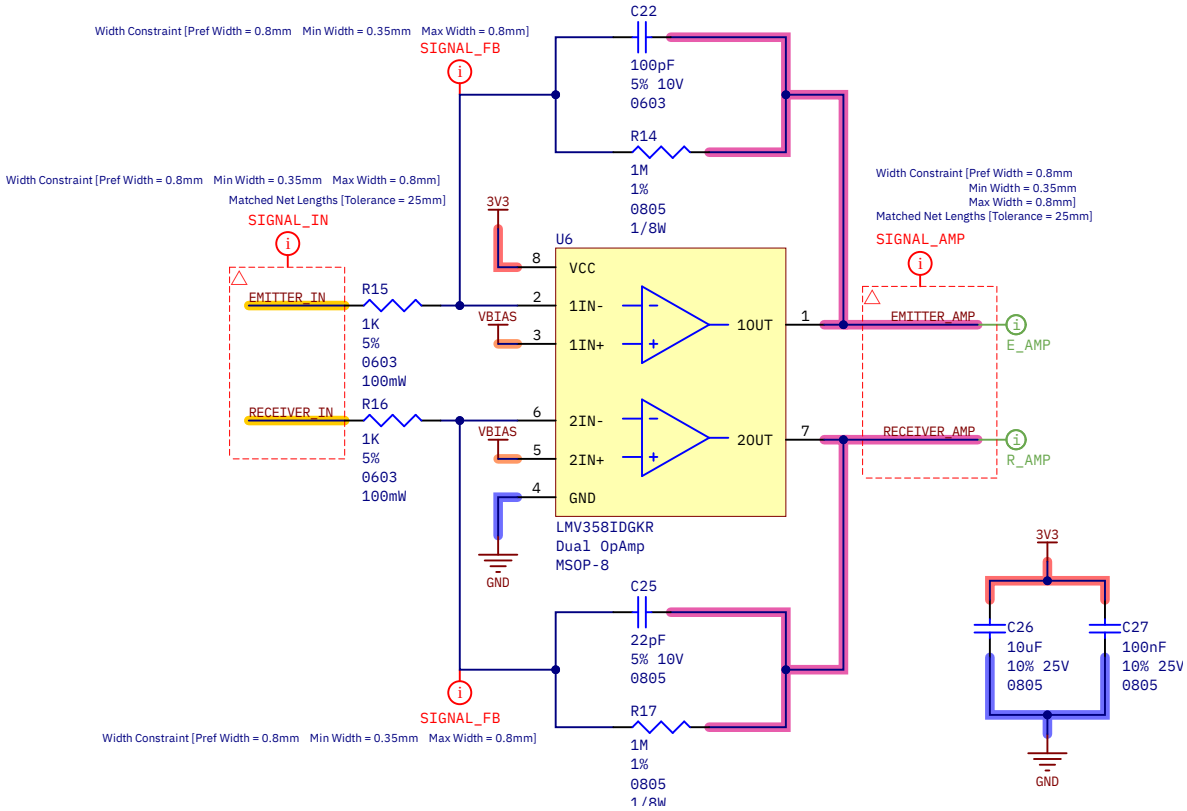

(b) *Operational Amplifier conditioning circuit.*

Figure 5.21 – *Expansion port circuit.*

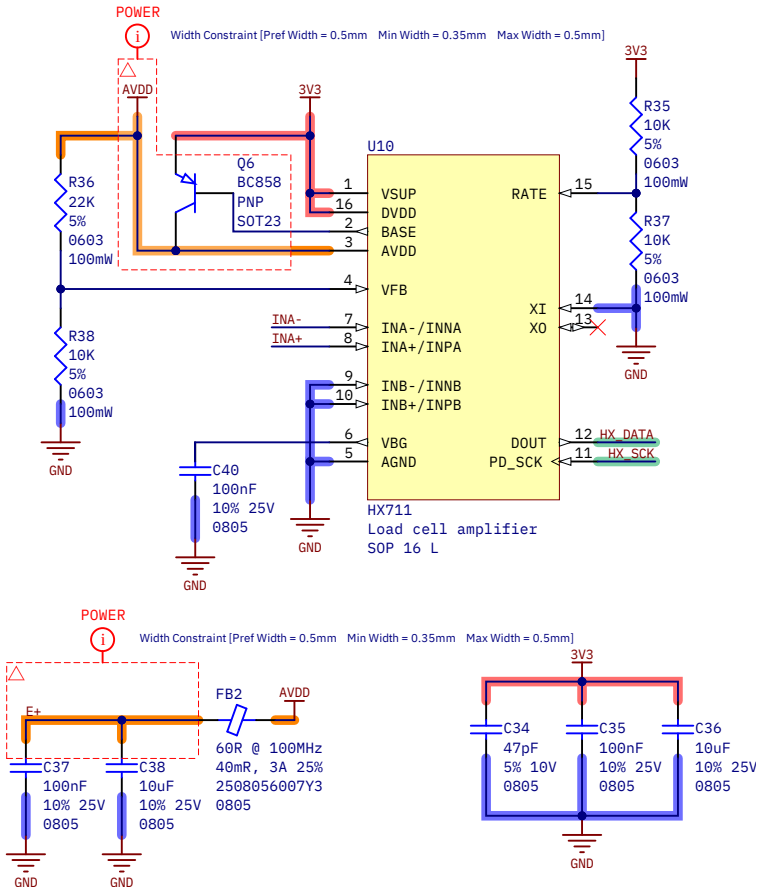

(a) *HX711 load cell amplifier configuration. AVDD regulation and filtering.*

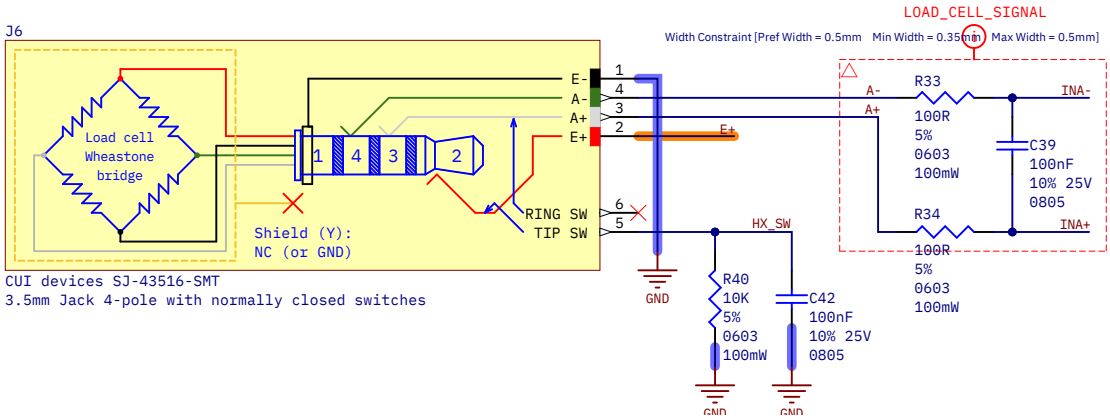

(b) *Load cell jack connector.*

Figure 5.22 – *Load cell amplifier circuit.*

extracting the readings' conversion factor for our specific design. On the other hand, the RATE pin configures the transmission rate. When pulled up the HX711 sends measurements at a "fast" rate of 80 Sps; and "slow" (10 Sps) when pulled down. In "fast" mode measurements are expected to be noisier. Only one of the R35 and R37 resistors should be populated at a time.

5.1.2.13 Expansion port

The expansion port uses another CUI Devices SJ-43516-SMT [153] 3.5 mm jack receptacle. As in the previous case, we are using a jack connector in a non-standard application, as we are not transferring audio but power and/or analog and digital signals of different nature. Nevertheless, we have adjusted the connector to somewhat fit the OMTP convention (in sleeve, signals in rings). Expansion port pins are connected both to two ESP32 input/output pins which are channels of the ADC1, so we are giving the maximum amount of functionality available to the expansion module.

The plug detection switches are normally closed, shorting pins 2-5 (tip) and 3-6 (ring). When the male jack connector is inserted, both switches open. We are only using the tip switch to allow mounting both SJ-43516 (6 pads) and SJ-43515 (5-pads) models. We prefer the 6-pad version as it offers more mechanical integrity. The pin 5 has a pull-down resistor, so normally EXP_SW is HIGH. When a connector is plugged in, the switch opens and EXP_SW changes to LOW.

To avoid shorting GND and VCC when inserting the connector, the 3.3 V rail is located at the tip, so it will make contact the last. This also allows us to easily add the tip switch circuitry. Since this is an external connector directly connected to the system's main power rail, a current limit switch and ESD protection IC (the Texas Instruments TPD3S014TDBVRQ1) is placed to avoid damaging the device.

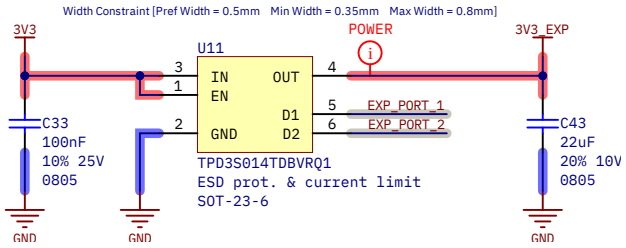

(a) *Expansion port jack current limit switch*

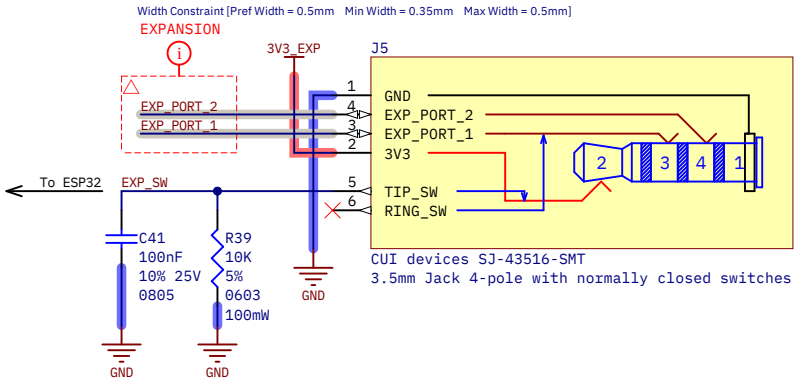

(b) *Expansion port jack connector.*

Figure 5.23 – *Expansion port circuit.*

5.1.3 PCB design

This section dives into the design of the PCB, where all the applied concepts are explained, as well as the different design decisions made and that make up the last version of TIK's printed circuit board.

5.1.3.1 PCB design rules

The Altium Designer PCB editor uses design rules to define all requirements and constraints of the design: trace widths, clearances, plane connection styles, routing via styles, and so on. These rules form an *instruction set* for the Design Rule Checker (DRC). Rules are classified in a hierarchy which defines their priority and scope [154].

As discussed in Section 6.1: PCB fabrication, the designed PCBs will be manufactured by JLCPCB. Therefore, we must stick to the design rules of this manufacturer, which can be found on its website [155, 156]. But instead of copying them one by one, we can import them all into Altium Designer thanks to the work of A. Özgür (@ayberkozgur), which collected these rules in a single `.rul` file and uploaded them to a public Github repository [157].

5.1.3.2 Form factor. Dimensions and mounting holes

The chosen form factor is simple: it is a 132x54 mm rectangle, with rounded corners with a radius of 2 mm. Rounded corners give a more finished appearance to the PCB and eliminate sharp corners, which can cause problems during assembly or handling. The shape of the PCB obeys many restrictions that appear during development, such as the size of the components that are mounted on it, the free space required for some of them, the necessary physical proximity of certain components or blocks... etc. The main components that have defined this shape are the larger ones: the LCD module (86x50 mm), the BNC connectors (15x36 mm) and the ESP32 (18x26 mm, plus antenna clearance). As said before, we inherit the LCD module mounting holes for our PCB.

A simple schematic of the PCB form factor is shown in Figure 5.24. For a more detailed mechanical description as well as more exhaustive dimensions, consult Appendix D: PCB schematics.

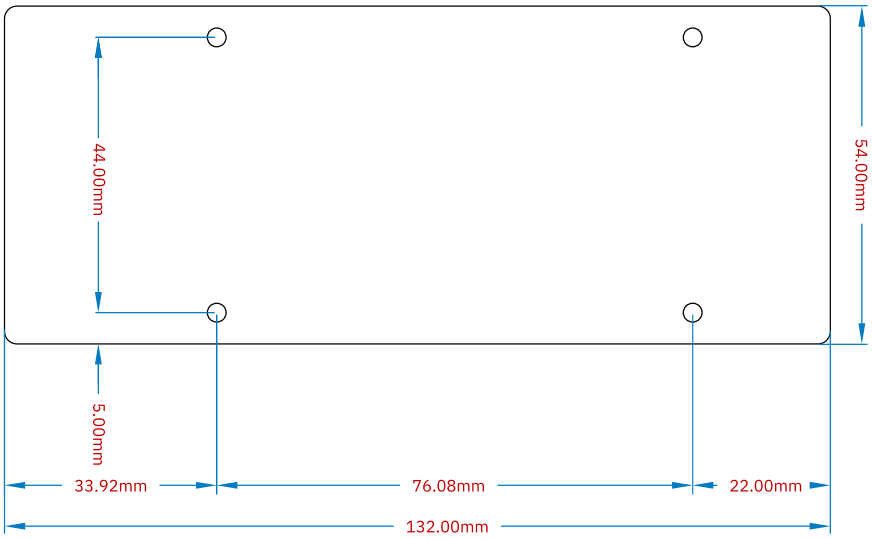

Figure 5.24 – *PCB form factor and fundamental dimensions.*

5.1.3.3 Layer stack-up

As explained in subsection 4.2.1, a Printed Circuit Board is made up of layers of copper and dielectric. The developed PCB has been implemented in only two layers of copper with a height of 35 um, with a dielectric type FR-4 of 1.5 mm thickness (Figure 5.25). The total thickness of the board is approximately 1.6mm, a typical value in the industry and standardized by PCB manufacturers.

It is true that the PCB could be thinner (other standardized values are 0.4, 0.6, 0.8, 1.0 and 1.2 mm) and therefore achieve better electrical characteristics, but it has been kept this way because the quality obtained is sufficient for our prototype, and because the thickness gives our PCB extra rigidity.

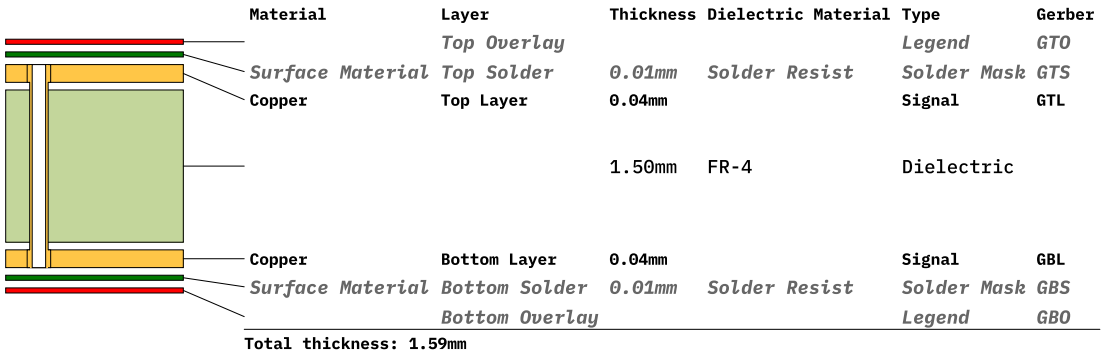

Figure 5.25 – *PCB layer stackup.*

5.1.3.4 Good design practices and EMI reduction techniques

This section details some relevant practices in the design of PCBs applied throughout our development. These techniques make it possible to avoid common manufacturing and operational problems.

- **Trace routing angle.** A common concern is having sharp-angle PCB tracks due to the possibility of causing radiated Electro-Magnetic Interference. A common assumption is that high-frequency signals emit RF radiation at every sharp turn of a copper track. However, electrons have minimal problems navigating even right-angle corners; with the exception of microwave and ultra high-frequency designs. Otherwise, they are not a major concern [158].

  Therefore, it has been decided to keep the default and traditional 45º routing shape.

- **Power planes.** The planes are large copper polygons belonging to a net. Power plans are those that belong to a power net, such as GND or a power rail. Planes have great benefits in terms of signal integrity and impedance control, as we will explain below [159]:

  – **Well-defined impedance:** Having a ground plane allows to approach the traces as *microstrip* (see Figure 5.26). Therefore, the design of the trace impedance becomes simpler.

  – **Clear return paths:** A ground plane provides the shortest and widest return path for currents. This helps to make our circuit loops small, and therefore with low inductance, ensuring low EMI coupling.

  – **Decoupling and stable power:** A pair of large power and ground planes will act like a big decoupling capacitor.

  Since we are using a two-layer design, we are going to restrict ourselves to using only ground planes, on both top and bottom layers.

- **Placement and values of decoupling capacitors.** As explained in detail in paragraph 5.1.2.4.1, a Bypass capacitor should be placed as close to an IC's power pins as possible in order to guarantee voltage stability and reduce loop inductance and thus noise coupling.

  The IC will first source power from a bulk capacitor when its consumption suddenly increases, since they provide the physically nearest charge reserve to the IC itself. This prevents the supply voltage from decaying in short pulses, thus avoiding causing supply voltage fluctuation on the rest of the components on the same power rail.

  Large capacitors are good power reservoirs and good low frequency noise filters, but they have a slow charge constant, increase power-on inrush current, and are not effective at high frequency. For this reason, as we saw in Figure 5.12, it is interesting to place several capacitors in parallel to filter a broad spectrum, specially in delicate components or those that cause noise, as is the case of ESP32, the DC/DC converter output, the LDO input, or the Operational Amplifier of the adequation circuit. For ICs that don't require as much care, a 100 nF decoupling capacitor is a common value that offers a good compromise between capacity, performance, and frequency response.

- **Via shielding.** Via shielding reduces crosstalk and EMI, and it is extensively used to shield RF traces. A *via shield* is created by placing one or more rows of vias alongside a signal's route path [160] (see Figure 5.28a).

  In our case it has been used to protect the analog signals from the piezoelectric sensors, and also to reduce the possible crosstalk between the SPI traces, which are high-speed and close together.

- **Via stitching.** Via stitching ties larger copper areas on the same net on different layers to create a strong vertical connection through the board structure, and tie areas of copper that might otherwise be isolated from their net. This maintains a low impedance and short current return loops [160] (see Figure 5.28b).

  In our design, it has been applied via stitching to the top and bottom GND planes, so that the quality of the ground is the best possible on the entire PCB.

- **Teardrops.** Teardrops are extra copper that fillets out from the trace to the edges of a pad or via's annular ring, and makes the connection stronger to thermal and mechanical stress. Examples are shown in Figure 5.27. The most common style of PCB teardrop is *rounded* because it modifies trace properties slightly while still being strong. This is a valuable feature when the design objects are small or for drilled pads and vias; since it paliates the effects of drill wander and layer misalignment during fabrication [161].

  There is no reason not to use this feature, which will be applied to all the traces.

- **Power trace over-dimension.** It is advisable to oversize the width of the power traces above the width calculated for the expected maximum current consumption. It can be helpful in order to respond correctly to sudden increases in power consumption (typical of the digital systems that have been implemented) or during the power-up inrush current; thus avoid heating or even burning traces. Traces will also have lower voltage and power losses due to decreased resistivity.

- **Plated mounting holes with screw head landing.** As pictured in Figure 5.29, there are various ways to design a PCB mounting hole [162]:

  - We can simply drill the PCB and create a clearance rule. The rule avoids exposing the copper to the hole edge, to prevent screws that may scratch the PCB from causing a short circuit. This option is the easiest and cheapest, but it can result in damage to the PCB surface when the screw is tightened against it.
  - Copper pads around the mounting holes usually have the purpose of connecting the screw to a circuit net such as GND or earth and usually include vias to electrically connect the pads on opposite sides of the board. This is since many mounting holes are not plated to prevent the screw from scratching the copper and generating conductive micro-particles. This mounting hole style is more resistant than the previous one.

We are going to use M3 plated mounting holes (with sufficient screw tolerance), with isolated head landings in both sides. In our case it is not important for the screws to be connected to ground, and thus we avoid injecting noise into the reference voltage, since metal screws can function as antennas if improperly used. Holes with copper do not imply an extra fabrication cost, since the manufacturer charges by the PCB area and not by copper surface.

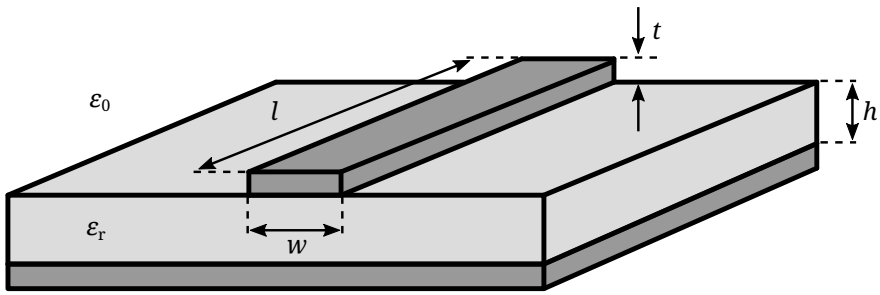

Figure 5.26 – *Representation of a microstrip line. Where ε_0 is the dielectric constant of vacuum, ε_r is the dielectric constant of the insulating material, w is the conductor width, l is the conductor length, t is the conductor thickness and h the dielectric height from the ground plane to the conductor. Credits: [163].*

5.1.3.5 Trace properties

To size the traces correctly to the requirements, we use a specialized calculation program called Saturn PCB Design Toolkit [164]. This application incorporates many features for PCB engineers, such as trace and via maximum current, capacitance and inductance, crosstalk, differential pairs, etc.

The designed properties for the different traces are detailed below. For DC characterization, a trace temperature increase of 10ºC over a standard ambient temperature of 25ºC in a FR-4 dielectric is considered.

- **10 mil (0.254 mm) wide traces.** This trace width is the default for our design. The trace conductor properties per centimetre can be consulted in Figure 5.30b. It is thin so we can save space when routing, but has the worst DC characteristics and should not be used for power delivery. Also, these are the kind of traces used by by the SPI bus. The skin depth is not optimal, but this will depend on frequency. Also, AC current is not a critical aspect here.
- **0.35 mm wide traces.** (Figure 5.30c) These traces are used to connect power pins to the power net in low-power components whose pins are very close together and cannot fit a wider trace without breaking design rules. This trace width has adequate DC and AC properties and smaller losses than the 0.254 mm ones, and they could be used for low-speed mixed-signal if needed, such as the expansion port data lines.
- **0.5 mm wide traces.** (Figure 5.30d) An optimal width in terms of area/specs for power delivery as it can withstand a lot of current (much more than the system will continuously need) with low losses.
- **0.8 mm wide traces.** (Figure 5.30e) This trace width is employed by the analog signals to maintain good signal integrity at low line impedance. It is also used as a power rail throughout the board to ensure low voltage losses by distance, and to deliver power for devices with a pulsed and aggressive consumption such as the ESP32 and the LCD.
- **Via characteristics.** We are using only use one type of via, with a 0.3 mm drilled diameter and a 0.6 mm diameter plating (see Figure 5.30a). This via is convenient as it is small, has very low parasite effects and thus our working spectrum is far from the resonant frequency, and the step response is very fast. In DC it can withstand large amounts of current. Nevertheless, it should be always used various in parallel to ensure a low resistance path for power and returning currents.

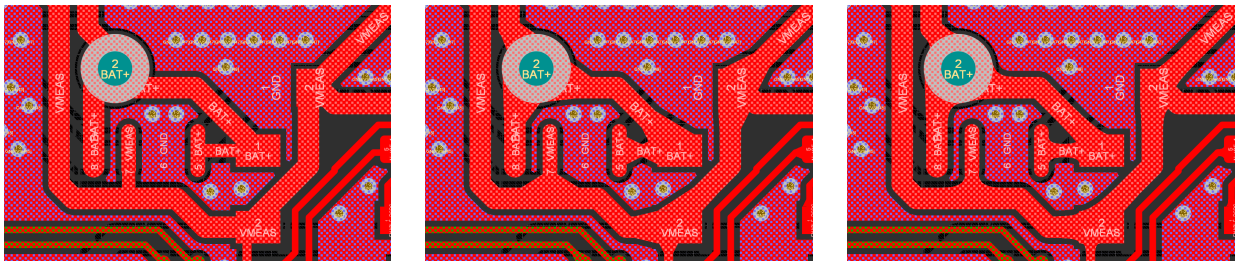

(a) *Without teardrops.* **(b)** *With line teardrops.* **(c)** *With round teardrops.*

Figure 5.27 – *Comparison of trace connection with pads, with and without teardrops.*

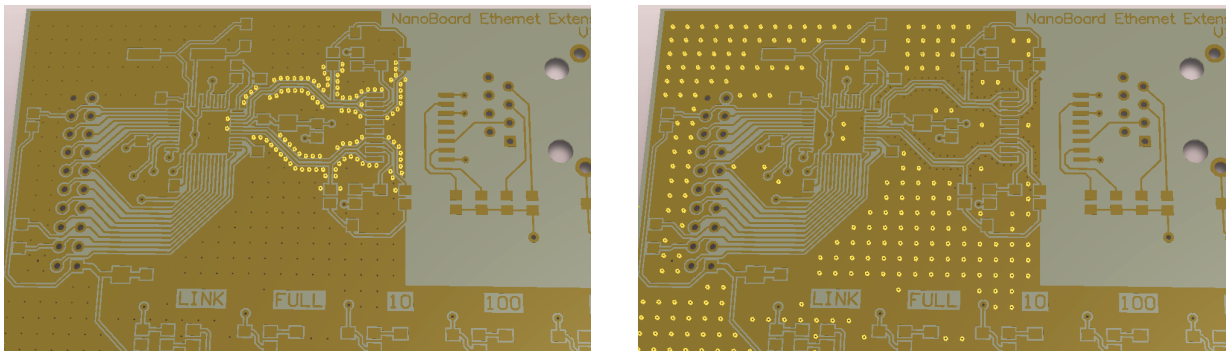

(a) *Via shielding.* **(b)** *Via stitching.*

Figure 5.28 – *Illustration of via shielding and via stitching. Source: [160].*

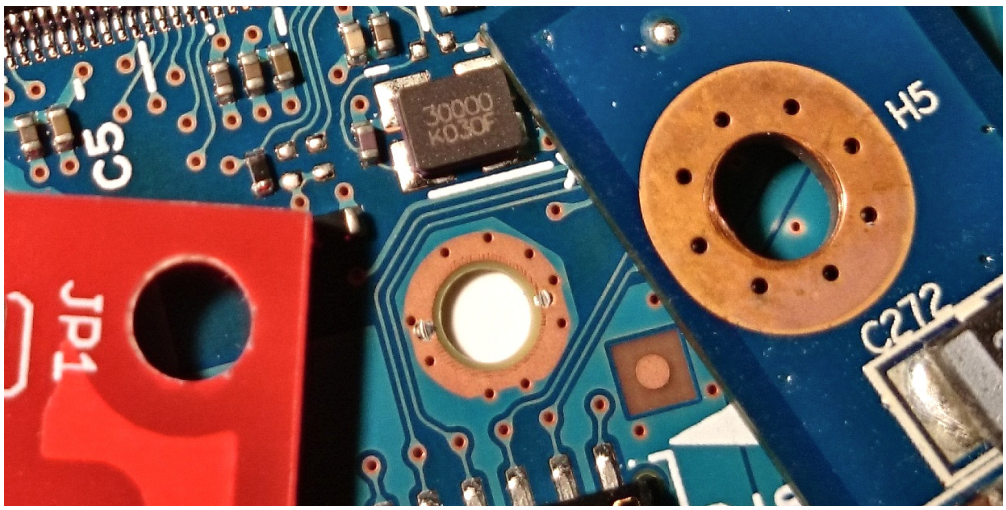

Figure 5.29 – *Different types of PCB mounting holes. Credits: [162]. Left: not plated, without head landing or vias, but with copper clearance. Middle and right: grounded, non-plated, with copper head landing and vias.*

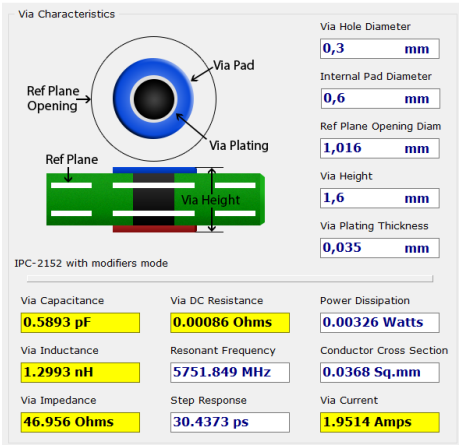

(a) *Characteristics and parasites of the vias.*

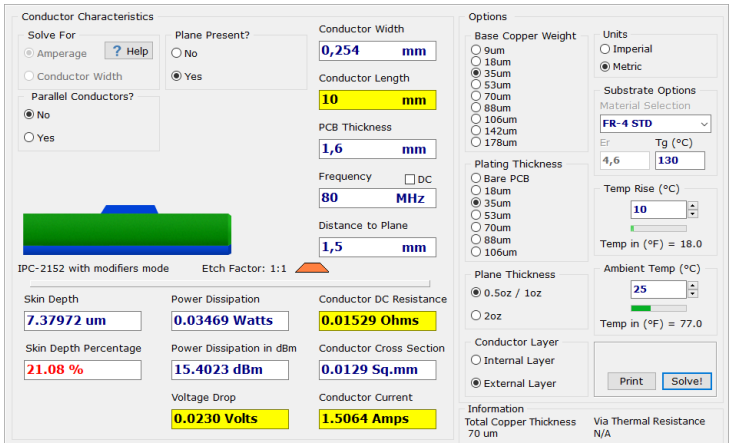

(b) *Conductor characteristics of 10 mil (0.254 mm) width traces.*

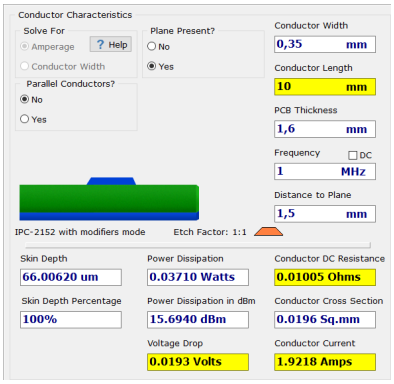

(c) *Conductor characteristics of 0.35 mm width traces.*

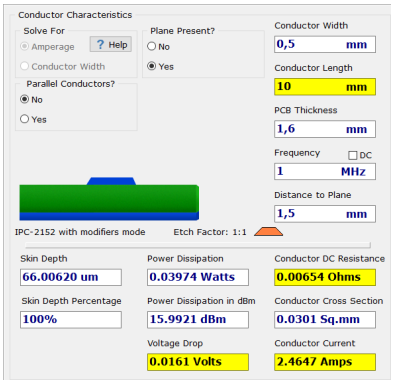

(d) *Conductor characteristics of 0.5 mm width traces.*

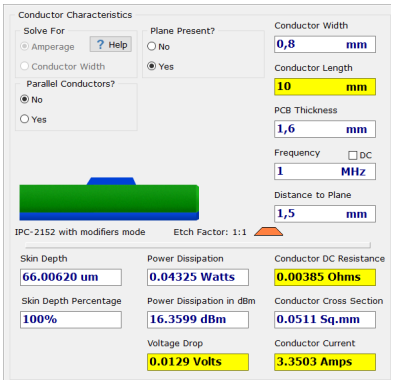

(e) *Conductor characteristics of 0.8 mm width traces.*

Figure 5.30 – *Characteristics of the vias and conductors used in the PCB.*

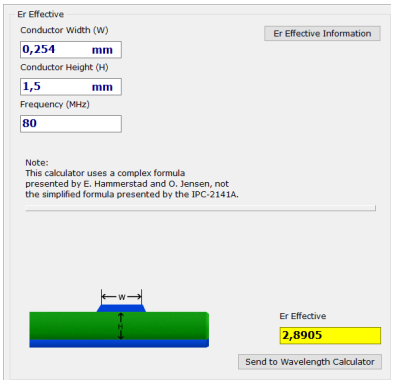

(a) *Calculus of the $\varepsilon_{r,\ eff}$ of the SPI bus traces.*

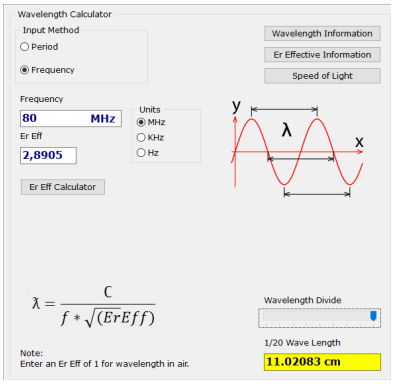

(b) *Calculus of the maximum SPI bus trace length given the $\varepsilon_{r,\ eff}$.*

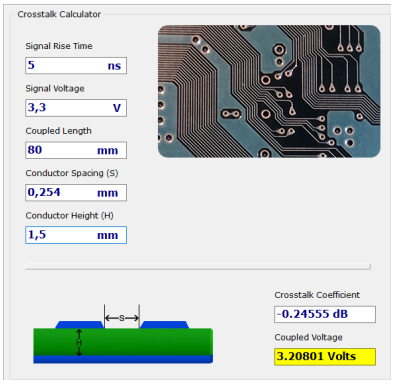

(c) *Calculus of the crosstalk between SPI lanes separated by 0.254 mm.*

Figure 5.31 – *Characteristics of the SPI bus traces.*

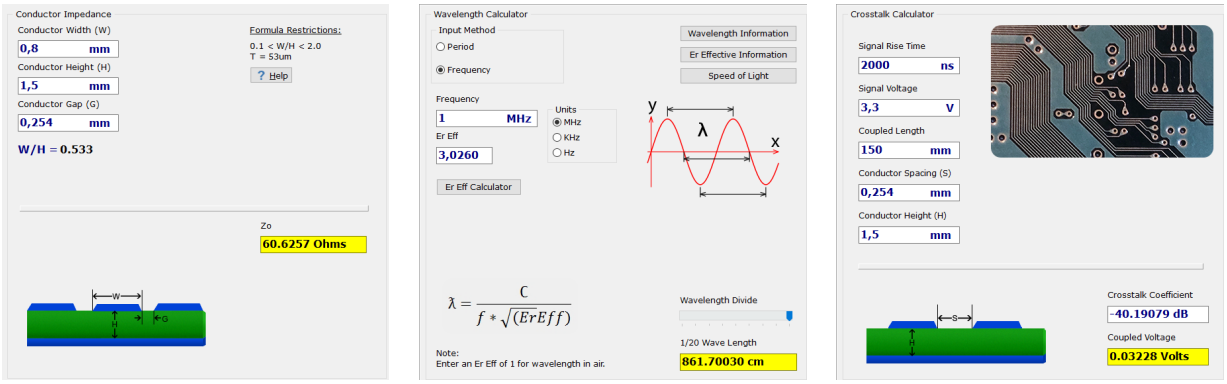

(a) *Characteristic impedance of the analog traces.*

(b) *Calculus of the maximum trace length given the* $\varepsilon_{r,\ eff}$.

(c) *Calculus of the crosstalk between analog lanes separated by 0.254 mm.*

Figure 5.32 – *Characteristics of the analog traces.*

- **SPI traces.** These lines carry the SPI bus lines. The ESP32's SPI clock can be set up to 80 MHz, which is the frequency that we will use to communicate with the LCD. They are the highest-speed digital signals of our entire design, and they require the highest bandwidth. In Figure 5.31a, the $\varepsilon_{\mathrm{r,eff}}$ (effective dielectric constant) of these signals has been estimated with JLCPCB's FR-4.

  These lines should not be very long in order to avoid transmission line effects, since electromagnetic signals propagate slower in conducted mediums than radiated in vacuum or air. According to our calculations, a SPI trace should not be longer than 11 cm (Figure 5.31b). Note that this is rather a pessimistic value, as we are dividing the real wavelength by 20.

  As you can clearly see in Figure 5.31c, a 2-layer, 1.6 mm PCB is not great for signal integrity as we have great crosstalk between SPI lines. A common solution is to include GND copper between lanes with good connection to ground (e.g. by using via stitching or shielding).

- **Traces for sensors' analog signals.** These lines are designed to have a characteristic impedance of 60 Ω (Figure 5.32a). The 50 Ω impedance cannot be matched unless the trace is much wider (another negative effect of 1.6 mm PCBs), so the 60 Ω mark is kept as a close enough solution. Besides, this is not by any means a critical design aspect in a low-speed design such as our case; and also there is no impedance control on the line terminations (amplifier input/output, ADC input, etc.).

  As seen in Figure 5.32b, length is not a problem. However, crosstalk and can become an issue given the needed signal precision (Figure 5.32c). Therefore, these lanes will be placed far from high-speed signals, they will be via-shielded, and we will try to maintain a GND plane below these traces.

5.1.3.6 Footprints

A footprint defines the interface required to solder a component to a PCB. Footprints are associated with schematic symbols, and their pins are mapped to the footprint's pads. Nowadays most PCB design software support 3D rendering, so footprints usually have their own embedded 3D model, which facilitates mechanical design. Manufacturers often specify a PCB landing pattern for their components in their datasheets, which we translate into a footprint. Some manufacturers make the footprints and/or 3D models available on their respective websites, which speeds up the implementation process by their costumers. Since many components follow standard packages, such as SOT, TSSOP, QFP etc. there are third-party libraries like Celestial [146] that gather many generic footprints of great quality.

Figures 5.33, 5.34 and 5.35 concentrate a collection of footprints, dimensions and 3D views of the most relevant components of the designed PCB.

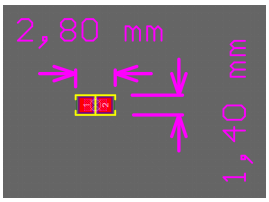

(a) *Generic 0603 footprint (MLCC capacitor).*

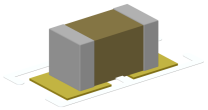

(b) *Generic 0603 3D model (MLCC capacitor).*

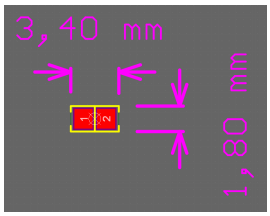

(c) *Generic 0805 footprint (MLCC capacitor).*

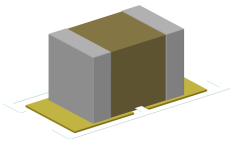

(d) *Generic 0805 3D model (MLCC capacitor).*

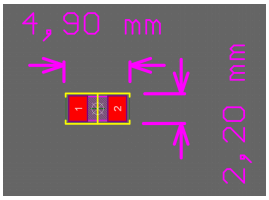

(e) *Generic 1206 footprint (MLCC capacitor).*

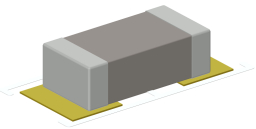

(f) *Generic 1206 3D model (MLCC capacitor).*

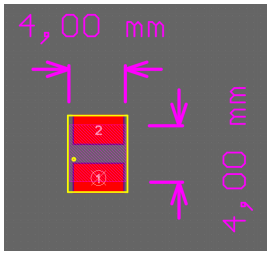

(g) *Inductor footprint.*

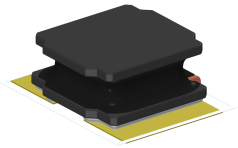

(h) *Inductor 3D model.*

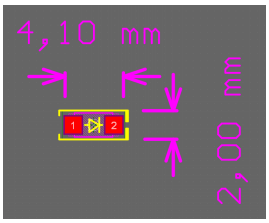

(i) *SOD123 footprint.*

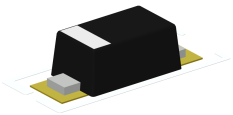

(j) *SOD123 3D model.*

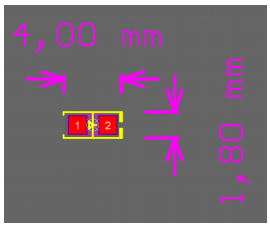

(k) *0805 LED footprint.*

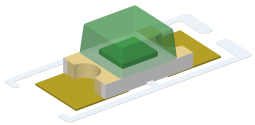

(l) *0805 LED 3D model.*

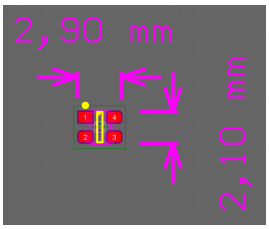

(m) *SC70 footprint.*

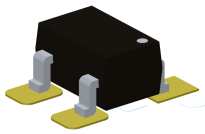

(n) *SC70 3D model.*

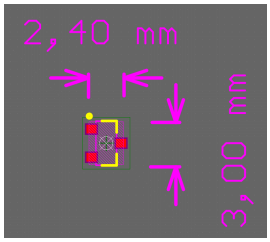

(o) *SOT-23-3 footprint.*

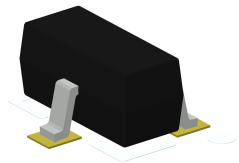

(p) *SOT-23-3 3D model.*

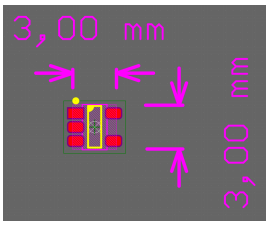

(q) *SOT-23-5 footprint.*

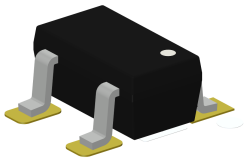

(r) *SOT-23-5 3D model.*

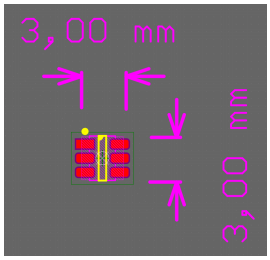

(s) *SOT-23-6 footprint.*

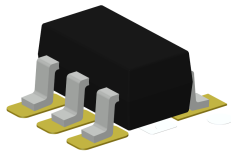

(t) *SOT-23-6 3D model.*

Figure 5.33 – *Footprints and 3D models of the different packages used in the PCB (part 1 of 3).*

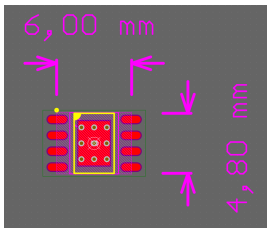

(a) *SOP-8 footprint.*

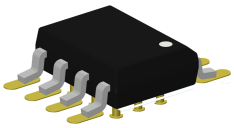

(b) *SOP-8 3D model.*

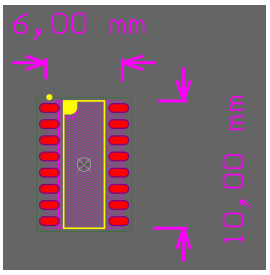

(c) *SOP-16 footprint.*

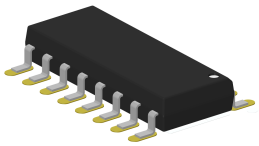

(d) *SOP-16 3D model.*

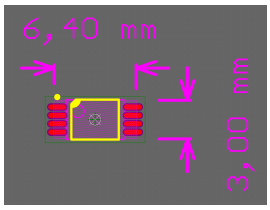

(e) *TSSOP-8 footprint.*

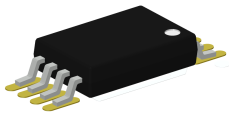

(f) *TSSOP-8 3D model.*

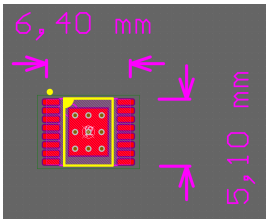

(g) *TSSOP-16 footprint.*

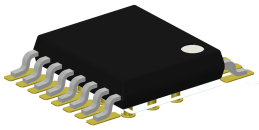

(h) *TSSOP-16 3D model.*

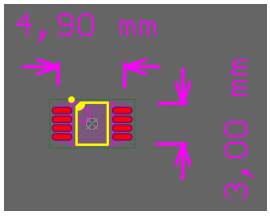

(i) *VSSOP-8 footprint.*

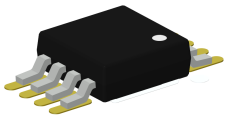

(j) *VSSOP-8 3D model.*

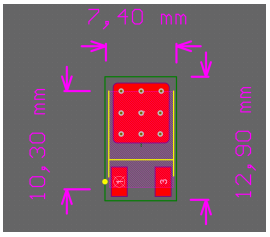

(k) *DPAK footprint.*

(l) *DPAK 3D model.*

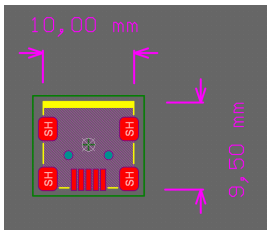

(m) *USB Mini-B footprint.*

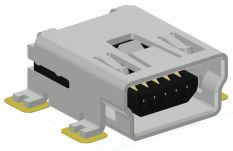

(n) *USB Mini-B 3D model.*

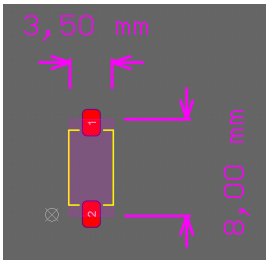

(o) *Generic 2-pad SMD button footprint.*

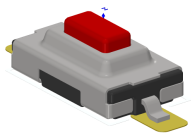

(p) *Generic 2-pad SMD button 3D model.*

Figure 5.34 – *Footprints and 3D models of the different packages used in the PCB (part 2 of 3).*

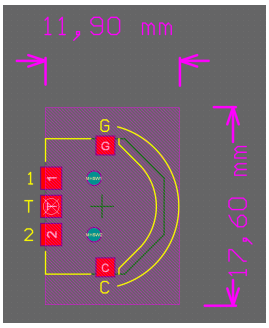

(a) *Thumb button footprint.*

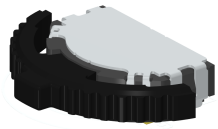

(b) *Thumb button 3D model.*

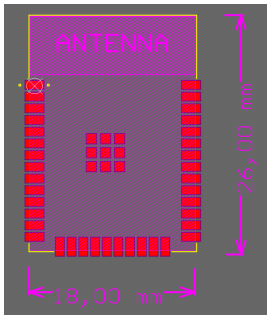

(c) *ESP32-WROOM-32D footprint.*

(d) *ESP32-WROOM-32D 3D model.*

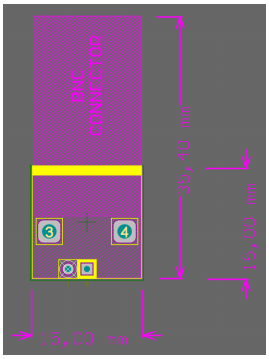

(e) *90º BNC footprint.*

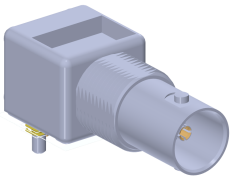

(f) *90º BNC 3D model.*

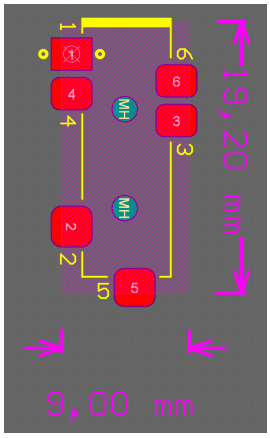

(g) *3.5 mm jack receptacle footprint.*

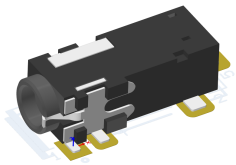

(h) *3.5 mm jack receptacle 3D model.*

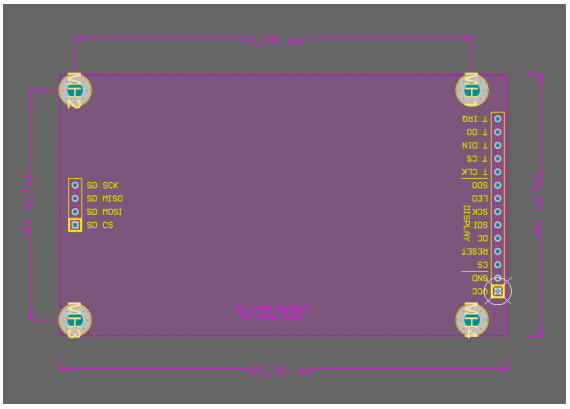

(i) *TFT LCD module footprint.*

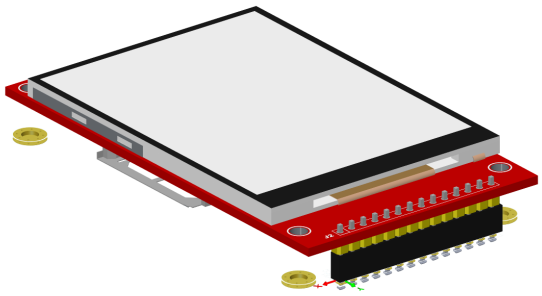

(j) *TFT LCD module 3D model.*

Figure 5.35 – *Footprints and 3D models of the different packages used in the PCB (part 3 of 3).*

5.1.3.7 Layout

This section summarizes the layout of the final version of the PCB. A *layout* defines the arrangement of components, mounting holes, cutouts, etc. on a PCB. Recalling some concepts introduced in Section 4.4: Mechanical architecture, below are a series of specifications and rules that have been followed for the final component layout, present in Figure 5.37 for more information and detailed mechanical drawings see Appendix D: PCB schematics.

- ESP32 needs copper and component clearance for its antenna (see Figure 5.36a). Also, the manufacturer's hardware design guidelines [1] recommends some placements on the PCB (Figure 5.36b). Sadly, this recommendation could not be fully met due to space and routing constraints. However, the ESP32 is placed a corner and far from metal parts to avoid as much RF reflections and interferences as possible.
- Screen is placed in portrait (vertical) orientation. Since the module has 2 rows of pins in each extreme, one with 14 (with 2 SPI interfaces: display and touchscreen) and the other 4 pin (with only one SPI interface: SD card), the larger row is placed closer to the ESP32.
- The muldi-direction 'thumb' button will be placed on the right side of the device, since statistically most of the users will be right-handed. No ports should be placed on this side.
- USB is at bottom-left, and not centered, due to design constraints with the needed area for the ESP32. Similarly, the power-on button is on the front, however, it is placed at the right side, not in the center.
- The battery chargers are placed as close as possible to the USB to minimize power losses. In the same way, the DC/DC is close to the battery connectors.
- CH340C and auto-programming circuit is placed close to both the USB and the ESP32.
- BNCs are placed at the top but with more separation between them to facilitate cable handling.
- The expansion port is placed also at the top, between the BNCs.
- The SD card slot is accessed by the left side, and so the load cell jack receptacle.

In general, components are amalgamated at the periphery of the PCB, with less component density in the center. This is a holdover from previous revisions where the battery was located between the LCD and PCB. In the latest version, it has been moved under the bottom layer to allow a larger battery to be mounted.

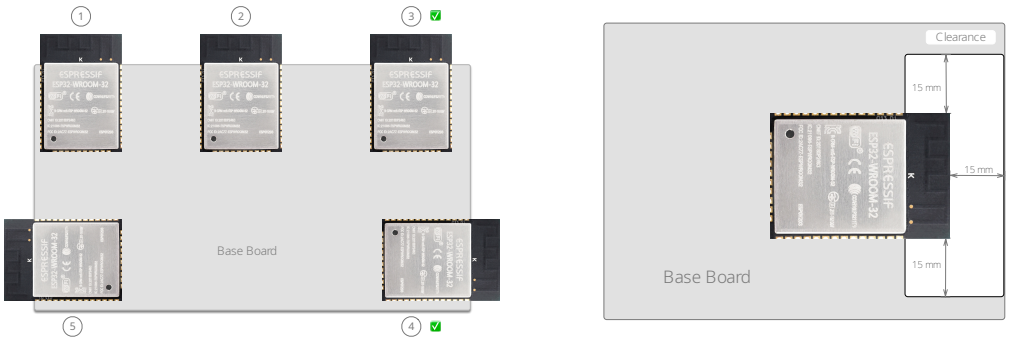

(a) *Recommended locations for the ESP32.* **(b)** *Required antenna keepout area.*

Figure 5.36 – *ESP32's recommended location and antenna clearance constraints [1].*

5.1.3.8 Final routing and renders

The routing of the final version of the PCB looks is presented in Figure 5.38. This is the result of multiple iterations and optimization of component placement, orientation and routing. This revision has zero design rule violations and was sent to manufacturing. As explained in paragraph 5.1.2.1.5, the traces are also highlighted here in different colors according to the net class they belong to. This allows a quick identification of the function the copper.

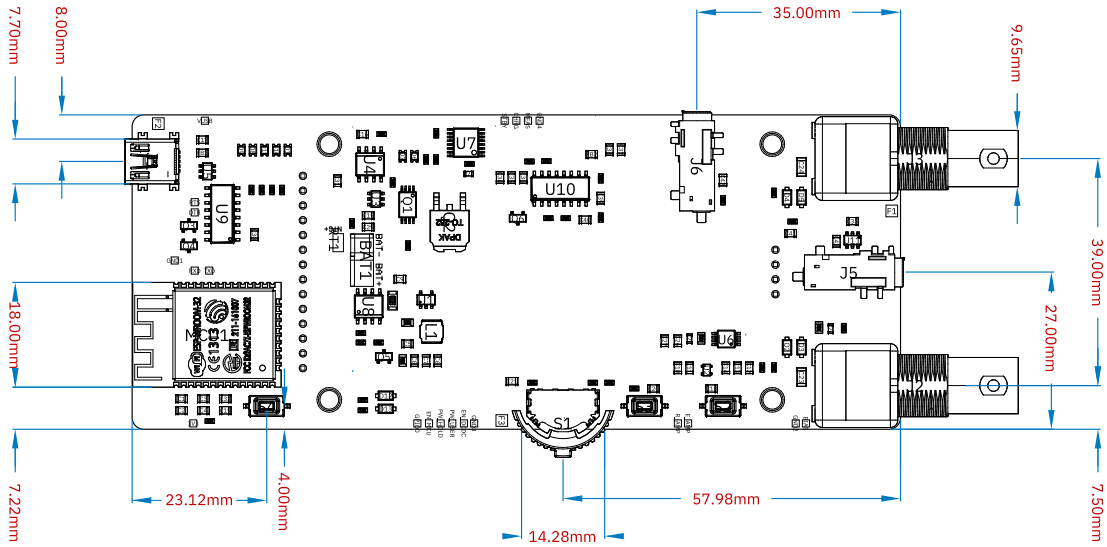

(a) *PCB layout without the LCD module.*

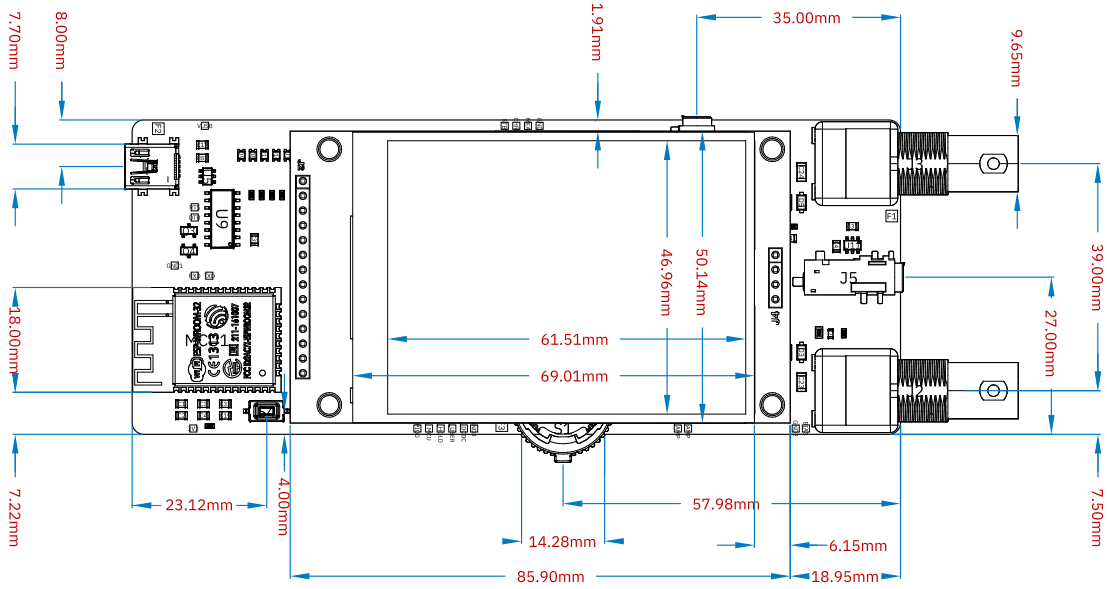

(b) *PCB layout with the LCD module.*

Figure 5.37 – *PCB layout and brief dimensions, with and without the LCD module.*

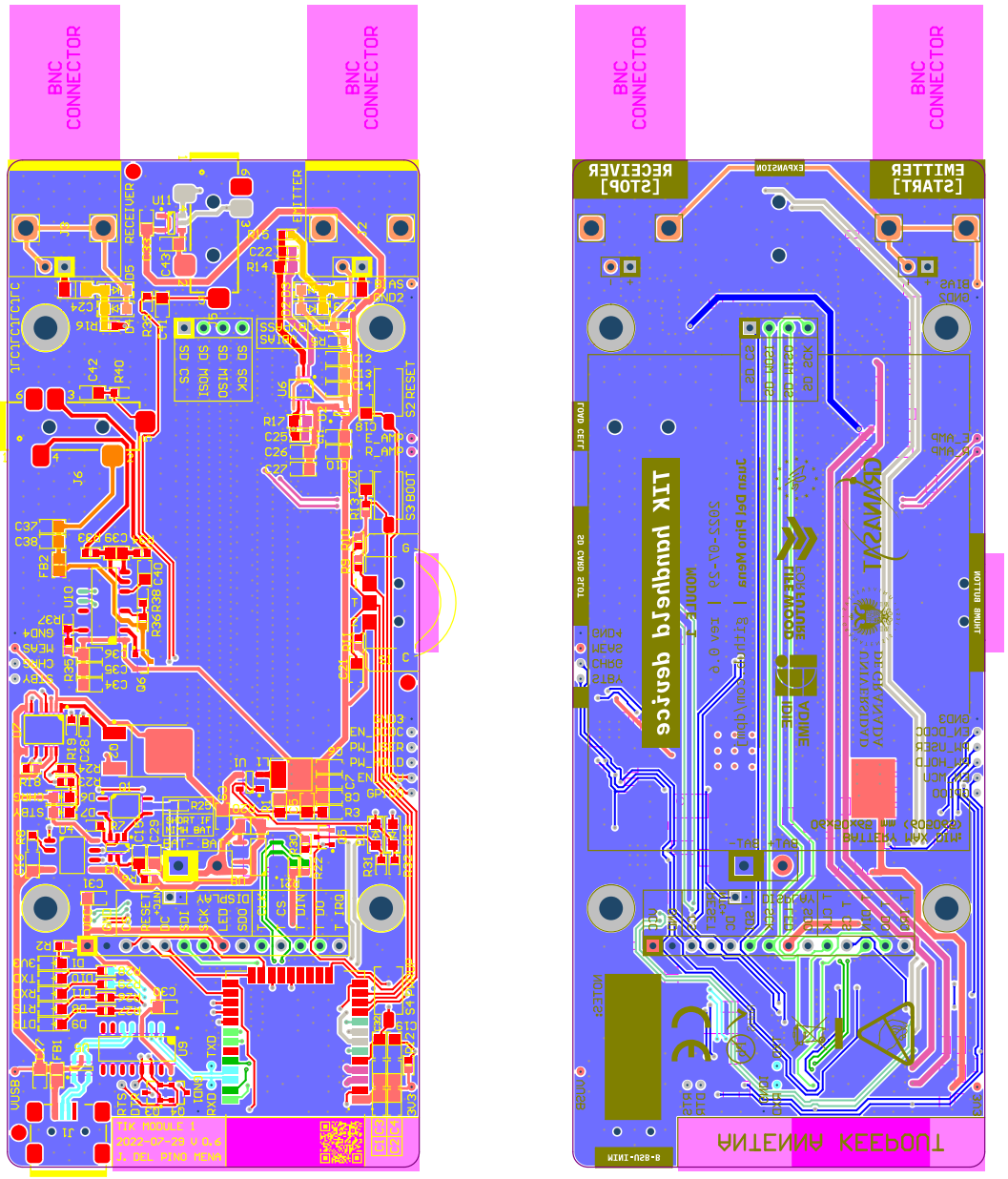

(a) *Top layer.*

(b) *Bottom layer.*

(c) *Legend.*

Figure 5.38 – *Top and bottom layer prints showing the final copper routing.*

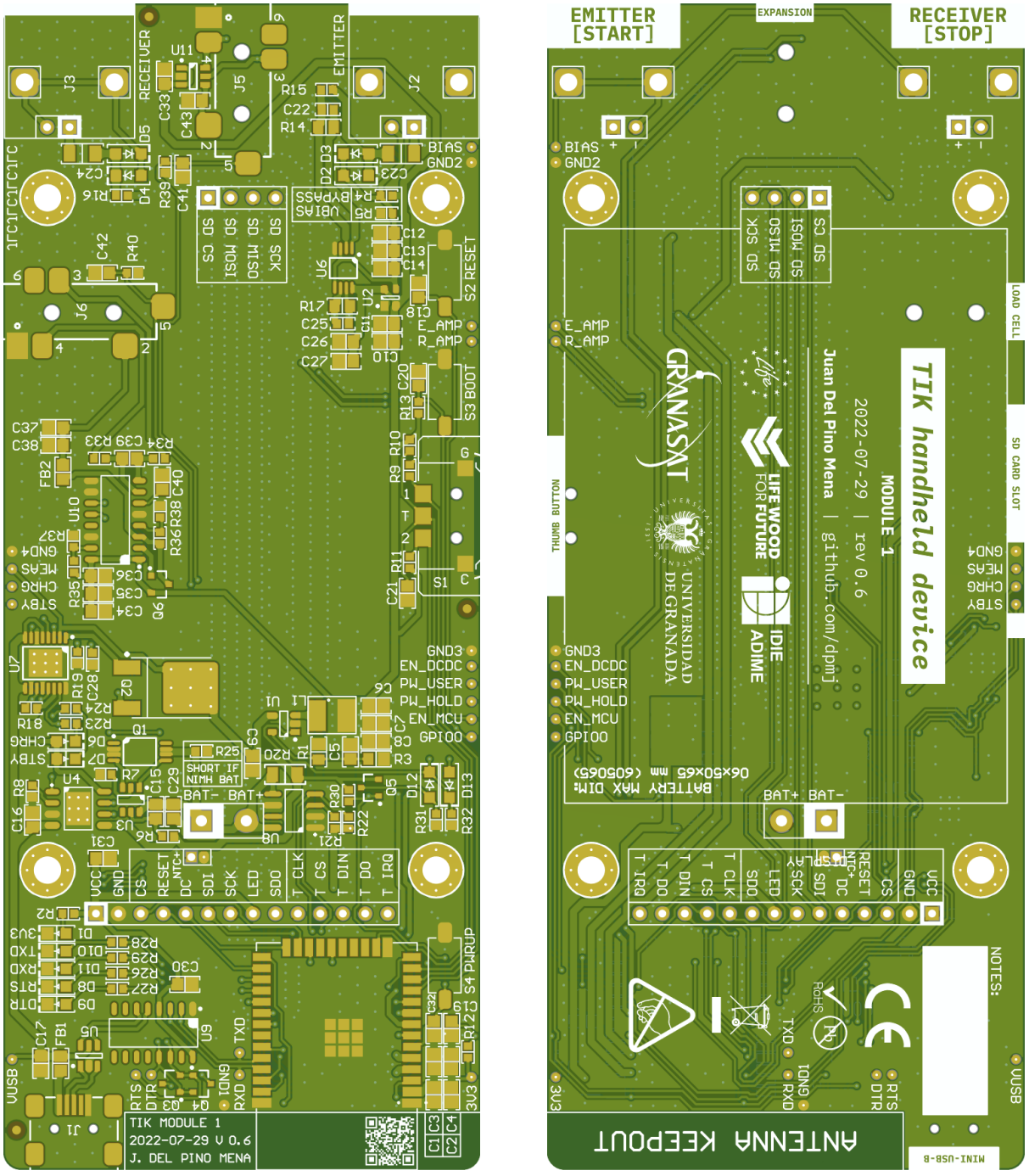

(a) *Front view.* **(b)** *Back view.*

Figure 5.39 – *Front and back views renderings of the final PCB, not populated.*

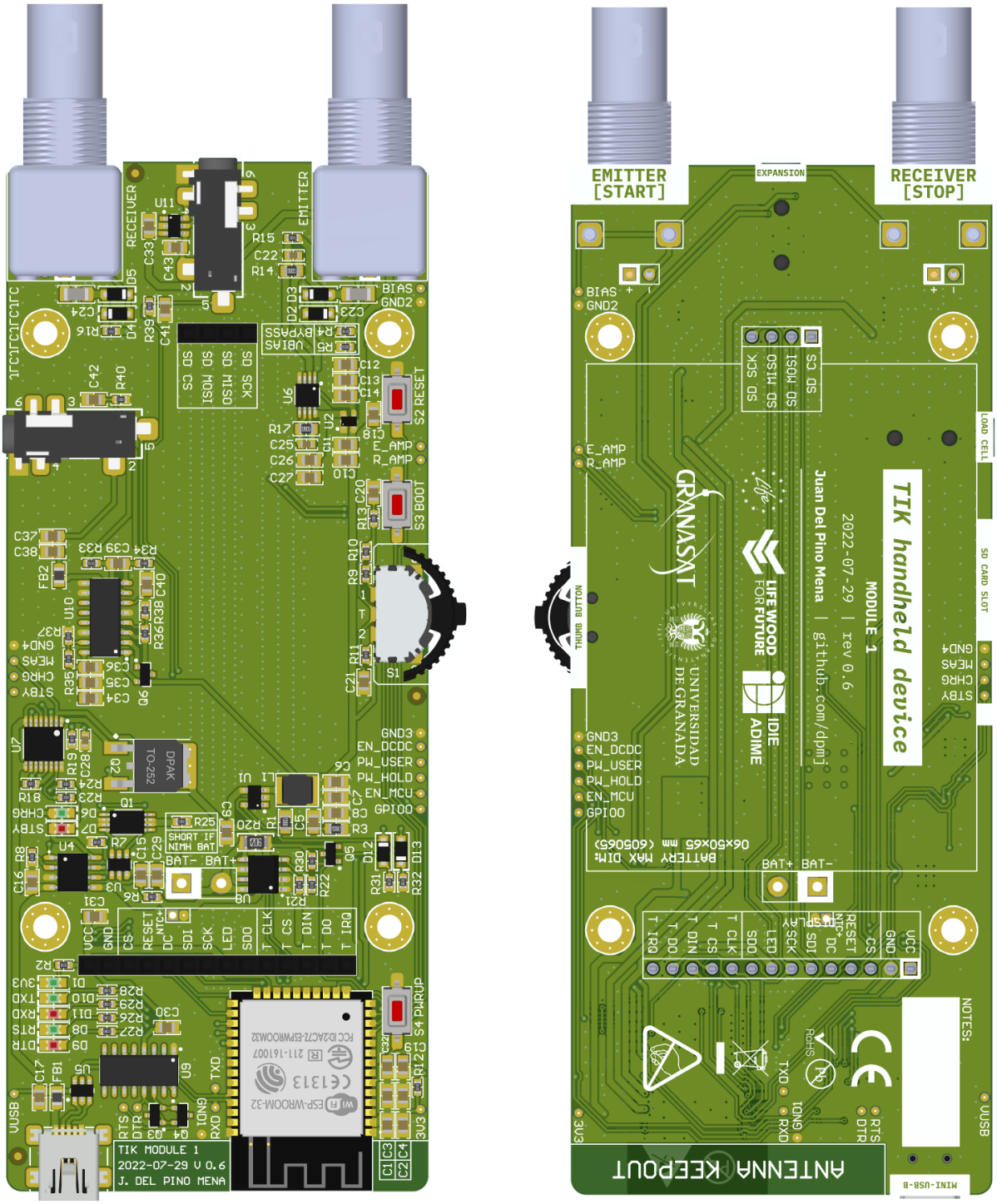

(a) *Front view.* **(b)** *Back view.*

Figure 5.40 – *Front and back views renderings of the final PCB, populated, without the LCD.*

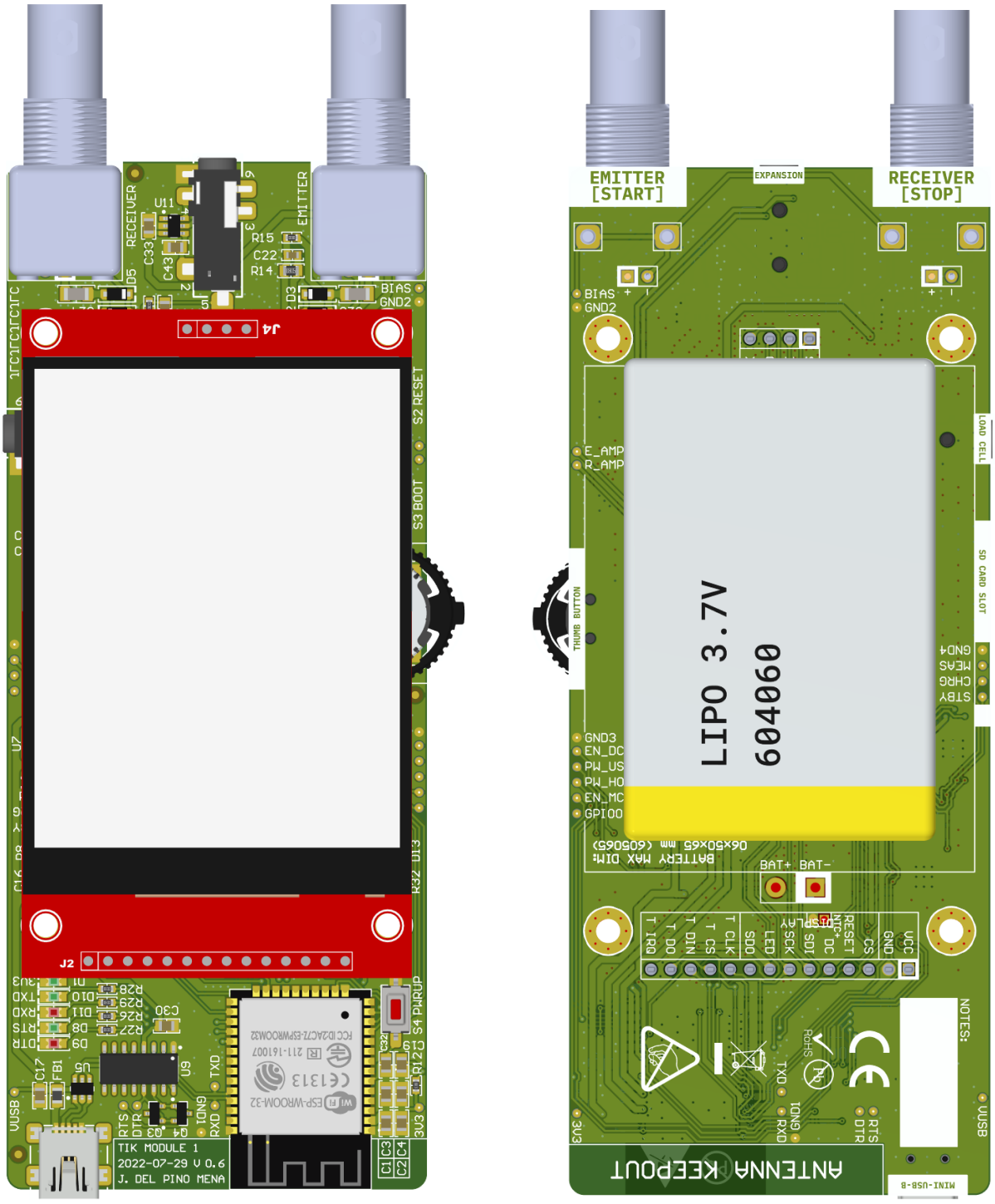

(a) *Front view.* **(b)** *Back view.*

Figure 5.41 – *Front and back views renderings of the final PCB, populated, with the LCD and battery.*

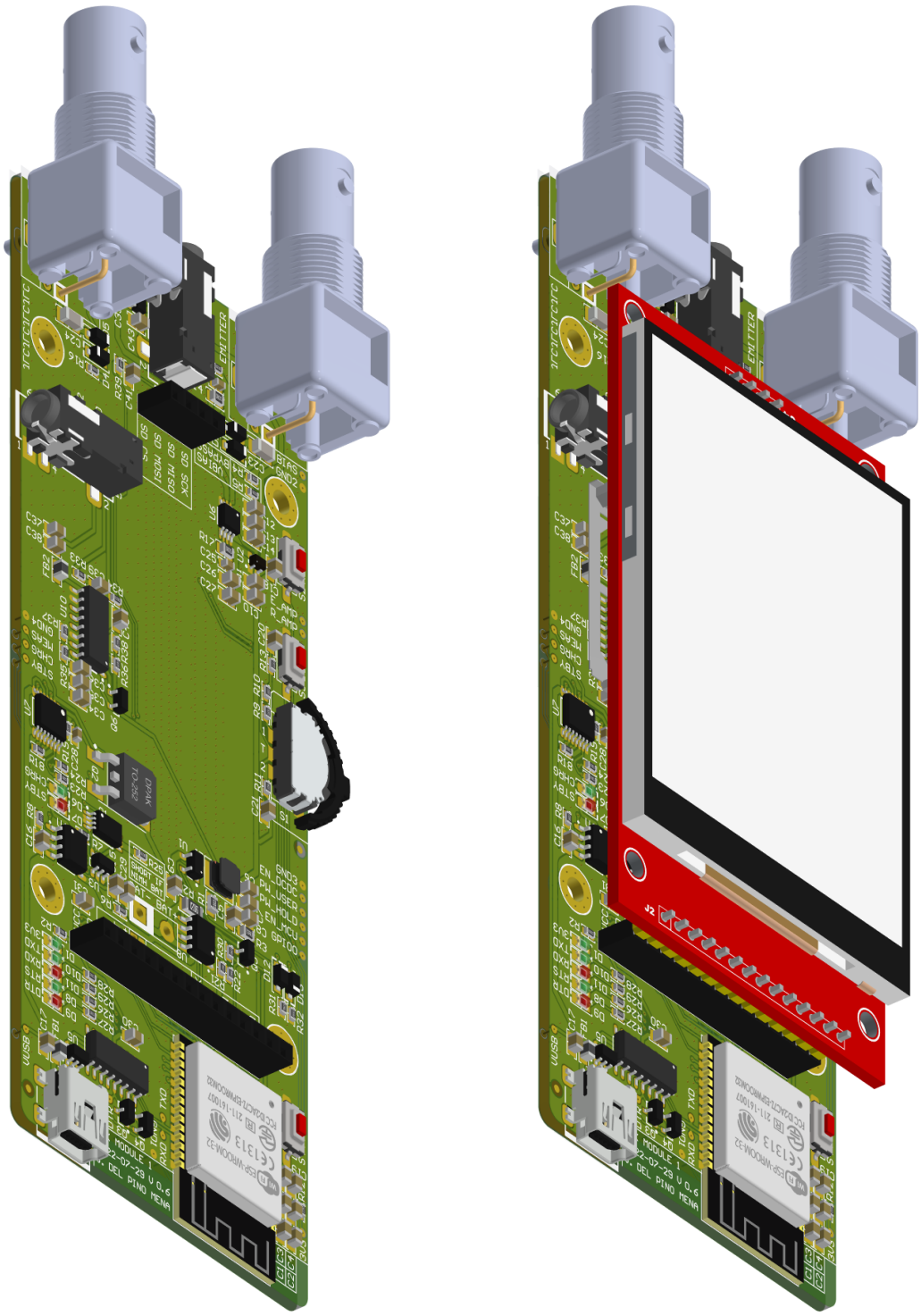

(a) *Without LCD.* **(b)** *With LCD.*

Figure 5.42 – *Front-side views renderings of the final PCB, populated, with and without the LCD and battery.*

5.2 Firmware design

This section describes the structure of the firmware developed to date.

5.2.1 Project organization, modules and dependencies

The source code is divided into several folders and files, according to the structure required by PlatformIO's projects. In Figure 5.43 is presented the breakdown of the files in the project, as well as a brief description of their function. The dependencies between the files, the libraries that each one requires, and the functions and methods of each module can be consulted in Figure 5.44.

Reviewing the most relevant blocks:

- **ADCSampler.** This module is responsible for configuring the ADC unit 1, taking samples and storing them directly in RAM using DMA and the I2S peripheral. The code has been forked from [140].

  Samples are stored in RAM using buffers. The amount of buffers reserved to this is set by a parameter named `dma_buf_count`, and the size of every buffer by `dma_buf_len`. Every buffer has a maximum length of 1024 positions. So, if we have 4 buffers with 1024 samples each with 16 bits per sample:

$$\text{RAM usage} = 4\,\text{buffers} \cdot 1024\,\text{Samples/buffer} \cdot \frac{16\,\text{bits/Sample}}{8\,\text{bits/Byte}} = 8192\,\text{Bytes} = 8\,\text{kB} \tag{5.2.1}$$

  The acquisition code is responsible for removing 4 header bits from the samples, leaving the 12 bits of the ADC measurement. Additionally, we must keep in mind that i2S sends data in pairs as if it were two channels even if the communication format is set to mono like with the `I2S_CHANNEL_FMT_ONLY_LEFT` parameter. This will be seen in the ADC tests performed in Section 6.4: Verification and debugging.

- **AIC.** This class implements the Akaike Information Criterion (AIC) calculus needed for the signal post-processing. This module contains methods that perform the auxiliary mathematical vector operations necessary for the calculation of the Akaike functions, such as the mean, variance, minimum and maximum locators, etc; and specialized functions such as one that define the calculation window relative to the properties of the signal, and another which sorts the stereo ADC samples in the correct order.

- **GUI.** This block contains all the necessary methods to draw the designed graphical interface on the LCD and manages the user touch input by using the TFT_eSPI library. It acts as an intermediary between said library and the rest of the system modules.

  For the buttons on the screen, a modified version of the Button class of TFT_eSPI (called **ButtonMod**) has been used to adapt it to our needs.

  The symbols that appear on the screen, such as those in the status bar (Bluetooth, Wi-Fi, state of charge, etc.) have been transformed from an bipmap to a C vector in which each position identifies a color. This information, plus the pixel dimensions, is interpreted by the library to represent images on screen as sprites.

- **main.cpp.** This is the primary file of the program. It is the compiler target, and contains the functions that are executed when ESP32 boots up. Since we are using the Arduino framework, these are the famous `setup()` and `loop()`. Main.cpp is the main file of the program. It is the compiler target, and contains the functions that are executed when ESP32 starts up. Since we are using the Arduino framework, these are the famous setup() and loop(). However, as we will see below, we don't need the loop() function because all system functions are implemented by tasks.

```
TIK_FIRMWARE/
├── .pio/   ...    Config files, PlatformIO toolkit and third-party
│                  libraries.
├── include/   ...    Folder in the compiler path, for third-party libs and
│                     files imported manually.
├── src/   ...    Contains our source code.
│   ├── ADC_SAMPLER/   ...    An I2S and DMA based fast sampler.
│   │   ├── ADCSampler.cpp
│   │   └── ADCSampler.h
│   ├── AIC/   ...    Class that implements the Akaike calculus.
│   │   ├── ADCSampler.cpp
│   │   └── ADCSampler.h
│   ├── GUI/   ...    All the GUI-related files.
│   │   ├── button/   ...    Modified TFT_eSPI/Button.h class.
│   │   │   ├── ButtonMod.cpp
│   │   │   └── ButtonMod.h
│   │   ├── sprites/   ...    Graphic symbols stored as sprites.
│   │   │   ├── BAT/
│   │   │   │   └── BAT_LEVELS_SPRITES.c
│   │   │   ├── BT/
│   │   │   │   └── BT_ICON_SPRITE.c
│   │   │   └── WIFI/
│   │   │       └── WIFI_SPRITES.c
│   │   ├── GUI.cpp
│   │   └── GUI.h   ...    Implements the GUI object itself, with configuration
│   │                      in defines.
│   ├── SIGNALS/   ...    Tree signal struct declaration.
│   │   └── SignalRE.h
│   ├── SYSTEM/   ...    System-related types and defines.
│   │   ├── SystemStatus.h
│   │   └── version.h
│   └── main.cpp   ...    Compilation target, program's main file, coordinates
│                         all tasks.
├── platformio.ini   ...    PlatformIO configuration.
└── README.md   ...    Brief project description.
```

Figure 5.43 – *PlatformIO project folder structure.*

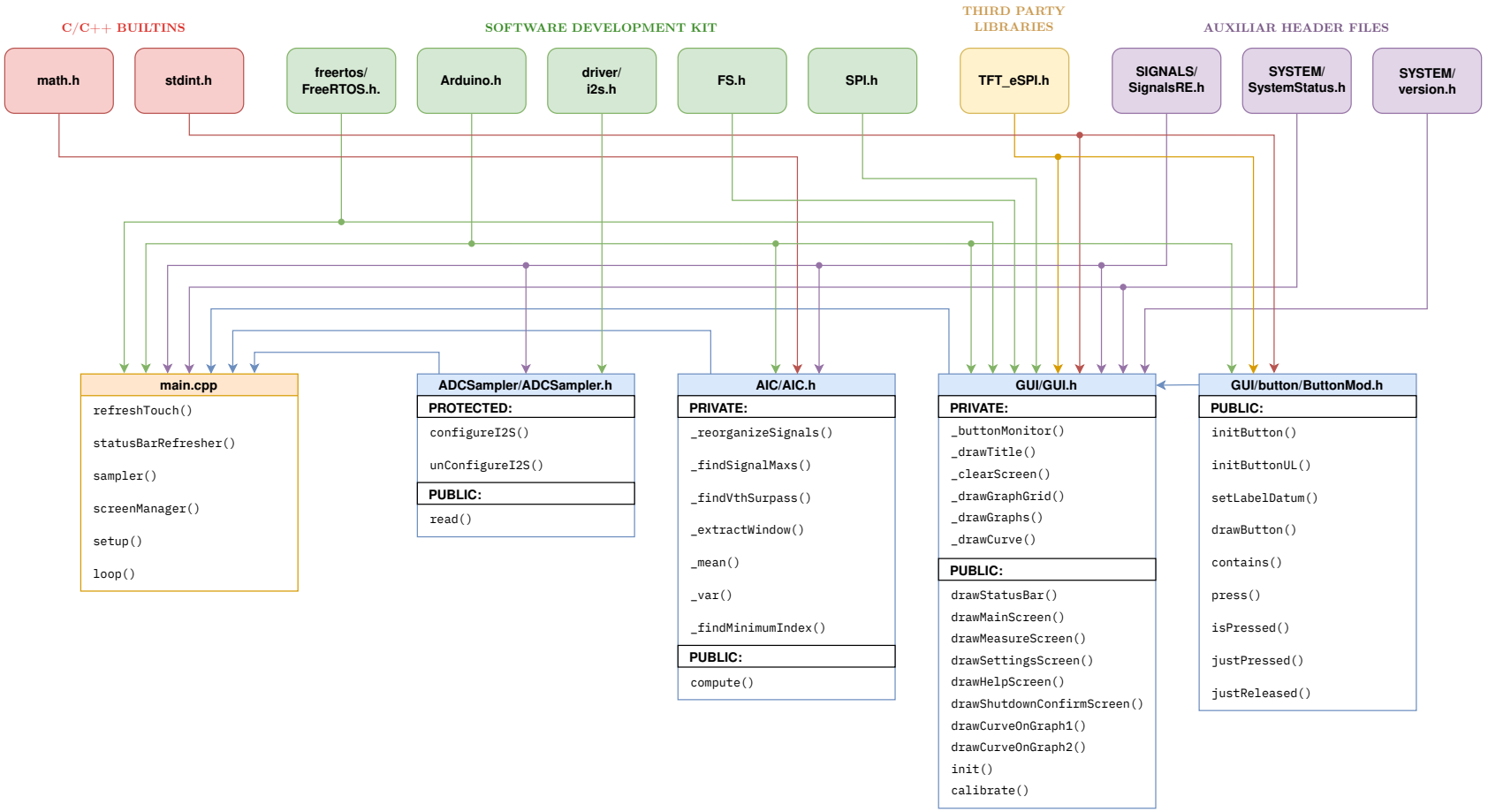

Figure 5.44 – *Firmware dependencies.*

5.2.2 Main program flow and tasks

Remembering the characteristics of ESP32, we have two symmetrical cores that can execute tasks independently through an RTOS. In Listing 5.1 appears a sample code illustrating the creation of a task assigned to a specific processor core in ESP-IDF's FreeRTOS in the Arduino Core SDK.

In Figure 5.46 we can see the flowchart of main.cpp. We can distinguish three different parts:

- The first one is in charge of importing the necessary headers, declaring the objects, structures, constants and necessary configuration, as well as the mutex for resource arbitration.
- Next, the functions of the tasks and their corresponding handlers are declared.
- Finally, we access `setup()`, which is responsible for initializing the objects and necessary configuration, performing a system status check, and finally starting the system tasks. Once finished, the function is exited and the associated task is automatically destroyed. In an ordinary Arduino fashion, `loop()` would now be executed indefinitely. However, since all of the system's functions are carried out by tasks, `loop()` is meaningless, and therefore its associated task is eliminated.

Tasks in FreeRTOS can adapt to 5 states: not created, ready, running, suspended, and blocked. The transitions between one and the other can be seen in Figure 5.45. As for the aforesaid implemented tasks, they are described below. In Figure 5.47 are drawn flowcharts showing the execution sequence of each individual task.

- **refreshTouch:** This task is responsible for updating the last position in which the user touched the screen. It is implemented as an infinite while loop. Before reading the position, it makes sure that the SPI is available by checking its Mutex, since the rest of the tasks also use it and the simultaneous access to this shared medium can lead to errors and even a forced reset of the processor. It then checks that no other task is accessing the global variable that stores the touch position. If both conditions are met, the task momentarily takes exclusivity of the resources by using xSemaphoreTake(). Once updated the variable, it frees the mutexes with xSemaphoreGive().

  The cycle repeats itself after a waiting period of 50 ms, in which other tasks can be executed. Since this task is not critical, it has been assigned a low priority and executed in core 0.

- **screenManager:** This task is responsible for changing the screen as the user navigates the interface. At the date of writing, 5 screens have been defined: main, measurement, settings, help, and shutdown confirmation. Although not explicitly listed, a check and takeover of the SPI mutex is performed within the gui module functions each time it is necessary to write to the screen. The priority of the task is low (1) and it is assigned to core 0.

- **statusBarRefresher:** Updates the information in the status bar every 5 seconds. It uses the updated information registered in the global SystemStatus structure, which contains data on the status and strength of the wi-fi signal, bluetooth, battery charge level, etc. Task priority is set to 1 in core 0.

- **sampler:** This task samples from the ADC1 using the ADCSampler object. Although it also has an infinite while loop, the task automatically suspended by using `TaskSuspend()` so as not to waste resources or processor time. It will be externally activated by another task that sends it the corresponding signal, through `vTaskResume(&TaskHandler)`.

  Since this task is considered critical for the speed and precision needed, it has been assigned a high priority of 10 and will be executed in core 1, to avoid interruptions.

```ino
#include <Arduino.h>            // Arduino framework
#include <freertos/FreeRTOS.h>  // FreeRTOS functionality

// ...

/* Function which implements the task. Tasks must never return (i.e. using a continuous
 * loop), or else they should be terminated by calling vTaskDelete(TaskHandler).
 */
void doSomething(void *parameters) {
    while (true) {
        // Task code here
    }
}

// Task handler (by which the created task can be referenced)
xTaskHandle doSomethingTask_TaskHandler;  // "doSomethingTask" task handler

void setup(void) {
    // ...

    xTaskCreatePinnedToCore(
        doSomething,                // pvTaskCode - Pointer to the task entry function
        "doSomething",              // pcName - A descriptive name for the task
        16384,                      // usStackDepth - The size of the task stack, in bytes
        NULL,                       // pvParameters - Pointer to the parameter for the task
        1,                          // uxPriority - The priority of the task
        &doSomething_TaskHandler,   // pvCreatedTask - Pointer to the task handler
        0);                         // xCoreID - Core in which to run task

    // ...
}

// ...
```

Listing 5.1 – *Example of task creation using the ESP-IDF FreeRTOS in Arduino Core.*

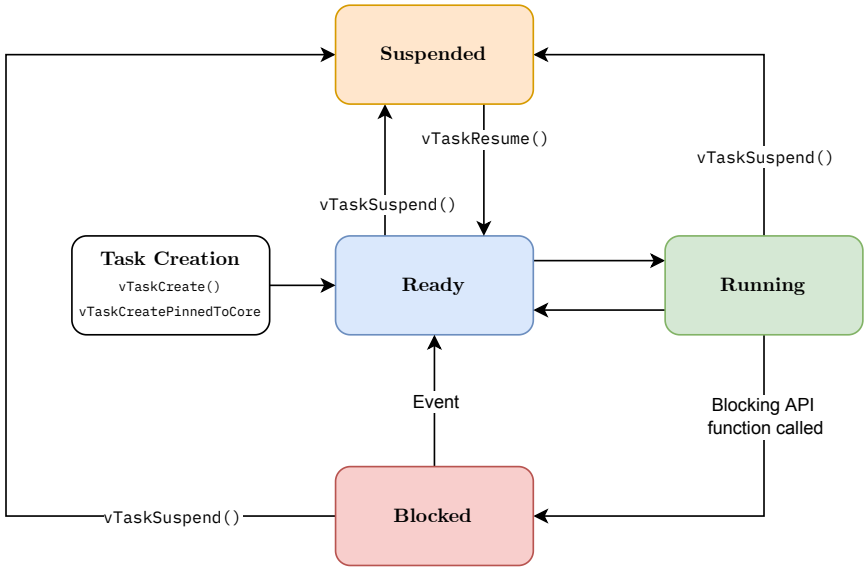

Figure 5.45 – *Valid task state and transitions. Own work, based on: [8] (Kernel > Developer Docs > Tasks and Co-routines > Task States).*

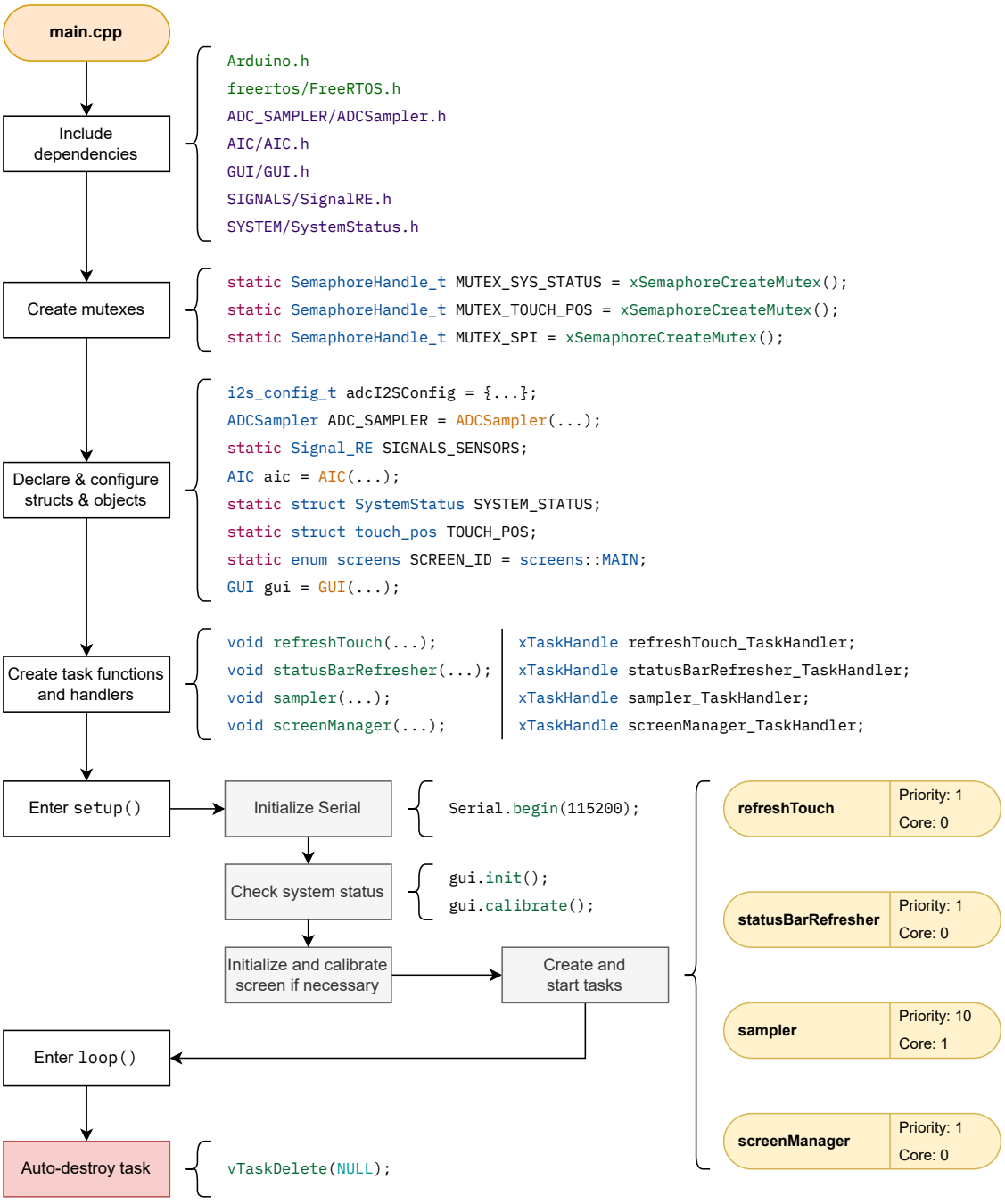

Figure 5.46 – *Flowchart of main.cpp.*

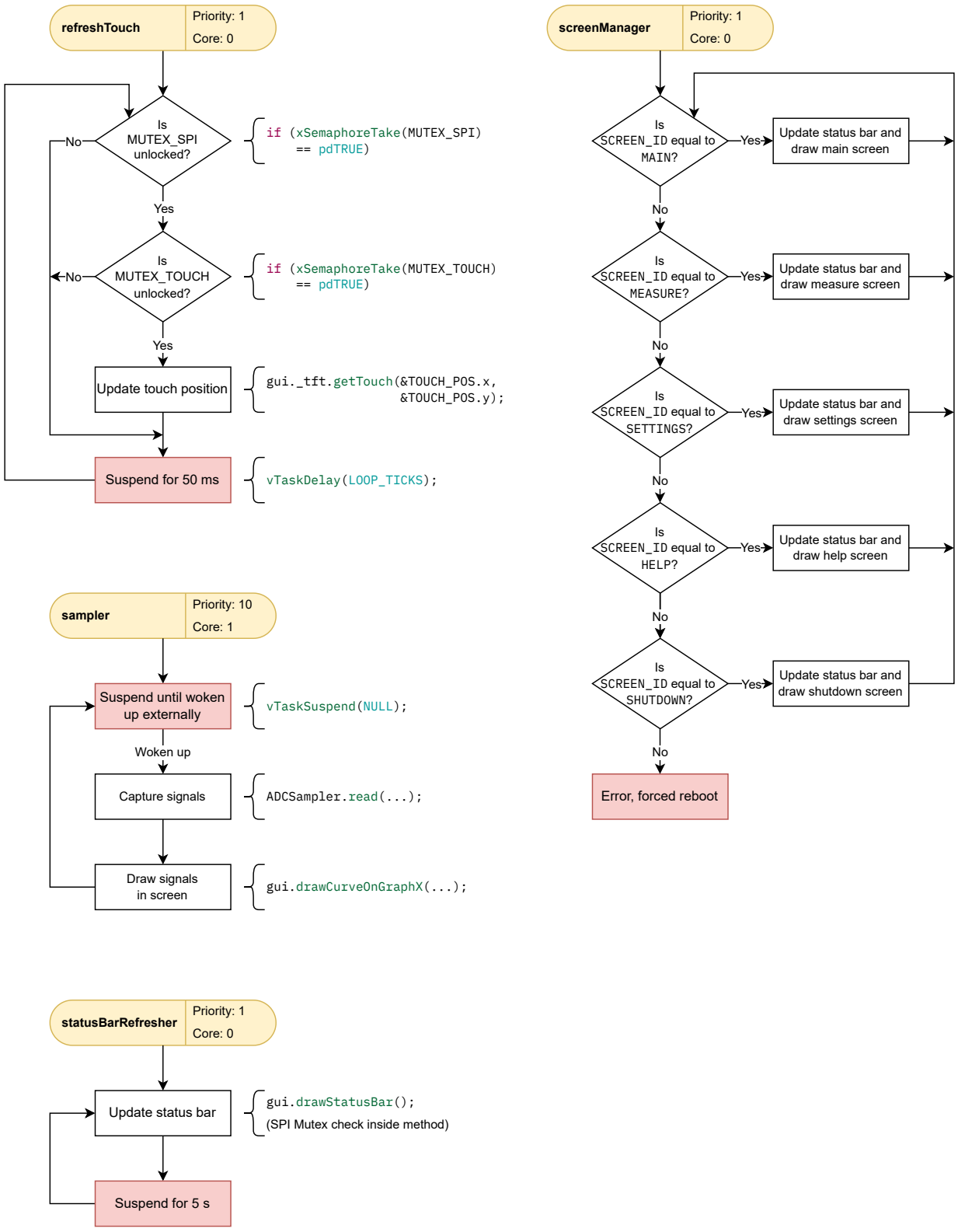

Figure 5.47 – *Flowcharts of the system's tasks.*

5.3 Mechanical design

This section is responsible for describing the mechanical design of the TIK casing and its assembly.

5.3.1 Case design

The case has been divided into two covers, called top and bottom, which fit together and enclose the electronics and have the corresponding ports holes. Some concepts exposed in Section 4.4: Mechanical architecture are recalled and applied in the design. However, the restriction of the PCB form factor greatly affects the original design that was conceptualized in Section 4.4.

- The size is comfortable enough to be manipulated with just one hand. The design is very rectangular, so grooves have been added to provide better grip and prevent the device from slipping from the hand.
- The design includes a hole to store the touchscreen stylus.
- It has an anchor point for a strap. This way, an operator can hang the strap around their neck preventing the device from falling, and leaving their hands free when they are not using the device.
- The areas surrounding the ports have a depression which levels the case wall with the connector itself, in order to avoid cables from colliding with the case wall.
- The multi-direction *'thumb'* has a groove in order to make it easy to find by touch.
- The screws placed on the exterior are flat-head, and the casing has the corresponding countersunks so the screws do not protrude from the profile of the case.
- Parts must be suitable for 3D printing.

The characteristics of the different pieces are specified below. Technical documentation of the casing pieces can be found in Appendix E, Section 1: Mechanical drawings of the case parts.

5.3.1.1 Top cover

Some of the features of this part are described below (see Figure 5.48):

- The top cover has a large cutout for the screen, which is surrounded by a raised frame to protect it from scratches and impacts. The idea of adding a visor has been scrapped because it increased too much the thickness of the device.
- This cover contains four 4 mm diameter holes at the top, near the screen cutout, to accommodate M3 size brass threaded inserts, which will be heat injected, melting the plastic and fixed to the case. The threaded inserts have a thread inside, and they will be the anchors for the screws that hold the PCB and the screen.
- The BNCs are surrounded by plastic with the appropriate dimensions so that they fit perfectly, providing mechanical fastening. In the same way, the rest of the ports that can suffer mechanical stress (the jack receptacles and the USB Mini-B) are supported with plastic walls.
- Just above the location of the power button a hole with rails is cut in order to accommodate the plunger that will actuate the button.
- This part has a quarter-ring hole which serves as an anchor for a strap.
- On the inner side faces there are holes designed to fit with clips from the bottom cover.

5.3.1.2 Bottom cover

Ditto as above, the most relevant characteristics of this piece are detailed next (see Figure 5.49).

- The back face of the bottom cover has large grooves that continue those in the top cover.
- There are three holes at the top and bottom faces which are meant for the threaded inserts that hold the exterior screws.
- There is a hole accessible from the bottom face with to accommodate the touch screen stylus. The part has the appropriate cuts to level it with the profile of the casing, and also to make it easy to remove with your finger.
- This piece has tabs that fit with the previously mentioned receptacles.

5.3.1.3 Extra parts

Two auxiliary pieces are described below. These pieces are not for the casing itself, but are part of the complete product.

- **Button plunger.** (Figure 5.50a) The plunger that allows the button to be actuated from the front of the device. It is a simple but fundamental piece. It fits into some rails of the top cover to prevent it from moving laterally.
- **Touchscreen stylus.** (Figure 5.50b) This part was not 3D printed, but was included with the LCD display module.

  Since it was necessary to take its measurements for the design of the casing, incidentally it was modeled in 3D in SolidWorks, which has allowed it to be incorporated into the layouts and renderings of the assembly.

  This piece is perfectly 3D-printable, if needed in the future.

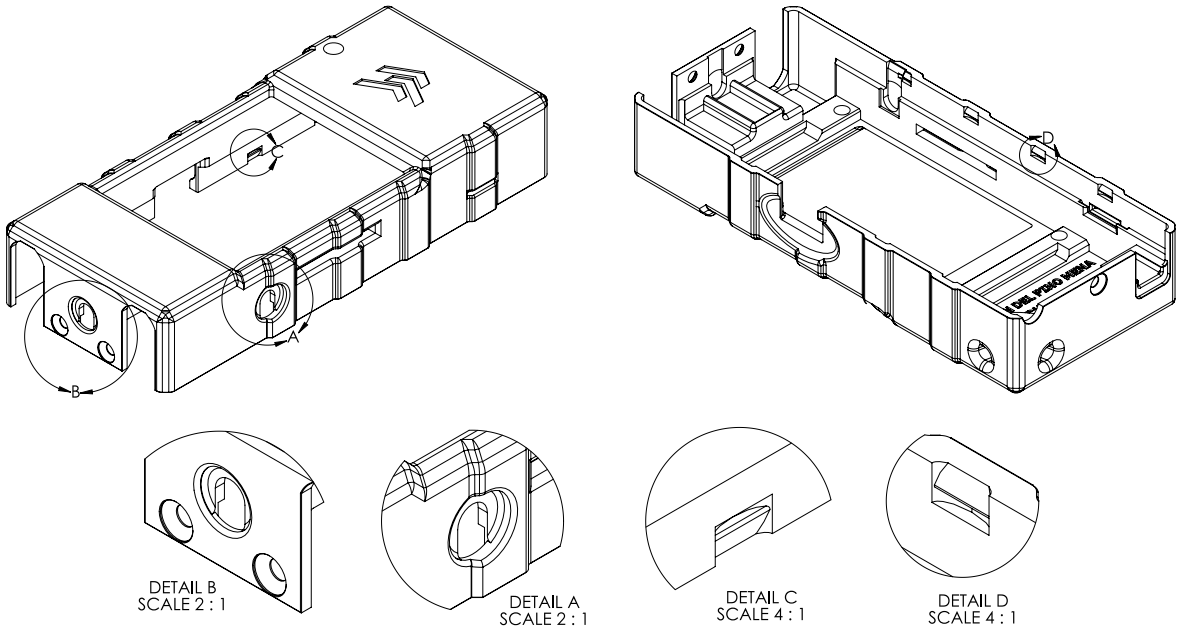

(a) *Isometric 3D views of the top cover, and details of some features.* ***Detail A:*** *depression for the jack receptacle of the load cell.* ***Detail B:*** *Screw countersunks and another depression for the expansion port.* ***Detail C:*** *Receptacle of the closing tabs, top view.* ***Detail D:*** *Receptacle of the closing tabs, bottom view.*

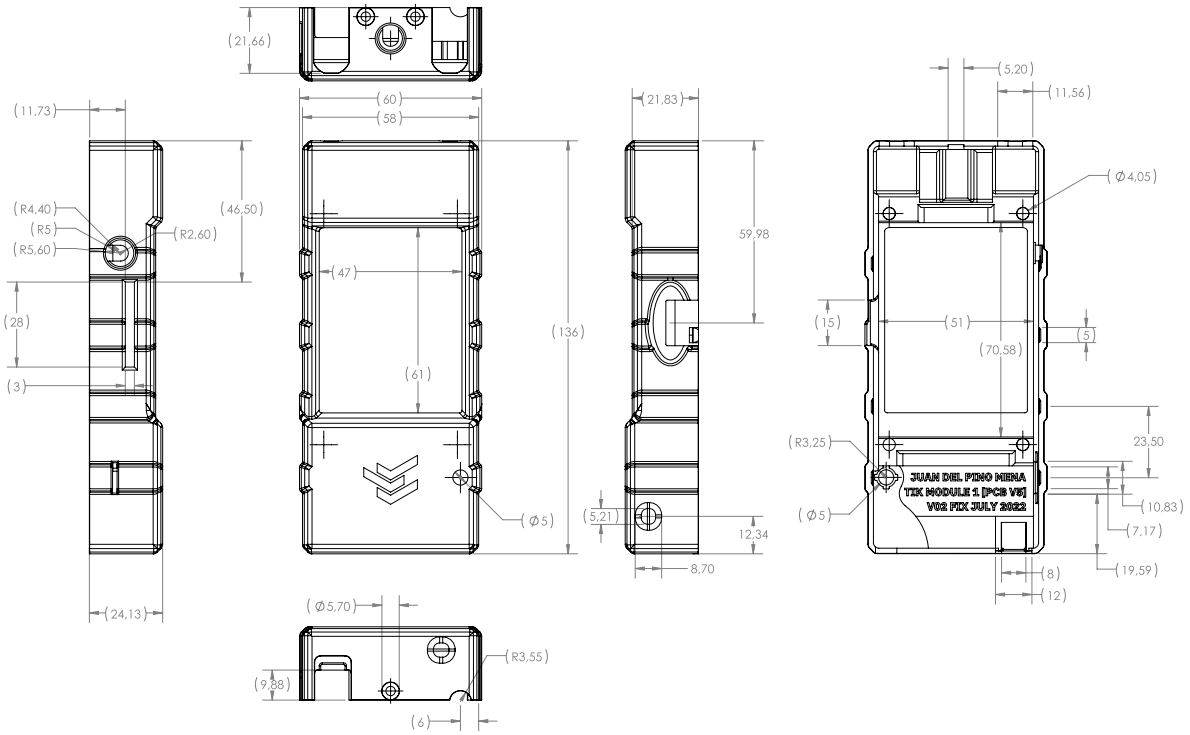

(b) *Views and dimensions of the top cover.*

Figure 5.48

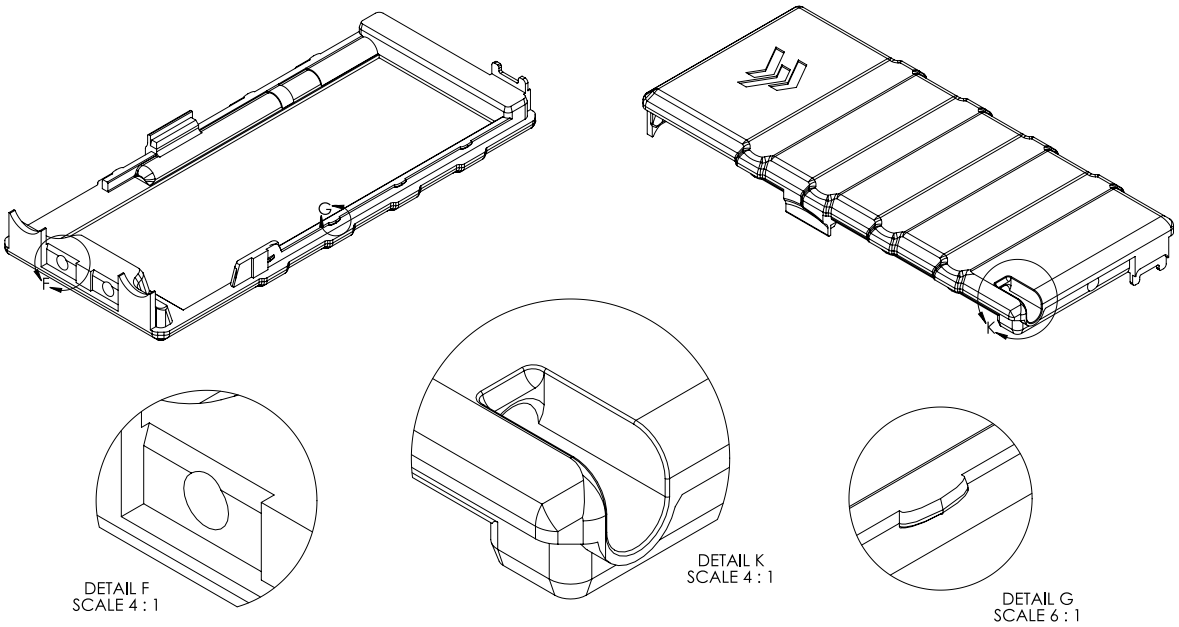

(a) *Isometric 3D views of the bottom cover, and details of some features.* ***Detail A:*** *depression for the jack receptacle of the load cell.* ***Detail F:*** *Hole for a threaded insert.* ***Detail K:*** *Hole for the stylus.* ***Detail G:*** *Closing tabs.*

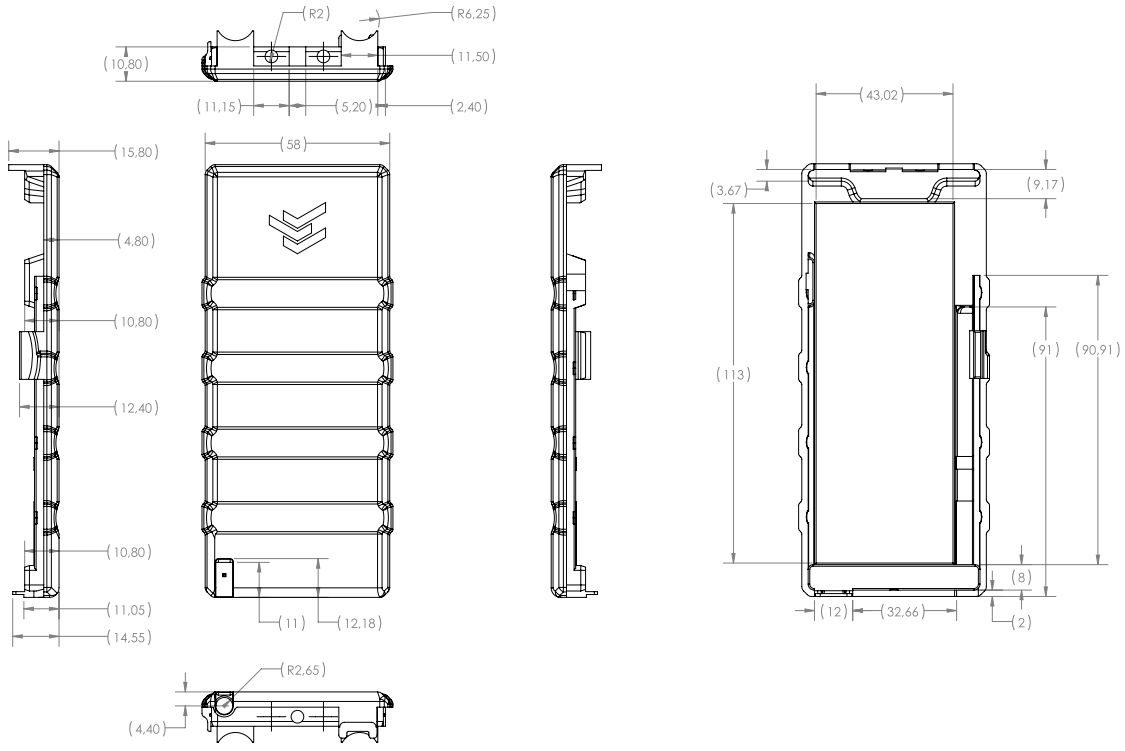

(b) *Views and dimensions of the bottom cover.*

Figure 5.49 – *Isometric 3D views, dimensions and details of the bottom cover.*

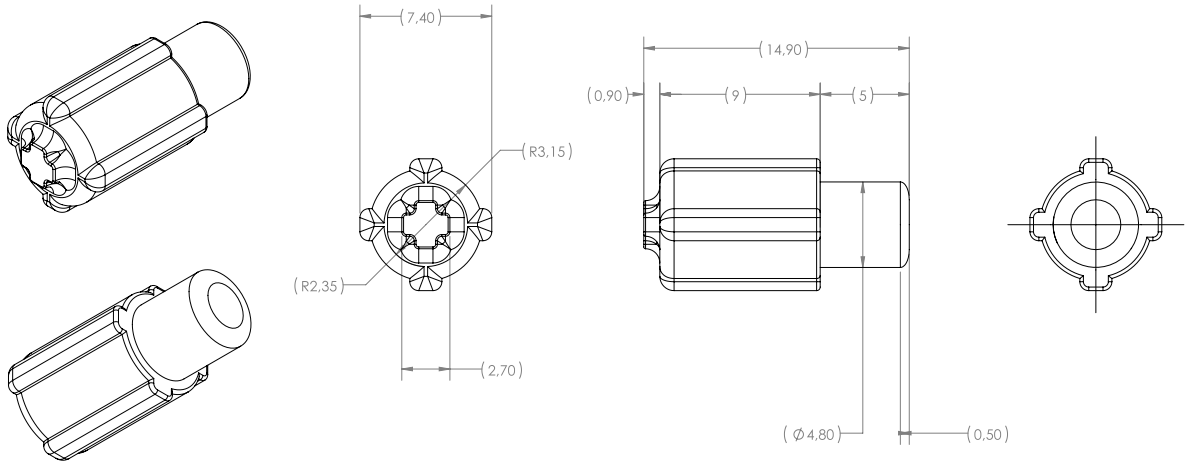

(a) *Views and dimensions of the button plunger.*

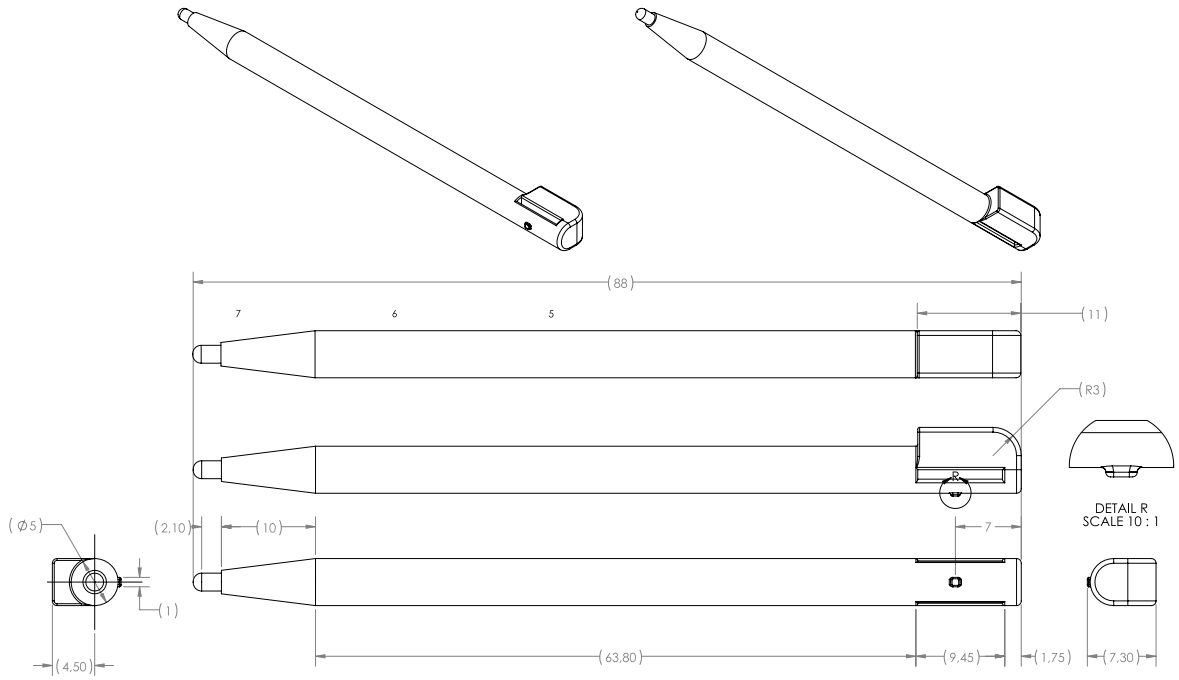

(b) *Views and dimensions of the stylus.*

Figure 5.50 – *Isometric 3D views, dimensions and details of the button plunger and the stylus.*

5.3.2 Complete assembly

This section illustrates the full assembly of the product. Diagrams and some renders of the device are represented in Figure 5.52, and the measurements of the product can be found in Figure 5.53; whereas Figure 5.54 shows a view and a render of the exploded assembly. For a reference of the ID number of each part in the schematics, consult Table 5.10. On the other hand, Video 5.1 shows an animation of the disassembly and reassembly process of the product.

There are 7 screws required for this assembly:

- **3x Flat head torx screw, ISO 10642, size M3, length: 8 mm** (Figure 5.51a), which are located on the upper and lower exterior faces of the device. Together with the clips, they are responsible of holding both covers together.
- **4x Socket-cap head hex screw, ISO 4762, size M3, length: 16 mm.** (Figure 5.51b), which hold the PCB and LCD module through their mounting holes to the top cover.

In addition, 7 M3 size threaded inserts (RS PRO 278-534) are required for each of them (Figure 5.51c).

A more extensive technical documentation with dimensions, details, section views and renderings of the product can be found in Appendix E, section 2: Mechanical drawings of the complete assembly.

Part ID in schematics	Component
1	Top cover (3D printed part).
2	Bottom cover (3D printed part).
3	Stylus for the touchscreen.
4	Threaded insert, size M3, length 5 mm.
5	Power-on/off button plunger (3D printed part).
6	Flat head torx screw, ISO 10642, size: M3, length: 8 mm.
7	Printed Circuit Board
8	Female 3.5 mm jack connector.
22	Female BNC connector.
36	Power-on push-button.
37	Multi-direction 'thumb' button.
44	Female USB-Mini-B connector.
46	LCD screen module PCB
52	TFT LCD screen
53	Socket Cap head hex screw, ISO 4762, size: M3 length: 16 mm.
54	Flat Li-Po battery, 604060 format (6x40x60 mm)

Table 5.10 – *Assembly part ID and the component it identifies.*

(a) *Flat head torx, ISO 10642.*

(b) *Socket-cap head hex, ISO 4762.*

(c) *Threaded insert RS PRO 278-534*

Figure 5.51 – *Exploded view and rendering of the complete assembly.*

Video 5.1 – *Rendered video in SolidWorks showing the animation of the disassembly and reassembly of the complete product. To play this video, please use a compatible viewer such as Adobe Acrobat Reader. If it does not play, you can still watch it if you extract it from the document by right clicking and selecting "save video as".*

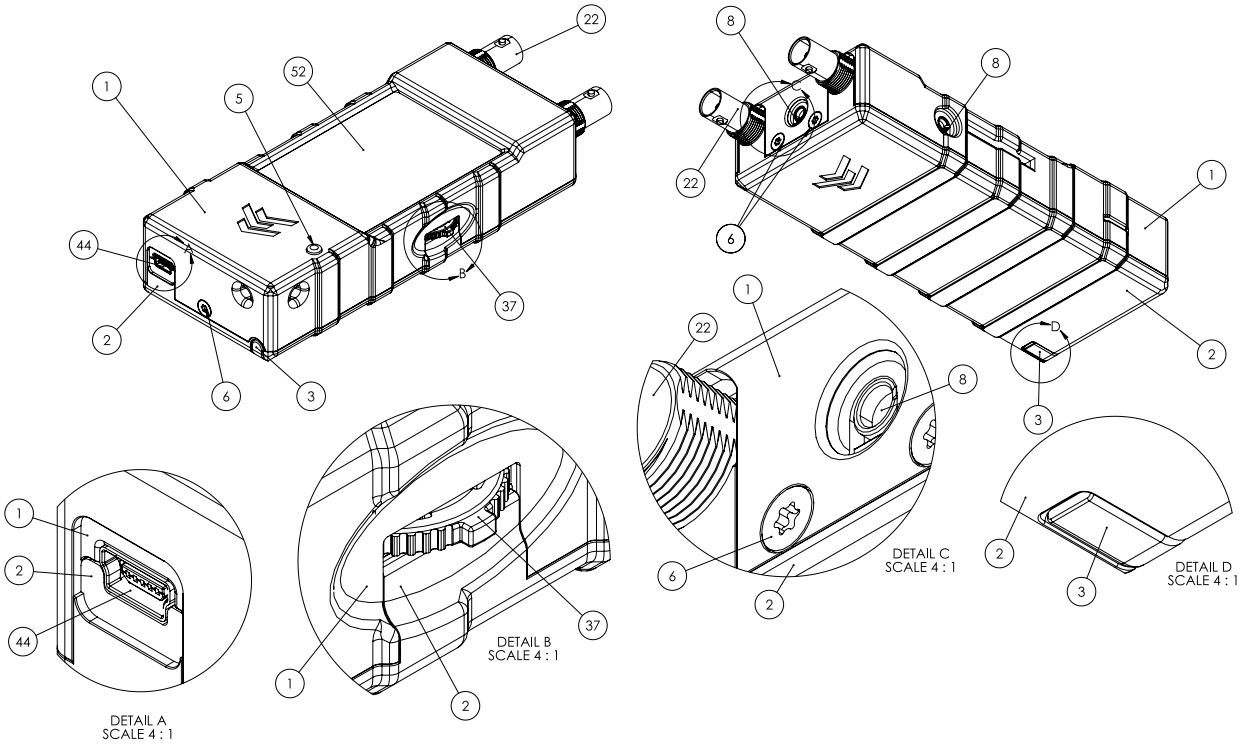

(a) *Collapsed view, schematic. See Table 5.10 for ID reference.*

(b) *Collapsed views, renderings.*

Figure 5.52 – *Exploded view and rendering of the complete assembly.*

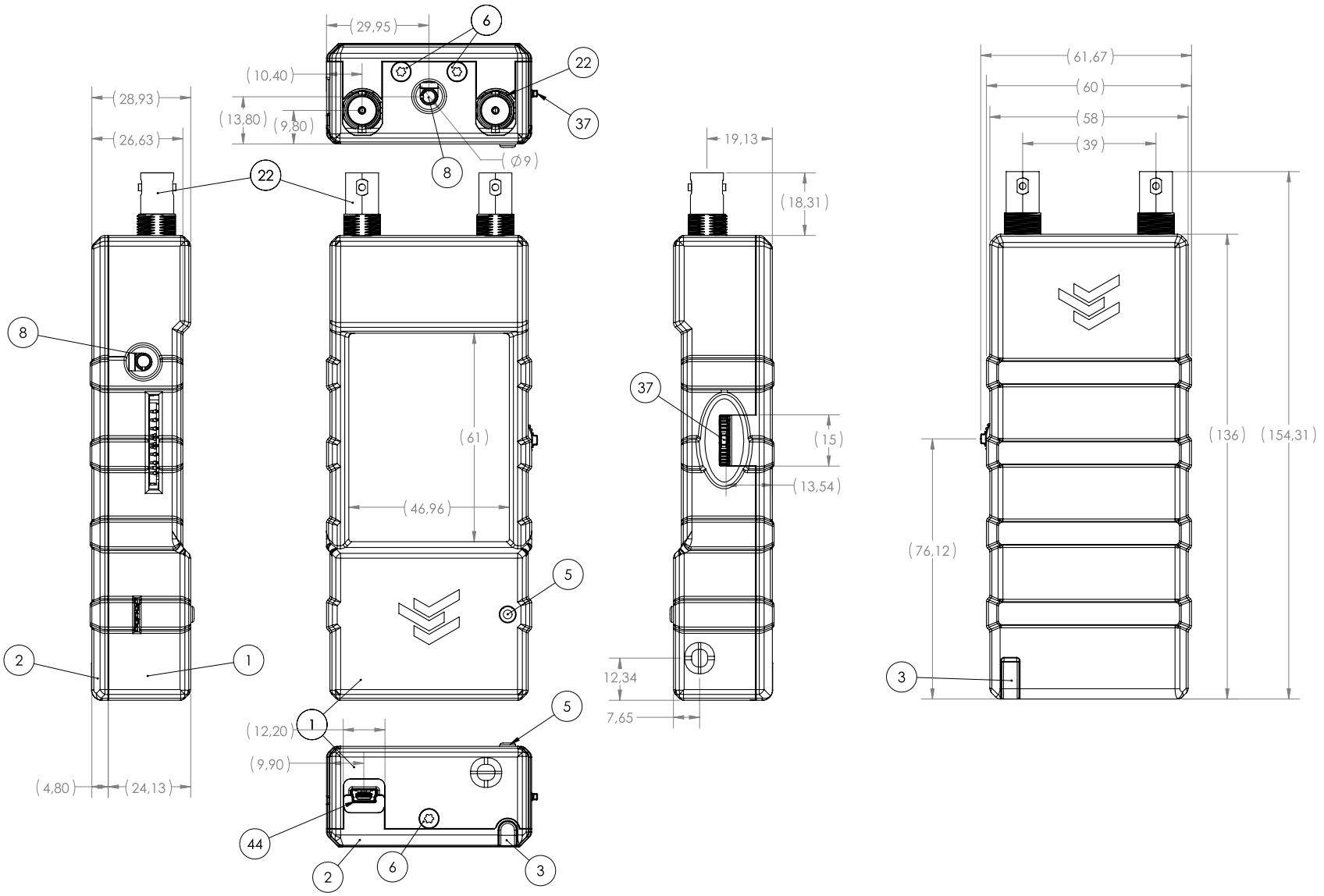

Figure 5.53 – *Views and dimensions of the collapsed assembly. See Table 5.10 for ID reference.*

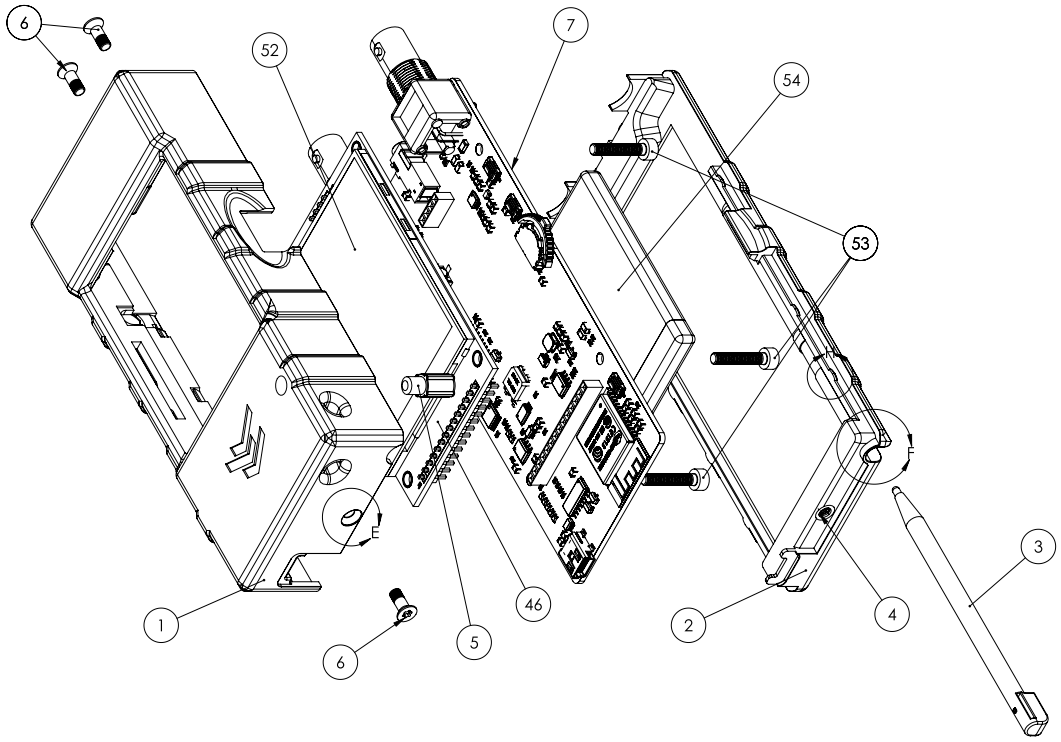

(a) *Exploded view, schematic. See Table 5.10 for ID reference.*

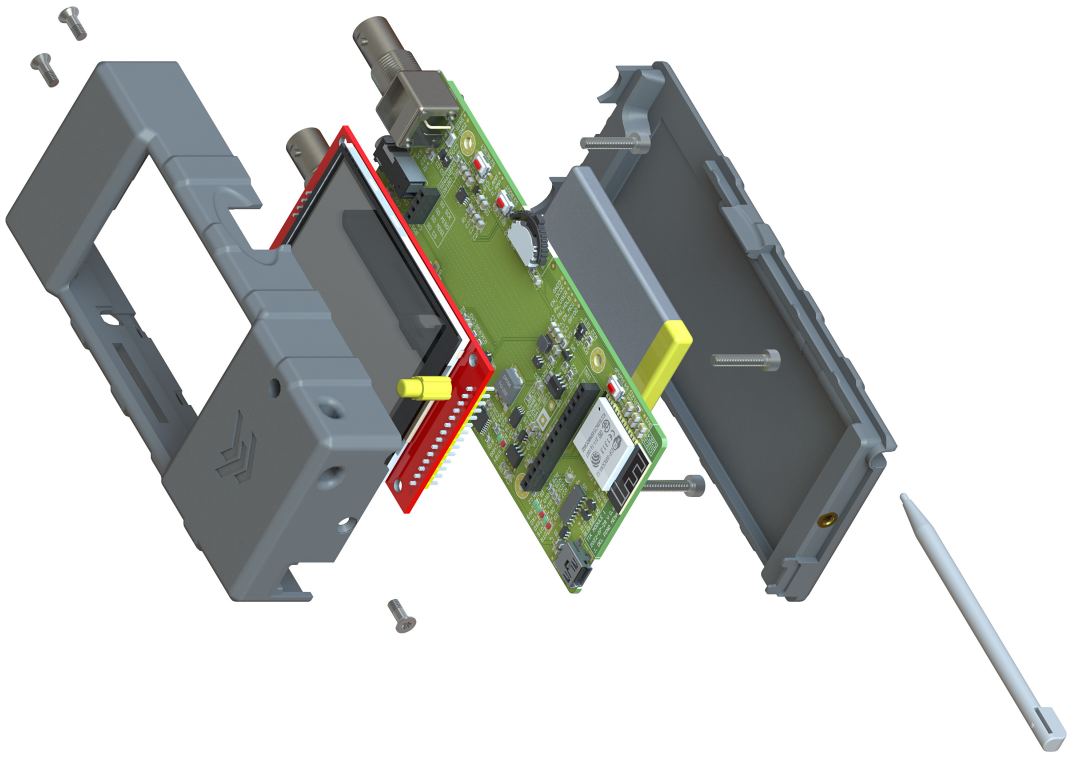

(b) *Exploded view, render.*

Figure 5.54 – *Exploded view and rendering of the complete assembly.*

Chapter 6

Fabrication, testing and validation.

This chapter is divided into several sections:

- First, the manufacturing process of the TIK prototype is detailed, through the **Printed Circuit Board fabrication** and the **3D printing process** of the different parts of the case, concluding with the **complete assembly**.
- Secondly, there is a process of **verification of the operation of the subsystems**, and to the solution of bugs and errors when necessary.

6.1 PCB fabrication

This section describes the Printed Circuit Board manufacturing process. Different fabrication options will be considered. Then, the necessary parameters will be adjusted, the production files that must be generated are detailed, and all the steps followed to solder the components to the board are explained. Finally, a visual inspection of the quality of the welds is performed, and the issues found are manually solved.

6.1.1 Manufacture options

In the GranaSat laboratory there are the necessary means to manufacture printed circuit boards with one or two layers, using a CNC machine to trace the copper polygons, and another electrolysis machine to plate vias and THT holes. However, at the time of writing it is not quite ready for production yet. And furthermore, this manufacturing process introduces new problems, restricts design freedom and introduces manufacturing difficulties: larger tolerances, larger vias, lower degree of miniaturization in general, no solder mask (and therefore copper oxidation) , without silkscreen, without SMD pads, or stencil, etc.

For all these reasons and given the complexity of our electronics, the decision was made to contract a commercial PCB manufacturing service instead. There are many similar options with competitive prices that give good results. To name a few: PCBway, JLCPCB or WellPCB.

Finally, JLCPCB has been selected for showing good results in previous students' works (such as: [105, 106, 165, 166]). This decision was made in agreement with the rest of the projects that are being developed in parallel in the GranaSat laboratory outside this bachelor's thesis, so that we all order the plates from the same place and share shipping costs, which make up the bulk of the cost of PCB manufacturing (see Annex A: Project costs). This decision was also made during early development stage, so that the PCB could be adapted to the manufacturer's design rules and capabilities.

Figure 6.1 – *JLCPCB logotype, extracted from: [167].*

Base Material	FR-4	Aluminum				
Layers	1	2	4	6		
Dimensions	132	*	54			
PCB Qty	5					
Product Type	Industrial/Consumer electronics	Aerospace	Medical			
Different Design	1	2	3	4		
Delivery Format	Single PCB	Panel by Customer	Panel by JLCPCB			
PCB Thickness	0.4	0.6	0.8	1.0	1.2	1.6	2.0
PCB Color	Green	Purple	Red	Yellow	Blue	White	Black
Silkscreen	White						
Silkscreen Technology	Ink-jet/Screen Printing Silkscreen	High-definition Exposure Silkscreen					
Surface Finish	HASL(with lead)	LeadFree HASL-RoHS	ENIG-RoHS				
Outer Copper Weight	1 oz	2 oz					
Gold Fingers	No	Yes					
Confirm Production file	No	Yes					
Flying Probe Test	Fully Test	Not Test					
Castellated Holes	No	Yes					
Remove Order Number	No	Yes	Specify a location				

Figure 6.2 – *PCB order fabrication details on JLCPCB.*

6.1.2 Fabrication files and parameters

Fabrication files are the ones needed by the manufacturer in order to make the PCB. There are various standards, but the most widespread are the Gerber files. [168]

Gerber files store all the information about shape and location for every primitive in a PCB layout, as well as configuration parameters. Each layer in your PCB layout data will be placed into its own Gerber file, identified by a three-letter code. For example, the most important layers in our design are GTL, GBL, GTO, GBO, GTS and GKO.

Each individual layer can be used to prepare *stencils* for each step in the fabrication and assembly process. We will use an stencil for the soldering process, which has been generated with the GTS. This file creates a mask of the SMD pads in top layer (see Figure 6.3). The stainless steel stencil has also manufactured by JLCPCB.

We must also provide the manufacturer with an NC Drill file that contains the positions and the caliber of the drilling holes necessary for the mounting holes, vias, etc.

On the other hand, when ordering from JLCPCB we need to specify some extra configuration parameters, such as the base material, thickness, solder resist color, or surface finish (Figure 6.2). The latter must be HASL-RoHS or ENIG-RoHS to ensure that we comply with European regulations.

6.1.3 PCB fabrication results

The results obtained are good, the manufacturer has perfectly met expectations. Figure 6.4 shows the top and bottom scans of one of the 5 ordered PCBs.

6.1.4 PCB assembly

This section details the PCB assembly procedure. First, the process of deposition of solder paste with the stencil is detailed, then, we will place the components, perform a reflow soldering in an oven, and finally we will carry out a visual inspection of the quality of the solders, and the correction of solder defects.

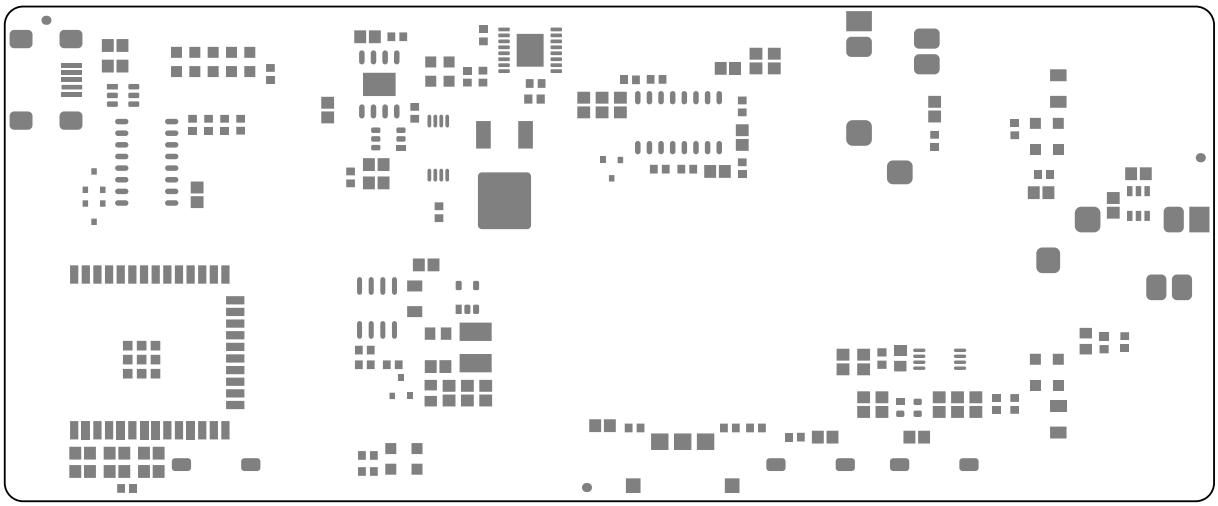

Figure 6.3 – *Representation of the Gerber Top Solder (GTS), which is a mask of the SMD pads in top layer.*

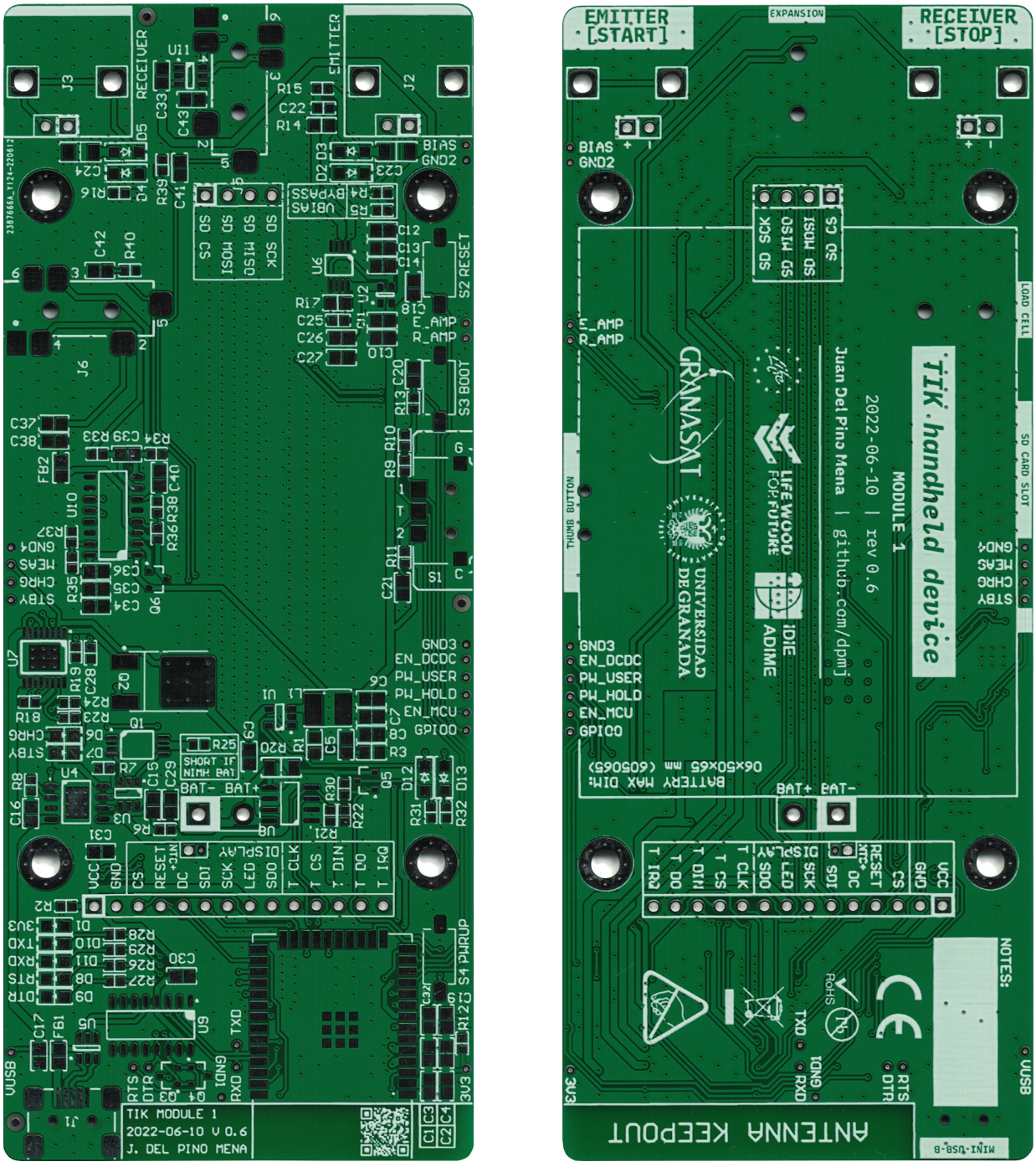

(a) *Top view* **(b)** *Bottom view*

Figure 6.4 – *Top and bottom view scans of the manufactured PCB.*

6.1.4.1 Stencil alignment and solder paste application.

1. The first step is to check that the stencil is correct, since only the openings for the top layer SMD pads should appear (Figure 6.5a).

2. We proceed to align the PCB with the stencil. For this, unpopulated and broken or disused PCBs of the same height as ours are used to form a tight frame around our PCB. This way it is completely fixed and will not move during the application of the solder paste (Figure 6.5b).

3. The next step is to deposit the solder paste itself, which comes in the tube pictured in Figure 6.6a. A specific applicator is used, which presses against the end of the tube (Figure 6.6b). Neither too small nor too abundant solder should be deposited (Figure 6.6d).

4. Finally, the solder paste is spread evenly (Figure 6.6e), with the help of spatulas (Figure 6.6c).

The result can be seen in Figure 6.7.

6.1.4.2 Component placing

This step consists on positioning each component on top of its corresponding footprint with tweezers, making sure that they have the correct orientation and enough solder. The components must be pressed lightly against the solder paste so that they are suspended in it. The process is pictured in Figure 6.8.

6.1.4.3 Oven reflow soldering

Using an oven allows us to solder all components at the same time, although we must be careful to ensure that they are solder correctly and that the solderings are uniform throughout the plate. Figure 6.9a shows the oven available for this purpose in the GranaSat laboratory.

The oven is preheated for 10 minutes until it reaches 250 ^{o}C. Then, we carefully insert the PCBs into the oven rack (6.9b). In order for the welding to be uniform, the PCB placement inside the oven is important: it should be away from the oven door, an area where the temperature is lower; and the components with more thermal inertia (such as the ESP32 or the USB Mini-B) are placed at the bottom of the oven, usually a hotter area (see Figure 6.9b).

PCBs should be left long enough for the solder paste to take on a smooth, shiny texture evenly across the board. This process takes longer for components with higher thermal inertia. Solder fumes are emitted during the process, which is expected. This should not be confused as smoke, which will only come out when the PCB has been inside for a long time and the board and its components are burning.

PCBs should be left long enough for the solder paste to take on a smooth, shiny texture evenly across the board. Thanks to the mixture of solder and flux, the solder paste tends to amalgamate on the pads during reflow, causing components to move and align themselves. This process takes longer for parts with higher thermal inertia. Solder fumes are emitted during the process, which are expected and should not be confused as smoke. After approximately 3 minutes inside the oven, the solderings are done. We turn off the oven, remove the PCBs and let them cool for 5 minutes.

The result of the two plates welded simultaneously can be seen in Figure 6.10. If the reader has a good eye, he will realize that solder defects have occurred, which we will review and correct in the next section.

In a more advanced manufacturing process, PCB manufacturing is automated by machines that apply just the right amount of solder, pick and place machines position components fast and without error, and specialized ovens with active airflow are configured to apply an optimum temperature curve for a specific design. This way, high quality solders with low defect rates are achieved.

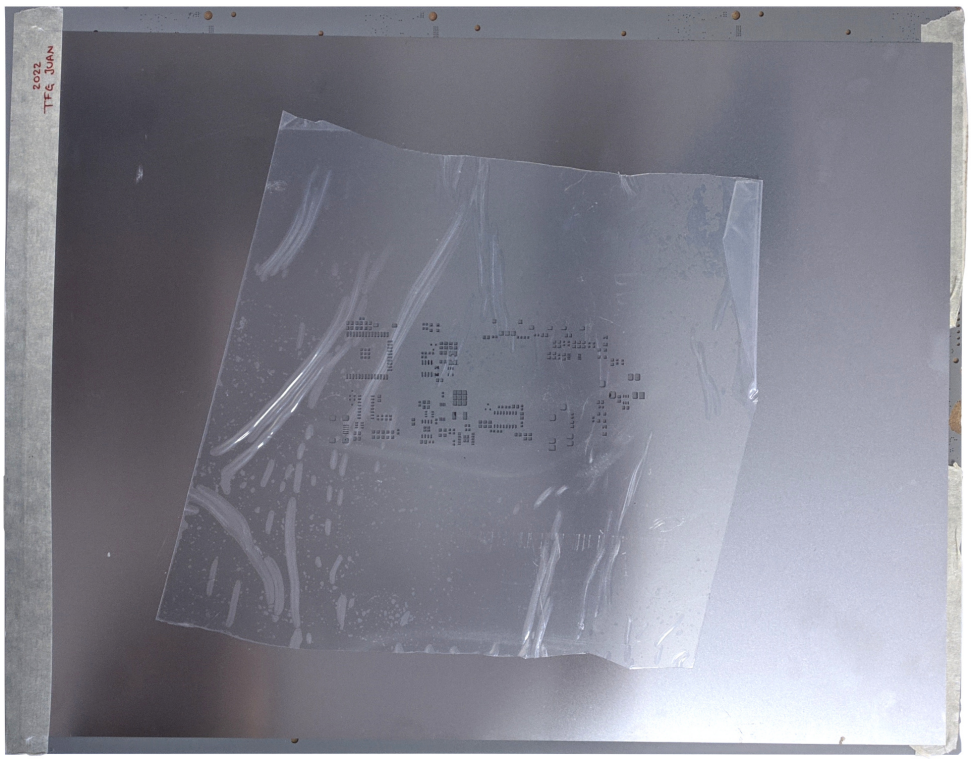

(a) *Stencil as delivered.*

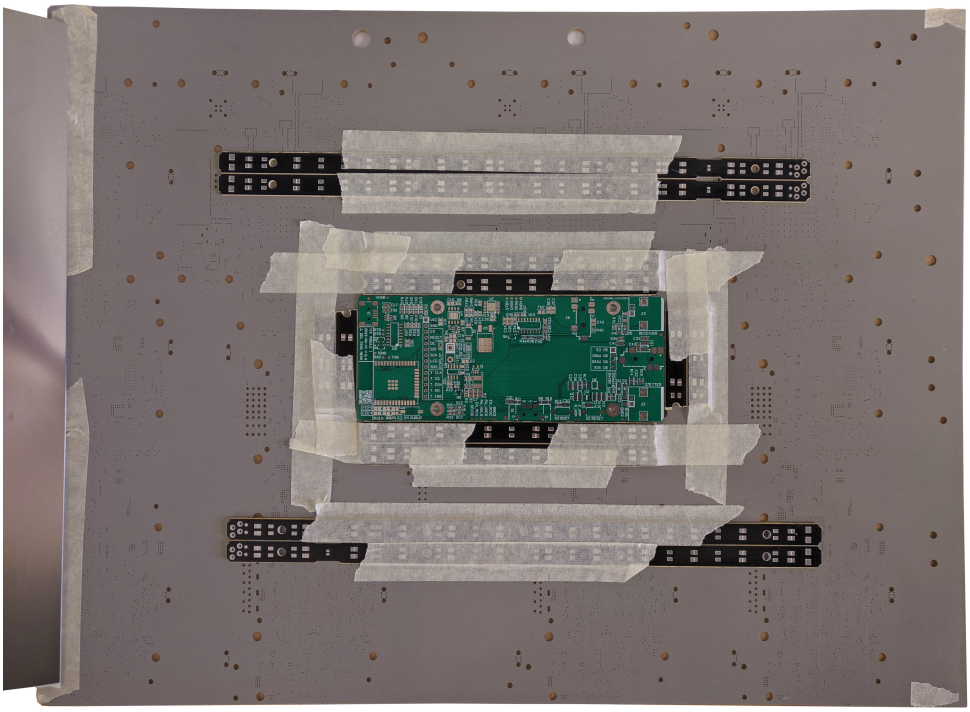

(b) *TIK's PCB held by other PCBs, and aligned with the stencil.*

Figure 6.5 – *Stencil and PCB alignment.*

(a) *Solder paste tube.*

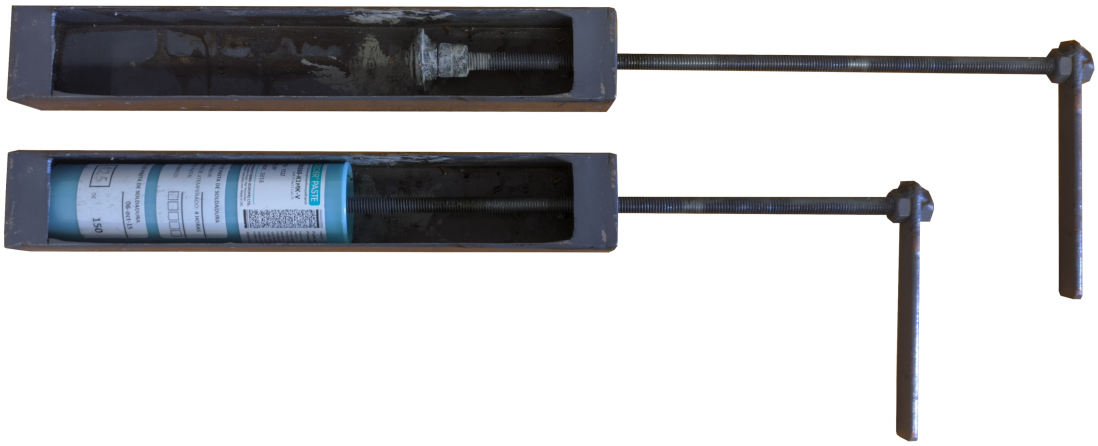

(b) *Solder paste applicator with and without the solder paste tube attached.*

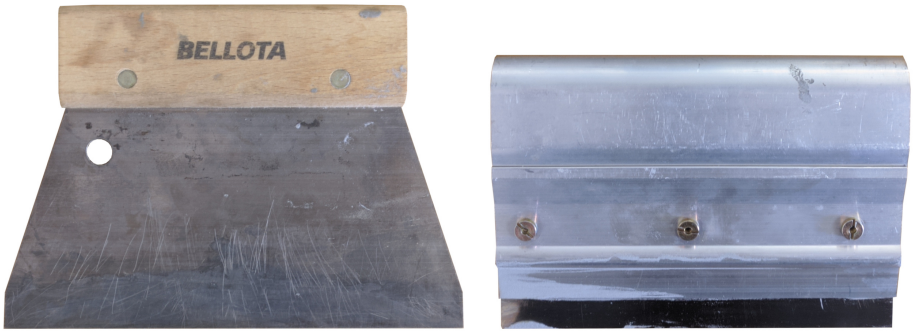

(c) *Spatulas used to spread the solder paste on the stencil.*

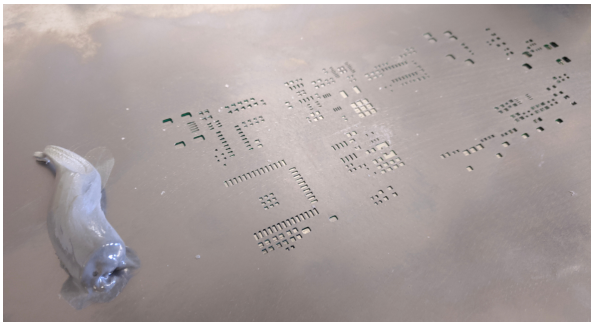

(d) *Stencil with solder paste not yet spread.*

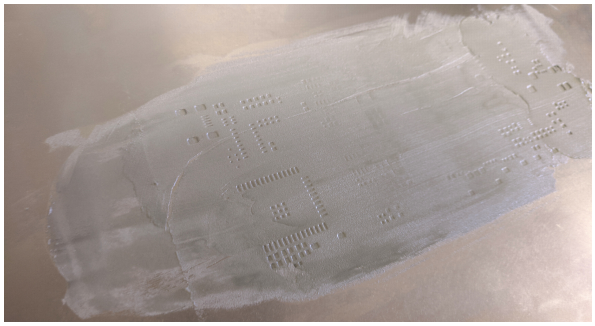

(e) *Stencil with solder paste spread.*

Figure 6.6 – *Application of the solder paste to the SMD pads of the PCB through the stencil.*

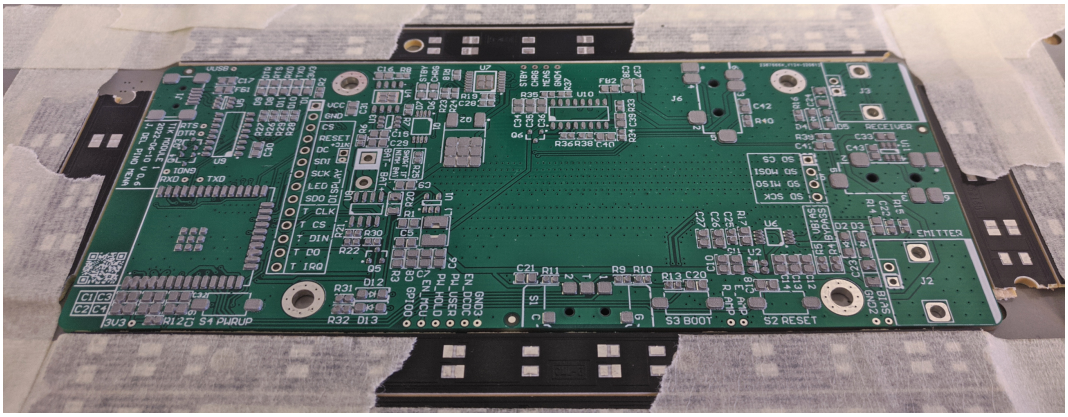

Figure 6.7 – *PCB with solder paste applied.*

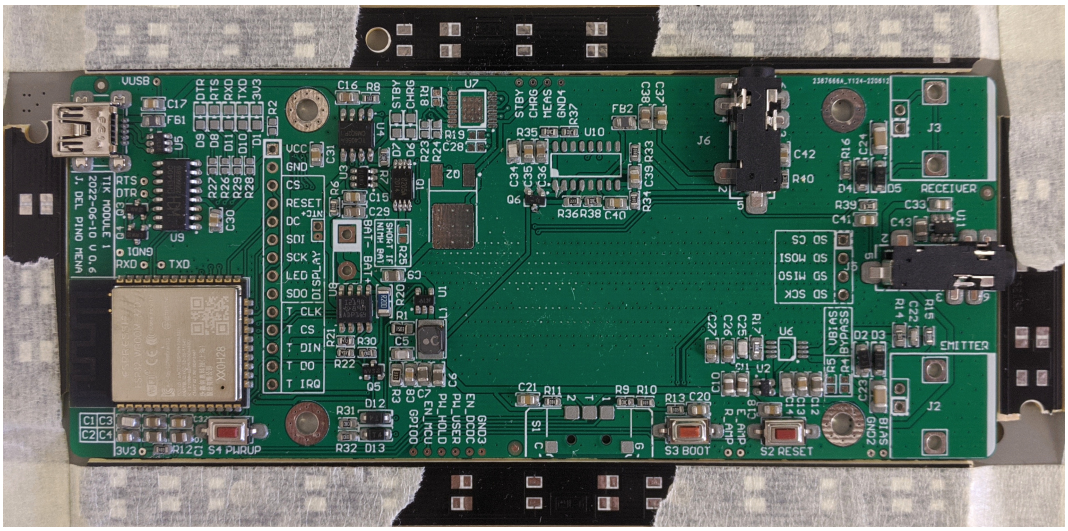

Figure 6.8 – *PCB with almost all components placed on top of the solder paste.*

(a) *Oven used for reflow soldering at GranaSat's.*

(b) *Placing the boards inside the oven.*

Figure 6.9 – *Oven for reflow soldering, and PCB placement inside it.*

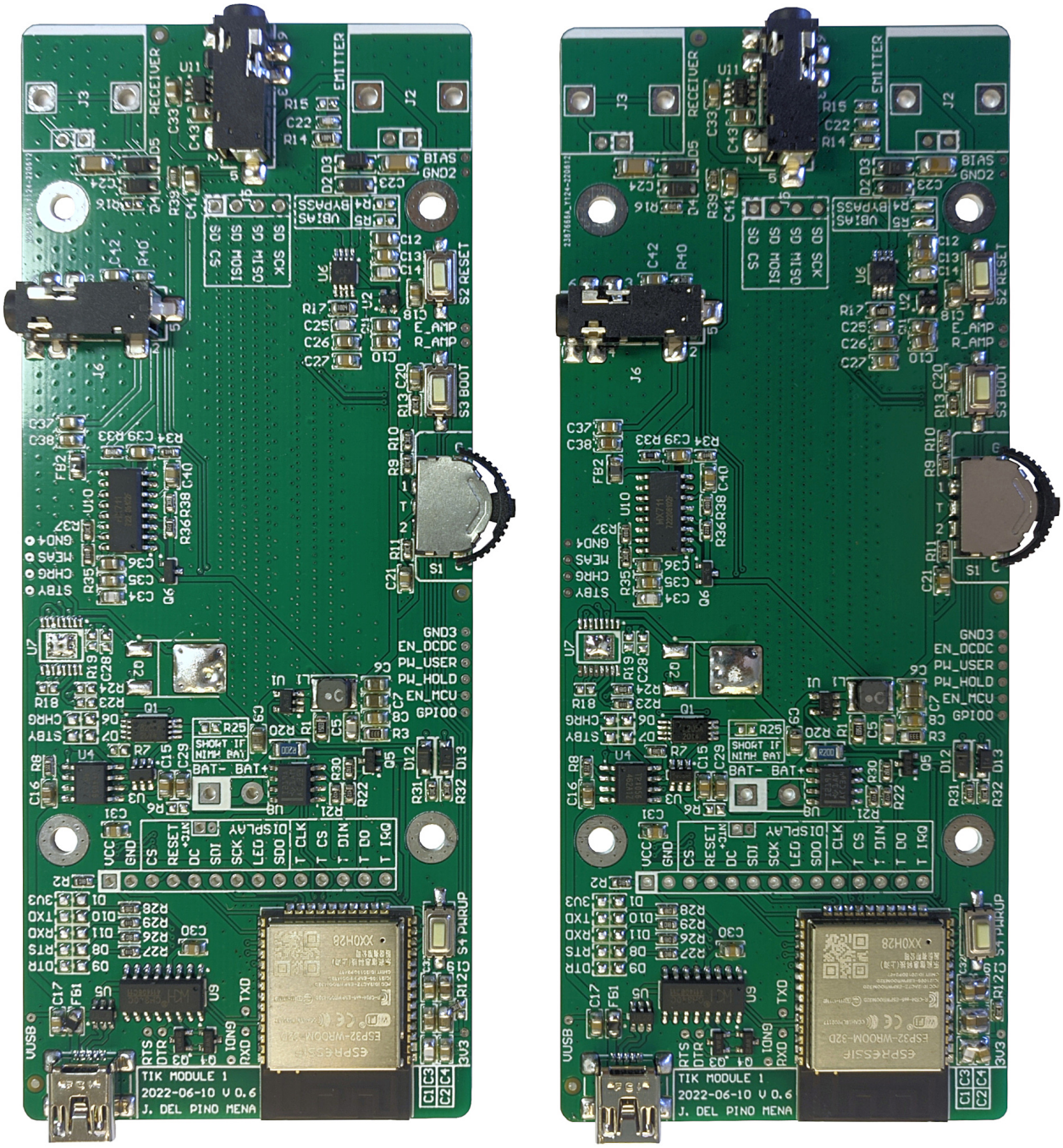

Figure 6.10 – *The two PCBs after being reflow-soldered in the oven, with solder defects.*

6.1.5 Visual inspection and correction of solder defects

That a manual soldering process comes out perfect the first time is very unlikely, and even less so with little experience in PCB manufacture. There are a lot of issues that can appear during soldering, even in mass production. Due to this, computer vision systems are introduced in the production line to automatically verify the quality of the solderings [169].

Next, a visual inspection of the solderings will be carried out in detail, to identify possible problems that will then be solved. In Figure 6.11, certain important PCB areas are zoomed-in so that solder defects are more apparent. The most serious errors are highlighted in red. We can observe multiple unwanted joints between components, which is mainly due to an excess of solder paste (as is evident in the case of Figure 6.11d), but also due to shocks or vibrations when moving and/or placing the PCB in the oven. (as is more likely to have occurred in Figure 6.11a).

6.1.5.1 Procedure to solve solder defects

These defects are solved manually. In the GranaSat laboratory there is an AOYUE Int 2702A+ soldering station, pictured in Figure 6.13a, which is specially suitable for this process. Said equipment has a solder iron with adjustable temperature and a solder fume absorber (Figure 6.13b); and a heat gun with changeable nozzle and adjustable air pressure and temperature (Figure 6.13c).

Defective solderings must be heated again using the most appropriate tool depending on the case. If the heat gun is used, both sides of the PCB must be heated in order to avoid damaging it.

Moved components can simply be repositioned using tweezers or desoldering needles.

Non-critical solder slack can be left as is, but those causing pin shorts should be corrected by reheating the solders and absorbing the excess by pressing solder wick (Figure 6.13d) against the component's pins with the solder iron.

Figure 6.12 illustrates some areas of the PCB after correcting the previously numbered defects.

6.1.6 PCB assembly result

After the correction of the SMD solder defects, THT components are soldered manually using the solder iron. The final result can be seen in Figure 6.14, where photos of two boards are shown, one of them with BNCs and the female pin strips for the LCD module soldered, and the one on the right shows the fit of the LCD on the PCB.

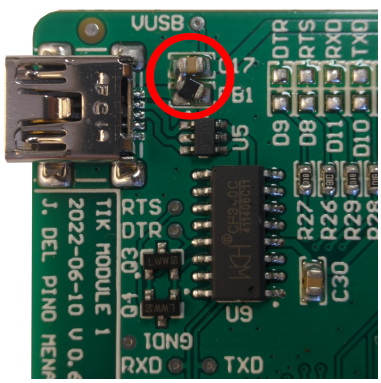

(a) *Detail of the USB Mini-B, CH340C and other surrounding components.*

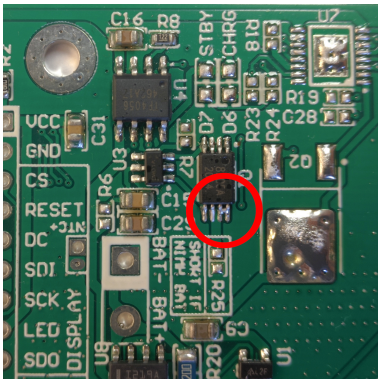

(b) *Detail of the TP4056-based charger.*

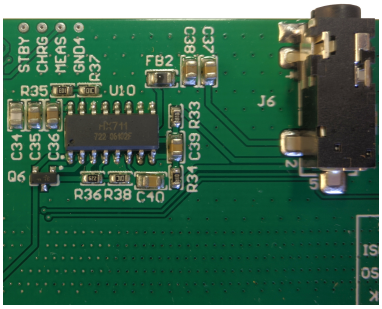

(c) *Detail of the HX-711 circuit.*

(d) *Detail of the ESP32 and its bypass capacitors.*

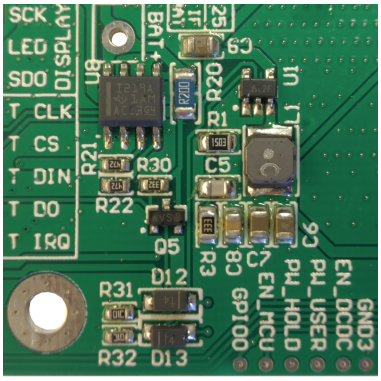

(e) *Detail of the DC/DC converter circuit, INA219 their surroundings.*

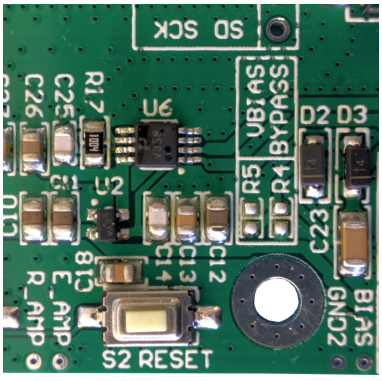

(f) *Detail of the adequation circuit and some buttons.*

Figure 6.11 – *Detail of some PCB areas with and without solder defects. Not all photos are of the same PCB, the details highlight errors on two different boards.*

(a) *Detail of the ESP32 after moving components and removing part of the solder with solder wick.*

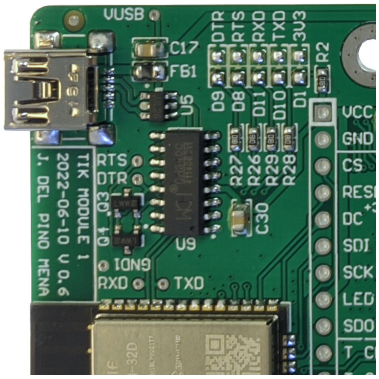

(b) *Detail of the USB circuit after repositioning the ferrite bead.*

Figure 6.12 – *Detail of some PCB areas after solving the solder defects.*

(a) *The AOYUE Int 2702A+ soldering station at GranaSat.*

(b) *Detail of the soldering iron with fume absorber.*

(c) *Detail of the heat gun.*

(d) *Desoldering wire (also known as soldering wick).*

Figure 6.13 – *AOYUE Int 2702A+ soldering station and its tools at GranaSat's laboratory.*

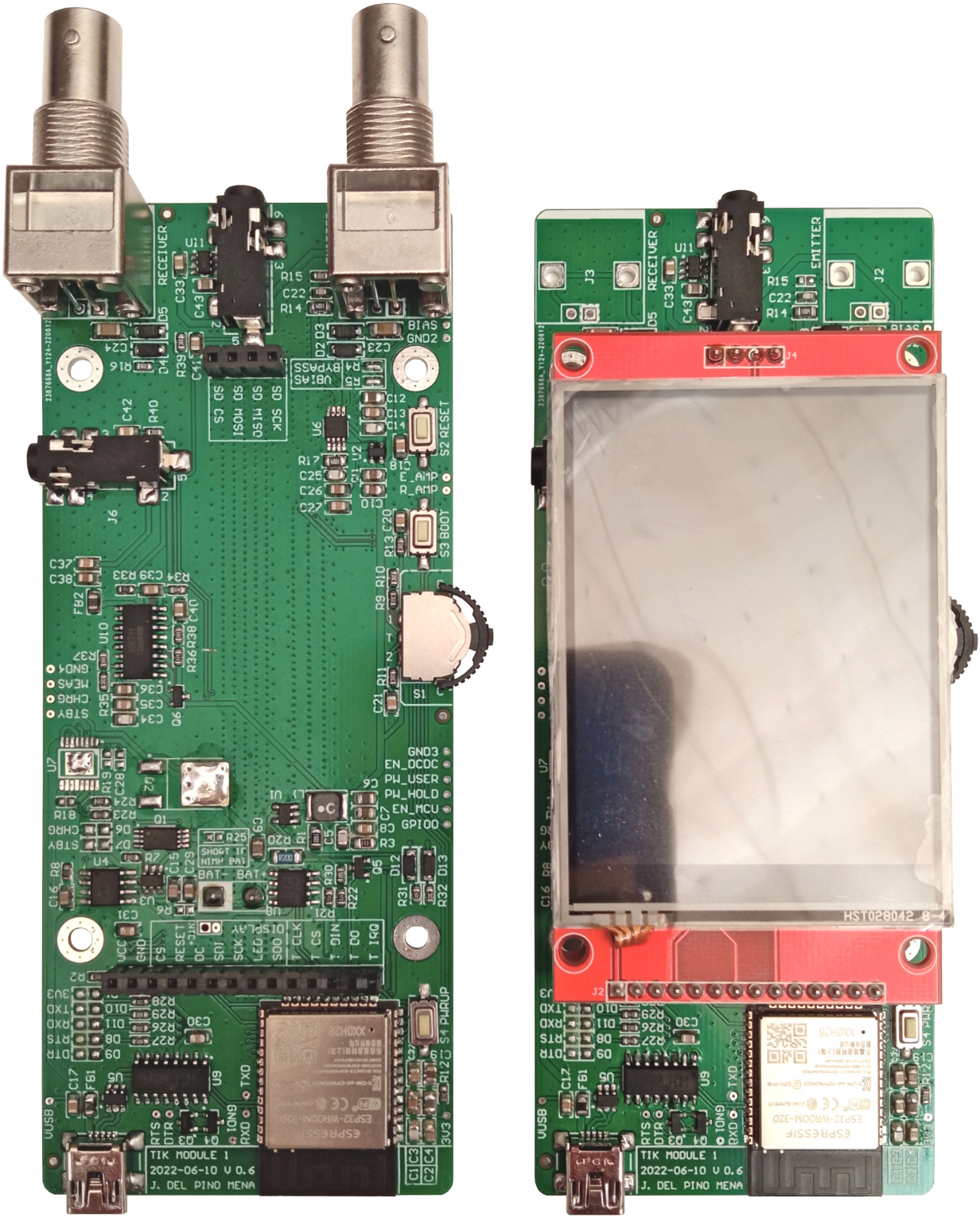

Figure 6.14 – *PCBs soldered with corrected solder defects. Version with and without BNCs and the LCD.*

6.2 Case 3D printing

As mentioned in previous sections, for a first approximation we will use 3D printing to create the prototype's casing. 3D printing is suitable for prototyping, but for product release to the market a more professional manufacturing process should be used (such as plastic molding). To print the pieces, we have used the 3D printers offered free of charge to students by BiblioMaker, the *"Maker"* space of the library of the Faculty of Sciences of the UGR [170].

Bibliomaker recently renewed all of its printers, now having eight Creality Ender 3 Pro (Figure 6.16a). These machines are meant to work with low-temperature plastic filaments such as PLA. Before printing, it is recommended to go through a preparation process that consists of leveling the nozzle in the 4 corners of the heated bed, cleaning and preheating the bed, and checking the condition of the filament and/or changing it. To print, the printers follow a series of instructions contained in a file with a `.gcode` extension.

To generate this `.gcode`, we must use 3D printing software such as Cura. Developed by Ultimaker, a 3D printer-manufacturing company, Cura is the most widely used application in this field, as it is an open source, high-quality software with advanced configuration and extensive support for many printers from many manufacturers. Ultimaker Cura is responsible for transforming a 3D model in `.STL` format to `.gcode` according to a configuration that we apply.

Bibliomaker's Ender 3 Pro machines work with a 1.75 mm diameter filament and are equipped with 0.2 mm nozzles, so the granularity will be large. The most relevant configuration parameters applied to Cura for the aforesaid printer can be consulted in Table 6.1. It is a compromise between resistance, quality and printing speed resulting from previous experience with this machine.

Even so, some pieces take up to 11 hours to print due to the large area they occupy, their particular shape and level of detail. The breakdown of printing hours of the corresponding parts is found in Table 6.2.

The part placement and the layered slicing can be seen in Figure 6.15, both for the case pieces (Figure 6.15a), and multiple power buttons printed at once in different positions to check which one is the most appropriate (Figure 6.15b). The back of the case is printed upside down and held by supports, as otherwise it would result in imperfections to the outside, visible surface; because the designed back cover part does not have good contact with the heated bed.

Photos of the printing process can be seen in Figure 6.16. In the first place, a test of the print settings and print quality was made with 3 orange buttons (Figure 6.16b), because they consume little filament and print in a short time. After the check, the two covers are printed (Figure 6.16c). Once the printing is finished, the parts are carefully detached off the heated bed using a spatula, and the supports are removed with the help of precision pliers to avoid damaging the piece.

The print result can be seen in Figure 6.17. This figure shows the parts from all perspectives to inspect method for quality and finish. As we can see, it is generally good for a filament printer, but with important flaws such as inconsistent ironing (softening of the last layers with the hot nozzle without releasing filament), separation between layers on some side areas, etc. For the parts to come out perfect it is necessary to fine-tune the print settings for the particular printer.

Also, some thinner walls, such as the surroundings of the USB Mini-B or the BNCs, have been broken after a few cycles of engaging and disengaging the two covers together. In addition, the walls of the top cover that interface with screws have suffered mechanical stress due to a tolerance problem in the complete assembly (which will be discussed in section 6.3), especially the wall next to the BNCs. And as a consequence, some of the wall layers have separated.

Trying to fit the buttons into their sockets showed that the tolerances were insufficient, having to reprint another batch with narrower plungers (Figure 6.18c). This time all were printed vertically, upside down and with supports (which was the option that resulted in a higher quality piece in the first batch).

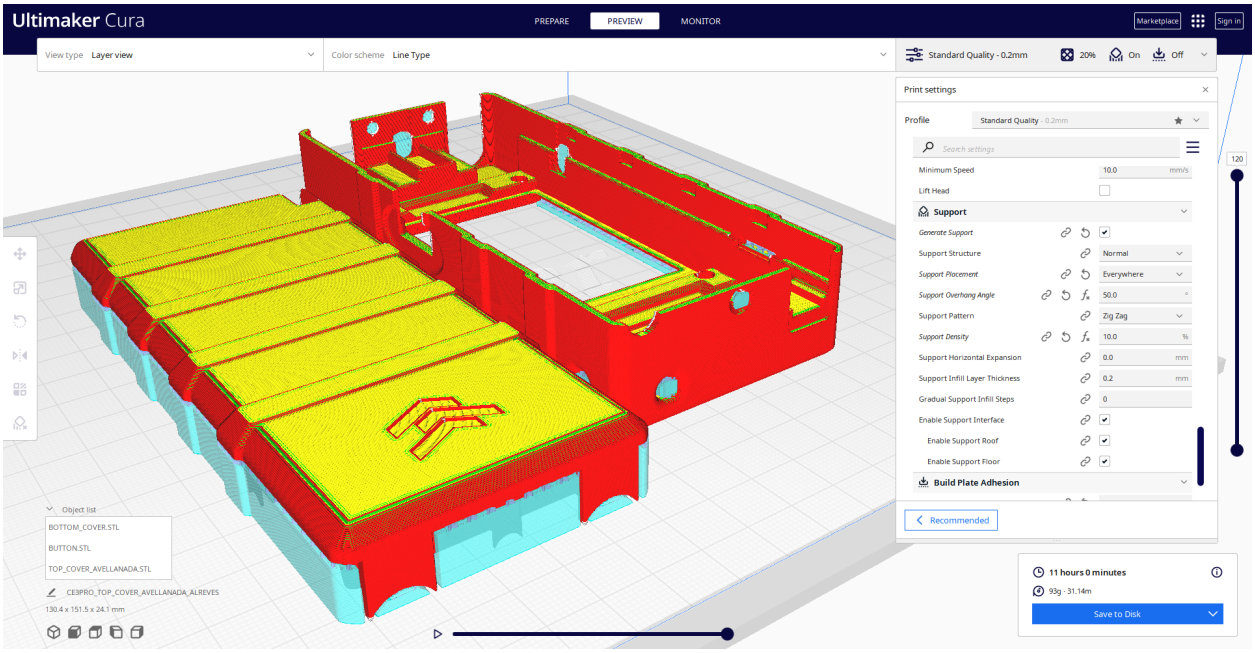

(a) *Case parts placement and slicing.*

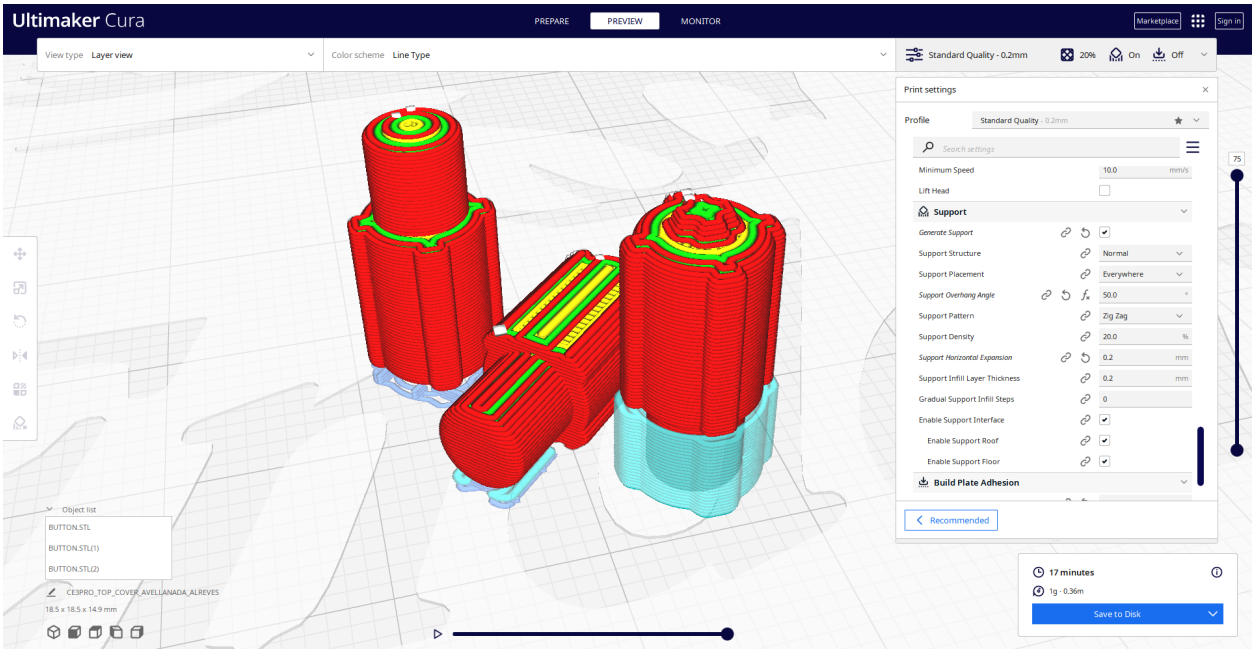

(b) *Button placement and slicing.*

Figure 6.15 – *Screenshot of Ultimaker Cura with the case pieces and buttons positioned and sliced. Estimation of the amount of filament and the printing time.*

Parameter type	Parameter	Value
Quality	Layer height	0.2 mm
	Initial layer height	0.2 mm
	Line width	0.4 mm
Walls	Wall thickness	1.2 mm
Top/Bottom	Top/Bottom thickness	1.2 mm
	Enable ironing	True
Infill	Infill density	30 %
	Infill pattern	Triangles
Material	Printing temperature	205ºC
	Build plate temperature	60ºC
Speed	Print speed	60 mm/s
	Wall speed	30 mm/s
	Top/Bottom speed	30 mm/s
	Travel speed	150 mm/s
	Initial layer speed	20 mm/s
Support	Generate support	True
	Support placement	Everywhere
	Support overhang angle	45º
	Support pattern	Zig-zag
	Support density	20 %
	Support horizontal expansion	0.2 mm
	Enable support interface	True
Build plate adhesion	Build plate adhesion type	None

Table 6.1 – *Set parameters in Ultimaker Cura for the Creality Ender 3 Pro.*

6

Part	Printing time	Weight (grams)	Filament amount (meters)
3x Buttons	17 minutes	1	0.36
Bottom cover	5 hours, 44 minutes	52	17.44
Top cover	5 hours, 12 minutes	41	13.70
Both covers simultaneously	11 hours, 0 minutes	93	31.14

Table 6.2 – *Printing time and material required for each part.*

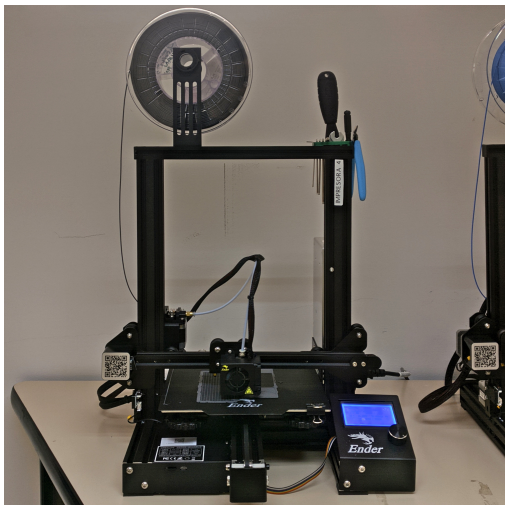

(a) *The Creality Ender 3 Pro printer at Bibliomaker.*

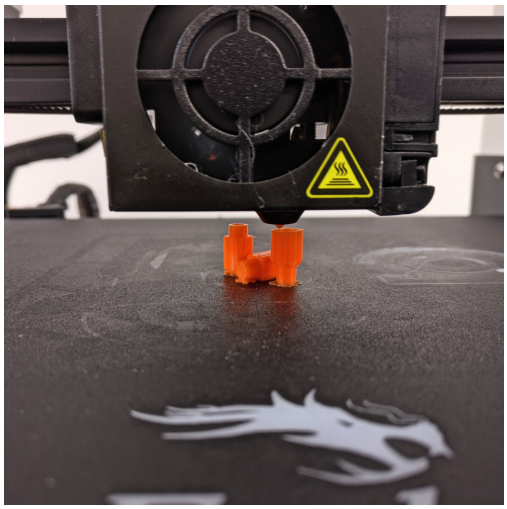

(b) *Printing test, first batch of buttons.*

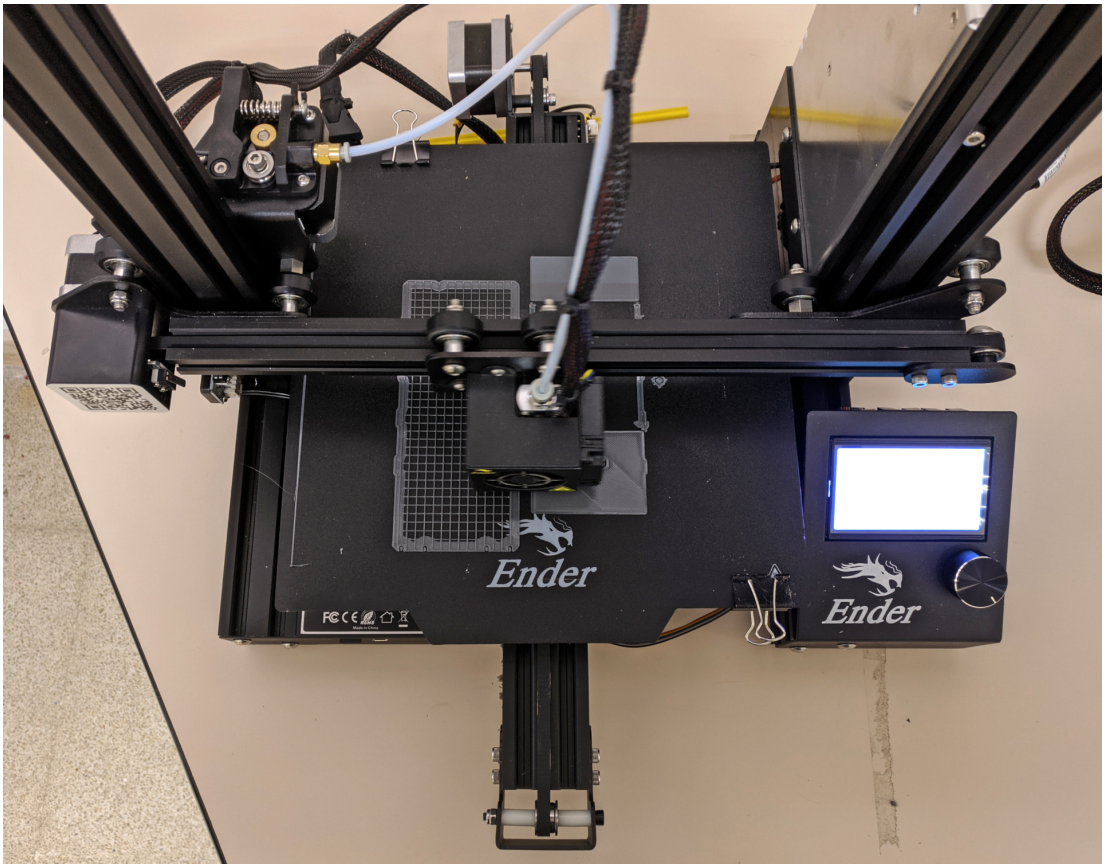

(c) *Printing the case parts.*

Figure 6.16 – *Photos of the printing process on the Creality Ender 3 Pro at Bibliomaker.*

Figure 6.17 – *Multiple views of the 3D-printed parts of the casing.*

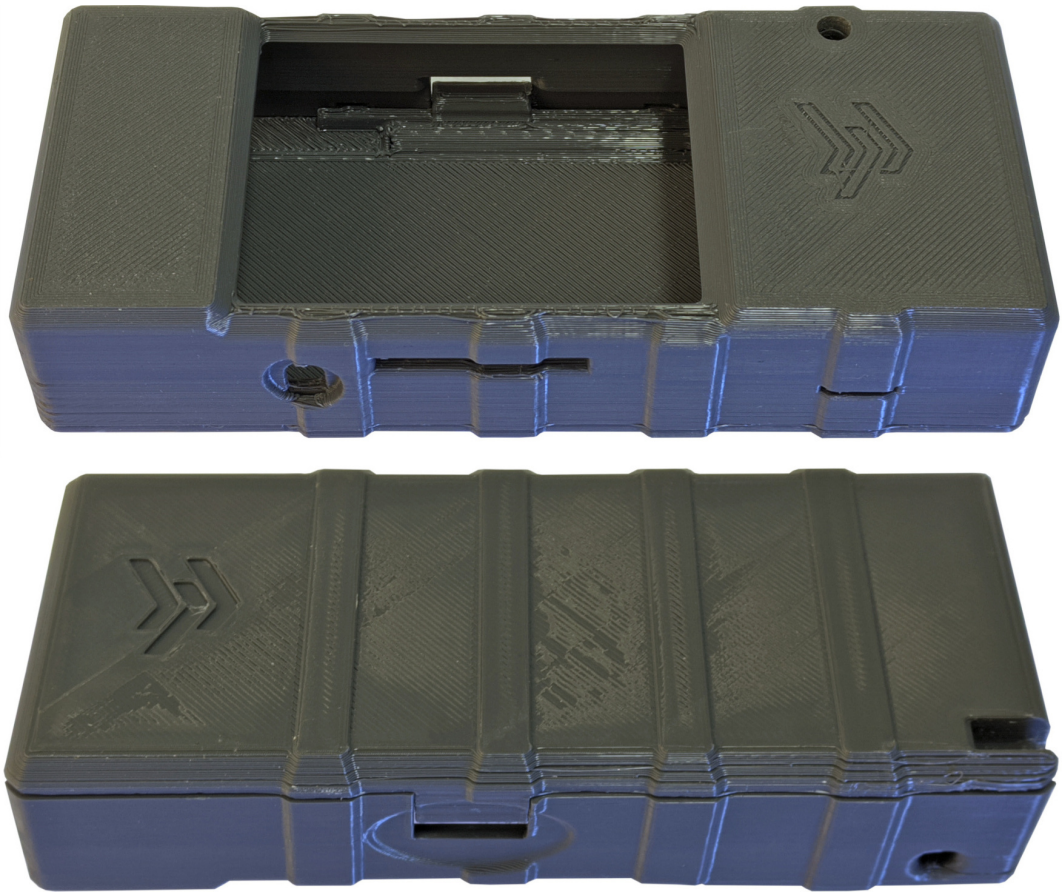

(a) *Front-side and back-side views. Fitting test of the two covers.*

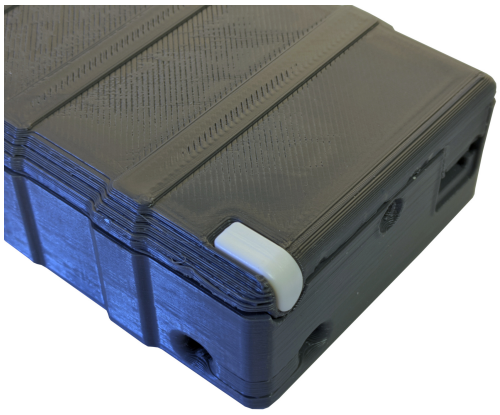

(b) *Detail of the bottom corner of the assembly. Stylus fit test.*

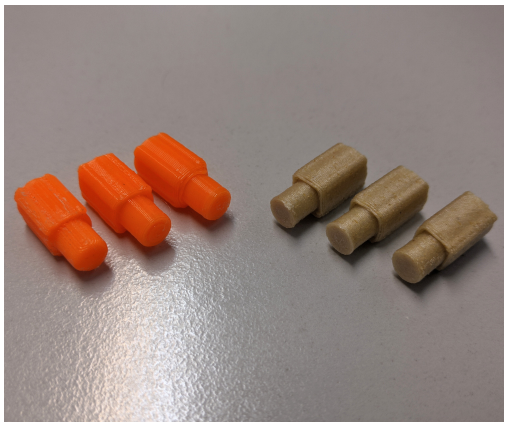

(c) *Detail of the printed buttons. First tests: left (orange), second batch: right (brown).*

Figure 6.18 – *Additional views of the 3D-printed parts: assembly test and buttons.*

6.3 Complete product assembly

As its name indicates, this section is dedicated to the assembly of the entire product. First of all, the fit of the PCB and the LCD module into the 3D printed case is checked Figure 6.19. Figure 6.20 shows the PCB fitted and screwed to the top cover. In said figure it can be seen how the head landings protect the PCB from the screws' heads. Once checked that the dimensions are correct, the entire product is then assembled as previously shown in Video 5.1. Figures 6.21 and 6.22 are photographs of the complete assembly while the device is on, showing the screen interface. The complete weight of the device with the electronics, battery, casing and screws is 210 grams.

As can be seen in the figures, the closure is not perfect. This is mainly due to two reasons: bad printing tolerance in certain layers of the lower cover which give it more height than expected; and because the BNCs datasheet [171] does not indicate the height of the component (having to rely on the manufacturer's 3D model) nor corresponds to the real product, which is almost 2 mm taller. So, the BNCs do not have enough room and the box do not close properly. Although the top cover has been reprinted with a fix, the problem persists because to correctly accommodate the BNCs deeper changes to the case design are required. This situation causes the top cover's horizontal layers near the outer screws to be stressed and separating.

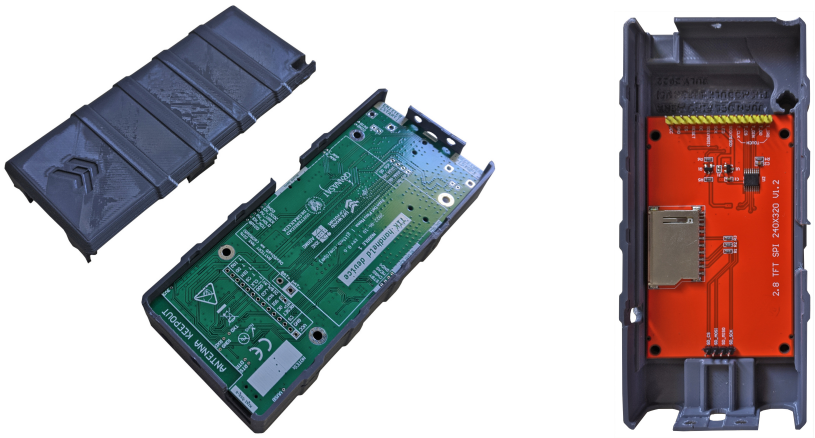

(a) *PCB fit check.* **(b)** *LCD fit check.*

Figure 6.19 – *Checking that the PCB and display module fit correctly into the 3D printed parts.*

Figure 6.20 – *PCB screwed to the top cover, with battery.*

Figure 6.21 – *Views of the complete assembly while the device is on.*

(a) *Front-side and Back-side views.*

(b) *Front view, with cables attached to all the ports.*

Figure 6.22 – *Extra views of the complete assembly while the device is on.*

6.4 Verification and debugging

This section highlights the most relevant aspects and the problems that appeared during the verification of the different circuits of the TIK. Not all subsystems were verified, either due to lack of time or software immaturity.

6.4.1 DC/DC converter

To get started with the system check, the first step is to check the power delivery. We start by checking the DC/DC converter circuit (with an AP3429K). To do this, an adjustable power supply was placed on the battery contacts, set to zero volts and limited to 500 mA for safety. The voltage was then rosen smoothly from zero volts to 4.2 volts. We were able to verify that the converter started working when 3.2 volts were reached (when the protective circuit governed by the DW01A allowed it) generating 2.7 volts at its output. The empirically found over-discharge voltage set by the DW01A is quite low and the battery could be damaged before even triggering the protection.

Nevertheless, as the DC/DC input voltage increased, so did its output voltage. When the supply tension exceeded 3.3 volts, the converter worked as intended, and its output was set to 3.3 V with not much noise.

6.4.2 Bias voltage LDO

On PCB mounts, V_{BIAS} is generated with the NCP562 LDO. This circuit does not involve any difficulty in design or implementation, and so it did not had any problems, outputting a constant 1.8 V DC without a remarkable noise level.

6.4.3 Auto-programming the ESP32-WROOM-32D from a PC

Once it is known that the system power supply is adequate, we proceed to verify that the system processing module, the ESP32-WROOM-32D, can be programmed automatically from a computer. This involves ESP32 itself, but also auxiliary components like the mini-USB and CH340C. This is a more complex process than it seems, and several *bugs* were found. The found problems, the debugging process and the solutions are explained below:

1. No detection by the computer, no activity on the differential USB data lines.

   Checking continuity and short-circuits with a multimeter, the root of the problem was identified as a solder defect in the USB Mini-B connector: a solder ball had formed, shorting the data lines. This phenomenon is known as *solder balling*, and occurs during reflow soldering [169]. This short circuit had escaped visual inspection because it was covered by the Mini-B's rear metal shield.

2. Detected by the computer, but failed to upload the program.

   The ESP32 was correctly identified by PlatformIO, as can be seen in Listing 6.1. This indicates that the ESP32 is alive, and that the USB to UART communication and conversion (the CH340C) is also working properly. The correct operation of the self-programming signaling circuit (via RTS and DTR) was also checked, and it operates as it should (Figure 6.23).

   However, when programming, a strange error appeared in the console (Listing 6.2) and the program could not be uploaded to the target. Pressing the Boot Selection button did not aid. There wasn't much information about it, but it seemed to be related to the ESP32's SPI flash memory. In the worst case, it could be due to a welding defect in the ESP32, either from manufacturing or caused during our reflow soldering. However, upon review of the circuitry, a very likely cause was found: improper use of non-recommended pins.

The problem is with the insertion detection circuit of the load cell amplifier and expansion port jack connectors (see Figure 6.24a): when nothing is connected to the ports, the tip switches are closed, and so GPIO6 and GPIO8 pins are in a HIGH state by being connected directly to the supply voltage, without a pull-up resistor. So the pins, which are connected to the internal SPI flash memory, cannot vary their voltage, therefore neither can receive nor send information and so reading and writing to the SPI fails.

The solution at the design level is simple: either stop using these pins, or add a series resistor between the `TP_SW` pins of the jacks and their corresponding GPIO. This resistor must be of a smaller value than the pull-down resistor, so that during programming information can be sent on the GPIO but the operation of the switch is not affected. The resistor should be placed immediately after the GPIO, so that the de-bounce capacitor does not load the GPIO directly (Figure 6.24b).

However, in the situation in which we find ourselves, with the PCB already manufactured and assembled, the simplest (albeit inelegant), solution is to cut traces with a razor, so that the problematic GPIOs get disconnected from the switches' circuits. The consequence is that this makes it impossible to detect the connectors in the prototype.

Once resolved these bugs, the ESP32 can be successfully programmed without issues.

Voltage on the Enable and GPIO0 pins on TIK and on an ESP32-DevKit during programming signaling.

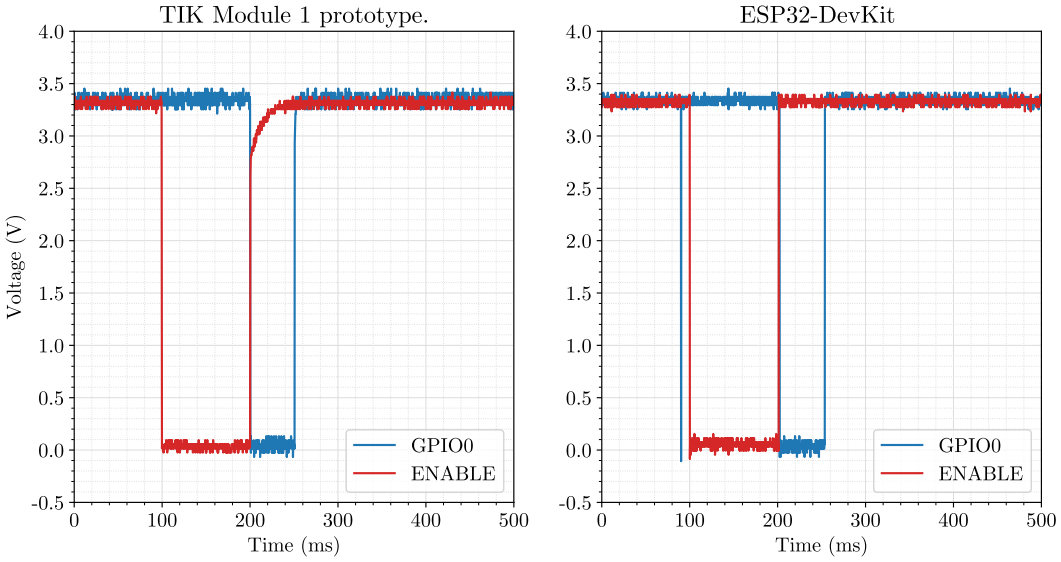

Figure 6.23 – *Comparison of the behaviour of the voltage on the ESP32's Enable and GPIO0 pins while sending a programming signal to the ESP32, on two different devices: the TIK Module 1 prototype and an ESP32-DevKit. Signals captured in a HAMEG HMO1024 digital oscilloscope.*

```
Auto-detected: /dev/ttyUSB0
Uploading .pio/build/esp32dev/firmware.bin
esptool.py v3.1
Serial port /dev/ttyUSB0
Connecting....
Chip is ESP32-D0WD (revision 1)
Features: WiFi, BT, Dual Core, 240MHz, VRef calibration in efuse, Coding Scheme None
Crystal is 40MHz
MAC: 98:cd:ac:[redacted]:[redacted]:[redacted]
```

Listing 6.1 – *ESP32 debug information given by PlatformIO's programmer, before failing.*

```
Configuring flash size...
Warning: Could not detect Flash size (FlashID=0xffffff, SizeID=0xff), defaulting to 4MB

A fatal error occurred: Timed out waiting for packet content.
```

Listing 6.2 – *Programming error thrown by PlatformIO after device identification and programming attempt.*

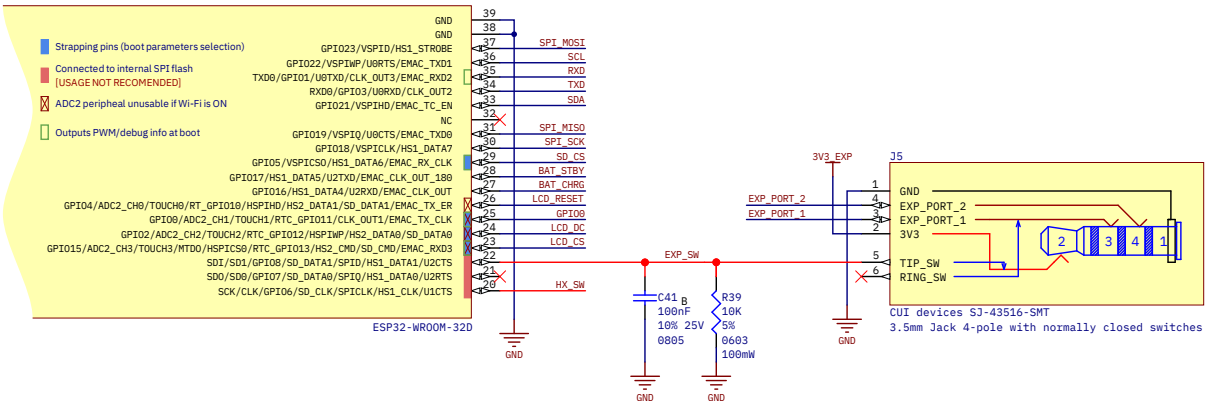

(a) *Current situation: cause of error illustrated with expansion port connector. Problematic nets highlighted in red. When nothing is connected to the port, the switch is closed and the GPIO6 and GPIO8 pins are connected directly to the supply voltage, without a pull-up. So the pins, which are connected to the SPI flash memory, are blocked and so the reading/writing in the SPI fails.*

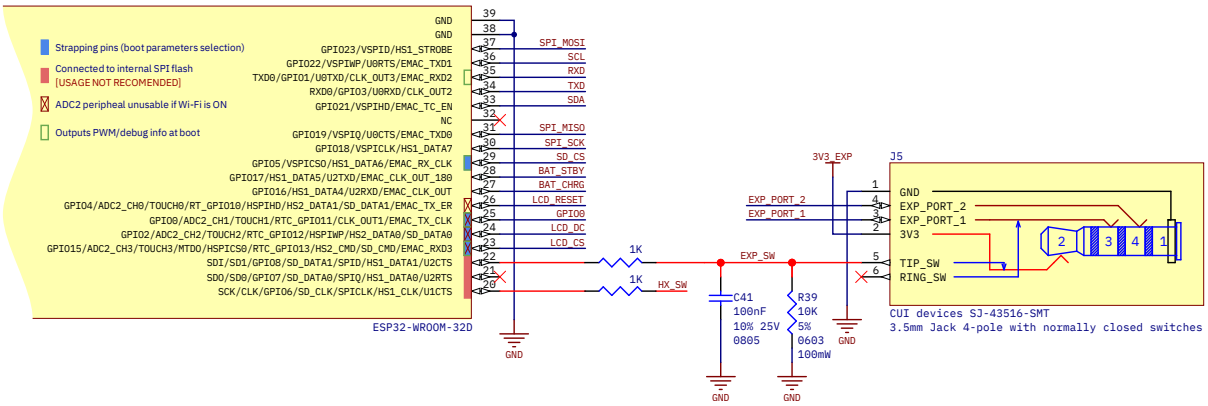

(b) *Proposed solution: resistors in series with the power supply, at least one order of magnitude smaller than the pull-down ones and close to the ESP32 pin. In this way, the GPIO can vary its voltage freely when programming and booting, and during program execution the state of the switch still can be read (with the GPIO in high-impedance mode).*

Figure 6.24 – *Explanation of the programming hardware bug and proposed solution.*

6.4.4 Battery charger

The Lithium charger works fine in the tested Li-Po battery, but the charge LED indicators do not lit correctly. The most likely cause is the impedance or voltage set by the ESP32 pins, since they are not configured for input/output at the moment, and the LEDs are not actively powered by the TP4056 but pulled down thought an open-drain.

Sometimes the protection circuit trips when using an external power supply, probably because there are two identical protection circuits in series (one in the battery and other in the PCB). A workaround is lowering the supply voltage below 3.0 V and slowly raising it until the system is powered up again.

The Ni-MH charger remains untested.

6.4.5 Power-up button

The power button circuit is not working properly. For a better understanding of this section, consult the circuit schematic in Section 5.1.2.8: Power-up button.

At first it was always on because the voltage on the `POWER_SW_USER` test point was very low, which caused the DC/DC to be always enabled. The most likely cause was that the ESP32 set a voltage or a pull-down on that pin even though it was disabled. Thus, the PMOS gate pull-up was reduced in steps until the circuit worked, which was at an unacceptably low 270 ohms (down from 100 kΩ).

But now, pressing the button raises the main supply voltage rail from zero to 3.3 V as expected. However, when the button is released, instead of going back to the reference voltage, it stays at 1.3 V. The cause is a new strange oscillating behavior in the PMOS drain which is transferred to the Enable pin of the DC/DC (Figure 6.25b). This signal intermittently turns the DC/DC on and off, and causes its capacitor-filtered output to be 1.3 volts.

After several unsuccessful tests, the cause of this behaviour is yet unknown. A deeper research needs to be done, maybe even a rework of the circuit itself (although this circuit has worked correctly in another student's work [105]).

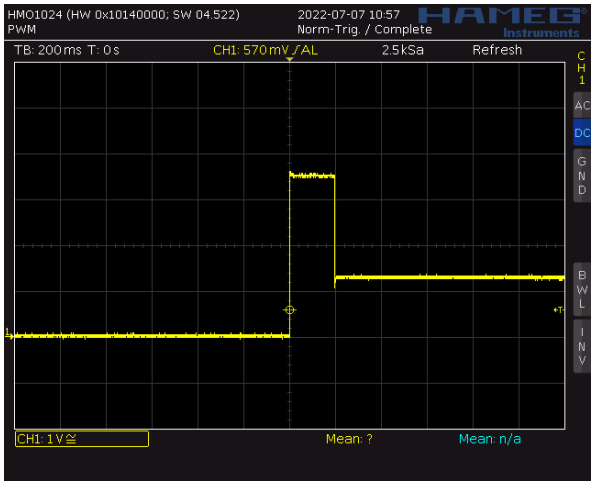

(a) *3V3 rail transient when the power-up button is pressed and released.*

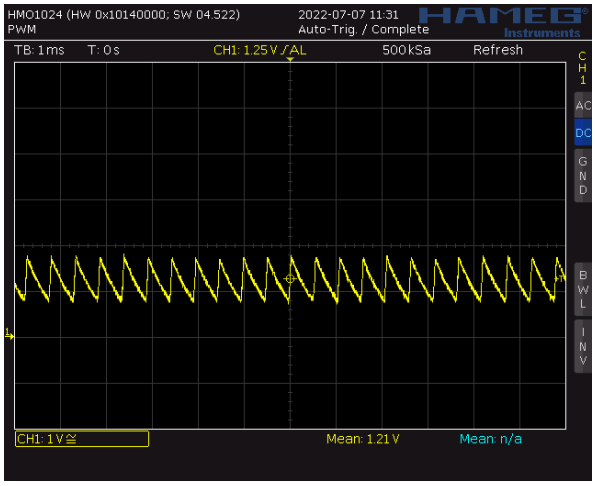

(b) *Oscillations in the PMOS drain.*

Figure 6.25 – *Power-up button behaviour captured in a HAMEG HMO1024 oscilloscope.*

6.4.6 ESP32's ADC

A test was carried out in order to characterize the behaviour of the ESP32's internal ADC. These tests were performed using channel 7 of the ADC unit 1, which has I2S and DMA support. A test program forked from [140] was configured to send samples via the serial port at 115 200 bauds, using 12 bits per sample in a 16384 samples long buffer in RAM. With this configuration, the manufacturer recommends a voltage input range from 150 mV to 2450 mV in order to avoid noise and non-linearity; but we are going to use the entire available range (from 0 V to 3 V). The tested ESP32 has its voltage reference factory-calibrated.

To start with, we generate a sine of amplitude 3 Vpp and with an offset of 1.5 V and inject it into the ADC pin. However, instead of a sinusoidal signal, we record the signal from the first graph in Figure 6.27: a signal that follows the frequency of the injected one, but has strange peaks as if it were overlaid by higher frequency harmonics. These signals did not show up on the oscilloscope, so the ESP32 must be the culprit.

Indeed, as can be seen in the Figure 6.27 this is an artificial degradation, a misinterpretation of the data from the I2S. Even in configured as a mono channel with the `I2S_CHANNEL_FMT_ONLY_LEFT` parameter, the I2S peripheral is hard-built for stereo, so samples are sent in pairs, but unsorted. If we interleave the even and odd samples in the correct order we get the clean sine of the last graph of Figure 6.27.

On the other hand, we evaluate the non-linearity of the ADC by introducing a low frequency ramp (see Figure 6.26). As can be seen, the extremes of the signal, which coincide with those of the supply, are very noisy. Linearity is acceptable until above the sample value of 3000, when the signal clearly bends due to non-linear distortion.

Finally, it is important to comment that by this sampling method a maximum sampling rate of 500 kHz was reached. However, any figure higher than this causes the ESP32 to lag behind the established sampling rate.

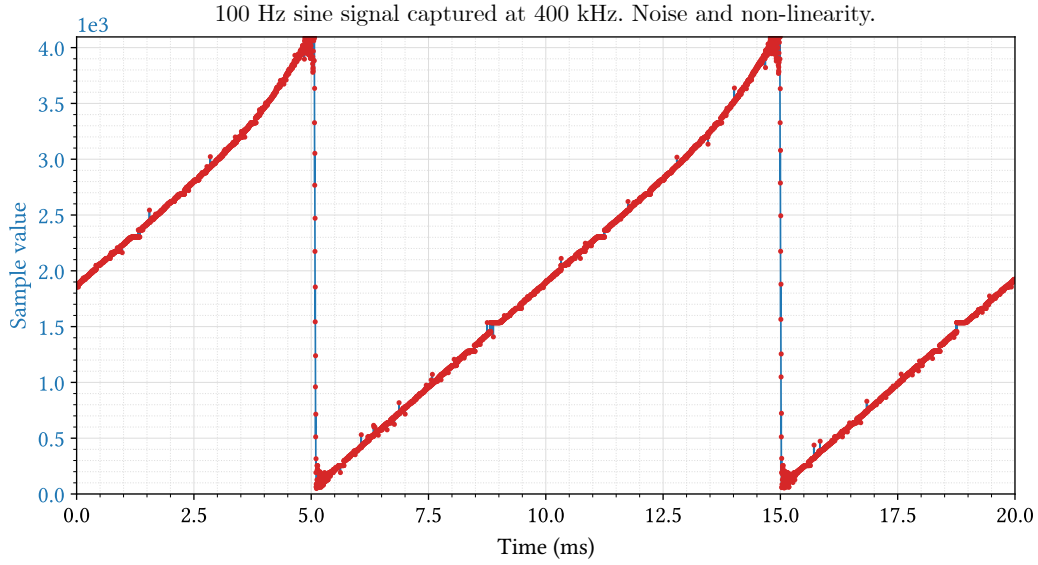

Figure 6.26 – *Caption*

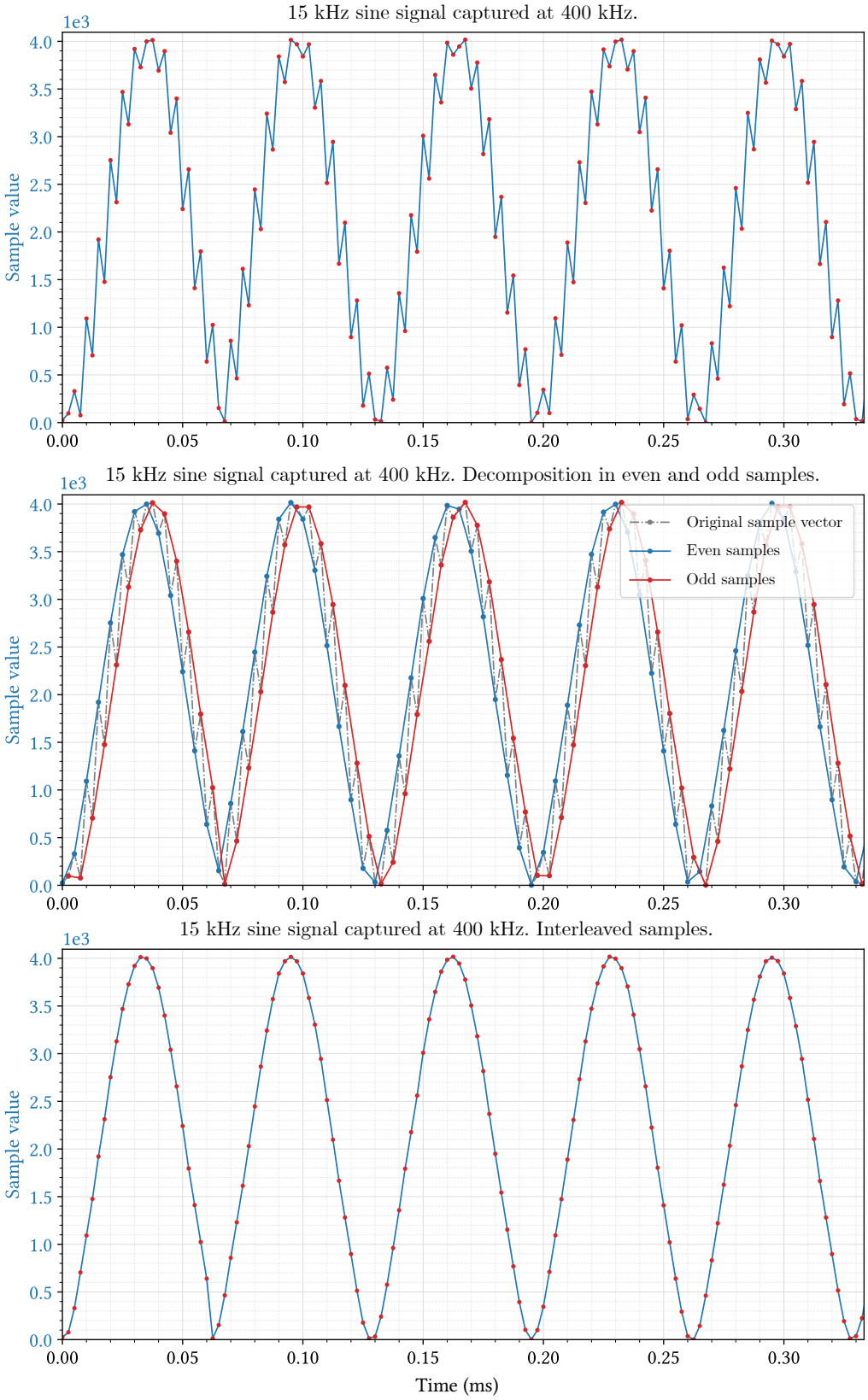

Figure 6.27 – *Original, divided and sorted sinusoidal signal captured by the ESP32's ADC using I2S and DMA.*

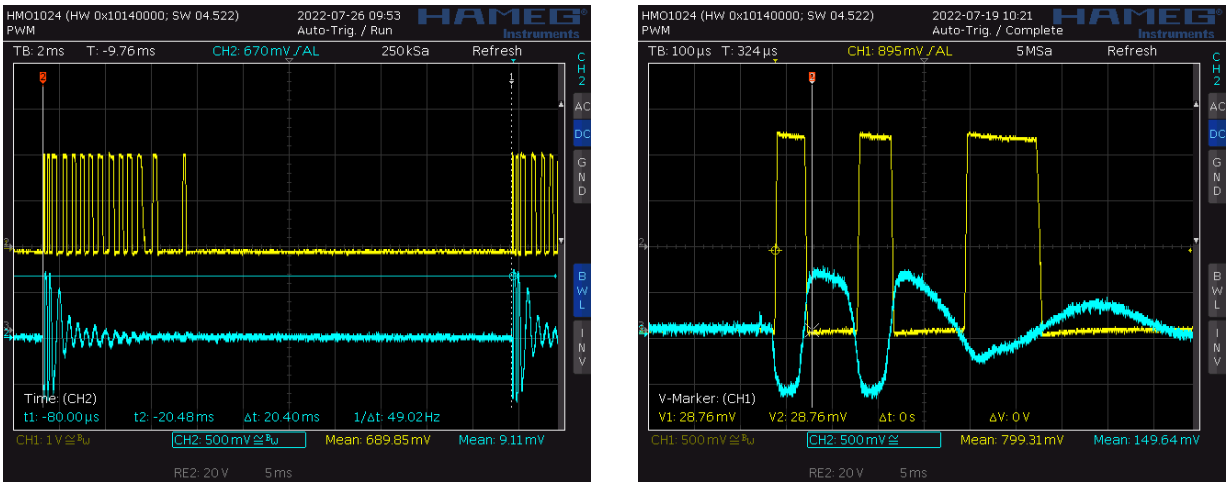

(a) *Zoom-out.* **(b)** *Zoom-in.*

Figure 6.28 – *Transient behaviour of the acquisition circuit captured in a HAMEG HMO1024 oscilloscope.*

6.4.7 Adequation circuit

We tested the transient of the adequation circuit that can be seen in Figure 6.28. Before commenting on the result, we must say that the fact that V_{BIAS} is not present in the captures seems to be due to the measurement instrumentation itself: when disconnecting the oscilloscope probes we measured with a battery multimeter that V_{BIAS} returns to 1.8 V.

Continuing with the results, you can see in Figure 6.28 how the OpAmp correclty performs the expected saturated amplification (Channel 1, yellow color) of the input clipped by the diodes (Channel 2, blue color).

The receiver signal was not tested.

To generate the replica of the sensors' signals seen in Figure 6.28, an SDG1062X arbitrary signal generator was used, configured through commands using a library written in Python. For more detail about the equipment and the developed library, see Appendix F: Instrumentation handling, Section 2: Siglent SDG1062X function/arbitrary waveform generator.

6.4.8 Power consumption

A Siglent SDM3065X digital multimeter was used to measure the total average current consumption. For more information about this tool and the measurement setup, consult Annex F: Instrumentation handling, Section 4: Siglent SDM3065X digital multimeter

During tests, the TIK prototype was running a demo program. Said program constantly sends information to the screen via SPI at a 80 MHz clock. The screen is updated at a rate of 60 Hz. Additionally, in the second core of ESP32, a task is executed that constantly reads values from one channel of ADC1 and outputs the raw values in the UART serial port at 115 200 bauds. This program uses a combination of code from the `TFT_Meters.ino` example from the TFT_eSPI library [138] (path: `./examples/320x240/TFT_Meters/`) and a fork of the `i2s_sampling` code made by Christopher Greening [140].

The program is considered to pose a equal if not higher stress than the final firmware, except for the wireless functionality.

The average measured consumption with the SDM3065X fluctuated around 40 to 45 mA only for the LCD screen, while 105 to 117 mA for the whole system (see Figure 6.29a and Figure 6.29b).

Then, a HAMEG HMO1024 digital oscilloscope and a power resistor in series with the power supply was used to characterize the fluctuations in current consumption of the whole system (Figure 6.29c).

As we can see, the average total power consumption is in line with the result given by SDM3065X and even around 15 mA less that the expected typical calculated in Section 5.1.2.3.5: Detailed typical and maximum power budget. The absolute maximum power consumption is close to 370 mA, which is not far from the maximum calculated in Section 5.1.2.3.5.

And so, we can ensure the power consumption of TIK will be similar to the results presented here.

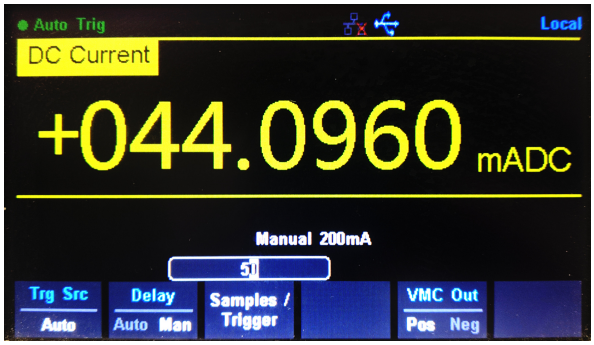

(a) *LCD-only average power consumption measured with a Siglent SDM3065X digital multimeter.*

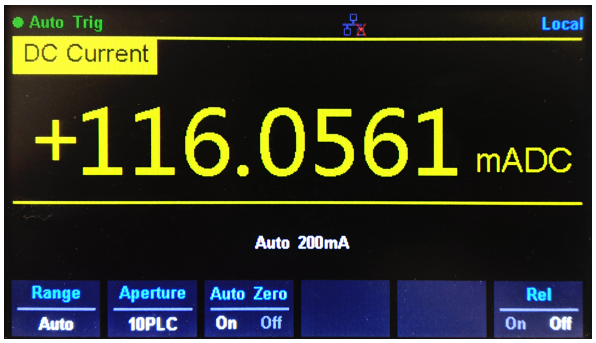

(b) *Average power consumption of the whole system measured with a Siglent SDM3065X digital multimeter.*

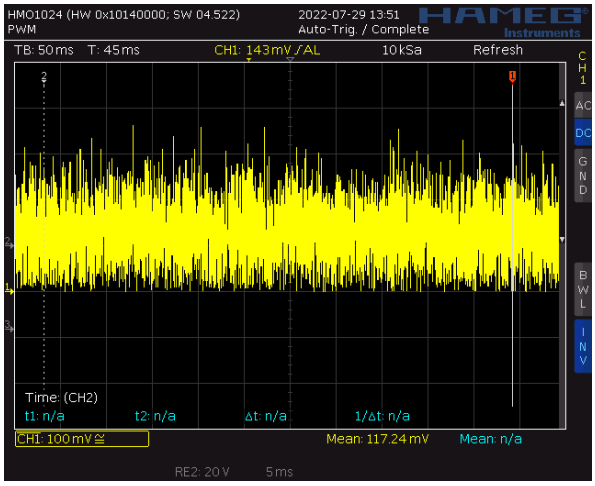

(c) *TIK's power consumption behaviour captured in a HAMEG HMO1024 oscilloscope*

Figure 6.29 – *Power consumption measurements while running a demo program on the TIK prototype.*

Chapter 7

Conclusions and future lines.

In this last chapter, the **milestones of the project** are included, as well as a **personal assessment** of the project itself. Also, a review of the loose ends of the project is made, along with self-criticism of errors and questionable design decisions and a list of possible **future improvements**. Finally, a reflection of **what direction should the project take** with all the experience gained throughout the course of the project.

7.1 Achieved milestones

This section reviews the merits achieved throughout the duration of this project:

- Exhaustive study of the properties of electrical signals captured with piezoelectric transducers, evaluation of digital signal processing algorithms and characterization of the piezoelectric sensors themselves.
- Establishment of the requirements, choice of the most appropriate architectures, circuit topologies, components and software for the different parts and tasks of this project.
- Design, development and fabrication of circuits of very different nature: from analog and digital signals to power management.
- Mechanical and electronic designs developed in unison with the aim of synthesizing an electronic product. Both areas were developed extensively and professionally, and with their corresponding technical documentation attached (see Annex B: Circuit schematics, Annex D: Printed Circuit Board schematics and Annex E: Mechanical drawings and renders).
- Firmware development has been started.
- Completed the first iteration of the TIK Engineering Model, starting from scratch and covering the hardware, firmware and mechanical design. The bases for subsequent development have been set.
- Development of electronic instruments management libraries, in order to simulate real measurements signals repeatedly and with configurable parameters (see Appendix F: Handling of electronic instrumentation).
- Managed with ease professional CAD and EDA programs for electronic and product design such as SolidWorks and Altium Designer.
- Collaboration with the GranaSat and ADIME R&D teams in a research line funded by the European Union, with the objective of exploiting local and sustainable resources.

7.2 Personal assessment

The project, lasting almost a full year, has been hard work for me but rewarding for all the experience and *know-how* that I have acquired. My experience throughout this project has been very positive educationally, professionally and personally.

I am satisfied that I have managed to combine the large amount of knowledge and methodologies learned throughout the Bachelor's Degree in a multidisciplinary project oriented to my specialization in electronics; and I consider that I have obtained more than satisfactory results.

In the professional side, I feel that I have matured considerably by being actively involved in a R&D team, and starting from scratch with the entire development process ahead: planification and organization, definition of requirements, brainstorming and concept evaluation, analysis, design, fabrication, validation, feedback and rectifications, etc; not to mention the frequent meetings. Collaterally, I have acquired more skill with LaTeX and the formatting and organization of large reports as this one, and by writing the documentation in English I have expanded my technical vocabulary. I also gained confidence with the Git version control software and with CAD and EDA programs.

The project has a considerable scope. It can be argued that this is enough work for a development team, not for a single student. I constantly felt overwhelmed by it, but with patience and perseverance I have pulled it through. I am proud of my results in the hardware section, especially when a year ago I knew absolutely nothing about PCB design. I've also gained a lot of perspective on firmware, mechanical and product design in a short amount of time. Still, I would have loved to have progressed certain areas further. For example, the firmware still needs tens of hours of work, and the mechanical aspect is very likely to need a rework from scratch (see Section 7.3: Future improvements and Section 7.4: New concepts). But again, the balance is positive, since it has been my first contact with complex fields such as RTOS-based and GUI-centric firmware development, mechanical and electronic co-design, etc.

Last but not least, I sincerely wish that the objective pursued by LIFE Wood For Future is successful, and that my work has been of help to achieve it. I hope to continue collaborating with them in the future.

7.3 Proposed future improvements.

This Thesis is a first approximation to the development of the final product and aims to create an engineering model to gain experience and perspective. The LIFE Wood For Future project is still far from being finished, and the market entry of the TIK tool is scheduled for 2024. The foundations have been laid, but there is still a lot of work to do to create a truly innovative and competitive product.

Once recognized the merits and the achieved educational and professional milestones of this Thesis, this section contains improvement propositions based on self-criticism and the experience gained during the development of the project. This allows new perspectives to be established, to advance the project in the right direction and to prevent mistakes from being repeated.

7

7.3.1 Improvements to the Printed Circuit Board

- **Use smaller components, improve the layout and increase component density.** In general, resistors of size 0603 and capacitors of size 0805 have been used in the PCB design. This decision was made because of the available stock in the GranaSat lab. In a latter design there is no reason not to make all passive chip sizes equal to 0603. The next smaller size, 0402, is too small to its manipulation. As for the IC packages, the sizes used have been adequate for assembly and debugging in the GranaSat laboratory, but relatively large packages with low lead density such as DPAK or SOP can be replaced by smaller options. On the contrary, if during the course of the project there were means for automatic manufacturing, the smaller-size parts and even QFN-type packages could be used.

On the other hand, the layout and placing of the components is adequate, but not optimal. During the manufacture and debugging of the boards it became clear that it would have been desirable for the parts of different blocks to be less mixed, creating easily identifiable regions of each system block.

Furthermore, although the density achieved on the board is good, there are certain unused regions. The extra unused area affects manufacturing costs: fewer PCBs per panel, and therefore higher cost per unit; and it also affects the size of the device and the available space inside its casing.

- **Migrate to 4-layer stackup design.** A denser and more compact design may already require 4 layers for routing. Even if this is not the case, a good 4-layer stackup on a 1.6mm thick PCB has significant advantages over a 2-layer-only board: More routing possibilities, physically closer and better ground planes and therefore lower overall trace impedance and better trace impedance control, and better Electro-Magnetic Compatibility performance.

- **Better impedance control.** Driven by the migration to a 4-layer design, it is desirable to more carefully control the impedance of critical traces, such as communication traces such as USB and SPI, and analog signal traces. Not only in the copper lines of the PCB, but also in the input/output impedance of the integrated circuits, to avoid reflections and ensure signal integrity.

- **Settle the battery chemistry, add a more advanced charger and a Battery Management System.** The advantages and disadvantages of various types of batteries for portable devices have been already discussed. However, since the type of battery to use was not yet decided at the design stage and the PCB was conceived as a test bed, two types of chargers were implemented. In the end, only the Li-Po/Li-Ion charger has been tested in this Thesis, since it was not feasible to mount the Ni-MH variant due to the price and lack of stock of its components. It is imperative to evaluate and definitively decide on the type of battery as soon as possible.

  Whichever technology is chosen a more modern, reliable and safe alternative than the proposed chargers should be used. The reasons being: the LTC4060 (the Ni-MH charger) is discontinued, and the TP4056 (Li-Po/Li-Ion) is not well documented and is not a reliable choice in the long term.

  Additionally, a battery fuel gauge IC and a BMS IC can be installed to accurately measure the state of charge and battery health. On top of all, some advanced ICs already include charging, protection circuitry and fuel gauge in one package.

- **Add a battery connector.** The battery is connected by two solder pads. A connector was ruled out due to the extra height, which would have required making the device taller. However, it is clear that a soldered battery is not practical for debugging, maintenance nor repair; and an standard XH254-2P 90-degree battery connector wouldn't have made the prototype any thicker.

- **Better GND test points.** The abundance of test points, their access from both the top and bottom layers and the fact that were drilled was very helpful for probing during hardware debugging. However, access to GND was difficult, since the test points are small for the alligator clips of the oscilloscope probes, regularly losing contact. For manual hardware testing and debugging, it is convenient to add one or more large double-sided pads specifically for the crocodile clips.

- **Change the USB Mini-B to an USB Type-C.** Currently, USB Type-C is replacing all other USB connectors. This way, the end user avoids having to use a specific USB cable, and he gets the impression of having a modern, universal and future-proof device. And although Mini-B are robust, they are also deprecated, and besides the Type-C can be just (if not more) robust: they are designed to withstand more current than traditional USBs, and generally have more connect/disconnect cycle durability. And in retrospective, an USB 2.0-only Type-C footprint is not so complex.

- **Add a way to power the device over USB without any batteries attached.** This is for convenience and ease of programming and debugging, as at the moment the device requires a connected battery to work even when connected to an USB source. The alternatives to do this are either by adding an additional DC/DC step-down converter from the 5V to 3.3V rail (more expensive, and it might cause

problems since it would be in parallel with the DC/DC coming from the battery), or by redesigning the charger stage, with *power path control*.

- **Add a more advanced USB-to-UART converter.** Working with the CH340C has been bittersweet. The CH340C has all the functionality required and proved to be capable, but only when it worked. It seems to have some hardware implementation peculiarities, and only one of the five total CH340C tested on identical assembled PCBs worked, for no apparent reason. Also, its power consumption is not ideal, it requires special drives in Windows and it is not well documented. An more reliable alternative would be desirable, for example the Silicon Labs CP2102N bridge chip is used on the open hardware ESP32-DevKitC reference design [172].

- **Add brightness control to the LCD.** The used TFT LCD module has a dedicated pin to control the display brightness by a PWM signal. Since the pins on the ESP32 were limited, this function was dismissed and brightness is set to the maximum. However, the implementation of brightness control would be a convenient, user-friendly and battery-saving feature.

- **Use a separate module for the LCD and the SD card.** This would make the display part smaller and allow to have the SD card slot in whichever location is required.

- **Change the load cell port.** There is not a standard load cell connector. However, the 4-pole jack connector is not very adequate, since it does not include a fifth connection for the commonly used cable shield. With proper redesign, a 6-pin RJ-11 type connector can be added.

- **Change the expansion port.** The 4-pole jack connector does the job for a prototype, but it is inadequate for a commercial product. It would be convenient to add a mechanically easier-to-couple connector, such as the already-discussed magnetic pogo-pins.

  However, it would be better if an expansion port was not needed in the first place, that is, to include the extended functionality in the same device. For this, a complete redesign is necessary. For more detail on the direction this could take, see Section 7.3.5: New concepts based on the experience gained with the prototype.

7.3.2 Improvements to the firmware and GUI

- **Add more languages.** At the moment only English is available, but it is planned to add translations to Spanish, Italian and French at least.

- **The dilemma about the programming SDK and the LCD library.** Although the Arduino Core framework was selected as the SDK, no Arduino functionality was used, so that the migration to ESP-IDF is easy to perform and we will gain control over some functionality not yet ported to the Arduino Core Framework.

  The only tether we have with Arduino Core is the TFT_eSPI library. The TFT_eSPI is a simple and lightweight library for our touchscreen, but it has close to zero documentation and it only works in the Arduino Core Framework. This has hampered firmware development, especially early on. A feasible and more advanced alternative is LVGL, which can create very appealing GUIs. The downside is that it introduces more complexity and alters the firmware design, requiring to program around its components. Also, the full version of LVGL requires more flash and RAM memory.

- **Idle mode.** A battery-saving functionality, similar to how smartphones and PCs work: after a time of no user input the display brightness would dim, and after waiting more time the display turns off and the device enters idle mode. In this state, it waits until an external interrupt occurs (e.g. the user presses a button).

- **Add wireless services.** For example, sharing measurement results via Bluetooth or a Wi-Fi access point to which the user can connect and download data via a web interface.

- **Secure boot and flash encryption.** Secure Boot prevents a device from running any unauthorized code by checking on boot that the program is signed. Flash Encryption encrypts the contents of the ESP32's flash memory to prevent the recovery of the flash contents by third parties. The product's EULA is not yet defined, but in case the hardware and firmware were intellectual property, these mechanisms can hinder the reverse engineering of our product.

7.3.3 Improvements to the signal acquisition and processing

- **Review the adequation circuit.** Diodes that clip less signal (higher V_f), OpAmp with better frequency response and slew rate, review the input impedance. Also, the inclusion of a PGA may be interesting.
- **Dedicated ADC with better specifications.** The ESP32 12-bit ADCs do their job, but they are not great for signal acquisition. The internal ADC units have major limitations for our use case, such as the highest achievable sampling speed, difficulty in multi-channel sampling and the impossibility to use both ADC units simultaneously since only the ADC1 supports DMA. Additionally, they have drawbacks such as significant non-linearity, noisy readings and limited voltage range.

  Also, we cannot use the noise reduction techniques recommended by Espressif due to, in the first place, the sensitivity of the analog signals to any distortion (rules out the use of a bypass capacitor on the ADC input); and secondly, the high sampling frequency required (dismisses the use of multisampling).

  For these reasons, albeit at the cost of increased price and complexity, it is worth including an external, faster, more accurate, more reliable, dual-channel ADC which also withstands a higher voltage range at its inputs. This ADC would use either I2S or SPI.
- **Implement the AIC-EMD method.** This entails a lot of development and improvement work, but could provide the processing algorithm with noise immunity, as described in [63].

7.3.4 Improvements to the mechanical design

- **Find a suitable material for the casing.** Given the fragility of PLA, it would be more appropriate to resort to higher performance materials that are also 3D printable, such as ABS, TPU, PETG, nylon, or PA12-CF. Although these requires more powerful printers than those available in Bibliomaker.
- **Dust and water resistant design.** Conduct an investigation of what methods can be used to make the case more dust and water proof. For example: use of rubber gaskets, coating for the screen, etc.
- **Design our own piezoeletric sensors.** As seen in Section 2.3: Piezoelectric sensor characterization, the frequency response of Fakopp's SD-02 transducers is not exactly ideal. Perhaps the development process would be easier if higher quality sensors were used. Among the options contemplated in the course of the project, it is possible to end designing our own probes which would be sold with the TIK; and thus we also avoid depending on a third-party product.

  Given this, we could also evaluate the possibility of changing the piezoelectric sensors' connectors. For example, some sensors used in ultrasound and resonance analysis use smaller SMA connectors instead of BNCs. However, BNCs are still quicker to connect/disconnect, and generally more resistant to mechanical stress.
- **Change the closing screws placement.** On the 3D printed case, the tolerance issue revealed that the lateral outer screws are inappropriate and were separating the printed layers. Whenever possible, we should stress a 3D part perpendicular to the layers.

  For example, the mounting holes positions could be reused, which would leave the screws visible only at the bottom of the device (and we would also save 3 screws); although you have to be very careful not to use the space reserved for the battery.

7.4 New concepts based on the experience gained with the prototype

In terms of usability, the developed device is correct: the size and weight are adequate and it is comfortable to manipulate with one or two hands. However, the coupling of the TIK Module 2 makes the resulting device too long, with most of the weight of the device farthest from the hand. This will cause it to be uncomfortable to hold and the device will tend to fall out of the hands.

A better solution must be found. Either we re-imagine the way to connect both modules, or the concept of two separate modules is abandoned and everything is integrated into a single tool, with proper weight distribution. Personally, I think that the second solution is the most appropriate and realistic. Besides, with the experience gained, it is now more feasible to create a more ergonomic tool, and co-design the electronics according to the selected product design.

In meetings with the GranaSat and ADIME teams, an interesting idea arose: to create a device with a grip like a pistol (similar to laser thermometers, for example). This way, it becomes very natural to grip it because the hand is kept in a comfortable position; especially when holding it against a vertical surface (as it occurs in measurements on logs and boards by the resonance method). Also, it becomes ambidextrous by design. This concept is significantly more complex to carry out than the one developed in this document both mechanically and electronically, but I think that the advantages of comfort, usability and the integration of all the functions in a single equipment are worth it.

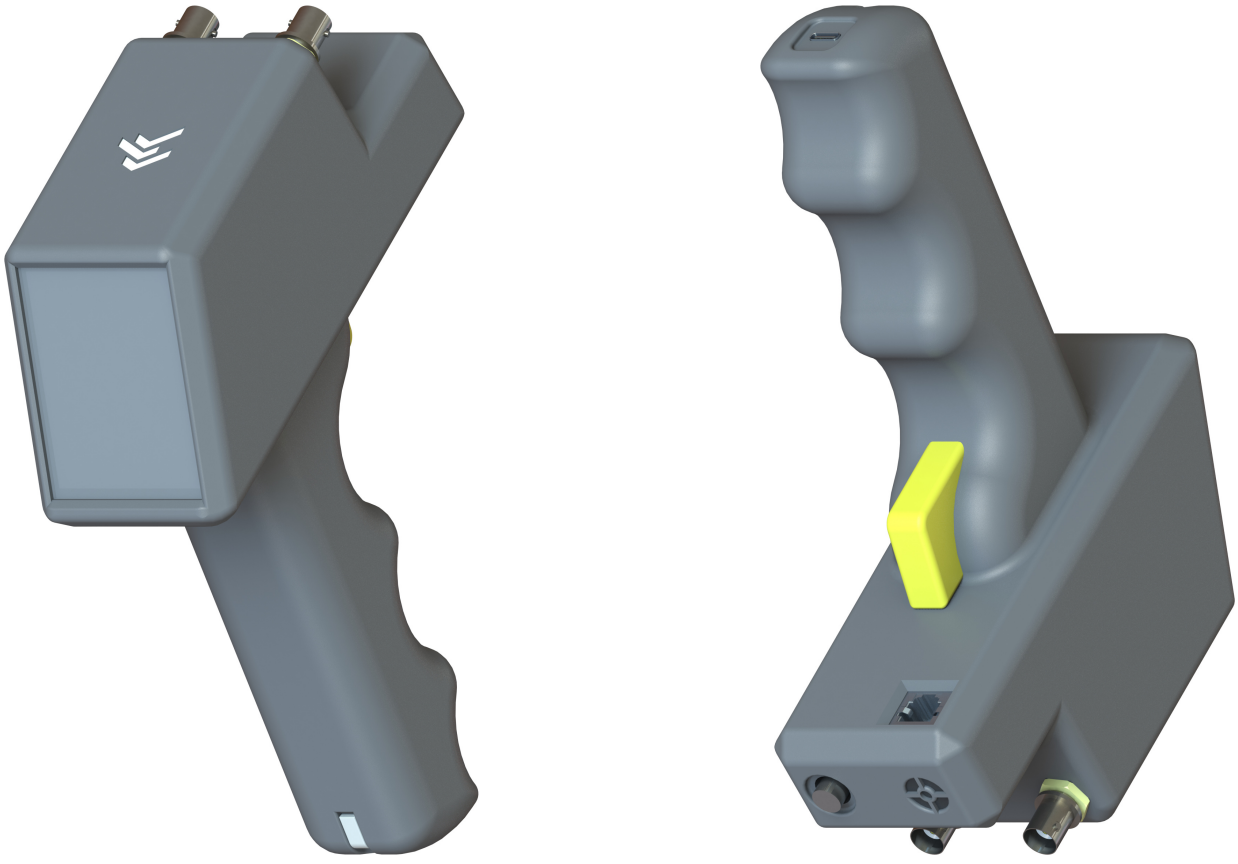

(a) *Top-side view.* **(b)** *Bottom-side view.*

Figure 7.1 – *Renders of the TIK pistol concept, in early design stage.*

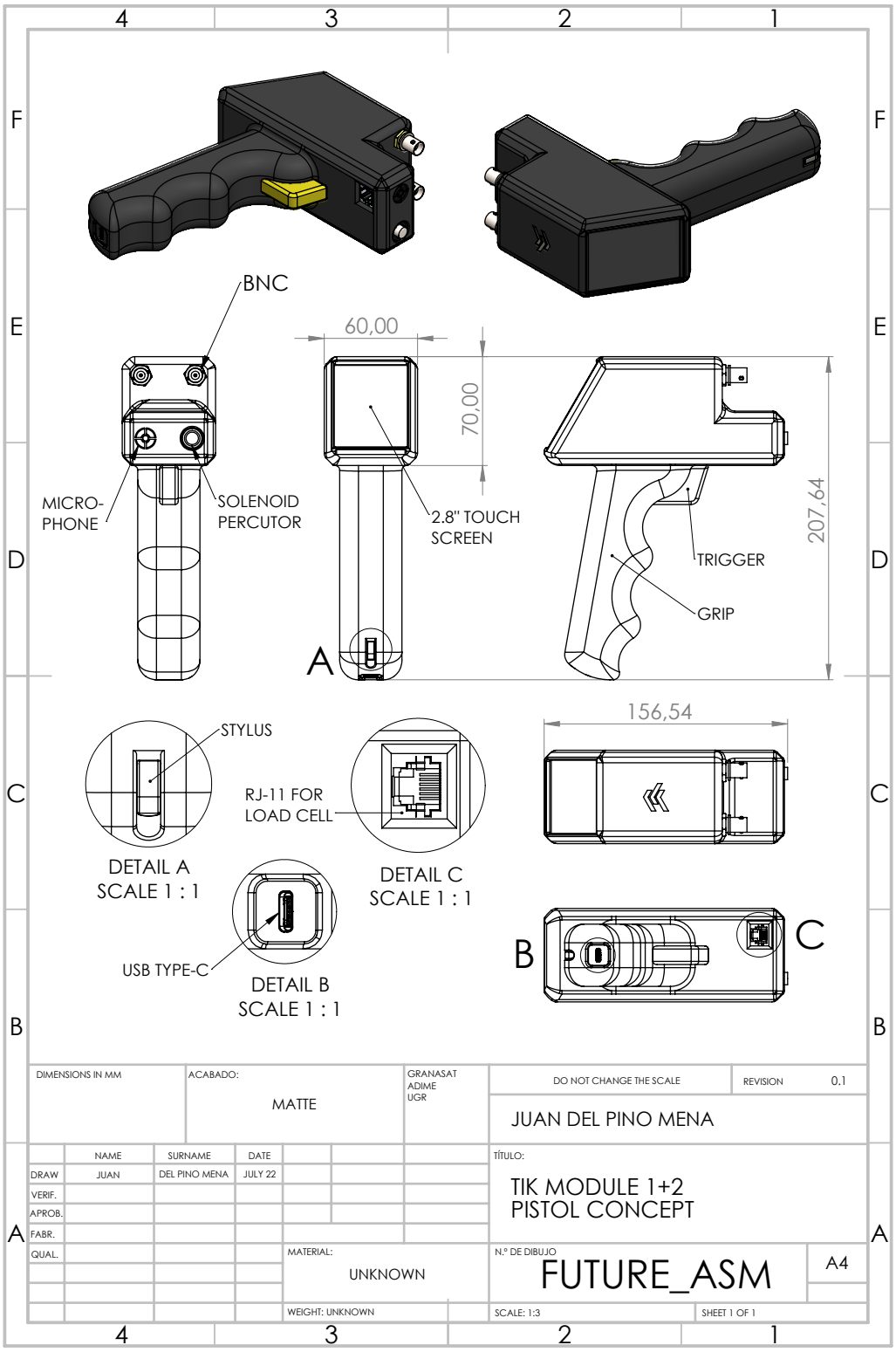

Figure 7.2 – *Schematics of the TIK pistol concept, in early design stage.*

7

Bibliography

[1] Espressif Systems Co. Ltd., *ESP32 Hardware Design Guidelines*, 2021. Version 3.2. https://www.espressif.com/sites/default/files/documentation/esp32_hardware_design_guidelines_en.pdf Accessed: November 2021.

[2] M. Bruneau, T. Scelo, and S. d'Acoustique, *Fundamentals of Acoustics*. ISTE, Wiley, 2013.

[3] IDIE-ADIME webpage. Information about the group, its research lines and projects and its technological services. https://idie.ugr.es/idie-adime/ (Spanish) Accessed: January 2022.

[4] Global Policy Forum, "Definition of conflict resources," 2007. https://archive.globalpolicy.org/component/content/article/198-natural-resources/40124-definition-of-conflict-resources.html Accessed: June 2022.

[5] D. R. Askeland, P. P. Fulay, and W. J. Wright, *Engineering Mechanics*. Cengage Learning, 6 ed., 2010.

[6] M. I. Montrose, *EMC and the Printed Circuit Board*. Wiley-Interscience, IEEE Press, 1997.

[7] S. Bhunia and M. Tehranipoor, *Hardware Security: A Hands-On Learning Approach*, ch. 4: Printed Circuit Board (PCB): Design and test, pp. 81–104. Morgan Kaufmann, 9 ed., 2019.

[8] The FreeRTOS project's main page. https://www.freertos.org/ Accessed: February 2022.

[9] GranaSat webpage. https://granasat.ugr.es (Spanish) Accessed: October 2021.

[10] IDIE webpage. Information about the research group and its technological services. https://idie.ugr.es/ (Spanish) Accessed: January 2022.

[11] R. S. Khandpur, *Printed Circuit Boards: Design, Fabrication, Assembly and Testing*, ch. 13: Soldering, Assembly and Re-working Techniques, pp. 453–560. McGraw-Hill, 1 ed., 2006.

[12] R. S. Khandpur, *Printed Circuit Boards: Design, Fabrication, Assembly and Testing*, ch. Glossary, pp. 635–666. McGraw-Hill, 1 ed., 2006.

[13] The Open Source Initiative, "Open Source Definition." https://opensource.org/osd Accessed: June 2022.

[14] "Directive 2011/65/EU of the European Parliament and of the Council of 8 June 2011 on the restriction of the use of certain hazardous substances in electrical and electronic equipment," 2011. Document number: 02011L0065-20211101. http://data.europa.eu/eli/dir/2011/65/2021-11-01 Accessed: June 2022.

[15] R. S. Khandpur, *Printed Circuit Boards: Design, Fabrication, Assembly and Testing*, ch. 8: Plating processes, pp. 310–364. McGraw-Hill, 1 ed., 2006.

[16] M. Rogríguez Marcos, "Determinación del Módulo de Elasticidad de la madera de chopo y nogal en árboles en pie mediante ondas acústicas," Master's Thesis, University of Granada, 2020.

[17] LIFE Wood for Future Action: Characterisation of wood: Development of the Tree Inspection Kit (TIK) tool to assess the quality of wood. https://life-woodforfuture.eu/en/actions/development-of-the-tree-inspection-kit-tool-to-assess-the-quality-of-wood/ Accessed: April 2022.

[18] LIFE Wood For Future (LIFE20CCM/ES/001656) on LIFE public database. https://webgate.ec.europa.eu/life/publicWebsite/project/details/5534 Accessed: April 2022.

[19] The LIFE programme objectives. https://ec.europa.eu/growth/industry/strategy/hydrogen/funding-guide/eu-programmes-funds/life-programme_en Accessed: May 2022.

[20] "Informe anual de evaluación de la calidad del aire en España 2020," tech. rep., Subdirección General de Aire Limpio y Sostenibilidad Industrial del Ministerio para la Transición Ecológica y el Reto Demográfico, 2021. NIPO: 665-21-045-X. Available online: https://www.miteco.gob.es/images/es/informeevaluacioncalidadaireespana2020_tcm30-529210.pdf (Spanish) Accessed: June 2022.

[21] F. Salmerón, "Contaminación y calidad del aire en el Área Metropolitana de Granada. parte 1," *Colegio Oficial de Aparejadores y Arquitectos Técnicos de Granada (COAATG)*, 2021. https://www.coaatgr.es/contaminacion-y-calidad-del-aire-en-el-area-metropolitana-de-granada-parte-1/ (Spanish) Accessed: June 2022.

[22] E. Abuín, "La Granada metropolitana respira el aire más contaminado de España," *Granada Hoy*, 2019. https://www.granadahoy.com/granada/Granada-metropolitana-respira-aire-contaminado-peor-calidad-Espana_0_1368763403.html (Spanish) Accessed: June 2022.

[23] E. Sánchez, "La contaminación se enquista en Granada," *El País*, 2018. https://elpais.com/sociedad/2018/11/17/actualidad/1542443705_032930.html (Spanish) Accessed: June 2022.

[24] M. J. Ramírez, "La contaminación del aire en Granada, un preocupante mal endémico," *Granada Digital*, 2019. https://www.granadadigital.es/la-contaminacion-del-aire-en-granada-un-preocupante-mal-endemico/ (Spanish) Accessed: June 2022.

[25] The LIFE Wood for Future Project webpage. https://life-woodforfuture.eu (Spanish) Accessed: April 2022.

[26] "Directive 2010/31/EU of the European Parliament and of the Council of 19 May 2010 on the energy performance of buildings," 2010. Document number: 02010L0031-20210101. http://data.europa.eu/eli/dir/2010/31/2021-01-01 Accessed: June 2022.

[27] "Directive 2012/27/EU of the European Parliament and of the Council of 25 October 2012 on energy efficiency, amending Directives 2009/125/EC and 2010/30/EU and repealing Directives 2004/8/EC and 2006/32/EC," 2021. Document number: 02012L0027-20210101. http://data.europa.eu/eli/dir/2012/27/2021-01-01 Accessed: June 2022.

[28] F. Stazi, E. Tomassoni, C. Bonfigli, and C. Di Perna, "Energy, comfort and environmental assessment of different building envelope techniques in a mediterranean climate with a hot dry summer," *Applied Energy*, vol. 134, pp. 176–196, 2014.

[29] The Choperas Vega Granada project. Accessed via the Internet Archive's Wayback Machine. https://web.archive.org/web/20211226004541/https://www.choperas-vegagranada.es/ (Spanish) Date of capture: 26/12/2021. Accessed: August 2022.

[30] International Poplar Commission webpage. Food and Agriculture Organization, United Nations. https://www.fao.org/ipc/en/.

[31] S. Verani, G. Sperandio, R. Picchio, R. Spinelli, and G. Picchi, *International Poplar Commission (IPC) Thematic Papers. FAO. Field handbook of poplar harvesting*, 2008. https://www.fao.org/3/k3305e/k3305e00.htm Accessed: July 2022.

[32] COMPOP webpage. Gallery of the project's works, thesis, papers and divulgation. http://compop.ugr.es/galeria.html (Spanish) Accessed: June 2022.

[33] C. I. Timbolmas, "Development of engineering wood products based on poplar boards and veneers with composite material insertions for use in construction," PhD Thesis, University of Granada, 2022. BIA2017-82650-R.

[34] F. J. Rescalvo, R. Duriot, G. Pot, A. Gallego, and L. Denaud, "Enhancement of bending properties of Douglas-fir and poplar laminate veneer lumber (LVL) beams with carbon and basalt fibers reinforcement," *Construction and Building Materials*, vol. 263, pp. 120–185, 2020.

[35] F. J. Rescalvo, C. Timbolmas, R. Bravo, I. Valverde-Palacios, and A. Gallego, "Improving ductility and bending features of poplar glued laminated beams by means of embedded carbon material," *Construction and Building Materials*, vol. 304, p. 124469, 2021.

[36] F. Sougnez (Pro-Populus asbl), "El chopo: el árbol del siglo XXI," 2018. https://propopulus.eu/wp-content/uploads/2018/07/Argumentaire-ES-Web.pdf (Spanish) Accessed: August 2022.

[37] "Actividades relativas al cultivo y la utilización del álamo y del sauce. Periodo 2012-2015. 25ª reunión en Berlín (Alemania)," tech. rep., Comisión Internacional del Álamo, 2016. Available online: https://www.miteco.gob.es/en/biodiversidad/temas/politica-forestal/2012-2015berlinalemania_tcm38-442796.pdf (Spanish) Accessed: June 2022.

[38] "II Simposio del Chopo. Valladolid, España. Libro de actas," 2018. https://www.simposiodelchopo.es/sites/default/files/actas/actas.pdf (Spanish) Accessed: August 2022.

[39] A. Gallego, M. Ripoll, and A. Martínez, "El chopo: Una oportunidad para el desarrollo sostenible en España y Andalucía.," 2018. II Simposio del Chopo. Valladolid, España http://compop.ugr.es/assets/Dossier_chopo_Granada_UGR.pdf (Spanish) Accessed: August 2022.

[40] A. Gallego, "La madera de chopo: un instrumento eficaz para la bioeconomía rural y la mitigación de cambio global en nuestro planeta," 2021. http://compop.ugr.es/assets/20210420_Presentation_Chopo_UniversidaddeHuelva.pdf (Spanish) Accessed: August 2022.

[41] "Actividades relativas al cultivo y la utilización del álamo y del sauce. Periodo 2008-2011. 24ª reunión en Dehradun (India)," tech. rep., Comisión Internacional del Álamo, 2012. Available online: https://www.miteco.gob.es/en/biodiversidad/temas/politica-forestal/2008-2011dehradunindia_tcm38-443024.pdf (Spanish) Accessed: June 2022.

[42] "Canuckguy" et al, 2007. Empty political world map https://commons.wikimedia.org/wiki/File:BlankMap-World-Compact.svg Accessed: July 2022.

[43] "Encuesta sobre Superficies Y Rendimientos de Cultivos (ESYRCE)," tech. rep., Ministerio de Agricultura, Pesca y Alimentación, 2019. Available online: https://www.mapa.gob.es/es/estadistica/temas/estadisticas-agrarias/boletin2019_tcm30-536911.pdf (Spanish) Accessed: June 2022.

[44] E. G. Fernández, 2005. Empty political map of Spain https://commons.wikimedia.org/wiki/File:Comunidades_autónomas_de_Espa~na_(blank).svg Accessed: July 2022.

[45] C. Hellier, *Handbook of Nondestructive Evaluation*. McGraw-Hill handbooks, Mcgraw-hill, 2001.

[46] X. Wang, "Acoustic measurements on trees and logs: A review and analysis," *Wood Science and Technology*, vol. 47, p. 965–975, 2013.

[47] P. Mix, *Introduction to Nondestructive Testing: A Training Guide*, ch. 11: Ultrasonic testing, pp. 457–520. Wiley, 2 ed., 2005.

[48] M. Meyers, *Dynamic Behavior of Materials*. Wiley-Interscience publication, Wiley, 1994.

[49] V. Bucur, *Theory of and Experimental Methods for the Acoustic Characterization of Wood*, ch. 4, pp. 39–104. Springer Berlin Heidelberg, 2006.

[50] A. Group, *Procedimiento de medición de la velocidad de propagación de ondas elásticas en árboles en pie por la técnica ToF*.

[51] Tree trunk layers, extracted from: https://courses.cit.cornell.edu/hort494/mg/specific.grafting/images/vascambx.big.jpg.html Accessed: August 2022.

[52] X. Wang, R. Ross, B. Brashaw, J. Punches, J. Erickson, J. Forsman, and R. Pellerin, "Diameter effect on stress-wave evaluation of modulus of elasticity of logs," *Wood and Fiber Science*, vol. 36, pp. 368–377, 2004.

[53] X. Wang, R. Ross, and P. Carter, "Acoustic evaluation of wood quality in standing trees. Part I: acoustic wave behavior," *Wood and Fiber Science*, vol. 39, pp. 28–38, 2007.

[54] Fakopp Enterprise Bt. webpage and product images. https://fakopp.com/en/ Accessed: June 2022.

[55] Brookhuis MTG handheld device webpage. https://brookhuis.com/wood-testing/strength-grading/strength-grading-handhelds/ Accessed: July 2022.

[56] Controls PULSONIC 58-E4900 Ultrasonic Pulse Analyzer webpage. https://www.controls-group.com/usa/ndt-quality-and-homogeneity-evaluation/ultrasonic-pulse-analyzer.php Accessed: July 2022.

[57] Brookhuis MTG handheld device during measurement, extracted from: https://www.volta.it/prodotti/misure/misuratori-di-umidita/umidita-linea-brookhuis/sistema-misurazione-resistenza-del-legno-portatile-mtg-timber-grader/.

[58] I. Gil Martín, "Evaluation system of the modulus of elasticity of wood in logs and boards through time-of-arrival techniques," Master's Thesis, University of Granada, 2022.

[59] G. E. Dieter and L. C. Schmidt, *EMC and the Printed Circuit Board*. McGraw-Hill, 4 ed., 2009.

[60] Science Buddies, "Engineering Design Process." https://www.sciencebuddies.org/science-fair-projects/engineering-design-process/engineering-design-process-steps Accessed: July 2022.

[61] Fakopp Enterprise Bt., *Fakopp Microsecond Timer Manual*, 2021. https://files.fakopp.com/mstimer/mstimer_manual.pdf Accessed: November 2021.

[62] Alpha Wire, *9058AC coaxial cable technical specifications*. https://www.alphawire.com/en/Products/cable/alpha-essentials/coaxial-cable/9058AC Accessed: February 2022.

[63] X. Li, X. Shang, A. Morales-Esteban, and Z. Wang, "Identifying p phase arrival of weak events: The Akaike Information Criterion picking application based on the Empirical Mode Decomposition," *Computers & Geosciences*, vol. 100, pp. 57–66, 2016.

[64] Tasker, *RG-58 CU coaxial cable technical specifications*. https://www.distrelec.ro/Web/Downloads/_t/ds/RG58CU_eng_tds.pdf Accessed: February 2022.

[65] I. Sommerville, *Software Engineering*, ch. 4: Requirements engineering, pp. 83–117. Pearson, 9 ed., 2011.

[66] S. Arar, "Common PCB stackups for a four-layer board," *All About Circuits*, 2019-09-04. https://www.allaboutcircuits.com/technical-articles/common-layer-stack-ups-for-a-four-layer-board/ Accessed: May 2022.

[67] R. Keim, "What is a Printed Circuit Board (PCB)?," *All About Circuits*, 2020-04-10. https://www.allaboutcircuits.com/technical-articles/what-is-a-printed-circuit-board-pcb/ Accessed: May 2022.

[68] Raspberry Pi 4 Model B Renders, extracted from: https://es.aliexpress.com/item/4000115074396.html Accessed: June 2022.

[69] Lead-free and RoHS logos, extracted from: https://seeklogo.com/vector-logo/119474/rohs Accessed: June 2022.

[70] M. Krüger. Conformité Européenne logo. Extracted from: https://en.wikipedia.org/wiki/CE_marking#/media/File:Conformité_Européenne_(logo).svg Accessed: June 2022.

[71] "Commission Notice - The 'Blue Guide' on the implementation of EU products rules 2016 (Text with EEA relevance)," 2016. Document number: 52016XC0726(02). https://eur-lex.europa.eu/legal-content/EN/ALL/?uri=CELEX:52016XC0726(02) Accessed: June 2022.

[72] VDE Testing and Certification Institute, "EU Directives: CE Telephone." https://www2.vde.com/en/Institute/TechnicsandRegulations/EUDirectives/Pages/CETelephone.aspx Accessed: June 2022.

[73] A. Usanov, M. de Ridder, and W. Auping, *Coltan, Congo and Conflict*. The Hague Centre for Strategic Studies, 6 ed., 2013.

[74] pighixxx, "SMD Cheat Sheet." Accessed via the Internet Archive's Wayback Machine. https://web.archive.org/web/20170509141102/http://www.pighixxx.com/test/2015/04/smd-cheat-sheet/ Date of capture: 9/5/2017. Accessed: July 2022.

[75] Espressif Systems Co. Ltd., *ESP32 Technical Reference Manual*, 2021. Version 4.6. https://www.espressif.com/sites/default/files/documentation/esp32_technical_reference_manual_en.pdf Accessed: November 2021.

[76] Espressif Systems Co. Ltd., *ESP-IDF documentation/programming guide.*, 2022. https://docs.espressif.com/projects/esp-idf/en/latest/esp32/ Accessed: February 2022.

[77] "ESP32 Arduino Core documentation." https://docs.espressif.com/projects/arduino-esp32/en/latest/ Accessed: April 2022.

[78] Espressif Systems Co. Ltd., *ESP32 Series datasheet*, 2021. Version 3.7. https://www.espressif.com/sites/default/files/documentation/esp32_datasheet_en.pdf Accessed: November 2021.

[79] Espressif Systems Co. Ltd., *ESP-IDF documentation/programming guide. Analog to Digital Converter (ADC) section*, 2022. ESP-IDF ver. 4.4 https://docs.espressif.com/projects/esp-idf/en/release-v4.4/esp32/api-reference/peripherals/adc.html Accessed: February 2022.

[80] Espressif Systems Co. Ltd., *ESP32-WROOM-32D and ESP32-WROOM-32U Datasheet*, 2021. Version 2.2. https://www.espressif.com/sites/default/files/documentation/esp32-wroom-32d_esp32-wroom-32u_datasheet_en.pdf Accessed: November 2021.

[81] Espressif Systems Co. Ltd., *ESP32-WROVER-E and ESP32-WROVER-IE datasheet*, 2021. Version 1.4. https://www.espressif.com/sites/default/files/documentation/esp32-wrover-e_esp32-wrover-ie_datasheet_en.pdf Accessed: December 2021.

[82] Espressif Systems Co. Ltd., *ESP32-S3 Series datasheet*, 2022. Version 1.0. https://www.espressif.com/sites/default/files/documentation/esp32-s3_datasheet_en.pdf Accessed: March 2022.

[83] Espressif Systems Co. Ltd., *ESP32-S3-WROOM-1 and ESP32-S3-WROOM-1U Series datasheet*, 2022. Version 0.6. https://www.espressif.com/sites/default/files/documentation/esp32-s3-wroom-1_wroom-1u_datasheet_en.pdf Accessed: March 2022.

[84] Espressif Systems Co. Ltd., *ESP8266EX series datasheet*, 2020. Version 6.6. https://www.espressif.com/sites/default/files/documentation/0a-esp8266ex_datasheet_en.pdf Accessed: February 2022.

[85] Espressif Systems Co. Ltd., *ESP-WROOM-02D and ESP-WROOM-02U datasheet*, 2022. Version 1.8. https://www.espressif.com/sites/default/files/documentation/esp-wroom-02u_esp-wroom-02d_datasheet_en.pdf Accessed: March 2022.

[86] Espressif Systems Co. Ltd., "ESP32 hardware reference: Chip series comparison." ESP-IDF Programming Guide. https://docs.espressif.com/projects/esp-idf/en/latest/esp32/hw-reference/chip-series-comparison.html Accessed: February 2022.

[87] STMicroelectronics, *STM32WB55 series datasheet*, 2022. Document number DS11929. Version 12. https://www.st.com/resource/en/datasheet/stm32wb55cc.pdf Accessed: April 2022.

[88] STMicroelectronics, *STM32WB5MMG module datasheet*, 2021. Document number DS13252. Version 2. https://www.st.com/resource/en/datasheet/stm32wb5mmg.pdf Accessed: April 2022.

[89] Texas Instruments Inc., *CC3200 datasheet*, 2013. Document number SWAS032F. https://www.ti.com/lit/gpn/cc3200 Accessed: April 2022.

[90] Texas Instruments Inc., *CC3200MOD module datasheet*, 2014. Document number SWRS166C. https://www.ti.com/lit/gpn/cc3200mod Accessed: April 2022.

[91] Microchip Technology Inc., *PIC32MZ W1 and WFI32E01 family datasheet*, 2020. Document number DS70005425D. https://www.microchip.com/en-us/product/WFI32E01PC Accessed: April 2022.

[92] Image of the ESP8266MOD Wi-Fi MCU module, extracted from: https://www.st.com/en/microcontrollers-microprocessors/stm32wb5mmg.html Accessed: June 2022.

[93] s. Image of the ESP-WROOM-02X series Wi-Fi MCU modules, extracted from: https://www.st.com/en/microcontrollers-microprocessors/stm32wb5mmg.html Accessed: June 2022.

[94] Image of the ESP-WROOM-32D Wi-Fi MCU module, extracted from: https://www.nabto.com/guide-to-iot-esp-32/ Accessed: June 2022.

[95] Image of the ESP-WROOM-32U Wi-Fi MCU module, extracted from: https://www.soselectronic.com/products/espressif/esp32-wroom-32u-esp32-wroom-32u-n16-287426 Accessed: June 2022.

[96] Espressif Systems Co. Ltd. Image of the ESP-WROVER-X series Wi-Fi MCU modules, extracted from: https://dl.espressif.com/dl/schematics/pictures/esp32-wrover.jpg Accessed: June 2022.

[97] M. T. Inc. Image of the WFI32E01 Wi-Fi MCU module, extracted from: https://www.microchip.com/en-us/products/wireless-connectivity/embedded-wi-fi/pic32mz-w1-wi-fi-soc-and-module-family# Accessed: June 2022.

[98] STMicroelectronics. Image of the STM32WB5MMG Wi-Fi MCU module, extracted from: https://www.st.com/en/microcontrollers-microprocessors/stm32wb5mmg.html Accessed: June 2022.

[99] Image of the CC3200MOD Wi-Fi MCU module, extracted from: https://spanish.alibaba.com/product-detail/IV-CC3200MOD-CC3200-wifi-module-CC3200-60777303886.html Accessed: June 2022.

[100] J. Karki, *Signal Conditioning Piezoelectric Sensors*, 2000. Application Report SLOA033A.

[101] Texas Instruments Incorporated, *LMV358 datasheet*, 1999. Document number SLOS263X. Last revised May 2020. https://www.ti.com/lit/ds/symlink/lmv358.pdf Accessed: March 2022.

[102] AVIA Semiconductor, *HX711 English datasheet*. https://cdn.sparkfun.com/assets/b/f/5/a/e/hx711F_EN.pdf Accessed: May 2022.

[103] N. Seidle and A. Wende (SparkFun Electronics), "Breakout board for HX711 load cell weight measuring amplifier repository." https://github.com/sparkfun/HX711-Load-Cell-Amplifier Accessed: May 2022.

[104] HRO Electronics Co., *K1-1502SA datasheet*, 2013. https://datasheet.lcsc.com/lcsc/2108131730_Korean-Hroparts-Elec-K1-1502SA-01_C145915.pdf Accessed: March 2022.

[105] I. Gil Martín, "Mechanical, electronic design and implementation of a CanSaT," Bachelor's Thesis, University of Granada, 2021.

[106] P. Hidalgo Rodulfo, "Industrialization of a characterization system for automotive LEDs on PCB," Bachelor's Thesis, University of Granada, 2021.

[107] N. Seidle (SparkFun Electronics), "Breakout board for CH340C usb to serial." https://github.com/sparkfun/Serial_Basic_Breakout-CH340C Accessed: April 2022.

[108] CUI Devices, *USB Type-B drawings*, 2022. Part number: UJ2-BH-2-TH. https://www.cuidevices.com/product/resource/pdf/uj2-bh-th.pdf Accessed: March 2022.

[109] Global Connector Technology, *USB Mini-B drawings*, 2020. Part number: USB2066. https://www.gct.co/files/drawings/USB2066.pdf Accessed: April 2022.

[110] Hirosi Electric Co. Ltd., *USB Micro-B drawings*, 2015. Part number: ZX62D-B-5PA8(30). https://www.hirose.com/en/product/document?documentid=0001147958 Accessed: April 2022.

[111] CUI Devices, *USB Type-C (USB 2.0 version) drawings*, 2022. Part number: UJ20-C-H-G-SMT-TR. https://www.cuidevices.com/product/resource/uj20-c-h-g-smt-tr.pdf Accessed: June 2022.

[112] Amphenol Communications Solutions, *USB Type-C (USB 3.2 version) drawings*, 2020. Part number: 12401598E4. https://cdn.amphenol-cs.com/media/wysiwyg/files/drawing/12401598xxx2a.pdf Accessed: April 2022.

[113] Nanjing Qinheng Microelectronics Co., *CH340C English datasheet*. Version 2C. https://cdn.sparkfun.com/datasheets/Dev/Arduino/Other/CH340DS1.PDF Accessed: March 2022.

[114] Cylindrical battery sizes, extracted from: https://www.gsl-energy.com/lifepo4-26650-3-2v-3800mah-lithium-ion-rechargeable-266500-battery Accessed: August 2022.

[115] Li-Po flat battery sizes, extracted from: https://www.takomabattery.com/ultimate-buying-guide-for-lithium-polymer-battery/ Accessed: August 2022.

[116] Y. Liang, C.-Z. Zhao, H. Yuan, Y. Chen, W. Zhang, J.-Q. Huang, D. Yu, Y. Liu, M.-M. Titirici, Y.-L. Chueh, H. Yu, and Q. Zhang, "A review of rechargeable batteries for portable electronic devices," *InfoMat*, vol. 1, no. 1, pp. 6–32, 2019.

[117] "Different types of batteries for electronic products (importer's guide)." https://www.sofeast.com/resources/different-types-of-batteries-for-electronic-products-guide/ Accessed: August 2022.

[118] NanJing Top Power ASIC Corporation, *TP4056 English datasheet*. https://www.tp4056.com/d/tp4056.pdf Accessed: March 2022.

[119] Fortune Semiconductor Corporation, *DW01A datasheet*, 2009. Document number DW01A-DS-10_EN. Revision 1.0. https://datasheet.lcsc.com/lcsc/1809191939_Fortune-Semicon-DW01A-G_C61503.pdf Accessed: March 2022.

[120] Fortune Semiconductor Corporation, *FS8205A datasheet*, 2009. Document number FS8205A-DS-12_EN. Revision 1.2. https://datasheet.lcsc.com/lcsc/1809050110_Fortune-Semicon-FS8205A_C16052.pdf Accessed: March 2022.

[121] Linear Technology (now Analog Devices), *LTC4060 datasheet*, 2004. Document number 4060f https://www.analog.com/media/en/technical-documentation/data-sheets/4060f.pdf Accessed: March 2022.

[122] D. Andrea, "Estimating the State Of Charge of Li-Ion batteries," *Li-Ion BMS*, 2009. Available online: https://liionbms.com/php/wp_soc_estimate.php Accessed: April 2022.

[123] Linear Technology (now Analog Devices), *LTC2990 datasheet*, 2018. Revision F https://www.analog.com/media/en/technical-documentation/data-sheets/LTC2990.pdf Accessed: March 2022.

[124] Linear Technology (now part of Analog Devices), *LTC4151 datasheet*, 2014. Document number 4151ff https://www.analog.com/media/en/technical-documentation/data-sheets/4151ff.pdf Accessed: March 2022.

[125] Texas Instruments Incorporated, *INA219 datasheet*, 2008. Document number SBOS448F. Last revision September 2011. https://www.ti.com/lit/gpn/ina219 Accessed: December 2021.

[126] Texas Instruments Incorporated, *INA226 datasheet*, 2011. Document number SBOS547A. Last revision August 2015. https://www.ti.com/lit/gpn/ina226 Accessed: March 2022.

[127] Texas Instruments Incorporated, *INA231 datasheet*, 2013. Document number SBOS644D. Last revision October 2014. https://www.ti.com/lit/gpn/ina231 Accessed: March 2022.

[128] Micrel Incorporated (now Microchip Inc.), *MIC22205 datasheet*, 2011. Document number M9999-082511-A. https://ww1.microchip.com/downloads/en/DeviceDoc/MIC22205.pdf Accessed: March 2022.

[129] Texas Instruments Incorporated, *LM3671 datasheet*, 2004. Document number M9999-082511-A. Last revision May 2016. https://www.ti.com/lit/gpn/lm3671 Accessed: March 2022.

[130] Texas Instruments Incorporated, *TLV62569, TLV62569P datasheet*, 2016. Document number SLVSDG1C. Last revision October 2017. https://www.ti.com/product/TLV62569 Accessed: May 2022.

[131] Diodes Incorporated, *AP3429/A datasheet*, 2015. Document number DS36561. Revision 3 - 2. https://www.diodes.com/assets/Datasheets/products_inactive_data/AP3429.pdf Accessed: December 2021.

[132] S. Cass, P. Kulkarni, E. Guizzo, and N. Diakopoulous, "Top programming languages 2021 (Ranking: IEEE Spectrum, Language Types: Embedded)," *IEEE Spectrum*, 2021. https://spectrum.ieee.org/top-programming-languages/#/index/2021/0/0/0/1/1/50/1/50/1/50/1/30/1/30/1/20/1/20/1/5/1/50/1/100/1/50/ Accessed: July 2022.

[133] Espressif Systems Co. Ltd., "Espressif IoT Development Framework (ESP-IDF) repository." https://github.com/espressif/esp-idf Accessed: April 2022.

[134] "MicroPython documentation for the ESP32." https://docs.micropython.org/en/latest/esp32/general.html Accessed: April 2022.

[135] Visual Studio Code logo, extracted from: https://code.visualstudio.com/brand Accessed: June 2022.

[136] PlatformIO logo, extracted from: https://commons.wikimedia.org/wiki/File:PlatformIO_logo.svg Accessed: June 2022.

[137] Arduino. Arduino trademark and copyright. https://www.arduino.cc/en/trademark Accessed: June 2022.

[138] @bodmer, "TFT_eSPI library repository." https://github.com/Bodmer/TFT_eSPI Accessed: March 2022.

[139] @lvgl (LVGL group), "The LVGL (Light and Versatile Graphics Library) repository." https://github.com/Bodmer/TFT_eSPI Accessed: March 2022.

[140] C. Greening (@cgreening), "I2S ADC1 DMA sampling repository." https://github.com/dpmj/esp32_adc_i2s_dma_sampling Accessed: February 2022.

[141] @bogde, "HX711 load cell weight measuring amplifier library repository." https://github.com/bogde/HX711 Accessed: May 2022.

[142] Espressif Systems Co. Ltd., "ESP-DSP library repository." https://github.com/espressif/esp-dsp Accessed: February 2022.

[143] D. Systèmes. SolidWorks logotype extracted from webpage. https://www.solidworks.com/ Accessed: August 2022.

[144] SmartMaterials PLA spool, extracted from: https://www.smartmaterials3d.com/en/pla-filament Accessed: August 2022.

[145] Altium. Altium Designer logotype extracted from webpage. https://www.altium.com/altium-designer Accessed: August 2022.

[146] @issus, "Celestial Altium library repository." https://github.com/issus/altium-library Accessed: April 2022.

[147] Institute of Electrical and Electronics Engineers (IEEE), "IEEE Standard American National Standard Canadian Standard Graphic Symbols for Electrical and Electronics Diagrams (Including Reference Designation Letters)," *IEEE Std 315-1975 (Reaffirmed 1993)*, pp. i–244, 1993.

[148] List of commonly used component designators, which do not necessarily comply with any standards. https://en.wikipedia.org/wiki/Reference_designator#Designators Accessed: June 2022.

[149] Semiconductor Components Industries, LLC, *NCP562, NCV562, NCP563, NCV563 datasheet*, 2019. Publication Order Number NCP562/D. Revision 15. https://www.onsemi.com/pdf/datasheet/ncp562-d.pdf Accessed: February 2022.

[150] S. Santos, "ESP32 Pinout Reference: Which GPIO pins should you use?," *Random Nerd Tutorials*, 2018. https://randomnerdtutorials.com/esp32-pinout-reference-gpios/ Accessed: March 2022.

[151] KEMET Corporation, "K-SIM 3." https://ksim3.kemet.com/capacitor-simulation Accessed: April 2022.

[152] HRO Electronics Co., *K2-1107ST datasheet*, 2021. https://datasheet.lcsc.com/lcsc/2108131530_Korean-Hroparts-Elec-K2-1107ST-A4DW-06_C118141.pdf Accessed: March 2022.

[153] CUI Devices, *SJ-4351X-SMT datasheet*, 2019. https://www.cuidevices.com/product/resource/sj-4351x-smt.pdf Accessed: March 2022.

[154] Altium, "Defining, Scoping and Managing PCB Design Rules in Altium Designer." https://www.altium.com/documentation/altium-designer/defining-scoping-managing-pcb-design-rules Accessed: April 2022.

[155] JLCPCB, "PCB manufacturing and assembly capabilities." https://jlcpcb.com/capabilities/Capabilities Accessed: April 2022.

[156] JLCPCB, *How to export Altium PCB to gerber files*. https://support.jlcpcb.com/article/42-how-to-export-altium-pcb-to-gerber-files Accessed: April 2022.

[157] A. Özgür (@ayberkozgur), "JLCPCB design rules and stackups for Altium Designer repository." https://github.com/ayberkozgur/jlcpcb-design-rules-stackups Accessed: April 2022.

[158] Altium, "PCB routing angle myths: 45-degree angle versus 90-degree angle," 2022. https://resources.altium.com/p/pcb-routing-angle-myths-45-degree-angle-versus-90-degree-angle Accessed: May 2022.

[159] Z. Peterson (Altium), "PCB ground plane best practices in your multilayer stackup," 2022. https://resources.altium.com/p/pcb-ground-plane-best-practices-your-multilayer-stackup Accessed: May 2022.

[160] Altium, "Adding via stitching and via shielding to a pcb in altium designer," 2022. https://www.altium.com/documentation/altium-designer/via-stitching-via-shielding-pcb Accessed: May 2022.

[161] Altium, "Use PCB teardrops to increase yield and design quality," 2017. https://resources.altium.com/p/how-to-increase-design-yield-quality-with-teardrops Accessed: May 2022.

[162] "@angs", "Mounting hole on a pcb," 2014. 3 mounting holes on three different PCBs, extracted from: https://electronics.stackexchange.com/questions/137394/mounting-hole-on-a-pcb, Accessed: August 2022.

[163] "7head7metal7", 2015. Three-dimensional view of a stripline on a dielectric substrate https://commons.wikimedia.org/wiki/File:Microstrip_scheme.svg Accessed: August 2022.

[164] Saturn PCB Design Toolkit https://saturnpcb.com/saturn-pcb-toolkit/ Accessed: January 2022.

[165] J.C. Martínez Durillo, "DATV receiver system design and development," Bachelor's Thesis, University of Granada, 2017.

[166] J.C. Martínez Durillo, "Design of a multidisciplinary 1U CubeSat simulation platform," Master's Thesis, University of Granada, 2018.

[167] JLCPCB. JLCPCB logotype extracted from webpage. https://jlcpcb.com/ Accessed: August 2022.

[168] Altium, "What is a Gerber file or release and how are they used in the PCB fabrication process?," 2017. https://resources.altium.com/p/what-gerber-file-pcb-fabrication-process Accessed: August 2022.

[169] C. Nash and D. R. C. Lasky, *Digital Communications: Fundamentals and Applications*. BR Publishing, Inc., 2004.

[170] BiblioMaker webpage. https://blogs.ugr.es/bibliomaker/ (Spanish) Accessed: August 2022.

[171] Amphenol Communications Solutions, *31-71043 BNC datasheet*, 2019. https://eu.mouser.com/datasheet/2/18/31_71043_customer_drawing-1621252.pdf Accessed: March 2022.

[172] Espressif Systems Co. Ltd., "ESP32-DevKitC-V4 Reference Design r2.1." https://www.espressif.com/sites/default/files/documentation/esp32-devkitc-v4_reference_design.zip Accessed: April 2022.

[173] "Informe socioprofesional COIT/AEIT. Mapa del titulado de Ingeniería de Telecomunicación," tech. rep., COIT/AEIT, 2017. https://www.coit.es/informes/informe-socioprofesional-coitaeit-mapa-del-titulado-de-ingenieria-de-telecomunicacion (Spanish) Accessed: June 2022.

[174] Ministerio de Inclusión, Seguridad Social y Migraciones, "Bases y tipos de cotización," 2022. https://www.seg-social.es/wps/portal/wss/internet/Trabajadores/CotizacionRecaudacionTrabajadores/36537#36538 (Spanish) Accessed: June 2022.

[175] "Estadística de convenios colectivos de trabajo. Avance Mensual.," tech. rep., Ministerio de Trabajo y Economía Social, 2022. CCT-2.1: Convenios, empresas, trabajadores afectados, variación salarial media pactada y revisada y jornada media pactada, según ámbito funcional, por año de efectos económicos y período de registro. Datos acumulados. https://www.mites.gob.es/estadisticas/cct/welcome.htm (Spanish) Accessed: June 2022.

[176] Ministerio de Inclusión, Seguridad Social y Migraciones, "Tarifa de Primas de Accidentes de Trabajo y Enfermedades Profesionales," 2019. https://www.seg-social.es/wps/portal/wss/internet/Trabajadores/CotizacionRecaudacionTrabajadores/48410 (Spanish) Accessed: June 2022.

[177] "Evolución del precio de la electricidad 2022," tech. rep., Organización de Consumidores y Usuarios (OCU), 2022. https://www.ocu.org/vivienda-y-energia/gas-luz/informe/precio-luz (Spanish) Accessed: August 2022.

[178] Siglent Technologies Co. Ltd., *SDG1000X series arbitrary waveform generator datasheet*, 2019. https://siglentna.com/download/2412/ Accessed: February 2022.

[179] Hewlett-Packard Co., *HP 33120A function generator / arbitrary waveform generator user's guide*, 1997. Version 2C. https://cdn.sparkfun.com/datasheets/Dev/Arduino/Other/CH340DS1.PDF Accessed: March 2022.

[180] Tektronix Inc., *TDS1000B and TDS2000B series digital storage oscilloscopes user's manual*, 2009. Document number 071-1817-02. https://www.tek.com/en/oscilloscope/tds1001b-manual/tds1000b-and-tds2000b-series Accessed: July 2021.

[181] HAMEG Instruments GmbH, *HAMEG HMO1022/HMO1024 mixed-signal digital oscilloscope datasheet*. https://cdn.rohde-schwarz.com/hameg-archive/HAMEG_DB_EN_HMO1022_1024.pdf Accessed: July 2021.

[182] "HP 33120A function / arbitrary waveform generator review." http://eereview.com/article/hp-33120a-function--arbitrary-waveform-generator-review Accessed: June 2022.

[183] E. Girlando, *Arduino UNO as a USB to GPIB controller - version 6.1*, 2014. https://egirland.blogspot.com/2014/03/arduino-uno-as-usb-to-gpib-controller.html Accessed: January 2021.

[184] Siglent Technologies Co. Ltd., *SDG1000X series arbitrary waveform generator user manual*, 2017. Document number UM0201X-E01D https://siglentna.com/download/2409/ Accessed: February 2022.

[185] Siglent Technologies Co. Ltd., *SDG1000X series arbitrary waveform generator service manual*, 2016. Document number SM0201X-E01A https://siglentna.com/download/2415/ Accessed: February 2022.

[186] Siglent Technologies Co. Ltd., *SDG series arbitrary waveform generator programming guide*, 2019. Document number PG02_E04A. https://siglentna.com/download/16164/ Accessed: February 2022.

[187] Siglent Technologies Co. Ltd., *Programming example: Create a stair-step waveform using Python and PyVISA using LAN (SDG1000X, SDG2000X, SDG6000X)*, 2020. https://www.siglenteu.com/application-note/programming-example-create-a-stair-step-waveform-using-python-and-pyvisa-using-lan/ Accessed: February 2022.

[188] Siglent SDG1062X function generator front and back photos. https://www.electrokit.com/produkt/funktionsgenerator-60mhz-siglent-sdg1062x/ Accessed: July 2022.

[189] G. Giesbrecht, *SDG2042X repair guide*. https://hackaday.io/project/169480-sdg2042x-repair Accessed: February 2022.

[190] D. Jones (EEVblog), *Siglent signal generator fix*, 2018. https://youtu.be/tM2j9zuBiRQ Accessed: February 2022.

[191] Siglent Technologies Co. Ltd., *Data recovery manual for SDG1000X*, 2017. Confidential, provided by Siglent's customer service.

[192] Yokogawa-Hewlett-Packard Ltd., *Model 4192A LF Impedance Analyzer. Operation and service manual*, 1984.

[193] Siglent SDG3065X digital multimeter front photo. https://www.saelig.com/pr/sdm3065x.html Accessed: July 2022.

[194] Siglent Technologies Co. Ltd., *SDM3065X Series digital multimeter user's manual*, 2022. Document number UM06036-E02B. Accessed: July 2022.

Appendix A

Project costs

In this appendix, the project expenditures will be detailed, including materials, human resources and an estimation of the energy consumption.

A.1 Materials costs

This section outlines the expenses linked to the necessary materials for the manufacture of the prototype: the Electronics, the manufacture of the casing and the Printed Circuit Board, in addition to the shipping costs.

A.1.1 Electronic components

In Table A.1 we can see the expenses breakdown of the electronic components of the TIK prototype that has been manufactured. These expenses correspond only to the costs of a single unit.

This version has the Li-Po battery charger. The cost of populating the Ni-MH charger instead of the Li-Po nearly doubles the charger expenses, as we can see in table Table A.2. The reason is because of the chosen components, since the LTC4060EFE is marked as obsolete by the manufacturer, and is at an exorbitant price in the common online electronics stores. Also, the IC's requirement for a precision resistor drives up the price considerably. The fact of having to buy 3 Ni-MH cells instead of a Li-Po does not change the price of the battery pack excessively. Nevertheless, this option was already discarded for the prototype as already discussed in the "Battery chemistry and capacity" section from the system specification chapter.

In addition, chip and stock shortage has negatively affected the total expenses of the project, with some specific chips being purchased for a significant amount compared to others, like the TLV62569DBVR step-down converter or the INA219AIDR current sensor Integrated Circuit. The choice of the mentioned Texas Instruments TLV62569DBVR over the identical and cheaper (1.13 € vs. 0.13 €) Diodes Incorporated AP3429KTTR-G1 is forced by the lack of stock of the latter.

A.1.2 PCB and stencil manufacturing

The 2-layer, RoHS compliant PCB and the stainless steel stencil were both ordered at JLCPCB. The PCBs must be manufactured in batches, with a minimum of 5 units per order. The costs of manufacturing are listed on Table A.3. Since they are being shipped from China relatively quickly, freight costs play a big role in the final price (see section A.1.4: Shipping costs).

A

Category	Item	Description	Units	Cost/unit (€)	Total (€)
Connectors	SJ-43516-SMT-TR	Jack 3.5 mm, female	2	0.9230	1.85
	10033526-N3212LF	USB Mini-B, female	1	0.5610	0.56
	031-71043	BNC, female	2	7.6800	15.36
	CES-120-01-T-S	Low profile socket strip	1	2.9600	2.96
Switches	K1-1502SA-01	Multi-Directional Switch	1	0.2417	0.24
	K2-1107ST-A4DW-06	Rectangle Button	3	0.0729	0.22
Mechanical	970070354	Brass spacer, M3, 7 mm	4	0.4990	1.97
	278-534	Brass threaded insert, M3	4	0.2420	0.97
	528-946	DIN 7985 screws	3	0.0570	0.17
	281-013	DIN 912 screws	4	0.2141	0.86
Transistors	NSV BC858 CLT1G	BJT PNP GP SOT-23	1	0.1430	0.14
	2N7002P	MOSFET N-Ch GP SOT-23	2	0.0490	0.10
	BSS84AK	MOSFET P-Ch GP SOT-23	1	0.0480	0.05
	FS8205A	MOSFETs N-Ch SOT-23-6	1	0.0593	0.06
Diodes	1N4148W	Power diode SOT-123	6	0.0900	0.54
	KP-1608SGC	Green LED 0805	4	0.1100	0.44
	OSR50805C1E	Red LED 0805	3	0.0800	0.24
Integrated Circuits	HX711	Load cell ADC, SOP-16	1	0.4846	0.48
	LMV358IDGKR-P	Dual OpAmp GP, MSOP-8	1	0.1333	0.13
	DW01A	Lithium bat. prot., SOT-23-6	1	0.0356	0.04
	TP4056	Lithium bat. charger, SOP-8	1	0.1494	0.15
	USBLC6-2SC6	USB ESD Prot., SOT-23-6	1	0.0628	0.06
	INA219AIDR	Current sensor, SOIC-8	1	1.5745	1.57
	CH340C	USB transceiver, SOP-16	1	0.3899	0.39
	TLV62569DBVR	Buck converter, SOT-23-5	1	1.1316	1.13
	TPD3S014TDBVRQ1	Current-limit, SOT-23-6	1	0.1100	0.11
	NCP562SQ18T1G	LDO 1.8V reg., SC82-AB	1	0.5970	0.60
Thick film resistors	–	5%, 0603, 0.1 W	33	[1] 0.0500	1.65
	–	5%, 0805, 0.1 W	5	[1] 0.0500	0.25
	RLC32-R200FTP	0.2 Ω, 1%, 1206, 0.5 W	1	0.2510	0.25
MLCC capacitors	CL21A226KPCLRNC	22uF, 10%, 10V, X5R, 0805	5	0.2610	1.31
	CL21A106KPFNNNF	10uF, 10%, 10V, X5R, 0805	6	0.0720	0.43
	C0805C105K4RAC7800	1uF, 10%, 10V, X5R, 0805	3	0.0860	0.26
	C0805C104J4RAUTO	100nF, 5%, 16V, X7R, 0805	19	0.0740	1.41
	C1206C104J1RECAUTO	100nF, 5%, 100V, X7R, 1206	2	0.1330	0.27
	CC603JRX7R9BB101	100pF, 5%, 50V, X7R, 0603	1	0.0440	0.04
	C0805C470J8HACTU	47pF, 5%, 10V, X8R, 0805	3	0.0640	0.06
	CC0805JRNPO9BN270	27pF, 5%, 50V, C0G, 0805	1	0.0390	0.04
	C0805C220J5RACTU	22pF, 5%, 50V, X7R, 0805	1	0.0640	0.06
Inductors & chokes	NRS4018T2R2MDGJ	2.2uH, 20%, 2.2A, shielded	1	0.1580	0.16
	2508056007Y3	60Ω@100MHz, 25%, 3A, 0805	2	0.0480	0.10
Other	ESP32-WROOM-32D	ESP32-D0WD, SPI flash, antenna	1	3.8800	3.88
	MIKROE-4473	Li-Po Bat., 3.7V, 1500mAh	1	10.3600	10.36
	JC2432S028R	ILI9341 2.8" touchscreen	1	5.3600	5.36
			Subtotal (before VAT) (€)		**57.28**
			Total (after 21% VAT) (€)		**69.31**

Table A.1 – *Bill of materials of the electronic components of the built prototype.*
[1] *Average value estimation.*

Charger type	Item	Description	Units	Cost/unit (€)	Total (€)
Li-Po/Li-Ion	TP4056	Lithium bat. charger, SOP-8	1	0.1494	0.15
	DW01	Lithium bat. prot., SOT-23-6	1	0.0356	0.04
	FS8205A	MOSFETs N-Ch SOT-23-6	1	0.0593	0.06
	Various resistors	Thick film, 5%, 0603, 0.1 W	3	0.0500	0.15
	MIKROE-4473	Li-Po Bat., 3.7V, 1500mAh	1	10.3600	10.36
				Li-Po Subtotal (before VAT) (€)	**10.76**
				Ni-MH Total (after 21% VAT) (€)	**13.02**
Ni-MH	LTC4060EFE	NiMH bat. charger, TSSOP-16	1	5.5667	5.57
	MJD210G	Power BJT PNP, DPAK	1	0.5990	0.60
	Various resistors	Thick film, 5%, 0603, 0.1 W	2	0.0500	0.10
	P-1206H4421DBT5	Thin film, 4.42KΩ, 0.5%, 1206	1	2.0100	2.01
	885012007007	MLCC, 470pF, 5%, 10V, 0805	1	0.0950	0.10
	HHR-150AAC8	NiMH, AA, 1.2V, 1500mAh	3	3.6300	10.89
				Ni-MH Subtotal (before VAT) (€)	**21.10**
				Ni-MH Total (after 21% VAT) (€)	**25.53**

Table A.2 – *Price comparison among the two charger variants.*

Item	Description	Units	Cost/unit (€)	Total (€)
Single PCB	132x54x1.6 mm, 2-layer, FR4, HASL-RoHS	5	1.5960	7.98
Stencil	Stainless steel, 380x280mm, top solder only	1	6.6500	6.65
			Subtotal (before VAT) (€)	**14.63**
			Total (after 21% VAT) (€)	**17.70**

Table A.3 – *Bill of materials of the PCB and stencil.*

Item	Description	Material amount (g)	Cost/unit (€)	Total (€)
Top cover	3D-printed, PLA, "antracite" color	41	0.9196	0.92
Bottom cover	3D-printed, PLA, "antracite" color	52	1.1664	1.17
Front button	3D-printed, PLA, "wood" color	1	0.0224	0.02
			Subtotal (before VAT) (€)	**2.11**
			Total (after 21% VAT) (€)	**2.55**

Table A.4 – *Bill of materials of the 3D-printed case parts.*

A

A.1.3 Case manufacturing

For manufacturing the housing of the handheld device we used a 3D printer borrowed from BiblioMaker, a 3D printing service for the UGR students. These printers make use of PLA polymer. The different parts were printed from spools of 1.75 mm diameter PLA filament which was acquired at 22.43 €/kg (before VAT), that is, 0.02243 €/g. Given that the total weight of the printed parts (including supports) was 94 grams, the cost of the case is 2.55 € (with VAT). This data is collected in Table A.4.

A.1.4 Shipping costs

Freight costs make up a substantial percentage of the total expending of items ordered online. In order to save some costs, the different projects which were being carried out simultaneously at GranaSat coordinated to order the necessary components on the same online stores. In this way, the shipping costs of the same order for a store are distributed among several projects. The subdivision of costs can be consulted in Table A.5.

A.1.5 Equipment costs

Although it would be desirable to account for the cost of the tools and machinery used (such as the cost of the 3D printer, the soldering stations, oven, the electronic instrumentation, the voltage sources, bench tools, etc.), estimating these costs is goes outside the scope of the expenditures of this project. Therefore, it is considered that the equipment belongs to the laboratory and is already amortized; thus without additional cost for this project. The same goes for the cost of the computers used.

A.1.6 Software costs

The software licenses are also an expense to be taken into account, which is detailed in Table A.6. Luckily, the software expenses of this project is nil thanks to the use of FOSS, freeware and student licenses.

A.2 Human resources: labor costs. Engineers' salaries and Social Security contribution

The average salary of a telecommunications engineer in Spain amounts to approximately 52 700 € gross per year [173]. In Spain, the Social Security withholding on the worker's gross salary is around 6.35 % [174], which translates into a net salary of over 53 600.00 €. However, as a junior engineer, a considerably lower salary is to be expected. For the calculations of the costs of human resources, an aspirated salary of 30 000.00 € gross per year (over 28 000.00 € net) is proposed. This amount is in line with the expectations of most telecommunication engineering students, according to the *"COIT/AEIT Socio-Professional Report of the Telecommunications Engineering Graduate"* [173].

The average number of hours worked in Spain from 2000 to 2021 has been 1 752 hours per year [175]. With a salary of 30 000.00 €/year, this translates into an approximate remuneration of 17.00 €/hour. This value will be used to estimate the payment for the junior engineer in the breakdown of hours dedicated to each task (Table A.7). In total, the junior engineer has spent around 1185 hours so his payment is 16 745.00 €.

The hours spent by the project supervisor are counted as those of a senior engineer. Therefore, the aforesaid average salary of a telecommunications engineer in Spain is taken as a reference (52 700.00 € gross per year). For the same estimate of 1 752 worked hours in a year, the senior's retribution is 30 €/hour. The supervisor has spent around 70 hours on the project, which constitutes a payment of 2 100.00 €.

Additionally, it is interesting to consider the payment that the employer must made to the Social Security

Online store	Shipping costs (€) (including VAT)	Nº of projects that share costs	Costs assumed by this project (€)
JLCPCB https://jlcpcb.com	40.64	2	20.32
LCSC Electronics https://lcsc.com	62.04	4	15.51
RS Components https://es.rs-online.com	7.00	4	1.75
Mouser Electronics https://www.mouser.es	0.00	3	0.00
Aliexpress https://es.aliexpress.com	1.83	1	1.83
Total assumed shipping costs (including VAT) (€)			**39.41**

Table A.5 – *Itemization of the shipping costs.*

Category	Software and version	Type of software and license/EULA	Cost
Operating System	Arch Linux	FOSS (license varies per package)	None
	Microsoft Windows 10	Proprietary, license owned by the student	None
Programming and data analysis	Jupyter Lab > 3.4	FOSS, BSD license	None
	Python > 3.6	FOSS, PSF license (GPL-compatible)	None
	Numpy > 1.20	FOSS, BSD 3-Clause revised	None
	Matplotlib > 3.5	FOSS, PSF-based (BSD-compatible)	None
	MatLab 9.9.0 (R2020b)	Proprietary, student license	None
	Visual Studio Code > 1.6	Source: MIT license, executable: Freeware	None
	PlatformIO (core > 6.0)	FOSS, Apache 2.0	None
	ESP-IDF > 4.4	FOSS, Apache 2.0	None
	PyCharm CE 2022	FOSS, Apache 2.0	None
	Arduino IDE > 1.8	FOSS, AGPL 3.0	None
Redaction of documents	Overleaf	Proprietary, free plan	None
	LaTeX (texlive) v. 2021	FOSS, GPL	None
	LibreOffice Suite > 7.1	FOSS, LGPL 3.0	None
EDA, electronic analysis and simulation	EasyEDA Std. > 6.5	Proprietary, free plan	None
	KiCad > 6.0	FOSS, GPL 3.0; libs: MIT or CC-BY-SA 4.0	None
	Altium Designer 21	Proprietary, student license	None
	LTSpice v. 2019	Proprietary, freeware	None
	Saturn PCB Toolkit > 8	Proprietary, freeware	None
CAD, mechanical design and 3D printing	SolidWorks 2021	Proprietary, student licence	None
	Ultimaker Cura > 5	FOSS, GPL 3.0	None
Image editors	Inkscape	FOSS, GPL 2.0	None
	GIMP	FOSS, GPL	None

Table A.6 – *List of the software used, its user licenses and the cost for the project.*

for having salaried workers. Table A.8 shows the contribution percentages and premiums due to the type of contract and occupational sector [174, 176]. The total ascends to a 32.5 % over the gross salary. For the junior engineer, this is a contribution of 6 547.13 €; and for the senior engineer, 682.50 €.

A

A.3 Electricity costs

The recent international events have shaken the economy and the European energy sector in particular; which has resulted in a much higher cost of electricity than in past years [177]. That is why it is interesting to consider the expense that this situation has caused in the costs of the project. In Figure A.1 we can see the evolution of the electricity prices for the PVPC rate. The average price from September 2021 to July 2022 was 0.293981 €/kW·h [177]. This value will be used to calculate the cost of the energy consumed. Fixed costs and taxes are unknown.

For the number of hours of usage of each device, an approximation is made based on the hours spent on every task (Table A.7). The Table A.10 presents an estimation of the energy consumption made during the development of the project. Since it's very difficult to know the exact consumption, the following approximation is proposed:

- **Student PCs'.** The signal analysis, software development, electronic and mechanical design, and all the written documents were carried out using the student's PCs. These consist of:
  - A desktop PC, whose components' maximum sustained power consumption is around 400 watts.
  - A laptop PC, whose maximum sustained power consumption is 60 W.

  Since the power consumption of a PC varies greatly depending of the tasks being performed, we will take half of these figures as reference. This is, 200 W for the desktop PC and 30 W for the laptop.
- **Electronic instrumentation.** Such as voltage sources, oscilloscopes, etc. We take the typical consumption of some used equipment. For example, the SDG1062X specifies 21 W [178], whereas the HP33120A states 28 W [179]. And for oscilloscopes, the Tektronix TDS1000B consumes "less than 30 W" [180] and the Hameg HMO1024 has a typical consumption of 35 W [181]. We will take the average of the four instruments, which is 29 watts.
- **Heat producers.** We can differentiate between large and small heat producers. The great heat producers are the reflow oven, the heat gun and the AOYUE Int 2702A+ soldering station, which are rated for 500 W. The small heat producer is the Ersa i-CON Nano soldering iron, which are rated for a maximum of 80 W.
- **Heavy tools.** Like the bench drill and grinder, which were used briefly but have a high power consumption of around a kilowatt.
- **Air conditioning.** It was essential to maintain a suitable work environment during the high temperatures of summer. The split AC units on GranaSat laboratories consume up to 1.8 kW. As an average, we will take half of that, 900 W.

A.4 Total costs

Finally, gathering all the subtotals from the previous sections, we can calculate the overall expenses of the project: the total amounts to 29 663.22 €; the vast majority being labor costs. As a digest, the costs of each part and the total are shown in a table in Table A.10 and in graphs in Figure A.2.

Task	Nº of hours spent	Task cost, at 17 €/hour
Meetings	46	782.00
Documentation and formation	23	391.00
Sampling and signal analysis	112	1 904.00
Developing instrumentation handling libraries	56	952.00
Circuit design	161	2 737.00
PCB design	167	2 839
Firmware development	104	1 768.00
Case design and printing	24	408.00
PCB check and assembly	11	187.00
Testing, verification and debugging	39	663.00
Writing the Bachelor's Thesis document	422	7 174.00
Defense preparation	20	340.00
	Total hours	**Engineer's payment (€)**
	985	**20 145.00**

Table A.7 – *Hours spent on every task and junior engineer's compensation.*

Concept	Kind of contribution	Percentage over salary
Common contingencies	–	23.60 %
Unemployment	Permanent contract	5.50 %
Work accidents/occupational diseases	Manufacture of computer, electronic and optical products	2.60 %
Professional Training	–	0.60 %
FOGASA (Fondo de Garantía Salarial)	–	0.20 %
	Total percentage over salary	**32.50 %**
	Junior engineer Social Security cost (€)	**6 547.13**
	Senior engineer Social Security cost (€)	**682.50**

Table A.8 – *Breakdown of the employer's payment to Social Security.*

Equipment	Estimated average power consumption (W)	Hours of usage	Energy consumed (kW·h)	Electricity cost (€)
Desktop PC	200	596	119.20	35.04
Laptop PC	30	217	6.51	1.91
Electronic instrumentation	29	97	2.81	0.83
Soldering station, oven and heat gun	500	10	5.00	1.47
Soldering iron	80	10	0.80	0.24
Bench tools	1000	1	1.00	0.29
Air conditioning	900	75	67.50	19.84
		Total electricity cost (€)		**59.62**

Table A.9 – *Estimation of the electricity costs.*

A

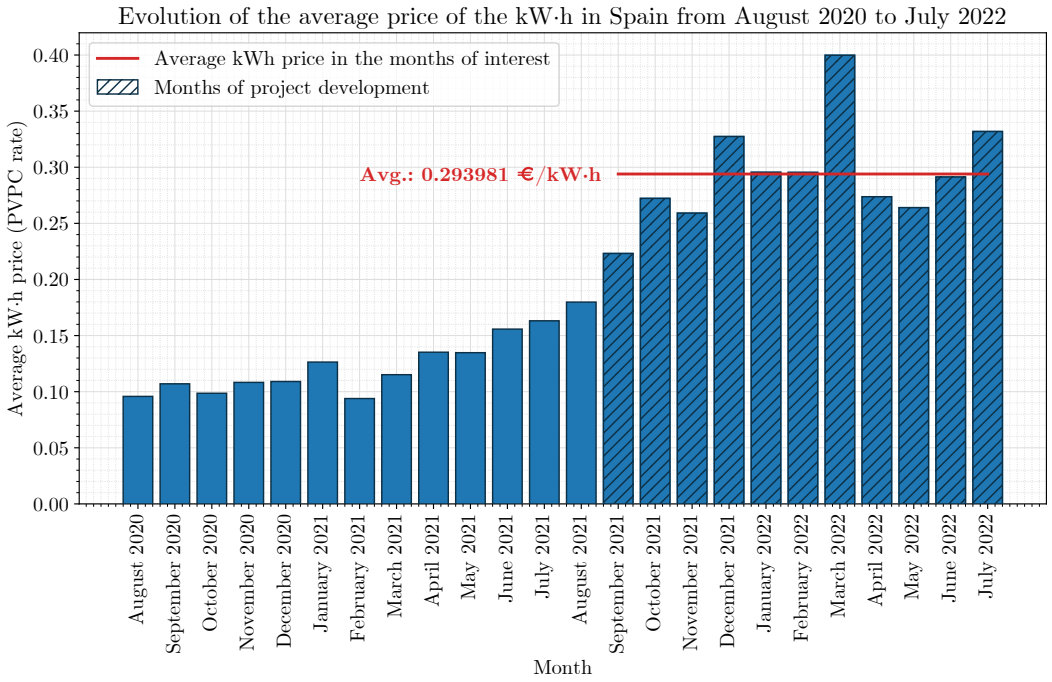

Figure A.1 – *Evolution of the average price of the kW·h in Spain from August 2020 to July 2022. Data extracted from OCU's monthly report [177].*

Type	Concept	Cost (€)
Materials	Electronic components	69.31
	PCB and stencil	17.70
	3D-printed case	2.55
	Shipping	39.41
	Total materials costs, including VAT (€)	**128.97**
Human resources	Junior engineer's payment	20 145.00
	Junior engineer's Social Security	6 547.13
	Senior engineer's payment	2 100.00
	Senior engineer's Social Security	682.50
	Total human resources costs (€)	**29 474.63**
Energy	Estimated electricity cost	59.62
	Total energy costs (€)	**59.62**
	TOTAL PROJECT EXPENSES (€)	**29 663.22**

Table A.10 – *Breakdown of the project's total costs.*

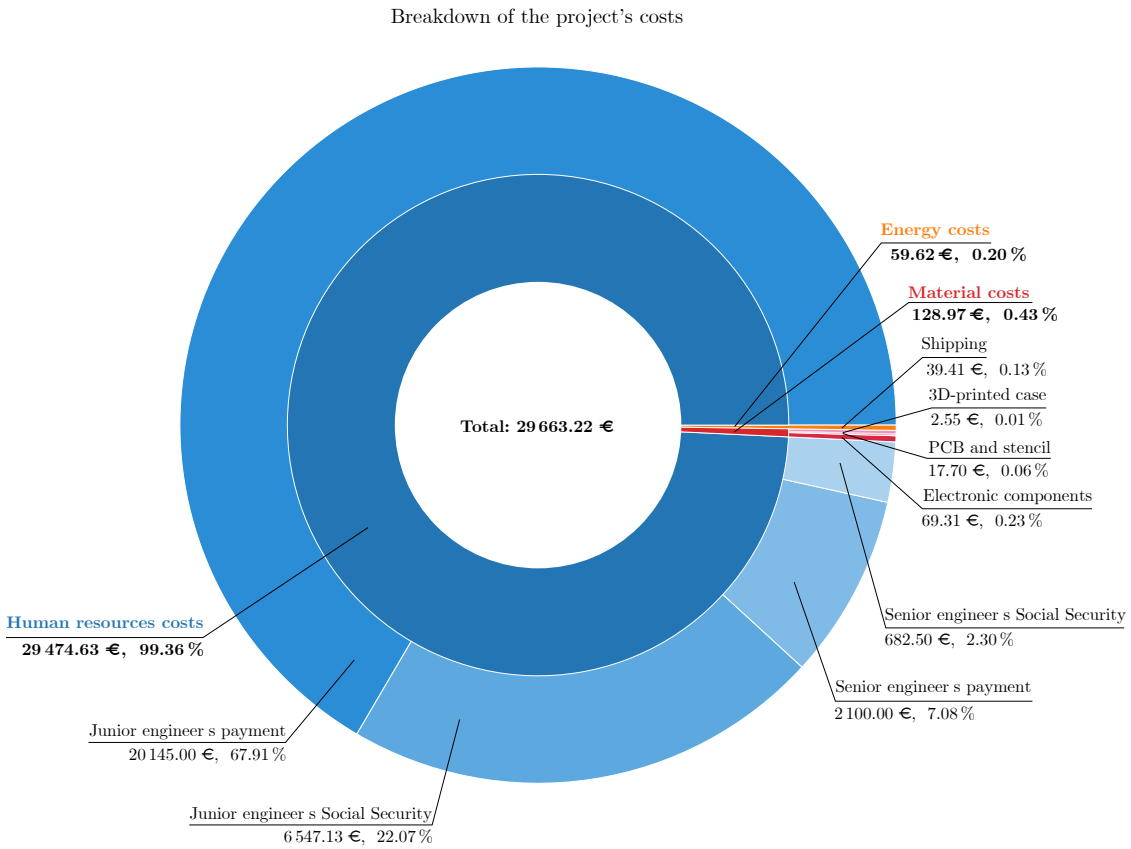

(a) *Nested pie chart of total project costs. The central ring indicates the type of expense (materials, human resources or energy), and the outer ring indicates the concept of the expense. For an enlarged view in detail of each part, see the figures below.*

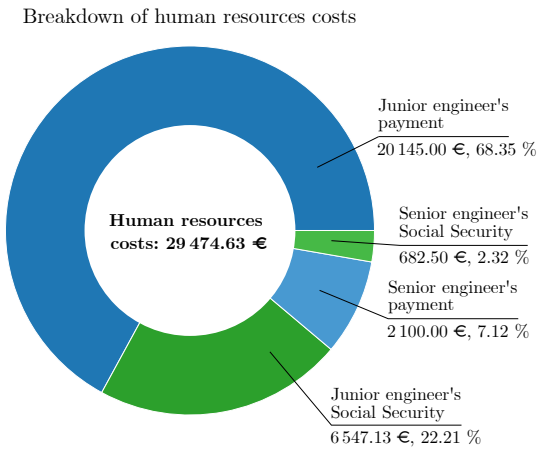

(b) *Detail of human resources costs.*

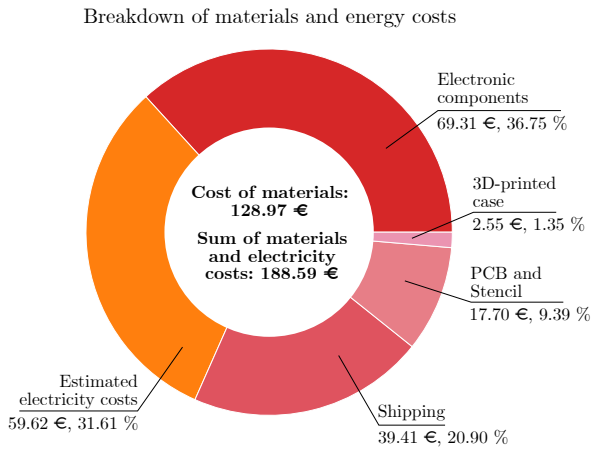

(c) *Joint perspective of material and energy costs.*

Figure A.2 – *Pie charts detailing the total and partial expenses of the project.*

A

Appendix B

Circuit schematics

The following 20 pages are the complete circuit schematics. The sheets were drawn in Altium Designer. For an explanation of the components and how the schematics should be interpreted, see Section 5.1.2 Circuit schematics.

The schematics contain diagrams and explanations of their operation, and the integrated ones have images of their corresponding footprint and package. That is, the schematics are self-contained and can be understood on their own, without the need for the explanation of the previous chapters.

BACHELOR'S DEGREE IN TELECOMMUNICATION ENGINEERING

ACADEMIC COURSE 2021/2022

Tree Inspection Kit handheld device

Part of the Bachelor's Thesis:

"Development of an acoustic measurement system of the Modulus of Elasticity in trees, logs and boards"

AUTHOR:

Juan Del Pino Mena

SUPERVISED BY:

Sr. Andrés M. Roldán Aranda

DEPARTMENT:

Electronics and Computer Technology

UNIVERSIDAD DE GRANADA

IDIE Investigación y Desarrollo en INGENIERÍA DE EDIFICACIÓN Universidad de Granada

ADIME Acústica y Diagnóstico de Materiales y Estructuras

LIFE WOOD FOR FUTURE

Project title: **TIK_HandheldDevice.PrjPcb**		
Date: **2022-07-29**	Revision: **0.6**	Sheet 1 of 21

Introduction

Objective

The present project has the goal of developing a handheld electronic device capable of measuring the MOE (Modulus Of Elasticity) of standing trees and logs from silviculture, so their wood can be classified for structural purpose.

The MOE (Modulus Of Elasticity) is the resistance of an object or substance to being elastically deformed when a stress is applied to it.

The device is equipped with the electronics needed to measure the delay between two signals which come from two piezoelectric sensors nailed into a piece of wood. It can be a standing tree, a tree trunk or a wooden board. The transit time of a wave travelling through the longitudinal axis of the wood is inversely related to the MOE and thus to the material rigidity. This device can also weight trunks to estimate its density by using a load cell.

At the right side you can see some renders of the PCB (version 0.5) which has been manufactured.

Motivation

The poplar silviculture has many environmental advantages such as high carbon sequestration, they conserve the quality of the soil and act as water cycle regulators.
For a sustainable explotation, it is necessary that the wood is of quality. One of the figures on which wood is selected is stiffness, specially for structural applications. The MOE and stiffness are direclty related. The development of a measuring instrument for the MOE is of interest to know the wood properties as soon as possible.

Collaborators

This work has been possible thanks to the GranaSat electronics team. Huge thanks to all the IDIE-ADIME research team and to the LIFE Wood For Future programme for offering and financing the project.

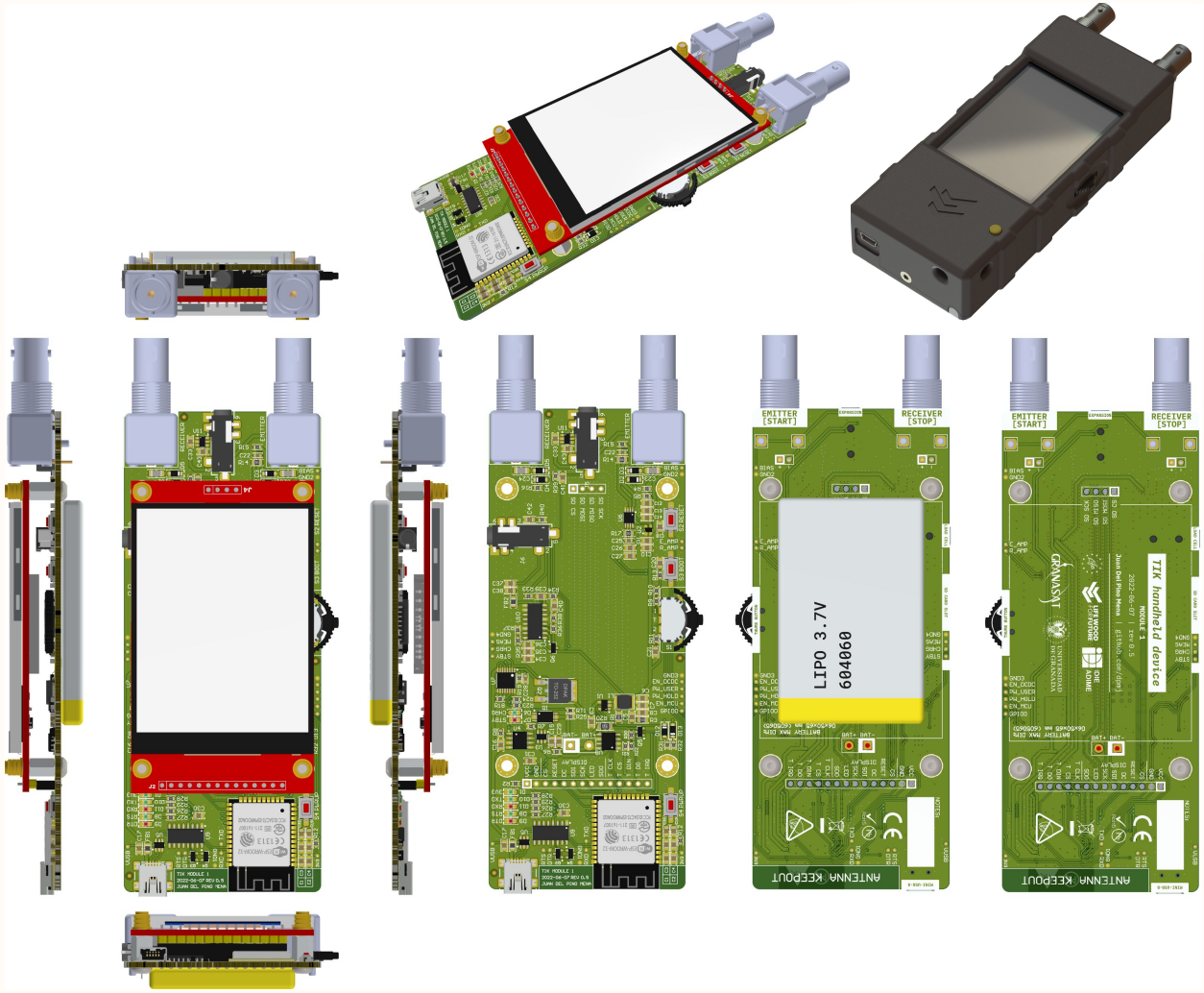

Tree Inspection Kit handheld device

A device capable of determining the microsecond delay between 2 signals coming from piezoelectric probes nailed into a tree, trunk or wood board. This allows the indirect calculus of the Modulus of Elasticity in a non-destructive way.

Designer's signature

Supervisor's signature

Sheet title:	**Introduction and PCB renders**
Project title:	**TIK_HandheldDevice.PrjPcb**
Desginer:	**Juan Del Pino Mena**
Date: **2022-07-29**	Revision: **0.6**
Sheet 2 of 21	

Supervisor:
Sr. Andrés Roldán Aranda
Dpto. Electrónica y Tecnología de Computadores
University of Granada
C/ Fuente Nueva, s/n, 18001
Granada, Granada, Spain

Index

Changelog

Revision 0.6 | 2022-07-29

NEW

- Completed documentation (final version)
- Added a DCDC converter substitute IC.
- Updated block diagram.

FIXED

- Changed 3D models to fit the real board.
- Added circuits' correction notes for future development.

Revision 0.5 | 2022-06-07 [MANUFACTURED VER.]

NEW

- Added multilayer connector to the battery
- Added a power budget & battery selection
- Adjusted the charging current resistor value of the TP4056.
- Added a expansion port and load cell connectors footprints. (4-pole jacks).
- Added support for jack plug switches.
- Applied JLCPCB design rules via .rul file.
- All vias are tented to avoid corrosion.
- Added detailed explanation of trace design with Saturn PCB toolkit.
- Applied a nice format to the BOM.
- Added an introduction, updated renders.
- Added mechanical drawings with 3D isometric views, part drawing views, measurements, layer stackup, drills, etc.
- Added Gerber and NC Drills fabrication jobs for ordering PCB and its stencil.

FIXED

- Corrected LEDs' series resistors values
- Relocated the battery below the PCB. This makes the product wider, but solves a lot of space constraints.
- Removed VBIAS plane to avoid splitting planes, for EMI considerations.
- A lot of cosmetic improvements and corrections on PCB top & bottom overlays.
- Replaced logos and added new ones.
- Improved routing.
- A few cosmetic changes on the schematic sheets and cover.
- Removed rooms.
- NTC connector changed, now it's meant for soldering the NTC cable from a battery.

Revision 0.4 | 2022-05-22

NEW

- Added parameters for fabrication groups and fabrication order
- Added a Bill of Materials. The one in this document is simple. Refer to the manually configured BOM of this project.
- Added a PCB track legend and description for visible layers.
- Given more info about ESP32 pins.
- Added a precise block diagram.
- Added support for an extension port.
- Added a HX711-based load cell adquisition system.

FIXED

- Corrected I2C pins on the ESP32.
- Removed "same length" directive on UART and I2C nets.
- Improved routing.
- Removed via shielding on I2C traces.
- Solved all DRC warnings and errors.
- Avoided disrupting the ESP32's strapping pins default configuration during boot.
- Corrected a pin assignment error between the schematic symbol and the footprint of the MDJ210 PNP BJT transistor.
- Removed PCB cutouts.

Revision 0.3 | 2022-04-28

NEW

- Changed rotary encoder vertical for horizontal, side-placed, SMD type multipurpuse 'thumb button'.
- Added a explanation of PCB trace widths.
- Adopted JLCPCB design rules.
- Full PCB component placement and routing, with no important DRC messages.
- Added silkscreen logos to the back of the PCB, as well as port markings, information and regulatory graphics: CE, WEEE, ESD sensitive warning and RoHS.

FIXED

- Changed numerical test point designators to net/rail names, to be quickly identified.
- Changed LEDs footprints.
- Corrected a faulty connection on the DW01A Lithium battery protection IC.
- The MCU has no longer the possibility to stop battery charging. This is because the ENABLE signals required by the chargers work on 5V and this could cause damage to the ESP32.

Revision 0.2 | 2022-04-23 [FIRST PCB]

NEW

- Schematic hierarchy and block diagram.
- Initial PCB layout
- Added a vertical rotary encoder. PCBLib contains a 90-degree alternative.
- Added an alternative Ni-MH charger.
- Added footprints for all neccessary components to the PCB Library.
- Added explanatory footprints and photos to schematic ICs.
- Added board mounting holes (making use of the TFT LCD module mounting hole positions)
- Added test points
- Added fiducials
- Added a power-up button
- Added net classes and parameter sets to most important nets: power, digital communications, analog signals, etc.

FIXED

- Removed errors in the lithium charger
- Removed errors in the adequation circuit
- Changed ESD USB Protection IC.
- Changed some adequation circuit values and made topology more clear.
- Revised all passive components values and sizes to match existing component disponibility.
- Corrected various pin definitions from the ESP32-WROOM-32D symbol

REVISION 0.1 | 2022-04-01 [FIRST VERSION]

NEW

- TFT LCD / SD card connections.
- First adequation circuit iteration
- LiPo battery charger with TP4056
- Auto programming circuit.

FIXED

--

Document index and revision history

Detailed changelog and complete document sheets index.
All along the schematic pages, a sheet title and description will be written on this corner.

Designer's signature

Supervisor's signature

Sheet title:	**Changelog and document index**		
Project title:	**TIK_HandheldDevice.PrjPcb**		
Desginer:	**Juan Del Pino Mena**		
Date: **2022-07-29**	Revision: **0.6**	Sheet 3 of 21	

Supervisor:
Sr. Andrés Roldán Aranda
Dpto. Electrónica y Tecnología de Computadores
University of Granada
C/ Fuente Nueva, s/n, 18001
Granada, Granada, Spain

SPI traces (@ 80 MHz, digital)

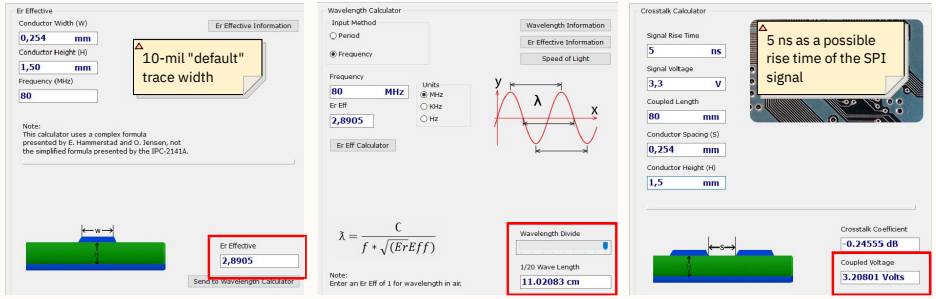

SPI traces should not be longer than this result to avoid a transmission line. Note that this is rather a pessimistic value, as we are dividing the real wavelength by 20. Er Eff has been estimated with the expected fabrication characteristics.

As you can clearly see, a 2-layer, 1-6 mm height PCB is not great for signal integrity. We have great crosstalk between SPI lines. A common solution is to include GND copper between SPI lines with good connection to ground. This can be achieved by using via shielding.

Sensor analog signals (1 MHz max BW)

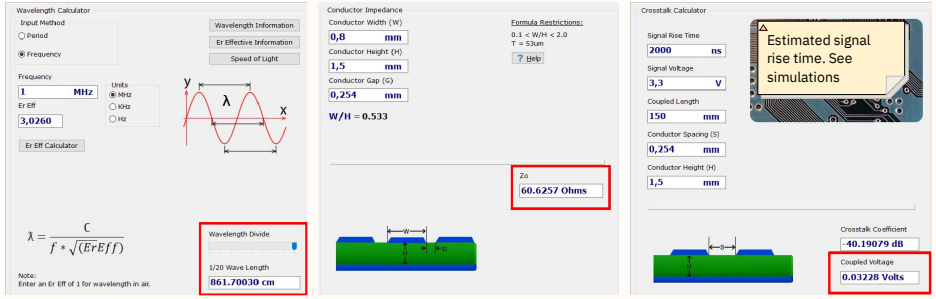

Er_Eff calculated with a 0.8 mm wide trace. Trace lenght will not be a problem.

We cannot totally match the 50-Ohm impedance of the cable but are fairly close. Besides, this is not by any means crytical in a low-speed design such as these, and there's no impedance control on the end of the lines

Crosstalk and EMI can be a problem given the needed precision. Place these far from high-speed, with via shielding, as well as a good GND/power planes below.

Via characteristics

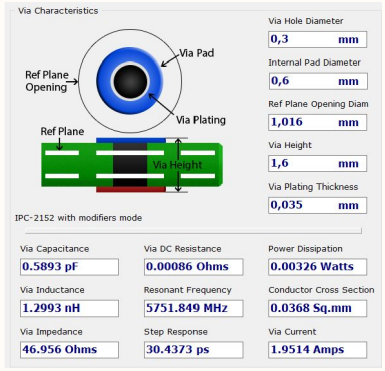

We are using only use one type of via. We are far from the resonant frequency and the step response is very fast. Parasites are very low. In DC it can stand the required amount of current. Nevertheless, it should be always used various in parallel to ensure a low resistance path for power and returning currents.

0.254 mm (10 mil) traces

Trace AC/DC characteristics in one centimetre of trace for a given frequency/DC and for a trace temperature increase of 10 ºC over a standard ambient temperature of 25ºC in a FR-4 dielectric.

0.254 mm (10 mil) is the default trace width. It's thin so we can save space, but has the worst DC characteristics and should not be used for power. These are the kind of traces used by by the SPI bus. The skin depth is not optimal but this will depend on frequency and again, AC current is not a crytical aspect here. It's a "good enough" approach.

0.35 mm traces

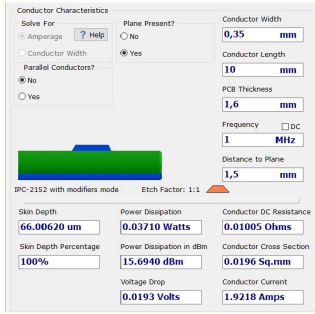

0.35 mm traces are used by connecting power pins to the power net in low-power components whose pins are very close together and cannot fit a trace of more width without breaking design rules.

This trace width has good properties and can be used even for low-speed analog signals if needed.

0.5 mm traces

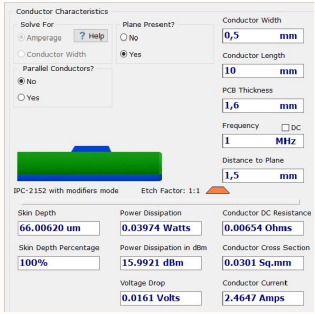

This is an optimal width in terms of area/specs for power delivery as it can withstand a lot of current (more than the system will continuosly need) with low losses.

0.8 mm traces

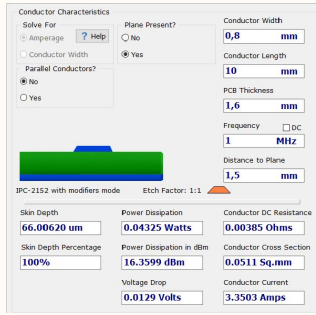

This trace width is employed by the analog signals to maintain good signal integrity at low line impedance.
It can also be used as a power main bus for ensuring low power losses across a distance and for devices with a pulsed, agressive power consumption such as the ESP32 and the LCD.

Trace & via characteristics

Trace width based on results from PCB Toolkit by Saturn PCB Design INC.
Used JLCPCB 2-layer, FR-4, 1.6 mm height, 35 um conductor height (1 oz/ft^2) board characteristics as reference.

Designer's signature

Supervisor's signature

Sheet title:	**Trace width design**		
Project title:	**TIK_HandheldDevice.PrjPcb**		
Desginer:	**Juan Del Pino Mena**		
Date: **2022-07-29**	Revision: **0.6**	Sheet 4 of 21	

Supervisor:
Sr. Andrés Roldán Aranda
Dpto. Electrónica y Tecnología de Computadores
University of Granada
C/ Fuente Nueva, s/n, 18001
Granada, Granada, Spain

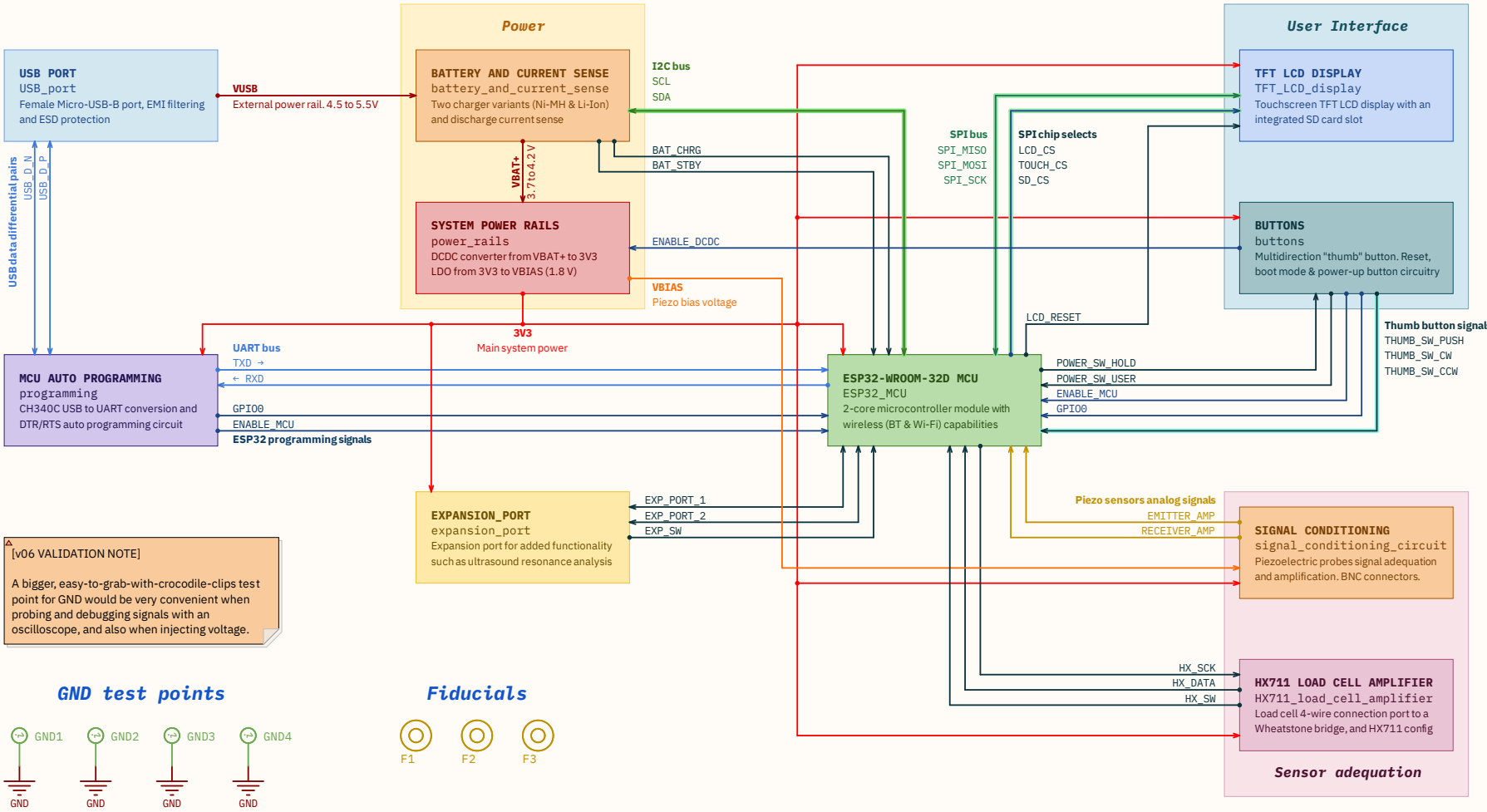

System blocks organization and connections

The project's global block diagram. Arrows show how modules are interconnected and include net names.
PCB includes 3 fiducials for fabrication purposes. GND test points are distributed along the PCB for easy access.

Designer's signature

Supervisor's signature

Sheet title:	**System blocks organization and connections**
Project title:	**TIK_HandheldDevice.PrjPcb**
Desginer:	**Juan Del Pino Mena**
Date:	**2022-07-29**
Revision:	**0.6**
Sheet	5 of 21

Supervisor:
Sr. Andrés Roldán Aranda
Dpto. Electrónica y Tecnología de Computadores
University of Granada
C/ Fuente Nueva, s/n, 18001
Granada, Granada, Spain

Some ESP32's pins behave in a way that prevent using them freely. They are marked on the legend below.

The ADC2 peripheal is not usable while using Wi-Fi or Bluetooth and should be left unused if not necessary. Digital I/O on those pins while on Wi-Fi or BT is fine.

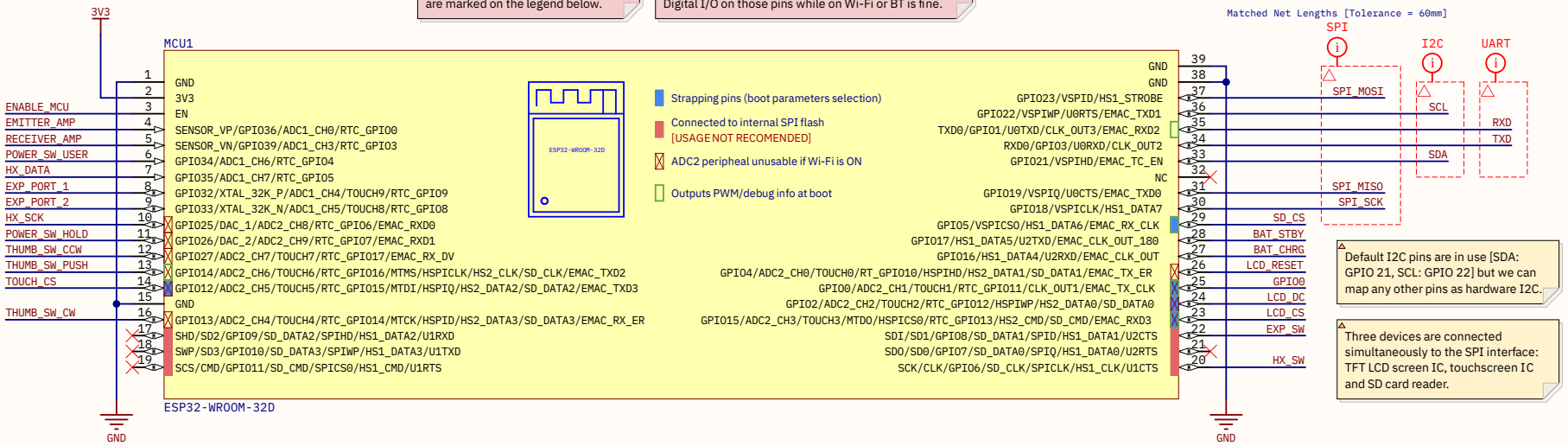

Default I2C pins are in use [SDA: GPIO 21, SCL: GPIO 22] but we can map any other pins as hardware I2C.

Three devices are connected simultaneously to the SPI interface: TFT LCD screen IC, touchscreen IC and SD card reader.

Strapping pins digital state are registered during reset and modify the boot sequence parameters according to the [ESP32 datasheet, table 5, page 21].
We must make sure that if pull-up/down resistors are connected to these pins (i.e for buttons) they do not alter the default configuration unintentionally.

Voltage of Internal LDO (VDD_SDIO)			
Pin	Default	3.3 V	1.8 V
MTDI	Pull-down	0	1
Booting Mode			
Pin	Default	SPI Boot	Download Boot
GPIO0	Pull-up	1	0
GPIO2	Pull-down	Don't-care	0
Enabling/Disabling Debugging Log Print over U0TXD During Booting			
Pin	Default	U0TXD Active	U0TXD Silent
MTDO	Pull-up	1	0
Timing of SDIO Slave			
Pin	Default	FE Sampling FE Output	FE Sampling RE Output	RE Sampling FE Output	RE Sampling RE Output
MTDO	Pull-up	0	0	1	1
GPIO5	Pull-up	0	1	0	1

Real model:

Footprint:

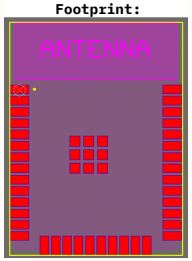

[v06 VALIDATION NOTE]

Footprint is adequate, no soldering errors found. SPI, I2C, UART and USB-to-serial work as expected. Programming circuit works and we can upload programs after cutting some tracks (see validation note on the right). Buttons are read correctly. ADC1 can register analog signals correctly.

Following the [ESP32-WROOM-32D datasheet, page 9] GPIO6 to GPIO11 (pins 17 to 22) will remain floating as they are connected to the integrated SPI flash memory and its usage is not recommended for other uses.

Although not recommended, GPIO6 and GPIO8 are used for a very basic task: reading plug switches.

[v06 VALIDATION NOTE]

The jack connector switches interfere with the SPI flash during programming resulting in a programming error. A different circuit (which doesn't pull up these pins) would be needed. As a temporary solution, both EXP_SW and HX_SW tracks were cut in the PCB.

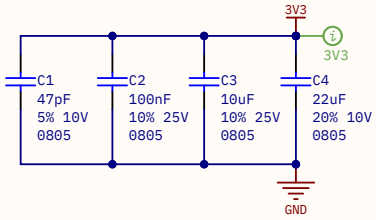

Recommended bucket/bypass capacitors are 0.1 µF and 10 µF, ceramic, low ESR. Should be placed close to the chip and with short return paths. [ESP32-WROOM-32D datasheet, page 21]

Added one extra MLC 22 µF electrolytic cap to filter current spikes during ESP32 RF usage and a small 47pF capacitor to be more effective filtering high frequencies

ESP32-WROOM-32D MCU, Wi-Fi + Bluetooth module

This module integrates an ESP32-D0WD chip, a 240 MHz, dual-core processor with Wi-Fi and Bluetooth capabilities.
This sheet describes its hardware configuration and I/O pins

Designer's signature

Supervisor's signature

Sheet title: **ESP32-WROOM-32D MCU**

Project title: **TIK_HandheldDevice.PrjPcb**

Desginer: **Juan Del Pino Mena**

Date: **2022-07-29** Revision: **0.6** Sheet 6 of 21

Supervisor:
Sr. Andrés Roldán Aranda
Dpto. Electrónica y Tecnología de Computadores
University of Granada
C/ Fuente Nueva, s/n, 18001
Granada, Granada, Spain

3.3 V rail: main system power

Typical Application Circuit. [AP3429/A datasheet, page 2]
with some values modified as needed and/or part availability.
Capacitors should be placed close to the chip and circuit should be traced in short loops.

Feedback voltage V_FB is regulated at 0.6 V.

Resistors are adjusted as a voltage divider. So, if 3.3V are needed at the converter output:

V_FB = 0.6V = V_out · (R2)/(R1+R2)
Thus, R2 = 2/9·R1

Resistor values must be high (kOhms) in order to maintain a low power consumption on the feedback circuit.

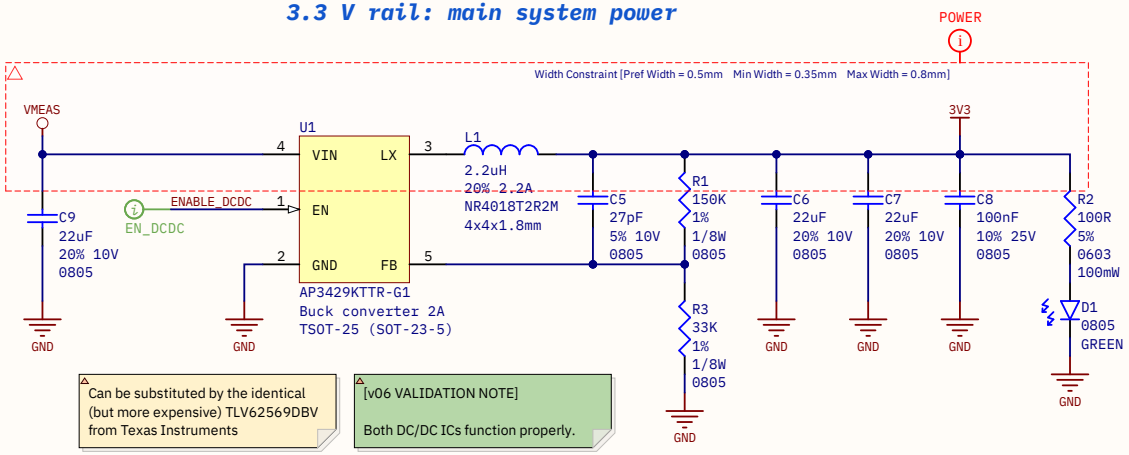

Can be substituted by the identical (but more expensive) TLV62569DBV from Texas Instruments

[v06 VALIDATION NOTE]

Both DC/DC ICs function properly.

Real model:

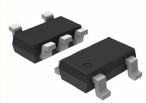

Footprint:

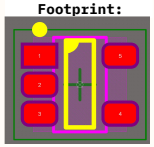

1.8 V rail: Vbias for signal conditioning circuit

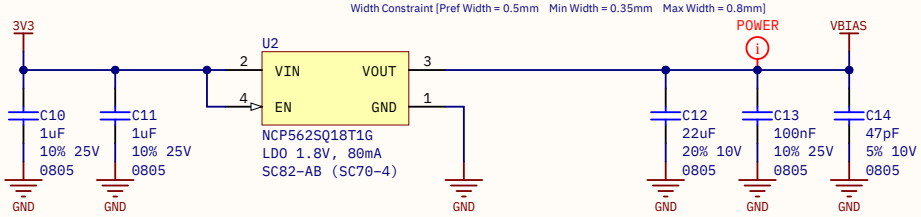

Usage of multiple input capacitors to reduce ESR and ESL. Recommended Cin is 1 uF. There are no recommended values for Cout but these 3 caps should probe more than enough for low ESR and ripple reduction at a wide frequency range. Datasheet specifies a typical 100 uVrms noise on Vout, somewhat high.

Real model:

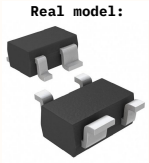

Footprint:

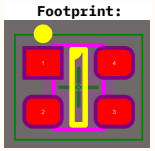

[v06 VALIDATION NOTE]

The LDO works as expected.

Optional 1V8 rail bypass jumpers

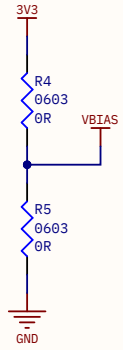

IMPORTANT:
1V8 rail is bypassable by soldering these optional 0-OHM resistors. This is for experimenting with different voltages and if it affects the overall performance of the adquisition circuit.

Do NOT connect both 0R resistors at the same time or it will jump VCC and GND. And keep the LDO disabled at all times.

This can also be used to insert a voltage divider. i.e.: if you want to reduce the rail voltage to VCC/2 you only have to add two >= 10 KOhm 0603 resistors. Just keep in mind that voltage won't be as stable as in a LDO as it will be greatly dependent on the load impedance.

If you do this, populate the LDO's output caps, so VBIAS it behaves as a small-signal GND.

Power rails

Battery DC/DC step-down converter and Vbias for signal conditioning circuit. 3V3 is the main system power and can deliver upto 2 amps. VBIAS is only for polarization of the probes and won't drag much current.

Designer's signature

Supervisor's signature

Sheet title:	**Power rails**		
Project title:	**TIK_HandheldDevice.PrjPcb**		
Desginer:	**Juan Del Pino Mena**		
Date: **2022-07-29**	Revision: **0.6**	Sheet 7 of 21	

Supervisor:
Sr. Andrés Roldán Aranda
Dpto. Electrónica y Tecnología de Computadores
University of Granada
C/ Fuente Nueva, s/n, 18001
Granada, Granada, Spain

Battery output current sense and voltage monitor. Charger selection jumper. Battery thermistor

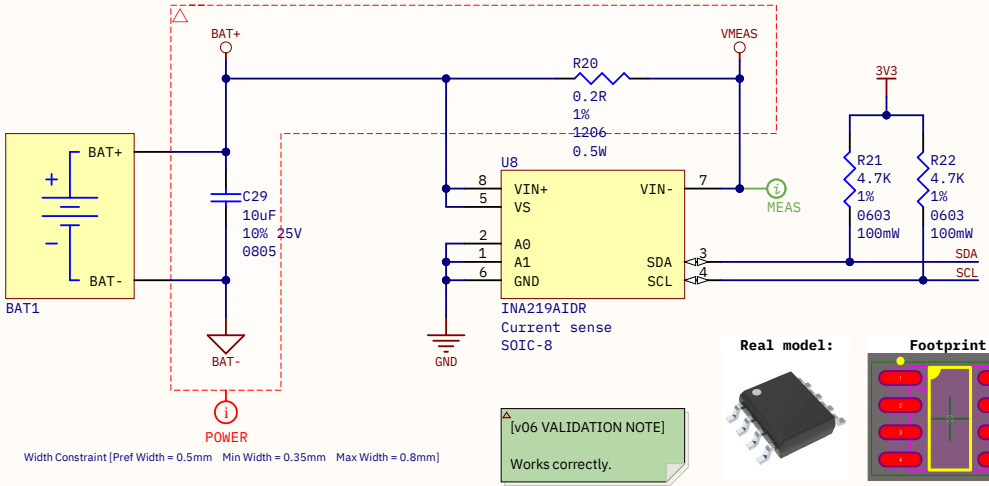

[v06 VALIDATION NOTE]

Works correctly.

Real model:

Footprint:

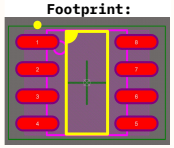

I2C bus termination resistors

Device's I2C address: 100000 (0x20) [INA219 datasheet, page 10, table 2]

All the current that passes by the battery also goes through the current sense resistor. When it's positive means that the battery is discharging and when it's negative means that it's charging. INA219 also reports the battery voltage.

This way we can monitor via software the energy the battery receives and supplies, building a BMS (Battery Monitoring System)

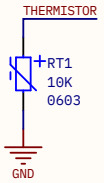

Battery NTC Thermistor, shared by both chargers. If not integrated onto the battery itselt (third cable), short the pads.

[v06 VALIDATION NOTE]

Unverified as our battery does not has an NTC.

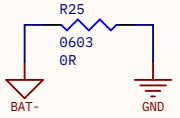

IMPORTANT: jumper for charger selection.

The battery connector is shared by the two possible chargers. However, on the Lithium charger BAT- is NOT connected to the system's global GND; but in the NiMH charger it is.

So, jump these pads ONLY IF USING THE NiMH charger.

Battery charging circuit variants

Two circuit variants are implemented BUT NOT USED SIMULTENEOSLY. Only one must be populated at a time.

The usage of one over the other will come by component disponibility.

[v06 VALIDATION NOTE]

The Lithium charger works fine for Li-Po batteries. Sometimes the protection circuit trips when using an external power supply. A workaround is lowering the voltage below 3 V and raising it again slowly until it powers on again. The Ni-MH charger remains untested.

CHARGER VARIANT #1: NiMH
battery_charger_Ni_MH
Charger to populate if battery chemistry is Nickel-Metal Hydride

CHARGER VARIANT #2: Li-Ion
battery_charger_Li-Ion
Charger to populate if battery chemistry is Lithium-Ion or Lithium-Polymer

Charging status indicator

These signals come from both charging IC's.

They are status outputs that are normally on high impedance and they are pulled LOW when activated.

We can use these pins to turn on some LEDs and to notify the microcontroller of the charging status.

[v06 VALIDATION NOTE]

They do not light properly, probably due to a soldering problem. Revision pending.

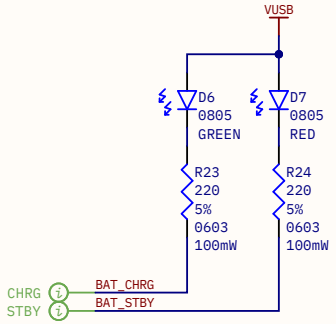

Battery and current sense

Two circuit variants that will be implemented but not used simultaneously. The usage of one over the other will come by component disponibility. INA219 current sensor is independent and common for both systems.

Designer's signature

Supervisor's signature

Sheet title:	**Battery and current sense**		
Project title:	**TIK_HandheldDevice.PrjPcb**		
Desginer:	**Juan Del Pino Mena**		
Date: **2022-07-29**	Revision: **0.6**	Sheet 8 of 21	

Supervisor:
Sr. Andrés Roldán Aranda
Dpto. Electrónica y Tecnología de Computadores
University of Granada
C/ Fuente Nueva, s/n, 18001
Granada, Granada, Spain

NiMH/NiCd battery charger IC

[v06 VALIDATION NOTE]

NOT POPULATED AND UNTESTED.

We can control the charging by pulling LOW the SHTD. This pin is normally pulled up (shutdown disabled).

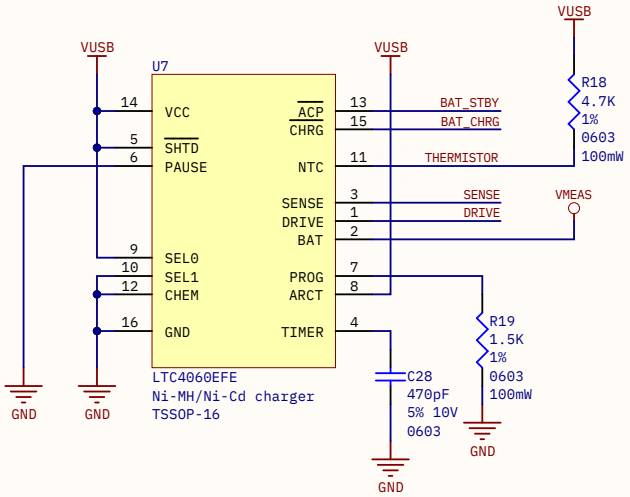

Following the [LTC4060 datasheet, page 13], if using a 10 K NTC thermistor, Its RHOT should be 4.42 kOhm, 1% to trigger the temperature warning at 45 ºC.
However, this value being too much specific is problematic.

This can be disabled by connecting a 0-ohm resistor in place of the thermistor.

[CURRENTLY NOT IMPLEMENTED] This IC can do power path control. This is, to power the load from external source while charging the battery.

Real model:

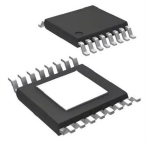

Footprint:

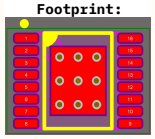

TIMER capacitor and PROG resistor program the charge Tmax (maximum charging time, a security measure). [LTC4060 datasheet, page 13]. These values should complete a full charge in at most 1 h 6'

These parameters are heavity dependant of battery capacity. A larger battery cell package should receive more time / current.

PROG resistor programs the maximum current that the battery will receive while charging. For 1.5 kOhm this is 0.93 A.

i.e.: a 1000 mAh battery will charge at approx 1C with this configuration, but can be insufficient time for a 3000 mAh one.

External PNP BJT current driver

Width Constraint [Pref Width = 0.5mm Min Width = 0.35mm Max Width = 0.8mm]

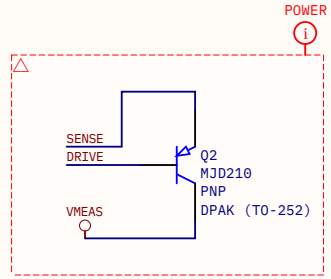

DRIVE pin on the LTC4060 provides a controlled sink current that drives the PNP base.
So, it's not necessary to have a base resistor.

Real model:

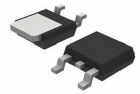

Footprint:

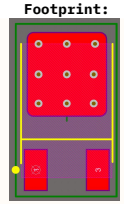

Battery charging circuitry for Ni-MH

Battery charger circuit variant #1. By default the device uses a Nickel-metal hydride battery which are chemically and thermally more stable (and safer) than Lithium-based ones; at the cost of a lower charge/volume ratio.

Designer's signature

Supervisor's signature

Sheet title: **Battery charger**			
Project title: **TIK_HandheldDevice.PrjPcb**			
Desginer: **Juan Del Pino Mena**			
Date: **2022-07-29**	Revision: **0.6**	Sheet 9 of 21	

Supervisor:
Sr. Andrés Roldán Aranda
Dpto. Electrónica y Tecnología de Computadores
University of Granada
C/ Fuente Nueva, s/n, 18001
Granada, Granada, Spain

Lithium battery charger IC

The TP4056 datasheet recommends to connect a resistor of 0.2 to 0.5 Ohm between VUSB and its VCC pin. It does not explain why, but probably for chip temperature concerns.

However, it is omitted as we don't have any resistor of these values available. As a note: not a single commercial TP4056 charger module uses any resistor at all (and they work fine at higher charge rates).

The TP4056 is only specified for charging single-cell Li-Ion batteries on its datasheet. However, many sites, forums and online stores list TP4056-based modules as compatible with both Li-Ion and Li-Po given the chemistry similatiry. Take this with caution.

Resistor in PROG regulates the maximum battery charging current. At 2 kOhm, this is 580 mA. At 1 kOhm, it is > 1 A. Change according to battery capacity. [TP4056 english datasheet, page 3]

TEMP expects a NTC thermistor (of unspecified value). On some Lithium-Ion batteries this NTC can be integrated on the package.

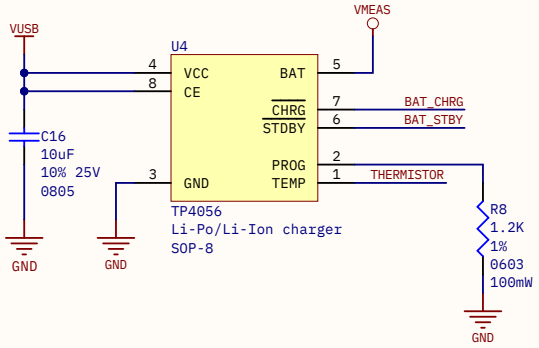

Real model:

Footprint:

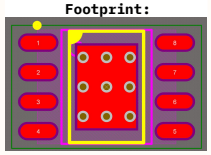

This device will get hot, and has a thermal pad to dissipate to PCB GND plane

Lithium battery protection

Width Constraint [Pref Width = 0.5mm Min Width = 0.35mm Max Width = 0.8mm]

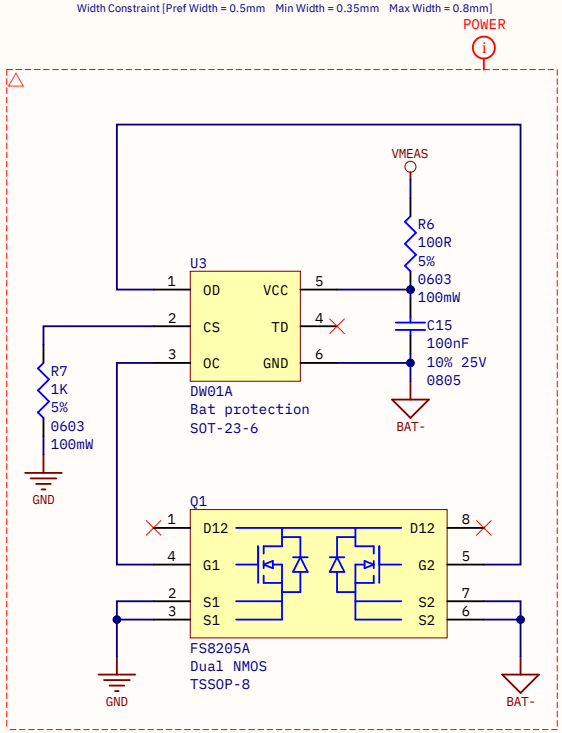

Real model:

Footprint:

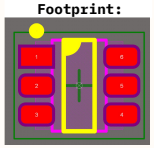

[v06 VALIDATION NOTE]

This charger works correctly and protection circuit trips under 2.8-3 V. Tested using a single-cell lithium-polymer battery.

Real model:

Footprint:

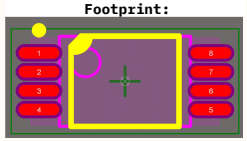

Battery charging circuitry for Li-Po & Li-Ion

Battery charger circuit variant #2. Li-Ion and Li-Po batteries offer much more power density at the cost of inestability. This circuit must NOT be placed if the Ni-MH charger is present on the board (and vice-versa).

Designer's signature

Supervisor's signature

Sheet title:	**Battery charger**
Project title:	**TIK_HandheldDevice.PrjPcb**
Desginer:	**Juan Del Pino Mena**
Date:	**2022-07-29**
Revision:	**0.6**
Sheet	10 of 21

Supervisor:
Sr. Andrés Roldán Aranda
Dpto. Electrónica y Tecnología de Computadores
University of Granada
C/ Fuente Nueva, s/n, 18001
Granada, Granada, Spain

'SH' pads are the USB connector metal shield, which is structural. This particular connector has 4 which are not connected to any circuit traces, not even GND. In any case, it should be connected to the device's metal chassy (as a faraday cage).

An USB-Mini-B has been chosen for various reasons:
- Over an USB-micro: because of the structural robustness of the mini-B.
- Over an USB-Type-C: because of the ease of implementation, less pins, and to make clear this device is not a host.

Real model:

Footprint:

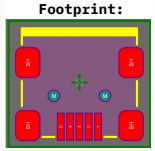

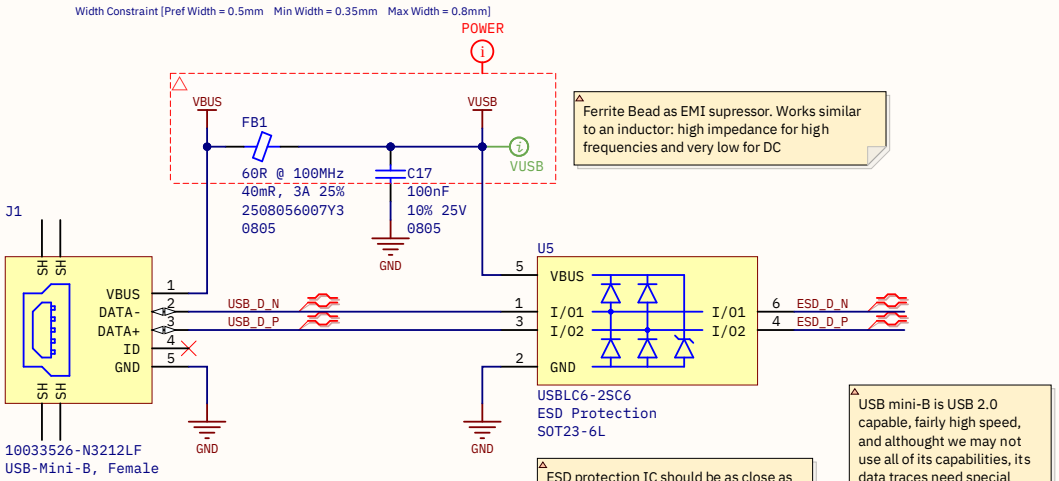

Ferrite Bead as EMI supressor. Works similar to an inductor: high impedance for high frequencies and very low for DC

ESD protection IC should be as close as possible to the USB connector to avoid damaging any other circuits.

USB mini-B is USB 2.0 capable, fairly high speed, and althought we may not use all of its capabilities, its data traces need special attention as they are differential.

[v06 VALIDATION NOTE]

The selected USB-mimi-B port is very stiff and has a good quality of construction, however one must be cautious while soldering as its plastic can melt resulting in an unusable connector.

Real model:

Footprint:

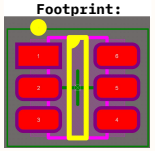

USB connector and ESD protection circuit

USB is used as a programming interface, as well as a power source for the charging circuit. Since it's an external connector, it needs to have a protection circuit against electro-static discharge (ESD) and noise.

Designer's signature

Supervisor's signature

Sheet title:	**USB connector and ESD protection circuit**		
Project title:	**TIK_HandheldDevice.PrjPcb**		
Desginer:	**Juan Del Pino Mena**		
Date: **2022-07-29**	Revision: **0.6**	Sheet 11 of 21	

Supervisor:
Sr. Andrés Roldán Aranda
Dpto. Electrónica y Tecnología de Computadores
University of Granada
C/ Fuente Nueva, s/n, 18001
Granada, Granada, Spain

USB to UART conversion

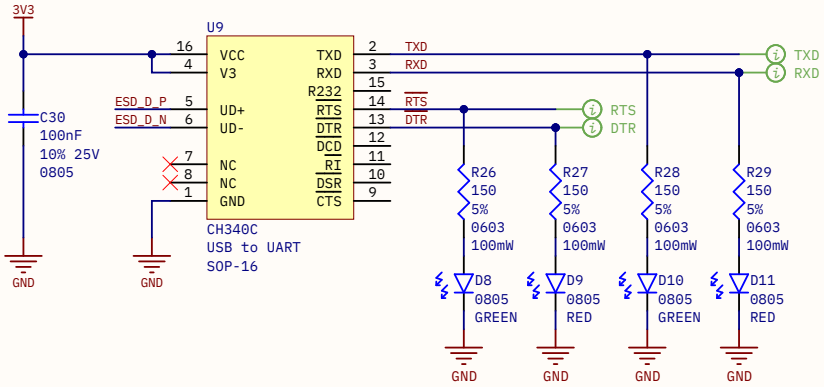

Real model:

Footprint:

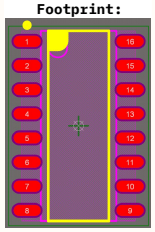

These LEDs serve as a visual testimonie of UART communication and help during debugging.

If they drag too much current they can be used with 1 kΩ resistors or be completely disconnected.

Should not be present on a commercial product.

[v06 VALIDATION NOTE]

This IC works correctly. However, debug LEDs are both not very visible (they blink fast for short times) and not very useful (sometimes redundant), so they can be removed.

Auto programming circuit

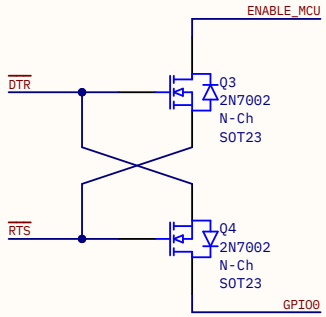

Real model:

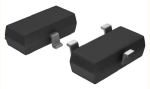

Footprint:

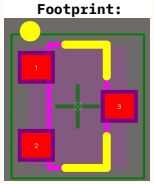

ESP32 GPIO0 is a Strapping pin. Strappin g pins modify the device's boot mode during chip reset. GPIO0 is pulled up during reset by default. ENABLE_MCU is pulled up by an external pullup resistor

When GPIO0 is HIGH, it boots from internal SPI memory, but when it's LOW the boot sequence changes to 'Download' and we can upload a program to the MCU.

[ESP32 Datasheet, section 2.4, pages 19-20]

Circuit truth table

DTR	RTS	ENABLE_MCU	GPIO0
0	0	1	1
0	1	1	0
1	0	0	1
1	1	1	1

*(DTR, RTS active low)

[v06 VALIDATION NOTE]

This circuit works correcly, the programming signaling sequence (RESET to Low, then GPIO0 to low) is correct and we can program the MCU.

USB to UART and MCU programming

This circuit allows a computer to the ESP32 via USB so it can be reprogrammed. This is possible by sending RTS and DTR signals with a determined timing so the device enters an alternative boot mode.

Designer's signature

Supervisor's signature

Sheet title:	**USB to UART and MCU programming**
Project title:	**TIK_HandheldDevice.PrjPcb**
Desginer:	**Juan Del Pino Mena**
Date:	**2022-07-29**
Revision:	**0.6**
Sheet	12 of 21

Supervisor:
Sr. Andrés Roldán Aranda
Dpto. Electrónica y Tecnología de Computadores
University of Granada
C/ Fuente Nueva, s/n, 18001
Granada, Granada, Spain

Reset

To ensure power stability to the microcontroller during powerup, this RC filter introduces a delay on the ENABLE pin. Usual values are 10 kΩ, 1 µF (τ = 10 ms, t_{10-90} = 22 ms).
[ESP32-WROOM-32D datasheet, page 22]

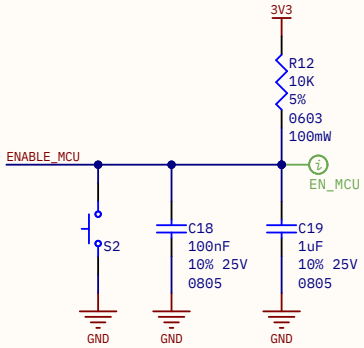

Boot mode selection (debug)

Allows to force 'Download' boot sequence

Same design as in ESP32 DevKit boards.
100 nF cap are for debouncing and should be placed close to the buttons

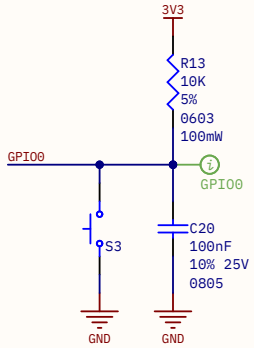

[V06 VALIDATION NOTE]

These buttons function properly.

POWERUP BUTTON
powerup_button
Power-up button circuitry for enabling the DCDC buck converter

Multidirection 'thumb' button (UI navigation)

Horizontal SMD device, multi-directional / muti-function rotary slider button. Accessed from the right side.

[V06 VALIDATION NOTE]

The 'thumb' button functions properly.

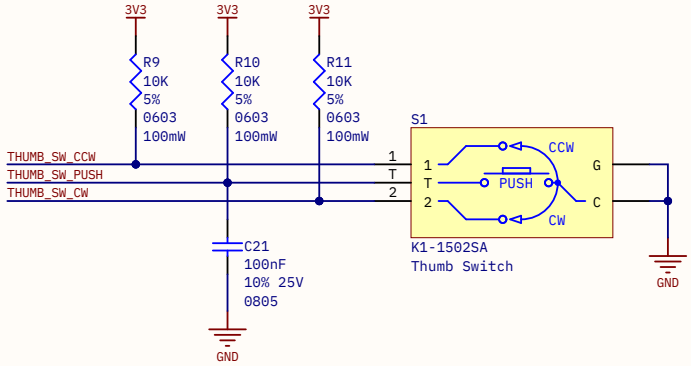

Real model:

Footprint:

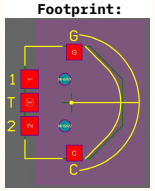

Buttons

TIK buttons. Some of them are meant for debugging like boot mode selection and reset, and will not be accesible to the end user. The power-up button and the "thumb" button are meant to be part of the UI.

Designer's signature	Sheet title: **Buttons**		
Supervisor's signature	Project title: **TIK_HandheldDevice.PrjPcb**		
	Desginer: **Juan Del Pino Mena**		
	Date: **2022-07-29**	Revision: **0.6**	Sheet 13 of 21

Supervisor:
Sr. Andrés Roldán Aranda
Dpto. Electrónica y Tecnología de Computadores
University of Granada
C/ Fuente Nueva, s/n, 18001
Granada, Granada, Spain

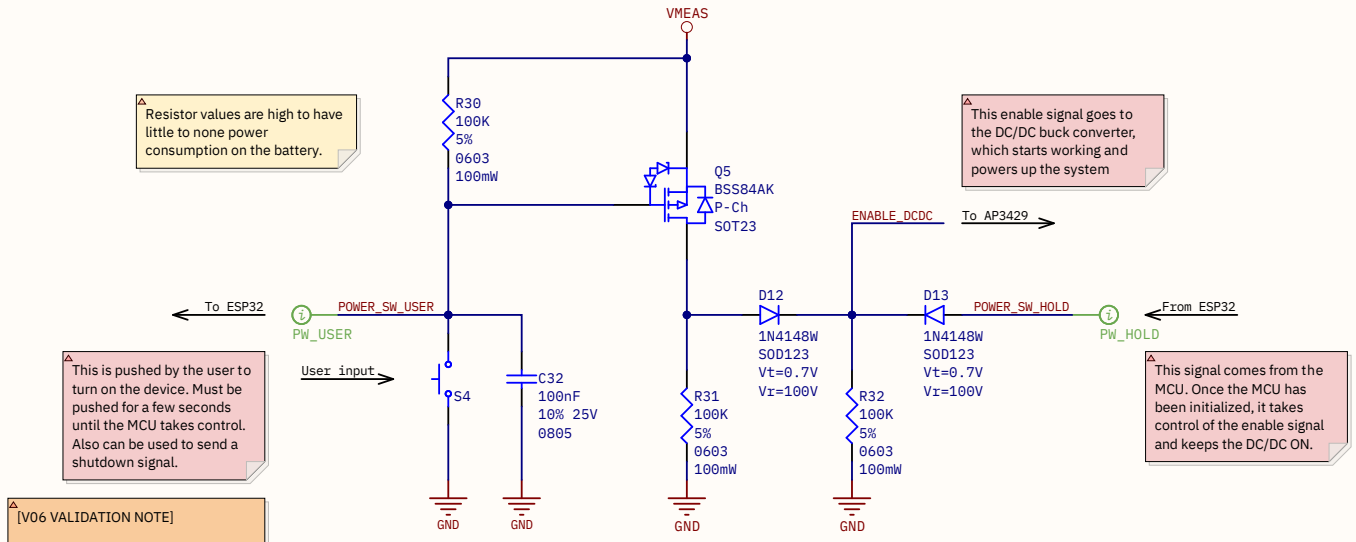

Resistor values are high to have little to none power consumption on the battery.

This enable signal goes to the DC/DC buck converter, which starts working and powers up the system

This is pushed by the user to turn on the device. Must be pushed for a few seconds until the MCU takes control. Also can be used to send a shutdown signal.

This signal comes from the MCU. Once the MCU has been initialized, it takes control of the enable signal and keeps the DC/DC ON.

[V06 VALIDATION NOTE]

In our tests, the node which this switch connects to exhibits a strong pull-down behaviour, son the PMOS is always active and so it prevents the system from turning off.

The most likely cause seems to be the microcontroller, which either pin has a non-high-impedance during startup that pulls-down the node; or it forces a certain voltage to its output.

In a later design, it should be tested on another pin.

When the button is not pressed, the tension in PMOS gate is BAT+; and thus V_sg is not greater than V_th and the PMOS is off.

When the button is pressed, gate voltage is GND, so V_sg > V_th and the PMOS turns on, letting the voltage rise on the diode anode and putting HIGH the ENABLE_DCDC net (enabling the DCDC converter).

This turns on the system and feeds the ESP32 (continues →)

The microcontroller boots over after the button has been pressed for a few seconds and pulls HIGH the POWER_SW_HOLD pin. The user can release the poweron button now.

The system will be on until the user sends a shutdown signal by software or by pressing this button again.

In this moment, the ESP32 will save all data and gets ready for shutdown. As last step, it pulls down POWER_SW_HOLD and the system powers off completely.

Powerup button

This circuit avoids using a power-up switch, which can shutdown the device without prior warning. The user pushes a button during a couple of seconds, in which the ESP32 will boot and keep the system on until a shutdown signal is sent.

Designer's signature

Supervisor's signature

Sheet title:	**Powerup button**
Project title:	**TIK_HandheldDevice.PrjPcb**
Desginer:	**Juan Del Pino Mena**
Date:	**2022-07-29**
Revision:	**0.6**
Sheet	14 of 21

Supervisor:
Sr. Andrés Roldán Aranda
Dpto. Electrónica y Tecnología de Computadores
University of Granada
C/ Fuente Nueva, s/n, 18001
Granada, Granada, Spain

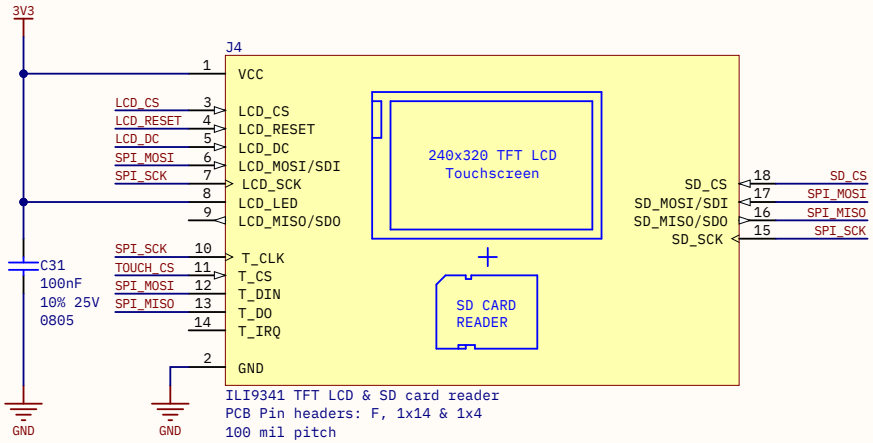

[v06 VALIDATION NOTE]

Screen and touch works with no problems.

Real model:

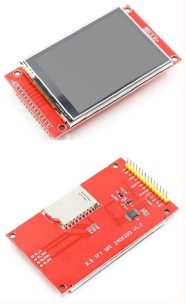

Footprint:

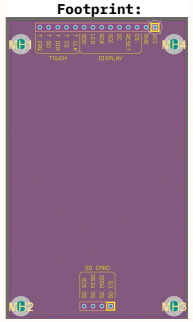

As ILI9341 2.8" TFT LCD module has the bigger footprint and needs mechanincal support. Our PCB inherits its mounting holes position.

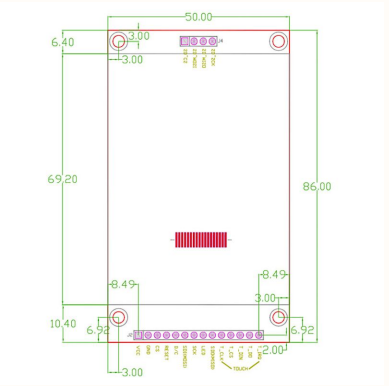

(Measures in mm)

LCD TFT touchscreen & SD card reader

TIK uses an ILI9341 2.8" TFT LCD display module as a graphic user interface. This module has touchscreen capabilities and also integrates a SD card reader on one of its sides. All three elements are managed via SPI.

Designer's signature

Supervisor's signature

Sheet title:	**LCD TFT touchscreen & SD card reader**		
Project title:	**TIK_HandheldDevice.PrjPcb**		
Desginer:	**Juan Del Pino Mena**		
Date: **2022-07-29**	Revision: **0.6**	Sheet 15 of 21	

Supervisor:
Sr. Andrés Roldán Aranda
Dpto. Electrónica y Tecnología de Computadores
University of Granada
C/ Fuente Nueva, s/n, 18001
Granada, Granada, Spain

SIGNAL_CONDITIONING_SIMULATIONS
signal_conditioning_sims1

signal_conditioning_sims2
Results of simulating the adequation circuit with SPICE and realistic input waveforms

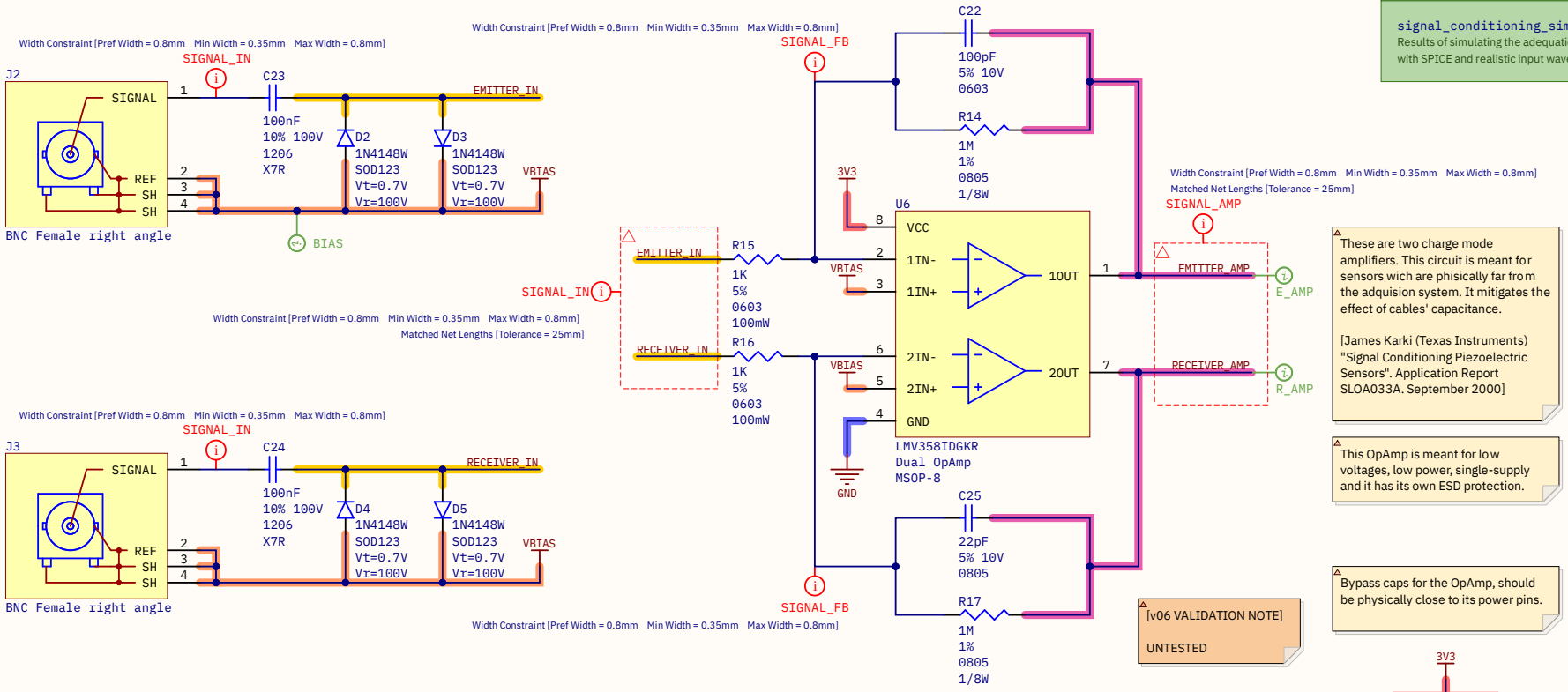

These are two charge mode amplifiers. This circuit is meant for sensors wich are phisically far from the adquision system. It mitigates the effect of cables' capacitance.

[James Karki (Texas Instruments) "Signal Conditioning Piezoelectric Sensors". Application Report SLOA033A. September 2000]

This OpAmp is meant for low voltages, low power, single-supply and it has its own ESD protection.

Bypass caps for the OpAmp, should be physically close to its power pins.

[v06 VALIDATION NOTE]

UNTESTED

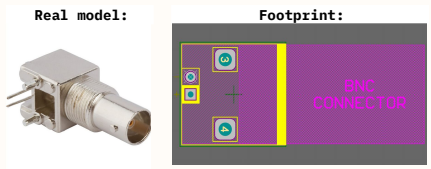

Emitter signal will be in the range of 15 V to 100 V and need to be clipped by the diodes. Then, the OpAmp will amplificate to saturation so the emitter can be perceived by the instrument as a flank; whereas the receiver signal will most likely be amplified without any clipping.

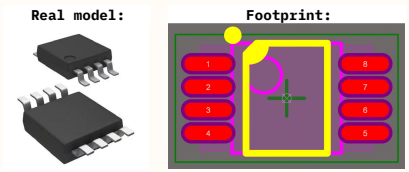

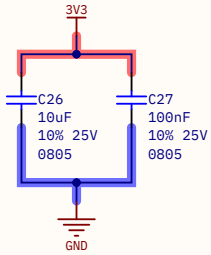

Piezoelectric sensors conditioning circuit

Two analog signals come from two piezoelectric sensors nailed into a tree or trunk. The way piezos work force us to use this circuit to convert charge into voltage. The piezo sensors used generated upto -100 V peak, so it needs clipping

Designer's signature

Supervisor's signature

Sheet title:	**Piezoelectric sensors conditioning circuit**
Project title:	**TIK_HandheldDevice.PrjPcb**
Desginer:	**Juan Del Pino Mena**
Date:	**2022-07-29**
Revision:	**0.6**
Sheet	16 of 21

Supervisor:
Sr. Andrés Roldán Aranda
Dpto. Electrónica y Tecnología de Computadores
University of Granada
C/ Fuente Nueva, s/n, 18001
Granada, Granada, Spain

Trunk signal's Voltage Spectral Density

Example VSD of a generic trunk signal captured by the Piezoelectric sensors using an oscilloscope

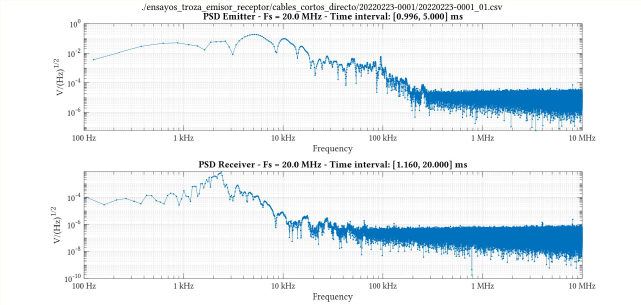

Analyzed frequecy characteristic of Fakkop's piezoelectric sensors

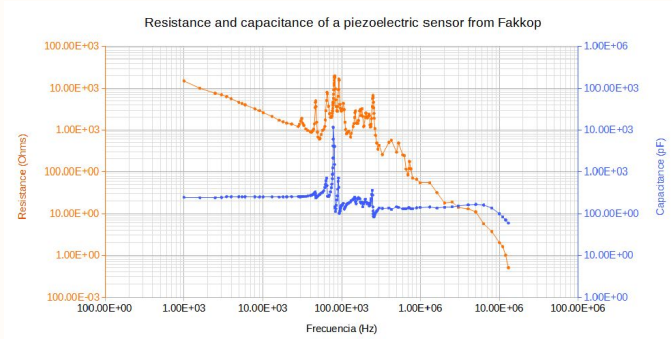

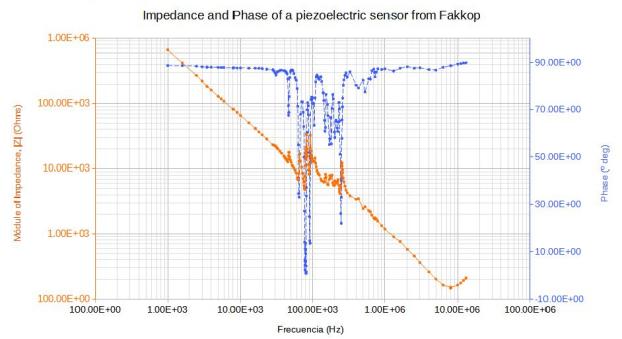

Circuit to simulate

Circuit from a subproject inside ./SIMULATIONS

[TOPOLOGY DOES NOT CHANGE, BUT COMPONENT VALUES MAY NOT BE UP TO DATE]

A piezoelectric is commonly modeled as a charge source in parallel with a resistor and a capacitor (charge model). This, however, is not practical for simulated analysis. Instead, we resorted to the voltage model, which is a voltage source in series with a resistor and a capacitor in parallel.

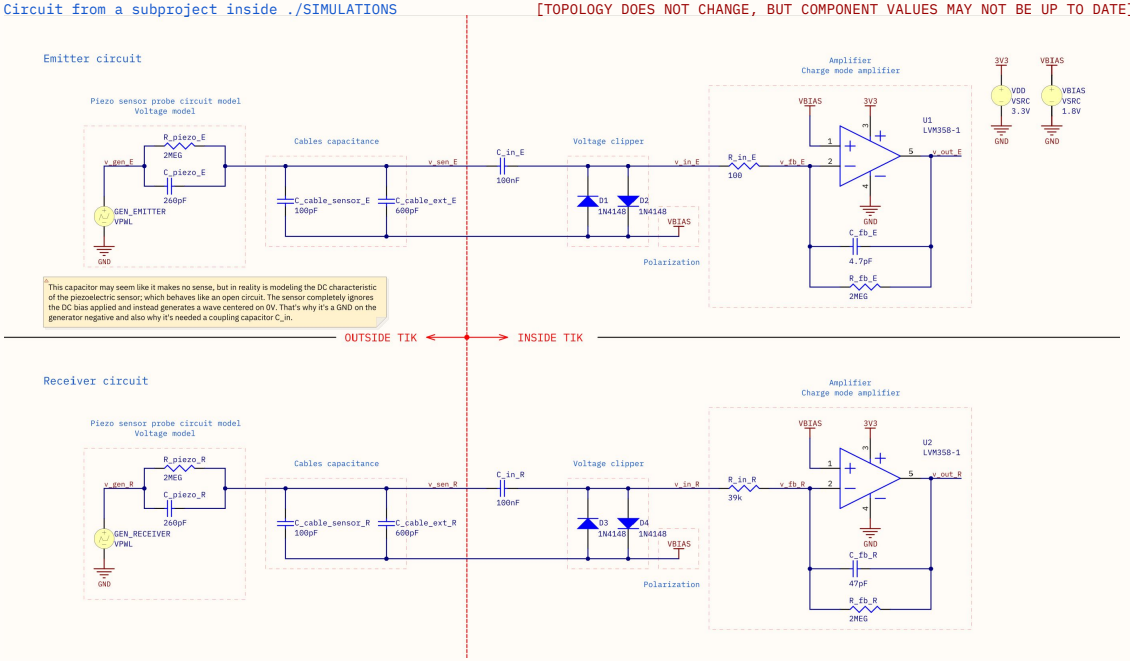

Nevertheless, in empirical analysis we found that our probes are far more complex than this simple model: They behave like an open circuit for DC (thus ignoring VBIAS). They have a great resistance and capacitance dependency on frequency, and a resonance around 100 kHz.

This is the reason behind the 100nF bypass capacitor. It allows us to center the input signals in the VBIAS DC voltage for our single-supply system. These caps should be rated for at least 50 V, as will have to stand a big voltage peak on their extremes.

Signal conditioning circuit simulations

SPICE simulations of the adequation circuit. These are only the results. You can find the simulation circuit and models on the ./SIMULATIONS/ folder inside this project.

Designer's signature

Supervisor's signature

Sheet title:	**Signal conditioning simulations. 1 of 2**		
Project title:	**TIK_HandheldDevice.PrjPcb**		
Desginer:	**Juan Del Pino Mena**		
Date: **2022-07-29**	Revision: **0.6**	Sheet 17 of 21	

Supervisor:
Sr. Andrés Roldán Aranda
Dpto. Electrónica y Tecnología de Computadores
University of Granada
C/ Fuente Nueva, s/n, 18001
Granada, Granada, Spain

Expected frequency response

Emitter adequation circuit

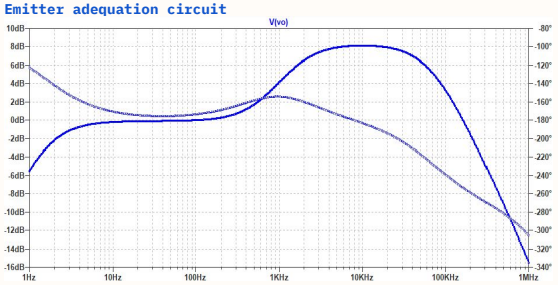

Receiver adequation circuit

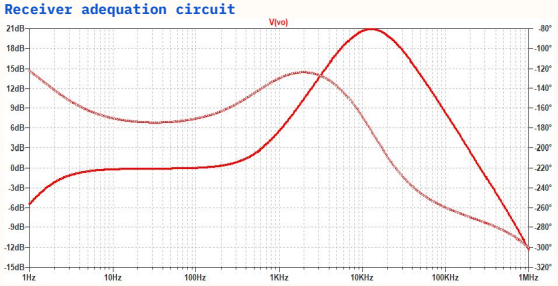

The adequation circuit for the emitter has more gain that it needs, so the output of the OpAmp is saturated.
This gives us a very step flank where the signal clearly begins and it's very easy to identify.
In this simulation it's clear that maybe it's not needed so much gain as the output is very noisy and could be easily false-triggered.

Expected transient behavior

Emitter

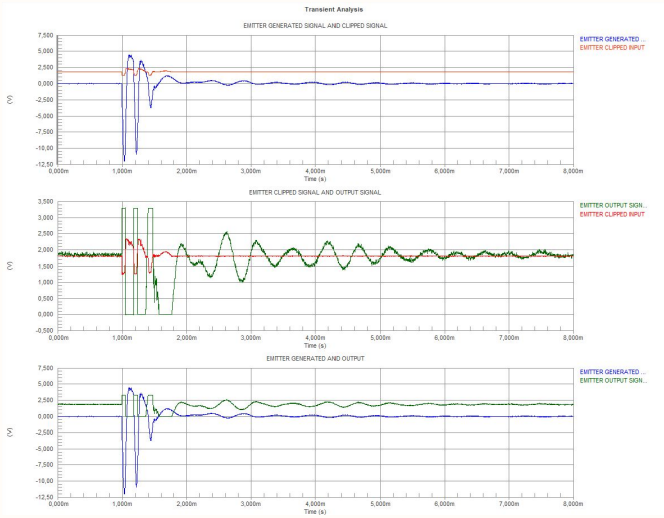

The emitter input signal can be of 10 to 20 V if the piezoelectric probe is hitted softly and over 100 V if hammered hard. This voltage can damage electronics. As a countermeasure we use two 4148 diodes on the input that clip the signal to ±0.7 volts around VBIAS, allowing us to manipulate it without risk.

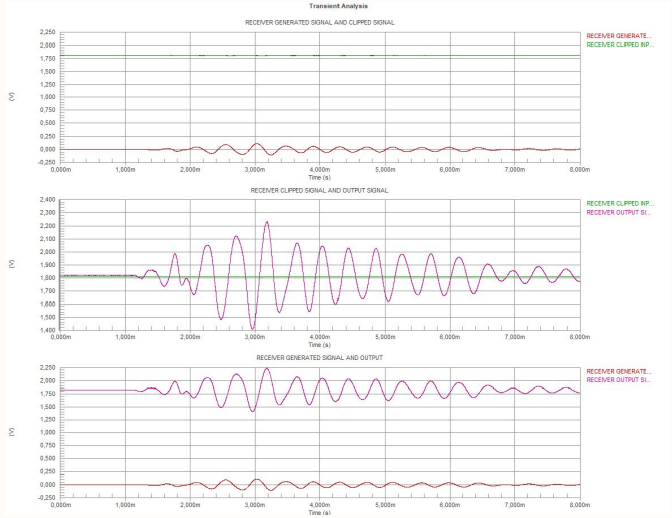

The receiver on the other hand has a very weak signal that needs to be amplified and centered over 1.8V.
We have to be more cautious in this case so we don't distort it as we have to sample and process it with precision.

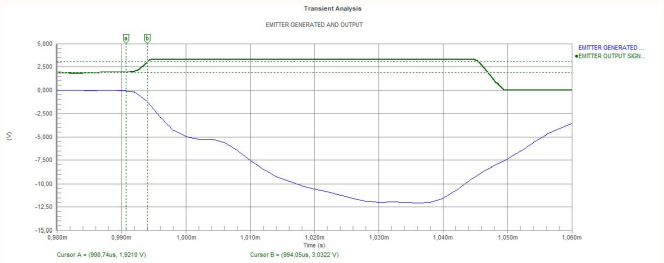

Zoom over the first pulse. The expected rise time will be around 3 us, so the delay is of 1 TO 2 samples (Fs = 500 kHz)

Signal conditioning circuit simulations

SPICE simulations of the adequation circuit. These are only the results. You can find the simulation circuit and models on the ./SIMULATIONS/ folder inside this project.

Designer's signature	Sheet title: **Signal conditioning simulations. 2 of 2**		
	Project title: **TIK_HandheldDevice.PrjPcb**		
Supervisor's signature	Desginer: **Juan Del Pino Mena**		
	Date: **2022-07-29**	Revision: **0.6**	Sheet 18 of 21

Supervisor:
Sr. Andrés Roldán Aranda
Dpto. Electrónica y Tecnología de Computadores
University of Granada
C/ Fuente Nueva, s/n, 18001
Granada, Granada, Spain

Current limiter and ESD protection

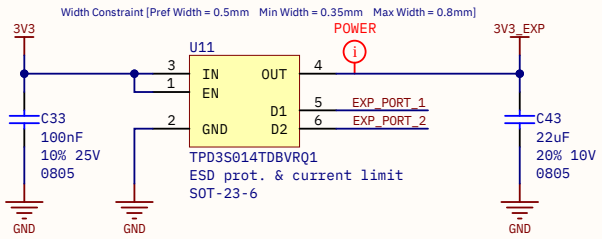

Since this is an external connector directly connected to the 3V3 rail, this will have a current limit switch and ESD protection IC to avoid damaging the device.

Expansion port connector

Expansion port pins are both Input/Output and are connected to the ADC1 so we give the maximum amount of functionality available to the expansion module.

Plug detection switch circuitry operation: The switch is normally closed. So, normally EXP_SW is HIGH. When plugged in, the switch opens and EXP_SW will be LOW

[v06 VALIDATION NOTE]

UNTESTED

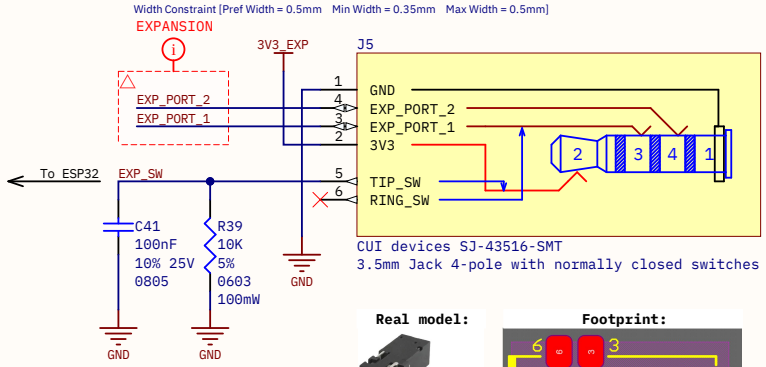

Real model:

Footprint:

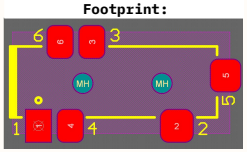

3.5mm jack connector considerations

We are using the 3.5mm jack connector in a non-standard application, as we are not transferring audio but power and/or analog and digital signals of different nature.

Nevertheless, we have adjusted the connector to somewhat fit the OMPT convention (GND in sleeve, signals in rings).

The mating socket and plug are connected as follows.
In this connector series there is the possibility of upto 6 pads, the additional 2 pads being connected to switches for detecting the plug insertion. We only use the tip switch (pin 5) to allow using both the SJ-43516 as well as the SJ-43515 models. We prefer the 6-pad version as it offers more mechanical integrity.
[CUI Devices SJ-4351X-SMT Datasheet, page 2]

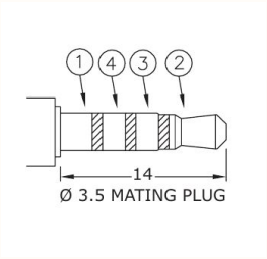

Model No.	SJ-43516-SMT
Schematic	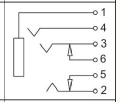
PIN	
1	sleeve
2	tip
3	ring 1
4	ring 2
5	tip switch
6	ring switch

To avoid shorting GND and VCC, the 3V3 rail is located at the tip, so it will make contact the last. This also allows us to easily add the tip switch circuitry.

Expansion port & jack connector

Expansion port for added functionality, such as an ultrasould resonance analysis for wood boards.
Also, this sheet includes a description of the jack connector properties.

Designer's signature

Supervisor's signature

Sheet title:	**Expansion port**		
Project title:	**TIK_HandheldDevice.PrjPcb**		
Desginer:	**Juan Del Pino Mena**		
Date:	**2022-07-29**	Revision: **0.6**	Sheet 19 of 21

Supervisor:
Sr. Andrés Roldán Aranda
Dpto. Electrónica y Tecnología de Computadores
University of Granada
C/ Fuente Nueva, s/n, 18001
Granada, Granada, Spain

HX711 load cell amplifier

This circuit is used to get weight measurements out from load cells in order to estimate the density of a trunk or board.
This design is based on the Sparkfun HX711 module by N. Seidle and A. Wende.

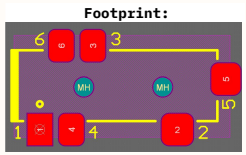

There's no "standard load cell connector". We have selected a 3.5mm jack 4-pole connector and organized the pins in the usual order and with usual colors. Nothe that the shield is unconnected. A more appropiate alternative could be a RJ-11 6-pin connector, but was discarded because of the large socket size.

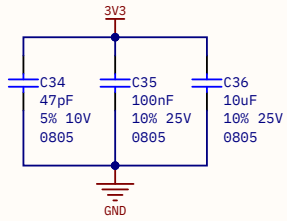

VCC/VDD bypass caps for noise filtering and voltage stabilization for the HX711.

[v06 VALIDATION NOTE]

UNTESTED

Resistors serve as a short circuit protection since A+ and A- are exposed pins and also input impedance. Capacitor prevents noise and rapid change. Signals from load cells are slow.

VBG = VFB is a reference bypass output. It stays fixed at 1.25 V.

AVDD is the analog voltage source with is generated by the HX711's internal regulator with the aid of the PNP BJT.

AVDD = VGB · (R1 + R2) / R1
It should always be less than (VSUP - 100 mV)
[HX711 datasheet, page 4]

In this design:

AVDD = 1.25 V·(22 kΩ+10 kΩ)/20 kΩ = 1.82 V

HX711 will serve 24 bit, 2's complement raw ADC data.
The system needs a software calibration with a known weight for extracting a correction factor for this design.

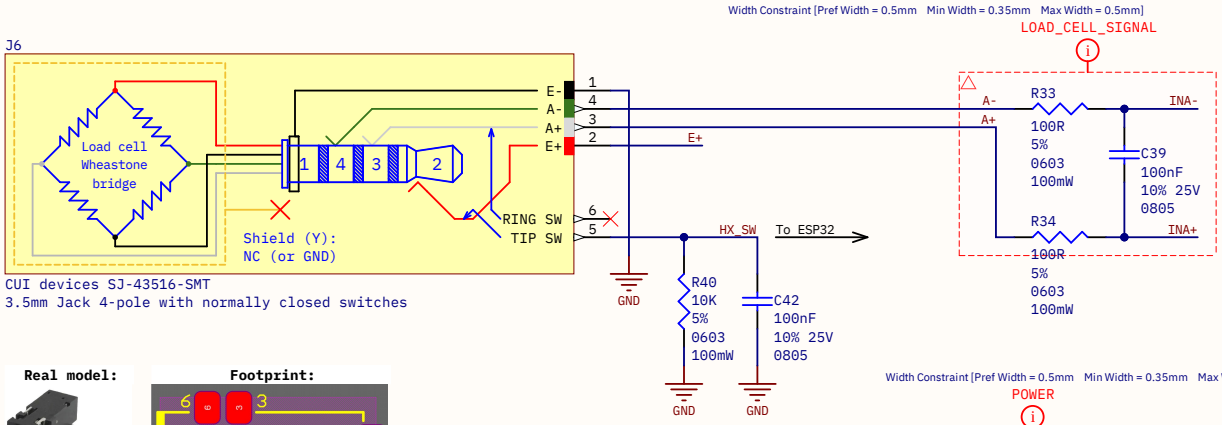

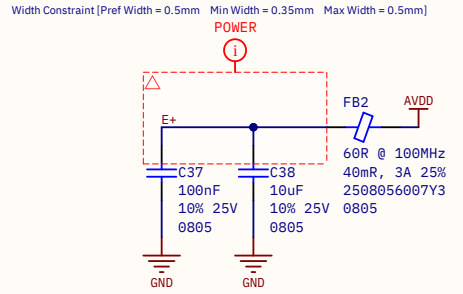

Noise/EMI filtering on AVDD. Sparkfun's design uses a 2.2 uH chip inductor. Instead we use a ferrite bead.

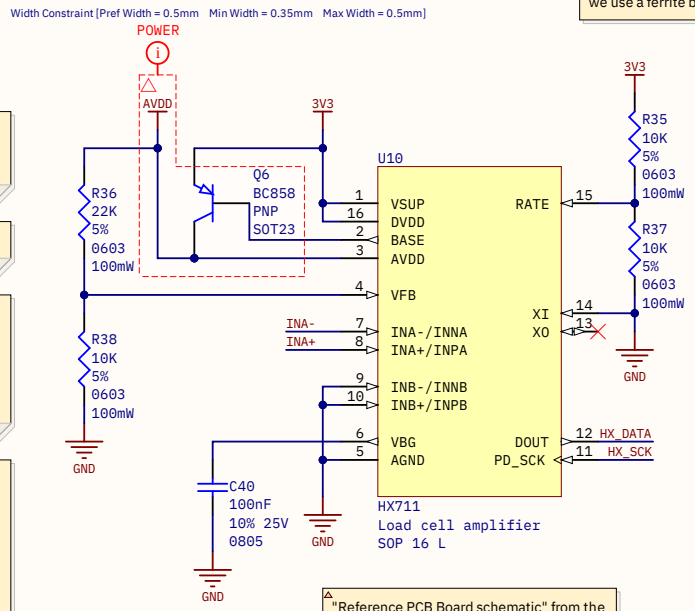

"Reference PCB Board schematic" from the [HX711 Datasheet, figure 4, page 6]

RATE pin config:
- Pulled down: normal mode, 10 Sps
- Pulled up: fast mode, 80 Sps, noisier

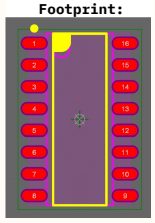

Designer's signature	Sheet title: **HX711 load cell amplifier**		
Supervisor's signature	Project title: **TIK_HandheldDevice.PrjPcb**		
	Desginer: **Juan Del Pino Mena**		
	Date: **2022-07-29**	Revision: **0.6**	Sheet 20 of 21

Supervisor:
Sr. Andrés Roldán Aranda
Dpto. Electrónica y Tecnología de Computadores
University of Granada
C/ Fuente Nueva, s/n, 18001 Granada, Granada, Spain

B

Appendix C

Circuit simulations

This appendix collects the results of circuit simulations that are of interest.

C.1 Reset button and enable delay

This simple simulation reproduces the behavior of the net `ENABLE_MCU` when a programming signal is sent from a PC. The simulated circuit is represented in Figure C.1a. Simulation performed in LTSpice. A comparison with the real, experimental behavior is also included. As we can see in Figure C.1b, the empirical response is considerably faster. This is probably because the simulator completely discharges the capacitor when shorted, while in reality it does not happen immediately, and that is why the voltage recovers so quickly.

On the other hand, Figure C.1 shows the delay when the device is first turned on. As you can see, there is a significant delay of about 23 ms of time from 10 % to 90 %, in line with what we had calculated in Section 5.1.1.7: Reset and boot selection buttons. In this case, there is no experimental signal to compare to.

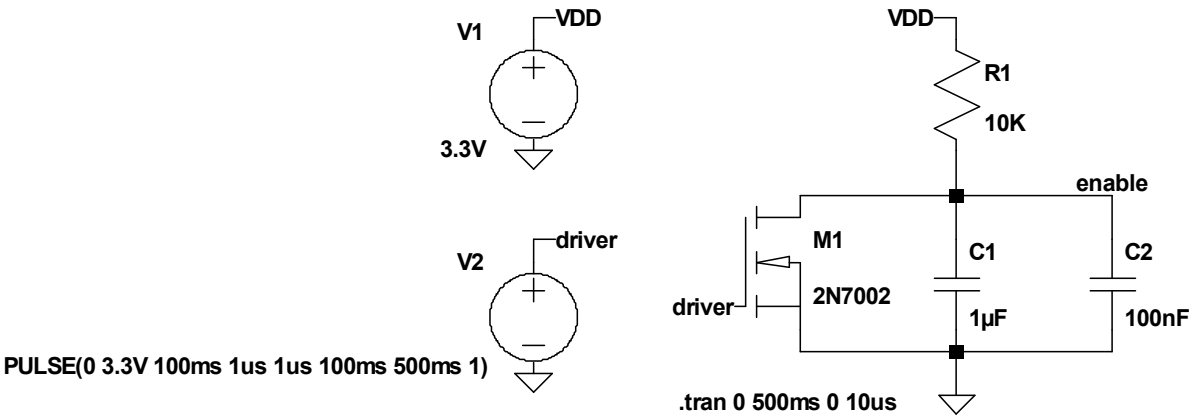

(a) *Simulated circuit for the reset activation.*

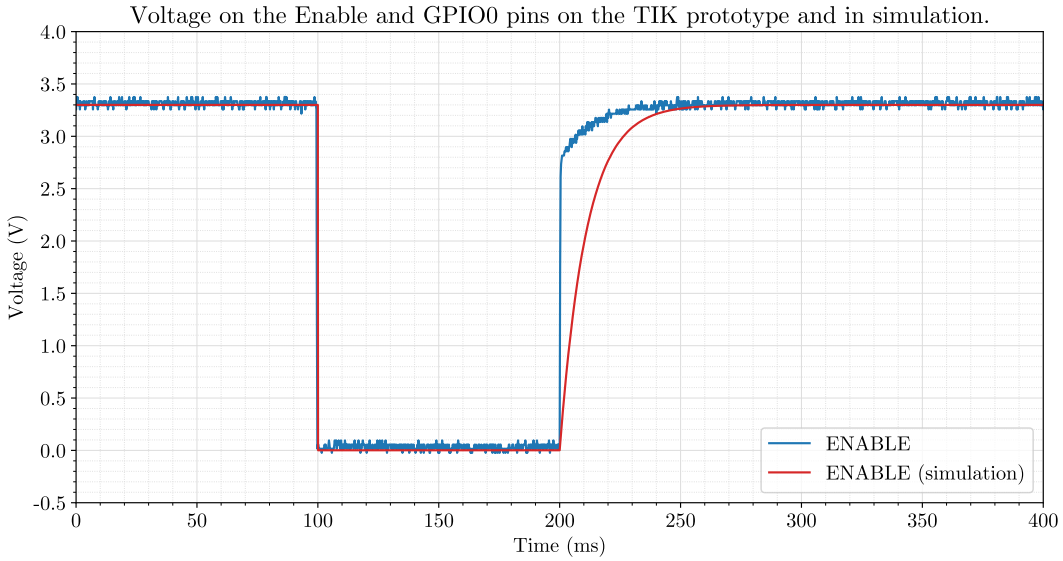

(b) *Simulation results compared with the signal captured with an oscilloscope in the real device.*

Figure C.1 – *Simulation circuit and results of the reset button activation.*

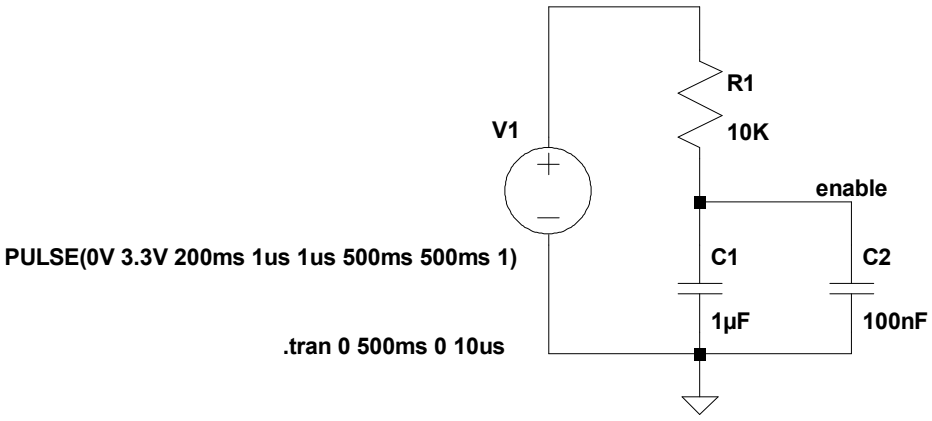

(a) *Simulated circuit for the enable delay.*

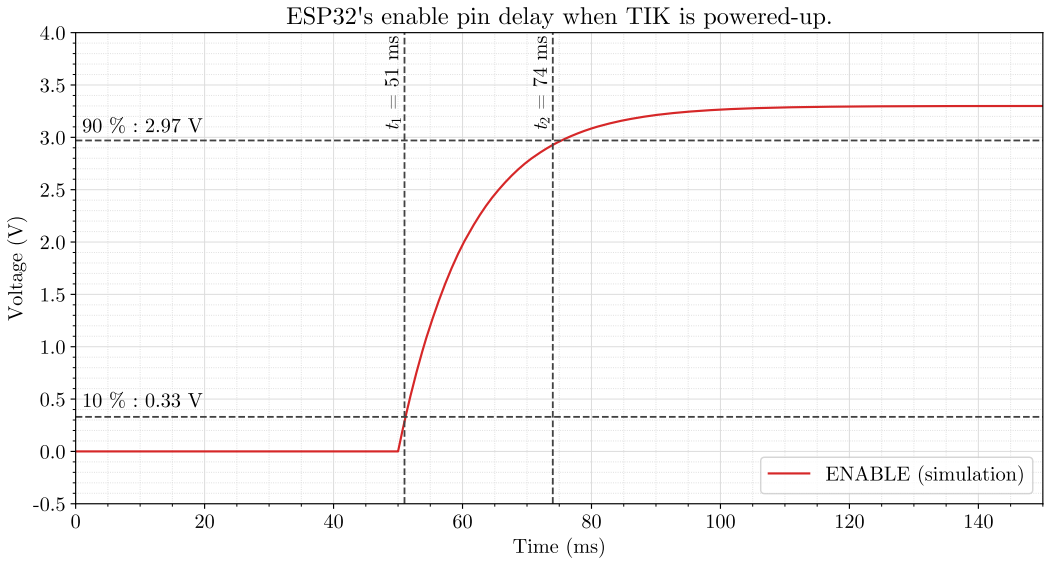

(b) *Simulation results. An enable delay of 23 ms (from 10 % to 90 %) is present.*

Figure C.2 – *Simulation circuit and results of the reset button.*

C.2 Adequation circuit

The simulations presented in this section have been divided into two classes: transient (in the time domain) and gain (in the frequency domain). For transient signals, we have transformed a tree log signal captured with a PicoScope into a PWL file suitable for SPICE-based simulators.

Gain simulations have been performed in LTSpice. However, the transients have been carried out in Altium Designer, because LTSpice has problems handling the large, high sample rate PWL signals in combination with the LMV358 Operational Amplifier spice model.

Moving on to the simulation constraints, some important decisions have been made. A piezoelectric is commonly modeled as a charge source in parallel with a resistor and a capacitor (charge model), as we saw in Section 4.2.4.3.4: Signal adequation circuit. However, the charge model is not practical for simulated analysis. Instead, we resorted to the voltage model, which is a voltage source in series with a resistor and a capacitor in parallel (see figures C.3 and C.6).

Nevertheless, as demonstrated in Section 2.3.1: Characterization of the piezoelectric sensors, in empirical analysis we found that our probes are far more complex than this simple model: They behave like an open circuit for DC (thus ignoring the offset set by V_{BIAS}). They have a great resistance and capacitance dependency on frequency, and a resonance around 80 kHz.

This is the reason behind the 100 nF coupling capacitor in both the simulation and in the circuit . It allows us to center the input signals in the VBIAS DC voltage for our single-supply system. These caps should be rated for at leas t 50 V, as will have to stand a big voltage peaks on their extremes as seen in chapter 3.

C.2.1 Gain

Gain depends on many factors. For example, the lower cutoff frequency is dominated by the high-pass of piezoelectric series resistor and the OpAmp feedback loop, whereas the top cutoff frequency mostly depends of the values of the feedback loop and the input resistance and it is ultimately limited by the frequency response of the LMV358 itself.

The results presented are the product of an iteration process to find the best compromise between gain and width of the flat band. In spite of this, given the simplicity of our simulation model, the results are expected to diverge from reality especially on the lower frequencies.

In the emitter, given that the signal does not require too much amplification but it does require an adequate frequency response for the marked beginning edge of the signal. However, the gain at the receiver needs to be considerably higher than the sender because of the weakness of the signal. And since its spectrum is centered at 10 kHz, the amplification has been optimized for that frequency.

C.2.2 Transient response

The adequation circuit for the emitter has more gain that it needs, so the output of the OpAmp is saturated to the supply voltages (see Figure C.7). This gives us a very step flank, where the signal has a clear beginning and it is easy to identify. The rise time is not immediate and so there will be a 2 µs to 3 µs delay in detection, which equals 1 to 2 samples at $f_s = 500\,\text{kHz}$ (Figure C.5). This simulation also makes clear that maybe the gain needs to be lowered, since the output is very noisy and the device could be false-triggered.

The receiver on the other hand has a very weak signal. We have to be more cautious in this case so we don't distort it as we have to sample and process it with precision (Figure C.8).

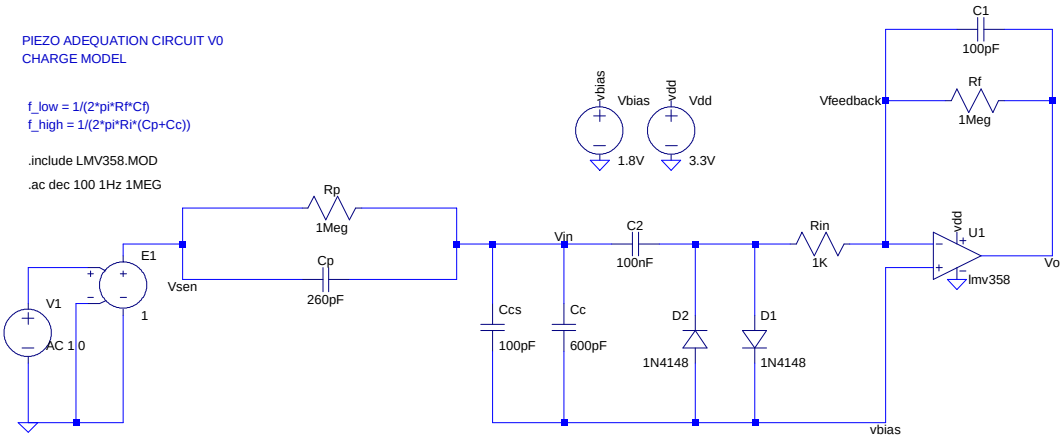

(a) *Emitter adequation circuit.*

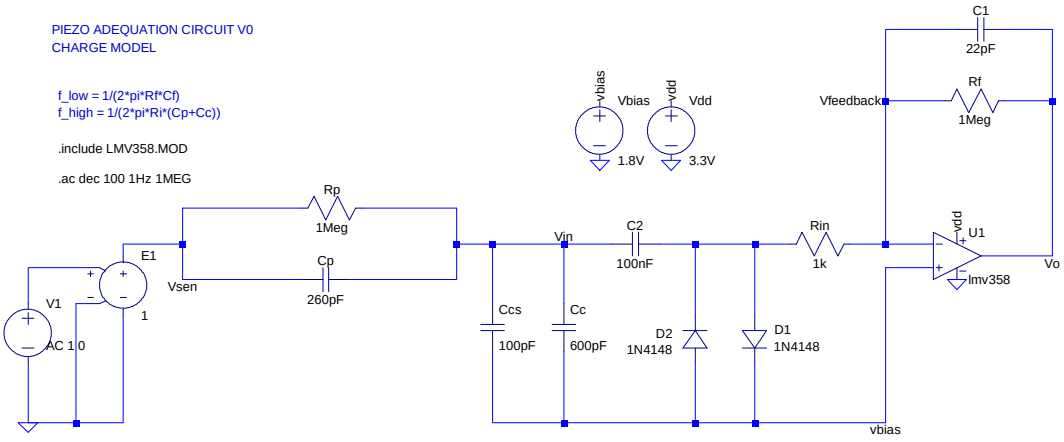

(b) *Receiver adequation circuit.*

Figure C.3 – *Simulation circuits for the amplifiers gains in LTSpice.*

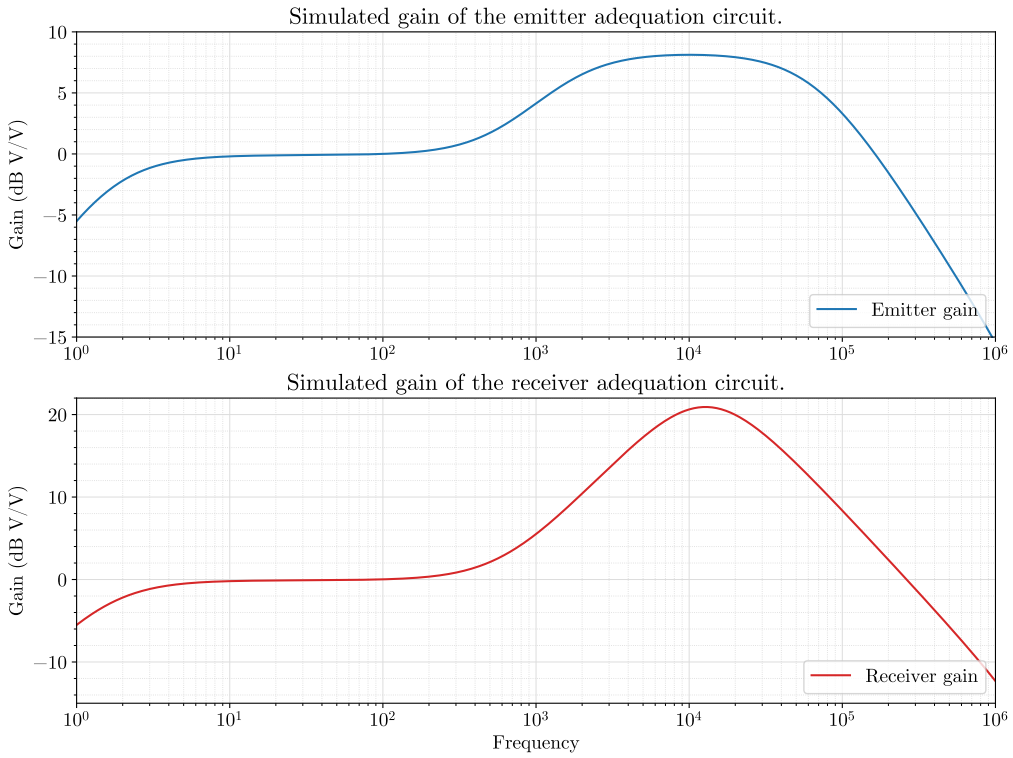

Figure C.4 – *Simulation result for the gains in LTSpice.*

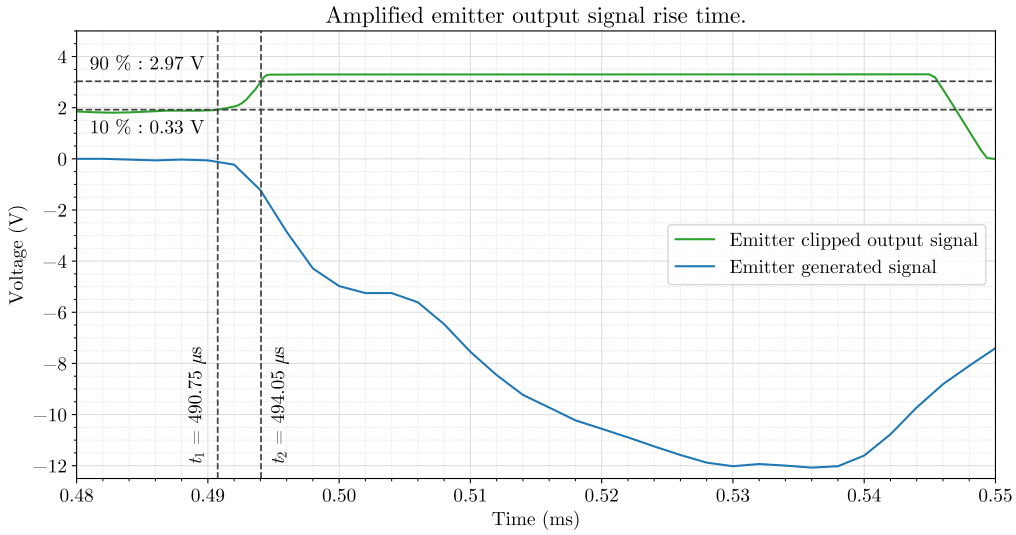

Figure C.5 – *Expected rise time of the emitter amplifier.*

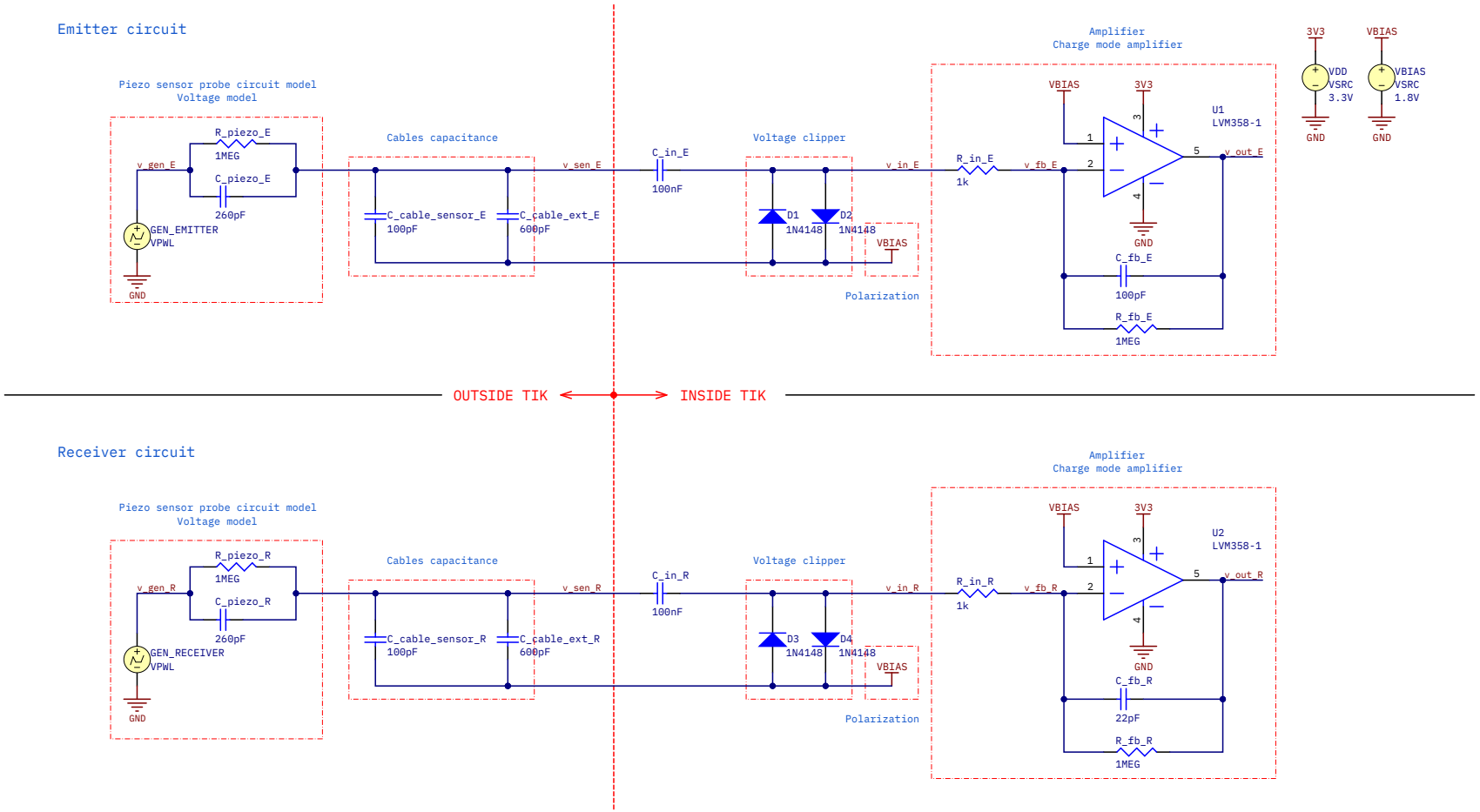

Figure C.6 – *Simulation circuit for the amplifiers transient response in Altium Designer.*

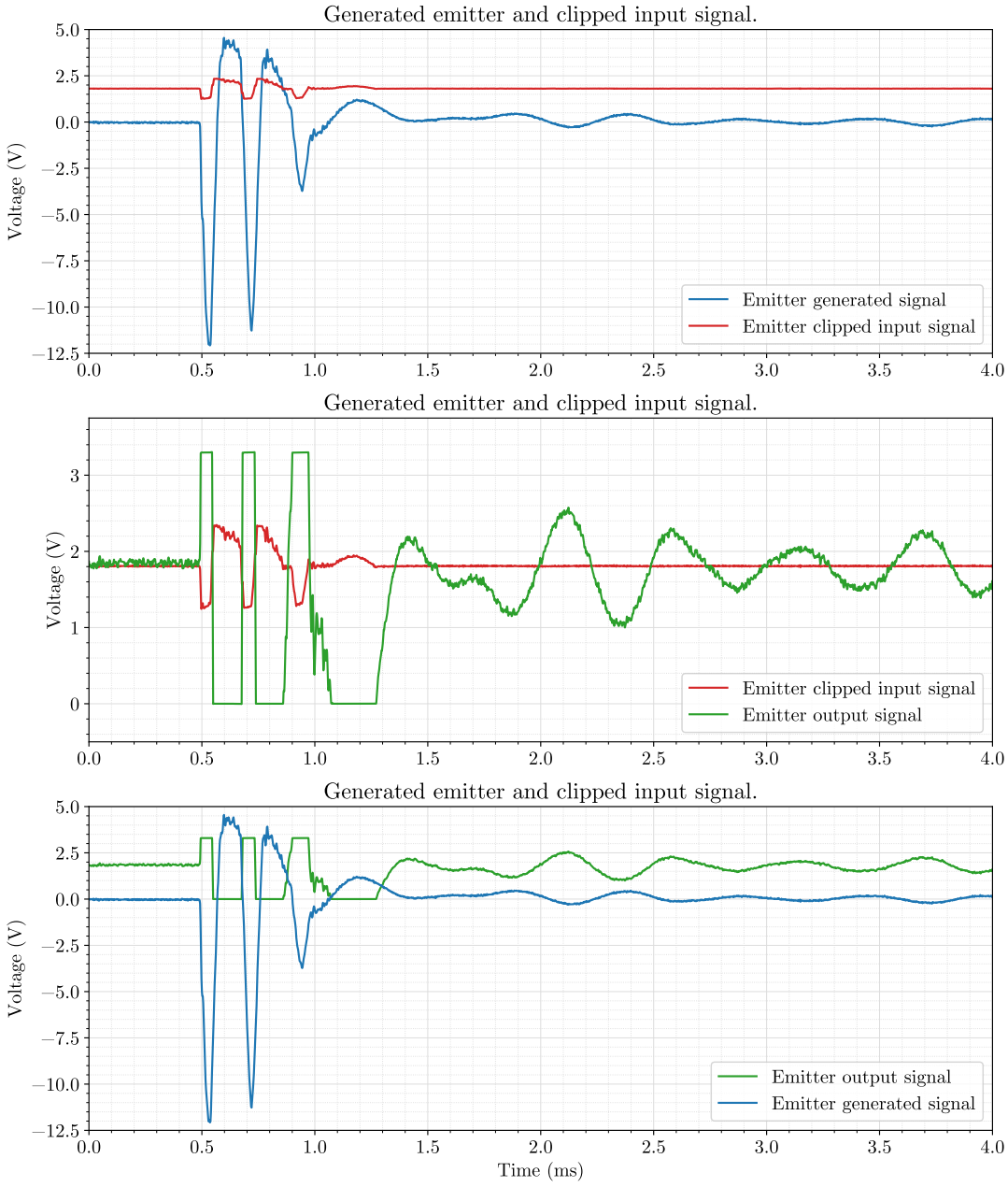

Figure C.7 – *Transient response simulation of the emitter adequation circuit.*

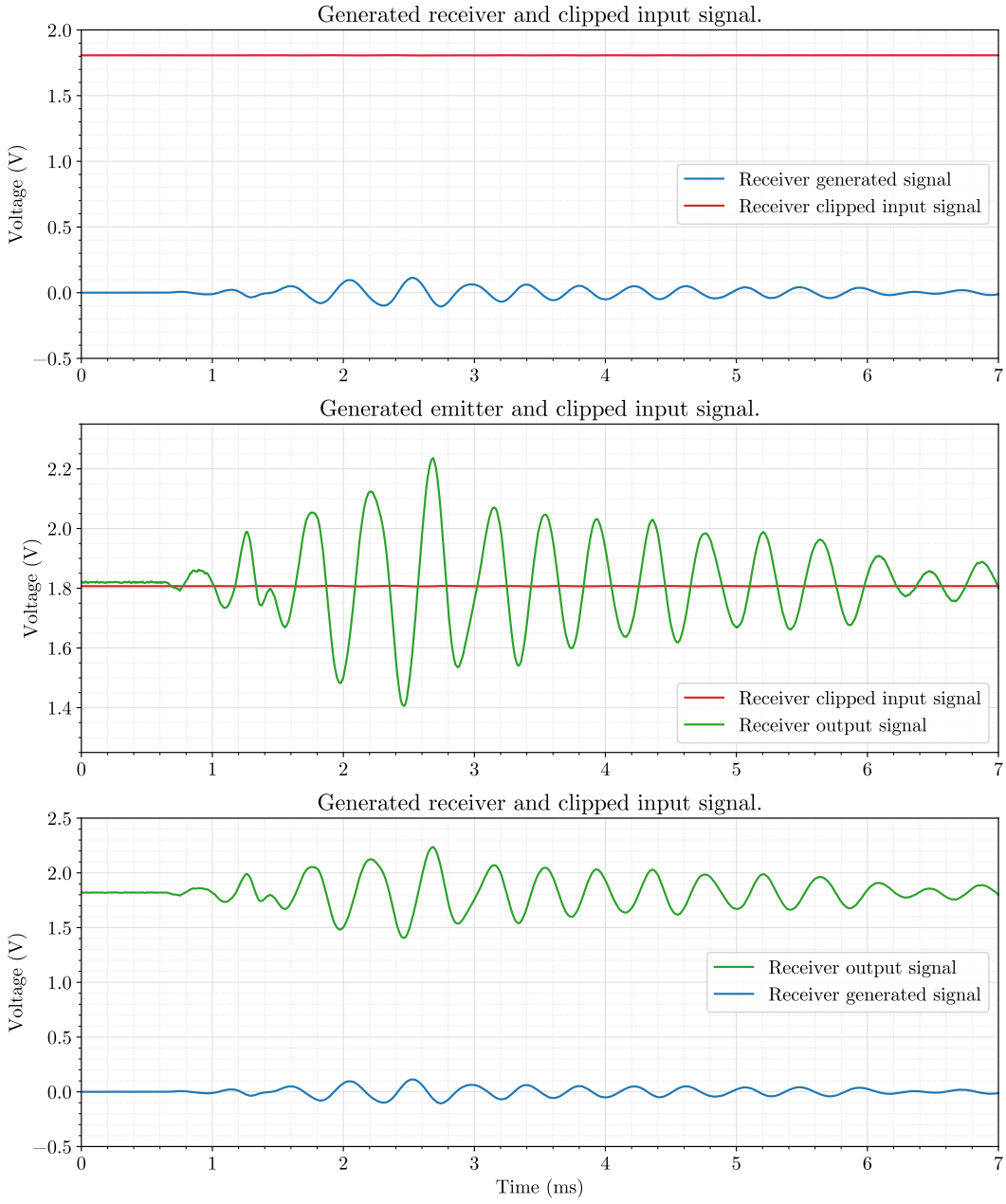

Figure C.8 – *Transient response simulation of the receiver adequation circuit.*

C

Appendix D

Printed Circuit Board schematics

This appendix contains drawings of the Printed Circuit Board layers as well as their mechanical information; both generated using Altium Designer.

D.1 Layout and routing

First, the PCB layers document is attached. It defines the form factor, the layout of the components on the board and their interconnection through the copper layers. The visible layers in each sheet are indicated clearly, and the legend on the right shows the colors that identify different net classes.

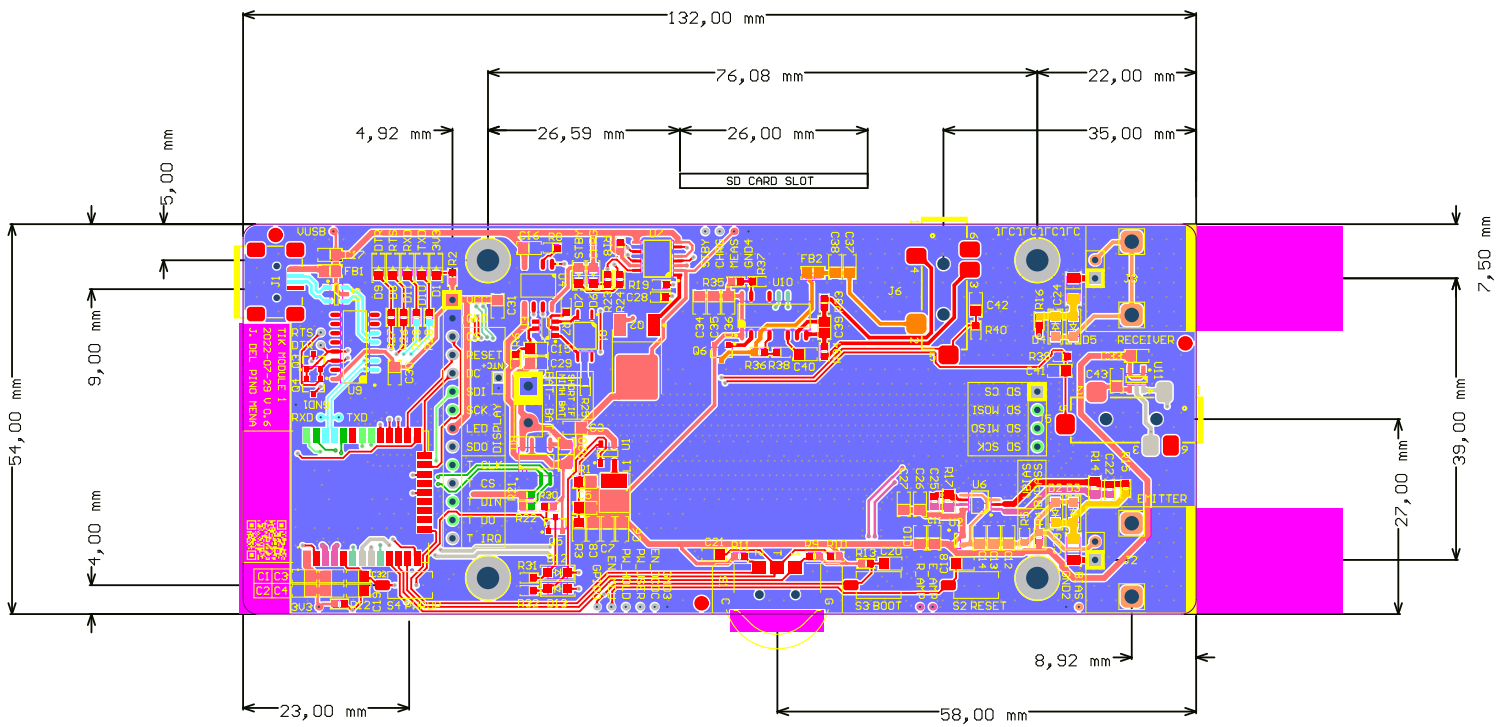

VISIBLE LAYERS:

Board outline + Multilayer + Top overlay + Top layer + Keep-out + dimensions

TRACKS & POLYGONS COLOR LEGEND:

- EMITTER/RECEIVER ANALOG SIGNALS
- GENERIC NET ON TOP LAYER
- GENERIC NET ON BOTTOM LAYER
- POWER REFERENCE GND/BAT-
- POWER RAIL 3V3/BAT+/VUSB/ VMEAS/VSENSE
- POWER RAIL VBIAS
- SPI
- I2C
- SERIAL UART/USB

TIK handheld device PCB

PCB orientation: vertical. Screen facing front, BNCs on top, USB at the bottom, SD Card reader at the left, powerup button at the bottom front right, and multipurpose button on the right side.

Designer's signature:

Supervisor's signature:

Sheet title: TIK Handheld Device PCB

Project title: TIK_HandheldDevice

Designer: Juan Del Pino Mena

Supervisor: Andres Roldan Aranda

Dpto. Electronica y Tecnologia de Computadores
University of Granada
C/ Fuente Nueva, s/n, 18001
Granada, Granada, Spain
Sr. Andres Roldan Aranda

Date: 2022-07-29
Revision: 0.6
Sheet 1 of 1

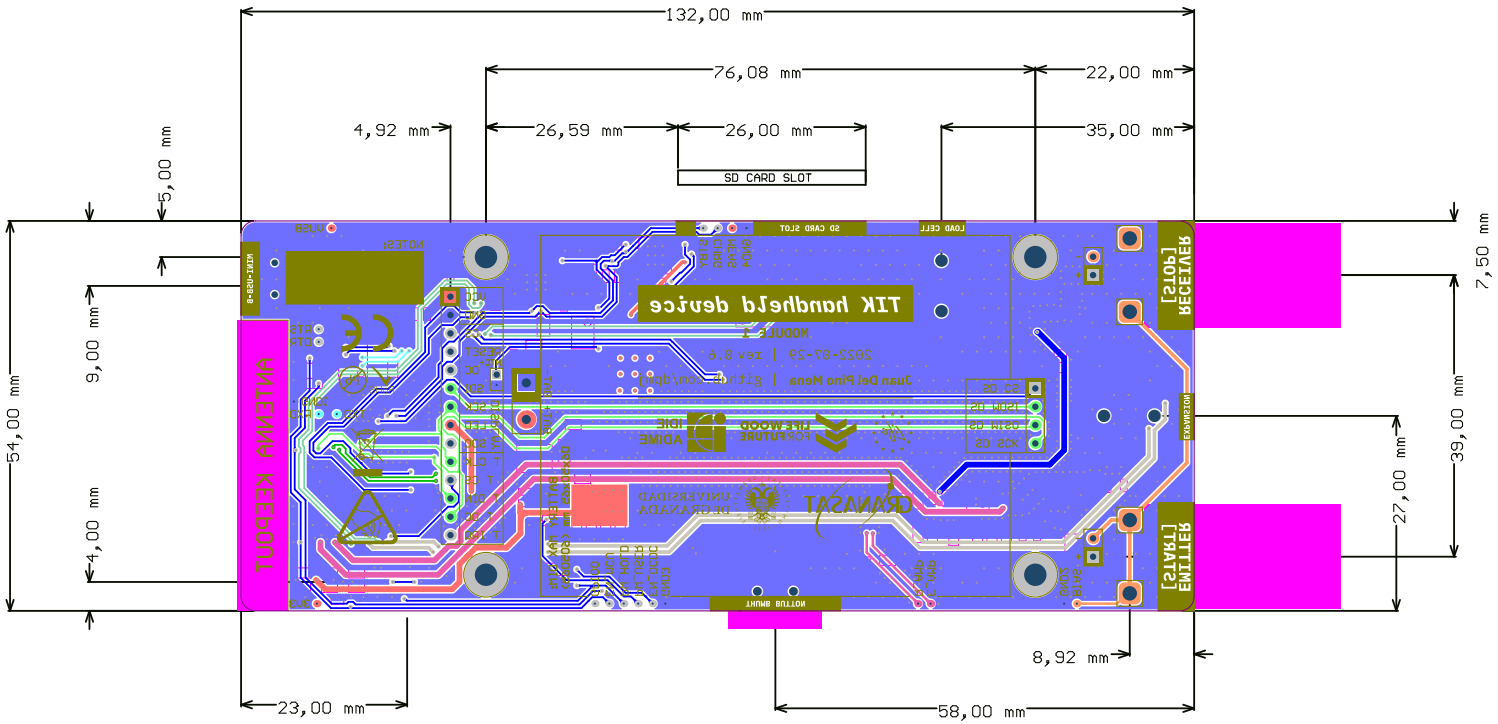

VISIBLE LAYERS:

Board outline + Multilayer + Bottom overlay + Bottom layer + Keep-out + dimensions

TRACKS & POLYGONS COLOR LEGEND:

- EMITTER/RECEIVER ANALOG SIGNALS
- GENERIC NET ON TOP LAYER
- GENERIC NET ON BOTTOM LAYER
- POWER REFERENCE GND/BAT-
- POWER RAIL 3V3/BAT+/VUSB/ VMEAS/VSENSE
- POWER RAIL VBIAS
- SPI
- I2C
- SERIAL UART/USB

TIK handheld device PCB

PCB orientation: vertical. Screen facing front, BNCs on top, USB at the bottom, SD Card reader at the left, powerup button at the bottom front right, and multipurpose button on the right side.

Designer's signature:

Supervisor's signature:

Sheet title: TIK Handheld Device PCB	Dpto. Electronica y Tecnologia de Computadores University of Granada C/ Fuente Nueva, s/n, 18001 Granada, Granada, Spain Sr. Andres Roldan Aranda
Project title: TIK_HandheldDevice	
Designer: Juan Del Pino Mena	
Supervisor: Andres Roldan Aranda	Date: 2022-07-29 Revision: 0.6 Sheet 1 of 1

D.2 Mechanical schematics

In this section, the Printed Circuit Board mechanical drawings are appended. They contain the dimensions of the board in exhaustive detail (they were necessary to design the case). Additionally, later pages include two top and bottom layer prints, a top solder layer print (the necessary mask for the stencil) and information on the layer stackup and the drill drawing. At the end of the document is a BOM, which is useful during component placing.

DWG NO: 1 REV: 6

REV STATUS OF SHEETS	REV										
	SHEET										

REVISIONS				
ZONE	REV	DESCRIPTION	DATE	APPROVED

View from Top side (Scale 1:1)

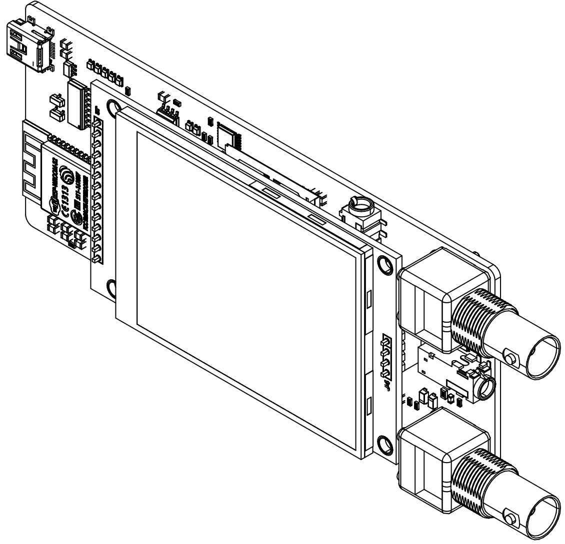

View from Bottom side (Scale 1:1)

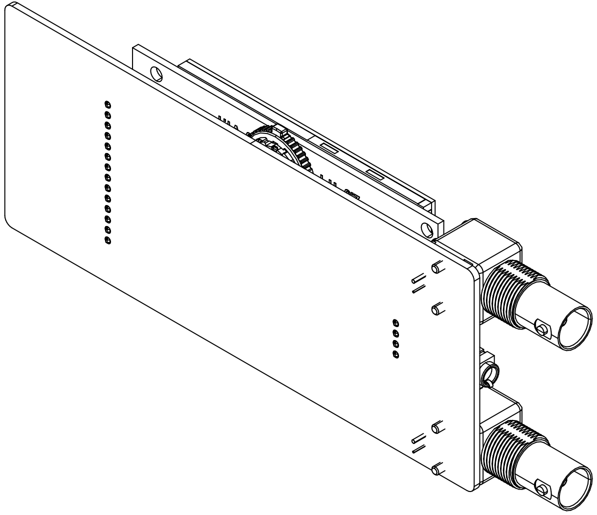

View from Back side (Scale 1:1)

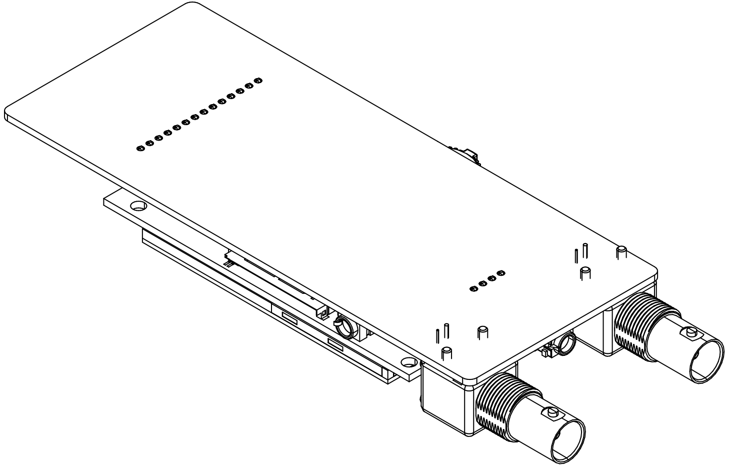

View from Front side (Scale 1:1)

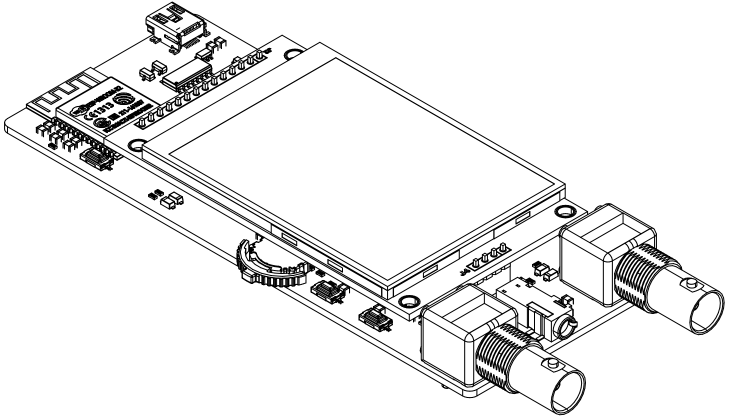

PART NO: =PCB_PART_NUMBER

APPROVALS		DATE
ENGINEER:	Juan Del Pino Mena	2022-07-29
DESIGNER:	Juan Del Pino Mena	2022-07-29
CHECKER:	Andrés M. Roldán	2022-07-29

Reference Documents
BOM DOC: BOM/bill_of_materials
ASSY DOC: --
SCH DOC: SCH/*
PCB DOC: PCB/TIK_PCB.PcbDoc

THIRD ANGLE PROJECTION

NEXT ASSY	USED ON
APPLICATION	

GRANASAT

Dpto. Electrónica y
tecnología de computadores
University of Granada, Spain
C/ Fuente Nueva, s/n, 18001

DESIGN ITEM: .Item
DESIGN ITEM REVISION: 6
TITLE: TREE INSPECTION KIT MECHANICAL DRAFTS
SIZE: A3
CAGE CODE: --
DWG NO: 1
REV: 6
SCALE: 1:1
FILE NAME: TIK_PCB.PCBDwf
SHEET: 1 OF 5

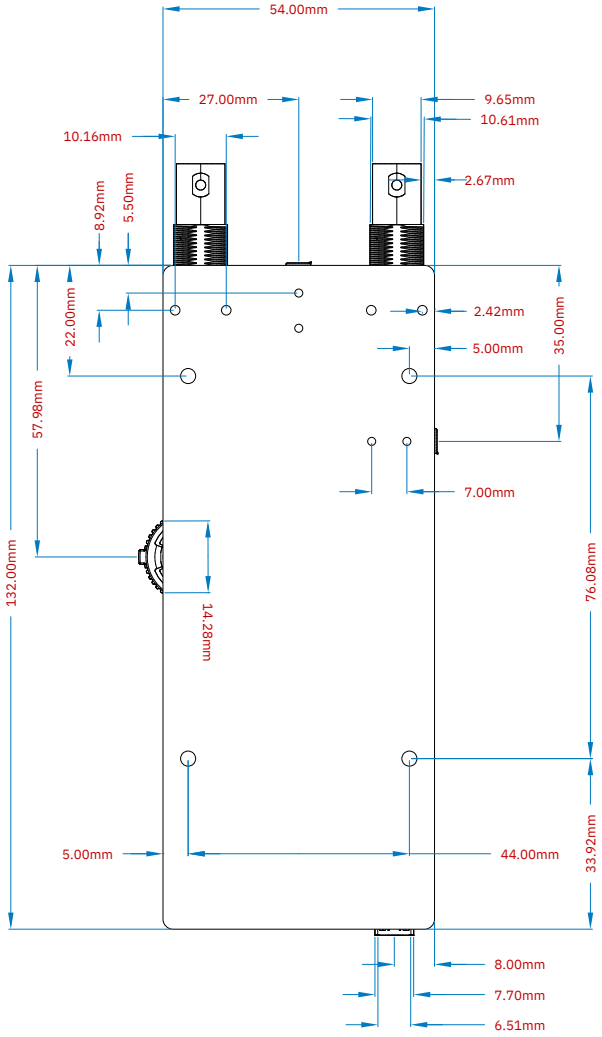

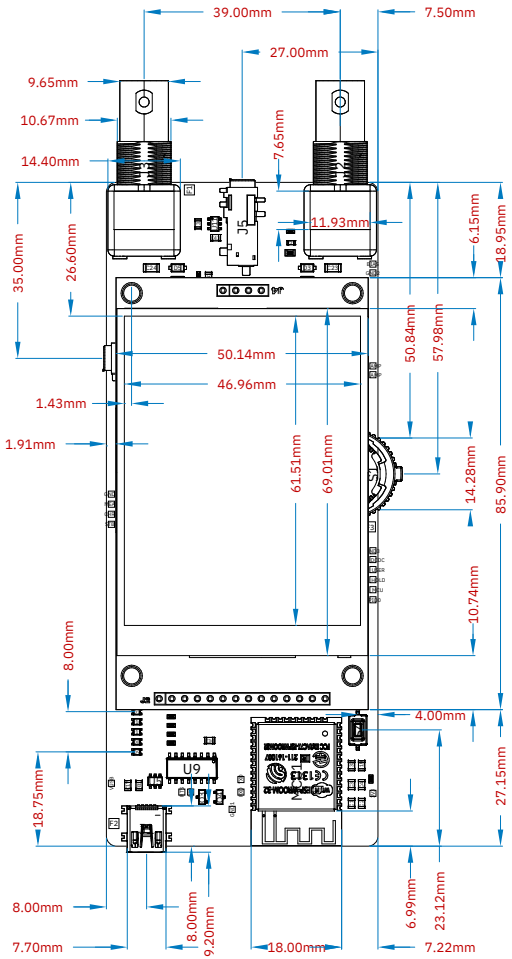

REVISIONS				
ZONE	REV	DESCRIPTION	DATE	APPROVED

PART NO: =PCB_PART_NUMBER

APPROVALS		DATE
ENGINEER:	Juan Del Pino Mena	2022-07-29
DESIGNER:	Juan Del Pino Mena	2022-07-29
CHECKER:	Andrés M. Roldán	2022-07-29

Reference Documents

BOM DOC: BOM/bill_of_materials

ASSY DOC: --

SCH DOC: SCH/*

PCB DOC: PCB/TIK_PCB.PcbDoc

NEXT ASSY | USED ON

APPLICATION

GRANASAT

Dpto. Electrónica y tecnología de computadores
University of Granada, Spain
C/ Fuente Nueva, s/n, 18001

DESIGN ITEM: .Item | DESIGN ITEM REVISION: 6

TITLE: TREE INSPECTION KIT MECHANICAL DRAFTS

SIZE: A3 | CAGE CODE: -- | DWG NO: | REV: 6

SCALE: | FILE NAME: TIK_PCB.PCBDwf | SHEET: 2 OF 5

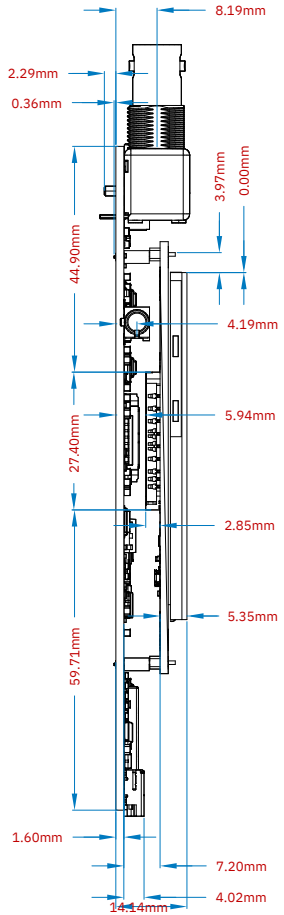

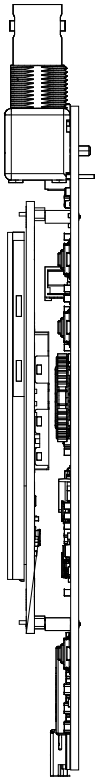

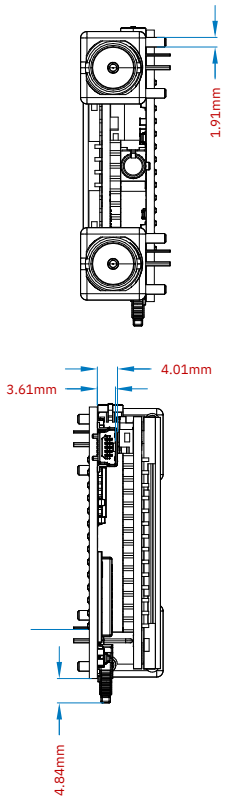

REVISIONS				
ZONE	REV	DESCRIPTION	DATE	APPROVED

REV STATUS OF SHEETS: REV | SHEET

DWG NO: 1 REV: 6

PART NO: =PCB_PART_NUMBER

APPROVALS		DATE
ENGINEER:	Juan Del Pino Mena	2022-07-29
DESIGNER:	Juan Del Pino Mena	2022-07-29
CHECKER:	Andrés M. Roldán	2022-07-29

Reference Documents

BOM DOC: BOM/bill_of_materials

ASSY DOC: --

SCH DOC: SCH/*

PCB DOC: PCB/TIK_PCB.PcbDoc

NEXT ASSY | USED ON

APPLICATION

THIRD ANGLE PROJECTION

GRANASAT

Dpto. Electrónica y tecnología de computadores
University of Granada, Spain
C/ Fuente Nueva, s/n, 18001

DESIGN ITEM: .Item | DESIGN ITEM REVISION: 6

TITLE: TREE INSPECTION KIT MECHANICAL DRAFTS

SIZE: A3 | CAGE CODE: -- | DWG NO: | REV: 6

SCALE: | FILE NAME: TIK_PCB.PCBDwf | SHEET: 3 OF 5

REV STATUS OF SHEETS	REV										
	SHEET										

DWG NO: 1 REV: 6

REVISIONS				
ZONE	REV	DESCRIPTION	DATE	APPROVED

Top Layer (Scale 1:1)

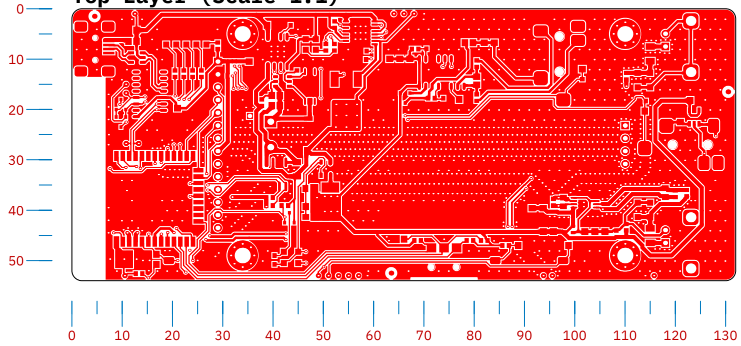

Top Paste (Scale 1:1)

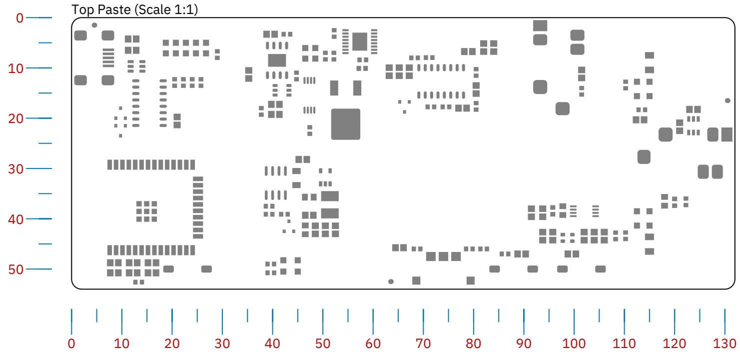

Bottom Layer (Scale 1:1)

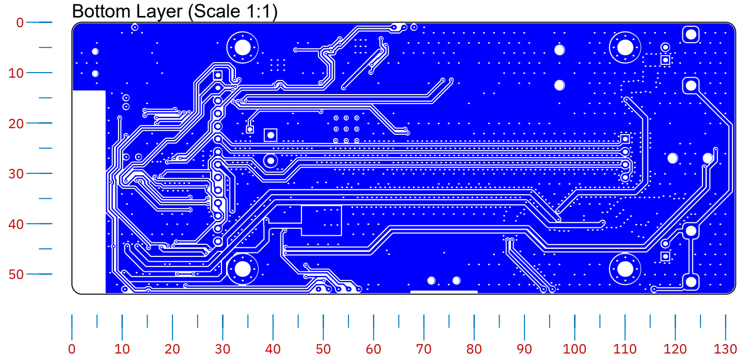

Drill Drawing View (Scale 1:1)

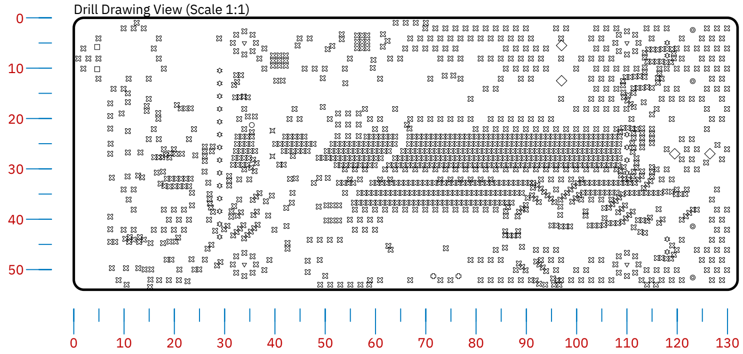

Layer Stack Legend

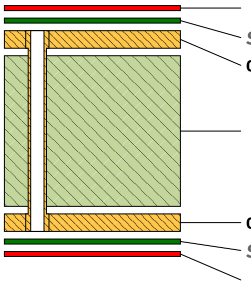

Material	Layer	Thickness	Dielectric Material	Type	Gerber
	Top Overlay			*Legend*	*GTO*
Surface Material	*Top Solder*	*0.01mm*	*Solder Resist*	*Solder Mask*	*GTS*
Copper	Top Layer	0.04mm		Signal	GTL
		1.50mm	FR-4	Dielectric	
Copper	Bottom Layer	0.04mm		Signal	GBL
Surface Material	*Bottom Solder*	*0.01mm*	*Solder Resist*	*Solder Mask*	*GBS*
	Bottom Overlay			*Legend*	*GBO*

Total thickness: 1.59mm

Drill Table

Symbol	Count	Hole Size	Plated	Hole Tolerance
⌧	1330	0.30mm	Plated	
☼	22	0.89mm	Plated	
□	2	0.90mm	Non-Plated	
○	1	0.90mm	Plated	
○	2	1.20mm	Non-Plated	
⌑	2	1.27mm	Plated	
◇	4	1.70mm	Non-Plated	
●	4	2.01mm	Plated	
▽	4	3.10mm	Plated	
	1371 Total			

PART NO: =PCB_PART_NUMBER

APPROVALS		DATE
ENGINEER:	Juan Del Pino Mena	2022-07-29
DESIGNER:	Juan Del Pino Mena	2022-07-29
CHECKER:	Andrés M. Roldán	2022-07-29

Reference Documents

BOM DOC: BOM/bill_of_materials
ASSY DOC: --
SCH DOC: SCH/*
PCB DOC: PCB/TIK_PCB.PcbDoc

THIRD ANGLE PROJECTION

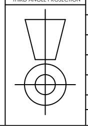

NEXT ASSY	USED ON
APPLICATION	

Dpto. Electrónica y
tecnología de computadores
University of Granada, Spain
C/ Fuente Nueva, s/n, 18001

DESIGN ITEM: .Item
DESIGN ITEM REVISION: 6
TITLE: TREE INSPECTION KIT MECHANICAL DRAFTS
SIZE: A3
CAGE CODE: --
DWG NO:
REV: 6
SCALE:
FILE NAME: TIK_PCB.PCBDwf
SHEET: 4 OF 5

Bill Of Materials

Designator	Value	Tolerance	Description	Type	PackageDescription	Quantity
C22	100pF	5% 10V	Ceramic cap size 0805		0603	1
C23, C24	100nF	10% 100V	Ceramic cap size 1206 C1206C104K1RACTU	X7R	1206	2
C25	22pF	5% 10V	Ceramic cap size 0805		0805	1
FB1, FB2	40mR, 3A 25%		0805, 60Ω, 3A, 25% SMT		0805	2
J5			3.5mm Jack 4-pole with normally closed switches			1
J6			3.5mm Jack 4-pole with normally closed switches		3.5mm Jack 4-pole with normally closed switches	1
L1	2.2uH	20% 2.2A	Shielded Power Inductor 2.2 uH 20% 2.2 A 50.4 mohms 3.11 A (sat) 60MHz 4018: 4x4x1.8mm		4x4x1.8mm	1
Q1			Dual N-channel Enhancement mode power MOSFET	Dual NMOS	TSSOP-8	1
Q2			MJD210 PNP BJT transistor DPAK (decawatt) 5A dc	PNP	DPAK (TO-252)	1
Q6			65 V, 100 mA PNP general-purpose transistor	PNP	SOT23	1
R1	150K	1%	Res size 0805 SMD mounting, low power Yageo-RC0805FR-07150KL		0805	1
R8	1.2K	1%	Res size 0603 SMD mounting, low power		0603	1
R14, R17	1M	1%	Res size 0805 SMD mounting, low power. Yageo-RC0805FR-071ML		0805	2
R23, R24	220	5%	Res size 0603 SMD mounting, low power		0603	2
R26, R27, R28, R29	150	5%	Res size 0603 SMD mounting, low power		0603	4
R36	22K	5%	Res size 0603 SMD mounting, low power		0603	1
RT1	10K		NTC THERMISTOR 10K for solding a cable from the battery NTC		0603	1
U1			1.0MHZ, 2A STEP-DOWN DC-DC BUCK CONVERTER, with latch-off protection	Buck converter 2A	TSOT-25 (SOT-23-5)	1
U2	LDO 1.8V, 80mA		Fixed output lowdropout linear regulator. 1.8 V 80 mA	LDO	SC82–AB (SC70–4)	1
U6			LMV358IDGKR Dual OpAmp; low voltage rail to rail opamp; 2.7V to 5V Vss; ESD protection; MSOP-8 Package.	Dual OpAmp	MSOP-8	1
U10			HX711 load cell amplifier		SOP 16 L	1
U11			TPD3S014TDBVRQ1 ESD prot. & current limit		SOT-23-6	1
C1, C14, C34	47pF	5% 10V	Ceramic cap size 0805		0805	3
C2, C8, C13, C15, C17, C18, C20, C21, C27, C30, C31, C32, C33, C35, C37, C39, C40, C41, C42	100nF	10% 25V	Ceramic cap size 0805		0805	19
C3, C16, C26, C29, C36, C38	10uF	10% 25V	Ceramic cap size 0805		0805	6
C5	27pF	5% 10V	Ceramic cap size 0805		0805	1
C4, C6, C7, C9, C12, C43	22uF	20% 10V	Ceramic cap size 0805 CC0805MKX5R6BB226 Yageo MLCC 22uF 10V 20% X5R		0805	6
C10, C11, C19	1uF	10% 25V	Ceramic cap size 0805		0805	3
C28	470pF	5% 10V	Ceramic cap size 0805		0603	1
D2, D3, D4, D5, D12, D13			SURFACE MOUNT FAST SWITCHING DIODE	Rectifier, General purpose	SOD123	6
D1, D6, D8, D10			Low power LED color Green	GREEN	0805	4
D7, D9, D11			Low power LED color Red	RED	0805	3
J1			USB-MINI-B Female, Manufacturer PN/ID: 10033526-N3212LF		USB-Mini-B, Female	1
J2, J3			BNC coaxial female connector	BNC Female right angle		2
J4			ILI9341 TFT LCD Jumper pin headers., plus SD card reader pins	PCB Pin headers: F, 1x14 & 1x4	100 mil pitch	1
MCU1			- Transceiver; 802.11 b/g/n _Wi-Fi, WiFi, WLAN_, Bluetooth Smart Ready 4.x Dual Mode For Use With ESP-WROOM-32			1
Q3, Q4				N-Ch	SOT23	2
Q5			PMOS BSS84AK	P-Ch	SOT23	1
R18, R21, R22	4.7K	1%	Res size 0603 SMD mounting, low power		0603	3
R3	33K	1%	Res size 0805 SMD mounting, low power		0805	1
R4, R5, R25	0R	5%	Res size 0603 SMD mounting, zero-ohm 0R Yageo RC0603JR-070RL		0603	3
R9, R10, R11, R12, R13, R35, R37, R38, R39, R40	10K	5%	Res size 0603 SMD mounting, low power		0603	10
R2, R6, R33, R34	100R	5%	Res size 0603 SMD mounting, low power		0603	4
R7, R15, R16	1K	5%	Res size 0603 SMD mounting, low power		0603	3
R19	1.5K	1%	Res size 0603 SMD mounting, low power		0603	1
R20	0.2R	1%	Res size 1206 SMD mounting, high power, shunt, current sense.		1206	1
R30, R31, R32	100K	5%	Res size 0603 SMD mounting, low power		0603	3
S1			SWITCH Multidirection Slide Push Button SMD TS-003	Thumb Switch		1
S2, S3, S4			Generic 2 pin button		SMD 2-pin	3
U3			DW01A One cell Li-Po/Li-ion Battery protection IC	Bat protection	SOT-23-6	1
U4			1A Standalone Linear Li-Ion Battery Charger with Thermal Regulation in SOP-8	Li-Po/Li-Ion charger	SOP-8	1
U5			Very low capacitance ESD protection	ESD Protection	SOT23-6L	1
U7			LTC4060EFE		TSSOP-16	1
U8			Zero-Drift, Bi-Directional CURRENT/POWER MONITOR with I2C. SOIC-8 (D) Package	Current sense	SOIC-8	1
U9			USB to serial chip CH340C, integrated oscillator.	USB to UART	SOP-16	1

REV STATUS OF SHEETS — REV / SHEET

REVISIONS

ZONE	REV	DESCRIPTION	DATE	APPROVED

DWG NO: 1 — REV: 6

PART NO: =PCB_PART_NUMBER

APPROVALS		DATE
ENGINEER:	Juan Del Pino Mena	2022-07-29
DESIGNER:	Juan Del Pino Mena	2022-07-29
CHECKER:	Andrés M. Roldán	2022-07-29

Reference Documents

BOM DOC: BOM/bill_of_materials

ASSY DOC: --

SCH DOC: SCH/*

PCB DOC: PCB/TIK_PCB.PcbDoc

NEXT ASSY | USED ON

APPLICATION

THIRD ANGLE PROJECTION

GRANASAT

Dpto. Electrónica y tecnología de computadores
University of Granada, Spain
C/ Fuente Nueva, s/n, 18001

DESIGN ITEM: .Item — DESIGN ITEM REVISION: 6

TITLE: TREE INSPECTION KIT MECHANICAL DRAFTS

SIZE: A3 — CAGE CODE: -- — DWG NO: — REV: 6

SCALE: — FILE NAME: TIK_PCB.PCBDwf — SHEET: 5 OF 5

D

Appendix E

Mechanical drawings and renders

In this appendix the PDF documents of mechanical drawings of the parts of the designed casing are attached, as well as the complete assembly with all the parts and the PCB. These documents have been generated with SolidWorks. Some high-quality 3D renderings are also included. These have been rendered using the *PhotoView 360* plugin for SolidWorks.

The drawings contain an exhaustive level of detail. They include the most relevant dimensions, details (the circular zoom zones) of areas of interest, and even section views. All dimensions are in millimeters. Other information of interest is located on the lower right corner, such as the material, finish, weight of the part, and the scale of the sheet. The scale of the different drawings and details within the page may vary, in which case it will be indicated. Note: the scale is only valid when using a suitable size paper, in this case the page format is ANSI B (279 x 432 mm).

E.1 Mechanical schematics of the case parts

The following pages contain a 7-sheet PDF with mechanical drawings of the top cover, the bottom cover, the power-on/off button plunger and the stylus for the touchscreen.

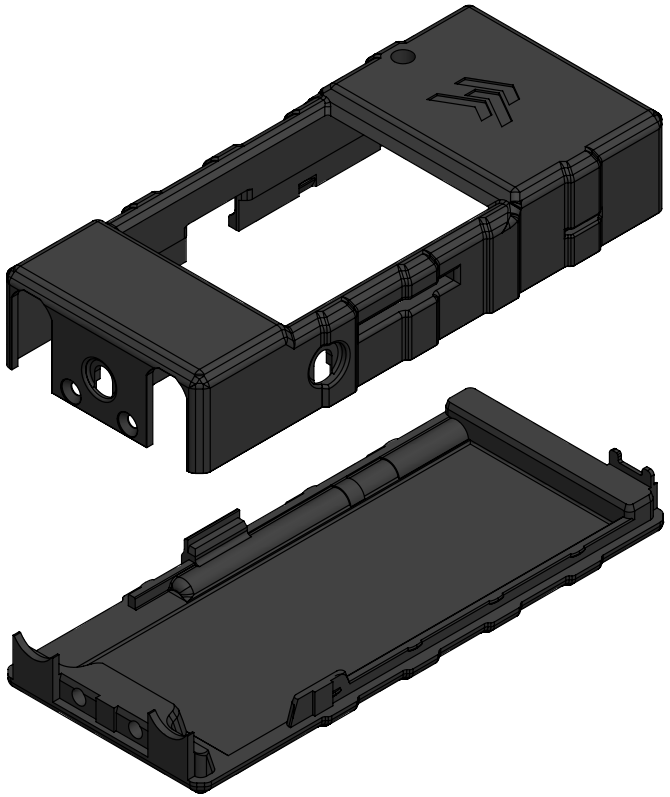

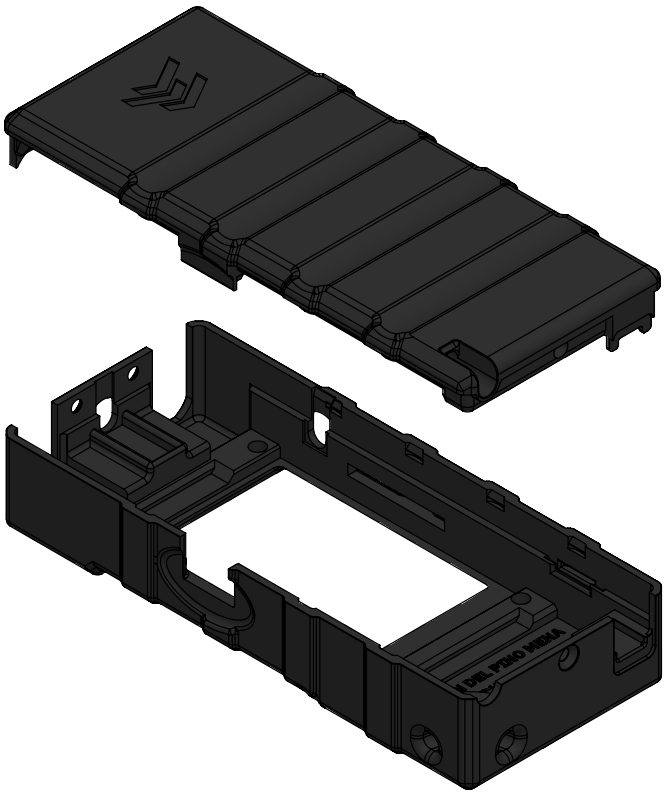

C/ FUENTE NUEVA S/N, 18001 GRANADA.	DO NOT SCALE DRAWING	

UNLESS OTHERWISE SPECIFIED:

DIMENSIONS ARE IN MILLIMETERS
TOLERANCES:
ANGULAR: MACH ±0°10'
ONE PLACE DECIMAL ±0.5
TWO PLACE DECIMAL ±0.1

INTERPRET GEOMETRIC TOLERANCING PER: ASME Y14.5

MATERIAL: Case: PLA

FINISH: Matte

	NAME	DATE
DRAWN	Juan Del Pino Mena	26/07/22
CHECKED	Andrés Roldán	
ENG APPR.		
MFG APPR.		
Q.A.		

COMMENTS:

AUTHOR: Juan Del Pino Mena

TITLE:

Case parts - Top & bottom covers

SIZE	DWG. NO.	REV
B	0 - Iso. views - Both	6

SCALE: 1:1	WEIGHT: 93 g	SHEET 1 OF 7

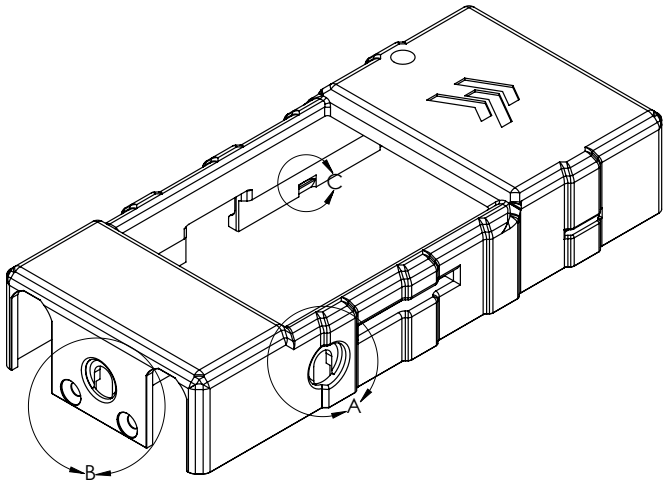

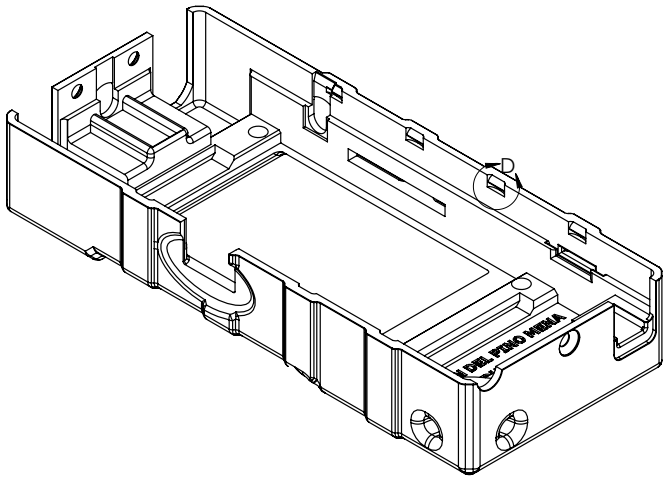

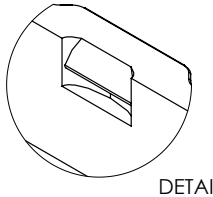

DETAIL D
SCALE 4 : 1

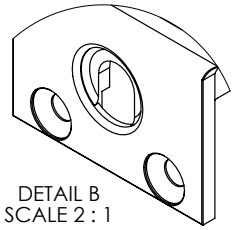

DETAIL B
SCALE 2 : 1

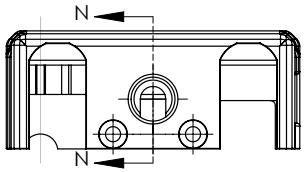

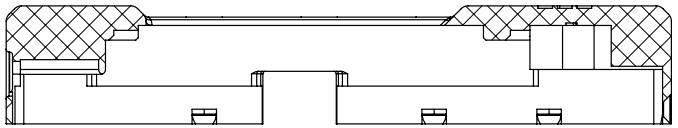

SECTION N-N

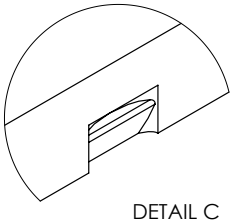

DETAIL C
SCALE 4 : 1

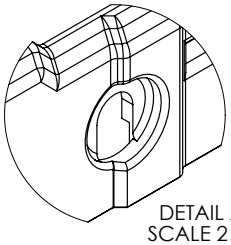

DETAIL A
SCALE 2 : 1

UNLESS OTHERWISE SPECIFIED:		
DIMENSIONS ARE IN MILLIMETERS TOLERANCES: ANGULAR: MACH ±0°10' ONE PLACE DECIMAL ±0.5 TWO PLACE DECIMAL ±0.1		
INTERPRET GEOMETRIC TOLERANCING PER: ASME Y14.5		
MATERIAL: Case: PLA		
FINISH: Matte		
C/ FUENTE NUEVA S/N, 18001 GRANADA.	DO NOT SCALE DRAWING	

	NAME	DATE
DRAWN	Juan Del Pino Mena	26/07/22
CHECKED	Andrés Roldán	
ENG APPR.		
MFG APPR.		
Q.A.		
COMMENTS:		

AUTHOR: Juan Del Pino Mena

TITLE:

Case parts. Top cover.

SIZE	DWG. NO.	REV
B	1.1 - Iso. views	6

SCALE: 1:1	WEIGHT: 41 g	SHEET 2 OF 7

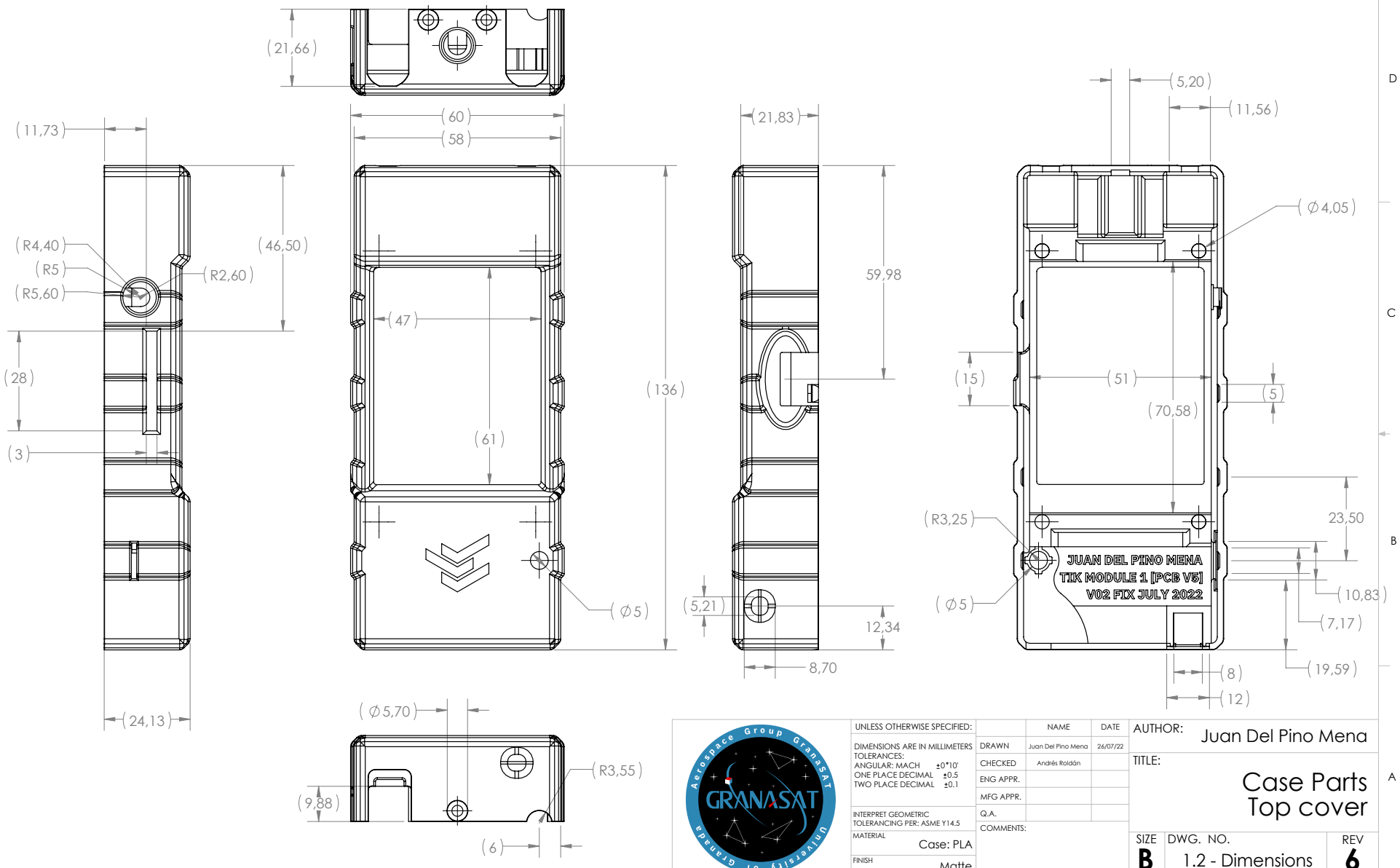

UNLESS OTHERWISE SPECIFIED:		NAME	DATE
DIMENSIONS ARE IN MILLIMETERS	DRAWN	Juan Del Pino Mena	26/07/22
TOLERANCES:	CHECKED	Andrés Roldán	
ANGULAR: MACH ±0°10'	ENG APPR.		
ONE PLACE DECIMAL ±0.5	MFG APPR.		
TWO PLACE DECIMAL ±0.1	Q.A.		
INTERPRET GEOMETRIC TOLERANCING PER: ASME Y14.5	COMMENTS:		
MATERIAL: Case: PLA			
FINISH: Matte			

C/ FUENTE NUEVA S/N, 18001 GRANADA.

DO NOT SCALE DRAWING

AUTHOR: Juan Del Pino Mena

TITLE: Case Parts Top cover

SIZE	DWG. NO.	REV
B	1.2 - Dimensions	6

SCALE: 1:1 | WEIGHT: 41 g | SHEET 3 OF 7

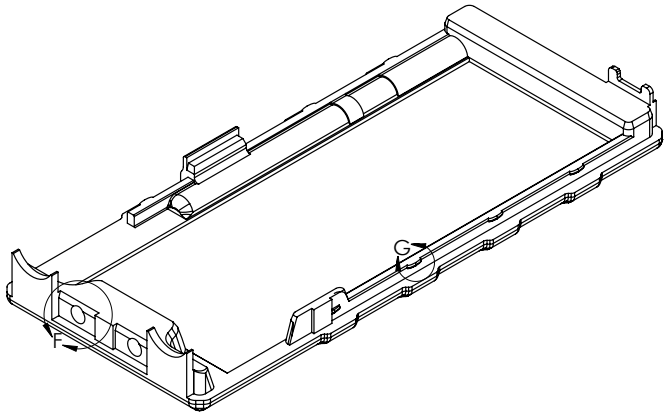

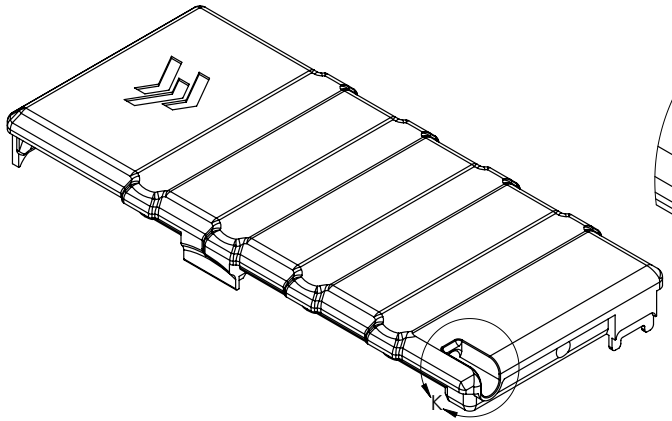

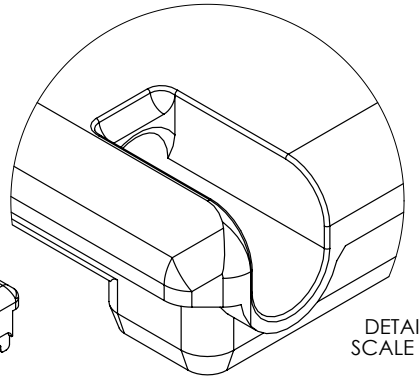

DETAIL K
SCALE 4 : 1

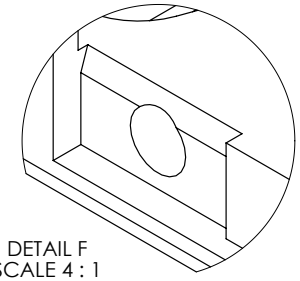

DETAIL F
SCALE 4 : 1

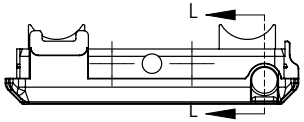

SECTION L-L

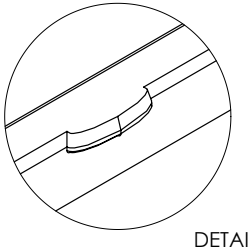

DETAIL G
SCALE 6 : 1

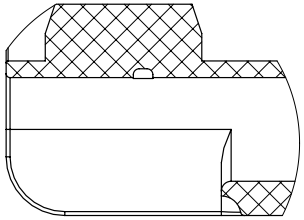

DETAIL M
SCALE 4 : 1

UNLESS OTHERWISE SPECIFIED:		
DIMENSIONS ARE IN MILLIMETERS TOLERANCES: ANGULAR: MACH ±0°10' ONE PLACE DECIMAL ±0.5 TWO PLACE DECIMAL ±0.1		
INTERPRET GEOMETRIC TOLERANCING PER: ASME Y14.5		
MATERIAL	Case: PLA	
FINISH	Matte	
C/ FUENTE NUEVA S/N, 18001 GRANADA.	DO NOT SCALE DRAWING	

	NAME	DATE
DRAWN	Juan Del Pino Mena	26/07/22
CHECKED	Andrés Roldán	
ENG APPR.		
MFG APPR.		
Q.A.		
COMMENTS:		

AUTHOR: Juan Del Pino Mena

TITLE:

Case parts
Bottom cover

SIZE	DWG. NO.	REV
B	2.1 - Iso. views	6

SCALE: 1:1	WEIGHT: 52 g	SHEET 4 OF 7

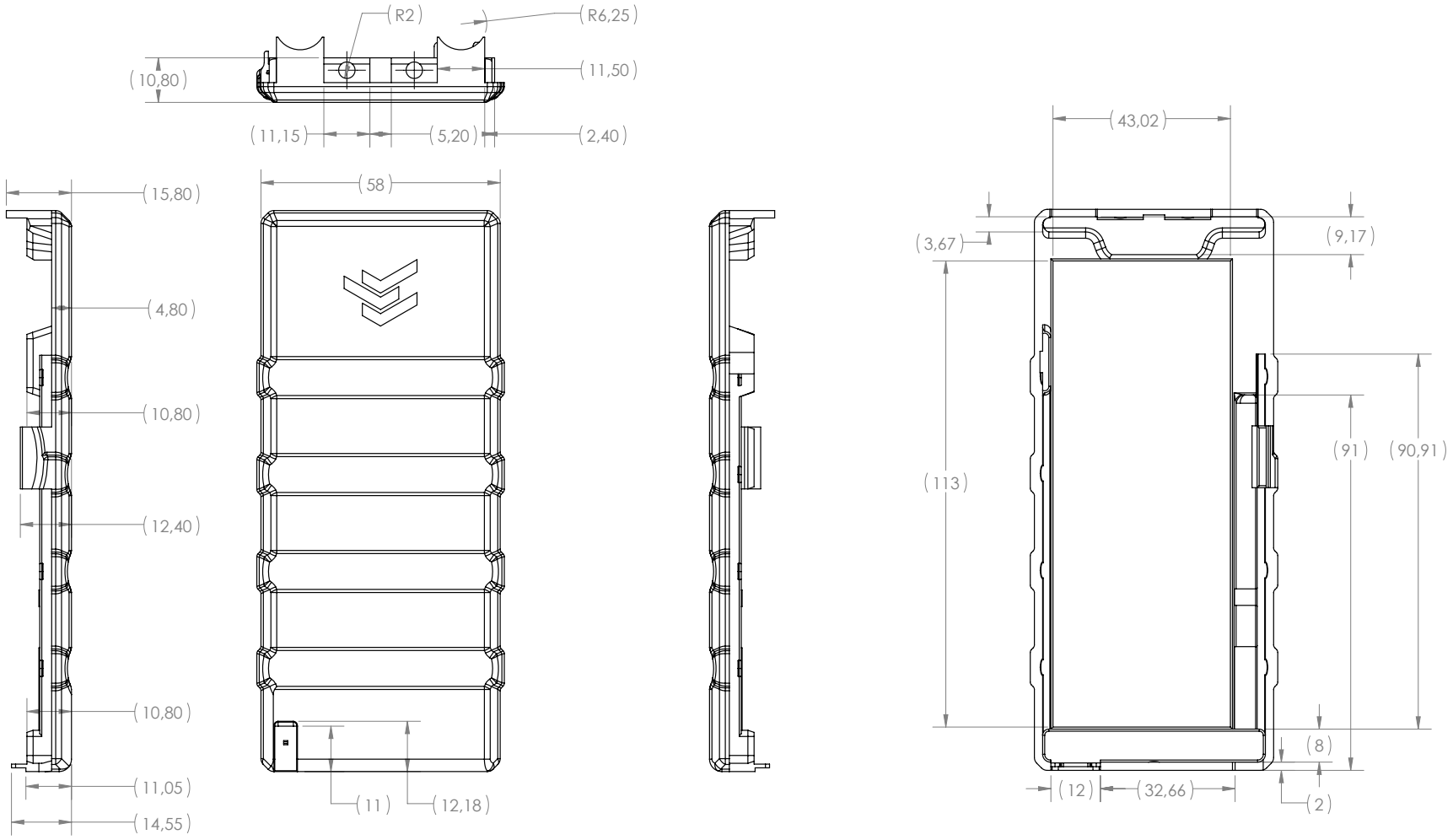

UNLESS OTHERWISE SPECIFIED:		
DIMENSIONS ARE IN MILLIMETERS		
TOLERANCES:		
ANGULAR: MACH ±0°10'		
ONE PLACE DECIMAL ±0.5		
TWO PLACE DECIMAL ±0.1		
INTERPRET GEOMETRIC TOLERANCING PER: ASME Y14.5		
MATERIAL: Case: PLA		
FINISH: Matte		
C/ FUENTE NUEVA S/N, 18001 GRANADA.	DO NOT SCALE DRAWING	

	NAME	DATE
DRAWN	Juan Del Pino Mena	26/07/22
CHECKED	Andrés Roldán	
ENG APPR.		
MFG APPR.		
Q.A.		
COMMENTS:		

AUTHOR: Juan Del Pino Mena

TITLE: Case parts Bottom cover

SIZE	DWG. NO.	REV
B	2.2 - Dimensions	6

SCALE: 1:1 | WEIGHT: 52 g | SHEET 5 OF 7

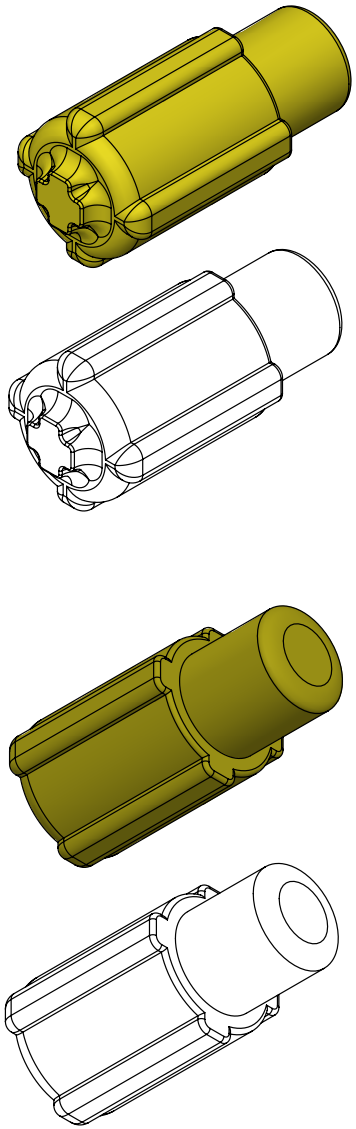

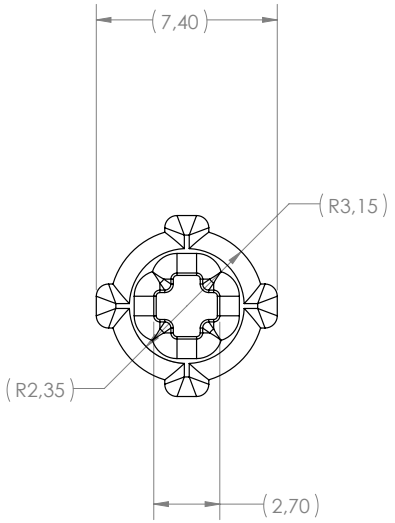

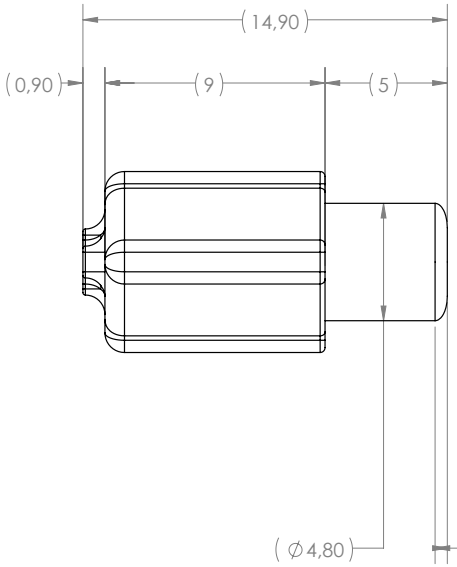

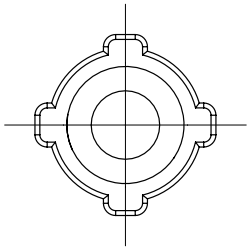

UNLESS OTHERWISE SPECIFIED:		
DIMENSIONS ARE IN MILLIMETERS TOLERANCES: ANGULAR: MACH ±0°10' ONE PLACE DECIMAL ±0.5 TWO PLACE DECIMAL ±0.1		
INTERPRET GEOMETRIC TOLERANCING PER: ASME Y14.5		
MATERIAL	Case: PLA	
FINISH	Matte	
C/ FUENTE NUEVA S/N, 18001 GRANADA.	DO NOT SCALE DRAWING	

	NAME	DATE
DRAWN	Juan Del Pino Mena	26/07/22
CHECKED	Andrés Roldán	
ENG APPR.		
MFG APPR.		
Q.A.		
COMMENTS:		

AUTHOR: Juan Del Pino Mena

TITLE: Case parts Button

SIZE	DWG. NO.	REV
B	3.1 - All	6

SCALE: 5:1	WEIGHT: 1 g	SHEET 6 OF 7

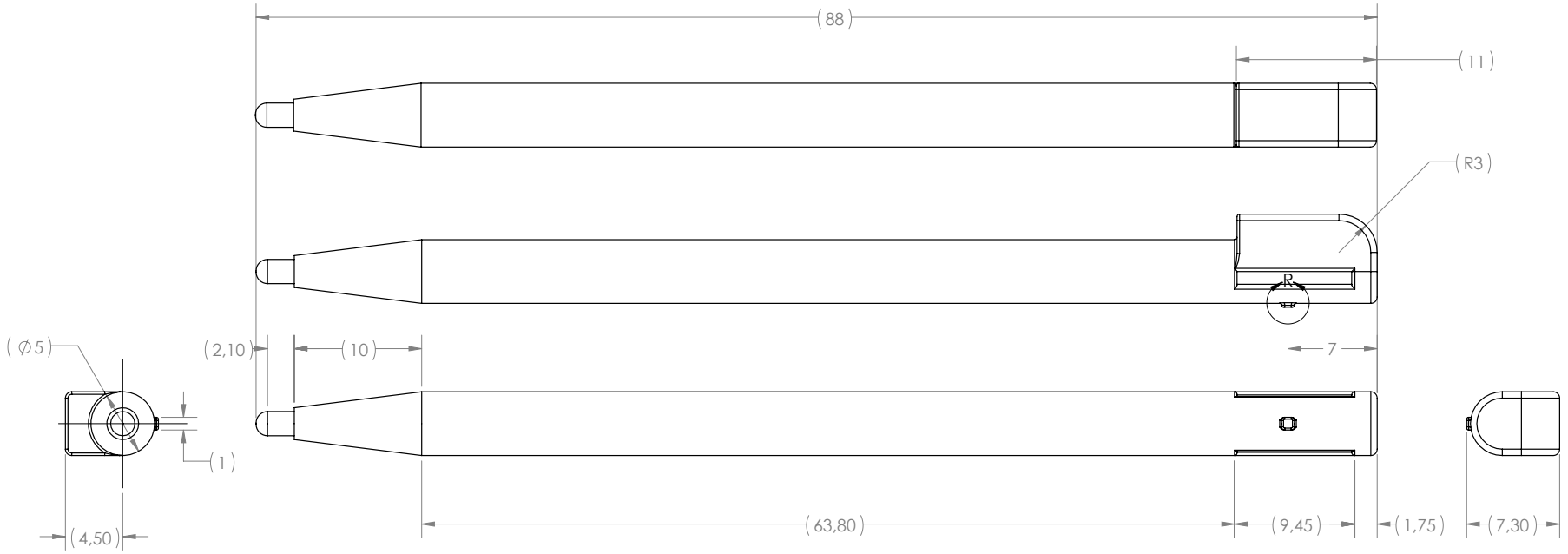

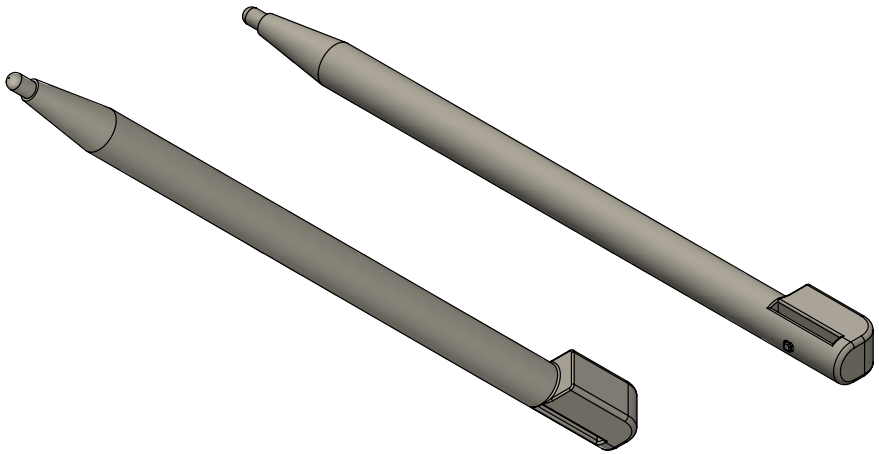

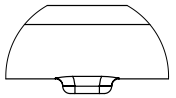

DETAIL R
SCALE 10 : 1

UNLESS OTHERWISE SPECIFIED:		
DIMENSIONS ARE IN MILLIMETERS TOLERANCES: ANGULAR: MACH ±0°10' ONE PLACE DECIMAL ±0.5 TWO PLACE DECIMAL ±0.1		
INTERPRET GEOMETRIC TOLERANCING PER: ASME Y14.5		
MATERIAL	Case: PLA	
FINISH	Matte	
C/ FUENTE NUEVA S/N, 18001 GRANADA.	DO NOT SCALE DRAWING	

	NAME	DATE
DRAWN	Juan Del Pino Mena	26/07/22
CHECKED	Andrés Roldán	
ENG APPR.		
MFG APPR.		
Q.A.		
COMMENTS:		

AUTHOR: Juan Del Pino Mena

TITLE: Case parts Stylus

SIZE	DWG. NO.	REV
B	4.1 - All	6

SCALE: 3:1 | WEIGHT: 10 g | SHEET 7 OF 7

E.2 Mechanical schematics of the complete assembly

The following pages contain a 4-sheet PDF with mechanical drawings of the complete assembly of the TIK prototype. The most relevant components are numbered, so the reader can easily recognize the parts on different views. Table E.1 relates each number to the part it identifies.

Part number in assembly	Description of the component
1	Top cover (3D printed part).
2	Bottom cover (3D printed part).
3	Stylus for the touchscreen.
4	Threaded insert, size M3, length 5 mm.
5	Power-on/off button plunger (3D printed part).
6	Flat head torx screw, ISO 10642, size: M3, length: 8 mm.
7	Printed Circuit Board
8	Female 3.5 mm jack connector.
22	Female BNC connector.
36	Power-on push-button.
37	Multi-direction 'thumb' button.
44	Female USB-Mini-B connector.
46	LCD screen module PCB
52	TFT LCD screen
53	Socket Cap head hex screw, ISO 4762, size: M3 length: 16 mm.
54	Flat Li-Po battery, 604060 format (6x40x60 mm)

Table E.1 – *Number in assembly and the component it identifies.*

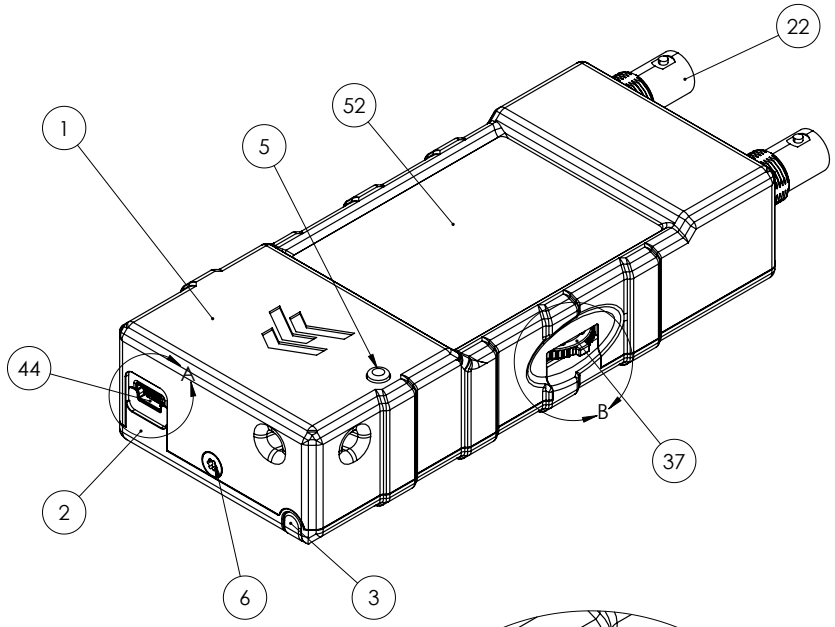

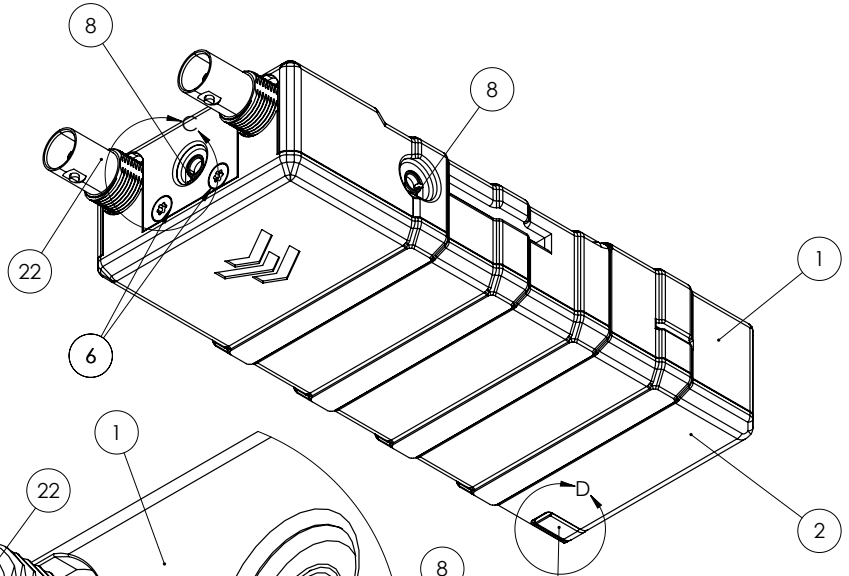

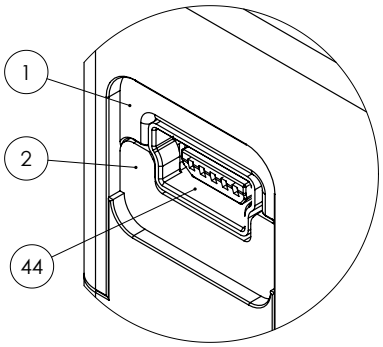

DETAIL A
SCALE 4 : 1

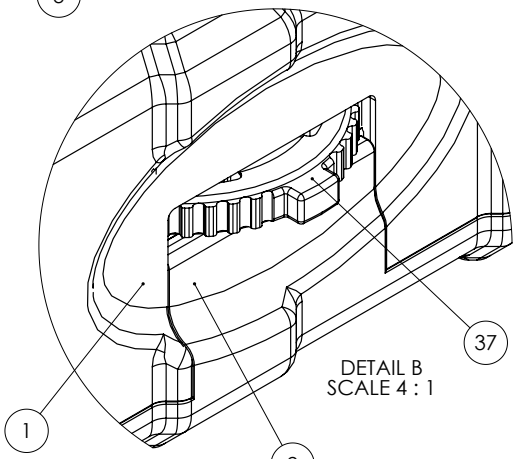

DETAIL B
SCALE 4 : 1

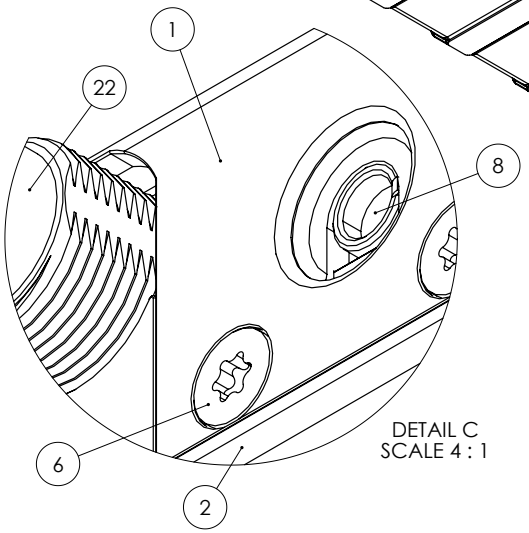

DETAIL C
SCALE 4 : 1

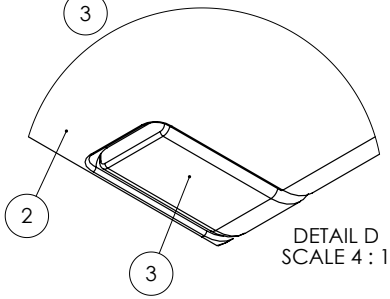

DETAIL D
SCALE 4 : 1

UNLESS OTHERWISE SPECIFIED:		
DIMENSIONS ARE IN MILLIMETERS TOLERANCES: ANGULAR: MACH ±0°10' ONE PLACE DECIMAL ±0.5 TWO PLACE DECIMAL ±0.1		
INTERPRET GEOMETRIC TOLERANCING PER: ASME Y14.5		
MATERIAL: Case: PLA		
FINISH: Matte		
C/ FUENTE NUEVA S/N, 18001 GRANADA.	DO NOT SCALE DRAWING	

	NAME	DATE
DRAWN	Juan Del Pino Mena	26/07/22
CHECKED	Andrés Roldán	
ENG APPR.		
MFG APPR.		
Q.A.		
COMMENTS:		

AUTHOR: Juan Del Pino Mena

TITLE: Case assembly with PCB

SIZE	DWG. NO.	REV
B	1 - Collapsed view	6

SCALE: 1:1 | WEIGHT: 210 g | SHEET 1 OF 4

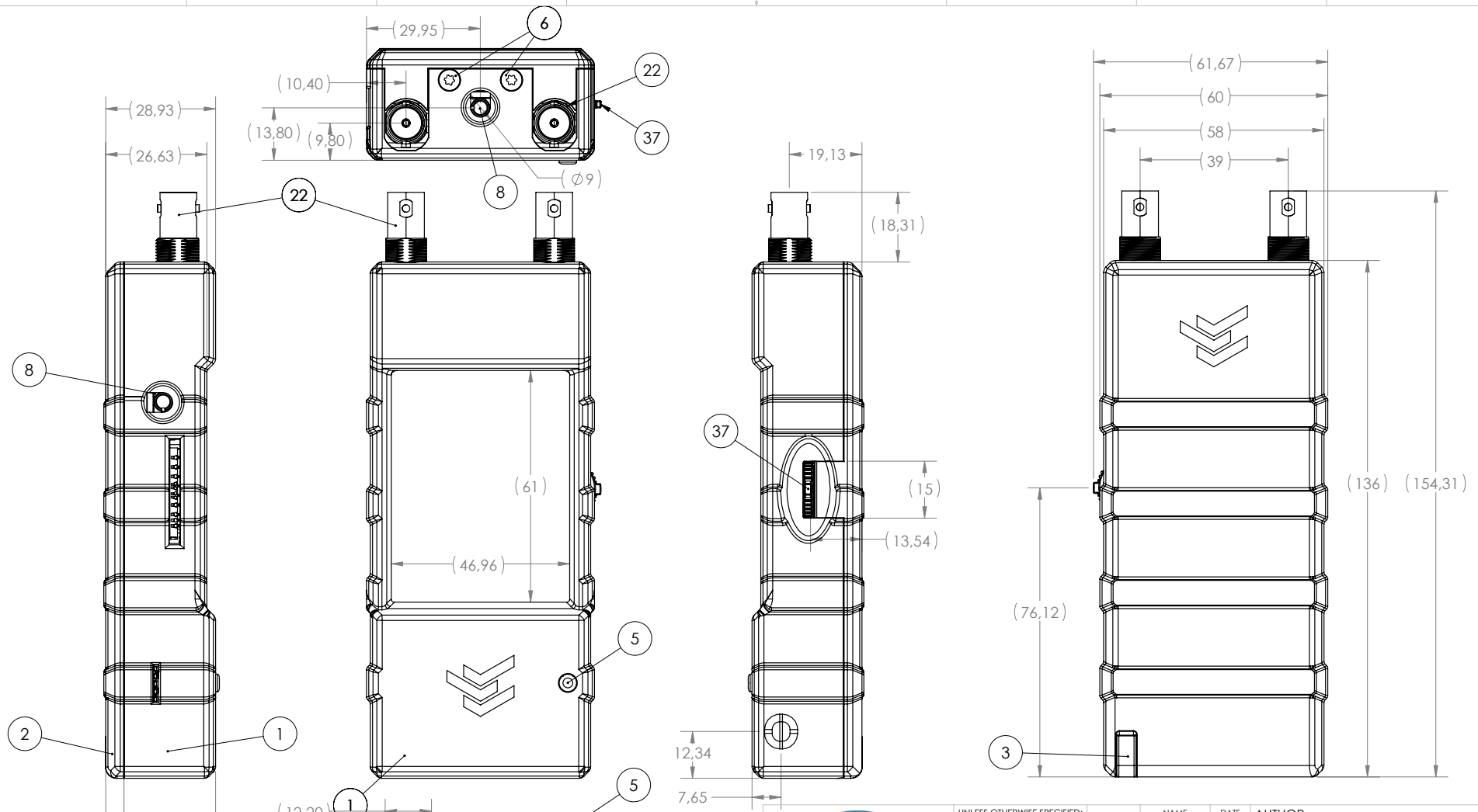

UNLESS OTHERWISE SPECIFIED:	NAME	DATE
DIMENSIONS ARE IN MILLIMETERS	DRAWN	Juan Del Pino Mena 26/07/22
TOLERANCES:	CHECKED	Andrés Roldán
ANGULAR: MACH ±0°10'	ENG APPR.	
ONE PLACE DECIMAL ±0.5	MFG APPR.	
TWO PLACE DECIMAL ±0.1	Q.A.	
INTERPRET GEOMETRIC TOLERANCING PER: ASME Y14.5	COMMENTS:	
MATERIAL Case: PLA		
FINISH Matte		

C/ FUENTE NUEVA S/N, 18001 GRANADA.

DO NOT SCALE DRAWING

AUTHOR: Juan Del Pino Mena

TITLE: Case assembly with PCB

SIZE	DWG. NO.	REV
B	2 - Dimensions	6

SCALE: 1:1 | WEIGHT: 210 g | SHEET 2 OF 4

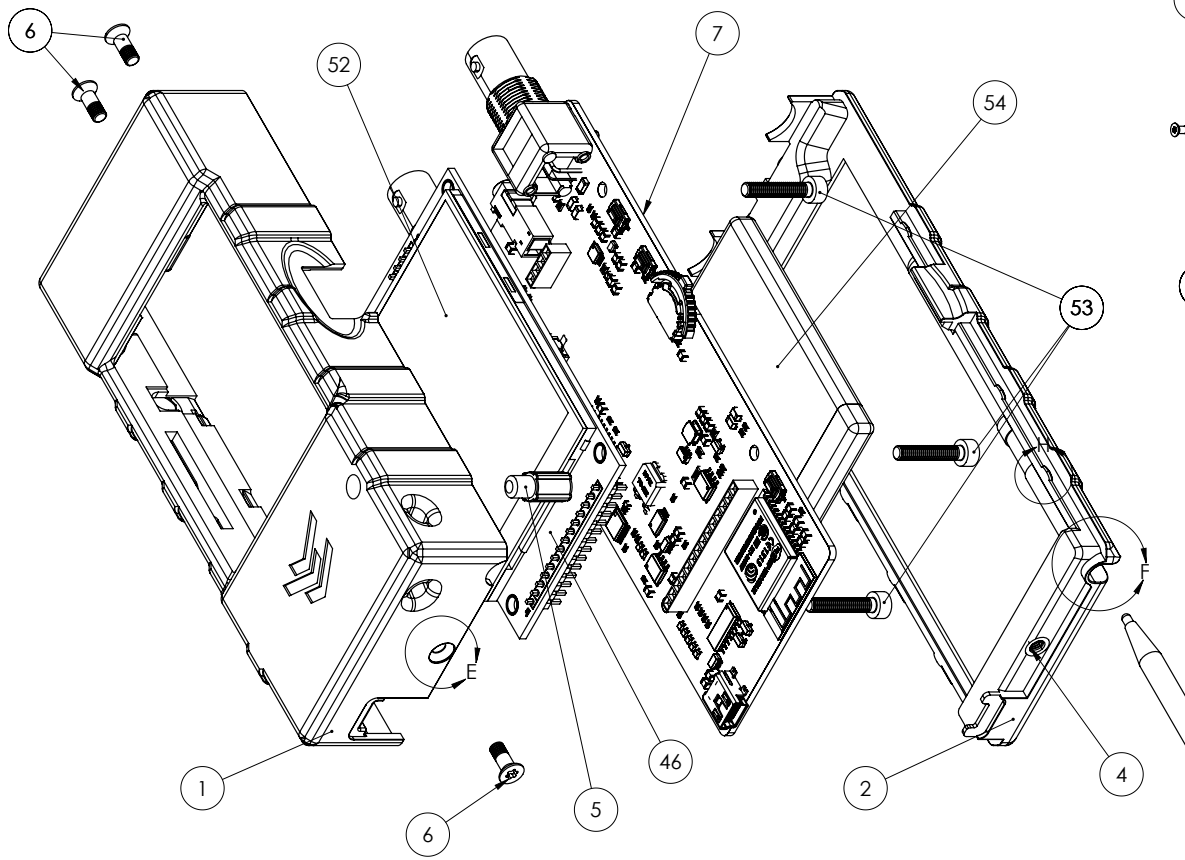

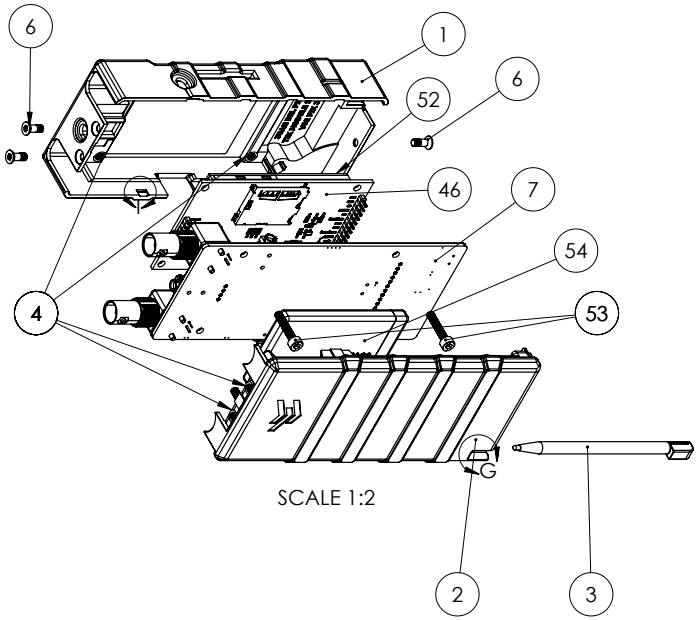

SCALE 1:2

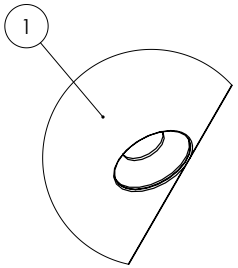

DETAIL E
SCALE 3 : 1

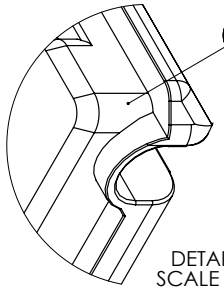

DETAIL F
SCALE 3 : 1

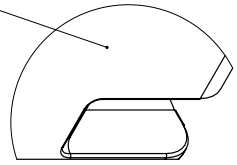

DETAIL G
SCALE 3 : 1

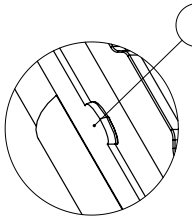

DETAIL H
SCALE 3 : 1

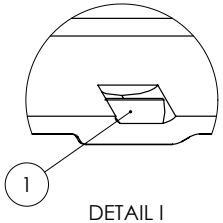

DETAIL I
SCALE 3 : 1

UNLESS OTHERWISE SPECIFIED:		
DIMENSIONS ARE IN MILLIMETERS TOLERANCES: ANGULAR: MACH ±0°10' ONE PLACE DECIMAL ±0.5 TWO PLACE DECIMAL ±0.1		
INTERPRET GEOMETRIC TOLERANCING PER: ASME Y14.5		
MATERIAL: Case: PLA		
FINISH: Matte		
C/ FUENTE NUEVA S/N, 18001 GRANADA.	DO NOT SCALE DRAWING	

	NAME	DATE
DRAWN	Juan Del Pino Mena	26/07/22
CHECKED	Andrés Roldán	
ENG APPR.		
MFG APPR.		
Q.A.		
COMMENTS:		

AUTHOR: Juan Del Pino Mena

TITLE: Case assembly with PCB

SIZE	DWG. NO.	REV
B	3 - Exploded view	6

SCALE: 1:1 | WEIGHT: 210 g | SHEET 3 OF 4

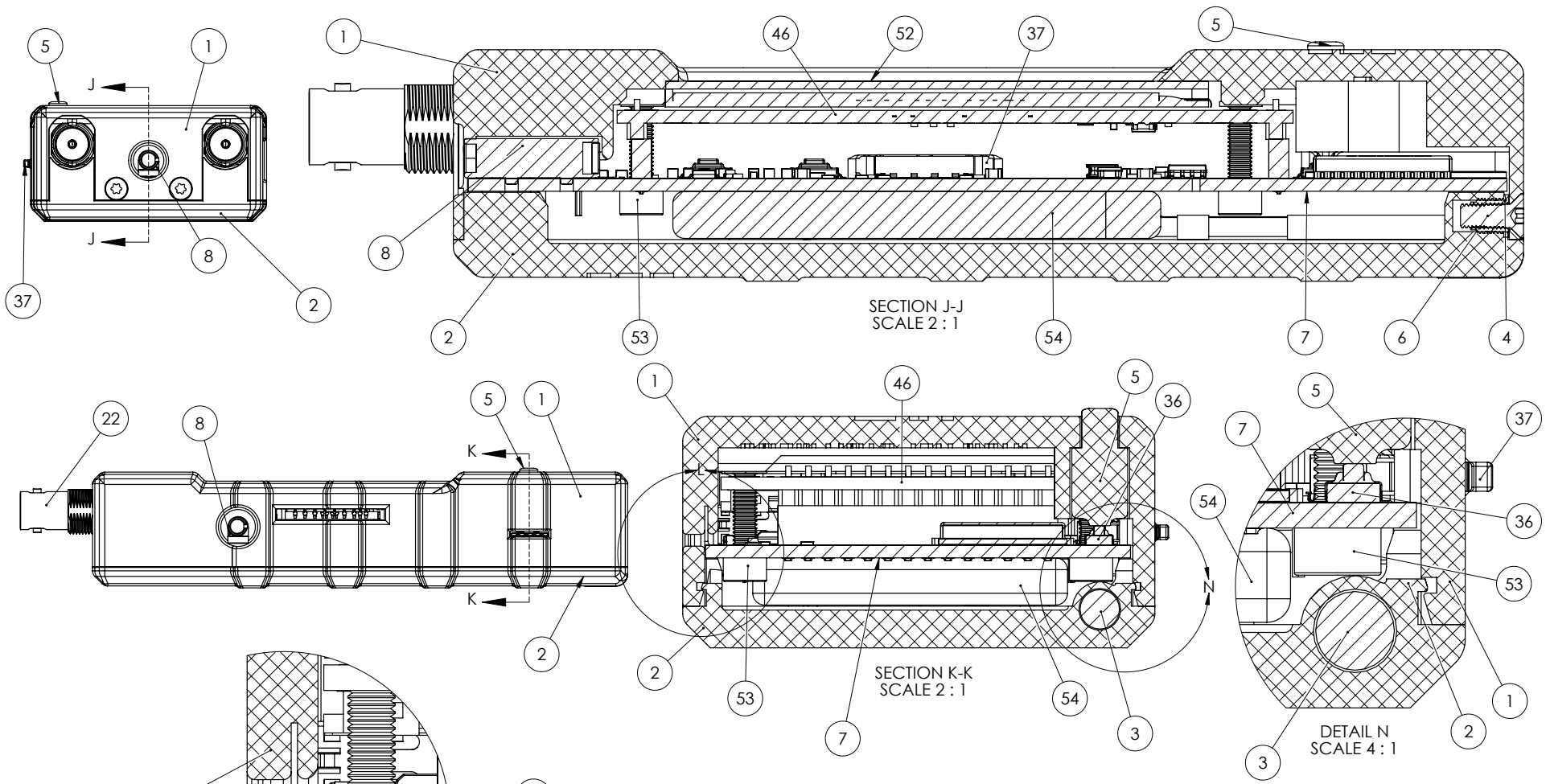

UNLESS OTHERWISE SPECIFIED:		
DIMENSIONS ARE IN MILLIMETERS TOLERANCES: ANGULAR: MACH ±0°10' ONE PLACE DECIMAL ±0.5 TWO PLACE DECIMAL ±0.1		
INTERPRET GEOMETRIC TOLERANCING PER: ASME Y14.5		
MATERIAL	Case: PLA	
FINISH	Matte	
C/ FUENTE NUEVA S/N, 18001 GRANADA.	DO NOT SCALE DRAWING	

	NAME	DATE
DRAWN	Juan Del Pino Mena	26/07/22
CHECKED	Andrés Roldán	
ENG APPR.		
MFG APPR.		
Q.A.		
COMMENTS:		

AUTHOR: Juan Del Pino Mena

TITLE: Case assembly with PCB

SIZE	DWG. NO.	REV
B	4 - Section views	6

SCALE: 1:1	WEIGHT: 210 g	SHEET 4 OF 4

E.3 Renders of the complete assembly of the product. Collapsed view

Figure E.1 – *Front, collapsed view render of the complete assembly.*

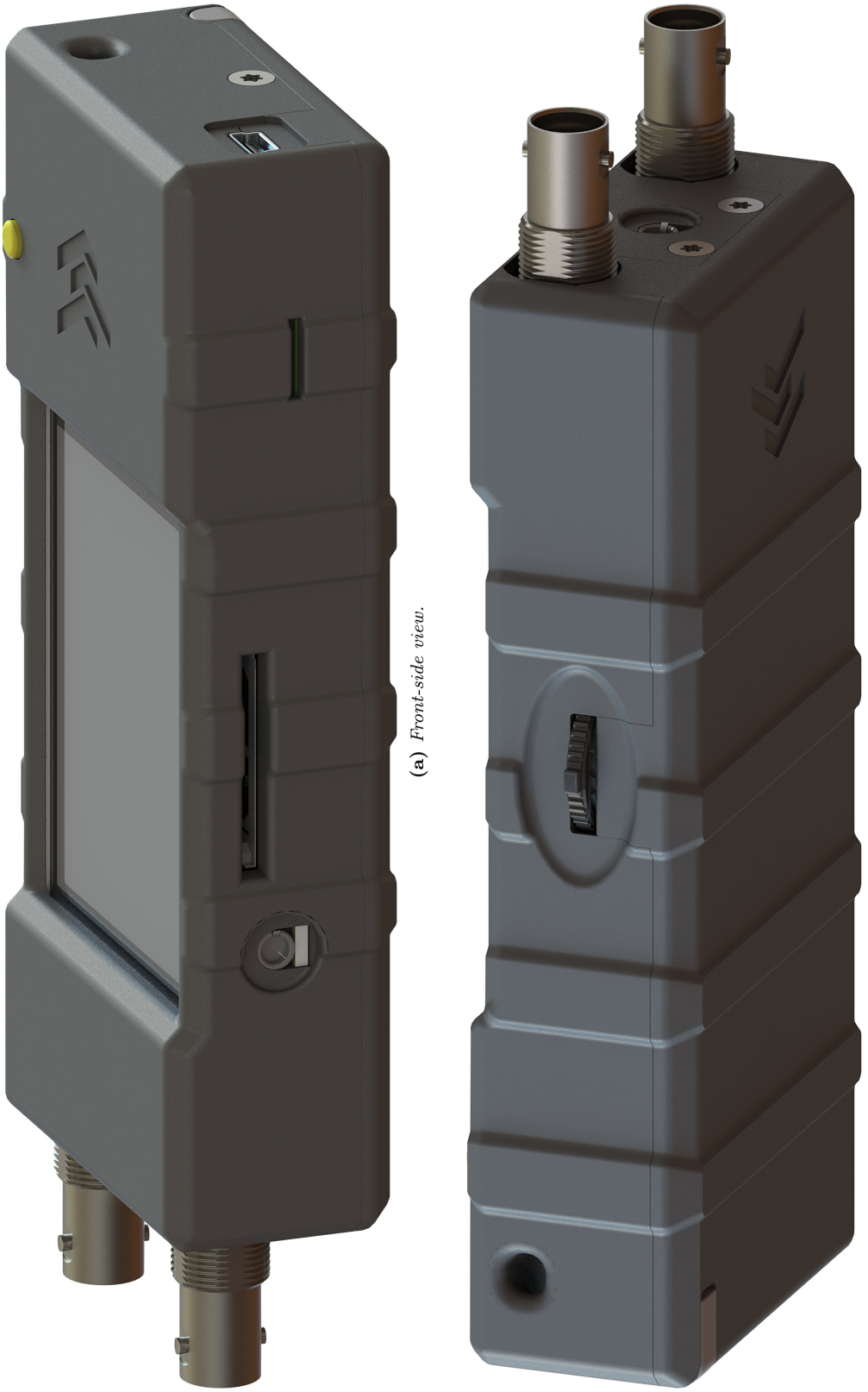

(a) *Front-side view.*

(b) *Back-side view.*

Figure E.2 – *Front-side and Back-side, collapsed view renders of the complete assembly.*

E.4 Renders of the complete assembly of the product. Exploded view

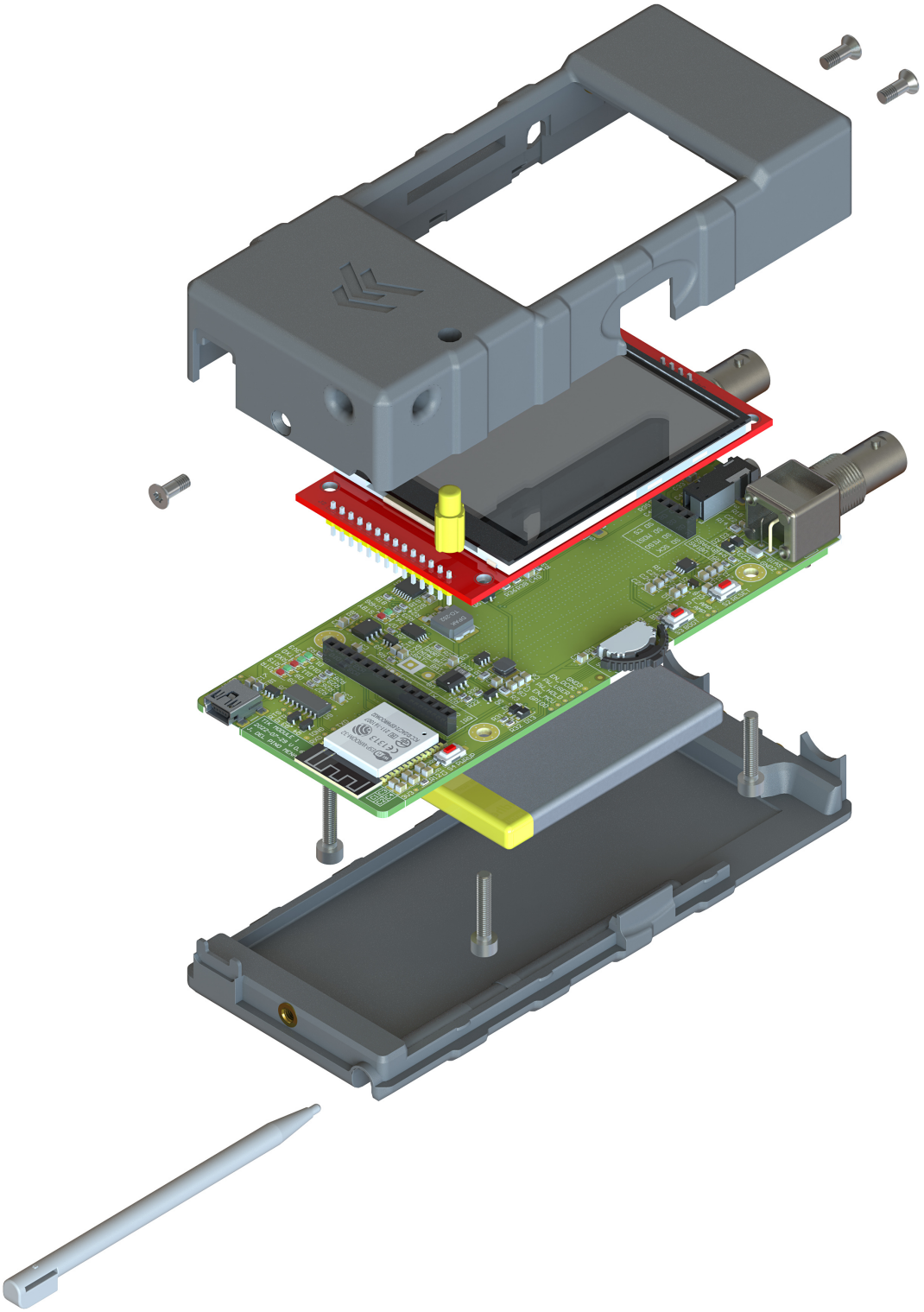

Figure E.3 – *Top-side exploded view render of the complete assembly.*

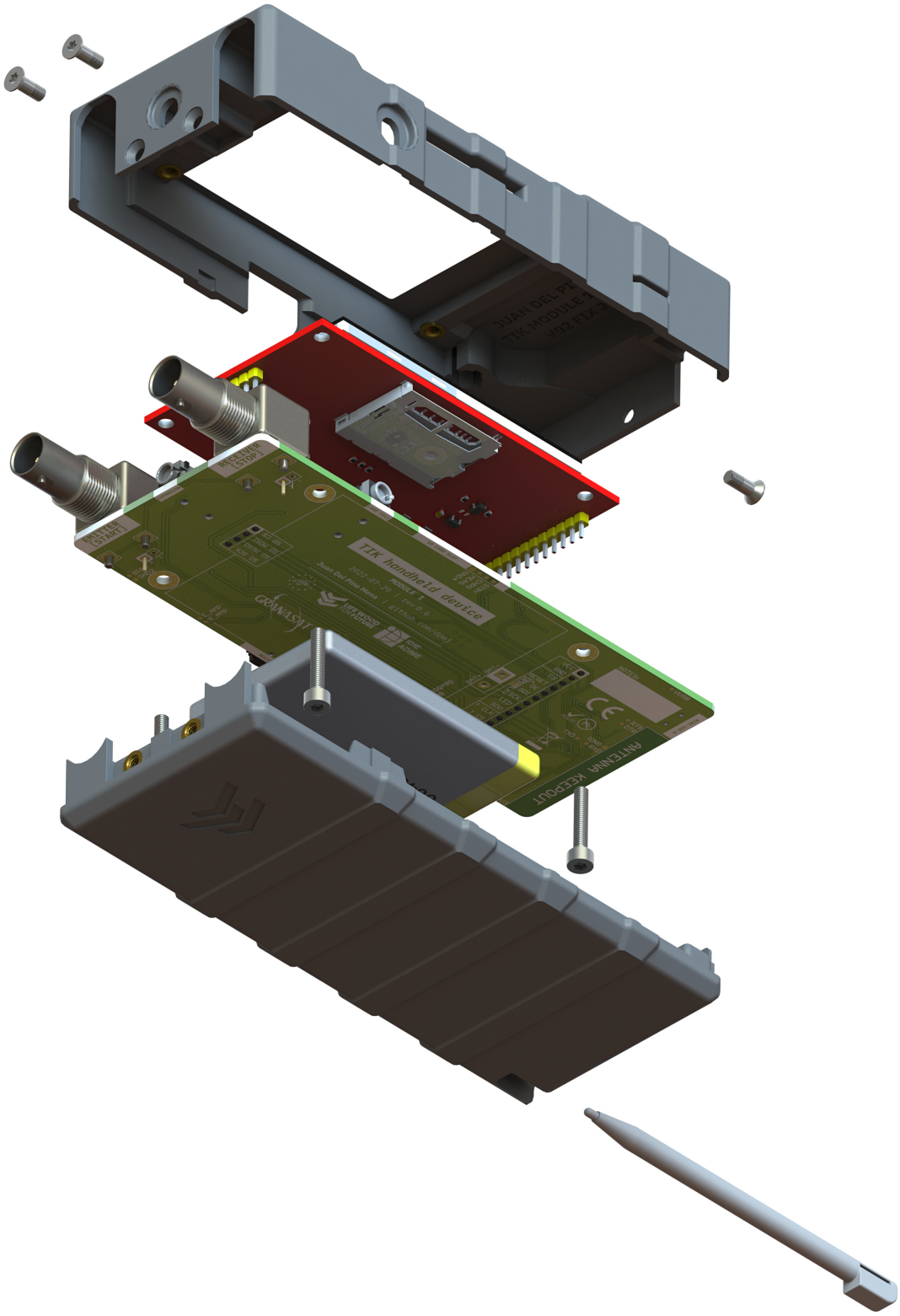

Figure E.4 – *Bottom-side exploded view render of the complete assembly.*

Appendix F

Handling of electronic instrumentation

During the development of this thesis it was necessary to resort to electronic instrumentation for various reasons:

- To generate replicas of the sensor signals under demand in a realistic but repeatable way. Diverse parameters will be configurable, such as amplitude and delay between emitter and receiver signals. For this, a **HP 33120A** and then a **Siglent SDG1062X** arbitrary waveform generators were used.

  At first, it was intended to use two HP33120A, one as the *emitter* signal generator and the other as the *receiver* signal generator. This last would be triggered by the first one. These devices can be controlled using a GPIB interface. As many modern computers do not include a GPIB port nowadays, a USB to GPIB (USB2GPIB) mediator was required.

  However, there seems to be a problem with the transfer of signal samples to the HP33120A, so we abandoned these equipment and focused our efforts on the SDG1062X.

  These instrumentation was managed through the development of two different Python utilities that send SCPI commands to the devices. These python libraries were written using the Jupyter Lab environment for easy simultaneous programming, debugging and documentation.

- To find the circuit equivalent of the piezoelectric sensors in frequency. For this purpose it was used an **Agilent/HP 4192A LF** impedance analyzer. Although this device allows to be controlled over a GPIB interface

- To measure the power consumption of different electronic components and the finished product itself. A **Siglent SDM3065X** digital multimiter was used.

F.1 HP33120A function/arbitrary waveform generator

The HP 33120A is a 15 MHz function generator with built-in arbitrary waveform capabilities. It has 10 standard waveforms already built-in, which synthesises using a 12-bit, 40 MSa/s DAC. This device may seen old-fashioned by nowadays standards, but its lifetime can be greatly extended since it's programmable and compatible with SCPI commands.

It has sufficient onboard memory to download up to four 16.000 point arbitrary waveforms via the GPIB port or via the RS-232 interface on the back of the instrument. It also has an external trigger port (input, on the back) and a sync port (output, on the front) which can be used to trigger both sources at the same time.

This device is well documented, with a complete User's Guide [179] with command references and even programming examples.

F.1.1 Development notes

- **Repository:** `https://github.com/granasat/HP3312A-jupyter-USB2GPIB-instrument-library`
- **Python version:** This utility was developed using Python 3.9.
- **Library requirements:** Third-party dependencies for running this application, with their corresponding versions used during the development.
  - `numpy`, version 1.22.

F.1.1.1 Changelog

- **v01 - 30/09/2021 - Prof. Andrés Roldán Aranda**
  - Initial implementation.
- **v02 - 31/01/2022 - Juan del Pino Mena**
  - Instructions for running the utility on GNU/Linux.
  - Code style standardization (comments, indent, spacing, etc.).
  - Code documentation.
  - Implementation of two Python classes:
    - `USB2GPIB` class: methods to communicate with the USB2GPIB mediator, using "++" commands.
    - `HP33120A` class: methods for handling the arbitrary waveform generator through commands.
  - Setup and output of built-in signals.
  - Setup of arbitrary waveforms and samples sending.
  - External trigger configuration.
  - Translation to English.

F.1.1.2 Known issues

This library is incomplete due to issues encountered during sample transmission. The device will accept samples until the command terminator is received, moment where the device will give an error of the kind: `103: Invalid separator`; which refers to a misuse of a comma, colon or semicolon. However, there's no incorrect usage in the developed utility. No solution has been found yet.

For a fully working program refer to the **SDG1062X generator** section.

F.1.2 Connection to the device

The connection between the operator's PC and the electronic instrument requires a USB to GPIB converter or mediator. Multiple devices can be connected to the same GPIB bus in parallel and will respond to different addresses (see Figure F.2). The role of this mediator is assumed by an Arduino UNO running Emanuele Girlando's USB2GPIB open source firmware [183]. The mediator is configured using commands which begin with the key characters "++".

As for how to detect and identify the device, it depends on the operating system used:

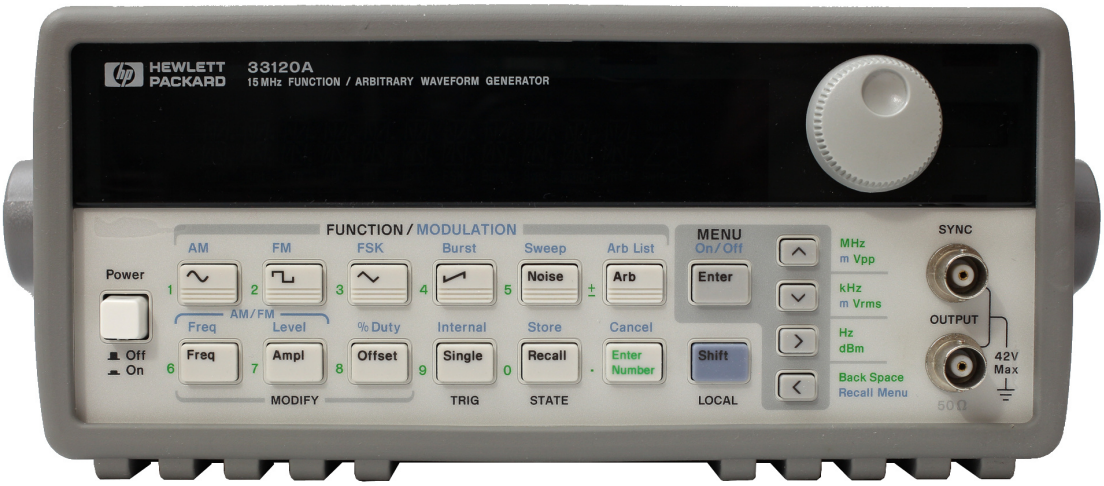

(a) *Front view.*

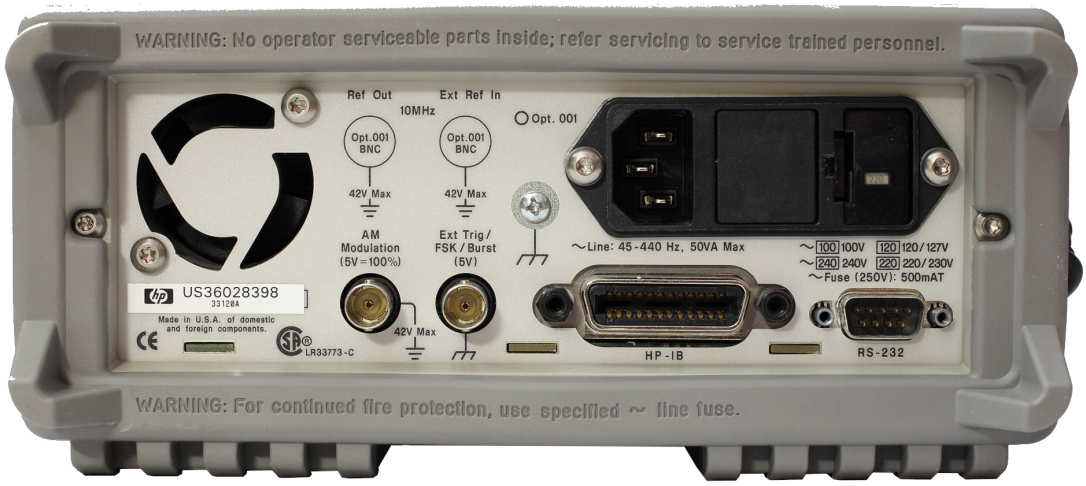

(b) *Back view.*

Figure F.1 – *The HP33120A function/arbitrary waveform generator. Credits: [182].*

F

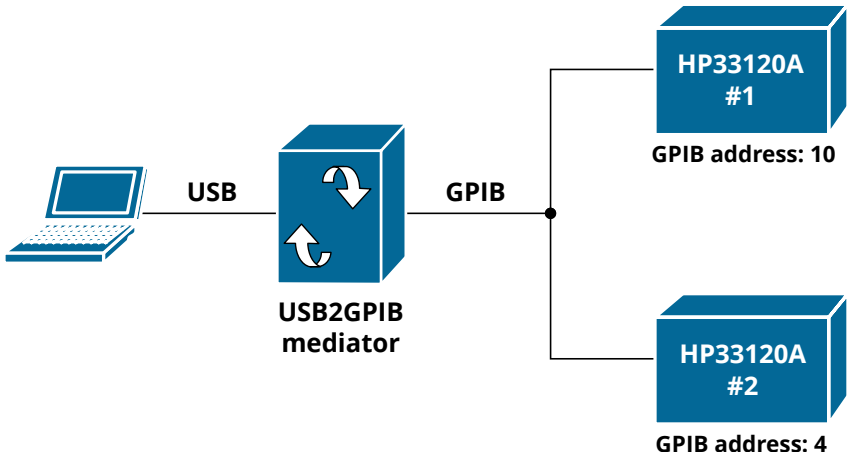

Figure F.2 – *Representation of the connection used to communicate the operator's PC and the HP3310A.*

- On Windows the mediator is identified as an USB-SERIAL CH340 on the Windows Device Manager, and will be accessible over a COM port. A CH340C driver install may be necessary for this to happen.
- On GNU/Linux, USB devices are listed as `/dev/ttyUSB*` (most often a single serial device will be just `/dev/ttyUSB0` regardless of which physical USB port it is connected to). No need to install any drivers, but the user may need to be added to a group (like `dialout` or `uucp`) in order to have permissions to access the USB device. In case there are more serial devices connected, we can quickly identify our target with some commands (Listing F.1):
  - `lsusb` lists USB devices. They are identified by an ID (in the case of CH340: `1a86:7523`).
  - `ls /dev/USB*` shows all USB devices plugged to the host.
  - `grep PRODUCT=/sys/bus/usb-serial/devices/ttyUSB0/../uevent` allows us to check which `ttyUSB` corresponds to which USB device, identified by its ID. We confirm that the ID of `ttyUSB0` is the same ID of the CH340.

```
$ lsusb
Bus 002 Device 001: ID 1d6b:0003 Linux Foundation 3.0 root hub
Bus 001 Device 008: ID 06cb:00a2 Synaptics, Inc. Metallica MOH Touch Fingerprint Reader
Bus 001 Device 003: ID 5986:2113 Acer, Inc SunplusIT Integrated Camera
Bus 001 Device 009: ID 1a86:7523 QinHeng Electronics CH340 serial converter
Bus 001 Device 001: ID 1d6b:0002 Linux Foundation 2.0 root hub

$ ls /dev/ttyUSB*
/dev/ttyUSB0

$ grep PRODUCT=/sys/bus/usb-serial/device4/ttyUSB0/../uevent
PRODUCT=1a86/7523/263
```

Listing F.1 – *Commands to identify the desired `/dev/ttyUSB*` port. Highlighted characters show the CH340 ID (blue) and its corresponding `ttyUSB` (red).*

F.1.3 Library implementation

Due to the USB2GPIB mediator, two python classes were written. The first, called `USB2GPIB` is a simple class that contains configuration functions for the mediator. It uses "++" commands sent over a serial port.

Not all the available commands that the firmware allows are implemented, only the most important ones that let us access the GPIB bus and configure the connected devices. The second class is called `HP33120A` and it is responsible for handling the commands sent to the arbitrary generator.

```
import serial
import time

# port_USB2GPIB = 'COM3'  # On Windows = COMx, with x={1, 2, ...}
port_USB2GPIB = '/dev/ttyUSB1'  # On Linux: /dev/ttyUSBx, with x = {0, 1, ...}
timeout = 0.5  # Global timeout in seconds

s = serial.Serial(port_USB2GPIB,        # Port
                  115200,               # Bauds
                  serial.EIGHTBITS,     # 8-bit payload
                  serial.PARITY_NONE,   # No parity bit
                  serial.STOPBITS_ONE,  # One stop bit
                  timeout=timeout,      # Dropout timeout
                  rtscts=False)         # RTS->CTS
```

Listing F.2 – *Prior serial initialization and configuration for the USB2GPIB mediator.*

```
class USB2GPIB:
    """
    Collection of methods to communicate with the USB2GPIB mediator running the
    "Arduino UNO as a USB to GPIB adapter / controller" v6.1 firmware by
    Emanuele Girlando.
    """

    def __init__(self, length_string_read=100):
        """
        Constructor.
        :param length_string_read: no. of characters to read from buffer. Defaults to 100.
        :type length_string_read int
        """
        self.length_string_read = length_string_read

    def _send(self, cmd, verbose=True):
        """
        Sends messages to the mediator. Resets the buffer every time it is called.
        :param cmd: Command to send
        :type cmd str
        """
        s.reset_input_buffer()  # reset del buffer
        s.write(cmd.encode() + b'\r\n')  # comando + caracteres de parada, bytes
        if verbose:
            print(f"Sent: {cmd}")

    def _read(self, verbose=True):
        """
        Reads messages coming from the mediator from the serial buffer.
        :returns out: incoming message
        :type out str
        """
        out = s.read(self.length_string_read)  # Reads from serial buffer
        if verbose:
            print(f"Read: {str(out)}")
        return out

    def identify(self, verbose=True):
        """
        Identifies the mediator
        Read ++ver
```

```
        """
        cmd = "++ver"
        self._send(cmd, verbose)
        return self._read(verbose)

    def set_auto_response(self, auto_mode=0, verbose=True):
        """
        Send command to establish the automatic response of the mediator and
        not have to do a ++read for each command sent.
        Send ++auto <auto_mode>
        :param mode: Response mode, defaults to 0 (auto_mode=0)
        """
        cmd = f"++auto {auto_mode}"
        self._send(cmd, verbose)

    def get_auto_response(self, verbose=True):
        """
        Queries the mediator its auto-response state.
        Send ++auto
        """
        cmd = "++auto"
        self._send(cmd, verbose)
        return self._read(verbose)

    def set_slave_address(self, address, verbose=True):
        """
        Establishes the GPIB slave address to talk to
        Send ++addr Address
        :param address: dirección del equipo esclavo a comunicar por GPIB.
        """
        cmd = f"++addr {str(address)}"
        self._send(cmd, verbose)

    def get_slave_address(self, verbose=True):
        """
        Consulta la dirección del esclavo
        Send ++addr
        """
        cmd = "++addr"
        self._send(cmd, verbose)
        return self._read(verbose)
```

Listing F.3 – *USB2GPIB mediator handler class.*

F

```
class HP33120A:
    """
    HP33120A Generator handler

    NOTE: The methods of this class expect the communication to be carried out by serial,
    requiring an intermediary USB2GPIB mediator. To communicate with each connected device,
    you must first specify the address corresponding to the mediator.
    """

    def __init__(self, length_string_read=100):
        """
        Constructor.
        :param length_string_read: no. of characters to read from buffer. Defaults to 100.
        This parameter affects commands that are too long, such as sending signal samples.
        :type length_string_read int
        """
        self.length_string_read = length_string_read

    def _send(self, cmd, verbose=True):
        """
```

```
        Sending messages to the mediator. It resets the buffer on each call.
        :param cmd: Command to send
        :type cmd str
        """
        s.reset_input_buffer()  # Buffer reset
        s.write(cmd.encode() + b'\r\n')  # Command + stop characters (encoded)
        if verbose:
            print(f"Sent: {cmd}")

    def _read(self, verbose=True):
        """
        Receives messages coming from the device
        :returns out: Incoming message
        :type out str
        """
        s.write(b'++read\r\n')
        out = s.read(self.length_string_read)  # Reads from serial buffer
        if verbose:
            print(f"Read: {str(out)}")
        return out

    # SYSTEM COMMANDS
    # System functions: management, queries, reset.

    def reset(self, verbose=True):
        """
        Sends a reset
        Send *RST
        User's Manual, pag. 190
        """
        cmd = "*RST"
        self._send(cmd, verbose)

    def identify(self, verbose=True):
        """
        Identifies the generator
        Send *IDN?
        User's Manual, pag. 190
        """
        cmd = "*IDN?"
        self._send(cmd, verbose)
        return self._read()

    def version(self, verbose=True):
        """
        Asks for the system's version
        Send SYSTem:VERSion?
        User's Manual, pag. 190
        """
        cmd = "SYSTem:VERSion?"
        self._send(cmd, verbose)
        return self._read()

    def error(self, verbose=True):
        """
        Read from the error stack. It is a FIFO stack.
        Send SYSTem:ERRor?
        User's Manual, pag. 110
        """
        cmd = "SYSTem:ERRor?"
        self._send(cmd, verbose)
        return self._read()

    # OUTPUT WAVEFORM COMMANDS
    # Functions to vary the output conditions: amplitude, frequency, offset and load type.

```

```
    def set_amplitude(self, vpp, verbose=True):
        """
        Peak-peak voltage of the signal (twice the amplitude).
        The value of the load at the output must be adjusted to obtain the desired value.
        Send VOLT <vpp>
        User's Manual, pag. 148
        """
        cmd = f"VOLT {vpp}"
        self._send(cmd, verbose)

    def set_frequency(self, freq, verbose=True):
        """
        Signal frequency. In arbitrary signals it is NOT the sampling frequency but the
        repetition frequency of the complete signal.
        Send FREQ <freq>
        User's Manual, pag. 146
        """
        cmd = f"FREQ {freq}"
        self._send(cmd, verbose)

    def set_offset(self, offset, verbose=True):
        """
        Sets the output DC voltage offset
        Send VOLT:OFFS
        User's Manual, pag. 149
        """
        cmd = f"VOLT:OFFS {offset}"
        self._send(cmd, verbose)

    def set_output_load(self, load, verbose=True):
        """
        Sets the type of load. For Hi-Z, specify "INF"
        Send OUTP:LOAD <load>. Load options: {50|INF}
        User's Manual, pag. 149
        """
        cmd = f"OUTP:LOAD {load}"
        self._send(cmd, verbose)

    def set_output_waveform(self, func, verbose=True):
        """
        Sets the output waveform
        Send FUNC:SHAP <func>. Signal options: SIN, SQU, TRI, RAMP, NOIS, DC
        User's Manual, pag. 145
        """
        cmd = f"FUNC:SHAP {func}"
        self._send(cmd, verbose)

    def get_output_waveform(self, verbose=True):
        """
        Gets the actual output waveform.
        Send FUNC:SHAP?
        """
        cmd = f"FUNC:SHAP?"
        self._send(cmd, verbose)
        return self._read(verbose)

    def get_output_parameters(self, verbose=True):
        """
        Gets the current output parameters.
        Send APPLy?
        """
        cmd = "APPLy?"
        self._send(cmd, verbose)
        return self._read(verbose)

    # BURST COMMANDS
```

```python
    # To generate two synchronized functions the trigger is not necessary,
    # but to use a burst modulation

    def enable_burst(self, mode : str, verbose=True):
        """
        Set up other modulation after setting other burst modulation
        Send BM:STATe {OFF|ON}
        User's Manual, pag. 84
        """
        cmd = f"BM:STATe {mode}"
        self._send(cmd, verbose)

    def set_burst_count(self, count : int, verbose=True):
        """
        Set the number of bursts
        Send BM:NCYC
        User's Manual, pag. 81
        """
        cmd = f"BM:NCYC {count}"

    # TRIGGER COMMANDS

    def set_trigger_source(self, mode : str, verbose=True):
        """
        Sets the trigger source
        Send TRIGger:SOURce <EXTernal|IMMediate|BUS>
        """
        cmd = f"TRIGger:SOURce {mode}"
        self._send(cmd, verbose)

    def get_trigger_source(self, verbose=True):
        """
        Gets the current trigger source
        Send TRIGger:SOURce?
        """
        cmd = f"TRIGger:SOURce?"
        self._send(cmd, verbose)
        return self._read(verbose)

    # ARBITRARY FUNCTION COMMANDS
    # Arbitrary function management functions.

    def arb_download_format_border(self, border, verbose=True):
        """
        Selects the bit order for binary data transfer.
        Send FORM:BORD {NORM|SWAP}
            NORM: The most significant bit (MSB) is sent first. Default.
            SWAP: The least significant bit (LSB) is sent first.
        You may have to use this function to switch to SWAP, the manual
        indicates that many PCs use the LSB-first format.
        User's Manual, pag. 180, 185

        :param border: type of transference
        :type border str
        """
        border = border.upper()
        if border != "NORM" or border != "SWAP":
            raise ValueError("Format border type must be 'NORM' or 'SWAP'.")
        cmd = "FORM:BORD {border}"
        self._send(cmd, verbose)

    def arb_download_binary_to_volatile(self, samples, verbose=True):
        """
        NOTE: IT DOESN'T WORK. Last modified: 03/1/22.
        - [ ] It seems that the binary format used is not correct.
        - [ ] It is necessary to send the data in chunks so as not to saturate the buffer.
```

```
219
220         Sending samples of an arbitrary signal. This function sends the
221         samples in binary to speed up the transmission:
222
223         [16000 samples per HP-IB (GPIB), floating point: 100 seconds]
224         [16000 samples per HP-IB (GPIB), integer: 51 seconds]
225         [16000 samples per HP-IB (GPIB), in binary: 8 seconds]
226         In RS-232 the times are greater. User's Manual, pag. 2
227
228         Send DATA:DAC VOLATILE, #XN <binary data>
229         Being #: the beginning character of the binary data block,
230                X: the number of digits below (# digits of N),
231                N: the number of bytes to send. It is equal to twice the number of
232                     signal samples: each sample will occupy 2 bytes: 12 bits
233                     per sample and the remaining 4 bits are padded with zeroes.
234         These parameters are automatically calculated by this function.
235         For example, to transmit 16000 samples, the message is sent:
236             b"DATA:DAC VOLATILE, #532000 <binary data>"
237
238         Any signal in volatile memory will be overwritten.
239         User's Manual, pag. 174, 179, 180
240
241         :param samples: array of samples. It is expected to be a list or tuple
242             of samples PRE-CONVERTED TO BINARY. To do this, use the function
243             attach samples_to_bin(). Length vector between 8 and 16000.
244         :type samples list, tuple
245         """
246
247         # Verification of input values
248         L = len(samples)
249         if L < 8 or L > 16000:
250             raise ValueError("No. of samples must be between 8 y 16000."
251                              f" Vector length is {L}.")
252         if type(samples[0]) is not bytes:
253             raise TypeError("Signal samples must be binary type.")
254
255         # Packing data for transfer
256         N = L * 2  # no of bytes to send
257         X = len(str(N))  # no. of digits of the no. of bytes
258         cmd = f"DATA:DAC VOLATILE, #{X}{N} "
259         #cmd = cmd.encode()
260         for item in samples:
261             cmd += item.decode("latin1")
262
263         cmd = cmd.encode()
264         # Transfer (can take a while)
265         if verbose:
266             print("Sending data, please wait.")
267         s.reset_input_buffer()  # Buffer reset
268         s.write(cmd + b'\r\n')  # Command + stop characters
269
270         if verbose:
271             print(f"Sent: DATA:DAC VOLATILE, #{X}{N} <samples>")
272
273     def arb_download_to_volatile(self, samples, verbose=True):
274         """
275         NOTE: IT DOESN'T WORK. Last modified: 03/1/22.
276         - Yes it works to send few samples, but when the buffer is full
277           gives error --> Implement sending by chunks [done]
278         - That does not solve the problem:
279           Gives an error of -103,"Invalid separator" at the end of the entire send
280           of the sample vector even with the shipment by chunks. When reading the "\r\n"
281           indicating the end of command gives the error.
282
283         Sending samples of an arbitrary signal to RAM. This function
284         sends the samples in integer or floating point.
```

```
285         [16000 samples per HP-IB (GPIB), integer: 51 seconds]
286         In RS-232 the times are greater. User's manual, pag. 2
287
288         Send DATA:DAC VOLATILE, <signed int list separated by comma>
289         User's manual, pag. 174, 179, 180.
290
291         A data list of length between 8 and 16000 samples is expected, of
292         signed integer and not greater than the 12-bit limit of the equipment:
293         The maximum amplitude of the signal corresponds to the sample with value 2047.
294         The minimum amplitude to the sample with value -2048.
295
296         :param samples: array of samples. It is expected to be a list or tuple
297             of samples in signed integer. Length vector between 8 and 16000.
298         :type samples list, tuple
299         """
300
301         # Verification of input values
302         L = len(samples)
303         if L < 8 or L > 16000:
304             raise ValueError("No. of samples must be between 8 y 16000."
305                              f" Vector length is {L}.")
306         maximo = max(samples)
307         if maximo > 2047:
308             raise ValueError(f"Sample value must not exceed 2047. "
309                              f"Max. value is: {maximo} at position "
310                              f"{samples.index(maximo)}")
311         minimo = min(samples)
312         if minimo < -2048:
313             raise ValueError(f"Sample value must not be below -2048. "
314                              f"Min. value is: {minimo} at position "
315                              f"{samples.index(minimo)}")
316
317         # Packing data for transfer
318         cmd = "DATA:DAC VOLATILE, "
319         for item in samples:
320             cmd += str(item) + ","
321         cmd = cmd[0:-1]  # removes final comma
322         cmd = cmd.encode() + b"\r\n"
323
324         # Transfer (can take a while)
325         if verbose:
326             print("Sending data, please wait.")
327
328
329         limit = 64  # Mediator's buffer length (Firmware restriction)
330         sleep_time = 1  # Sleep between chunks (seconds)
331
332         s.reset_input_buffer()  # Input buffer reset
333         s.reset_output_buffer()
334
335         longitud = len(cmd)
336         if longitud >= limit:
337             iterations = int(longitud / limit)
338             restante = longitud % limit
339
340             if verbose:
341                 print(f"Data is long: {longitud} chars. Slicing it into "
342                       f"{iterations} chunks of length {limit} characters.")
343
344             for i in range(iterations):
345                 chunk = cmd[i*limit:(i+1)*limit]
346                 print(f"iter: {i}: sent: {str(chunk)}")
347                 s.write(chunk)  # escribe en chunks
348                 print(f"done. sleep {sleep_time}")
349                 time.sleep(sleep_time)  # wait sleep_time seconds before sending more
                     samples
```

```
350
351             if restante:  # remaining to send
352                 chunk = cmd[(i+1)*limit:]
353                 print(f"iter (remaining): {i+1}: sent: {str(chunk)}")
354                 s.write(chunk)
355                 print(f"DONE.")
356
357         else:
358             s.write(cmd)
359             if verbose:
360                 print(cmd)
361
362     def arb_copy_to_non_volatile(self, arb_name, verbose=True):
363         """
364         Copies the samples of a downloaded function to volatile memory at the
365         nonvolatile memory. Data is always copied from volatile memory to
366         a region of non-volatile memory, identified by the name put on the sign.
367         It will overwrite any saved function with the same name, except
368         built-in functions, which cannot be overridden.
369         Send DATA:COPY <arb_name>
370         Page 182 of the manual
371
372         :param arb_name: name of the function to store in memory. The name of
373         the function identifies the samples. It must be a maximum of 8 characters,
374         must start with a letter. Can contain numbers and underscore ('_').
375         It is not case sensitive.
376         :type arb_name str
377         """
378         cmd = f"DATA:COPY {arb_name}"
379         self._send(cmd, verbose)
380
381     def arb_list_waveforms(self, verbose=True):
382         """
383         Lists the name of the selectable arbitrary functions.
384         Send DATA:CAT?
385         User's manual pag. 176
386         """
387         cmd = "DATA:CAT?"
388         self._send(cmd, verbose)
389         return self._read(verbose)
390
391     def arb_del_waveform(self, arb_name, verbose=True):
392         """
393         Deletes an arbitrary function. Built-ins cannot be removed.
394         It can be used to erase the content stored in volatile memory.
395         Send DATA:DEL <arb_name>
396         User's manual pag. 183
397
398         :param arb_name: name of function to erase, or "VOLATILE".
399         :type arb_name str
400         """
401         cmd = f"DATA:DEL {arb_name}"
402         self._send(cmd, verbose)
403
404     def arb_set_waveform(self, arb_name, verbose=True):
405         """
406         Selection of the arbitrary wave to generate at the output. does not generate
407         the wave to the output, it just selects it. To enable the output, you must
408         use the .arb_output_waveform() method.
409
410         Send FUNC:USER {<arb_name>|VOLATILE}
411         Where VOLATILE specifies that the signal loaded in the
412         RAM. <arb_name> is the name of a stored token. Can be
413         any of the options listed with .arb_list_waveforms().
414         User's manual pag. 175, 176
415
```

```
416         :param arb_name: name of function to erase, or "VOLATILE".
417         :type arb_name str
418         """
419         cmd = f"FUNC:USER {arb_name}"
420         self._send(cmd, verbose)
421 
422     def arb_get_waveform(self, verbose=True):
423         """
424         Get current user waveform.
425         Send FUNC:USER?
426         """
427         cmd = f"FUNC:USER?"
428         self._send(cmd, verbose)
429         return self._read(verbose)
430 
431     def arb_set_output_waveform(self, verbose=True):
432         """
433         Generate selected arbitrary waveform.
434         Send FUNC:SHAP USER
435         User's manual pag. 175, 177
436         """
437         cmd = f"FUNC:SHAP USER"
438         self._send(cmd, verbose)
```

Listing F.4 – *HP33120A instrument handler class.*

F.1.4 Usage Examples

```
In [1]:
1 Mediator = USB2GPIB()
2 Mediator.identify()
3 
4 Mediator.set_auto_response(auto_mode=0)  # Since the HP33120A does not support it
5 Mediator.set_slave_address(address=10)  # Address of slave no. 1
6 
7 Mediator.get_auto_response()  # Confirm parameters sets
8 Mediator.get_slave_address()
```

```
Out [1]:
1 Sent: ++ver
2 Read: b'ARDUINO GPIB firmware by E. Girlando Version 6.1\r\n'
3 Sent: ++auto 0
4 Sent: ++addr 10
5 Sent: ++auto
6 Read: b'0\r\n'
7 Sent: ++addr
8 Read: b'10\r\n'
```

Listing F.5 – *Usage Example of the mediator.*

```
In [2]:
1 Mediador.set_slave_address(address=4)  # Generator 2
2 Generador.identify()
3 Generador.version()
```

```
Out [2]:
1 Sent: ++addr 4
2 Sent: *IDN?
3 Read: b'HEWLETT-PACKARD,33120A,0,7.0-2.0-1.0\n'
4 Sent: SYSTem:VERSion?
5 Read: b'1993.0\n'
```

Listing F.6 – *Example identification of the instrument.*

```
In [3]: Generador.arb_list_waveforms(verbose=True)
```

```
Out [3]: Sent: DATA:CAT?
         Read: b'"SINC","NEG_RAMP","EXP_RISE","EXP_FALL","CARDIAC","PRUEBA"\n'
```

```
In [4]: Generador.arb_set_waveform(arb_name="NEG_RAMP")
        Generador.arb_set_output_waveform()
```

```
Out [4]: Sent: FUNC:USER NEG_RAMP
         Sent: FUNC:SHAP USER
```

```
In [5]: Generador.arb_get_waveform()
```

```
Out [5]: Sent: FUNC:USER?
         Read: b'NEG_RAMP\n'
```

Listing F.7 – *Example showing how to output an built-in arbitrary signal.*

F.1.5 Burst mode and external triggering

This code snippets configure the generator 2 to generate a 10 kHz square signal, and through the sync port it will emit the trigger that uses generator 1 as an external trigger to its own signal, a 5 µs square pulse.

It exists a noticeable delay between the two signals, usually around 1.25 µs (see Figure F.3). It is significant for the signals that we handle and it is comparable to the sampling period used.

```
In [6]: Mediator.set_slave_address(address=10)  # Generator 1
        Generator.reset()  # Reset
        Generator.set_output_load("INF", verbose=True)  # High Z
        Generator.set_output_waveform("SQU", verbose=True)  # Square signal
        Generator.set_amplitude("1 VPP", verbose=True)  # 1 Vpp
        Generator.set_offset(0, verbose=True)  # No offset
        Generator.set_frequency(100e3, verbose=True)  # 100 kHz for 5 us pulse

        Generator.enable_burst(mode="ON")  # Activate burst mode
        Generator.set_burst_count(count=1)  # No. of repetitions of the signal
        Generator.set_trigger_source(mode="EXTernal")  # External trigger setup
```

```
Out [6]: Sent: ++addr 10
         Sent: *RST
         Sent: OUTP:LOAD INF
         Sent: FUNC:SHAP SQU
         Sent: VOLT 1 VPP
         Sent: VOLT:OFFS 0
         Sent: FREQ 100000.0
         Sent: BM:STATe ON
         Sent: TRIGger:SOURce EXTernal
```

Listing F.8 – *Trigger setup on the first generator.*

```
In [7]: Generator.get_trigger_source()  # Wait a second before sending
        Generator.get_output_parameters()  # Confirm parameters
        Generator.get_output_waveform()
```

```
Out [7]: Sent: ++addr 10
```

```
Sent: *RST
Sent: OUTP:LOAD INF
Sent: FUNC:SHAP SQU
Sent: VOLT 1 VPP
Sent: VOLT:OFFS 0
Sent: FREQ 100000.0
Sent: BM:STATe ON
Sent: TRIGger:SOURce EXTernal
```

Listing F.9 – *Confirmation of parameter sets in the first generator.*

F.1.6 Example for sending samples to the arbitrary waveform generator from a CSV file

The Listing F.10 shows an example code snippet that automates sending samples from a CSV file which contains signals previously captured with a PicoScope. Please notice that this code is not very flexible since it was conceived only for testing. Refer to the Siglent SDG1062X arbitrary waveform generator utility implementation example of sending samples for a more advanced and elegant solution.

Note that this code works only for short signals. For some reason, the generator refuses to accept long signals (Listing F.11), even though the sent command have the correct format; and even signals are divided in chunks to avoid overflowing the mediator buffer.

In [8]:
```python
import numpy as np

filename = "samples/Arbol_42_original/Arbol_42_A1_1.csv"
t, ch_a, ch_b = np.loadtxt(filename, delimiter=',', unpack=True, skiprows=3)

# Unit adjustments
time_offset = 1e-3 * abs(t[1])  # Time offset to start at t=0
t = t * 1e-3 + time_offset
ch_b = ch_b * 1e-3  # mV to V

L = len(ch_a)
Ts = t[-1] / L  # periodo de muestreo
Fs = int(1/Ts)  # frecuencia de muestreo

print(f"Sampling frequency: {Fs/1e3:.3f} kHz")

sample_init = 2900
sample_end = 10900
sample_num = sample_end - sample_init

t2 = np.arange(0, sample_num, 1) * Ts  # new time vector
tmax = sample_num * Ts  # max time, vector end
freq_rep = int(1/tmax)  # frequency of full-signal repetition

emitter = ch_a[sample_init:sample_end]
receiver = ch_b[sample_init:sample_end]

print(f"Maximum time: {tmax*1e3:.3f} ms; Complete signal frequency: {freq_rep:.3f} Hz")
print(f"Sample vector length: t2: {len(t2)}, emitter: {len(emitter)}, receiver: {len(
 receiver)}")

vmax_emitter = max(abs(emitter))
vmax_receiver = max(abs(receiver))
print(f"vmax,emitter: {vmax_emitter:.3f} V\nvmax,receiver: {vmax_receiver*1e3:.3f} mV")
```

Out [8]:
```
Sampling frequency: 392.196 kHz
Maximum time: 20.398 ms;  Complete signal frequency: 49.000 Hz
Sample vector length: t2: 8000, emitter: 8000, receiver: 8000
```

```
vmax,emitter: 7.221 V
vmax,receiver: 69.039 mV
```

```
In [9]:
emitter_sint = samples_to_signed_int(emitter, v_max=vmax_emitter)
print(f"Emitter length: {len(emitter_sint)}, max: {max(emitter_sint)}, min: {min(
 emitter_sint)}")
receiver_sint = samples_to_signed_int(receiver, v_max=vmax_receiver)
print(f"Receiver length: {len(receiver_sint)}, max: {max(receiver_sint)}, min: {min(
 receiver_sint)}")
```

```
Out [9]:
Emitter length: 8000, max: 1089, min: -2047
Receiver Length: 8000, max: 2047, min: -1768
```

```
In [10]:
Mediador.set_slave_address(address=4)
Generator.reset()
s.reset_input_buffer()
s.reset_output_buffer()
```

```
Out [10]:
Sent: ++addr 4
Sent: *RST
```

```
In [11]:
Mediator.set_slave_address(address=4)  # Generator no. 1
Generator.arb_download_to_volatile(samples=emitter_sint)  # won't work with long signals
```

```
Out [11]:
Sent: ++addr 4
Sending data, please wait.
Data is long: 21098 chars. Slicing it into 329 chunks of length 64 characters.
iter: 0: sent: b'DATA:DAC VOLATILE, 3,3,0,1,0,-2,3,0,0,-27,-210,-451,-594,-646,-7'
done. sleep 1
...
iter: 328: sent: b'3,1,0,-3,-2,-2,0,-3,-2,1,3,-3,-2,0,-2,-2,3,0,-2,1,1,-2,-3,0,-2,-'
done. sleep 1
iter adicional: 329: sent: b'2,0,1,0,-2,-2,0,-3,-2,0,0,1,3,1,-2,4,0,0\r\n'
DONE.
```

Listing F.10 – *Snippet for sending samples to the HP33120A arbitrary waveform generator.*

```
In [12]:
Generador.error()
```

```
Out [12]:
Sent: SYSTem:ERRor?
Read: b'-103,"Invalid separator"\n'
```

Listing F.11 – *Error that appears when sending long vectors of samples.*

F.1.7 Generators repair process

When the sources were first turned on, they both showed no signal at their outputs, but the Sync ports were working just fine. A common failure, especially in old equipment, is that either the output resistance or a fuse has burned or deteriorated due to misuse or the passage of time.

When opening the power supply casing (Figure F.5), the first thing that was done was to check the status of the fuse at the generator output, which is marked on the PCB as F801 (Figure F.6). It is a simple 250 mA THT fuse fitted in a socket. It did not give continuity with the multimeter, so it was obviously fused. When changing it for a new one, it was verified that the generator worked correctly. This same fix was made to the second source, with identical result.

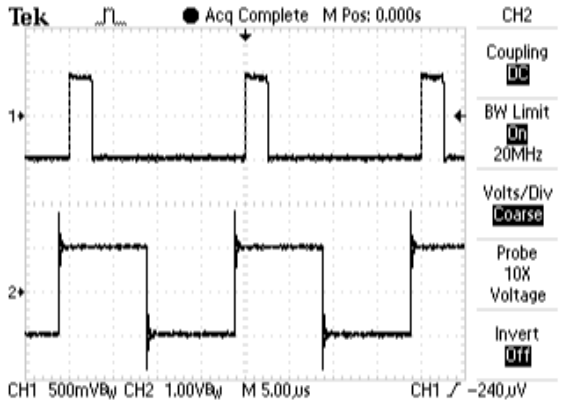

(a) *Channel 2: 50 kHz signal being generated with the second generator. This device also produces its corresponding "sync" signal that is being used by the first generator (channel 1) as trigger for its own 2.5 µs square signal.*

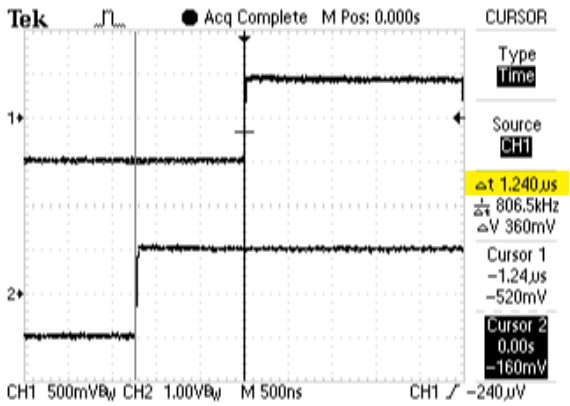

(b) *Detail over the pulses. The delay between the triggering signal (below, ch2) and triggered signal (above, ch1) is approximately 1.240 µs. Precision of the cursors: 20 ns.*

Figure F.3 – *The HP33120A trigger delay measured on a Tektronix TDS1001B oscilloscope.*

(a) *Both HP33120A generators with the mediator on top.*

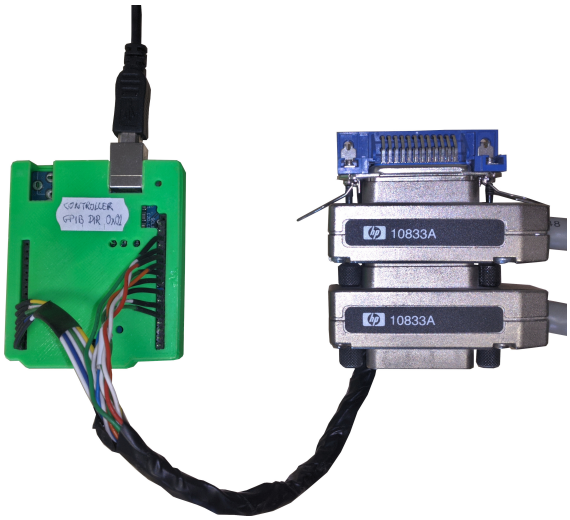

(b) *Detail of the Arduino UNO mediator and GPIB adapter and connectors.*

Figure F.4 – *Both HP33120A generators and the USB2GPIB mediator.*

F

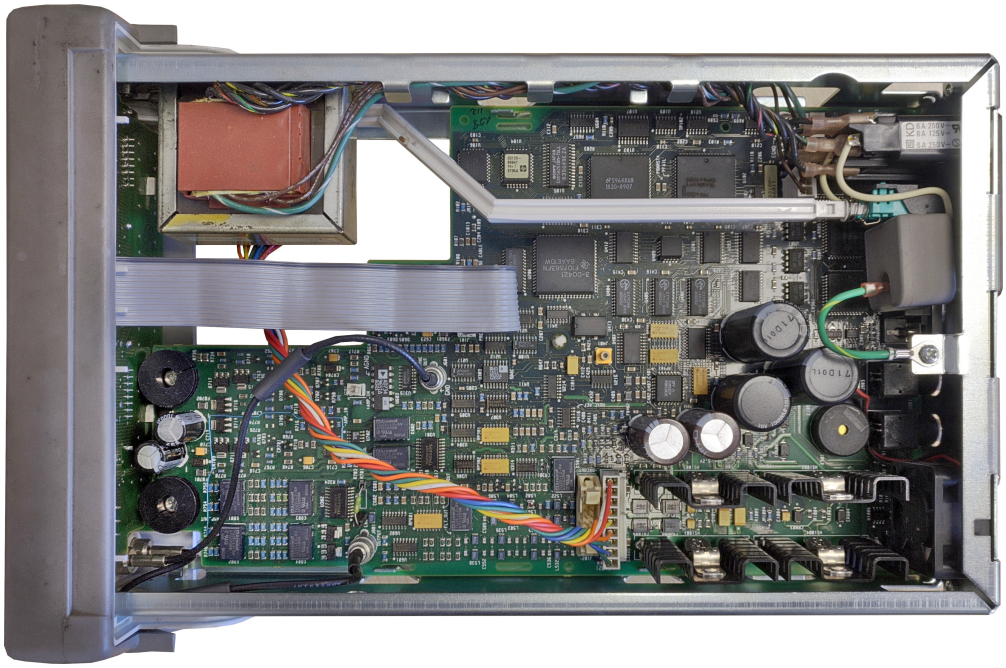

Figure F.5 – *Photo of the internals of the HP33120A.*

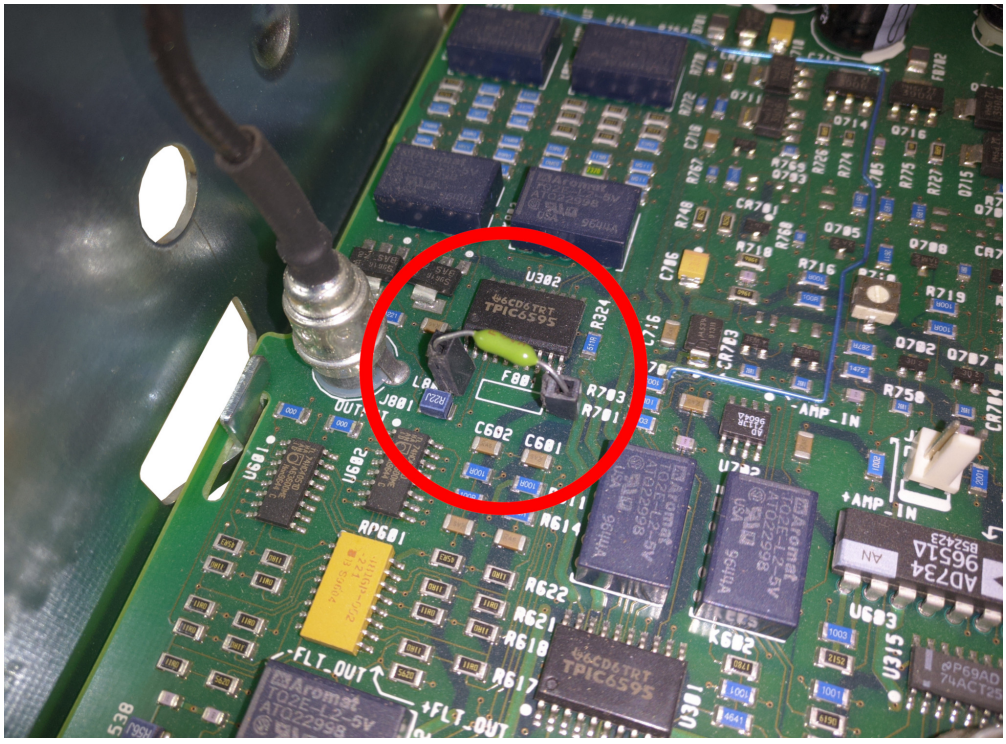

Figure F.6 – *Detail of the HP33120A's output fuse.*

F.2 Siglent SDG1062X function/arbitrary waveform generator

The most important specifications of the Siglent SDG1062X generator for our scope of use are: 2 output channels, up to 60 MHz of bandwidth, a maximum sampling rate of 150 MSa/s, and 14-bit of vertical resolution over a range of ±10 V. This device can output samples using both TARB (True Arbitrary) which respects the sampling frequency of the arbitrary waveform; or DDS (Direct Digital Synthesis), which interpolates samples for a smoother output (see Figure F.12). It also has a *burst* function which allows to generate a single period of a given signal. It can save arbitrary signals up to 16.000 points in its internal memory as binary files.

Some recommended reading beforehand are the SDG1000X series user manual [184], its service manual [185] and its programming guide [186]. Part of the code of this application is based on Siglent's programming example for creating a stair-step waveform using PyVISA over a LAN [187].

F.2.1 Development notes

- **Repository:** `https://github.com/granasat/SDG1000X-jupyter-pyVISA-instrument-library`
- **Python version:** This program was developed using Python 3.9.
- **Library requirements:** Third-party dependencies for running this application, with their corresponding versions used during the development.
  - `numpy`, version 1.22
  - `matplotlib`, version 3.5.1
  - `pyvisa`, version 1.10

F.2.1.1 Changelog

- **v01 - 01/02/2022**
  - Initial implementation.
  - Setup and output of built-in signals.
  - Methods for selecting the output signal and setting the output parameters, per channel.
  - Methods for sending samples to the arbitrary waveform generator.
- **v02 - 30/03/2022**
  - Implementation of burst commands, to trigger signals under demand, per channel.
- **v03 - 05/04/2022**
  - Translation to English.

F.2.1.2 Known issues

Seems like sending long samples vectors causes the generator to not detect the command termination. This causes the next command to be interpreted as samples and to output some weird, digital shapes at the end of the desired function. This can be palliated by sending immediately after the samples an empty command, only containing the command termination characters (`\r\n`).

The small remnant of this effect that has not been possible to eliminate can be seen for example in the waveforms of Figure F.12a and Figure F.12c. It manifests itself in a small hill or peak at the end of the signal period (therefore, it also appears just before the start of a new period). Thus, signals generated with *burst* mode signals are unaffected at the beginning of its periods.

(a) *Front panel.*

(b) *Back panel.*

Figure F.7 – *The SDG1062X front and back panels. Extracted from: [188].*

F

F.2.2 Network interface configuration

1. Connect the function generator and your PC to the same local network:
   (a) This library was developed using wired Ethernet LAN cables for both devices. The router and network hub on GranaSat's 11th laboratory share the `192.168.1.0/24` LAN.
   (b) The router has Wi-Fi disabled. To avoid problems, you may need to deactivate the Wi-Fi connection of your laptop (can be troublesome as they can use different wired and wireless networks simultaneously).
   (c) For convenience, this guide sets a fixed IP to the generator and assumes DHCP is enabled for the operator's PC. This way, there is no need to figure out what IP is the generator using every time you power it up.

   Make sure your PC is connected to the same LAN as the equipment by typing `ipconfig` (on Microsoft Windows CLI), or `ifconfig` or `ip addr` (on a GNU/Linux terminal emulator).
2. Access the LAN interface setup on the function generator and configure a fixed IP:
   (a) Press the "Utility" button » Go to page 2 » Enter in the "Interface" section » Press "LAN setup".
   (b) Set the equipment's IP address to a known free IP e.g.: `192.168.1.101`.
   (c) Set the network mask to: `255.255.255.0` (equivalent to /24).
   (d) Set the gateway address to: `192.168.1.1`
   (e) Press accept. A message pops, which says: "Set up successfully".
   (f) Make sure DHCP is off.
3. Check if the device is accessible from the operator's PC:ç
   (a) Do a ping to the device: `ping 192.168.1.101` (on Windows and GNU/Linux). The device should reply (Listing F.12).
   (b) (Optional) The Nmap network tool can provide some more information about the device's network status. `# nmap -O 192.168.1.101` (on GNU/Linux). It should appear as a 'Texas Instruments' network device, as seen on Listing F.13.

```
$ ping 192.168.1.101
PING 192.168.1.101 (192.168.1.101) 56(84) bytes of data.
64 bytes from 192.168.1.101: icmp_seq=1 tt1=64 time=0.662 ms
64 bytes from 192.168.1.101: icmp_seq=2 tt1=64 time=0.370 ms
64 bytes from 192.168.1.101: icmp_seq=3 tt1=64 time=0.293 ms
^C
--- 192.168.1.101 ping statistics ---
3 packets transmitted, 3 received, 0% packet loss, time 2021ms
rtt min/avg/max/mdev = 0.293/0.441/0.662/0.158 ms
```

Listing F.12 – *Result of doing a 'ping' to the equipment.*

```
# nmap -O 192.168.1.101
Starting Nmap 7.92 ( https://nmap.org ) at 2022-02-02 10:29 CET
Nmap scan report for 192.168.1.101
Host is up (0.00028s latency).
All 1000 scanned ports on 192.168.1.101 are in ignored states.
Not shown: 1000 filtered tcp ports (no-response)
MAC Address: E8:EB:11:[redacted] (Texas Instruments)
Too many fingerprints match this host to give specific OS details
Network Distance: 1 hop
```

Listing F.13 – *Nmap scan results of the device.*

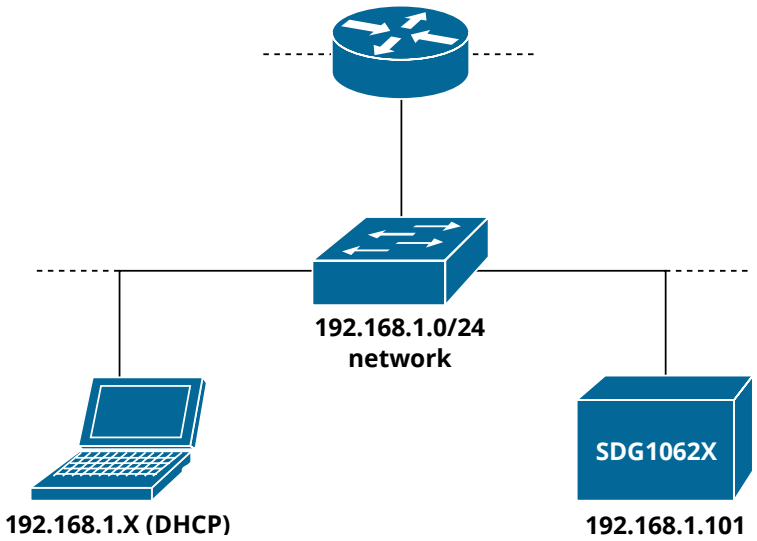

Figure F.8 – *Representation of the LAN network used to connect the operator's PC and the SDG1062X.*

F.2.3 Library implementation

The communication library with the instrument has been coded in the following Python class (Listing F.14)

```python
import pyvisa as visa
import binascii

class SDG1062X:
    """
    Methods to communicate with the Siglent SDG1062X arbitrary waveform generator. May be
    compatible with other device series like SDG1000X, 2000X and 6000X/X-E (untested).
    These functions send SCPI commands according to the SDG1000X series programming guide.
    """

    def __init__(self, device_resource : str, timeout=50, chunk_size=24*1024*1024):
        """
        Constructor. Default configuration based on Siglent's python example.
        :param device_resource: Device resource identification.
        """
        self.timeout = timeout
        self.chunk_size = chunk_size
        self.device_resource = device_resource
        self.device_resource_manager = visa.ResourceManager('@py')
        self.device = self.device_resource_manager.open_resource(self.device_resource,
                                                                 timeout=self.timeout,
                                                                 chunk_size=self.chunk_size
                                                                 )
        self.device.write_termination = ''

    def query(self, cmd: str):
        """
        Sends a command and waits for a reply.
        :param cmd: command to send
        """
        return self.device.query(cmd)

    def write(self, cmd: str, termination="", encoding="latin1"):
```

```
        """
        Sends a command without expecting a reply.
        :param cmd: command to send
        """
        return self.device.write(cmd, encoding=encoding, termination=termination)

    # SYSTEM COMMANDS

    def identify(self):
        """
        Asks the function generator to identify itself.
        Sends: *IDN?
        """
        cmd = "*IDN?"
        return self.query(cmd)

    def reset(self):
        """
        Resets the function generator.
        Sends: *RST
        """
        cmd = "*RST"
        return self.write(cmd)

    # OUTPUT COMMANDS

    def output_config(self, channel: int, enabled: bool, load: str):
        """
        Output channels configuration.
        C<channel>:OUTPut ON|OFF,LOAD,<load>
        Programming Guide pag. 17

        :param channel: Output channel (1 or 2).
        :param enabled: Wether if output is enabled. True: ON, False: OFF
        :param load: Output load, in ohms. Can be "HZ" (High Impedance).
        """
        if enabled:
            output = "ON"
        else:
            output = "OFF"
        cmd = f"C{str(channel)}:OUTPut {output},LOAD,{load}"
        return self.write(cmd)

    def output_basic_wave(self,
                          channel: int,
                          wave_type: str,
                          freq: int,
                          amp: float):
        """
        Generates a basic wave.
        C<channel>:BaSic_WaVe WVTP,<wave_type>,FRQ,<freq>,AMP,<amp>
        Programming guide pag 18,19,20
        :param channel: Output channel (1 or 2).
        :param wave_type: Output signal name. Only tested with "SINE" and "ARB"
        :param freq: Frequency of the signal period repetition.
        :param amp: signal Vpp amplitude.
        """
        cmd = f"C{str(channel)}:BaSic_WaVe WVTP,{wave_type},FRQ,{freq},AMP,{amp}"
        return self.write(cmd)

    # ARBITRARY WAVE COMMANDS

    def arb_output(self, channel, wave_name):
        """
        Output a device-stored arbitrary waveform.
        Programming guide pag 30, 31
```

```
        :param channel: Output channel (1 or 2).
        :param wave_name: Name of the signal to output.
        """
        cmd = f"C{channel}:ARWV NAME,{wave_name}"
        return self.write(cmd)

    def arb_sample_rate(self,
                        channel: int,
                        sample_rate: int,
                        interpolation="LINE",
                        sample_rate_mode="DDS"):
        """
        Sets the sampling mode and rate of the arbitrary function generator.
        <channel>:SampleRATE MODE,<mode>,VALUE,<sample_rate>,INTER,<interpolation>
        Programming guide pag 48, 49

        For the SDG1062X model, I strongly recommend using DDS (Direct Digital
        Synthesis) over TARB (True ARB), as SDG1062X does not have linear or
        sinc interpolation. in DDS, samples are stair-interpolated but in TARB
        are not, and signal is much more step.

        :param channel: Output channel (1 or 2).
        :param sample_rate: Sampling frequency (only for TARB)
        :param sample_rate_mode: "DDS" or "TARB"
        :param interpolation: "LINE", "HOLD" or "SINC". Doesn't work on SDG1062X
        """
        cmd = f"C{channel}:SRATE MODE,{sample_rate_mode},VALUE,{sample_rate},INTER,{
         interpolation}"
        return self.write(cmd)

    def arb_send_samples(self,
                         channel: int,
                         wave_name: str,
                         freq: int,
                         amp: float,
                         bin_data: str,
                         len_data: int):
        """
        Send arbiatry function data to the signal generator. Must be
        pre-converted to binary-ascii. Use the utils to convert data to the
        right format. (at the end of this class, marked as staticmethods)

        C<channel>:WVDT WVNM,<wave_name>,FREQ,<freq>,AMPL,<amp>,WAVEDATA,<wave_data>
        Programming guide pag 42,43

        :param wave_name: The name your signal will be stored as.
        :param wave_data: Sample vector with samples formatted as binascii
        """
        cmd = f"C{channel}:WVDT WVNM,{wave_name},FREQ,{freq:.3f},AMPL,{amp:.3f},OFST,0.0,
         PHASE,0.0,WAVEDATA,{bin_data}"
        print(f"bytes: {len(cmd)}")
        return self.write(cmd, encoding='latin1', termination='')

    def arb_get_samples(self, wave_name):
        """
        Get user-defined wave data
        C<channel>:WVDT? USER,<wave_name>
        Programming guide pag 43

        :param wave name:
        :type wave_name str
        """
        cmd = f"WVDT? USER,{wave_name}"
        return self.query(cmd)

    # BURST COMMANDS
```

```
164
165     def burst_config(self, channel: int, state: str, trigger_source='INT'):
166         """
167         Busrt configuration.
168
169         <channel>:BursTWaVe <parameter>,<value>
170         Programming guide pag 27, 28
171
172         :param channel Generator channel (1 or 2)
173         :param state {'ON', 'OFF'} Enable/Disable burst
174         :param trigger_source {'EXT', 'INT', 'MAN'} (External, Internal, Manual)
175         :param trigger_delay seconds to wait to trigger the generator.
176         """
177         cmd = f"C{channel}:BursTWaVe STATE,{state},TRSR,{trigger_source}"
178         self.write(cmd)
179
180     def burst_send_manual_single_channel(self, channel: int, trigger_delay=0):
181         """
182         Sends a manual trigger to a channel.
183
184         <channel>:BursTWaVe <parameter>,<value>
185         Programming guide pag 27, 28
186
187         :param channel Generator channel (1 or 2)
188         :param trigger_delay seconds to wait to trigger the generator.
189         """
190         cmd = f"C{channel}:BursTWaVe STATE,ON,TRSR,MAN,DLAY,{trigger_delay}"
191         self.write(cmd)
192         cmd = f"C{channel}:BursTWaVe MTRIG"
193         self.write(cmd)
194
195     def burst_send_manual_both_channels(self,
196                                         ch1_trigger_delay=0,
197                                         ch2_trigger_delay=0):
198         """
199         Sends a manual trigger to both channels.
200
201         <channel>:BursTWaVe <parameter>,<value>
202         Programming guide pag 27, 28
203
204         :param ch1_trigger_delay trigger delay of channel 1
205         :param ch2_trigger_delay trigger delay of channel 2
206         """
207         cmd = f"C1:BursTWaVe STATE,ON,TRSR,MAN,DLAY,{ch1_trigger_delay}"
208         self.write(cmd)
209         cmd = f"C2:BursTWaVe STATE,ON,TRSR,MAN,DLAY,{ch2_trigger_delay}"
210         self.write(cmd)
211
212         cmd = f"C1:BursTWaVe MTRIG"
213         self.write(cmd)
214         cmd = f"C2:BursTWaVe MTRIG"
215         self.write(cmd)
216
217     # STATIC METHODS, UTILS
218
219     @staticmethod
220     def samples_int_C2_to_bytes(samples_int_C2 : list):
221         """
222         Standalone function (util) to convert a sample vector in two's
223         complement-ready format (unsigned int) to binascii.
224
225         The generator expects a two's complement, littl-endian, 2-bytes samples.
226         Based on Siglent's Python example: first transforms the data to hex,
227         switches byte order and then converts to binany-ascii using
228         binascii.unhexlify() from binascii python library.
229
```

```
230         :param samples_int_C2: list of samples in C2, unsigned.
231         :returns samples_bytes: list of samples in binary ascii ready to be sent
232         """
233 
234         # Transforms integers to hexadecimal in a much more compact way than the
             programming example.
235         samples_hex = [f"{(sample):04x}" for sample in samples_int_C2]
236 
237         # Inverts the byte order in hexadecimal (little)
238         samples_hex_little = [sample[2:4] + sample[:2] for sample in samples_hex]
239 
240         # Transforms HEX little to ASCII-codified binary
241         samples_bytes = [binascii.unhexlify(sample) for sample in samples_hex_little]
242 
243         return samples_bytes
244 
245     @staticmethod
246     def samples_float_to_int_C2(samples_float : list, amp=None):
247         """
248         Standalone function (util) to convert a sample vector in floating point
249         to integer. Negatives are transformed to two's complement unsigned int.
250 
251         Sample values are selected from the amp param. All values are scaled by
252         this value. If no amplitude is specified, the function will select the
253         absolute maximum as signal amplitude.
254 
255         IMPORTANT: Although the function generator datasheet indicates a 14 bit
256         vertical resolution, the device expects 16-bit samples which i suspect
257         transforms internally to the DAC maximum resolution.
258         This means the maximum sample value range it's not [-8192, +8191] but
259         [-32768, +32767].
260 
261         :param samples_float list of samples in float, can be signed.
262         :param amp: maximum absolute signal amplitude.
263         :type amp float
264         :returns samples_int_C2: list of samples on int C2, unsigned format.
265         """
266         if not amp:  # Uses the signal's full range by default
267             amp = max(abs(samples_float))
268 
269         n_bits_dac = 16  # no. of bits of the DAC. Supposed to be 14, but the instrument
              understands 16
270         n_points_totales = 2 ** n_bits_dac
271         n_points = (n_points_totales / 2) - 1  # no. of steps of the DAC, from zero to the
              positive extreme
272         factor = n_points / amp  # Scaling factor of the samples
273 
274         samples_int_signed = [int(round(sample * factor))
275                               for sample in samples_float]
276         samples_int_C2 = []
277         for sample in samples_int_signed:
278             if sample < 0:
279                 samples_int_C2.append(sample + n_points_totales)
280             else:
281                 samples_int_C2.append(sample)
282 
283         return samples_int_C2
```

Listing F.14 – *SDG1062X arbitrary waveform generator communication class.*

F.2.4 Usage examples

This section introduces how to use the previous class and teaches the basics of how the communication works. `DEVICE_IP` is a constant defined globally. It is a string that identifies the instrument's fixed IP. If you are using any other interface you'll need to find how to identify the resource. Check the documentation of pyVISA for help.

```
In [1]:
DEVICE_IP = "192.168.1.178"  # The IP of the instrument

# Initialize class
Generator = SDG1062X(device_resource=f"TCPIP0::{DEVICE_IP}::inst0::INSTR")
Generator.identify()  # Ask the device to identify itself.
```

```
Out [1]:
'Siglent Technologies,SDG1062X,SDG1XCAD1R3295,1.01.01.33R1B6\n'
```

Listing F.15 – *Initialization of the class object and identification of the instrument.*

```
In [2]:
# Output a sine wave of 10 kHz and 2 Vpp with a HZ load on channel 1.
Generator.output_config(channel=1, enabled=True, load="HZ")
Generator.output_basic_wave(channel=1, wave_type="SINE", freq=1e4, amp=2)
```

Listing F.16 – *Example of output setup for a sine wave of 10 kHz, 2 Vpp, high-impedance load.*

F.2.5 Burst control. Triggering of individual periods

By default, the signal generator outputs repetitive and continuous signal periods. However, real tree signals, read by the piezoelectric sensors, consists of single events that can be missed. In order to realistically simulate this behaviour, *burst* mode is used.

Burst mode triggers individual signal periods when a specific condition is met. Both channels of the SDG can be triggered manually and independently, allowing us to imitate a real signal and even configure the delay between the emitter and the receiver (see Figure F.14c and Figure F.14d).

Since there's no way to trigger both channels truly simultaneously, we could think that an additional delay will be inherently added to the signals. Nevertheless, this effect is not noticeable (compare Figure F.14a and Figure F.14b). And if necessary, it could be corrected by setting a small trigger delay on channel 1.

Listing F.17 shows the usage of the implemented *burst* methods.

```
In [3]:
# Deactivates burst
Generator.burst_config(channel=1, state="OFF")
Generator.burst_config(channel=2, state="OFF")

# Activates burst and sends a manual trigger to both channels
# This is what you want to execute if are outputting TIK singals
Generador.burst_send_manual_both_channels()
```

```
In [4]:
# Activates both channels burst mode and sends a manual trigger for both
# channels, but with a configurable delay on every channel.
# This can be used to test if TIK equipment detects the arrival time correctly.

emitter_delay_s = 100e-6  # Emitter delay in seconds. Moves signal closer to each other.
receiver_delay_s = 0  # Receiver delay. in seconds. Moves signals away from each other.

```

```
Generador.burst_send_manual_both_channels(ch1_trigger_delay=emitter_delay_s,
                                          ch2_trigger_delay=receiver_delay_s)
```

Listing F.17 – *Configuration of burst mode triggering.*

F.2.6 Sending samples directly from CSV files with PicoScope format

Listing F.19 shows a complete, standalone function called `send_samples_file()` which implements a program using the developed library. The function does all the operations necessary to send samples to the arbitrary waveform generator from a .csv file. This file must follow the PicoScope CSV format: plain text, with 3 columns separated by commas, and with a header which indicates the corresponding units, and with a point as the decimal separator (see format at Listing F.18). In Listing F.19, `graphSamples()` is an auxiliary function which represents the sent data to ease visual verification of the signal waveform and its properties (Figure F.9). The code of the graph function has been omitted in this Appendix as it was considered irrelevant.

In Listing F.20 we can observe an example usage and output of this function.

```
 Time,        Channel A,   Channel B       # Channel names
 (ms),        (V),         (mV)            # Channel units

-7.50678836,  0.00488341,  0.30521300      # sequence of N data rows
-7.50423836, -0.01587108,  0.30521300
...          ...          ...
```

Listing F.18 – *Default expected format of the samples files.*

```
import numpy as np
import time
import os

Generator = SDG1062X(device_resource=f"TCPIP0::{DEVICE_IP}::inst0::INSTR")

def send_samples_file(path_to_file : str,
                      sample_init : int,
                      sample_end : int,
                      delimiter=","):
    """
    Does all the operations necessary to send samples to the arbitrary waveform
    generator from a .csv file. Generator channel 1 will be the Emitter (column
    ChannelA) and channel 2 will be the receiver (column ChannelB). By default
    this signal repeats itself periodically. To avoid this, set the burst
    configuration. NOTE: The number of samples must not exceed 16000.

    :param path_to_file relative path to the .csv file to send
    :sample_init: sample index from where to begin sending
    :sample_end: sample index to where end sending.
    """

    # ------------------------- GENERATOR OBJECT ---------------------------- #

    Generator.identify()
    Generator.reset()
    time.sleep(1)

    # --------------------------- FILE READING ------------------------------ #

    # Reads the 2nd row as string, to identify units
```

```
    units = np.loadtxt(path_to_file, delimiter=delimiter, dtype=str, skiprows=1, max_rows
     =1)

    # lectura de los datos como números en coma flotante
    t, ch_a, ch_b = np.loadtxt(path_to_file, delimiter=delimiter, unpack=True, skiprows=3,
     dtype=float)

    # ------------------------- DATA TRANSFORMATION ------------------------- #

    t = t - t[0]  # start at t0 = 0

    if units[0] == "(ms)":
        t *= 1e-3;  # ms to s
    elif units[0] == "(us)":
        t *= 1e-6;  # us to s

    if units[1] == "(mV)":
        ch_a *= 1e-3;  # mV to V
    if units[2] == "(mV)":
        ch_b *= 1e-3;  # mV to V

    L = len(t)      # length of the vector of samples
    Ts = t[-1] / L  # sampling period
    Fs = int(1/Ts)  # sampling frequency

    sample_num = sample_end - sample_init

    print(f"Sampling frequency: {Fs/1e3:.3f} kHz")

    t2 = np.arange(0, sample_num, 1) * Ts  # New temporal vector
    tmax = t2[-1]  # Maximum time
    freq_rep = int(1/tmax)  # Frequency of a complete signal's period

    emitter = ch_a[sample_init:sample_end]
    receiver = ch_b[sample_init:sample_end]

    print(f"Complete signal period: {tmax*1e3:.3f} ms\n"
          F"Complete signal frequency: {freq_rep:.3f} Hz")
    print(f"Length of the sample vector: {len(t2)}")

    vmax_emitter = max(abs(emitter))
    vmax_receiver = max(abs(receiver))

    print(f"vmax,emitter: {vmax_emitter:.3f} V (abs)\n"
          f"vmax,receiver: {vmax_receiver*1e3:.3f} mV (abs)")
    print(f"2*vmax,emitter: {2*vmax_emitter:.3f} V (abs)\n"
          f"2*vmax,receiver: {2*vmax_receiver*1e3:.3f} mV (abs)")

    vpp_emitter = max(emitter) - min(emitter)
    vpp_receiver = max(receiver) - min(receiver)

    print(f"vpp,emitter: {vpp_emitter:.3f} V\n"
          f"vpp,receiver: {vpp_receiver*1e3:.3f} mV")

    # ------------------------- BINARY CONVERSION ------------------------- #

    # EMITTER

    emitter_intC2 = Generator.samples_float_to_int_C2(emitter)
    emitter_bytes = Generator.samples_int_C2_to_bytes(emitter_intC2)

    emitter_bytearray = b""
    for item in emitter_bytes:
        emitter_bytearray += item
    emitter_binascii = emitter_bytearray.decode("latin1")

```

```
    # RECEIVER

    receiver_intC2 = Generator.samples_float_to_int_C2(receiver)
    receiver_bytes = Generator.samples_int_C2_to_bytes(receiver_intC2)

    receiver_bytearray = b""
    for item in receiver_bytes:
        receiver_bytearray += item
    receiver_binascii = receiver_bytearray.decode("latin1")

    # ---------------------- SAVING INTO A .BIN FILE ------------------------ #

    arbol_file = str(path_to_file.split('/')[-1]).split('.')[0]
    save_folder = str(path_to_file.split('.')[0])

    try:
        os.mkdir(save_folder)
    except FileExistsError:
        print("Overwriting data!")
    print(f"save_folder = {save_folder}")


    # Guardando el binario
    with open(f"{save_folder}/{arbol_file}_e.bin", "wb") as f:  # Emisor
        f.write(emitter_bytearray)
    with open(f"{save_folder}/{arbol_file}_r.bin", "wb") as f:  # Receptor
        f.write(receiver_bytearray)

    # Lectura del archivo binario
    with open(f"{save_folder}/{arbol_file}_e.bin", "rb") as f:
        emitter_bindata = f.read().decode("latin1")
    with open(f"{save_folder}/{arbol_file}_r.bin", "rb") as f:
        receiver_bindata = f.read().decode("latin1")

    print(f"Length of binary data: {len(emitter_bindata)}")

    # --------------------- SEND DATA TO THE GENERATOR ---------------------- #

    # EMITTER to CHANNEL 1

    emitter_wave_name = f"{arbol_file}_e"
    Generator.arb_send_samples(channel=1,
                               wave_name=emitter_wave_name,
                               freq=freq_rep,
                               amp=vmax_emitter,
                               bin_data=emitter_bindata,
                               len_data=len(emitter_bindata))
    Generator.write("\r\n")
    time.sleep(1)
    Generator.arb_output(channel=1, wave_name=f"{emitter_wave_name}")

    time.sleep(1)

    # RECEIVER to CHANNEL 2

    receiver_wave_name = f"{arbol_file}_r"
    Generator.arb_send_samples(channel=2,
                               wave_name=receiver_wave_name,
                               freq=freq_rep,
                               amp=vmax_receiver,
                               bin_data=receiver_bindata,
                               len_data=len(receiver_bindata))
    Generator.write("\r\n")
    time.sleep(1)
    Generator.arb_output(channel=2, wave_name=f"{receiver_wave_name}")

```

```
    print("\nDONE")

    graphSamples(t2, emitter, receiver,
                 title=f"{path_to_file} | Sent signals. [COMPLETE]")
    graphSamples(t2, emitter, receiver,
                 title=f"{path_to_file} | Sent signals. [ZOOM]", xlim=[0, 5])
```

Listing F.19 – *Standalone function which uses the developed class to automatically send samples to the arbitrary waveform generator from a CSV file.*

In [5]:
```
# Path to the .csv samples file. (a .bin file will be saved on the same path)
# Expects a plain text file with '.' as decimal separator and ',' delimiter.
path_to_file = "samples/Arbol_42_original/Arbol_42_A1_5.csv"

# Sets the configuration and sends samples to the arbitrary waveform generator.
# Channel 1 will be the Emitter
# Channel 2 will be the Receiver
send_samples_file(path_to_file,
                  sample_init=2900,  # These parameters sets the init and end of
                  sample_end=10900)  # Sample vector to send. Must not be longer than 16000
```

Out [5]:
```
Sampling frequency: 392.176 kHz
Complete signal period: 20.396 ms
Complete signal frequency: 49.000 Hz
Length of the vector of samples: 8000
vmax,emitter: 7.074 V (abs)
vmax,receiver: 68.307 mV (abs)
2*vmax,emitter: 14.147 V (abs)
2*vmax,receiver: 136.613 mV (abs)
vpp,emitter: 11.043 V
vpp,receiver: 131.242 mV
save_folder = samples/Arbol_42_original/Arbol_42_A1_5
Length of binary data: 16000
bytes: 16080
bytes: 16080

DONE
```

Listing F.20 – *Example usage of the* `send_samples_file()` *function.*

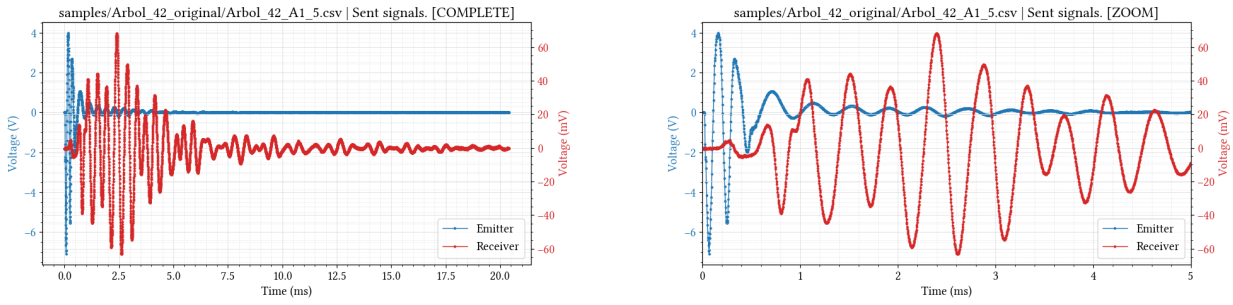

(a) *Normal view: complete sent signal.*

(b) *Zoom view: Detail of the signal beginning*

Figure F.9 – *Matplotlib-generated graphs of samples sent to the generator, for visual inspect, and to compare expected results with the generator output.*

F.2.7 Verification of generated waveforms

The logical subsequent task is the inspection of the implemented functionality, and that it serves our purposes of simulating a real tree signal. Below are some tests that were performed on the team with an arbitrary, real, typical signal previously captured with a PicoScope on a standing tree.

For visualizing the generated waveforms, a Tektronix TDS1001B oscilloscope was used (Figure F.10).

1. In the first place, we realized the poor noise conditions and SNR, specially in the weaker receiver signal. Whether it's coming from the generator, or from the environment (in the GranaSat laboratory there are multiple nearby radio-communications equipment, as well as power electronics) and/or the combination of both, results in noisy signals. This is an important limitation when simulating real signals to verify the correct behavior of our prototype.

   To address this problem at least for measuring the output signals properties, average acquisition mode was used (Figure F.11) which artificially suppresses noise.

2. We also studied the signal's wave form in detail. Since it's artificially generated by a DAC this can lead to distorted, staggered signals. As we can see in figure Figure F.12, DDS mode gives a more natural look to the waveform, as this model has not got access to advanced interpolation methods in TARB mode.

3. In Figure F.13 the generated signal properties are compared to the desired one. As we can see, in terms of signal characteristics accuracy, Siglent's source delivers.

4. Finally, we examined the delays that may occur when using burst mode as we did with the HP33120A units. In this case, the result is much more convenient as no noticeable delay was added. On top on that, this device allows for easy tweaking of the delay between the receiver and emitter signals.

F.2.8 Generator repair process

During the use of the equipment, in a cycle of switching on and off the generator completely stopped working. The symptoms were:

- The screen turned on, showed the logo, the LCD stayed off indefinitely.
- It did not respond to the buttons on the front panel.
- It was detected by the Nmap network scanning tool, but did not respond to any *pings*.

These symptoms are typical of an internal logical error, rather than hardware. However, guided by a user who had problems with a power rail [189], it was decided to open the case and inspect the internal test points of two PCBs of the device. However, as we can see on Table F.1, all the rails were working on their nominal voltages with tolerable margins of error.

In view of the results, this possibility was ruled out. Another user had problems with the firmware of the device: certain versions of the firmware seem to clutter the internal storage of the device with logs without control or self-maintenance, preventing the system from being able to write during boot and therefore blocking the power on [190].

We got in touch with Siglent Europe technical support, who were very kind and sent us a copy of a recovery firmware and instructions for its installation [191]. After successfully recovering the system and formatting it to its factory state, its software was updated to the latest version available to prevent the aforementioned error from reoccurring.

Figure F.10 – *Siglent SDG1062X outputting emitter/receiver signals, and visualization with a Tektronix TDS1001B oscilloscope on GranaSat's laboratory. Both devices are directly connected one another. The arbitrary generator is configured for a high-impedance (Hi-Z) load.*

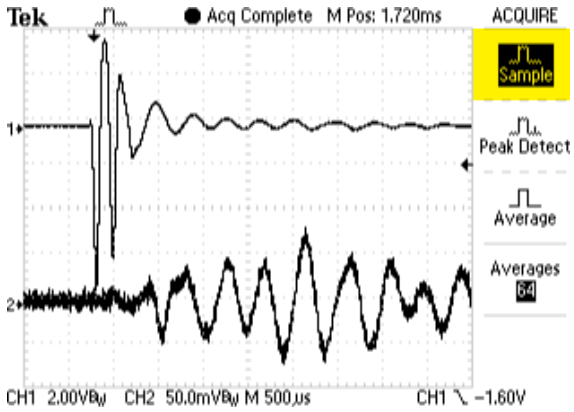

(a) *Sample mode. A lot of noise is captured on the oscilloscope, even with a 20 MHz bandwidth limit applied to its input.*

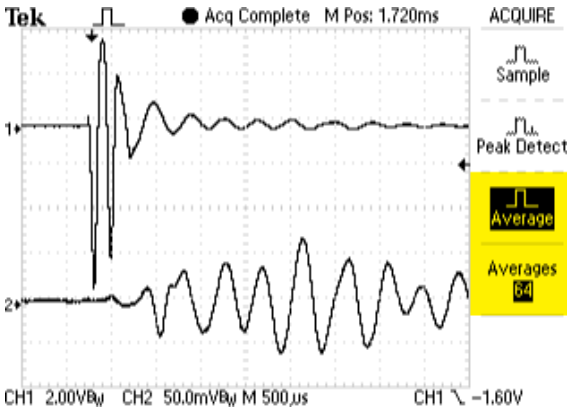

(b) *Average mode. What we see is a mean of 64 successive periods. A lot of noise is artificially suppressed, and we can now easily measure the signal properties.*

Figure F.11 – *Comparison of waveforms and noise between sample acquisition mode and average acquisition mode.*

F

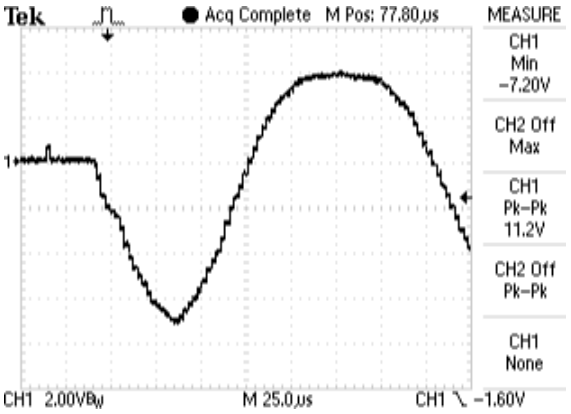

(a) *Analysis of the DAC distortion on TARB (True Arbitrary) mode. This mode places a sample on the generator output respecting the sampling period of the original signal, unlike the DDS mode. But on the downside, this makes the signal look staggered and artificial.*

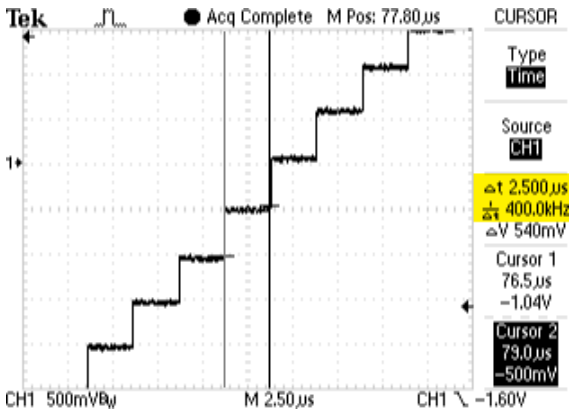

(b) *If we zoom in, we can confirm the original sampling frequency is respected in TARB mode. (the precision of the cursors is 0.1 µs)*

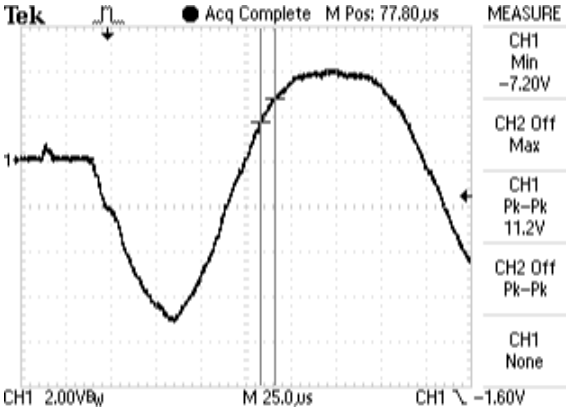

(c) *Analysis of the DAC distortion on DDS mode. This mode interpolates samples, and makes the signal look more natural and clean.*

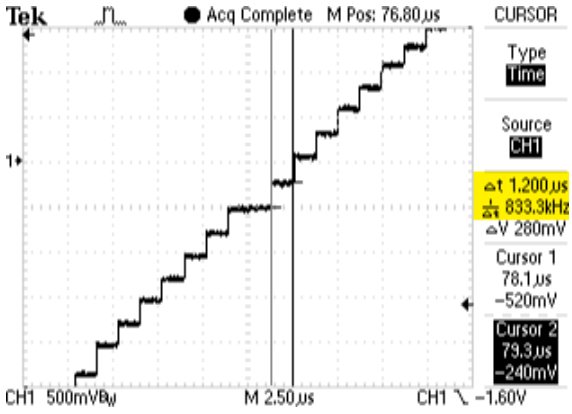

(d) *Zooming in the same region as before we can clearly see the sampling frequency has approximately doubled in comparison to the TARB mode, and steps are smaller (the precision of the cursors is 0.1 µs)*

Figure F.12 – *Comparison of waveforms and noise between sample acquisition mode and average acquisition mode.*

F

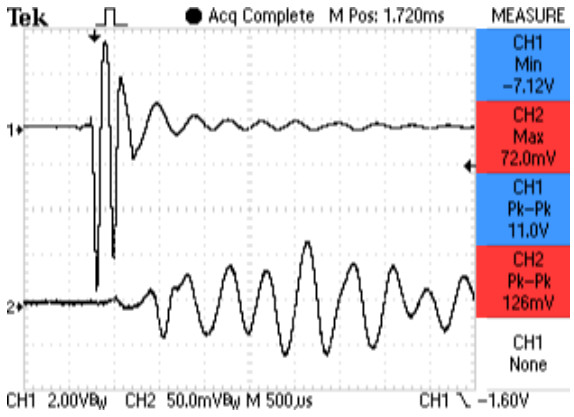

(a) *Measurements of simulated signals generated with the equipment and acquired with 64 averages. For the emitter, we measure the minimum voltage (the negative peak) and for the receiver the maximum, as it will be always positive. For both channels, we also measure the peak-to-peak voltage.*

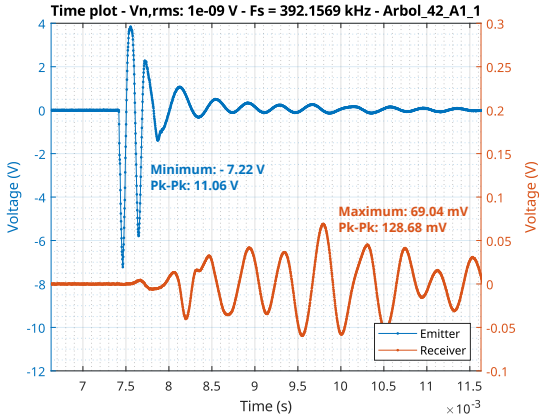

(b) *Original signal graphed in the same time interval and scale than the image on the left, for visual comparison. As we can see, the wave form is accurate and its properties are almost identical.*

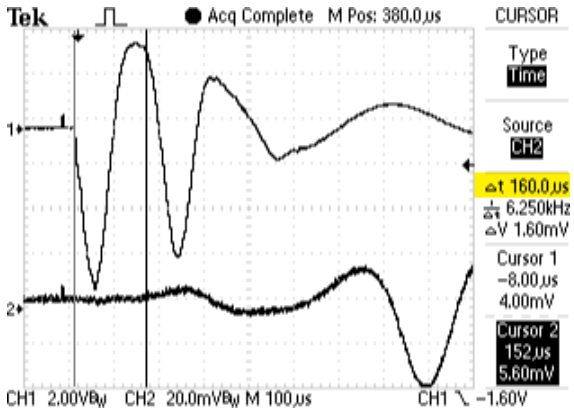

(c) *Zoom in to the signal beginning, in order to measure the delay between the two signals (the precision of the cursors is 4 µs). The result on the original signal estimated with the Akaike method is 163.2 µs (see graph on the right).*

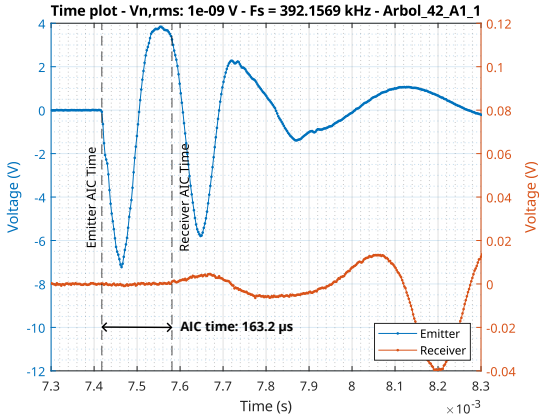

(d) *Original signal graphed in the same time interval and scale than the image on the left. The result estimated with the Akaike method is 163.2 µs.*

Figure F.13 – *Comparison of signal properties and waveforms between the original sent signal and the generated one acquired in average mode.*

F

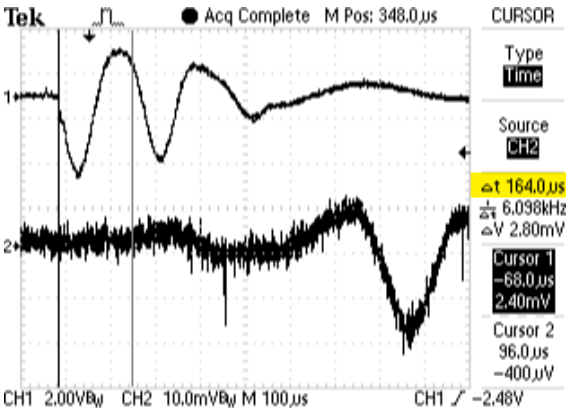

(a) *Visual identification of the signal's beginning and delay estimation with cursors (the precision of the cursors is 4 µs). In this case, both signals were generated simultaneously by the SDG's internal trigger and continuously, without a burst setting.*

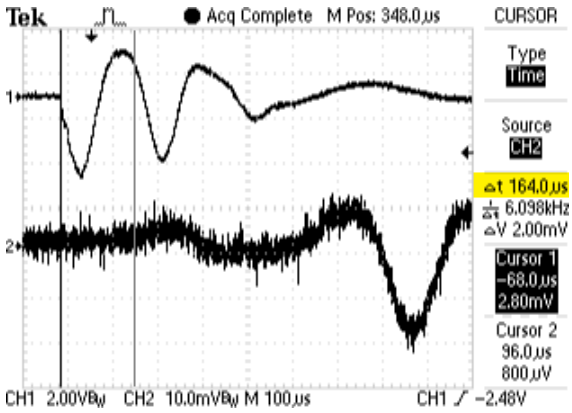

(b) *Visual identification of the signal's beginning and delay estimation with cursors. In this case, both signals were manually triggered and only generated once. As we can observe, the difference is imperceptible and negligible.*

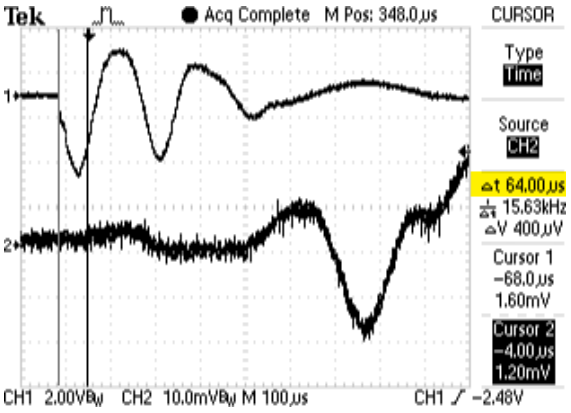

(c) *Delay control on simulated signals. In this case, the delay was reduced in 100 µs.*

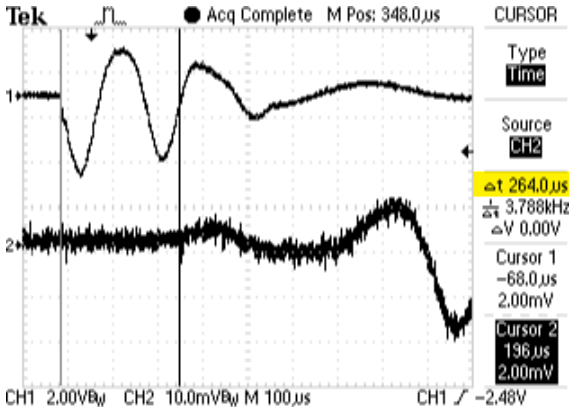

(d) *Delay control on simulated signals. The delay between signals was increased in 100 µs.*

Figure F.14 – *Demonstration of burst mode capabilities.*

F

PCB name	Test Point	Description	Nominal signal	Read signal	Discrepance
Main board	TP22	CPU clock	CLK @ 25 MHz	24.88 MHz	0.5 %
	TP86	VCC16V	16 V DC	14.93 V DC	6.7 %
	TP87	VCC5V	5 V DC	5.06 V DC	1.2 %
	TP88	VCC3V3	3.3 V DC	3.37 V DC	2.1 %
Channel board	TP11	VCC3V3	3.3 V DC	3.34 V DC	1.2 %
	TP12	AVCC15V	15 V DC	15.20 V DC	2.0 %
	TP13	VCC5V	5 V DC	4.95 V DC	1.0 %
	TP14	AVCC-15V	-15 V DC	-14.97 V DC	0.2 %
	TP15	VCC1V2	1.2 V DC	1.24 V DC	3.3 %
	TP16	AVEE5V	5 V DC	4.98 V DC	0.4 %
	TP18	AVEE-5V	-5 V DC	-5.03 V DC	0.6 %
	R19	FPGA clock	CLK @ 25 MHz	24.94 MHz	0.2 %

Table F.1 – *Result of reading the test points of both PCBs of the SDG1062X.*

Figure F.15 – *Photo of the internals of the SDG1062X.*

F

F.3 Agilent/HP4192A LF impedance analyzer

The Agilent/HP4192A LF impedance analyzer (Figure F.16) is a 4½-digit test instrument designed to measure impedance parameters in frequency, as well as gain, phase, and group delay. It provides a 5 Hz to 13 MHz, 5 mV to 1.1 V stimulus signal for the DUT. In impedance measurements, the HP4192A can measure:

- Absolute value of impedance |Z|
- Absolute value of admittance |Y|
- Phase angle $|\theta|$
- Resistance |R|
- Reactance |X|
- Conductance |G|
- Susceptance |B|
- Inductance |L|
- Capacitance |C|
- Dissipation factor |D|
- Quality factor |Q|

For the characterization of the piezoelectric sensors, only the resistance and capacitance (and sometimes inductance) were needed. All measurements have a basic accuracy of 0.01 %, given the equipment is correctly calibrated. Measurements were taken manually, as the development of another SCPI management library was dismissed as an unnecessary and time-consuming effort.

Some usage guidelines will be given in order to properly characterize an unknown impedance on frequency. The information presented here has been extracted from the operation and service manual [192]. For more information on the capabilities and operation of the equipment, consult said document.

F.3.1 Preliminary setup, tests and calibration

F.3.1.1 Power up and self-test

1. Press the `LINE ON/OFF` key to turn the 4192A on. Following turn on, the instrument will perform an automatic operational check, sets the GPIB address and displays it on the display A; and performs an initial control setting. Once finished, the trigger should flash.
2. Press the `BLUE` (*shift*) key and then the `SELF TEST` key to check the basic operation of the instrument. "PASS" message should be displayed on the display A.
3. Since the 16047A Direct Coupled Test Fixture will be used, `CABLE LENGTH` switch must be in the "0" position. Connect the 16047A test fixture to the `UNKNOWN` BNC terminals (Figure F.17).

F.3.1.2 Short-Open zero calibration at a given frequency

1. Select which parameter to show on Display A by selecting one from the list using the left `UP` and `DOWN` keys. The indicator LED adjacent to the selected parameter will turn on.
2. Select which parameter to show on Display B by pressing the right `DOWN` key.
3. Press `SPOT FREQ` to set the calibration frequency with the keypad, then press `ENTER`. Default is 1 kHz.
4. Press `OSC LEVEL` to adjust the amplitude of the oscillator. Default is 1 V. In our case, it is left as is.
5. Set the equivalent `CIRCUIT MODE` to series.
6. Ensure the test fixture is correctly coupled. Insert a low impedance shorting lead to the 16047A. In case of using extension cables to reach the DUT, short the ends of the cables instead.

7. Press the BLUE key and then ZERO SHORT. An offset adjustment is automatically made by the equipment, at the spot frequency. "CAL" is displayed on display A.
8. Remove the shorting bar from the test fixture and the equivalent CIRCUIT MODE to parallel. In case of using extension cables to reach the DUT, leave open the ends of the cables instead.
9. Press the BLUE key and the ZERO OPEN key. Another offset adjustment calibration is performed. "CAL" is displayed again on display A. A value of approximately zero should then be displayed on screens A and B. If not, perform another calibration.

   Note: The 4192A requires a one-hour warm-up time to satisfy the stipulated accuracy and all the other listed specifications.

F.3.2 Impedance Measurements in frequency. Operating Instructions

F.3.2.1 Setting the measurement conditions

1. Select the desired equivalent CIRCUIT MODE: series or parallel.
2. Select which parameter to show on Display A and Display B.
3. Set the measurement frequency and oscillator voltage.
4. Perform a Short-Open zero calibration.
5. Press the BLUE key and then the AVERAGE key. The rate of information in the screens will be reduced, since they now show the average of several samples.
6. Connect the DUT to the test fixture (the polarization is not relevant). Make sure the DUT leads are making good connection with the 16047A metal contacts. The DUT (or its cables) should not move during measurement.

F.3.2.2 Measuring in frequency and re-calibration

1. By connecting a DUT to the terminals, the HP4192A automatically calculates its electrical parameters at the set frequency and displays them on the screens.
2. Record the result of the measurement. The equivalent circuit mode and the parameters to show in each screen can be adjusted at any moment.
3. Increase/decrease the spot frequency in the desired steps.

   Note: The equipment can become uncalibrated in the course of usage by switching to a significantly different frequency from the original calibration frequency. Therefore, regular re-calibration at the new frequencies is recommended.

   When a re-calibration is performed, it is advisable to retake some samples close to the re-calibration frequency measured before the re-calibration; and check that there is not a large variance between the old and new values.

   During the measurements for this project, it was found that calibrating once a decade is sufficient to maintain reasonable sample consistency.

Figure F.16 – *Front panel of the HP4192A LF impedance analyzer in the L-4 laboratory of the Faculty of Sciences; with the 16047A test fixture coupled.*

Figure F.17 – *Detail of the 16047A test fixture and HP4192A UNKNOWN port.*

F

F.4 Siglent SDM3065X digital multimeter

The Siglent SDM3065X is a 6½ high-precision digital multimeter capable of voltage and current measurements. Although it is a programmable device, measurements were taken manually as in the case of the HP4192A, since developing another library for few measurements was not time-effective.

F.4.1 Current measurements

1. Turn on the SDM3065X digital multimeter.
2. To measure the current supplied to a device, the instrument must be in series with the power supply and the device (see Figure F.19. Supply cables must be connected to the SDM3065X terminals as indicated in Subfigure H.20c. Do not connect the power supply cables yet.
3. Select DCI (DC intensity) measurement by pressing `Shift` and then `DCI`.
4. Turn on the adjustable power supply, adjust the output voltage in a safe range, from 3.6 V to 4.2 V and a maximum output current of 500 mA. Connect the power supply cables to the circuit.
5. Once connected, the DUT turns on. The TIK prototype runs a demo program; and the SDM3065X shows the average current consumption.

   More information about the demo program is detailed in Section 6.4.8: Power consumption. The program is considered to pose a equal if not higher stress than the final firmware.

This equipment measures assuming a constant DC current supply. As already discussed in Chapter 6: Fabrication, testing and validation, this is not the appropriate way to characterize the current consumption of a digital device, which is not constant but very noisy, and varies greatly depending on the tasks and operations of the microcontroller and the rest of the integrated circuits. Furthermore, we did not use wireless communication in the demo program (in the moments of wireless communication, the current consumption of the ESP32 skyrockets). However, it gives an idea of the average power consumption of the device and can be used to estimate the battery discharge time.

Figure F.18 – *Front panel of the SDM3065X digital multimiter. Extracted from: [193].*

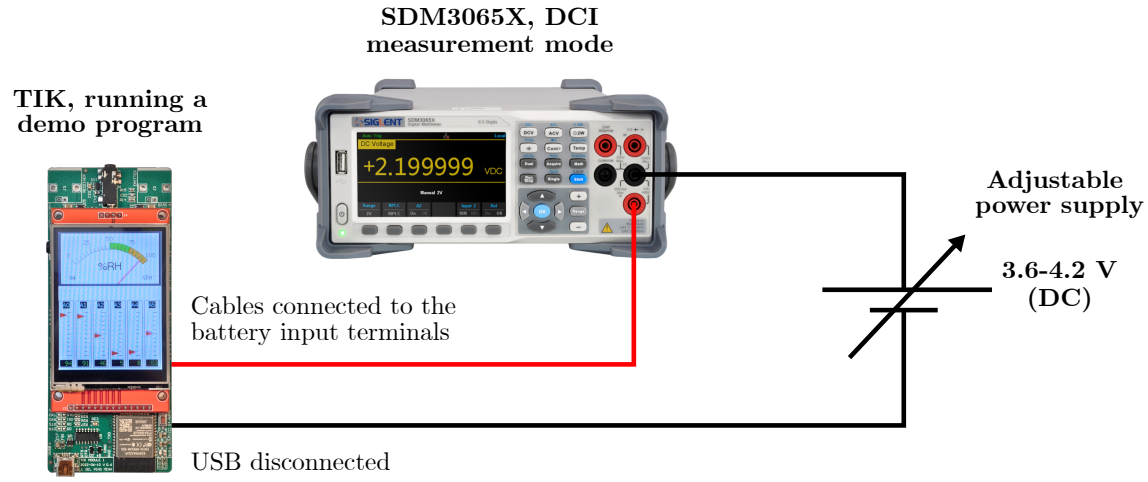

Figure F.19 – *Arrangement of the equipment to measure the DC current supplied to the TIK.*

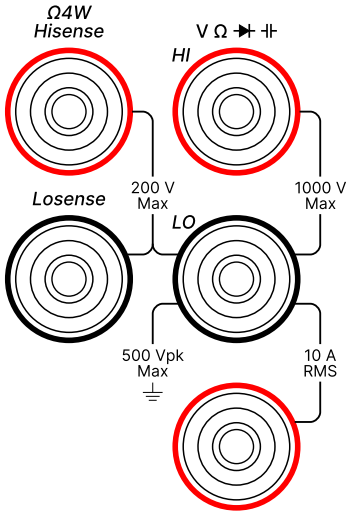

(a) *SDM3065X Front panel measurement connectors.*

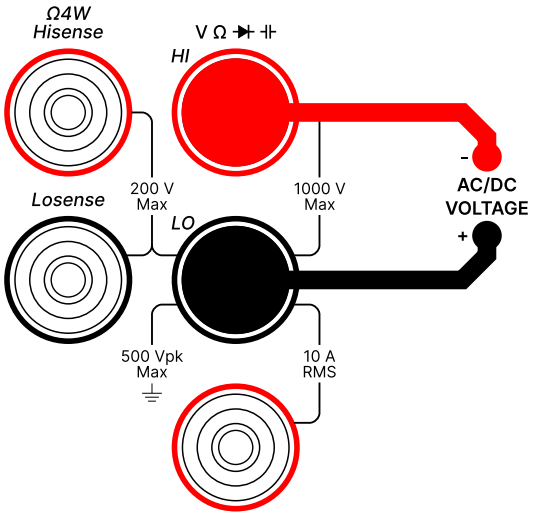

(b) *Needed connections for ACV/DCV (AC/DC voltage) measurements.*

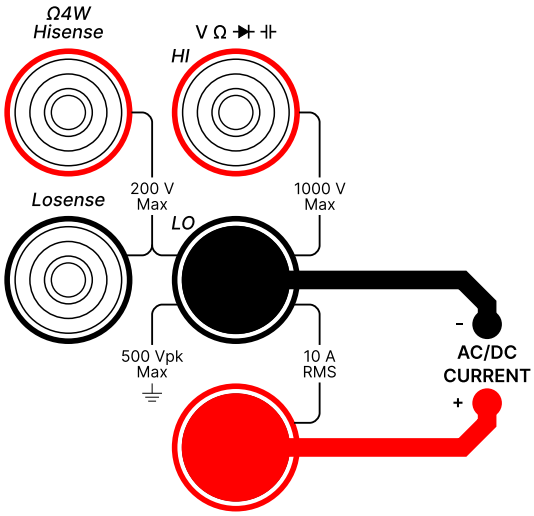

(c) *Needed connections for ACI/DCI (AC/DC intensity) measurements.*

Figure F.20 – *SDM3065X measurement connections. Own work, based on the drawings found on [194].*

F

Thank you for reading this Bachelor's Thesis.